# CAMx
**Ozone
Particulates
Toxics**

## User's Guide
### COMPREHENSIVE AIR QUALITY MODEL
**WITH EXTENSIONS**
Version 6.0

ENVIRON

Copyright: ENVIRON International Corporation,

1997 – 2013

This publication may be reproduced for

non-commercial purposes with appropriate attribution.

## ACKNOWLEDGMENTS

ENVIRON acknowledges the following groups for their contributions to the development of CAMx:

- The Texas Commission on Environmental Quality (TCEQ), for sponsoring the development, testing, and review of numerous components of the model;

- The Lake Michigan Air Directors Consortium (LADCo), for sponsoring the development, testing and review of numerous components of the model;

- The Coordinating Research Council (CRC), for sponsoring the development, testing, and review of numerous components of the model;

- The Carnegie-Mellon University, Department of Chemical Engineering, for providing full-science PM algorithms, assistance in incorporating them into CAMx, and testing the implementation;

- The University of Texas, Center for Energy and Environmental Resources, for assistance in developing and testing the Open-MP multi-processor capability;

- Atmospheric, Meteorological, and Environmental Technologies (ATMET), for providing libraries and implementation support for the HDF5 output format and the MPI parallel processing capability;

- The Midwest Ozone Group (MOG), for sponsoring the development and testing of the MPI parallel processing capability;

- The U.S. Environmental Protection Agency (EPA), for sponsoring the development, testing, and review of the MPI parallel processing capability.  Special thanks to Dr. Jon Pleim for assistance with our implementation of ACM2;

- The San Francisco Bay Area Air Quality Management District (BAAQMD), for supporting and testing the coupling of SAPRC99 gas-phase chemistry to the PM chemistry algorithm;

- The American Petroleum Institute (API), for sponsoring the development and testing of improvements to the vertical advection algorithm;

- Atmospheric and Environmental Research (AER), for developing the mercury chemistry algorithm.

**CONTENTS**

**TABLES**

**FIGURES**

## 1. OVERVIEW

The **C**omprehensive **A**ir quality **M**odel with e**x**tensions (CAMx) is an Eulerian photochemical dispersion model that allows for integrated "one-atmosphere" assessments of air pollution (ozone, particulates, air toxics, and mercury) over spatial scales ranging from neighborhoods to continents.  It is designed to unify all of the technical features required of "state-of-the-science" air quality models into a single open-source system that is computationally efficient, flexible, and publicly available.  The model's Fortran source code is modular and well-documented.  The Fortran binary input/output file formats are based on the Urban Airshed Model (UAM) convention and are compatible with many existing pre- and post-processing tools.  Meteorological fields are supplied to CAMx from separate weather prediction models.

CAMx simulates the emission, dispersion, chemical reaction, and removal of pollutants in the troposphere by solving the pollutant continuity equation for each chemical species (*l*) on a system of nested three-dimensional grids.  The Eulerian continuity equation describes the time dependency of the average species concentration ($c_l$) within each grid cell volume as a sum of all of the physical and chemical processes operating on that volume.  This equation is expressed mathematically in terrain-following height (*z*) coordinates as follows:

$$\frac{\partial c_l}{\partial t} = -\nabla_H \cdot V_H c_l + \left[ \frac{\partial (c_l \eta)}{\partial z} - c_l \frac{\partial^2 h}{\partial z\, \partial t} \right] + \nabla \cdot \rho K \nabla (c_l / \rho)$$

$$+ \left. \frac{\partial c_l}{\partial t} \right|_{Emission} + \left. \frac{\partial c_l}{\partial t} \right|_{Chemistry} + \left. \frac{\partial c_l}{\partial t} \right|_{Removal}$$

where $V_H$ is the horizontal wind vector, $\eta$ is the net vertical transport rate, $h$ is the layer interface height, $\rho$ is atmospheric density, and $K$ is the turbulent exchange (or diffusion) coefficient.  The first term on the right-hand side represents horizontal advection, the second term represents net resolved vertical transport across an arbitrary space- and time-varying height grid, and the third term represents sub-grid scale turbulent diffusion.  Chemistry is treated by simultaneously solving a set of reaction equations defined from specific chemical mechanisms.  Pollutant removal includes both dry surface uptake (deposition) and wet scavenging by precipitation.

CAMx can perform simulations on three types of Cartesian map projections: Universal Transverse Mercator, Rotated Polar Stereographic, and Lambert Conic Conformal.  CAMx also offers the option of operating on a curvi-linear geodetic latitude/longitude grid system.  The vertical grid structure is defined externally, so layer interface heights may be specified as any arbitrary function of space and/or time.  This flexibility in defining the horizontal and vertical grid structures allows CAMx to be configured to match the grid of any meteorological model that is used to provide environmental input fields.

## 1.1  CAMx Features

In addition to the attributes it shares with most photochemical grid models, some of the most notable features of CAMx are:

Two-Way Nested Grid Structure:  This feature allows CAMx to be run with variable grid spacing. Use a coarse grid for regional domains where high spatial resolution is not particularly needed, while in the same run, nest finer grids in specific areas of interest.  Two-way nesting propagates information both up- and down-scale across all grids.

Flexi-Nesting:  Arbitrarily introduce and/or remove nested grids at any point during a simulation.  Upon model restart, CAMx automatically diagnoses any changes to the grid system. You can supply complete information for new grids (emissions, meteorology, surface characteristics) or allow CAMx to interpolate any or all of these inputs from parent grids.

Multiple Photochemical Gas Phase Chemistry Mechanisms:  CAMx offers three version of Carbon Bond chemistry (CB05, CB6 and CB6r1; CAMx Mechanisms 6, 7, and 2, respecitively) and the 1999 version of the Statewide Air Pollution Research Center chemistry (SAPRC99; CAMx Mechanism 5).  Variants of these mechanisms that include reactions involving oceanic halogens (chlorine and iodine compounds) are also available.

Particulate Matter Chemistry:  CAMx features detailed algorithms for aqueous chemistry (RADM-AQ), inorganic aerosols (ISORROPIA), and secondary organic aerosols (SOAP).  These algorithms use products from the gas-phase photochemistry for the production of sulfate, nitrate, condensable organic gases, and chloride.  CAMx provides two options to represent the particle size distribution: a static two-mode coarse/fine (CF) scheme, and an evolving multi-section (CMU) scheme.

Mercury Chemistry:  CAMx optionally treats the chemistry of five mercury species (two gases and three particulates) via gas-phase and aqueous pathways.  The mercury chemistry module requires total PM concentrations, so mercury can only be modeled with the "CF" two-mode PM mechanism by including mercury species among the list of modeled species.  All of the rate and equilibrium constants for the mercury mechanism are hard-coded within the chemistry module.

User-Defined Chemistry Mechanism:  "Mechanism 10" provides a simple way to define your own chemistry mechanism.  This option is intended to define simple chemical decay or transformations between gas and/or aerosol species.  You must develop your own Mechanism 10 subroutine and chemistry parameters file.

Chemical Kinetics Solver Options:  Three options are available to solve gas-phase chemistry. The Euler-Backward Iterative (EBI) solver is fast and accurate.  Alternatively, the Implicit-Explicit Hybrid (IEH) solver accuracy is comparable to reference methods such as LSODE but is several times slower than EBI.  The fully explicit Gear-type LSODE solver can be used to "benchmark" a simulation to evaluate the performance of EBI or IEH.  We do not recommend LSODE for typical applications as the model will run ***much*** more slowly.

Plume-in-Grid (PiG) Module: PiG treats the chemistry and dispersion of point source emission plumes at sub-grid scales using a Lagrangian puff model, until such time as the pollutant mass can be adequately represented within the grid model framework.  Both gas-phase and PM chemistry can be treated.  PiG includes a "sampling grid" capability to passively sample plume surface concentrations at any resolution, which is particularly useful to visualize near-source sub-grid scale impacts.

Horizontal Advection Solver Options: CAMx offers the Piecewise Parabolic Method (PPM) of Colella and Woodward (1984), and the area-preserving advection solver of Bott (1989).  Both possess high-order accuracy, little numerical diffusion, and are sufficiently quick for applications on very large grids.

Vertical Diffusion (Mixing) Options:  By default, CAMx employs a standard "K-theory" approach for vertical diffusion to account for sub-grid scale mixing layer-to-layer.  Version 2 of the Asymmetric Convective Model (ACM2; Pleim, 2007) is available as an alternative to the K-theory approach.  ACM2 is a hybrid of local K-theory and non-local convective transport between the surface and layers aloft.  Note that ACM2 increases CAMx runtime considerably relative to the default K-theory, so use of parallelization with ACM2 is encouraged.  ACM2 does not work with the Integrated Process Rate (IRP) component of the Process Analysis (PA) tool.

Dry Deposition Options:  CAMx offers two dry deposition options: an older approach based on the models of Wesely (1989) and Slinn and Slinn (1980); and an updated approach based on the algorithims of Zhang et al. (2001; 2003).  The Wesely/Slinn model is formulated for 11 landuse categories, while the Zhang model uses 26 landuse categories.

Advanced Photolysis Model: The TUV radiative transfer and photolysis model, developed and distributed by the National Center of Atmospheric Research (NCAR, 2011), is used as a CAMx preprocessor to provide the air quality model with a multi-dimensional lookup table of clear-sky photolysis rates.  CAMx internally adjust clear-sky rates for the presence of clouds and aerosols using a fast in-line version of TUV.

Parallel Processing: CAMx supports two types of parallelization: (1) OpenMP (OMP), which allows parallel processing on shared-memory (e.g., multi-core) computers; and (2) Message Passing Interface (MPI), which allows parallel processing across distributed memory (networked) computer cluster environments.  Both OMP and MPI can be used in combination to maximize speed performance.  To use OMP, your Fortran compiler must include libraries to enable in-code directives.  To use MPI, you must have external MPI libraries installed on your system.

## 1.2 CAMX Extensions

The CAMx "extensions" include the following Probing Tools:

Ozone and Particulate Source Apportionment Technology (OSAT/PSAT): Source apportionment technology tracks source region and source category contributions to predicted ozone and/or PM species concentrations.  OSAT also reports information as to whether the ozone at the selected time and location would likely respond to upwind $NO_x$ or VOC controls.  OSAT/PSAT informs the user as to how ozone/PM is attributed to source regions/categories for a given emissions matrix, but does not provide quantitative information as to how ozone/PM would change as those emissions are altered.

Decoupled Direct Method (DDM) and High-Order DDM (HDDM) Source Sensitivity:  This technology calculates first-order (DDM) and second-order (HDDM) sensitivity coefficients for all gas concentrations to changes in emissions, initial conditions and boundary conditions.  Conversely to OSAT, (H)DDM estimates how pollutant concentrations change as a result of region- and category-specific emission changes, but does not provide information on source attribution.  DDM provides accurate sensitivity estimates for relatively small changes (~10%), whereas HDDM allows for more accurate sensitivity estimates for larger changes.

Process Analysis (PA):  This probing tool provides in-depth information on the physical and chemical processes occurring during a CAMx run.  Through PA, one can more fully understand the complex interactions of the different processes, explain simulation results within the context of model formulation, and improve the design of control strategies.  PA is available for CB05, CB6, and SAPRC99 chemical mechanisms, and for EBI, IEH, and LSODE chemistry solvers.  Three components of PA are implemented in CAMx:

1) Integrated Processes Rate (IPR): Provides detailed process rate information for each bulk process in CAMx (i.e., advection, diffusion, deposition, emissions, chemistry, etc.) for selected grid cells and selected species;

2) Integrated Reaction Rate (IRR): Provides detailed reaction rate information for all reactions in the chemical mechanism for selected grid cells; and

3) Chemical Process Analysis (CPA): Closely related to the IRR method, it is designed to be more user friendly and accessible.

Reactive Tracers (RTRAC):  RTRAC provides a flexible add-on to simulate the emission, dispersion, chemistry, and deposition of multiple gas and particle tracers that are not otherwise included in the model's core gas/PM chemistry mechanisms, such as toxics.  Gas-phase chemistry can be simply defined as a set of decay rates by species (via photolysis and radical oxidation from the core model), or as a complex non-linear system defined by the user through the RTRAC Chemical Mechanism Compiler (RTCMC).

## 1.3  Updates In CAMX Version 6.0

CAMx version 6.0 includes the following major updates and additional capabilities over version 5.4:

Revised Input Formats:  All major gridded input/output fields are now in a common format, including all input meteorology, initial/boundary conditions, emissions, and output concentration and deposition fields.  While the format is consistent with the CAMx/UAM format employed up to this version, the file headers have been updated to include additional meta data, such as map projection, grid specifications, time zone, and various field-specific flags.  The biggest change is to meteorological and landuse file formats.  These are now provided in 5 files: 2-D time-invariant, 2-D time-variant, 3-D time-variant, 3-D vertical diffusivities, and 3-D cloud/rain.  Landuse must now be developed for 26 Zhang landuse categories; CAMx internally maps these to 11 categories if Wesely deposition is invoked.  Only the headers of initial/boundary conditions, emissions and output concentration/deposition files have been changed.  ***Pre-existing initial/boundary condition and emission files can be used with v6.00 for backward compatibility, but meteorological input files must be generated specifically for v6.00.***

Photoloysis Rate Updates:  The process to generate photolysis (J) rates and their use in CAMx has changed.

First, the albedo/haze/ozone file now contains only ozone column data.  Surface albedo is internally set within CAMx from input landuse and snow cover.  Haze is internally set within CAMx from the PM simulation, or a default haze profile is set for non-PM runs.  Optional snow-cover has been moved to the 2-D time-varying meteorology file.  Optional drought and surface roughness have been removed.  Optional land/ocean mask is still allowed.  The CAMx namelist variable "`Albedo_Haze_Ozone`" is now "`Ozone_Column`".  ***Use the new "O3MAP" pre-processor to generate this file.***

Second, the TUV photolysis pre-processor generates a clear-sky J lookup table for the following dimensions: ozone column, altitude above ground, terrain height, albedo, and solar zenith.  A single default haze profile is used in TUV.  ***Use the latest version of TUV to generate this file.***

Third, CAMx interpolates lookup J rates to cell-specific values of solar zenith, height above ground, terrain height, and albedo; then photolysis rates are adjusted for clouds and haze using the in-line TUV; then certain photolysis rates are adjusted for temperature and pressure.

Finally, the RADM cloud adjustment has been removed.  In-line TUV is now the only cloud/haze adjustment scheme.  CAMx namelist variables "`TUV_Cloud_Adjust`" and "`TUV_Aero_Adjust`" have been removed.

New Gas-Phase Chemistry Mechanisms:  Two new chemical mechanims were added in CAMx v5.41 and are now documented in this user's guide: Mechanism 1 is the Carbon Bond 6 (CB6) with iodine chemistry intended for modeling ozone in marine environments; Mechanism 2 is CB6 "revision 1" (CB6r1), which revises isoprene and aromatics extensively, and has additional

NOx recycling from organic nitrates.  PM chemistry has not been extensively tested with either mechanism.  Probing tools are not available with Mechanism 1.  OSAT and DDM are available for Mechanism 2, but not Process Analysis.

Mercury Chemistry Updates:  Mercury chemistry has been updated to include adsorption of Hg(II) to PM and gas-phase reactions with ambient bromine.  Gas-phase reactions with ambient molecular chlorine ($Cl_2$) have been removed.  The dry deposition velocity for Hg(0) is set to zero for ocean cells.

Removed Vertical Nesting:  This rarely used feature was removed as it does not contribute significantly to runtime efficiency, leads to numerical problems along nested grid boundaries, and complicates code structures in several areas.  ***NOTE: Namelist variable `"Number_of_Layers"` has been changed from an array to a scalar.***

## 2. THE CAMX MODELING SYSTEM

CAMx comprises the core component of an overall air quality modeling system, as illustrated in Figure 2-1. CAMx inputs are developed using independent third-party models and processing tools that characterize meteorology, emissions, and various other environmental conditions (land cover, radiative/photolysis properties, and initial/boundary conditions). Interface programs are needed to translate the products of each of these models/processors into the specific input fields and formats required by CAMx. After the air quality simulation is completed, additional programs are used to post-process the concentration fields, develop model performance statistics and measures, manipulate Probing Tool output into various reportable formats, and further translate raw results into forms necessary for regulatory purposes. While third-party visualization software, meteorological models, and emission processors are not distributed with CAMx, ENVIRON does provide many of the necessary interface programs and post-processors on the CAMx web site (www.camx.com). A brief description of each of these is provided at the end of this section.
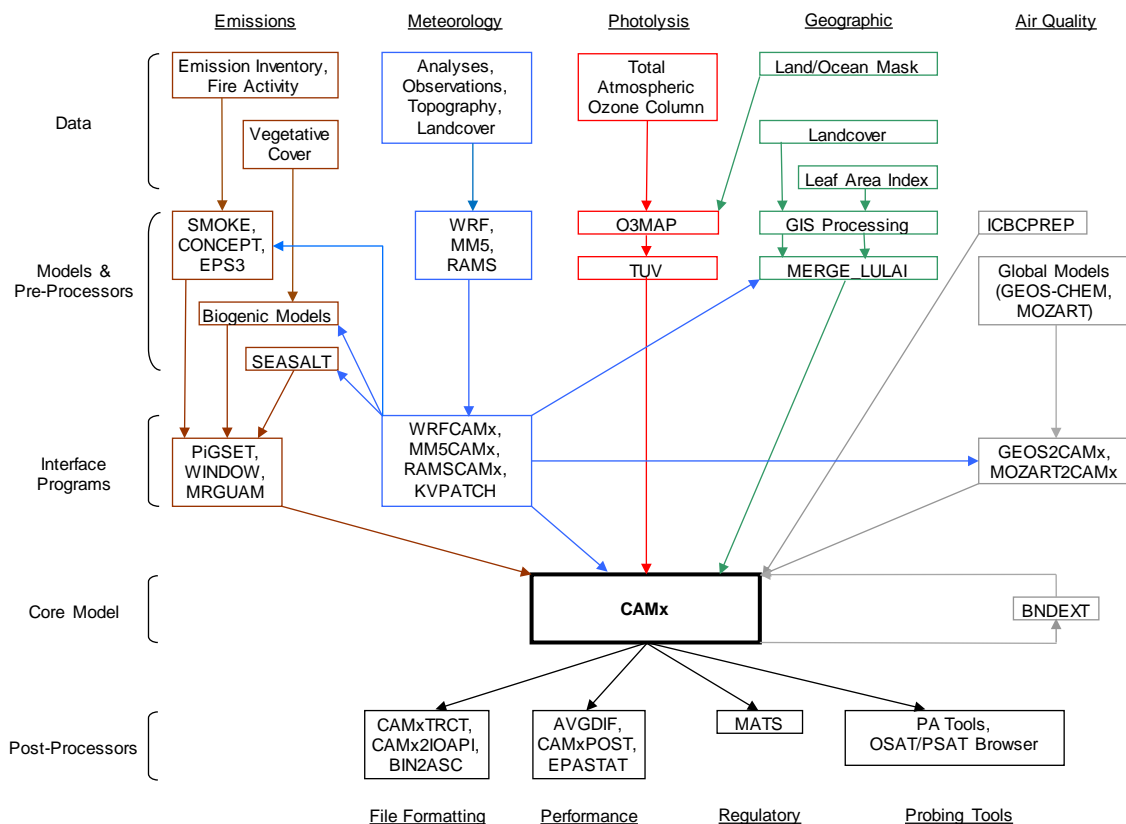


**Figure 2-1. Schematic diagram of the CAMx modeling system. See Table 3-1 for a detailed list of specific model input requirements for the five major data classes shown at the top of the figure. Certain pre- and post-processor programs shown in the figure are described in this section. Third-party models, processors, and visualization software are not described in this User's Guide and are not distributed with CAMx.**

## 2.1 CAMx Program Structure

The core CAMx model is written in Fortran90, but includes some utilities written in C to interface with MPI and HDF5.  The program is highly modular and well documented to ease code review, mofications and substitution of alternate routines.  The source code is arranged in several directories, grouped according to function.  The main source directory contains version release notes, the GNU user license, the "Makefile" compile utility, and a control file namelist template.  Sub-directories contain source code for the core model and ancillary routines according to the following:

| | |
|---|---|
| `CAMx/` | Source code for the main driver routine `CAMx.f` and core model routines. |
| `CF_AERO/` | Source code for inorganic aerosol chemistry (aqueous and thermodynamic partitioning) for the 2-mode CF scheme. |
| `CMC/` | Source code for the gas-phase chemical mechanism routines. |
| `CMU_AERO/` | Source code for inorganic aerosol chemistry (aqueous and thermodynamic partitioning) for the multi-section CMU scheme. |
| `DDM/` | Source code for the (H)DDM Probing Tool, consisting of I/O and core routines that are unique to (H)DDM. |
| `HG/` | Source code for the mercury chemistry routines. |
| `Includes/` | Fortran "include" files, consisting of program parameters and memory management code. |
| `IO_bin/` | Source code for Fortran binary (unformatted) I/O. |
| `IO_hdf/` | Source code for HDF5 I/O. |
| `Mod_src/` | Source code for F90 memory management modules. |
| `MPI/` | Source code for routines specific to MPI parallelization. |
| `OSAT/` | Source code for the OSAT/PSAT Probing Tools, consisting of I/O and core routines that are unique to OSAT/PSAT. |
| `PA/` | Source code for the Process Analysis Probing Tool, consisting of I/O and core routines that are unique to PA. |

| | |
|---|---|
| `PiG/` | Source code for the Plume-in-Grid sub-model, consisting of I/O and core routines that are unique to PiG. |
| `RTRAC/` | Source code for the Reactive Tracer Probing Tool, consisting of I/O and core routines that are unique to RTRAC/RTCMC. |
| `SOAP/` | Source code for secondary organic aerosol thermodynamic partitioning. |

### 2.1.1  Memory Management

All of the model's global data structures are dynamically allocated when the model starts.  The data necessary to allocate memory space for a given model run are read from the CAMx control file developed by the user (see Section 2.3).  However, to alleviate compiler dependency on speed performance, CAMx utilizes some hard-coded Fortran parameters to statically allocate local arrays in low-level subroutines.  All of these parameters are defined in the `Includes/camx.prm` file.  The distribution version of this "include" file sets key array parameters to default values that should be sufficiently large to accommodate most applications: see Table 2-1 for a description of parameters and their default values.  However, you may want to customize these values to ensure that they are large enough to accommodate all of your model configurations, or to exactly match your specific application, thus preventing wasted memory.

*If any parameter is set to a value that is too small to support your application the model will stop, displaying an informative error message.  To conserve memory, default values of 1 are set for Probing Tool tracers, PiG sampling grids, and sampling grid dimensions.  These must be increased accordingly if Probing Tools or sampling grids are to be used.*

**Table 2-1.  Parameters and their defaults in `Includes/camx.prm` used to statically dimension local arrays in low-level subroutines.**

| Parameter Name | Description | Default Value |
|---|---|---|
| MXCELLS | Number of cells in X/Y direction for any grid | 200 |
| MXLAYER | Number of layers | 30 |
| MXSPEC | Number of species (could be number of radicals, number of input species, or total number of model species) | 138 |
| MXREACT | Number of reactions (depends on the mechanism; see the user's guide for the value for each mechanism) | 288 |
| MXGRID | Number of grids | 10 |
| MXPTSRC | Number of point sources | 100000 |
| MXTRSP | Number of Probing Tool tracer species | 1 |
| MXPIG | Number of PiG puffs | 50000 |
| MXSAMPLE | Number of PiG sampling grids | 1 |
| MXCOLSMP | Number of PiG sampling grid columns | 1 |
| MXROWSMP | Number of PiG sampling grid rows | 1 |

All of the parameters in the table above can be determined before starting a simulation except for `MXPIG`. A value of 10,000 is usually sufficient for most applications in which PiG is used; set this parameter to 1 if PiG is not used to conserve memory. If this parameter is exceeded during a simulation, the model will stop with an informative error message. If this happens, simply increase `MXPIG`, recompile the model executable, and restart the simulation. The other parameters in `camx.prm` beyond those listed in Table 2-1 will not normally need to be changed and are not discussed further.

### 2.1.2  Parallel Processing

Parallel processing refers to distributing a model application to multiple processors (CPUs) that share the computational load. CAMx supports two types of parallelization: (1) OpenMP (OMP), which allows parallel processing on shared-memory (e.g., multi-core) computers; and (2) Message Passing Interface (MPI), which allows parallel processing across distributed memory (networked) computer cluster environments. Both OMP and MPI can be used in combination to maximize speed performance.

To use OMP, your Fortran compiler must include libraries to enable the in-code parallelization directives. OMP distributes calculations for individual processes, such as chemistry within a single grid cell or advection/diffusion along a single row of cells, to a number of CPUs defined by the user. Once each CPU has completed its calculations, it works on the next individual process until all processes over the entire grid are completed.

To use MPI, you must have an external MPI library installed on your system. MPICH is a specific open source MPI library widely used in the numerical modeling community; CAMx has been specifically developed and tested using MPICH. With MPI, the CAMx modeling grid is divided into sub-regions and each is assigned to a CPU on the user-defined network. Each CPU operates the entire model on its assigned sub-region and passes common information needed by other CPUs via large data "messages".

MPI in CAMx is designed using a "master/slave" parallel processing approach. The CPU on which the program is launched (process ID 0 under MPI) serves as the master node and will not conduct any model computations on any part of the modeling domain. This process will perform all of the model setup, the vast majority of I/O, and manage the communication between the slave or compute nodes. Since the master node handles the important I/O it is the only CPU that needs access to the disk volume containing the input files and the location of the output directory. This approach allows for a minimal amount of network traffic to/among the compute nodes by eliminating the need for them to manage NFS mounts. The master node may need access to the LAN for data access, but the compute nodes only need access to the internal cluster network. However, the compute nodes will need access to a copy of the executable program. This can be accomplished in a number of ways: (1) have an NFS mount on the master node accessible to the internal cluster network and launch the model from that location; or (2) port a copy of the executable program, using `rcp` or `scp`, to the user's home directory on each compute node and launch the model from the user's home directory on the master node.

During each model time step, when computations are performed by the compute nodes, some information is written to the diagnostic and message output files. Rather than just eliminate this information altogether, we decided to create node-specific versions of each of these two files and have each compute node write the information to its own version. However, in order to prevent the need to have the output directory available to the compute node across the network, we have designed the model so that the node-specific files are created in the current working directory. This means that if the model is launched from an NFS-mounted directory, all of the node-specific files will all be created in that location. On the other hand, if the model is launched from a user's home directory on the compute nodes, you will have to log in to the specific compute node to view the files.

## 2.2  Compiling CAMx

A single "Makefile" script is provided in the main source directory. The Makefile will compile all CAMx source code into an executable program, and it supports platforms running Linux (Portland Group and Intel compilers) and Macintosh OSX (Absoft compiler). All gas-phase chemistry mechanisms and solvers are compiled together into the model executable from the `CMC/` sub-directory. The choice of which chemistry mechanism and solver to use is selected at model run-time as defined in the chemistry parameters and run control files. Similarly, all OSAT, PSAT, DDM, Process Analysis, and RTRAC source code is compiled into the model executable from their respective sub-directories. The choice of which (or none) of these "extensions" to use is selected at model run-time in the run control file.

***The choice for OMP and MPI parallelization, HDF formatted output, and the memory configuration for probing tools are set during model compilation. All other CAMx options are selected at run time.***

CAMx is compiled by issuing the following command at a shell prompt within the main source directory:

```
make platform <DOMAIN=domain_name> <MPI=true> <HDF=true>
```

where the text within the brackets "`<>`" is optional, and `platform` is one of the following:

> `pg_linux` or `pg_linuxomp` (Portland Group compiler for Linux)
> `i_linux` or `i_linuxomp` (Intel compiler for Linux)
> `ab_linux` or `ab_linuxomp` (Absoft compiler for Macintosh OSX)

These keywords inform the Makefile of the type of system/compiler being used to compile and run the model, so that the Makefile can invoke the proper compiler-specific commands and flags. If an OMP platform is not specified then CAMx will not be able to run with OMP parallelization.

The optional `domain_name` allows the CAMx executable program to be labeled for a specific memory configuration as defined within the CAMx parameters file (`Includes/camx.prm`)

described above.  You may want to customize some applications, for example to configure the Probing Tool extensions, and it is convenient to be able to distinguish between these executables.  The Makefile will search for a CAMx parameters file called:

*Includes/camx.prm.domain_name.*

If the Makefile variable "DOMAIN" is not defined on the make command line, the Makefile will compile CAMx using the default parameters file, camx.prm.v6.00.

The optional MPI=true flag will compile CAMx to utilize MPI parallel processing.  This requires that the third-party MPICH libraries have been installed and built on the machine that is running this Makefile script and compiling CAMx.  If the MPI flag is not set on the command line, the Makefile script will ignore the MPI library and CAMx will not be able to run with MPI parallelization.

*You should check that the variable MPI_INST in the CAMx Makefile, as well as in the Makefile in the MPI/util sub-directory, is correctly set to your system's MPI installation path.*

*ENVIRON has developed and tested CAMx with MPICH using only the Portland Group and Intel Fortran90 compilers.*

CAMx supports the use of both OMP and MPI in a single run.  To utilize OMP in your MPI application, run the command "make pg_linuxomp MPI=true" or "make i_linuxomp MPI=true" or "make ab_linuxomp MPI=true".  In this case, the executable will have the OMP directives for shared-memory parallelization built in.

The optional HDF=true flag will compile CAMx to include HDF5 I/O libraries.  This requires that HDF5 libraries have been installed and built on the machine that is running this Makefile script and compiling CAMx.  If the HDF flag is not set on the command line, the Makefile script will ignore the HDF libraries and CAMx will not be able to write HDF5 files.

*You should check that the variables HDF_LIB and HDF_INC in the CAMx Makefile are correctly set to your system's HDF5 library and include-file installation path.*

The Makefile will generate a CAMx executable program named

CAMx.*<domain_name>.noMPI.platform* (compiled without MPI)

or

CAMx.*<domain_name>.MPI.platform* (compiled with MPI)

which will reside in the main source directory.  For example, a default compilation using the Portland Group compiler wil result in an executable named

`CAMx.v6.00.noMPI.pg_linux`.

If you need to rebuild CAMx using different Makefile arguments we recommend typing "`make clean`" between builds. Make clean will delete all existing object files and force a complete re-build.

### 2.2.1 A Note on Fortan Binary Input/Output Files

Large CAMx input and output data fields are contained within Fortran "unformatted" (binary) files. This means that the data are read and written as represented in memory, without translation between binary and ASCII character sets as is performed for "text" files. Binary files reduce file volume and improve program read/write speed, but the user cannot directly view or manually edit them. There are two ways to represent binary information in memory: "big endian" and "little endian." The difference between these is essentially the order of bits in a word, and which order is used depends on the computer chipset. Historically, big endian has been used in many Unix workstations (Sun, SGI, HP, and IBM). The x86 processors on personal computer platforms (e.g., Intel and AMD) use little endian, while PowerPC chips are big endian.

CAMx can be compiled and run on machines that use either big or little endian binary representations, as long as the model and all of its pre- and post-processors are consistently compiled and run on the same type of platform. If any component of the modeling system is compiled on a different platform using the opposite binary representation, I/O files will not be properly read and will likely lead to a program crash.

***A typical run-time error message from trying to read the wrong binary format is "input record too long," so if you get this error message, check for big endian / little endian consistency between your binary files and Fortran compiler options.***

Compilers for little endian machines (e.g., x86 PC chipsets) provide compile-time switches that allow binary files to be read and written as big endian. The Portland Group compiler option is "`-byteswapio`", whereas the Intel compiler option is "`-convert big_endian`." The CAMx Makefile sets compiler flags to consistently use big endian to maximize platform portability. Therefore, use of the CAMx Makefile will by default result in the model reading and writing big endian binary files. In practice, users should use the default binary format that is built into the CAMx Makefile and that is used for the CAMx distribution test case.

## 2.3 Running CAMx

### 2.3.1 Control File Namelist Input

CAMx reads a text (ASCII) run control file named "`CAMx.in`" that must exist locally in the directory from which the model is run. This file must be in the Fortran "namelist" format, and contains all user-specified control parameters for a given simulation, including model configuration, option-specific inputs, and I/O filenames. The run control file must contain the primary namelist module labeled "`&CAMx_Control`", which provides all of the information to configure the core model. Additional namelist modules may be provided in the run control file

to configure the various CAMx Probing Tool extensions. These optional namelist modules are ignored if no Probing Tools are selected in the primary namelist.

Each record in the CAMx control file contains a variable name that is explicitly set to a numerical, logical, or character value. The variable names are used by the program directly, and therefore cannot be changed without source code modifications. Character strings must be enclosed by single quotes, and all variable assignments must be delimited with commas. The order of the records may be arranged in any fashion that the user prefers. Any number of comment statements may be included anywhere within the namelists, provided that they do not interrupt variable assignments (`variable_name = value,`). The "`!`" character is the Fortran namelist comment delimiter.

Certain variables are multi-dimension arrays; the user may provide a comma-delimited list of values to fill the array or assign values to specific array elements. Certain other variables are optional or associated with option flags; these do not need to appear in the namelist if their associated options are not invoked, and they will be ignored if they remain in the file.

***If the user does not provide necessary inputs, the model will stop with a descriptive error message.***

### 2.3.1.1  Common Errors When Creating a Namelist

Fortran programs ingest the entire contents of namelist modules using a single READ statement. If the program experiences an error reading the namelist, it echoes a simple error message like "error reading namelist" and the program stops. It is therefore difficult to determine the cause of the read error, especially if the namelist is lengthy and contains a variety of data types. When experiencing an error reading the CAMx control file namelist, you must carefully inspect the file for any syntax errors. These errors can be subtle and difficult to spot. Here are a few of the common reasons an error occurs when reading a namelist:

- *Mistyped variable name*:

  All variables to be assigned within a namelist must be recognized as a declared namelist variable within the reading program. If a variable is misspelled or an unknown variable is assigned a value, a read error will occur.

- *Incorrect data type for the assigned variable*:

  If the data type of the value assigned to a namelist variable does not match the variable's declared data type within the reading program, an error will occur. Some compilers will allow real type variables to be assigned to integer values, but not the converse.

- *Missing period around a logical value*:

  The logical values `.true.` and `.false.` must be surrounded by a period.

- *Missing quotes around a character variable*:

  Any character data type must be surrounded by quotes.

- *Overflow when assigning values to an array*:

The values in an array can be assigned using array index notation. If the index used to assign an array value exceeds the declared dimension of the array, a read error occurs. Check the "MXNAM" parameter in the `Includes/namelist.inc` include file to see if this value needs to be increased. Alternatively, check your namelist file to be sure all of your array indices are correct.

- *Wrong number of dimensions when assigning values to a multi-dimensional array*:

  When assigning values to an array using array index notation, the number of subscripts in the assignment must match the declared dimensions of the array (e.g., assignments to an array dimensioned `var(i,j)` must be referenced using two indices).

- *Missing comma following a variable definition*:

  A comma must be the last character in a variable assignment (`variable = value,`). A comment may be placed after the comma (delimited using the "`!`" symbol, see below) on the same file record. This restriction on the use of commas is ignored on some compilers.

- *Too many commas following a scalar variable definition*:

  More than one comma following a scalar variable assignment will result in a read error.

- *Too many commas following the variable assignment list for an array*:

  The entire contents of an array can be assigned using a single statement by listing the values of each element separated by commas. The read will fail if there are more commas than the dimension of the array.

- *Comment does not begin with !*:

  The character that delimits a comment in a namelist is the exclamation point. Comments can appear anywhere within the namelist. However, all text in the namelist must either be part of a namelist variable assignment or part of an identified comment.

**We suggest that new CAMx users start with the `CAMx.namelist.template` that is provided with the source code.**

### 2.3.1.2  The Primary Namelist Module

This section describes the primary namelist module; detailed descriptions of each of the Probing Tool modules are provided in their respective sections (Sections 7 through 11). A listing of all namelist variables necessary to run the core model is presented on the following pages.

**Description of CAMx Run Control File Variables**

| | |
|---|---|
| `&CAMx_Control` | Label for the primary namelist module that configures the core model; it must begin in column 2 |
| `&` | Flag ending a namelist module; it must be in column 2 |
| `Run_Message` | 60-character simulation message, written to output files to label the run |

The short simulation "run message" is written to all output files to describe and label the run.

Model Clock Control

| | |
|---|---|
| `Time_Zone` | Integer time zone (0=UTC, 5=EST, 6=CST, 7=MST, 8=PST) |
| `Restart` | Logical model restart flag (TRUE=read restart file, FALSE=read initial conditions file) |
| `Start_Date_Hour` | Integer array start time (YYYY, MM, DD, HHmm) |
| `End_Date_Hour` | Integer array end time (YYYY, MM, DD, HHmm) |
| `Maximum_Timestep` | Real maximum allowable timestep (minutes) |
| `Met_Input_Frequency` | Real input frequency of environmental fields (minutes) |
| `Ems_Input_Frequency` | Real input frequency of emissions (minutes) |
| `Output_Frequency` | Real output frequency (minutes) |

The user specifies the simulation start/end year, month, day, and hour; the model uses julian dates internally. All times must be given in military format (e.g., 1:30 PM must be given as 1330). The simulation time zone must match the time zone in which the emission and environmental inputs are developed.

Map Projection Parameters

| | |
|---|---|
| `Map_Projection` | Character mapping projection keyword (LAMBERT, POLAR, UTM, LATLON) |
| `UTM_Zone` | Integer UTM zone |
| `POLAR_Longitude_Pole` | Real longitude of projection pole (degrees, west<0) |
| `POLAR_Latitude_Pole` | Real latitude of projection pole (degrees, south<0) |
| `LAMBERT_Center_Longitude` | Real central longitude of modeling domain (degrees, west<0) |
| `LAMBERT_Center_Latitude` | Real central latitude of modeling domain (degrees, south<0) |
| `LAMBERT_True_Latitude1` | Real first true latitude of projection (degrees, south<0) |
| `LAMBERT_True_Latitude2` | Real second true latitude of projection (degrees, south<0) |

The grid projection may be selected as Cartesian (fixed physical distance coordinates on a flat plane) or curvi-linear geodetic (following the curved surface of the Earth). The Cartesian options include Universal Transverse Mercator (UTM), Lambert Conic Conformal (LAMBERT), and Rotated Polar Stereographic (POLAR). The geodetic option performs the simulation on a latitude/longitude grid (LATLON). All gridded input files must be defined on the grid projection specified for the CAMx simulation.

Parameters For The Master (First) Grid

| | |
|---|---|
| `Number_of_Grids` | Integer number of grids in simulation |
| `Master_Origin_XCoord` | Real x-coordinate of domain southwest corner (km, or degrees for LATLON) |
| `Master_Origin_YCoord` | Real y-coordinate of domain southwest corner (km, or degrees for LATLON) |
| `Master_Cell_XSize` | Real cell size in x (km, or degrees for LATLON) |
| `Master_Cell_Ysize` | Real cell size in y (km, or degrees for LATLON) |
| `Master_Grid_Columns` | Integer number of master grid columns (E-W grid cells) |
| `Master_Grid_Rows` | Integer number of master grid rows (N-S grid cells) |
| `Number_of_Layers` | Integer number of grid layers (applies to all grids) |

The master grid is defined by its location (southwest corner point in the chosen projection space), number of grid cells (east-west, north-south, vertically), and horizontal resolution. Vertical resolution is defined by the layer structure specified in the input 3D meteorological file.

Parameters For The Nested Grids

| | |
|---|---|
| `Nest_Meshing_Factor` | Integer array (by grid) nested grid cell size relative to master grid |
| `Nest_Beg_I_Index` | Integer array (by grid) master grid column containing western edge of nest |
| `Nest_End_I_Index` | Integer array (by grid) master grid column containing eastern edge of nest |
| `Nest_Beg_J_Index` | Integer array (by grid) master grid row containing southern edge of nest |
| `Nest_End_J_Index` | Integer array (by grid) master grid row containing northern edge of nest |

The definition of nested grids is specified in the `CAMx.in` file in terms of the range of master grid cells that each nested grid spans (see Section 4). The "meshing factor" sets the resolution or cell size of the nested grids relative to the master grid. The CAMx diagnostic output file provides information on the location and size of each nested grid to help ensure proper setup.

Model Options

| | |
|---|---|
| `Diagnostic_Error_Check` | Logical model startup diagnostic flag (TRUE=stops before first timestep indicating successful model initialization, FALSE=continues with simulation after model initialization) |
| `Flexi_Nest` | Logical flexi-nesting flag (TRUE=allow some/all nested input fields to be interpolated from the parent grid, FALSE=all data must be provided for all nests) |
| `Advection_Solver` | Character horizontal advection solver keyword (PPM, BOTT) |
| `Chemistry_Solver` | Character chemistry solver keyword (EBI, IEH, LSODE) |
| `PiG_Submodel` | Character PiG submodel keyword (NONE, GREASD, IRON) |

| | |
|---|---|
| Probing_Tool | Character Probing Tool keyword (NONE, OSAT, GOAT, APCA, PSAT, DDM, HDDM, PA, IPR, IRR, RTRAC, RTCMC) |
| Chemistry | Logical chemistry flag (TRUE=chemistry on, FALSE=chemistry off) |
| Drydep_Model | Character dry deposition model keyword (NONE, WESELY89, ZHANG03) |
| Wet_Deposition | Logical wet deposition flag (TRUE=deposition on, FALSE=deposition off) |
| ACM2_Diffusion | Logical ACM2 vertical diffusion flag (TRUE=ACM2 on, FALSE=standard K-theory diffusion) |
| Super_Stepping | Logical super-stepping flag (TRUE=use super-stepping for horizontal advection to maximize model speed, FALSE=do not use super-stepping). |
| Gridded_Emissions | Logical gridded emissions flag (TRUE=gridded emissions will be used, FALSE=gridded emissions will be ignored) |
| Point_Emissions | Logical elevated point source flag (TRUE=point emissions will be used, FALSE=point emissions will be ignored) |
| Ignore_Emission_Dates | Logical date-insensitive emission flag (TRUE=dates on emission files will be ignored, FALSE=dates on emission files will be checked against simulation date) |

The user has the option of selecting among the Bott or Piecewise Parabolic Method horizontal advection solvers by specifying "BOTT" or "PPM" as keywords in the run control file. The user also has the option to use the EBI, IEH, or LSODE chemistry solvers for gas-phase chemistry by specifying these respective keywords. Probing Tools are selected by specifying one of the allowed keywords; no Probing Tool will be run if this keyword is set to "None". The description of the PiG submodel is provided in Section 6.

Super stepping maximizes the model's speed performance by setting the largest grid-specific driving time steps possible. This results in the need for potentially many sub-steps to be applied in horizontal advection on a layer-by-layer basis to maintain a stable solution. While super stepping has little impact on surface concentrations in non-MPI mode, larger differences are seen using MPI. A "super-stepping" flag was added to the control namelist that allows users to specifically turn off super stepping when they wish to compare concentrations between MPI and non-MPI runs in the most consistent manner possible. Super stepping can reduce the accuracy of the vertical transport solution, especially in high wind conditions over complex terrain. Turning super stepping off will cause the model to run much more slowly.

<u>Output Specifications</u>

| | |
|---|---|
| Root_Output_Name | Character root output path/filename (see Table 2-2 for description of file suffixes) |
| Average_Output_3D | Logical 3-D average output file flag (TRUE=output full 3-D concentration fields, FALSE=output surface layer concentration fields) |

| | |
|---|---|
| `Output_3D_Grid` | Logical array (by grid) 3-D average output file flag (TRUE=output full 3-D concentration fields for specified grid, FALSE=output surface layer concentration fields) |
| `HDF_Format_Output` | Logical HDF average output format flag (TRUE=output additional HDF format files, FALSE=do not output HDF format files) |
| `HDF_File_Root` | Character HDF root output path/filename |
| `Output_Species_Names` | Character array (by output species) species names to be written to average and deposition output files |
| `PiG_Sampling_Grid` | Logical sampling grid flag for IRON PiG output (TRUE=sampling grids are specified, FALSE=sampling grids will not be generated) |
| `Sample_Background` | Logical flag to include background concentrations (TRUE=background concentrations from the host computational grid will be added to puff increments, FALSE=only puff increments will be shown) |
| `Number_of_Sampling_Grids` | Integer number of sampling grids |
| `SG_Beg_I_Index` | Integer array (by sampling grid) master grid column containing western edge of sampling grid |
| `SG_End_I_Index` | Integer array (by sampling grid) master grid column containing eastern edge of sampling grid |
| `SG_Beg_J_Index` | Integer array (by sampling grid) master grid row containing southern edge of sampling grid |
| `SG_End_J_Index` | Integer array (by sampling grid) master grid row containing northern edge of sampling grid |
| `SG_Mesh_Factor` | Integer array (by sampling grid) cell size relative to master grid |

The user specifies a "root" path and filename that will be used for all standard CAMx core model output files. The model appends suffixes to these root names according to the file type generated. Alternatively, the user may select HDF5 output files. In this case, a separate HDF root path and filename is required, and CAMx will automatically generate grid- and hour-specific average concentration and sampling grid output files in HDF5 format in lieu of the CAMx Fortran binary file formats.

The types of CAMx output files are listed in Table 2-2. A subset of state and radical species may be output to the average concentration output files; see the description of output file formats in Section 3. There are two flags that control whether 3-D average output files are generated. The first (original) flag will toggle 3-D output for all grids in the run. The second is the "`Output_3D_Grid`" flag array, which allows 3-D average output to be set for specific grids. The original flag supersedes the grid-specific flag.

PiG sampling grids are set identically to the way nested grids are specified for the host model, with one exception: there are no vertical levels to define (sampling grids are currently only 2-D surface fields). The same rules that apply for the specification of nested grids holds for the specification of all sampling grids (see Section 4).

Input Files

| | |
|---|---|
| `Chemistry_Parameters` | Character input chemistry parameters path/filename |
| `Photolyis_Rates` | Character input photolysis rates path/filename (optional according to Chemistry flag and Chemistry_Parameters file) |
| `Ozone_Column` | Character input ozone column path/filename (ignored if Chemistry=FALSE) |
| `Initial_Conditions` | Character input master grid initial conditions path/filename (ignored if Restart=TRUE) |
| `Boundary_Conditions` | Character input master grid boundary conditions path/filename |
| `Point_Sources` | Character input elevated point source emissions path/filename (ignored if Point_Emissions=FALSE) |
| `Master_Grid_Restart` | Character input master grid restart path/filename (ignored if Restart=FALSE) |
| `Nested_Grid_Restart` | Character input nested grid restart path/filename (ignored if Restart=FALSE or Number_of_Grids=1) |
| `PiG_Restart` | Character input PiG restart path/filename (ignored if Restart=FALSE or PiG_Submodel=FALSE) |
| `Surface_Grid` | Character array (by grid) input static 2D surface path/filename (optional for nested grids) |
| `Met2D_Grid` | Character array (by grid) input time-variant 2D surface meteorology path/filename (optional for nested grids) |
| `Met3D_Grid` | Character array (by grid) input time-variant 3D meteorology path/filename (optional for nested grids) |
| `Vdiff_Grid` | Character array (by grid) input time-variant 3D vertical diffusivity path/filename (optional for nested grids) |
| `Cloud_Grid` | Character array (by grid) input time-variant 3D cloud/rain path/filename (optional but required if Wet_Deposition=TRUE, optional for nested grids) |
| `Emiss_Grid` | Character array (by grid) input gridded emissions path/filename (ignored if Gridded_Emissions=FALSE, optional for nested grids) |

If CAMx cannot find or open a non-blank input filename provided in the run control file, the model will stop with an error.  CAMx will accept blank input filenames for only those files that are optional.

**Table 2-2. CAMx output file suffixes and their corresponding file types.**

| Suffix | CAMx File Type |
|---|---|
| .out | Text simulation tracking file (CPU, input files read, error/warning messages) |
| .diag | Text simulation diagnostic file (repeat of run control inputs, PiG diagnostics, miscellaneous diagnostic output) |
| .mass | Text mass budget file for subsequent postprocessing |
| .inst | Fortran binary master grid instantaneous concentration file at the end of the simulation (used for restarts) |
| .finst | Fortran binary nested grid instantaneous concentration file at the end of the simulation (used for restarts) |
| .pig | Fortran binary PiG sub-model file (used for restarts) |
| **Standard CAMx Output Option** | |
| .avrg.grd*nn* | Fortran binary average concentration file for grid *nn*; optionally contains 2-D layer 1 concentration field or full 3-D concentration field |
| .depn.grd*nn* | Fortran binary surface deposition file for grid *nn* |
| .smp*nn* | Fortran binary average surface concentration file for PiG sampling grid *nn* (optional) |
| **HDF5 Output Option** | |
| -CX-YYYY-MM-DD-HHMMSS-head.txt | Text header file for all grids at specific date/time |
| -CX-YYYY-MM-DD-HHMMSS-g*nn*.h5 | HDF average concentration file for grid *nn* at specific date/time; optionally contains 2-D layer 1 concentration field or full 3-D concentration field |
| -CS-YYYY-MM-DD-HHMMSS-head.txt  (optional) | Text header file for all sampling grids at specific date/time |
| -CS-YYYY-MM-DD-HHMMSS-g*nn*.h5  (optional) | HDF average surface concentration file for sampling grid *nn* at specific date/time |

### 2.3.2 Using Scripts to Run CAMx

The generation of the run control file is most easily accomplished in the job script that actually runs the model; Figure 2-2 shows an example of a CAMx job script that builds a "CAMx.in" file and runs the model for each day to be simulated. Alternatively, the run control file could be written separately with a name specific to a given simulation, then linked or copied to the standard "CAMx.in" filename before the model is executed at a command line or in a job script.

```
#!/bin/csh
#
# CAMx 6.00
#
setenv OMP_NUM_THREADS 4
setenv MPSTKZ 128M
limit stacksize unlimited
#
set EXEC      = "../../src/CAMx.v6.00.noMPI.pg_linuxomp"
#
set RUN     = "v6.00.midwest.36.12.noMPI"
set INPUT   = "../inputs"
set MET     = "../inputs/met"
set EMIS    = "../emiss"
set PTSRCE  = "../ptsrce"
set OUTPUT  = "../outputs"
#
mkdir -p $OUTPUT
#
#  --- set the dates and times ----
#
set RESTART = "NO"
foreach today (03.154 04.155)
set JUL = $today:e
set CAL = $today:r
set YESTERDAY = `echo ${CAL} | awk '{printf("%2.2d",$1-1)}'`
#
if( ${RESTART} == "NO" ) then
        set RESTART = "false"
else
        set RESTART = "true"
endif
#
#  --- Create the input file (always called CAMx.in)
#
cat << ieof > CAMx.in

 &CAMx_Control

 Run_Message       = 'CAMx 6.00 Test Problem -- Mech6 CF CB05 $RUN',

!--- Model clock control ---

 Time_Zone         = 0,                     ! (0=UTC,5=EST,6=CST,7=MST,8=PST)
 Restart           = .${RESTART}.,
 Start_Date_Hour  = 2002,06,${CAL},0000,   ! (YYYY,MM,DD,HHmm)
 End_Date_Hour    = 2002,06,${CAL},2400,   ! (YYYY,MM,DD,HHmm)

 Maximum_Timestep    = 15.,              ! minutes
 Met_Input_Frequency = 60.,              ! minutes
 Ems_Input_Frequency = 60.,              ! minutes
 Output_Frequency    = 60.,              ! minutes
```

**Figure 2-2.  A sample CAMx job script that generates a "CAMx.in" file and runs the model with OMP parallelization.**

```
!--- Map projection parameters ---

 Map_Projection           = 'LAMBERT', ! (LAMBERT,POLAR,UTM,LATLON)
 LAMBERT_Central_Meridian = -97.,       ! deg (west<0,south<0)
 LAMBERT_Center_Longitude = -97.,       ! deg (west<0,south<0)
 LAMBERT_Center_Latitude  =  40.,       ! deg (west<0,south<0)
 LAMBERT_True_Latitude1   =  45.,       ! deg (west<0,south<0)
 LAMBERT_True_Latitude2   =  33.,       ! deg (west<0,south<0)

!--- Parameters for the master (first) grid ---

 Number_of_Grids      = 2,
 Master_Origin_XCoord = -792.,          ! km or deg, SW corner of cell(1,1)
 Master_Origin_YCoord = -1656.,         ! km or deg, SW corner of cell (1,1)
 Master_Cell_XSize    = 36.,            ! km or deg
 Master_Cell_YSize    = 36.,            ! km or deg
 Master_Grid_Columns  = 68,
 Master_Grid_Rows     = 68,
 Number_of_Layers     = 16,

!--- Parameters for the second grid ---

 Nest_Meshing_Factor(2) = 3,            ! Cell size relative to master grid
 Nest_Beg_I_Index(2)    = 22,           ! Relative to master grid
 Nest_End_I_Index(2)    = 51,           ! Relative to master grid
 Nest_Beg_J_Index(2)    = 22,           ! Relative to master grid
 Nest_End_J_Index(2)    = 58,           ! Relative to master grid

!--- Model options ---

 Diagnostic_Error_Check = .false.,       ! True = will stop after 1st timestep
 Advection_Solver       = 'PPM',         ! (PPM,BOTT)
 Chemistry_Solver       = 'EBI',         ! (EBI,IEH,LSODE)
 PiG_Submodel           = 'None',        ! (None,GREASD,IRON)
 Probing_Tool           = 'None',        ! (None,OSAT,GOAT,APCA,PSAT,DDM,
                                          !  HDDM,PA,IPR,IRR,RTRAC,RTCMC)
 Chemistry              = .true.,
 Drydep_Model           = 'WESELY89',    ! (NONE, WESELY89, ZHANG03)
 Wet_Deposition         = .true.,
 ACM2_Diffusion         = .false.,
 Super_Stepping         = .true.,
 Gridded_Emissions      = .true.,
 Point_Emissions        = .true.,
 Ignore_Emission_Dates  = .true.,

!--- Output specifications ---

 Root_Output_Name         = '$OUTPUT/CAMx.$RUN.200206${CAL}',
 Average_Output_3D        = .false.,
 HDF_Format_Output        = .false.,
 Output_Species_Names(1)  = 'NO',
 Output_Species_Names(2)  = 'NO2',
 Output_Species_Names(3)  = 'O3',
 Output_Species_Names(4)  = 'SO2',
 Output_Species_Names(5)  = 'H2O2',
 Output_Species_Names(6)  = 'HNO3',
 Output_Species_Names(7)  = 'NH3',
 Output_Species_Names(8)  = 'PNO3',
 Output_Species_Names(9)  = 'PSO4',
 Output_Species_Names(10) = 'PNH4',
 Output_Species_Names(11) = 'POA',
```

**Figure 2-2 (continued).**

```
 Output_Species_Names(12)  = 'PEC',
 Output_Species_Names(13)  = 'FPRM',
 Output_Species_Names(14)  = 'CPRM',
 Output_Species_Names(15)  = 'CCRS',
 Output_Species_Names(16)  = 'FCRS',
 Output_Species_Names(17)  = 'SOA1',
 Output_Species_Names(18)  = 'SOA2',
 Output_Species_Names(19)  = 'SOA3',
 Output_Species_Names(20)  = 'SOA4',
 Output_Species_Names(21)  = 'SOA5',

!--- Input files ---

 Chemistry_Parameters = '$INPUT/CAMx6.0.chemparam.6_CF',
 Photolyis_Rates      = '$INPUT/tuv.200206.STL.txt',
 Ozone_Column         = '$INPUT/o3col.200206.STL_36_68X68_12_92X113.txt',
 Initial_Conditions   = '$INPUT/IC.vistas_2002gt2a_STL_36_68X68_16L.2002081',
 Boundary_Conditions  = '$INPUT/BC.vistas_2002gt2a_STL_36_68X68_16L.2002${JUL}',
 Point_Sources        = '$PTSRCE/ptsrce.stl.36km.2002${JUL}.a0.bin',
 Master_Grid_Restart  = '$OUTPUT/CAMx.$RUN.200206${YESTERDAY}.inst',
 Nested_Grid_Restart  = '$OUTPUT/CAMx.$RUN.200206${YESTERDAY}.finst',
 PiG_Restart          = ' ',

 Flexi_Nest       = .false.
 Emiss_Grid(1)    = '$EMIS/emiss.stl.36km.200206${CAL}.a1.bin',
 Surface_Grid(1) = '$INPUT/met/camx.lu.36k.bin',
 Met2D_Grid(1)    = '$INPUT/met/camx.2d.200206${CAL}.36k.bin',
 Met3D_Grid(1)    = '$INPUT/met/camx.3d.200206${CAL}.36k.bin',
 Vdiff_Grid(1)    = '$INPUT/met/camx.kv.200206${CAL}.36k.bin',
 Cloud_Grid(1)    = '$INPUT/met/camx.cr.200206${CAL}.36k.bin',
 Emiss_Grid(2)    = '$EMIS/emiss.stl.12kmsmall.200206${CAL}.a1.bin',
 Surface_Grid(2) = '$INPUT/met/camx.lu.12ksmall.bin',
 Met2D_Grid(2)    = '$INPUT/met/camx.2d.200206${CAL}.12ksmall.bin',
 Met3D_Grid(2)    = '$INPUT/met/camx.3d.200206${CAL}.12ksmall.bin',
 Vdiff_Grid(2)    = '$INPUT/met/camx.kv.200206${CAL}.12ksmall.bin',
 Cloud_Grid(2)    = '$INPUT/met/camx.cr.200206${CAL}.12ksmall.bin',

 /
!-------------------------------------------------------------------------------

ieof
#
#  --- Execute the model ---
#
if( ! { $EXEC } ) then
   exit
endif

end
```

**Figure 2-2 (concluded).**

### 2.3.3 MPI Parallel Processing

Using CAMx with MPI requires the same job script as the standard version, with a few modifications to support multi-processing.  Here, we explain the approach we have taken.  We provide this as guidance; it is not necessary to follow these steps to run CAMx with MPI.  Others may have a different way of handling the MPI portion of the execution.

1. Put the CAMx input files somewhere on the network that is accessible by the computer that will serve as the master node.  Also, identify a location where the output will be written.

2. Create a directory on the local disk of the master node that will serve as the launching point for the CAMx execution.  Copy the standard CAMx job script, and any scripting support programs to this location.

3. Modify the job script so that the variable identifying the executable program points to the local directory.

4. Modify the job script so that the pathnames for input and output files are correct.

5. Add a section, similar to the one shown below, to the top of the job script:

   For MPICH1 use the following:

   ```
   cat << ieof > nodes
   10.1.4.2
   10.1.4.3
   10.1.4.4
   10.1.4.5
   10.1.4.6
   10.1.4.2
   10.1.4.3
   10.1.4.4
   ieof
   set NUMPROCS = `wc -l nodes | awk '{print $1+1}'`
   ```

   This will create a file containing the IP addresses of the computers that will get a computational slice of the domain on which to work.

   ***NOTE: THE MASTER NODE SHOULD NOT BE LISTED for an MPICH1 run, and will not get a computational slice.***

   The computer on which the program is launched is included in the MPI simulation by default and is given a process ID of 0.  Notice that some computers are listed twice.  This example is utilizing a cluster containing dual processor computers.  The computer must be listed once for each CPU that is to be used in the simulation.  Notice that the `NUMPROCS` variable is assigned to a value equal to one more than the number of computers listed.  This is because the master node is included in the count of processors.  This example will utilize 9 processors: one to serve as the master node and

8 that will receive a computational slice. If the names of the computers are known to the master node, hostnames can be used in place of IP addresses.

For MPICH2 use the following:

```
cat << ieof > nodes
10.1.4.2:3
10.1.4.3:2
10.1.4.4:2
10.1.4.5:2
ieof
set NUMPROCS = 9
set RING = `wc -l nodes | awk '{print $1}'
```

Notice that the syntax for each entry differs from the MPICH1 version in that the addresses are followed by a colon and a numeric value. This is the convention adopted in MPICH2 for utilizing several processors on a single host. Do not list a machine multiple times in the `nodes` file. Unlike MPICH1 the `NUMPROCS` variable is set to the number of total nodes listed after the colon. In this example, the `nodes` file will also be used to launch a node "ring" using the MPICH2 utilities.

***For this reason you must include the master node in the list for an MPICH2 run – the master node must be part of the MPICH ring.***

6.  Change the line that launches the executable program, at the bottom of the script.

    For MPICH1 use the following:

```
mpirun –v –machinefile nodes –np $NUMPROCS $EXEC
```

This will use the `mpirun` utility to launch the CAMx model using the file called "`nodes`" to identify the computers to be included. Of course, this assumes that the `mpirun` utility is in the current user's path. In fact, the `mpich` package must be installed on each compute node and the `mpirun` utility must be available in the user's path on each system. A complete absolute path to `mpirun`, such as `/usr/local/bin/mpirun`, could be used instead.

For MPICH2 use the following:

```
mpdboot –n $RING –f nodes --verbose
mpiexec –machinefile nodes –np $NUMPROCS $EXEC
mpdallexit
```

The `mpdboot` command will initialize the MPD environment, establishing a ring using all of the machines listed in the nodes file. The `mpiexec` command will launch the

model using the specified number of processors, utilizing the machines in the established ring. The `mpdallexit` command will terminate the ring. If your script is looping over several days, which is typical, you should put the `mpdboot` command before the start of the loop, the `mpiexec` command inside the loop, and the `mpdallexit` command after the point where the loop is terminated.

### 2.3.4 OMP Parallel Processing

You may implement OMP parallel processing alone or in combination with MPI. In either case, it is necessary to add environment variables to the CAMx job script that define the number of OMP threads (the examples below use the c-shell syntax):

```
setenv OMP_NUM_THREADS 4
```

There have been problems with some parallel programs on Linux systems when the per-thread stack size is set to the default (2 MB). If you have unexplained failures such as segmentation faults/violations, try setting the `MPSTKZ` environment variable to a larger value, for example:

```
setenv MPSTKZ 32M
```

For large applications, you will probably also need to increase the stack size available to the shell executing the model by using the limit command as shown below:

```
limit stacksize unlimited
```

To use a hybrid MPI/OMP approach, follow all of the steps for running an MPI application and include the `OMP_NUM_THREADS` environment variable (and others if needed). The domain will be divided into slices in the usual way as part of MPI, but when operating on a particular slice, the host will spawn multiple OMP threads to parallelize the portions of the code where OMP directives have been included.

## 2.4 Benchmarking Model Run Times

Two cases with very different model configurations were used to test CAMx v5.00 with MPI/OMP. Note that runtimes and parallelization scalability for the current version of CAMx have been improved according to updates to the MPI implementation since v5.00 – however, conclusions drawn from these test remain valid. The first model configuration is the standard CAMx test case available for download from www.camx.com: it employs two relatively small grids at 36 and 12 km resolution, centered over St Louis, Missouri:

- Grids: 68×68 and 92×115
- 16 layers
- No PiG
- Mechanism 6 (CB05, no PM)

The second configuration was provided by the EPA/OAQPS, and employs two larger grids, the 36-km RPO domain covering most of North America and a 12-km grid covering the entire eastern U.S.:

- Grids: 148×112 and 281×242
- 14 layers
- No PiG
- Mechanism 4 CF (CB4, with PM)

Results from both test cases are shown in Tables 2-3 and 2-4, respectively. These results consistently show that MPI is most advantageous for larger applications in which overhead processes (e.g., model setup, I/O, etc.) are a much smaller fraction of total model run time. In other words, CAMx applications on expansive multiple grids, employing extensive chemistry (PM and RTRAC), and/or including Probing Tools (OSAT, PSAT, DDM) would benefit most from MPI parallelization.

**Table 2-3.  CAMx v5.00 speed performance with MPI and OMP for the distribution test case available at www.camx.com (processed on 2.83 Ghz Intel Xeon chipsets).**

| MPI Slices | OMP threads / Slice | Total CPU | Minutes /Sim Day | Equivalent Processors |
|---|---|---|---|---|
| 1 | 1 | 1 | 106 | ///////////// |
| 2 | 1 | 2 | 57 | 1.9 |
| 4 | 1 | 4 | 32 | 3.3 |
| 8 | 1 | 8 | 21 | 5.0 |
| 16 | 1 | 16 | 18 | 5.9 |
| 1 | 4 | 4 | 43 | 2.5 |
| 2 | 4 | 8 | 25 | 4.3 |
| 4 | 4 | 16 | 17 | 6.2 |

*Equvalent Processors is defined as the ratio of runtime for multiple processors to the runtime for a single processor.

**Table 2-4.  CAMx v5.00 speed performance with MPI and OMP for the EPA/OAQPS test case (processed on 2.83 Ghz Intel Xeon chipsets).**

| MPI Slices | OMP threads / Slice | Total CPU | Minutes / Sim Day | Equivalent Processors* |
|---|---|---|---|---|
| 1 | 1 | 1 | 503 | ///////////// |
| 2 | 1 | 2 | 266 | 1.9 |
| 4 | 1 | 4 | 138 | 3.6 |
| 8 | 1 | 8 | 81 | 6.2 |
| 12 | 1 | 12 | 76 | 7.0 |
| 16 | 1 | 16 | 61 | 8.2 |
| 24 | 1 | 24 | 49 | 10.3 |
| 1 | 8 | 8 | 111 | 4.5 |
| 2 | 8 | 16 | 79 | 6.4 |
| 4 | 4 | 16 | 71 | 7.1 |
| 3 | 8 | 24 | 52 | 9.7 |

*Equvalent Processors is defined as the ratio of runtime for multiple processors to the runtime for a single processor.

## 2.5  CAMx Pre- And Post-Processors

This section describes a variety of CAMx pre- and post-processors that we have made available to the user community.  Since they support CAMx I/O, these programs are written in Fortran77 and Fortran90 and distributed by ENVIRON as free software.  As such, they contain notices like this in the source code:

```
cccccccccccccccccccccccccccccccccccccccccccccccccccccccccccccc
c Copyright (C) 2003  ENVIRON
c
c This program is free software; you can redistribute it and/or
c modify it under the terms of the GNU General Public License
c as published by the Free Software Foundation; either version 2
c of the License, or (at your option) any later version.
c
c This program is distributed in the hope that it will be useful,
c but WITHOUT ANY WARRANTY; without even the implied warranty of
c MERCHANTABILITY or FITNESS FOR A PARTICULAR PURPOSE.  See the
c GNU General Public License for more details.
c
c To obtain a copy of the GNU General Public License
c write to the Free Software Foundation, Inc.,
c 59 Temple Place - Suite 330, Boston, MA  02111-1307, USA.
cccccccccccccccccccccccccccccccccccccccccccccccccccccccccccccc
```

ENVIRON occasionally posts updates for certain widely-used programs when necessary, but does not actively support or maintain every one.  Users can e-mail questions, comments, suggestions or improvements to ask-camx@environ.org.  A few of the more important pre- and post-processors are briefly described below.  Each come with README files, makefiles, and sample job scripts that document their purpose and usage.

### 2.5.1  Emissions

Most emission models (those shown in Figure 2-1) can provide speciated, temporally-allocated, gridded and point source emission input files in the CAMx-ready format.  Further processing may be required, however, to select point sources for the PiG treatment, translate the point source files from a common ASCII text format to CAMx-ready binary files, or to refine the domain size/resolution for gridded emissions.

PIGSET:  This program allows the user to select and set certain point sources for the Plume-in-Grid (PiG) treatment in a CAMx simulation.  It also converts ASCII point source files commonly generated by emission models such as SMOKE, CONCEPT, and EPS3 to CAMx-ready binary format.  See the source code for more information, and the sample job for usage.  Also see Section 6 for guidance in selecting PiG point sources and manipulating day-specific point source files.

WINDOW:  This program is used to "window" out a sub-section of the surface emissions grid for use on a smaller CAMx grid.  It can also be used to aggregate or interpolate surface emissions to coarser or finer resolution, respectively.  See the sample job for usage.

SEASALT:  This program generates aerosol emissions of sodium and chloride, and gaseous emissions of chlorine and halo-methane compounds, using CAMx-ready meteorological and landuse files.  A separate merging program is included that allows sea salt emissions to be merged in with pre-existing CAMx-ready gridded emission files.

## 2.5.2  Meteorology

The recommended approach to develop meteorological inputs for CAMx is through the use of prognostic meteorological models.  ENVIRON provides interface programs for three specific models: WRF, MM5, and RAMS;  This does not necessarily preclude other meteorological models to be used, but users will need to develop interface programs on their own.

WRFCAMx:  This program generates CAMx v6 meteorological input files from WRF (ARW core) v2 and v3 output files.  See the README in the archive for a description of the program and how it is applied.

MM5CAMx:  This program generates CAMx v6 meteorological input files from MM5 v3 output files.  See the README in the archive for a description of the program and how it is applied.

RAMSCAMx:  This program generates CAMx v6 meteorological input files from RAMS v4/5/6 output files.  See the README in the archive for a description of the program and how it is applied.

METCONVERT:  This program converts older meteorological files from CAMx v4 and v5 to the CAMx format introduced with CAMx v6.

KVPATCH:  This program applies minimum Kv values within a user-defined surface layer depth based on an input landuse grid.  It optionally allows Kv profiles to be extended into daytime boundary-layer capping convection as defined by input cloud/rain files.  See the source code for more information.  Use of this program to adjust Kv inputs is entirely optional.

## 2.5.3  Photolysis Rates

The development of photolysis rate inputs for CAMx is crucial for the photochemical mechanisms, but is not needed for inert or simple chemistry (e.g., Mechanism 10) applications. Two programs are available to assist the user in developing photolysis and ozone column input files.

O3MAP:  This program prepares ozone column input files for CAMx, and must be run prior to running the TUV model as it defines the atmospheric ozone column intervals based on input data.  Ozone column data files (http://toms.gsfc.nasa.gov/ozone/ozone.html) must be supplied as input.  NOTE: gaps in day-specific ozone column data at low latitudes, and high latitudes during winter, may result in zero values over portions of the modeling grid (see Figure 2-3).  This results from the inability of polar-orbiting satellite instruments to cover the entire globe on a daily basis.  The user may instead use seasonal-average ozone column files (no data gaps); alternatively, O3MAP provides

## OMI Total Ozone Mar 18, 2009
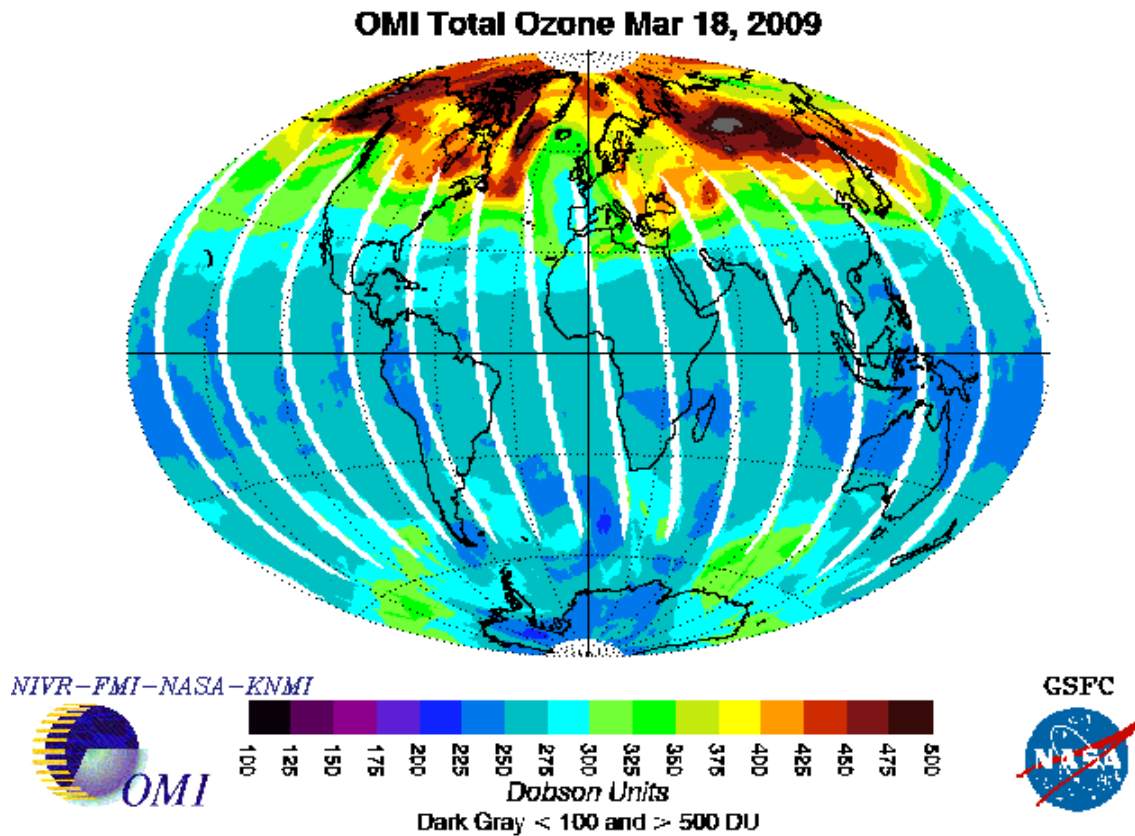
**Figure 2-3.  An example of global ozone column from the Ozone Monitoring Instrument (OMI) platform.  White areas denote missing data.  From http://toms.gsfc.nasa.gov/ozone/ozone.html.**

an option to fill these day-specific gaps with an average determined from valid data processed for the extraction domain.  See the Readme file and job script in the archive for usage.

TUV:  This is a radiative transfer model that develops clear-sky photolysis rate inputs for all CAMx photochemical mechanisms.  TUV is developed and distributed by NCAR (2011). The program specifies default intervals for 5 surface UV albedos, 3 terrain heights, 11 altitudes above ground, and 10 solar zenith angles.  Five total atmospheric ozone column intervals are defined from the O3MAP program.  See the sample job in the archive for usage.

### 2.5.4  Air Quality

There are numerous approaches for defining initial and boundary concentration inputs for CAMx.  The level of possible detail ranges from time- and space-constant values for all pollutants, to specific time and space profiles for each.  The level of detail depends on available measurements or modeling datasets, the particular focus and detail of the modeling exercise, and scale considerations (e.g., local vs. continental domains).  ENVIRON provides a simple

program that generates space and time-constant initial and boundary conditions for use in simple CAMx applications and testing. The more common approach for regional applications is to extract initial and boundary conditions from the output of global-scale chemical transport models. Users will need to develop their own programs if they choose an alternative methodology to generate initial/boundary conditions.

ICBCPREP: This program prepares CAMx initial and boundary condition files. Values are constant in space and time, but unique values may be specified for each chemical species to be modeled; they are defined in a simple text file. See the sample job in the archive for usage.

GEOS2CAMx: This program generates CAMx initial and boundary condition input files from GEOS-Chem global model output. See the Release Notes and job scripts in the archive for a description of the program and how it is applied.

MOZART2CAMx: This program generates CAMx and CMAQ initial and boundary condition input files from MOZART4 output (using both GEOS5 and NCEP meteorology). See the README in the archive for a description of the program and how it is applied. You will need I/O-API and NetCDF libraries to compile and run this program.

### 2.5.5 Landuse

Approaches for developing landuse/landcover inputs for CAMx are about as varied as they are for initial/boundary conditions. Popular approaches have included: (1) translating gridded spatial allocation surrogates developed during emissions processing into the CAMx categories described in Section 3; (2) translating the gridded landuse/landcover fields from the meteorogical model; or (3) separately developing landuse input fields from raw data (such as from the USGS or NLCD) using GIS or other programs. The advantages of (1) are consistency with input emissions estimation methodologies, and the fact that land cover processing is done just once. The advantages of (2) are similar consistency with the meteorological modeling and one-time processing, but most models assign a single dominant landuse to each grid cell, which may not be representative for coarse-resolution grids (CAMx allows a distribution of multiple land cover types per cell). ENVIRON provides meteorological interface programs (described above) that translate the meteorological model landuse/landcover fields to the CAMx definitions and grid configuration.

MERGE_LULAI: This program merges independently-developed landuse and/or LAI fields (for example via GIS processing of common terrestrial datasets) with an existing CAMx 2D surface file generated by the meteorological interface programs. See the sample job and source code for a description of the program and how it is applied.

### 2.5.6 Post-processors

Most of the CAMx post-processors provided by ENVIRON provide some manner of concentration file manipulation, either to extract certain information from the raw output files, to re-format for use in other programs and applications, to concatenate files, etc. A few others

are provided to assist in evaluating Probing Tool output.  As stated above, ENVIRON does not provide any visualization or graphics software other than a few Excel® spreadsheet macros.

AVGDIF:  This program is used to compare two CAMx format output average files and print a table of differences.  This is useful for checking differences between CAMx runs on different machines or different compile options for the test case.  See the sample job in the archive for usage.

BNDEXTR:  Use this program to extract boundary conditions for a nested grid when you apply CAMx in one-way nesting mode.  One-way nesting means that CAMx is run successively for each grid, with BNDEXTR as the interface between each run.  This program is not needed when CAMx is run in the more standard two-way nesting mode, where all grids are run in a single simulation.  See the example job for usage.

CAMxPOST:  This is a suite of post-processing utilities designed to facilitate the evaluation of model performance.  It is used to combine observations and predictions, calculate statistics, and plot time series.  See the README file in the archive for usage.

CAMxTRCT:  This program extracts specified chemical species for specified grids from the output average concentration and deposition files, and from input emission files. Output from this program can be written in the standard CAMx format, or alternatively to a text (ASCII) format in Surfer® "GRD" format for subsequent plotting.  It also has the capability to convert units.  See the sample job in the archive for usage.

CAMx2IOAPI:  This program converts CAMx output average concentration and deposition files to I/O-API format.  You will need I/O-API and NetCDF libraries to compile and run this program.  This program allows you to use various third-party manipulation and visualization software that handle I/O-API format.

PA_Tools:  This is a suite of post-processing utilities designed to extract IPR, IRR, and CPA data from CAMx Process Analysis output files and reformat the data suitable for subsequent analysis (e.g. using spreadsheets).

OSAT/PSAT_Browser:  These are separate suites of Fortran and Excel macro tools that support the evaluation of the source apportionment output at receptor locations.  The macro plots ranked source contributions at receptor locations using Excel (compatible with MS Office 2007).  See the README file for usage.

# 3. CORE MODEL INPUT/OUTPUT STRUCTURES

Most CAMx input/output (I/O) files are Fortran binary and based on the Urban Airshed Model (UAM) convention. This allows the user to employ widely available software designed specifically for these formats to develop the input files or to post-process and visualize the output files.

CAMx requires input files that define the chemical mechanism and describe the photochemical conditions, surface characteristics, initial/boundary conditions, emission rates, and various meteorological fields over the entire modeling domain. Table 3-1 summarizes the input data requirements of CAMx. Preparing this information requires several preprocessing steps to translate "raw" emissions, meteorological, air quality and other data into final input files for CAMx. We expect that most CAMx applications will utilize output from a prognostic meteorological model that can generate all of the required time varying three-dimensional meteorological fields.

**Table 3-1. Data requirements of CAMx.**

| Data Types | Data Fields |
|---|---|
| Meteorology<br>*Supplied by Prognostic Meteorological Models* | • 3-Dimensional Gridded Fields:<br>  - Vertical Grid Structure<br>  - Horizontal Wind Components<br>  - Temperature<br>  - Pressure<br>  - Water Vapor<br>  - Vertical Diffusivity<br>  - Clouds/Precipitation<br>  - Snow Cover |
| Air Quality<br>*Developed from Other Models or Measurement Data* | • Gridded Initial Concentrations<br>• Gridded Boundary Concentrations |
| Emissions<br>*Supplied by Emissions Models and Processors* | • Elevated Point Sources<br>  - Industrial Facilities<br>  - Prescribed, Agricultural, Wild Fires<br>  - Lightning NOx<br>• Combined Gridded Sources<br>  - Low-Level Point<br>  - On-Road and Non-Road Mobile<br>  - Area<br>  - Biogenic<br>  - Oceanic |
| Geographic<br>*Developed from Terrain, Landuse/Landcover, and Vegetation Density Datasets* | • Gridded Surface Characteristics<br>  - Landuse/LandCover<br>  - Terrain Elevation<br>  - Leaf Area Index (LAI)<br>  - Land/Ocean Mask |
| Photolysis<br>*Derived from Satellite Measurements and Radiative Transfer Models* | • Atmospheric Radiative Properties<br>  - Gridded Ozone Column Codes<br>  - Photolysis Rates Lookup Table |

CAMx produces gridded time-averaged concentration output files; the user selects the time interval (usually hourly), the species to be output (both "state" and "radical" species), and whether the output contains just two-dimensional surface layer fields or entire three-dimensional fields. A separate average output file is written for each grid employed in the simulation. Surface deposition fields for the same user-selected species are also written to output files with the same structure as the average concentration files. Gridded three-dimensional instantaneous concentrations of all species on all grids are written at the end of the simulation to allow for a model restart. Commonly available graphical visualization and animation software can be used to view CAMx average and deposition output files. The CAMx Probing Tool options provide their own information in separate output files in the same CAMx output format that can be viewed directly or further post-processed for detailed analysis. Diagnostic output files include three files that track computer resources, echo input selections, provide mass budget and diagnostic summaries, and provide error/warning messages.

## 3.1  CAMx Chemistry Parameters File

Chemistry parameters are provided in a text (ASCII) file that specifies the chemical mechanism be used and associated details on species properties and reaction types and rates. The chemistry parameters file format is defined in Table 3-2, and samples are given in Figure 3-1. Some records in this file are labeled (columns 1-20) to indicate the type of information to supply on that line (starting in column 21). For records that are not labeled, data start in column 1. Some chemistry parameter records are optional, depending upon the logical flags indicated for such records, and are shown in Table 3-2 by a check in the third column; if the indicated option is not invoked these records should not appear in the file. The first record of the chemistry parameters file must contain the string "`VERSION6.0`", which indicates that the file is specific to this version of CAMx.

If the chemistry flag is set "true" on the `CAMx.in` file, CAMx checks that certain properties of the selected mechanism are consistent with parameters supplied on the input file (e.g., number of reactions, photolysis reactions and species). If any discrepancies are found, they are reported in the output message file and the simulation is halted. The user may also specify an inert simulation by setting the chemistry flag to "false". In this case, any number of arbitrarily named species may be listed, and chemistry reaction parameters are ignored.

Gas-phase chemistry is controlled by the Mechansim ID (5, 6, 7, or 2 for SAPRC99, CB05, CB6, or CB6r1, respectively). Aerosol chemistry is controlled by the keywords "NONE", "INERT", "CF" or "CMU". In the "INERT" case, the user can define any number of arbitrary particulate names and sizes. The "CF" and "CMU" options invoke aerosol chemistry and treat aerosol size using either static coarse and fine modes (CF) or an evolving size section model (CMU). Both CF and CMU options require a minimum set of specific aerosol names with associated chemistry.

The chemistry parameters file controls how photolysis rates are calculated in CAMx. So-called "primary" photolysis rates are input to CAMx via the photolysis rates file. The primary photolysis reactions are identified by number in the chemistry parameters file and the photolysis rates file must match this declaration. So-called "secondary" photolysis rates are set by scaling factors to one of the primary reactions. Use of secondary rates requires at least one primary photolysis reaction.

**Table 3-2.  Description of the CAMx chemistry parameters file.  The record labels exist in columns 1-20, and where given, the input data for that record start in column 21.  The format denoted "list" indicates a free-format list of numbers (comma or space-delimited).**

| Record Label (columns 1-20) | Record Optional | Format | Description |
|---|---|---|---|
| CAMx version | | A | Model version keyword (VERSION6.0) |
| Mechanism ID | | list | ID number of chemical mechanism (see Table 5-1) |
| Aerosol Option | | A | Keyword for aerosol scheme (NONE, INERT, CF, or CMU)[1] |
| Description | | A | Message record to describe this file |
| No of gas species | | list | Number of radical and state gas species (NGAS ≥ 1) |
| No of aero species | | list | Number of aerosol species (NAERO ≥ 0) Aerosol chemistry timestep (min) (**if NAERO > 0**) Number of size bins (NBIN ≥ 1) (**if NAERO > 0**)[2] Aerosol diameter (μm) for NBIN+1 cut points (**if NAERO > 0**) |
| No of reactions | | list | Number of reactions (NREACT ≥ 0) |
| Prim photo rxns | | list | Number of primary photolysis reactions (NPHOT1 ≥ 0) List of primary photolysis reaction ID numbers (must match the photolysis rates input file) |
| No of sec photo rxn | | list | Number of secondary photolysis reactions (NPHOT2 ≥ 0) |
| ID, prim ID, scale | √ | list | *If NPHOT2 > 0*, repeat this record for each secondary photolysis reaction ID number of the secondary photolysis reaction ID number of the primary photolysis reaction used for scaling Secondary reaction scale factor |
| Species Records | | | Heading |
| Gas Spec ... | | | Heading |
| | | 5X, A10, E10.0, E10.0, F10.0, F10.0, F10.0 F10.0 | Repeat this record for each gas species (start in column 1) Gas species name (radicals first, followed by state species) Lower bound concentration (ppm) Henry's law constant (M/atm) Henry's law temperature dependence (K) Molecular weight (g/mol) Wesley's reactivity parameter Surface resistance scaling factor for strong acids (0-1) |

**Table 3-2 (continued).  Description of the CAMx chemistry parameters file.  The record labels exist in columns 1-20, and where given, the input data for that record start in column 21.  The format denoted "list" indicates a free-format list of numbers (comma or space-delimited).**

| Record Label (columns 1-20) | Record Optional | Format | Description |
|---|---|---|---|
| `Aero Spec ...` | √ | | Heading (*if NAERO > 0*) |
| | √ | 5X,<br>A10,<br>E10.0,<br>F10.0<br>F10.0<br>I10<br>F10.0<br>I10 | *If NAERO > 0*, repeat this record for each aerosol species (start in column 1)<br>Aerosol species name<br>Lower bound concentration ($\mu g/m^3$)<br>Species density ($g/cm^3$)<br>Dry extinction efficiency ($m^2/\mu m$)<br>Hygroscopic extinction adjustment (0 = no adjustment, 1 = RH-dependent)<br>Single-scattering albedo<br>Assigned size bin (INERT and CF aerosols only – references cut points in record 6) |
| `Reaction Records` | √ | | Heading (*if NREACT > 0*) |
| `Rxn Typ Param ...` | √ | | Heading (*if NREACT > 0*) |
| | √ | list | *If NREACT > 0*, repeat this record for each gas-phase reaction (start in column 1)<br>Reaction ID number<br>Rate constant expression ID number (1-7, as shown in Table 3-3)<br>Rate constant parameters (depending on expression type in Table 3-3).  For reactions identified as photolysis reactions above, the rate constant is not used and is customarily set to zero. |

1 NONE = gas-phase chemistry only; INERT = user-defined inert PM species; CF = Coarse/Fine aerosol chemistry scheme; CMU = multi-sectional aerosol chemistry scheme;.
2 For the CF scheme, NBIN *must be set to 2*, and the user specifies the coarse/fine size ranges.

```
CAMx Version        |VERSION6.0
Mechanism ID        |6
Aerosol Option      |CF
Description         |CB05 plus PM (CF) with Hg: PNA rates set to 0; molecular units
No of gas species   |67
#aero, dt, bins     |24 15.0 2 0.039 2.5 10.0
No of reactions     |156
Prim photo rxns     |19 1 8 9 14 15 25 36 51 52 53 62 65 75 76 87 91 102 143 152
No of sec photo rxn |4
ID, prim ID, scale  |72  65 1.0
                    |97  65 0.0
                    |106 91 1.0
                    |138 75 9.0
```

Species Records

| | Gas Spec | lower bnd | H-law | T-fact | Molwt | Reactvty | Rscale |
|---|---|---|---|---|---|---|---|
| 1 | O1D | 1.00E-25 | 1.00E+00 | 0. | 0.00 | 0.0 | 0. |
| 2 | O | 1.00E-25 | 1.00E+00 | 0. | 0.00 | 0.0 | 0. |
| 3 | OH | 1.00E-25 | 1.00E+00 | 0. | 0.00 | 0.0 | 0. |
| 4 | HO2 | 1.00E-25 | 1.00E+00 | 0. | 0.00 | 0.0 | 0. |
| 5 | C2O3 | 1.00E-25 | 1.00E+00 | 0. | 0.00 | 0.0 | 0. |
| 6 | XO2 | 1.00E-25 | 1.00E+00 | 0. | 0.00 | 0.0 | 0. |
| 7 | XO2N | 1.00E-25 | 1.00E+00 | 0. | 0.00 | 0.0 | 0. |
| 8 | CXO3 | 1.00E-25 | 1.00E+00 | 0. | 0.00 | 0.0 | 0. |
| 9 | MEO2 | 1.00E-25 | 1.00E+00 | 0. | 0.00 | 0.0 | 0. |
| 10 | TO2 | 1.00E-25 | 1.00E+00 | 0. | 0.00 | 0.0 | 0. |
| 11 | ROR | 1.00E-25 | 1.00E+00 | 0. | 0.00 | 0.0 | 0. |
| 12 | HCO3 | 1.00E-25 | 1.00E+00 | 0. | 0.00 | 0.0 | 0. |
| 13 | CRO | 1.00E-25 | 1.00E+00 | 0. | 0.00 | 0.0 | 0. |
| 14 | AACD | 1.00E-12 | 5.00E+03 | -4000. | 60.03 | 1.0 | 1. |
| 15 | ALD2 | 1.00E-09 | 6.30E+03 | -6492. | 44.04 | 1.0 | 1. |
| 16 | ALDX | 1.00E-12 | 6.30E+03 | -6492. | 58.06 | 1.0 | 1. |
| 17 | CO | 1.00E-04 | 1.00E-10 | 0. | 28.00 | 0.0 | 1. |
| 18 | CRES | 1.00E-09 | 2.70E+03 | -6492. | 108.12 | 1.0 | 1. |
| 19 | ETH | 1.00E-09 | 1.00E-02 | -4000. | 28.05 | 0.0 | 1. |
| 20 | ETHA | 1.00E-04 | 1.73E-03 | -4000. | 30.06 | 0.0 | 1. |
| 21 | ETOH | 1.00E-09 | 2.20E+02 | -4932. | 46.05 | 1.0 | 1. |
| 22 | FACD | 1.00E-12 | 5.68E+03 | -6060. | 46.00 | 1.0 | 1. |
| 23 | FORM | 1.00E-09 | 6.30E+03 | -6492. | 30.01 | 1.0 | 1. |
| 24 | H2O2 | 1.00E-09 | 7.40E+04 | -6643. | 33.99 | 1.0 | 0. |
| 25 | HNO3 | 1.00E-09 | 2.10E+05 | -8707. | 62.98 | 0.0 | 0. |
| 26 | HONO | 1.00E-09 | 5.90E+01 | -4781. | 46.99 | 1.0 | 1. |
| 27 | IOLE | 1.00E-12 | 5.00E-03 | -4000. | 56.10 | 0.0 | 1. |
| 28 | ISOP | 1.00E-09 | 1.00E-02 | -4000. | 68.11 | 0.0 | 1. |
| 29 | ISPD | 1.00E-09 | 6.30E+03 | -6492. | 70.07 | 1.0 | 1. |
| 30 | MEOH | 1.00E-09 | 2.20E+02 | -4932. | 32.03 | 1.0 | 1. |
| 31 | MEPX | 1.00E-12 | 3.05E+02 | -5250. | 48.02 | 0.8 | 0. |
| 32 | MGLY | 1.00E-09 | 2.70E+03 | -6492. | 72.04 | 1.0 | 1. |
| 33 | N2O5 | 1.00E-12 | 1.00E+05 | -4000. | 107.95 | 0.1 | 0. |
| 34 | NO | 1.00E-15 | 1.90E-03 | -1480. | 29.99 | 0.0 | 1. |
| 35 | NO2 | 1.00E-09 | 1.00E-02 | -2516. | 45.98 | 0.8 | 1. |
| 36 | NO3 | 1.00E-12 | 1.00E+05 | -4000. | 61.97 | 0.1 | 0. |
| 37 | NTR | 1.00E-09 | 9.40E+03 | -8706. | 119.07 | 0.0 | 1. |
| 38 | O3 | 1.00E-09 | 1.10E-02 | -2415. | 47.97 | 1.0 | 1. |
| 39 | OLE | 1.00E-09 | 5.00E-03 | -4000. | 42.07 | 0.0 | 1. |
| 40 | OPEN | 1.00E-12 | 2.70E+03 | -6492. | 84.05 | 1.0 | 1. |
| 41 | PACD | 1.00E-12 | 5.00E+03 | -4000. | 76.02 | 1.0 | 1. |
| 42 | PAN | 1.00E-09 | 3.60E+00 | -5910. | 120.99 | 0.6 | 1. |
| 43 | PANX | 1.00E-09 | 3.60E+00 | -5910. | 135.02 | 0.6 | 1. |
| 44 | PAR | 1.00E-04 | 1.00E-03 | -4000. | 72.13 | 0.0 | 1. |
| 45 | PNA | 1.00E-09 | 2.00E+04 | -5910. | 78.97 | 1.0 | 1. |
| 46 | ROOH | 1.00E-12 | 1.00E+02 | -4000. | 90.09 | 0.8 | 0. |
| 47 | SO2 | 1.00E-09 | 1.22E+00 | -3156. | 64.04 | 0.0 | 1. |
| 48 | SULF | 1.00E-12 | 1.00E+10 | 0. | 98.03 | 0.0 | 0. |

**Figure 3-1a. Example CAMx chemistry parameters file for Mechanism 6 (CF scheme), including the mercury species HG0, HG2, and HGP.**

```
49   TERP        1.00E-12  4.90E-02   -4000.    136.21       0.0        1.
50   TOL         1.00E-09  1.20E+00   -4000.     92.13       0.0        1.
51   XYL         1.00E-09  1.40E+00   -4000.    106.15       0.0        1.
52   NH3         1.00E-09  5.76E+01   -4100.     16.94       0.0        0.
53   HCL         1.00E-12  1.00E+05   -4000.     36.30       0.0        0.
54   TOLA        1.00E-09  1.20E+00   -4000.     91.94       0.0        1.
55   XYLA        1.00E-09  1.40E+00   -4000.    106.29       0.0        1.
56   ISP         1.00E-09  1.00E-02   -4000.     67.74       0.0        1.
57   TRP         1.00E-12  4.90E-02   -4000.    136.13       0.0        1.
58   SQT         1.00E-12  4.90E-02   -4000.    204.42       0.0        1.
59   CG1         1.00E-12  1.00E+05   -4000.    150.34       0.0        1.
60   CG2         1.00E-12  1.00E+05   -4000.    150.34       0.0        1.
61   CG3         1.00E-12  1.00E+05   -4000.    130.25       0.0        1.
62   CG4         1.00E-12  1.00E+05   -4000.    130.25       0.0        1.
63   CG5         1.00E-12  1.00E+05   -4000.    179.74       0.0        1.
64   CG6         1.00E-12  1.00E+05   -4000.    179.74       0.0        1.
65   CG7         1.00E-12  1.00E+05   -4000.    210.54       0.0        1.
66   HG0         1.00E-12  1.11E-01   -4970.    200.80       0.0        1.
67   HG2         1.00E-12  2.00E+05   -4000.    254.48       0.0        0.
     Aero Spec   lower bnd  Density  Dry Bext RH Adjust     SSA    SizeBin
 1   PNO3        1.00E-09     1.5       7.0        1       0.99       1
 2   PSO4        1.00E-09     1.5       7.0        1       0.99       1
 3   PNH4        1.00E-09     1.5       7.0        1       0.99       1
 4   POA         1.00E-09     1.0       7.0        0       0.80       1
 5   SOA1        1.00E-09     1.0       7.0        0       0.80       1
 6   SOA2        1.00E-09     1.0       7.0        0       0.80       1
 7   SOA3        1.00E-09     1.0       7.0        0       0.80       1
 8   SOA4        1.00E-09     1.0       7.0        0       0.80       1
 9   SOA5        1.00E-09     1.0       7.0        0       0.80       1
10   SOA6        1.00E-09     1.0       7.0        0       0.80       1
11   SOA7        1.00E-09     1.0       7.0        0       0.80       1
12   SOPA        1.00E-09     1.0       7.0        0       0.80       1
13   SOPB        1.00E-09     1.0       7.0        0       0.80       1
14   PEC         1.00E-09     2.0      18.0        0       0.25       1
15   FPRM        1.00E-09     3.0       0.4        0       0.70       1
16   FCRS        1.00E-09     3.0       0.4        0       0.70       1
17   CPRM        1.00E-09     3.0       0.4        0       0.70       2
18   CCRS        1.00E-09     3.0       0.4        0       0.70       2
19   NA          1.00E-09     2.0       1.5        1       0.99       1
20   PCL         1.00E-09     2.0       1.5        1       0.99       1
21   PH2O        1.00E-09     1.0       0.0        0       0.99       1
22   HGP         1.00E-15     8.0       0.0        0       0.99       1
23   HGIIP       1.00E-20     8.0       0.0        0       0.99       1
24   HGIIPC      1.00E-20     8.0       0.0        0       0.99       2
Reaction Records
Rxn Typ Order Parameters (1 to 12, depending upon Typ)
1   1  1  0.000E+00
2   3  3  6.000E-34   0.0        -2.40        300.0
3   3  2  3.000E-12   1500.0      0.00        300.0
4   3  2  5.600E-12   -180.0      0.00        300.0
5   4  2  2.500E-31   0.0        -1.80        300.0        2.200E-11   0.0          -
0.70      300.0        0.60        1.00
6   4  2  9.000E-32   0.0        -1.50        300.0        3.000E-11   0.0          0.00
300.0        0.60        1.00
7   3  2  1.200E-13   2450.0      0.00        300.0
8   1  1  0.000E+00
9   1  1  0.000E+00
10  3  2  2.100E-11   -102.0      0.00        300.0
11  1  2  2.200E-10
12  3  2  1.700E-12   940.0       0.00        300.0
13  3  2  1.000E-14   490.0       0.00        300.0
14  1  1  0.000E+00
15  1  1  0.000E+00
16  3  2  1.500E-11   -170.0      0.00        300.0
```

**Figure 3-1a (continued).**

```
17  3  2  4.500E-14   1260.0      0.00       300.0
18  4  2  2.000E-30   0.0        -4.40       300.0       1.400E-12   0.0        -
0.70       300.0       0.60       1.00
19  1  2  2.500E-22
20  1  3  1.800E-39
21  4  1  1.000E-03   11000.0    -3.50       300.0       9.700E+14   11080.0    0.10
300.0       0.45       1.00
22  3  3  3.300E-39   -530.0      0.00       300.0
23  1  3  5.000E-40
24  4  2  7.000E-31   0.0        -2.60       300.0       3.600E-11   0.0        -
0.10       300.0       0.60       1.00
25  1  1  0.000E+00
26  3  2  1.800E-11   390.0       0.00       300.0
27  1  2  1.000E-20
28  4  2  2.000E-30   0.0        -3.00       300.0       2.500E-11   0.0        0.00
300.0       0.60       1.00
29  6  2  2.400E-14   -460.0      0.00       300.0       2.700E-17   -2199.0    0.00
300.0       6.500E-34   -1335.0     0.00       300.0
30  3  2  3.500E-12   -250.0      0.00       300.0
31  1  2  0.000E+00
32  1  1  0.000E+00
33  1  2  0.000E+00
34  7  2  2.300E-13   -600.0      0.00       300.0       1.700E-33   -1000.0    0.00
300.0
35  7  3  3.220E-34   -2800.0     0.00       300.0       2.380E-54   -3200.0    0.00
300.0
36  1  1  0.000E+00
37  3  2  2.900E-12   160.0       0.00       300.0
38  1  2  1.100E-10
39  3  2  5.500E-12   2000.0      0.00       300.0
40  3  2  2.200E-11   -120.0      0.00       300.0
41  3  2  4.200E-12   240.0       0.00       300.0
42  4  2  6.900E-31   0.0        -1.00       300.0       2.600E-11   0.0        0.00
300.0       0.60       1.00
43  3  2  4.800E-11   -250.0      0.00       300.0
44  3  2  3.000E-11   -200.0      0.00       300.0
45  3  2  1.400E-12   2000.0      0.00       300.0
46  1  2  1.000E-11
47  1  2  2.200E-11
48  1  2  3.500E-12
49  1  2  1.000E-17
50  3  2  8.500E-13   2450.0      0.00       300.0
51  1  1  0.000E+00
52  1  1  0.000E+00
53  1  1  0.000E+00
54  3  2  2.600E-12   -365.0      0.00       300.0
55  3  2  2.600E-12   -365.0      0.00       300.0
56  3  2  7.500E-13   -700.0      0.00       300.0
57  3  2  7.500E-13   -700.0      0.00       300.0
58  1  2  6.800E-14
59  1  2  6.800E-14
60  1  2  6.800E-14
61  3  2  5.900E-13   360.0       0.00       300.0
62  1  1  0.000E+00
63  4  2  3.000E-31   0.0        -3.30       300.0       1.500E-12   0.0        0.00
300.0       0.60       1.00
64  3  2  3.010E-12   -190.0      0.00       300.0
65  1  1  0.000E+00
66  7  2  1.440E-13   0.0         0.00       300.0       3.430E-33   0.0        0.00
300.0
67  3  2  2.450E-12   1775.0      0.00       300.0
68  3  2  2.800E-12   -300.0      0.00       300.0
69  3  2  4.100E-13   -750.0      0.00       300.0
70  3  2  9.500E-14   -390.0      0.00       300.0
```

**Figure 3-1a (continued).**

```
71  3  2  3.800E-12    -200.0       0.00        300.0
72  1  1  0.000E+00
73  3  2  7.300E-12     620.0       0.00        300.0
74  1  2  9.000E-12
75  1  1  0.000E+00
76  1  1  0.000E+00
77  3  2  3.400E-11    1600.0       0.00        300.0
78  1  2  5.800E-16
79  3  2  9.700E-15    -625.0       0.00        300.0
80  3  1  2.400E+12    7000.0       0.00        300.0
81  1  2  5.600E-12
82  3  2  5.600E-15   -2300.0       0.00        300.0
83  1  2  4.000E-13
84  3  2  1.800E-11    1100.0       0.00        300.0
85  3  2  5.600E-12    -270.0       0.00        300.0
86  3  2  1.400E-12    1900.0       0.00        300.0
87  1  1  0.000E+00
88  3  2  8.100E-12    -270.0       0.00        300.0
89  4  2  2.700E-28     0.0        -7.10        300.0       1.200E-11   0.0         -
0.90       300.0       0.30         1.00
90  4  1  4.900E-03   12100.0       0.00        300.0       5.400E+16   13830.0     0.00
300.0        0.30        1.00
91  1  1  0.000E+00
92  3  2  4.300E-13   -1040.0       0.00        300.0
93  3  2  2.000E-12    -500.0       0.00        300.0
94  3  2  4.400E-13   -1070.0       0.00        300.0
95  3  2  2.900E-12    -500.0       0.00        300.0
96  3  2  4.000E-13    -200.0       0.00        300.0
97  1  1  0.000E+00
98  3  2  4.000E-13    -200.0       0.00        300.0
99  3  2  1.300E-11     870.0       0.00        300.0
100 3  2  5.100E-12    -405.0       0.00        300.0
101 1  2  6.500E-15
102 1  1  0.000E+00
103 3  2  6.700E-12    -340.0       0.00        300.0
104 4  2  2.700E-28     0.0        -7.10        300.0       1.200E-11   0.0         -
0.90       300.0       0.30         1.00
105 4  1  4.900E-03   12100.0       0.00        300.0       5.400E+16   13830.0     0.00
300.0        0.30        1.00
106 1  1  0.000E+00
107 1  2  3.000E-13
108 3  2  4.300E-13   -1040.0       0.00        300.0
109 3  2  2.000E-12    -500.0       0.00        300.0
110 3  2  4.400E-13   -1070.0       0.00        300.0
111 3  2  2.900E-12    -500.0       0.00        300.0
112 3  2  2.900E-12    -500.0       0.00        300.0
113 3  2  8.700E-12    1070.0       0.00        300.0
114 3  2  6.900E-12     230.0       0.00        300.0
115 1  2  8.100E-13
116 3  1  1.000E+15    8000.0       0.00        300.0
117 1  1  1.600E+03
118 1  2  1.500E-11
119 3  2  1.000E-11     280.0       0.00        300.0
120 1  2  3.200E-11
121 3  2  6.500E-15    1900.0       0.00        300.0
122 3  2  7.000E-13    2160.0       0.00        300.0
123 3  2  1.040E-11     792.0       0.00        300.0
124 4  2  1.000E-28     0.0        -0.80        300.0       8.800E-12   0.0         0.00
300.0        0.60        1.00
125 3  2  1.200E-14    2630.0       0.00        300.0
126 3  2  3.300E-12    2880.0       0.00        300.0
127 1  2  2.300E-11
128 3  2  1.000E-11    -550.0       0.00        300.0
129 3  2  8.400E-15    1100.0       0.00        300.0
```

**Figure 3-1a (continued).**

```
130 3  2  9.600E-13    270.0       0.00        300.0
131 3  2  1.800E-12   -355.0       0.00        300.0
132 1  2  8.100E-12
133 1  1  4.200E+00
134 1  2  4.100E-11
135 1  2  2.200E-11
136 1  2  1.400E-11
137 1  2  5.500E-12
138 1  1  0.000E+00
139 1  2  3.000E-11
140 3  2  5.400E-17    500.0       0.00        300.0
141 3  2  1.700E-11   -116.0       0.00        300.0
142 1  2  1.700E-11
143 1  1  0.000E+00
144 1  2  3.600E-11
145 3  2  2.540E-11   -407.6       0.00        300.0
146 3  2  7.860E-15   1912.0       0.00        300.0
147 3  2  3.030E-12    448.0       0.00        300.0
148 1  2  1.500E-19
149 1  2  3.360E-11
150 1  2  7.100E-18
151 1  2  1.000E-15
152 1  1  0.000E+00
153 1  2  3.600E-11
154 3  2  1.500E-11   -449.0       0.00        300.0
155 3  2  1.200E-15    821.0       0.00        300.0
156 3  2  3.700E-12   -175.0       0.00        300.0
```

**Figure 3-1a (concluded).**

```
CAMx Version        |VERSION6.0
Mechanism ID        |0
Aerosol Option      |NONE
Description         |inert test
No of gas species   |1
No of aero species  |0
No of reactions     |0
Prim photo rxns     |0
No of sec photo rxn |0
Species Records
     Gas Spec   lower bnd    H-law    T-fact    Molwt   Reactvty    Rscale
  1  TRACER     1.00E-09   1.00e-10      0.      1.00       0.0        1.
```

**Figure 3-1b.  Example inert chemistry parameters file (requires chemistry flag to be set false – see the description of the CAMx control file).**

The section of the file that lists gas species must include the names of radical and state species, according to the selected chemical mechanism, along with each species' lower bound value, Henry's Law solubility parameters, molecular weight, and surface reactivity and resistance scaling parameters for use in the dry deposition calculations.  The lower bound values set the minimum concentration "floor" for any chemical or physical process that reduces concentrations to "zero".  The lower bound is also used to set initial and/or boundary conditions for species that are omitted from the initial and/or boundary condition files.

The section of the file that lists aerosol species names must include a lower-bound value, particle density, dry extinction efficiency, a hygroscopic flag, and single-scattering albedo.  In the case of INERT or CF options, the user must also specify the size bin assigned to each species at the end of each particulate species record (CMU automatically applies each species to all size bins).  Since the effect of aerosol water on optical parameters is taken into account through an internal relative humidity adjustment, the dry extinction efficiency for particle species PH2O must be set to zero.

CAMx supports several equations for specifying gas-phase rate constants, as shown in Table 3-3a.  The type of equation used for each reaction is identified by the second parameter specified for each reaction – a number between 1 and 7 (Table 3-3a).  The number of additional parameters required depends upon the expression type and varies between 2 and 13, as shown in Table 3-3b.  The CB mechanisms use types 1, 3, 4, and 7, and SAPRC99 uses types 1, 3, 4, 6 and 7.  Expression type 4 (Troe expression) allows for a complete description of dependencies on temperature and pressure; background information on Troe expressions may be found in the NASA and IUPAC rate constant compilations (NASA, 1997; IUPAC, 1992).

Rate constants can be specified in molecular units (e.g., $cm^3$ molecule$^{-1}$ s$^{-1}$) or ppm units (e.g., ppm$^{-1}$ min$^{-1}$).  All the rate constants must be in a single units system; CAMx will determine which units system is being used from the magnitude of the rate constants.  Diagnostic information on the rate constants and units system is output by CAMx at run-time.

## 3.2  Photolysis Rates File

The rates for the primary photolysis reactions are supplied via the photolysis rates file in units of minute$^{-1}$.  This file must be supplied if chemistry is invoked.  The photolysis rates file comprises a large look-up table of clear-sky photolysis rates specific to the gas-phase chemistry mechanism to run.  Rates are arranged in a matrix of five dimensions, including variations over 10 solar zenith angles, 11 altitudes above ground, 5 total ozone column values, 5 ultraviolet (UV) surface albedos, and 3 terrain heights.  This table is generated using the TUV preprocessor, which internally specifies the ranges of solar zenith, albedo, and terrain heights.  The ranges of altitude are controlled by the user, while the ranges of ozone column are taken from the ozone column file (Section 3.3).  TUV is run with a typical aerosol profile defined by Elterman (1968).

**Table 3-3a.  Rate constant expression types supported in CAMx and order of expression parameters for the chemistry parameters file.**

| Expression Type | Description | Expression |
|:---:|:---|:---:|
| 1 | Constant | $k = k_{298}$ |
| 2 | UAM (Arrhenius expression) | $k = k_{298} \exp\left[ E_a\left( \dfrac{1}{298} - \dfrac{1}{T} \right) \right]$ |
| 3 | General temperature dependence | $k = A\left( \dfrac{T}{T_R} \right)^B \exp\left( -\dfrac{E_a}{T} \right)$ |
| 4 | Troe-type temperature and pressure dependence | $k = \left( \dfrac{k^0[M]}{1 + k^0[M]/k^\infty} \right) F^G$ <br><br> $k^0 = A\left( \dfrac{T}{T_R} \right)^B \exp\left( -\dfrac{E_a}{T} \right)$ <br><br> $k^\infty = A'\left( \dfrac{T}{T_R'} \right)^{B'} \exp\left( -\dfrac{E_a'}{T} \right)$ <br><br> $G = \left[ 1 + \left( \dfrac{\log\left(k^0[M]/k^\infty\right)}{n} \right)^2 \right]^{-1}$ |
| 5 | Equilibrium with a previously defined reaction ($k_{ref}$) | $k = k_{ref} A\left( \dfrac{T}{T_R} \right)^B \exp\left( -\dfrac{E_a}{T} \right)$ |
| 6 | Lindemann - Hinshelwood as used for OH + HNO3 | $k = k^0 + \dfrac{k_3[M]}{1 + k_3[M]/k_2}$ |
| 7 | Simple pressure dependence used for OH + CO | $k = k_1 + k_2[M]$ |

Notes:
      $T$ is temperature (K)
      $T_R$ is reference temperature of 300 K
      $E_a$ is an Arrhenius activation energy (K)
      $k^0$ is the low pressure limit of the rate constant
      $k^\infty$ is the high pressure limit of the rate constant
      $[M]$ is the concentration of air

**Table 3-3b. List of parameters that must be provided in the CAMx chemistry parameter file for each of the seven types of rate constant expressions. Use ppm/minute units for A and Kelvin for $E_a$ and $T_R$. The variable O is the order of the reaction (1 to 3).**

| Expression Type | Parameters | | | | | | | | | | | | |
|---|---|---|---|---|---|---|---|---|---|---|---|---|---|
| | 1 | 2 | 3 | 4 | 5 | 6 | 7 | 8 | 9 | 10 | 11 | 12 | 13 |
| 1 | O | $k_{298}$ | | | | | | | | | | | |
| 2 | O | $k_{298}$ | $E_a$ | | | | | | | | | | |
| 3 | O | A | $E_a$ | B | $T_R$ | | | | | | | | |
| 4 | O | A | $E_a$ | B | $T_R$ | A′ | $E_a′$ | B′ | $T_R′$ | F | n | | |
| 5 | O | $k_{ref}$ | A | $E_a$ | B | $T_R$ | | | | | | | |
| 6 | O | $A^o$ | $E_a^o$ | $B^o$ | $T_R^o$ | $A^2$ | $E_a^2$ | $B^2$ | $T_R^2$ | $A^3$ | $E_a^3$ | $B^3$ | $T_R^3$ |
| 7 | O | $A^1$ | $E_a^1$ | $B^1$ | $T_R^1$ | $A^2$ | $E_a^2$ | $B^2$ | $T_R^2$ | | | | |

The photolysis rates file is a readable text (ASCII) format and it has the following structure:

```
TUV4.8CAMx6
Loop from 1 to nozn ozone column intervals:
    Loop from 1 to nalb UV albedo intervals:
        Loop from 1 to ntht terrain height intervals:
            ozcl,albcl,trncl                (12X,f7.3,8X,f7.3,11X,f7.3)
            Loop from 1 to nalt altitudes above ground:
                height                      (*)
                Loop from 1 to nphot photolysis reactions:
                    (pk(n),n=1,nsol)        (1X,10F12.0)
```

where the first record labels the version of TUV used to generate the file, and where variables have the following definitions:

| | |
|---|---|
| ozcl | Ozone column value for the current interval (Dobson units) |
| albcl | UV albedo value for the current interval (unitless) |
| trncl | Terrain height value for the current interval (km MSL) |
| height | Altitude (km AGL) |
| pk | Photolysis rates (min$^{-1}$) for *nsol* solar zenith angles |

Figure 3-2 presents an example of a photolysis rates file for the first several panels of data.

## 3.3 Ozone Column File

This file defines the intervals of total atmospheric ozone column to be used by TUV, as well as its spatial and temporal distributions for a specific CAMx domain and episode. This parameter is essential for photochemical simulations as it determines the spatial and temporal variation of photolysis rates. Therefore, this file must be supplied if chemistry is invoked. Additionally, the ozone column file may also provide an optional field defining a land/ocean mask (for mercury chemistry).

```
TUV4.8CAMx6
O3 Column =  0.290 Albedo=  0.040 Terrain  =  0.000
   0.000    km above surface
    4.562E-01   4.526E-01   4.416E-01   4.224E-01   3.934E-01   3.516E-01   2.921E-01   2.065E-01   1.148E-01   3.074E-02
    1.670E-03   1.643E-03   1.563E-03   1.427E-03   1.236E-03   9.889E-04   6.936E-04   3.747E-04   1.502E-04   2.570E-05
    2.211E-03   2.186E-03   2.107E-03   1.973E-03   1.776E-03   1.506E-03   1.152E-03   7.108E-04   3.352E-04   7.560E-05
    2.078E-03   2.007E-03   1.801E-03   1.485E-03   1.097E-03   6.925E-04   3.382E-04   1.034E-04   2.201E-05   2.056E-06
    3.131E-04   3.058E-04   2.841E-04   2.491E-04   2.027E-04   1.482E-04   9.100E-05   4.015E-05   1.264E-05   1.517E-06
    8.728E-05   8.638E-05   8.364E-05   7.891E-05   7.189E-05   6.212E-05   4.892E-05   3.166E-05   1.580E-05   3.934E-06
   0.150    km above surface
    4.866E-01   4.830E-01   4.717E-01   4.521E-01   4.223E-01   3.794E-01   3.179E-01   2.284E-01   1.308E-01   3.760E-02
    1.855E-03   1.827E-03   1.742E-03   1.598E-03   1.394E-03   1.130E-03   8.102E-04   4.566E-04   1.956E-04   3.701E-05
    2.443E-03   2.416E-03   2.334E-03   2.193E-03   1.986E-03   1.701E-03   1.322E-03   8.415E-04   4.159E-04   1.000E-04
    2.327E-03   2.249E-03   2.024E-03   1.677E-03   1.250E-03   8.008E-04   4.035E-04   1.337E-04   3.383E-05   4.166E-06
    3.489E-04   3.410E-04   3.177E-04   2.799E-04   2.297E-04   1.704E-04   1.075E-04   5.024E-05   1.755E-05   2.556E-06
    9.553E-05   9.460E-05   9.176E-05   8.684E-05   7.952E-05   6.928E-05   5.530E-05   3.672E-05   1.910E-05   5.068E-06
   0.360    km above surface
    5.050E-01   5.013E-01   4.900E-01   4.702E-01   4.402E-01   3.968E-01   3.343E-01   2.426E-01   1.412E-01   4.171E-02
    1.974E-03   1.945E-03   1.857E-03   1.708E-03   1.497E-03   1.222E-03   8.862E-04   5.096E-04   2.245E-04   4.415E-05
    2.587E-03   2.560E-03   2.477E-03   2.333E-03   2.120E-03   1.826E-03   1.432E-03   9.258E-04   4.673E-04   1.152E-04
    2.494E-03   2.411E-03   2.174E-03   1.806E-03   1.353E-03   8.740E-04   4.474E-04   1.536E-04   4.129E-05   5.492E-06
    3.722E-04   3.640E-04   3.396E-04   3.002E-04   2.475E-04   1.851E-04   1.183E-04   5.679E-05   2.067E-05   3.210E-06
    1.006E-04   9.970E-05   9.681E-05   9.180E-05   8.433E-05   7.382E-05   5.940E-05   3.999E-05   2.122E-05   5.763E-06
   0.640    km above surface
    5.230E-01   5.193E-01   5.080E-01   4.882E-01   4.581E-01   4.143E-01   3.510E-01   2.574E-01   1.520E-01   4.577E-02
    2.092E-03   2.062E-03   1.972E-03   1.819E-03   1.601E-03   1.315E-03   9.632E-04   5.633E-04   2.535E-04   5.126E-05
    2.731E-03   2.703E-03   2.618E-03   2.471E-03   2.254E-03   1.951E-03   1.544E-03   1.011E-03   5.191E-04   1.304E-04
    2.664E-03   2.577E-03   2.327E-03   1.939E-03   1.459E-03   9.497E-04   4.928E-04   1.738E-04   4.872E-05   6.809E-06
    3.958E-04   3.872E-04   3.618E-04   3.207E-04   2.656E-04   2.000E-04   1.294E-04   6.343E-05   2.378E-05   3.860E-06
    1.057E-04   1.047E-04   1.018E-04   9.672E-05   8.912E-05   7.839E-05   6.354E-05   4.331E-05   2.336E-05   6.448E-06
   0.980    km above surface
    5.409E-01   5.373E-01   5.260E-01   5.062E-01   4.760E-01   4.321E-01   3.682E-01   2.727E-01   1.635E-01   4.989E-02
    2.210E-03   2.179E-03   2.087E-03   1.930E-03   1.705E-03   1.409E-03   1.041E-03   6.178E-04   2.827E-04   5.837E-05
    2.873E-03   2.845E-03   2.758E-03   2.609E-03   2.387E-03   2.077E-03   1.656E-03   1.099E-03   5.718E-04   1.454E-04
    2.837E-03   2.746E-03   2.483E-03   2.074E-03   1.567E-03   1.028E-03   5.396E-04   1.944E-04   5.611E-05   8.121E-06
    4.195E-04   4.106E-04   3.842E-04   3.414E-04   2.840E-04   2.152E-04   1.407E-04   7.017E-05   2.689E-05   4.509E-06
    1.107E-04   1.097E-04   1.068E-04   1.016E-04   9.392E-05   8.299E-05   6.775E-05   4.673E-05   2.556E-05   7.133E-06
   1.380    km above surface
    5.593E-01   5.556E-01   5.444E-01   5.247E-01   4.947E-01   4.507E-01   3.863E-01   2.892E-01   1.760E-01   5.427E-02
    2.329E-03   2.298E-03   2.203E-03   2.042E-03   1.811E-03   1.505E-03   1.122E-03   6.743E-04   3.128E-04   6.563E-05
    3.016E-03   2.988E-03   2.900E-03   2.749E-03   2.524E-03   2.207E-03   1.773E-03   1.190E-03   6.270E-04   1.609E-04
    3.015E-03   2.920E-03   2.644E-03   2.215E-03   1.681E-03   1.109E-03   5.887E-04   2.158E-04   6.364E-05   9.454E-06
    4.437E-04   4.345E-04   4.071E-04   3.627E-04   3.029E-04   2.310E-04   1.524E-04   7.716E-05   3.009E-05   5.169E-06
    1.157E-04   1.148E-04   1.118E-04   1.066E-04   9.883E-05   8.772E-05   7.213E-05   5.031E-05   2.789E-05   7.835E-06
   1.840    km above surface
    5.782E-01   5.746E-01   5.635E-01   5.440E-01   5.141E-01   4.702E-01   4.056E-01   3.069E-01   1.897E-01   5.904E-02
    2.451E-03   2.419E-03   2.322E-03   2.157E-03   1.920E-03   1.605E-03   1.206E-03   7.338E-04   3.445E-04   7.312E-05
    3.162E-03   3.133E-03   3.045E-03   2.892E-03   2.664E-03   2.341E-03   1.894E-03   1.286E-03   6.856E-04   1.769E-04
    3.200E-03   3.101E-03   2.811E-03   2.361E-03   1.799E-03   1.196E-03   6.407E-04   2.385E-04   7.141E-05   1.082E-05
    4.685E-04   4.589E-04   4.307E-04   3.846E-04   3.224E-04   2.473E-04   1.647E-04   8.451E-05   3.341E-05   5.848E-06
    1.209E-04   1.199E-04   1.169E-04   1.117E-04   1.039E-04   9.263E-05   7.671E-05   5.412E-05   3.039E-05   8.570E-06
   2.350    km above surface
    5.974E-01   5.939E-01   5.829E-01   5.636E-01   5.340E-01   4.904E-01   4.257E-01   3.258E-01   2.046E-01   6.425E-02
    2.572E-03   2.540E-03   2.441E-03   2.273E-03   2.031E-03   1.706E-03   1.292E-03   7.955E-04   3.775E-04   8.077E-05
    3.307E-03   3.278E-03   3.190E-03   3.036E-03   2.805E-03   2.477E-03   2.019E-03   1.386E-03   7.476E-04   1.934E-04
    3.389E-03   3.285E-03   2.983E-03   2.512E-03   1.922E-03   1.285E-03   6.952E-04   2.622E-04   7.936E-05   1.221E-05
    4.934E-04   4.836E-04   4.544E-04   4.068E-04   3.424E-04   2.641E-04   1.774E-04   9.214E-05   3.685E-05   6.538E-06
    1.261E-04   1.251E-04   1.221E-04   1.169E-04   1.090E-04   9.763E-05   8.142E-05   5.811E-05   3.305E-05   9.333E-06
   2.910    km above surface
    6.169E-01   6.134E-01   6.026E-01   5.836E-01   5.543E-01   5.111E-01   4.466E-01   3.458E-01   2.209E-01   7.003E-02
    2.694E-03   2.661E-03   2.561E-03   2.390E-03   2.143E-03   1.810E-03   1.382E-03   8.602E-04   4.124E-04   8.867E-05
    3.452E-03   3.423E-03   3.335E-03   3.180E-03   2.948E-03   2.615E-03   2.148E-03   1.492E-03   8.140E-04   2.106E-04
    3.582E-03   3.474E-03   3.159E-03   2.667E-03   2.049E-03   1.379E-03   7.528E-04   2.874E-04   8.761E-05   1.363E-05
    5.187E-04   5.086E-04   4.786E-04   4.294E-04   3.628E-04   2.814E-04   1.906E-04   1.002E-04   4.045E-05   7.246E-06
    1.312E-04   1.303E-04   1.273E-04   1.221E-04   1.142E-04   1.027E-04   8.630E-05   6.231E-05   3.593E-05   1.014E-05
   3.530    km above surface
    6.368E-01   6.334E-01   6.228E-01   6.041E-01   5.754E-01   5.328E-01   4.687E-01   3.673E-01   2.389E-01   7.670E-02
    2.818E-03   2.784E-03   2.683E-03   2.510E-03   2.258E-03   1.917E-03   1.476E-03   9.296E-04   4.505E-04   9.704E-05
    3.599E-03   3.571E-03   3.482E-03   3.328E-03   3.094E-03   2.759E-03   2.283E-03   1.605E-03   8.871E-04   2.291E-04
    3.783E-03   3.670E-03   3.343E-03   2.830E-03   2.184E-03   1.478E-03   8.148E-04   3.147E-04   9.644E-05   1.512E-05
    5.446E-04   5.343E-04   5.034E-04   4.528E-04   3.840E-04   2.996E-04   2.046E-04   1.088E-04   4.434E-05   7.989E-06
    1.365E-04   1.355E-04   1.326E-04   1.274E-04   1.195E-04   1.080E-04   9.142E-05   6.681E-05   3.911E-05   1.103E-05
   4.210    km above surface
    6.569E-01   6.536E-01   6.433E-01   6.250E-01   5.969E-01   5.550E-01   4.917E-01   3.902E-01   2.588E-01   8.447E-02
    2.943E-03   2.909E-03   2.807E-03   2.632E-03   2.376E-03   2.029E-03   1.574E-03   1.004E-03   4.925E-04   1.060E-04
    3.747E-03   3.719E-03   3.631E-03   3.477E-03   3.243E-03   2.906E-03   2.424E-03   1.725E-03   9.679E-04   2.493E-04
    3.992E-03   3.875E-03   3.534E-03   3.000E-03   2.325E-03   1.585E-03   8.818E-04   3.447E-04   1.060E-04   1.668E-05
    5.711E-04   5.605E-04   5.289E-04   4.769E-04   4.060E-04   3.186E-04   2.195E-04   1.181E-04   4.859E-05   8.775E-06
    1.417E-04   1.408E-04   1.379E-04   1.327E-04   1.249E-04   1.135E-04   9.674E-05   7.161E-05   4.262E-05   1.202E-05
O3 Column =  0.290 Albedo=  0.040 Terrain  =  1.000
   0.000    km above surface
    4.655E-01   4.615E-01   4.493E-01   4.279E-01   3.958E-01   3.499E-01   2.855E-01   1.957E-01   1.048E-01   2.871E-02
    1.688E-03   1.660E-03   1.576E-03   1.435E-03   1.237E-03   9.833E-04   6.824E-04   3.626E-04   1.414E-04   2.142E-05
    2.240E-03   2.212E-03   2.129E-03   1.987E-03   1.780E-03   1.498E-03   1.132E-03   6.858E-04   3.159E-04   6.495E-05
    2.098E-03   2.025E-03   1.815E-03   1.492E-03   1.098E-03   6.883E-04   3.334E-04   1.009E-04   2.101E-05   1.716E-06
    3.162E-04   3.086E-04   2.863E-04   2.503E-04   2.029E-04   1.473E-04   8.961E-05   3.896E-05   1.193E-05   1.254E-06
    8.857E-05   8.761E-05   8.467E-05   7.961E-05   7.213E-05   6.180E-05   4.802E-05   3.042E-05   1.483E-05   3.488E-06
   0.150    km above surface
    5.004E-01   4.963E-01   4.839E-01   4.623E-01   4.296E-01   3.828E-01   3.163E-01   2.220E-01   1.237E-01   3.1E-02
    1.870E-03   1.841E-03   1.752E-03   1.604E-03   1.394E-03   1.123E-03   7.976E-04   4.424E-04   1.847E-04   3.188E-05
    2.473E-03   2.445E-03   2.359E-03   2.211E-03   1.994E-03   1.697E-03   1.306E-03   8.179E-04   3.956E-04   8.840E-05
    2.338E-03   2.259E-03   2.030E-03   1.677E-03   1.245E-03   7.929E-04   3.960E-04   1.294E-04   3.180E-05   3.572E-06
    3.509E-04   3.428E-04   3.189E-04   2.803E-04   2.292E-04   1.690E-04   1.056E-04   4.859E-05   1.651E-05   2.187E-06
    9.713E-05   9.614E-05   9.312E-05   8.789E-05   8.013E-05   6.934E-05   5.476E-05   3.574E-05   1.823E-05   4.615E-06
```

**Figure 3-2.  Example of the first several panels of lookup data in the photolysis rates input file.**

There are two mandatory and one optional header records in the ozone column file. The first record contains an arbitrary file label. The second record defines the intervals for 5 ozone column values for the domain and temporal period to be simulated. These intervals must exactly match those defined in preparing the photolysis rates file, so the ozone column file is also read by the TUV preprocessor to define the photolysis rates lookup table (Section 3.2).

If the optional land/ocean mask is included, then a third header record must be added to inform CAMx that this field is to be read. The time-invariant land/ocean mask is used for mercury chemistry to define profiles of ambient halogens; it is simply a map of 0 (land and fresh water bodies) and 1 (ocean) that must be located directly under its header record. A value must be supplied for each cell of the master grid and optionally any nested grids.

Gridded fields of time-varying ozone column follow the header records and optional land/ocean mask data. The gridded fields are maps of the respective "codes" for each interval, as defined in the header. For example, 5 ozone column intervals are specified in TUV and in the ozone column header record, so the map must consist of a distribution of integers ranging from 1 to 5. Ozone column is supplied for the master grid only; CAMx internally assigns master cell values to all nested grids cells. Multiple maps of these codes may be provided for arbitrary time intervals that span the entire simulation period.

The ozone column file is a readable text (ASCII) format and it has the following structure:

```
    text                              (A)
    ozname,(ozncl(n),n=1,nozn)        (A10,5F10.0)
    loname,igrd,nx,ny                 (A10,3I10)        -- Optional
    Loop from j = ny grid rows to 1                     -- Optional
        (jocn(i,j),i=1,nx)            (999I1)           -- Optional
    loname,igrd,nx,ny                 (A10,3I10)        -- Optional
    ozname,idt1,tim1,idt2,tim2        (A10,I10,F10.0,I10,F10.0)
    Loop from j = ny master grid rows to 1
        (jozn(i,j),i=1,nx)            (9999I1)
```

where the variables in the ozone column file have the following definitions:

| | |
|---|---|
| text | Text identifying file and any messages |
| ozname | Text string "OZONE COL" |
| ozncl | Ozone column (Dobson units) for each of *nozn* ozone values |
| loname | Text string "OCEAN" |
| igrd | Grid index (1 = master grid, 2+=nested grid, 0 = end of data) |
| nx | Number of grid columns for this grid index |
| ny | Number of grid rows for this grid index |
| jocn | Grid *igrd,* row *j* land/ocean codes for *nx* grid columns |
| idt1 | Beginning date (YYJJJ) of time span |
| tim1 | Beginning hour (HHMM) of time span |
| idt2 | Ending date of time span |

tim2            Ending hour of time span

jozn            Master grid row *j* ozone column codes for *nx* master grid columns

An example of a small ozone column file is given in Figure 3-3.

```
Sample ozone column file with optional land ocean mask
OZONE COL      0.285      0.315      0.345      0.375      0.405
OCEAN              1         64         10
00000000000000000000011111111100000000000000000000000000000000
00000000000000000000000001111111110000000000000000000000000000
00000000000000000000000011111111111110000000000000000000000000
00000000000000000000000011111111111100000000000000000000000000
00000000000000000000000011111111111111000000000000000000000000
00000000000000000000000011111111111111110000000000000000000000
00000000000000000000000011111111111111111000000000000000000000
0000000000000000000001111111000000000111111100000000000000000
0000000000000000000001111111100000000001111111100000000000000
0000000000000000000001111111110000000001111111110000000000000
OCEAN              0          0          0
OZONE COL      05213       0.00      05213    2400.00
33333333333333333333333333333333333333333333333333333333333333
33333333333333333333333333333333333333333333333333333333333333
22222222222223333333333333333333333333333333333333333333333333
22222222222222333333333333333333333333333333333333333333333333
22222222222222333333333333333333333333333333333333333333333333
22222222222222333333333333333333333333333333333333333333333333
22222222222222333333333333333333333333333333333333333333333333
22222222222222333333333333333333333333333333333333333333333333
22222222222222333333333333333333333333333333333333333333333333
22222222222222222222233333333333333333333333333333333333333333
```

**Figure 3-3.  Example structure of a single-grid ozone column input file showing panels for the optional time-invariant land-ocean mask and time-varying ozone column field.**

## 3.4  Fortran Binary Input/Output Files

### 3.4.1  What is a Fortran Binary File?

Large CAMx input and output data fields are contained within Fortran "unformatted" (binary) files.  This means that the data are read and written as represented in memory, without translation between binary and ASCII character sets as done for "text" files.  Binary files reduce file volume and improve program read/write speed, but the user cannot directly view or manually edit them.  There are two ways to represent binary information in memory: "big endian" and "little endian."  The difference between these is essentially the order of bits in a word, and which order is used depends on the computer chipset.  Historically, big endian has been used in many Unix workstations (Sun, SGI, HP, and IBM).  The x86 processors on personal computer platforms (e.g., Intel and AMD) use little endian, while PowerPC chips are big endian.

CAMx can be compiled and run on machines using their native big or little endian binary representations, as long as the model and all of its pre- and post-processors are consistently compiled and run on the same type of platform.  If any component of the modeling system is

compiled for a different platform using the opposite binary representation, I/O files will not be properly read and will likely lead to a program crash. A typical run-time error message from trying to read the wrong binary format is "input record too long," so if you get this error message, check for consistency between your binary files and Fortran compiler options.

Compilers for little endian machines provide compile-time switches that allow binary files to be read and written as big endian. The "makefile" compiler script that is distributed with CAMx sets compiler flags to consistently use big endian to maximize platform portability. Therefore, use of the CAMx Makefile will by default result in the model reading and writing big endian binary files. Additional information on this topic is provided in Section 2.

### 3.4.2  CAMx Binary File Headers

The format of all binary CAMx I/O files follows the convention established by the Urban Airshed Model (EPA, 1990). CAMx binary files contain a set of time-invariant header records, followed by a set of data records that contain time- and variable-specific fields. All input gridded emissions, initial conditions, meteorology[1], and output concentration and deposition files share the same basic format. The input boundary condition and point source emissions files are similar but include additional records specific to their data structures. The input 3D meteorological file may provide wind fields in a staggered or un-staggered grid arrangement. A flag to indicate the wind staggering is included in the second header record and is checked only when the 3D meteorological file is read.

The four header records within all CAMx binary files have the following structure:

```
name,note,itzon,nvar,ibdate,btime,iedate,etime
plon,plat,iutm,xorg,yorg,delx,dely,nx,ny,nz,iproj,istag,tlat1,tlat2,rdum
ione,ione,nx,ny
(namvar(l),l=1,nvar)
```

The header variables have the following definitions:

Record 1

| | | |
|---|---|---|
| name | Text string describing file contents (character*4(10) array): | |
| | AIRQUALITY | Initial conditions |
| | BOUNDARY | Boundary conditions |
| | EMISSIONS | Gridded emissions |
| | PTSOURCE | Point source emissions |
| | AVERAGE | Average output concentrations/deposition and input meteorology/surface variables |
| | INSTANT | Instantaneous output concentrations |
| note | Text string containing user note (character*4(60) array) | |
| itzon | Integer time zone (0=UTC, 5=EST, etc.) | |
| nvar | Integer number of variables on file | |

---

[1] NOTE: Starting with CAMx v6.00, all binary meteorological files have been converted to the UAM convention.

| | |
|---|---|
| `ibdate` | Integer beginning date span on file (YYJJJ) |
| `btime` | Real beginning decimal hour (e.g., 1:30 PM = 13.5) |
| `iedate` | Integer ending date span on file (YYJJJ) |
| `etime` | Real ending decimal hour (e.g., 1:30 PM = 13.5) |

Record 2

| | |
|---|---|
| `plon` | Real projection pole longitude (degrees; west is negative) |
| `plat` | Real projection pole latitude (degrees; south is negative) |
| `iutm` | Integer UTM zone (ignored for other projections) |
| `xorg` | Real grid x-origin at southwest corner of domain (m or degrees longitude) |
| `yorg` | Real grid y-origin at southwest corner of domain (m or degrees latitude) |
| `delx` | Real cell size in x-direction (m or degrees longitude) |
| `dely` | Real cell size in y-direction (m or degrees latitude) |
| `nx` | Integer number of grid columns (east-west) |
| `ny` | Integer number of grid rows (north-south) |
| `nz` | Integer number of vertical layers |
| `iproj` | Integer projection index: |
| | 0 = geodetic (lat/lon) |
| | 1 = Universal Transverse Mercator (UTM) |
| | 2 = Lambert Conic Conformal (LCP) |
| | 3 = Polar Stereographic (PSP) |
| `istag` | Integer flag to indicate wind staggering (1=staggered, 0=not staggered) |
| `tlat1` | Real LCP first true latitude (degrees; south is negative) |
| `tlat2` | Real LCP second true latitude (degrees; south is negative) |
| `rdum` | Real dummy variable |

Record 3

| | |
|---|---|
| `ione` | Integer dummy variable (=1) |
| `ione` | Integer dummy variable (=1) |
| `nx` | Integer number of grid columns (east-west) |
| `ny` | Integer number of grid rows (north-south) |

Record 4

| | |
|---|---|
| `namvar` | Text names for *nvar* variables (character*4(10,nvar) array) |

### 3.4.3 Input Files

The Fortran binary input files include initial/boundary conditions, gridded and elevated point source emissions, and several meteorological files. All times on input files must match the time zone specified in the CAMx control file (CAMx.in).

Initial/boundary condition files may include a single time interval covering the entire simulation period, or more detailed hour-by-hour (or other interval) variations. The time intervals are allowed to be entirely arbitrary to maximize flexibility in defining these inputs. A subset of the pollutant species to be simulated may be defined in the initial/boundary condition files; any species that are missing will be set to "lower bound" values as defined in the chemistry parameters file.

Emission inputs are usually developed at one hour intervals, but the file structures allow for any other interval as long as a consistent interval is used throughout the file (all one hour, or all three hour, but no mixing of these). The time interval on all emission files must match the emission update frequency defined in the CAMx control file. A subset of species to be simulated may be included in the emission files; zero emission rates will be applied for any species that are missing.

Meteorological fields are separated into two-dimensional and three-dimensional fields. The core meteorological file contains the basic parameters needed for most model processes, and includes winds and basic thermodynamic properties. Separate vertical diffusivity and cloud files allow for easy substitution of alternative inputs without the need to re-generate all of the core fields. The time interval on all meteorological files must match the meteorological update frequency defined in the CAMx control file.

### 3.4.3.1  Input Static 2-D Surface File

The static 2-D surface file contains time-invariant gridded fields of landuse and topographic elevation, and optionally leaf area index (LAI). This file must be developed for the master grid, and optionally any of the nested fine grids. The fractional distribution of 26 landuse categories, consistent with the Zhang dry deposition scheme, is supplied for each grid cell. If the Wesely dry deposition option is invoked, CAMx internally maps the 26 categories to the 11 WESELY89 categories. These are used to define surface UV albedo, surface resistances for dry deposition calculations, and to set seasonal default surface roughness lengths and LAI values (if LAI is not specified in the file). The landuse categories are described in Tables 3-4 and 3-5.

**Table 3-4.  The 11 WESELY89 landuse categories, their default UV surface albedos, and their surface roughness values (m) by season.  Winter is defined for conditions where there is snow present; winter months with no snow are assigned to the Fall category.  Roughness for water is calculated from the function** $z_0 = 2 \times 10^{-6} w^{2.5}$**, where** *w* **is surface wind speed (m/s).**

| Category Number | Land Cover Category | Surface Roughness (meters) | | | | UV Albedo |
|---|---|---|---|---|---|---|
| | | Spring | Summer | Fall | Winter | |
| 1 | Urban | 1.0 | 1.0 | 1.0 | 1.0 | 0.08 |
| 2 | Agricultural | 0.03 | 0.2 | 0.05 | 0.01 | 0.05 |
| 3 | Rangeland | 0.05 | 0.1 | 0.01 | 0.001 | 0.05 |
| 4 | Deciduous forest | 1.0 | 1.3 | 0.8 | 0.5 | 0.05 |
| 5 | Coniferous forest, wetland | 1.3 | 1.3 | 1.3 | 1.3 | 0.05 |
| 6 | Mixed forest* | 1.15 | 1.3 | 1.05 | 0.9 | 0.05 |
| 7 | Water | f(w) | f(w) | f(w) | f(w) | 0.04 |
| 8 | Barren land | 0.002 | 0.002 | 0.002 | 0.002 | 0.08 |
| 9 | Non-forested wetlands | 0.2 | 0.2 | 0.2 | 0.05 | 0.05 |
| 10 | Mixed agricultural/range* | 0.04 | 0.15 | 0.03 | 0.006 | 0.05 |
| 11 | Rocky (with low shrubs) | 0.3 | 0.3 | 0.3 | 0.15 | 0.05 |

* Roughness for these categories is taken to be the average of their components.

**Table 3-5. The 26 ZHANG03 landuse categories, their UV albedos, and their default annual minimum and maximum LAI and surface roughness (m) ranges. Roughness for water is calculated from the function** $z_0 = 2 \times 10^{-6} w^{2.5}$**, where** *w* **is surface wind speed (m/s).**

| Category Number | Land Cover Category | Roughness (meters) | | LAI | | UV Albedo |
|---|---|---|---|---|---|---|
| | | Min | Max | Min | Max | |
| 1 | Water | f(*w*) | f(*w*) | 0.0 | 0.0 | 0.04 |
| 2 | Ice | 0.01 | 0.01 | 0.0 | 0.0 | 0.5 |
| 3 | Inland lake | f(*w*) | f(*w*) | 0.0 | 0.0 | 0.04 |
| 4 | Evergreen needleleaf trees | 0.9 | 0.9 | 5.0 | 5.0 | 0.05 |
| 5 | Evergreen broadleaf trees | 2.0 | 2.0 | 6.0 | 6.0 | 0.05 |
| 6 | Deciduous needleleaf trees | 0.4 | 0.9 | 0.1 | 5.0 | 0.05 |
| 7 | Deciduous broadleaf trees | 0.4 | 1.0 | 0.1 | 5.0 | 0.05 |
| 8 | Tropical broadleaf trees | 2.5 | 2.5 | 6.0 | 6.0 | 0.05 |
| 9 | Drought deciduous trees | 0.6 | 0.6 | 4.0 | 4.0 | 0.05 |
| 10 | Evergreen broadleaf shrubs | 0.2 | 0.2 | 3.0 | 3.0 | 0.05 |
| 11 | Deciduous shrubs | 0.05 | 0.2 | 0.5 | 3.0 | 0.05 |
| 12 | Thorn shrubs | 0.2 | 0.2 | 3.0 | 3.0 | 0.05 |
| 13 | Short grass and forbs | 0.04 | 0.04 | 1.0 | 1.0 | 0.05 |
| 14 | Long grass | 0.02 | 0.1 | 0.5 | 2.0 | 0.05 |
| 15 | Crops | 0.02 | 0.1 | 0.1 | 4.0 | 0.05 |
| 16 | Rice | 0.02 | 0.1 | 0.1 | 6.0 | 0.05 |
| 17 | Sugar | 0.02 | 0.1 | 0.1 | 5.0 | 0.05 |
| 18 | Maize | 0.02 | 0.1 | 0.1 | 4.0 | 0.05 |
| 19 | Cotton | 0.02 | 0.2 | 0.1 | 5.0 | 0.05 |
| 20 | Irrigated crops | 0.05 | 0.05 | 1.0 | 1.0 | 0.05 |
| 21 | Urban | 1.0 | 1.0 | 0.1 | 1.0 | 0.08 |
| 22 | Tundra | 0.03 | 0.03 | 0.1 | 2.0 | 0.05 |
| 23 | Swamp | 0.1 | 0.1 | 4.0 | 4.0 | 0.05 |
| 24 | Desert | 0.04 | 0.04 | 0.0 | 0.0 | 0.08 |
| 25 | Mixed wood forest | 0.9 | 0.9 | 3.0 | 5.0 | 0.05 |
| 26 | Transitional forest | 0.9 | 0.9 | 3.0 | 5.0 | 0.05 |

**Th**e data records for the static 2-D surface file have the following structure:

```
    ibdate,btime,iedate,etime
    Loop from l = 1 to nvar variables:
        ione,namvar(l),((var(i,j),i=1,nx),j=1,ny)
```

The variables have the following definitions:

Record 1

| | |
|---|---|
| ibdate | Integer beginning date span on file (YYJJJ) |
| btime | Real beginning decimal hour (e.g., 1:30 PM = 13.5) |
| iedate | Integer ending date span on file (YYJJJ) |
| etime | Real ending decimal hour (e.g., 1:30 PM = 13.5) |

<u>Record 2 through *nvar+1*</u>

| | |
|---|---|
| `ione` | Integer dummy variable (=1) |
| `namvar` | Text names for *nvar* variables (character*4(10,nvar) array): |

| | |
|---|---|
| `WATER` | Water fraction (Zhang 1) |
| `ICE` | Ice fraction (Zhang 2) |
| `LAKE` | Lake fraction (Zhang 3) |
| `ENEEDL` | Evergreen needle leaf forest fraction (Zhang 4) |
| `EBROAD` | Evergreen broad leaf forest fraction (Zhang 5) |
| `DNEEDL` | Deciduous needle leaf forest fraction (Zhang 6) |
| `DBROAD` | Deciduous broad leaf forest fraction (Zhang 7) |
| `TBROAD` | Tropical broad leaf forest fraction (Zhang 8) |
| `DDECID` | Drought deciduous tree fraction (Zhang 9) |
| `ESHRUB` | Evergreen shrub fraction (Zhang 10) |
| `DSHRUB` | Decidous shrub fraction (Zhang 11) |
| `TSHRUB` | Thorn shrub fraction (Zhang 12) |
| `SGRASS` | Short grass fraction (Zhang 13) |
| `LGRASS` | Long grass fraction (Zhang 14) |
| `CROPS` | Cropland fraction (Zhang 15) |
| `RICE` | Rice crop fraction (Zhang 16) |
| `SUGAR` | Sugar crop fraction (Zhang 17) |
| `MAIZE` | Corn crop fraction fraction (Zhang 18) |
| `COTTON` | Cotton crop fraction (Zhang 19) |
| `ICROPS` | Irrigated cropland fraction (Zhang 20) |
| `URBAN` | Urban fraction (Zhang 21) |
| `TUNDRA` | Tundra fraction (Zhang 22) |
| `SWAMP` | Swamp fraction (Zhang 23) |
| `DESERT` | Desert fraction (Zhang 24) |
| `MWOOD` | Mixed woodland fraction (Zhang 25) |
| `TFOREST` | Transitional forest fraction (Zhang 26) |
| `TOPO_M` | Topographic elevation above sea level (m) |
| `LAI` | Optional Leaf Area Index |

| | |
|---|---|
| `var` | Real variable field values for *nx* grid columns and *ny* grid rows |

### 3.4.3.2  Input Time-Variant 2-D Surface File

The time-variant 2-D surface file contains gridded fields of surface temperature and snow cover.  This file must be developed for the master grid, and optionally any of the nested fine grids.  The surface temperature is used for dry deposition calculations and to establish surface-layer atmospheric stability.  Snow cover is simply a map of 0 (no snow) and 1 (snow); this impacts surface roughness, surface resistances for dry deposition, and photochemistry by setting UV albedo to snow values.

The data records for the time-variant 2-D surface file have the following structure and are repeated for each time interval on file:

```
    ibdate,btime,iedate,etime
    Loop from l = 1 to nvar variables:
        ione,namvar(l),((var(i,j),i=1,nx),j=1,ny)
```

The variables have the following definitions:

Record 1

| | |
|---|---|
| ibdate | Integer beginning date of time interval (YYJJJ) |
| btime | Real beginning decimal hour (e.g., 1:30 PM = 13.5) |
| iedate | Integer ending date of time interval  (YYJJJ) |
| etime | Real ending decimal hour (e.g., 1:30 PM = 13.5) |

Record 2 through *nvar+1*

| | |
|---|---|
| ione | Integer dummy variable (=1) |
| namvar | Text names for *nvar* variables (character*4(10,nvar) array): |
| | TSURF_K          Surface temperature (K) |
| | SNOWCOVER     Snow cover (1=present, 0=absent) |
| var | Real variable field values for *nx* grid columns and *ny* grid rows |

CAMx time-interpolates surface temperature to each model timestep for each grid, and so the model requires that data be available on file for an additional update time at the end of the simulation.  For example, in the case of hourly fields, a 24-hour simulation requires 25 input fields on file.  The time interval of the data records must match the time zone and input frequency of the meteorology as specified in the CAMx.in file.

3.4.3.3  Input Time-Variant 3-D Meteorological File

The time-variant 3-D meteorological file contains gridded fields of state meteorological parameters.  This file must be developed for the master grid and optionally any fine grid nest specified for a given simulation.  The layer interface heights define the vertical grid structure for each grid.  The number of vertical layers and the vertical grid definition must be consistent among all grids in a simulation; otherwise CAMx will stop with an error message if this condition is not met.  The layer interface heights may be specified to vary in space and/or time (e.g., to follow the layer structure of meteorological models), or they may be set to a constant field.  CAMx allows the user to optionally supply wind components at cell center, in which case the model will interpolate the components to their respective positions on cell interfaces, or the user may supply these components directly on the staggered Arakawa C configuration (recommended).  In any case, the user must supply a full *nx×ny×nz* array of wind values for each component (even though the CAMx Arakawa C configuration uses only *(nx-1)×(ny-1)* values in the horizontal).  The wind staggering flag is set in the second header record.  The pressure, wind, temperature, and humidity fields are used for transport, plume rise, PiG, dry and wet deposition, and chemistry calculations.

The data records for the time-variant 3-D meteorological file have the following structure and are repeated for each time interval on file:

```
        ibdate,btime,iedate,etime
        Loop from l = 1 to nvar variables:
            Loop from k = 1 to nz layers:
                ione,namvar(l),((var(i,j,k),i=1,nx),j=1,ny)
```

The variables have the following definitions:

Record 1

| | |
|---|---|
| `ibdate` | Integer beginning date of time interval (YYJJJ) |
| `btime` | Real beginning decimal hour (e.g., 1:30 PM = 13.5) |
| `iedate` | Integer ending date of time interval (YYJJJ) |
| `etime` | Real ending decimal hour (e.g., 1:30 PM = 13.5) |

Record 2 through *nvar*×*nz+1*

| | |
|---|---|
| `ione` | Integer dummy variable (=1) |
| `namvar` | Text names for *nvar* variables (character*4(10,nvar) array): |

| | |
|---|---|
| `ZGRID_M` | Layer interface heights (m AGL) |
| `PRESS_MB` | Pressure (mb) |
| `TEMP_K` | Temperature (K) |
| `HUMID_PPM` | Humidity as mixing ratio (ppm) |
| `UWIND_MpS` | U-component (east-west) wind (m/s) |
| `VWIND_MpS` | V-component (north-south) wind (m/s) |

| | |
|---|---|
| `var` | Real layer *k* variable field values for *nx* grid columns and *ny* grid rows |

CAMx time-interpolates these meteorological variables to each model timestep for each grid, and so the model requires that data be available on file for an additional update time at the end of the simulation. For example, in the case of hourly fields, a 24-hour simulation requires 25 input fields on file. The time interval of the data records must match the time zone and input frequency of the meteorology as specified in the CAMx.in file.

### 3.4.3.4  Input Time-Variant 3-D Vertical Diffusivity File

The time-variant 3-D vertical diffusivity file contains gridded fields of layer-interface diffusivity (i.e., turbulent exchange or diffusion coefficients). This file must be developed for the master grid, and optionally any fine grid nests. This file is kept separate from the main meteorological data file to facilitate the substitution of alternative vertical mixing rates. Diffusivity is used for vertical diffusion and PiG puff growth calculations.

The data records for the time-variant 3-D meteorological file have the following structure and are repeated for each time interval on file:

```
        ibdate,btime,iedate,etime
        Loop from l = 1 to nvar variables:
            Loop from k = 1 to nz layers:
                ione,namvar(l),((var(i,j,k),i=1,nx),j=1,ny)
```

The variables have the following definitions:

<u>Record 1</u>

| | |
|---|---|
| `ibdate` | Integer beginning date of time interval (YYJJJ) |
| `btime` | Real beginning decimal hour (e.g., 1:30 PM = 13.5) |
| `iedate` | Integer ending date of time interval (YYJJJ) |
| `etime` | Real ending decimal hour (e.g., 1:30 PM = 13.5) |

<u>Record 2 through *nvar×nz+1*</u>

| | |
|---|---|
| `ione` | Integer dummy variable (=1) |
| `namvar` | Text names for *nvar* variables (character*4(10,nvar) array): |
| | `KV_M2pS`          Vertical diffusivity ($m^2/s$) |
| `var` | Real layer *k* variable field values for *nx* grid columns and *ny* grid rows |

CAMx time-interpolates the diffusivity to each model timestep for each grid, and so the model requires that data be available on file for an additional update time at the end of the simulation. For example, in the case of hourly fields, a 24-hour simulation requires 25 input fields on file. The time interval of the data records must match the time zone and input frequency of the meteorology as specified in the CAMx.in file.

<u>3.4.3.5  Input Time-Variant 3-D Cloud/Precipitation File</u>

The time-variant 3-D cloud/precipitation file contains gridded fields of cloud and precipitation parameters to be used for photochemistry, aqueous chemistry, and wet/dry deposition calculations. Note that precipitation rate is not explicitly provided to the model; instead, it is internally calculated from the three precipitation water content forms provided on the cloud/rain file. This file also contains layer-specific cloud optical depth to scale down photolysis rates for layers within or below clouds to account for UV attenuation, or to scale up the rates for layers above clouds to account for UV reflection. This file must be developed for the master grid, and optionally any fine grid nests, if chemistry, dry, and/or wet deposition are invoked.

The data records for the time-variant 3-D cloud/precipitation file have the following structure and are repeated for each time interval on file:

```
        ibdate,btime,iedate,etime
        Loop from l = 1 to nvar variables:
            Loop from k = 1 to nz layers:
                ione,namvar(l),((var(i,j,k),i=1,nx),j=1,ny)
```

The variables have the following definitions:

Record 1

| | |
|---|---|
| `ibdate` | Integer beginning date of time interval (YYJJJ) |
| `btime` | Real beginning decimal hour (e.g., 1:30 PM = 13.5) |
| `iedate` | Integer ending date of time interval  (YYJJJ) |
| `etime` | Real ending decimal hour (e.g., 1:30 PM = 13.5) |

Record 2 through *nvar*×*nz*+1

| | |
|---|---|
| `ione` | Integer dummy variable (=1) |
| `namvar` | Text names for *nvar* variables (character*4(10,nvar) array): |

| | |
|---|---|
| `CLODW_GpM3` | Cloud water content ($g/m^3$) |
| `RAINW_GpM3` | Rain water content ($g/m^3$) |
| `SNOWW_GpM3` | Snow water content ($g/m^3$) |
| `GRPLW_GpM3` | Graupel water content ($g/m^3$) |
| `CLOUDOD` | Layer-specific cloud optical depth |

| | |
|---|---|
| `var` | Real layer *k* variable field values for *nx* grid columns and *ny* grid rows |

The CAMx cloud fields are assumed to be time-averaged, so the model does not require an additional update time at the end of the simulation.  For example, in the case of hourly fields, a 24-hour simulation requires only 24 cloud input fields on file.  The time interval of the data records must match the time zone and input frequency of the meteorology as specified in the CAMx.in file.

### 3.4.3.6  Input 3-D Initial Conditions File

The input 3-D initial conditions file contains gridded concentration fields on the master grid. Initial concentration fields may be specified for a sub-set of the total number of modeled species.  An initial condition file must be developed for the master grid, and contain concentration fields for at least one species.  For those species not on the initial condition file, CAMx sets up uniform fields using the "lower bound" values specified in the chemistry parameters file.  CAMx then interpolates all master grid initial conditions to each fine grid nest at the start of the simulation.

The data records for the initial conditions file have the following structure and are repeated for each time interval on file:

```
    ibdate,btime,iedate,etime
    Loop from l = 1 to nspec species:
        Loop from k = 1 to nz layers:
            ione,namspec(l),((conc(i,j,k),i=1,nx),j=1,ny)
```

The variables have the following definitions:

<u>Record 1</u>

| | |
|---|---|
| `ibdate` | Integer beginning date of time interval (YYJJJ) |
| `btime` | Real beginning decimal hour (e.g., 1:30 PM = 13.5) |
| `iedate` | Integer ending date of time interval  (YYJJJ) |
| `etime` | Real ending decimal hour (e.g., 1:30 PM = 13.5) |

<u>Record 2 through *nspec*×*nz+1*</u>

| | |
|---|---|
| `ione` | Integer dummy variable (=1) |
| `namspec` | Text names for *nspec* species (character*4(10,nvar) array): |
| `conc` | Real layer *k* concentration field values (ppm for gases, µg/m$^3$ for aerosols) for *nx* grid columns and *ny* grid rows |

The time interval of the data records must match the time zone as specified in the CAMx.in file.

<u>3.4.3.7  Input 3-D Lateral Boundary Conditions File</u>

The input 3-D lateral boundary conditions file contains gridded concentration fields on the lateral faces of the master grid boundary.  Boundary concentration fields may be specified for a sub-set of the total number of modeled species.  However, if a boundary concentration is specified for a given species, it must be supplied for all four boundaries.  A boundary concentration file must be developed for the master grid, and contain concentration fields for at least one species.  For those species not on the boundary conditions file, CAMx sets up uniform fields using the "lower bound" values specified in the chemistry parameters file.  The time span of each set of boundary data records may be set arbitrarily; e.g., a set of boundary conditions may be specified for a six hour span, followed by a set spanning just an hour.

The boundary conditions file adds an additional set of four header records, resulting in a total of eight header records altogether (note that first four records are identical to the header records described above):

```
name,note,ione,nspec,ibdate,btime,iedate,etime
plon,plat,iutm,xorg,yorg,delx,dely,nx,ny,nz,iproj,istag,tlat1,tlat2,rdum
ione,ione,nx,ny
(namspec(l),l=1,nspec)
Loop from 1 to 4 boundaries:
    ione,iedge,ncell,(icell(n),idum,idum,idum,n=1,ncell)
```

The additional header variables have the following definitions:

<u>Records 5-8</u>

| | |
|---|---|
| `ione` | Integer dummy variable (=1) |
| `iedge` | Integer boundary edge number (1=west, 2=east, 3=south, 4=north) |
| `ncell` | Integer number of rows or columns on this edge |
| `icell` | Integer index of first cell modeled (edges 1,3), or last cell modeled (edges |

2,4): if "0", this row/column is omitted from the simulation

    `idum`           Integer dummy variable

The data records for the boundary conditions file have the following structure, and are repeated for each time interval on file:

```
ibdate,btime,iedate,etime
Loop from l = 1 to nspec species:
    Loop from 1 to 4 boundaries:
        ione,namspec(l),iedge,((bc(i,k,iedge,l),k=1,nz),i=1,ncell)
```

The variables have the following definitions:

<u>Record 1</u>

| | |
|---|---|
| `ibdate` | Integer beginning date of time interval (YYJJJ) |
| `btime` | Real beginning decimal hour (e.g., 1:30 PM = 13.5) |
| `iedate` | Integer ending date of time interval  (YYJJJ) |
| `etime` | Real ending decimal hour (e.g., 1:30 PM = 13.5) |

<u>Record 2 through *nspec×4+1*</u>

| | |
|---|---|
| `ione` | Integer dummy variable (=1) |
| `namspec` | Text names for nspec species (character*4(10,nvar) array): |
| `bc` | Real edge *iedge* boundary concentrations (ppm for gases, $\mu g/m^3$ for aerosols) for *ncell* grid rows/columns, and *nz* layers |

The time interval of the data records must match the time zone as specified in the CAMx.in file.

### 3.4.3.8  Input Elevated Point Source File

The input elevated point source emissions file contains stack parameters and emission rates for all elevated point sources, and for all emitted species, to be modeled.  If elevated point sources are to be modeled, only one point source emissions file must be developed for the entire modeling domain.  The point source file also flags the individual stacks to be treated by the CAMx PiG sub-model by setting the stack diameter as a negative value.  The file offers the ability to optionally specify the effective plume height or the vertical plume distribution for each point source and to bypass the internal plume rise calculation.

The elevated point source file adds two additional set of header records that specify time-invariant stack parameters, resulting in a total of six header records altogether (note that first four records are identical to the header records described above):

```
    name,note,ione,nspec,ibdate,btime,iedate,etime
    plon,plat,iutm,xorg,yorg,delx,dely,nx,ny,nz,iproj,istag,tlat1,tlat2,rdum
    ione,ione,nx,ny
    (namspec(l),l=1,nspec)
    ione,nstk
    (xstk(n),ystk(n),hstk(n),dstk(n),tstk(n),vstk(n),n=1,nstk)
```

The additional header variables have the following definitions:

Record 5

| | |
|---|---|
| `ione` | Integer dummy variable (=1) |
| `nstk` | Integer number of elevated point source stacks |

Record 6

| | |
|---|---|
| `xstk` | Real stack x-coordinate (m or degrees longitude) |
| `ystk` | Real stack y-coordinate (m or degrees latitude) |
| `hstk` | Real stack height (m) |
| `dstk` | Real stack diameter (m); negative value flags source for PiG |
| `tstk` | Real stack exit temperature (K) |
| `vstk` | Real stack exit velocity (m/hr) |

The time-variant data records for the elevated point source file have the following structure, and are repeated for each time interval on file:

```
    ibdate,btime,iedate,etime
    ione,nstk
    (idum,idum,kcell(n),flow(n),plmht(n),n=1,nstk)
    Loop from l = 1 to nspec species:
        ione,namspec(l),(ptems(n,l),n=1,nstk)
```

The variables have the following definitions:

Record 1

| | |
|---|---|
| `ibdate` | Integer beginning date of time interval (YYJJJ) |
| `btime` | Real beginning decimal hour (e.g., 1:30 PM = 13.5) |
| `iedate` | Integer ending date of time interval  (YYJJJ) |
| `etime` | Real ending decimal hour (e.g., 1:30 PM = 13.5) |

Record 2

| | |
|---|---|
| `ione` | Integer dummy variable (=1) |
| `nstk` | Integer number of elevated point source stacks |

Record 3

| | |
|---|---|
| `idum` | Integer dummy variable |

kcell          Zero or positive: Ignored
               Negative: integer flag for OSAT/PSAT source region override
flow           Zero: ignored (plume rise calculation uses time-invariant exit velocity)
               Positive: real stack flow rate ($m^3$/hr) for plume rise calculations
               Negative: real plume bottom (m) for vertical plume distribution override
plmht          Zero or positive: ignored (plume rise calculation is performed)
               Negative (flow $\geq$ 0): real effective plume rise override (m)
               Negative (flow < 0): real plume top (m) for vertical plume distribution
               override

<u>Record 4 through *nspec+4*</u>

ione           Integer dummy variable (=1)
namspec        Text names for *nspec* species (character*4(10,nvar) array):

ptems          Real point emission rate (mol/time period for gases, g/time period for
               aerosols) for *nstk* point sources

Note that the emission time interval (the denominator for the emissions rate) is normally, but not necessarily, 1 hour.  The time interval of the emission records must match the time zone and input frequency of the emissions as specified in the CAMx.in file.

<u>3.4.3.9  Input Gridded Emissions File</u>

The input gridded emissions file contains gridded fields of low-level (i.e., surface) emission rates for all emitted species to be modeled.  If gridded emissions are to be modeled, a gridded emissions file must be developed for the master grid and optionally any nested fine grids.

The data records of the gridded emissions file have the following structure, and are repeated for each time interval on file:

```
    ibdate,btime,iedate,etime
    Loop from l = 1 to nspec species:
        ione,namspec(l),((emiss(i,j,l),i=1,nx),j=1,ny)
```

The variables have the following definitions:

<u>Record 1</u>

ibdate         Integer beginning date of time interval (YYJJJ)
btime          Real beginning decimal hour (e.g., 1:30 PM = 13.5)
iedate         Integer ending date of time interval  (YYJJJ)
etime          Real ending decimal hour (e.g., 1:30 PM = 13.5)

<u>Record 2 through *nspec×nz+1*</u>

ione           Integer dummy variable (=1)
namspec        Text names for *nspec* species (character*4(10,nvar) array):

emiss          Real gridded emission field values (mol/time period for gases, g/time period for aerosols) for *nx* grid columns and *ny* grid rows

Note that the emission time interval (the denominator for the emissions rate) is normally, but not necessarily, 1 hour.  The time interval of the emissions record must match the time zone and input frequency of the emissions as specified in the CAMx.in file.

### 3.4.4  Output Files

Master and nested grid instantaneous files contain full three-dimensional fields of all species modeled, while the gridded average and deposition files contain only those species specified in the run control file.  For flexibility, CAMx offers the option to write full three-dimensional average concentration fields, or just surface layer two-dimensional fields (see the "3-D average file" option in the CAMx control file).  It is permissible to change the number of species on the average file, or change between 2-D and 3-D average files, from one CAMx simulation period to the next (provided the periods are configured as separate CAMx runs).  As the instantaneous concentration files are used for CAMx restarts, the model only writes instantaneous fields at the end of the simulation.  PiG output files possess a unique format, and are used primarily for model restarts.

#### 3.4.4.1  Output Concentration Files

The output average files for all grids, and the coarse (master) grid instantaneous file, are all written in the CAMx Fortran binary format as described earlier.  There are three differences between the output concentration files and the input initial concentration files.  First, the file name given in the file description header record (header record #1) is "AVERAGE" for the average output file, "INSTANT" for the instantaneous output file, and "AIRQUALITY" for the input initial concentration file.  Second, the "note" in the file description header record of the output concentration files is the message supplied in the first line of the CAMx run control file, whereas the "note" in the air quality file is set as part of the input file preparation.  Third, the species lists can be different among the files: the output instantaneous file contains all species modeled (as specified in the chemistry parameters file), the average output file contains only the species specified in the run control file, and the input initial concentration file may contain any subset of modeled species as determined when that file is prepared.

Two other differences exist between the average and instantaneous output files.  As noted above, the average file may contain only surface-level fields or the entire three-dimensional fields, as selected by the user.  Also, gas concentration fields are output as ppm in average files, but as $\mu mol/m^3$ in instantaneous files (aerosols are in $\mu g/m^3$ in both files).  Because of these differences, and because average files usually do not contain all modeled species, CAMx does not allow the average output concentration file to be used for simulation restarts.

#### 3.4.4.2  Ouput Deposition Files

The output deposition file is identical in format to the two-dimensional surface-level output average concentration file.  The file name given on the first record of the deposition file is "AVERAGE" so that existing post-processing software will recognize the format.  However, the output deposition file differs from the output average concentration file in one important way.

The species list is identical to the list on the average concentration output files, except that four parameters are output for each species:

| | |
|---|---|
| `species_DV` | Real 2-D dry deposition velocity field for *species* (m/s) |
| `species_DD` | Real 2-D dry deposited mass field for *species* (mol/ha for gases, g/ha for aerosols) |
| `species_WD` | Real 2-D wet deposited mass field for *species* (mol/ha for gases, g/ha for aerosols) |
| `species_LC` | Real 2-D precipitation liquid concentration for *species* (mol/l for gases, g/l for aerosols) |

### 3.4.4.3 Nested (Fine) Grid Instantaneous Output File

The nested (or "fine") grid Fortran binary output instantaneous file is unique and contains the three-dimensional concentration fields for all nested grids together, as opposed to separate files for each grid. All grid definition parameters given in these files are referenced relative to the master grid, so specific absolute information about grid cell size or projection coordinates for each nested grid must be determined from master grid parameters. If the user utilizes the Flexi-nesting capability of CAMx, then the gridded fields output to the nested fine grid files will change according to how nests are altered, added, and/or removed during the course of a simulation.

The header portion of the nested grid output files contain 3+*nnest* records with the following structure:

```
message
nnest,nspec
(mspec(l),l=1,nspec)
Loop from 1 to nnest grid nests
    ibeg,jbeg,iend,jend,mesh,ione,nx,ny,nz,iparnt,ilevel
```

The time-variant portion of the nested grid output files have the following structure, where the following records are repeated for each output time:

```
time,idate
Loop from 1 to nnest grid nests
    Loop from l = 1 to nspec species:
        Loop from k = 1 to nz layers:
            ((conc(i,j,k,l),i=1,nx),j=1,ny)
```

The variables on the nested grid output concentration files have the following definitions:

|  |  |
|---|---|
| message | Text string containing file description (character*60) |
| nnest | Number of fine grid nests on file |
| nspec | Number of species on file |
| mspec | Species names for nspec species |
| ibeg | Grid *n* x-direction starting index of grid (master grid cell) |
| jbeg | Grid *n* y-direction starting index of grid (master grid cell) |
| iend | Grid *n* x-direction ending index of grid (master grid cell) |
| jend | Grid *n* y-direction ending index of grid (master grid cell) |
| mesh | Grid *n* meshing factor (number of nested cells per master) |
| ione | Dummy integer = 1 |
| nx | Grid *n* number of grid rows |
| ny | Grid *n* number of grid columns |
| nz | Grid *n* number of layers |
| iparnt | Grid *n's* parent grid (grid index within which this fine grid is nested; 0 = master grid) |
| ilevel | Grid *n's* grid level (depth at which this grid is nested; 1=master grid is parent) |
| time | Time of output (HHMM); ending hour for average output |
| idate | Date of output (YYJJJ) |
| conc | Grid *n*, species *l*, layer *k* concentrations (ppm for average gases, µg/m$^3$ for average aerosols, µmol/m$^3$ for instantaneous gas species) for *nx* grid columns, and *ny* grid rows |

### 3.4.4.4 PiG Restart File

When the PiG option is invoked, CAMx outputs all puff parameters each hour for model restart capabilities. This file is Fortran binary and is analogous to the instantaneous gridded concentration output files in that it represents a "snapshot" of data at the top of each hour. The file format is unique and contains information for each puff, including coordinates, grid location, size specifications, age, and mass of each of the chemical species carried. While this file contains PiG information for the entire simulation, it would be of limited use for certain analyses such as plotting puff trajectories. This is because the instantaneous nature of the data, and the dynamic memory allocation utilized in the PiG submodel, leads to insufficient information to identify and track individual puffs hour to hour.

The PiG restart file contains two records with the following structure, and these are repeated for each output time:

```
      idatpig,timpig,npig,nreactr
      (ingrd(n),idpig(n),xpigf(n),xpigb(n),ypigf(n),ypigb(n),zpig(n),
     &      axisy(n),axisz(n),sigy(n),sigx(n),sigz(n),pufftop(n),puffbot(n),
     &      htfms(n),htfmb(n),vtfms(n),vtfmb(n),agepigf(n),agepigb(n),fmspig(n),
     &      ipufmap(n),ipufgrp(n),
     &      ((puffrad(i,nr,n),i=1,nrad),nr=1,nreactr),
     &      ((puffmass(i,nr,n),i=1,nspec),nr=1,nreactr),n=1,npig
```

The variables on the PiG restart file have the following definitions:

| | |
|---|---|
| idatpig | Date of output (YYJJJ) |
| timpig | Time of output (HHMM) |
| npig | Number of PiG puffs active at this output time |
| nreactr | Number of chemical reactors in each puff |
| ingrd | Grid index for *npig* puffs |
| idpig | Point source index for *npig* puffs |
| xpigf | x-coordinate of puff front (km from master grid origin) for *npig* puffs |
| xpigb | x-coordinate of puff back (km from master grid origin) for *npig* puffs |
| ypigf | y-coordinate of puff front (km from master grid origin) for *npig* puffs |
| ypigb | y-coordinate of puff back (km from master grid origin) for *npig* puffs |
| zpig | Puff height (m AGL) for *npig* puffs |
| axisy | Puff lateral width (m) for *npig* puffs |
| axisz | Puff vertical depth (m) for *npig* puffs |
| sigy | Puff Gaussian lateral dimension (m) for *npig* puffs |
| sigx | Puff Gaussian longitudinal dimension (m) for *npig* puffs |
| sigz | Puff Gaussian vertical dimension (m) for *npig* puffs |
| pufftop | Puff top height (m AGL) for *npig* puffs |
| puffbot | Puff bottom height (m AGL) for *npig* puffs |
| htfms | Puff horizontal turbulent flux moment, shear ($m^2$/s) |
| htfmb | Puff horizontal turbulent flux moment, buoyancy ($m^2$/s) |
| vtfms | Puff vertical turbulent flux moment, shear ($m^2$/s) |
| vtfmb | Puff vertical turbulent flux moment, buoyancy ($m^2$/s) |
| agepigf | Puff front age since release (s) for *npig* puffs |
| agepigb | Puff back age since release (s) for *npig* puffs |
| fmspig | Puff volume parameter (unitless) for *npig* puffs |
| ipufmap | Puff OSAT region map pointer (unitless) for *npig* puffs |
| ipufgrp | Puff OSAT group poing (unitless) for *npig* puffs |
| puffrad | Puff radical concentrations (ppm) for *nrad* species, *nreactr* reactors, and *npig* puffs |
| puffmass | Puff pollutant mass (μmol) for *nspec* species, *nreactr* reactors, and *npig* puffs |

3.4.4.5  PiG Sample Grid Files

The optional PiG sampling grid concentrations are time-averaged in the same manner as the output average concentrations provided on the computational grids.  The same user-defined set of output species are written to the sampling grid files, but only two-dimensional surface layer concentrations are reported.  The sampling grid file format is identical to the CAMx average and deposition files, with one file generated per sampling grid, so that they may be readily viewed and manipulated with CAMx post-processing software.

## 3.5  HDF5 Output Files

CAMx provides the option to output two-dimensional or three-dimensional average concentrations to HDF5 files in lieu of the CAMx Fortran binary format.  The HDF conventions employed in CAMx were taken from the Regional Atmospheric Modeling System (RAMS), version 6.0 (http://www.atmet.com/html/docs/documentation.shtml).  Standard HDF5 utilities can be used to view and manipulate the CAMx HDF5 average output files.  Deposition and instantaneous restart files cannot be output in HDF5 format, and will continue to be written in the standard formats as described above if the HDF option is invoked.

Two basic types of files are generated when this option is invoked:

- A text "header" file, containing various grid, species and pointer information defining the data contained in each HDF concentration file (labeled "…`head.txt`");
- HDF5 format concentration files, one for each output time and for each grid (labeled "…`gnn.h5`", where *nn* is grid index).

Each file is labeled first with a user-supplied root path/filename (`root`) and then the year, month, day, and time (`YYYY-MM-DD-HHMMSS`).  The standard computational grid output fields are written to files labeled with the letters "`CX`".  The optional PiG sampling grid output fields are written to files labeled "`CS`".

Both types of files contain core model species, labeled with a prefix of "`CH-`" to indicate standard chemistry species (e.g., NO and O3 are output to HDF files as "`CH-NO`" and "`CH-O3`").  If the RTRAC Probing Tool is used, then both computational and PiG sampling grid files will also contain all the RTRAC species with a prefix of "`PT-`" to indicate Probing Tool species (e.g., the arbitrary RTRAC species TRAC1 is output to HDF files as "`PT-TRAC1`").

See Section 2 for information on how to compile CAMx with HDF5 libraries.

# 4.  CORE MODEL FORMULATION

This section outlines the numerical approach employed in CAMx, and describes the technical formulation of the emissions, transport and removal processes.  The specific chemical mechanisms and their numerical solvers are discussed in detail in Section 5.

## 4.1  Numerical Approach

The physical representations and the numerical methods used for each term of the pollutant continuity equation (described in Section 1) are summarized in Table 4-1.  CAMx includes peer-accepted algorithms and component formulations, and its modular framework eases the addition and/or substitution of alternative algorithms in the future.

**Table 4-1.  Summary of the CAMx models and methods for key physical processes.**

| Process | Physical Models | Numerical Methods |
|---|---|---|
| Horizontal advection | Eulerian continuity equation | • Bott (1989)<br>• PPM (Colella and Woodward,1984) |
| Horizontal diffusion | K-theory $1^{st}$ order closure | Explicit simultaneous 2-D solver |
| Vertical advection | Eulerian continuity equation | Implicit backward-Euler (time) hybrid centered/upstream (space) solver |
| Vertical diffusion | • K-theory $1^{st}$ order closure<br>• Non-local mixing | • Implicit backwards-Euler (time) centered (space) solver<br>• Explicit ACM2 non-local convection/diffusion (Pleim, 2007) |
| Gas-Phase Chemistry | • Carbon Bond 2005 (Yarwood et al., 2005b)<br>• Carbon Bond 6 (Yarwood et al., 2010, 2012a,b)<br>• SAPRC99 (Carter, 2000)<br>• Inorganic/organic aerosol precursors | • EBI (Hertel et al., 1993)<br>• IEH (Sun et al., 1994)<br>• LSODE (Hindmarsh, 1983) |
| Aerosol Chemistry | • Aqueous inorganic chemistry<br>• Inorganic thermodynamics/partitioning<br>• Organic thermodynamics/partitioning<br>• Static 2-mode or multi-section size models | • RADM-AQ (Chang et al., 1987)<br>• ISORROPIA (Nenes et al., 1998)<br>• SOAP (Strader et al., 1999)<br>• CMU (Pandis et al., 1993) |
| Dry deposition | • Resistance model for gases (Wesely, 1989) and aerosols (Slinn and Slinn, 1980)<br>• Resistance model for gases (Zhang et al., 2003) and aerosols (Zhang et al., 2001) | Deposition velocity as surface boundary condition in vertical diffusion solver |
| Wet deposition | Scavenging model for gases and aerosols (Seinfeld and Pandis, 1998) | Exponential decay as a function of scavenging coefficient |

The continuity equation is numerically marched forward in time over a series of time steps.  At each step, the continuity equation is integrated by way of an operator-splitting approach that calculates the separate contribution of each major process (emission, advection, diffusion, chemistry, and removal) to concentration change within each grid cell.  The specific equations that are solved individually in the operator-splitting process are shown in order below:

$$\left.\frac{\partial c_l}{\partial t}\right|_{Emission} = m^2 \frac{E_l}{\partial x\,\partial y\,\partial z}$$

$$\left.\frac{\partial c_l}{\partial t}\right|_{X\ advection} = -\frac{m^2}{A_{yz}}\frac{\partial}{\partial x}\left(\frac{uA_{yz}c_l}{m}\right)$$

$$\left.\frac{\partial c_l}{\partial t}\right|_{Y\ advection} = -\frac{m^2}{A_{xz}}\frac{\partial}{\partial y}\left(\frac{vA_{xz}c_l}{m}\right)$$

$$\left.\frac{\partial c_l}{\partial t}\right|_{Z\ transport} = \frac{\partial(c_l\eta)}{\partial z} - c_l\frac{\partial^2 h}{\partial z\,\partial t}$$

$$\left.\frac{\partial c_l}{\partial t}\right|_{Z\ diffusion} = \frac{\partial}{\partial z}\left[\rho K_v\frac{\partial(c_l/\rho)}{\partial z}\right]$$

$$\left.\frac{\partial c_l}{\partial t}\right|_{XY\ diffusion} = m\left\{\frac{\partial}{\partial x}\left[m\rho K_X\frac{\partial(c_l/\rho)}{\partial x}\right] + \frac{\partial}{\partial y}\left[m\rho K_Y\frac{\partial(c_l/\rho)}{\partial y}\right]\right\}$$

$$\left.\frac{\partial c_l}{\partial t}\right|_{Wet\ Scavenging} = -\Lambda_l\,c_l$$

$$\left.\frac{\partial c_l}{\partial t}\right|_{Chemistry} = Mechanism-specific\ reaction\ equations$$

where $c_l$ is species concentration ($\mu$mol/m$^3$ for gasses, $\mu$g/m$^3$ for aerosols), $E_l$ is the local species emission rate ($\mu$mol/s for gasses, $\mu$g/s for aerosols), $\partial t$ is timestep length (s), $u$ and $v$ are the respective east-west ($x$) and north-south ($y$) horizontal wind components (m/s), $A_{yz}$ and $A_{xz}$ are cell cross-sectional areas (m$^2$) in the $y$-$z$ and $x$-$z$ planes, respectively, $m$ is the ratio of the transformed distance on the various map projections to true distance ($m$=1 for curvi-linear latitude/longitude coordinates), and $\Lambda_l$ is the wet scavenging coefficient (s$^{-1}$).

A master driving time step for the model is dynamically determined during the simulation for the largest and coarsest (master) grid.  Time steps typically range from 5-15 minutes for grid cell sizes of 10-50 km, to a minute or less for small cell sizes of 1-2 km.  As a result, nested grids require multiple driving time steps per master step depending on their grid sizes relative to the master grid spacing.  Furthermore, multiple transport and chemistry time steps per driving step are used as necessary to ensure accurate solutions for these processes on all grids.

The first process in each time step for a given grid is the injection of emissions from all sources. CAMx then performs horizontal advection and vertical advection, followed by vertical diffusion, horizontal diffusion, chemistry, and finally wet scavenging.

Although advection is performed separately in the *x* (east-west), *y* (north-south), and *z* (vertical) directions, the numerical linkage between these components has been developed in a mass consistent fashion to preserve the density field at each time step.  This maintains the flexibility to allow many types of meteorological models, and modeling grid resolutions, projections, and layer structures, to characterize transport in CAMx.

Trace gases and particles are removed from the atmosphere via deposition to the ground.  Dry deposition refers to the direct sedimentation and/or diffusion of material to various terrestrial surfaces and uptake into biota.  Wet deposition refers to the uptake of material into cloud water and precipitation, and its subsequent transfer to the surface.  The efficiency with which wet and dry deposition processes can remove pollutants from the air depends upon the physical and chemical properties of the pollutants, local meteorological conditions, the type of surface on which they are being deposited, and on the frequency, duration, and intensity of precipitation events.  Dry deposition is an important removal mechanism, but it is not explicitly treated as a separate process in the time-splitting approach.  Instead, deposition velocities for each species are used as the lower boundary condition for vertical diffusion.  This appropriately couples the surface removal of pollutants through each column of cells via the vertical mixing process.

## 4.2  CAMX Grid Configuration

### 4.2.1  Grid Cell Arrangement

CAMx carries pollutant concentrations at the center of each grid cell volume, representing the average concentration over the entire cell.  Meteorological fields are supplied to the model to quantify the state of the atmosphere in each grid cell for the purposes of calculating transport, chemistry, and removal.  CAMx internally carries these variables in an arrangement known as an "Arakawa C" grid configuration (Figure 4-1).  State variables such as temperature, pressure, water vapor, and cloud water are located at cell center along with pollutant concentration, and represent grid cell average conditions.  Wind components and diffusion coefficients are carried at cell interfaces to describe the transfer of mass in and out of each cell face.  Note in Figure 4-1, for example, that horizontal wind components *u* and *v* are staggered from each other.  This facilitates the solving of the transport equations in "flux form".

Depending upon the source of meteorological data, it is recommended that the user directly provide the gridded horizontal wind fields in the staggered Arakawa C configuration.  However, this is not always feasible, and so CAMx offers the option for the user to supply all meteorological variables, including horizontal wind components, at cell center; in this case CAMx internally interpolates the winds to cell interfaces.  Note that this leads to a slight smoothing effect on the horizontal wind fields.

Figure 4-1 also describes the horizontal cell indexing convention used in CAMx.  Each cell is defined by the index pair (*i,j*), where *i* ranges from 1 to *nx* (the number of cells in the east-west direction), and *j* ranges from 1 to *ny* (the number of cells in the north-south direction).  The eastern and northern faces of the cell are indexed (*i,j*), while the western and southern faces are indexed (*i*-1,*j*) and (*i,j*-1), respectively.
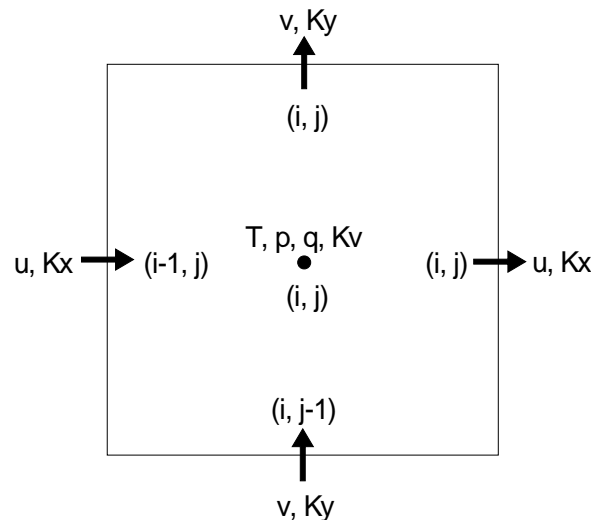
**Figure 4-1. A horizontal representation of the Arakawa C variable configuration used in CAMx.**

In the vertical, most variables are carried at each layer midpoint (defined as exactly half way between layer interfaces). Again the exceptions are those variables that describe the rate of mass transport across the layer interfaces, which include the vertical diffusion coefficient $K_V$ and the vertical transport rate $\eta$. These variables are carried in the center of each cell horizontally, but are located at the top of the layer (i.e., the interface) vertically.

### 4.2.2 Grid Nesting

CAMx incorporates two-way grid nesting, which means that pollutant concentration information propagates into and out of all grid nests during model integration. Any number of grid nests can be specified in a single run, where horizontal grid spacings can vary from one grid nest to another (note that vertical grid structures must be consistent among all grids). The nested grid capability of CAMx allows cost-effective application to large regions in which regional transport occurs, yet at the same time providing fine resolution to address small-scale impacts in selected areas.

Each grid nest is defined over a subset of master (coarsest) grid cells. The range of master grid row and column indices that define the coverage of each nested grid must be specified in the run control file. An integer number of nested grid cells must span one master grid cell; this number is referred to as a "meshing factor". "Buffer" cells are added around the perimeter of each nested grid to hold boundary conditions. Buffer cells are added automatically within CAMx and should not be specified by the user in the run control file. All nested grid output files contain data for the entire array of computational and buffer cells; however, buffer cell concentrations are considered invalid and should be ignored. Additionally, all nested grid input files must contain data for the entire array of computational and buffer cells. An example of a horizontal nesting arrangement is shown in Figure 4-2. Here, two telescoping fine grid nests are defined: one with a meshing factor of 2 spanning master grid cells (5,4) to (8,8), and one with a meshing factor of 4 spanning master grid cells (6,6) to (6,7).
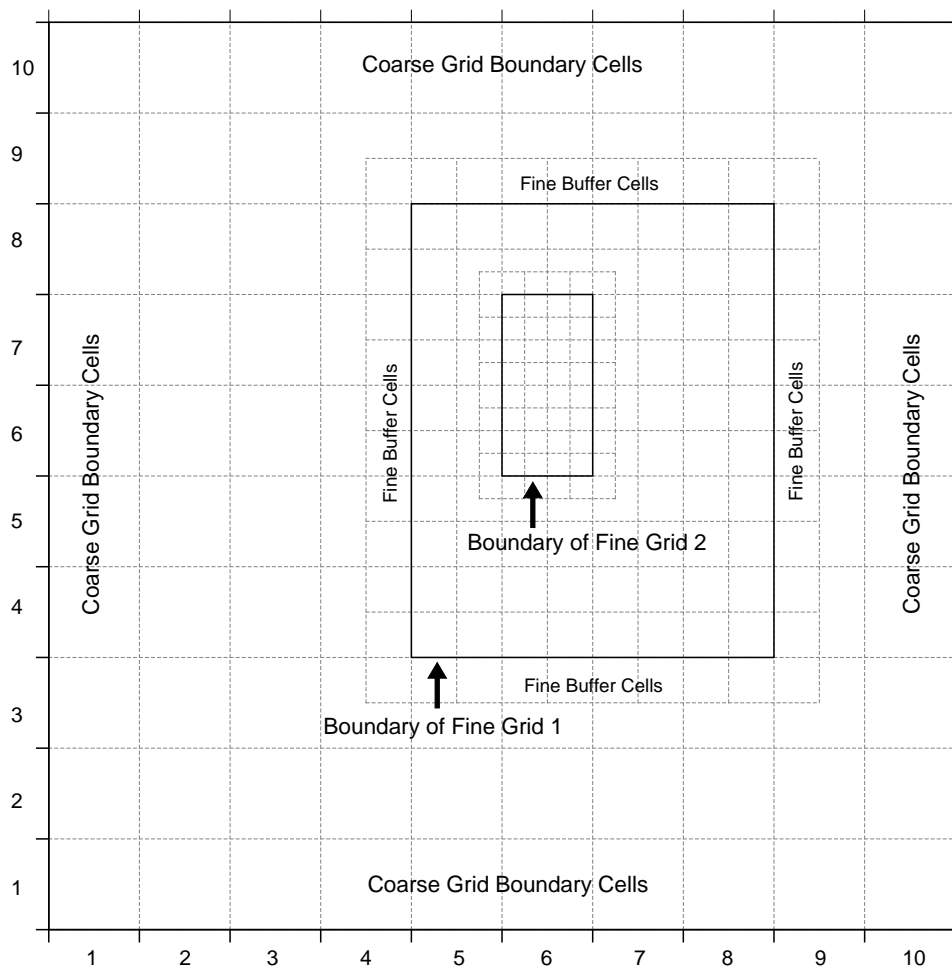
**Figure 4-2. An example of horizontal grid nesting, showing two telescoping nested grids within a 10×10 cell master grid. The outer nest contains 10×12 cells (including buffer cells to hold internal boundary conditions), and the inner nest contains 6×10 cells (including buffer cells).**

Restrictions on specifying the size and resolution of all grid nests include the following:

1) The ratio of master grid cell size to nested grid cell size must be an integer (e.g., a "meshing factor" of 3 means that 3 nested cells span the distance of 1 master cell, resulting in an area of 9 nested cells per master cell);

2) For telescoping grids (a nested grid containing an even finer grid), the cell size of the finest grid must be a common denominator for all parent grids above it (e.g., a 36-12-4 km or 36-12-2 km arrangement is allowed, but a 36-12-9 km is not);

3) The restriction in (2) above does not apply to parallel nested grids of the same generation (e.g., 4 km and 5 km grids can be located in different areas of a master grid provided that the master cell size is some multiple of 20 km);

4) Nested grids cannot overlap, although they may share a common boundary or edge;

5) Nested grids cannot extend into a boundary, or non-modeled, area of the master grid;

6) CAMx is currently configured to allow four "generations" of nests (e.g., four levels of telescoping grids); this can be extended in the code if more than four levels of nests are required;

7) The total vertical depth of each nested grid must exactly match the depth of the master grid, and nested grid vertical layer structures must be consistent with the master grid in terms of the number of layers and their thicknesses;

### 4.2.3 Flexi-Nesting

The following Fortran binary I/O files must be provided for the master grid, and optionally provided for each nested grid:

- gridded surface emissions;
- landuse and LAI distribution;
- height/pressure (defines the layer interface structure);
- horizontal wind components;
- temperatures;
- vertical diffusivities;
- water vapor;
- clouds and precipitation

Any of these input files may be supplied for each nested grid, or none at all. If any of these files are not supplied for a particular nested grid, the Flexi-Nest algorithm within CAMx interpolates the missing fields from the parent grid. Clearly it is desirable to provide nested grid data whenever possible. However, the ability to interpolate data is useful for testing sensitivity to grid configurations or for situations when it is not possible to run a meteorological model for all grid nests.

The Flexi-Nest option also allows users to redefine the nested grid configuration at any point in a simulation. Nested grids can be introduced or removed only at the time of a model restart since a new CAMx user control file must be used to redefine the grid configuration. For example, the user may wish to "spin-up" the model using a regional-scale master grid and a single nest over an area of interest for two days. Starting at 6 AM on the third day, the user might introduce one or more nests within the original nested grid for more detailed analysis. This would require that the model be restarted at 6 AM of the third day with a new control file that defines the position of the two new nests and (optionally) provides any additional input fields for these grids. CAMx will internally reconcile the differences in grid structure between the nested grid restart files and the new user control file, and then interpolate any data fields not supplied to CAMx for the new nests from the parent grid(s).

## 4.3 Treatment of Emissions

Pollutant emissions are treated in two basic ways within CAMx: low-level (gridded) emissions that are released into the lowest (surface) layer of the model; and elevated stack-specific (point) emissions with buoyant plume rise that can be emitted into any model layer. Emission

rates are held constant (not time interpolated) between reading intervals (usually 1 hour) but are injected at every grid-specific time step during the simulation.  Gridded and point emissions are provided to CAMx in separate input files.  External emission processing systems are used to develop gridded and point, time- and space-resolved, chemically-speciated input files for CAMx.  These external programs are not discussed in this User's Guide; see Section 2 for more information on emission systems that are used to support CAMx applications.

### 4.3.1  Gridded Emissions

Two-dimensional gridded low-level emissions are defined by space- and time-varying rates for each individual gas and PM species to be modeled.  Gridded emissions represent sources that emit near the surface and that are not sufficiently buoyant to reach into the upper model layers.  Such emission categories include:

- Low-level stack (point) emissions that are too small to result in plume rise above the model surface layer;
- Other non-point industrial sources (fugitive leaks, tanks, etc.);
- Mobile sources (cars, trucks, non-road vehicles, railroad, marine, aircraft, etc.);
- Residential sources (heating, cooking, consumer products);
- Commercial sources (bakeries, refueling stations, dry cleaners);
- Biogenic sources;
- Natural sources (small fires, wind-blown dust).

The spatial distribution of each individual source within these categories is defined by the modeling grid.  Information such as population distribution, housing density, roadway networks, vegetative cover, etc. is typically used as a surrogate to distribute regional emission estimates for each source to the grid system.  Processing tools are used to combine emissions from all sources into a single input file for each grid (see Sections 2 and 3).

### 4.3.2  Elevated Point Emissions

Similarly to gridded emissions, elevated point emissions are defined by space- and time-varying rates for each individual gas and PM species to be modeled.  The only difference is that these sources emit from individual stacks with buoyant rise that may take them into upper model layers.  These types of sources are almost always associated with large industrial processes, such as electric generators, smelters, refineries, large factories, etc. but can also represent natural elevated sources such as wildfires and lightning NOx.  The spatial distribution of these points is specifically given by the coordinates of the stacks themselves (grid locations are determined within CAMx).  Plume rise is determined within CAMx as a function of stack parameters (height, diameter, exit velocity and temperature) and ambient meteorological conditions, so the point source file provides speciated time-resolved emission rates and stack parameters for each individual source.  A single point source file provides the definition of all stacks and their emissions over the entire modeling domain (see Sections 2 and 3).

Plume rise is calculated using the multi-layer stability-dependent algorithm of Turner et al. (1986).  This approach calculates the momentum and buoyant plume rise energy from the

stack, takes the larger of these two values, and determines the dissipation of that energy via mixing with ambient air according to the meteorological conditions through the host model layer.  If sufficient energy remains to reach into the next model layer, the calculation for buoyant rise repeats for the meteorological conditions of that layer, and so on, until a layer is found where the plume cannot rise any farther.  All emissions from this source are then injected into the grid cell directly above the stack at this layer height.  This algorithm was adopted for CAMx because it provides a more realistic handling of stable layers aloft that can trap plume rise, whereas this effect would not be realized based on meteorological conditions at stack top alone.

Under neutral/unstable conditions, momentum rise at the stack top is calculated from

$$H_{mu} = \frac{3 d_s v_s}{w}$$

while buoyancy rise is the lesser of

$$H_{bu} = 30 (f/w)^{3/5} + z_b$$

and

$$H_{bu} = 24 (f/w^3)^{3/5} \left[ h_s + 200 (f/w^3) \right]^{2/5} + z_b$$

In these expressions $d_s$ is stack diameter (m), $v_s$ is stack exit velocity (m/s), $h_s$ is stack height (m), $w$ is ambient wind speed (m/s), and $z_b$ is the distance between the stack top and the base of the current model layer.  A minimum wind speed of 1 m/s is specified to avoid unrealistically large plume rise.  Buoyancy flux $f$ is initially calculated from stack parameters, but is set to residual flux entering the bottom of any higher layer.  The initial buoyancy flux at stack top is given by

$$f_0 = g v_s d_s^2 \left( \frac{T_s - T}{4 T_s} \right)$$

where $g$ is gravitational acceleration (9.8 m$^2$/s), $T_s$ is stack exit temperature (K), and $T$ is ambient temperature (K).  The residual flux calculation into the next higher layer depends on which neutral/unstable buoyancy rise equation was originally used in the current layer:

$$f = w \left( \frac{H_{bu} - z_t}{30} \right)^{5/3}$$

or

$$f = 5.5 \times 10^{-3} w^3 (H_{bu} - z_t) \left( 1 + \frac{h_s}{H_{bu} - z_t} \right)^{-2/3}$$

where $z_t$ is the distance between stack top and the top of the current model layer.

Under stable conditions, momentum rise at the stack top is calculated from the lesser of $H_{mu}$ and

$$H_{ms} = 0.646 T^{1/2} \left( \frac{v_s^2 d_s^2}{T_s w} \right)^{1/3} \left( \frac{\partial \theta}{\partial z} \right)^{-1/6}$$

while buoyancy rise is the lesser of

$$H_{bs} = \left[ \frac{1.8 f T}{w} \left( \frac{\partial \theta}{\partial z} \right)^{-1} + z_b^3 \right]^{1/3}$$

and

$$H_{bs} = \left[ \frac{4.1 f T}{f_0^{1/3}} \left( \frac{\partial \theta}{\partial z} \right)^{-1} + z_b^{8/3} \right]^{3/8}$$

In these expressions, $\partial \theta / \partial z$ is the potential temperature gradient (a measure of atmospheric stability). Here also, buoyancy flux is initially calculated from stack parameters, but is set to residual flux if the plume extends into the next higher layer. The residual flux calculation depends on which stable buoyancy rise equation was originally used:

$$f = f - 0.56 \frac{\partial \theta}{\partial z} \frac{w}{T} \left( z_t^3 - z_b^3 \right)$$

or

$$f = f - 0.24 \frac{\partial \theta}{\partial z} \frac{f_0^{1/3}}{T} \left( z_t^{8/3} - z_b^{8/3} \right)$$

When final plume rise is reached using stable buoyancy rise, it is adjusted downward to two-thirds of the rise through the stable depth. After final plume rise is determined, the rise is further adjusted downward by stack tip downwash according to a critical Froude number and ambient wind speed. The stack Froude number is given by

$$F = \frac{T v_s^2}{g d_s (T_s - T)}$$

For $F<3$, no downwash adjustment is made to final plume rise. Above that value, the following downwash factors ($D$) are applied depending upon the ambient wind speed at stack top:

$$
\begin{aligned}
D &= 0, & v_s < w \quad (no\ plume\ rise) \\
D &= 3 \frac{v_s - w}{v_s}, & \frac{2}{3} v_s \leq w < v_s \\
D &= 1, & w < \frac{2}{3} v_s
\end{aligned}
$$

CAMx injects point source emissions into all model layers spanned by the plume depth at final (adjusted) rise. Plume depth is determined as a function of stack diameter, plume temperature, plume velocity, time of plume rise, and ambient wind and temperature conditions. A uniform mass distribution through plume depth is assumed. If this depth is wholly contained within a single layer, that layer receives all emission mass. If this depth spans several layers, then fractions of the emissions are injected into these layers according to the fraction of plume depth spanning those layers. We apply the "rule-of-thumb" that plume depth equals plume rise (Turner and Schulze, 2007) as a maximum limit for plume depth.

The following equations are used to define the plume depth after reaching final rise. These are based on the approach used in the SCIPUFF model (EPRI, 2000) and were developed for use in the CAMx plume-in-grid (PiG) submodel. The plume depth $D_p$ at final rise is given by

$$D_p = 3\left(2D_s^2 + 2Kt\right)^{1/2}$$

where $D_s$ is stack diameter, $K$ is plume diffusivity during rise, and t is the time of rise. The time of rise is determined by dividing final plume rise by the mean plume rise speed $V_p$; the latter is set to half the stack exit velocity. A lower limit of 1 m/s is applied to the exit velocity, so the minimum value of $V_p$ is 0.5 m/s. The plume diffusivity is determined by scaling initial plume width (according to stack diameter) by the turbulent flux moment $q_p^2$:

$$K = 0.15\left(\sqrt{2}D_s\right)\sqrt{q_p^2}$$

where

$$q_p^2 = f_p V_p^2\left[0.4 + \left(\frac{3v^2}{v^2 + V_p^2}\right)\right]$$

The turbulent flux moment is a function of the mean plume rise speed $V_p$, the ambient wind speed $v$ taken at the level of final rise, and a plume entrainment coefficient $f_p$:

$$f_p = 1 + 4\left(\sqrt{2}D_s\right)g\left(\frac{T_p - T}{TV_p^2}\right)$$

where $g$ is the gravitational constant (9.8 m$^2$/s), $T$ is ambient temperature at the level of final rise, and $T_p$ is the mean plume temperature, taken as the mean of the stack exit temperature and the ambient temperature at final rise.

## 4.4 Transport Fundamentals

The CAMx transport algorithm is both mass conservative and mass consistent. Mass conservation refers to the ability to accurately account for all sources and sinks of mass in the

model, with no spurious loss or gain of mass during model integration. To be mass conservative, CAMx internally carries concentrations of each species as a density ($\mu$mol/m$^3$ for gases, $\mu$g/m$^3$ for aerosols), and solves the advection/diffusion equations in flux form. This also serves to simplify mass budget accounting, which is used by the various source apportionment and process analysis options. Gas concentrations are internally converted to volumetric mixing ratio (parts per million, or ppm) for the chemistry step, and when they are written to the average output files.

Mass consistency refers to the model's ability to transport pollutant mass exactly equivalent to the input atmospheric momentum field. For example, a model that is perfectly mass consistent will preserve a unity pollutant mixing ratio field in a divergent momentum field given constant unity boundary and initial conditions and zero sources and sinks. Sources of poor mass consistency in air quality models are typically related to the following (in order of importance):

1) supplying meteorology that is inherently inconsistent, e.g., from an interpolative objective analysis or diagnostic model in which wind, temperature, moisture, and pressure fields are all independently developed;

2) spatially interpolating or averaging meteorological model fields, especially *three-dimensional* wind vector fields, to an air quality model grid of different resolution and/or different mapping projection;

3) relying on a nested grid model to internally interpolate coarse grid meteorological parameters to finer grids;

4) employing numerical techniques within the air quality model that are mass inconsistent, e.g., holding input wind and density fields constant between meteorological update times, assuming non-divergent three-dimensional winds, etc.; and

5) employing different numerical and/or physical methods in the air quality and meteorological models.

***It is expected that CAMx users will prepare high quality, mass consistent meteorological fields using advanced prognostic models so as to minimize inconsistencies in the inputs themselves. The practice of developing meteorological input fields using objective analysis or "diagnostic" approaches is highly discouraged.***

CAMx operates on the map projections and grid systems employed in several widely used meteorological models (e.g., WRF, MM5, and RAMS) so that translation of meteorological data to CAMx requires as little manipulation as possible.

However, CAMx provides a very important flexibility that allows the air quality grid to differ from the meteorological grid in terms of projection and/or resolution when necessary. This, of course, leads to a potentially large source of mass consistency error as noted in point (2) above, and if nested grids are specified where higher resolution meteorological fields are unavailable, additional error may occur as in point (3). Therefore, adjustments must be made to correct for the external inconsistencies coming into the model. Such adjustments could be applied to the meteorological fields during the interpolation/averaging procedure, but this approach would not account for internal sources of inconsistency within the air quality model itself (points 3-5

above).  To account for all sources of error while maintaining flexibility on input requirements and grid configuration, CAMx internally minimizes the sources of mass inconsistency as the model integrates forward in time.  As discussed below, the model does this in several ways.

First, the transport equations are written and solved in mass "flux" form.  Gridded meteorological inputs are carried in an "Arakawa C" arrangement (Figure 4-1), which optimizes the calculation of mass flux divergences while ensuring mass conservation.  These points are important for the calculations described further below.  Solutions based on the alternative "advective" form cannot guarantee mass conservation or consistency.

Second, CAMx can accept input meteorological fields for each individual nested grid, if available from a meteorological model.  This reduces errors stemming from internal interpolations from parent to nested grids.  Input gridded fields of layer heights, temperature, pressure, horizontal winds, water vapor, and vertical diffusivity are then interpolated in time to the unique time steps for each modeling grid.  Since the vertical grid structure is defined via external inputs, layer interface heights may be specified as any arbitrary function of space and/or time.  This allows the CAMx vertical grid system to exactly match all or a subset of any meteorological model layer structures, whether they are defined in terms of physical height above ground, normalized height coordinates (i.e., "sigma-z"), or normalized pressure coordinates (i.e., "sigma-p").  Therefore, total vertical transport is the combination of resolved vertical advection and mass exchange across undulating layer interfaces.

Third, and most importantly, the grid- and timestep-specific horizontal momentum fields are used to determine an instantaneous vertical velocity field that balances the local atmospheric continuity equation for the specific grid configuration employed.  The presumption of a non-divergent momentum field ($\nabla \cdot \rho V = 0$) is usually invalid within air quality models since the externally supplied wind and density fields are not balanced in the first place (see points 1-3 above).  In CAMx, such a density-momentum balance obviously does not exist since a linear rate of temperature, pressure and horizontal wind change is imposed at each time step between meteorological update times.   To calculate a vertical velocity profile for a given grid column, the divergent atmospheric continuity equation

$$\frac{\partial \rho}{\partial t} = -\nabla \cdot \rho V$$

is locally integrated through the depth of the column

$$\rho w(z) = -\int_0^z \left( \frac{\partial \rho}{\partial t} + \nabla_H \cdot \rho V_H \right) dz$$

where the local time-rate change of atmospheric density $\partial \rho / \partial t$ in each grid cell is known from the input meteorological fields.  In this approach, a vertical velocity profile $w(z)$ is constructed that provides a balance between the imposed density tendency and the resolved horizontal momentum divergence in each grid cell at each time step.

The total vertical transport rate $\eta$ at a particular layer interface is defined as the combination of resolved vertical velocity and the local time-rate of change of the layer interface height:

$$\eta \;=\; \frac{\partial h}{\partial t} \;-\; w$$

The total vertical transport rate is used for subsequent vertical transport calculations for all pollutants.  A zero vertical velocity is specified at the ground, while a column- and pollutant-specific zero-gradient mixing ratio condition is applied at the top of the model.

The fourth way CAMx ensures mass consistency is to calculate the horizontal flux divergence of atmospheric density in a manner that is numerically consistent with the procedure used to horizontally transport pollutants.  Atmospheric density is advected in and out of each cell using the same equation as for pollutants:

$$\nabla_H \cdot \rho V_H \;=\; \frac{m^2}{A_{yz}} \frac{\partial}{\partial x}\left(\frac{uA_{yz}\rho}{m}\right) \;+\; \frac{m^2}{A_{xz}} \frac{\partial}{\partial y}\left(\frac{vA_{xz}\rho}{m}\right)$$

and this equation is solved using either the Bott (1989) or PPM (Colella and Woodward, 1984) advection solvers, as selected by the user (see Section 4.5 below).  Total three-dimensional transport thus includes resolved momentum convergence/divergence rates as well as any artificial divergences caused by the horizontal and vertical grid specifications (e.g., spatially varying vertical grid structure, or systematic distortions associated with the map projections).  In simple tests in which a uniform pollutant field of unity mixing ratio is transported throughout a single regional grid over several days using actual episodic meteorological inputs, this approach has been shown to provide nearly exact (to within $10^{-3}$-$10^{-4}$%) consistency between the density and pollutant fields.

## 4.5  Transport Algorithms

Horizontal advection is performed using the area preserving flux-form advection solver of Bott (1989) or the Piecewise Parabolic Method (PPM) of Colella and Woodward (1984) as implemented by Odman and Ingram (1993).  These two finite difference schemes were incorporated into CAMx because they provide higher order accuracy with minimal numerical diffusion, yet are equivalent in execution speed compared to other simpler advection algorithms when operating on equivalent time steps.  In CAMx, the Bott scheme is allowed to take larger time steps than PPM because Bott remains stable for Courant-Friedrichs-Levy (CFL) numbers up to 1 (i.e., the ratio of wind speed to grid spacing per timestep).  Time steps are determined for Bott using a CFL number of 0.9, while time steps for PPM are restrained by a CFL number of 0.5.  Therefore, the Bott option results in a faster simulation than the PPM option, perhaps at the price of some accuracy.  We recommend testing both for your specific application.

As discussed by Yamartino (2000) the latest advection solvers such as Bott and PPM reduce numerical diffusion to the point where modelers need to be concerned about including

appropriate levels of explicit horizontal diffusion.  Currently, there is very little information on the appropriate level of horizontal diffusion for Eulerian grid models.  We see this issue becoming increasingly important as more accurate advection solvers are utilized in grid models. This issue is not limited to CAMx.

Explicit horizontal diffusion coefficients are determined within CAMx using a deformation approach based on the methods of Smagorinsky (1963):

$$K_{X/Y} \quad = \quad K_o + \frac{\Delta x \Delta y}{4\sqrt{2}}\left[\left(\frac{\partial u}{\partial y}+\frac{\partial v}{\partial x}\right)^2 + \left(\frac{\partial u}{\partial x}-\frac{\partial v}{\partial y}\right)^2\right]^{1/2}$$

Separate diffusivity components are generated for fluxes in the *x*- and *y*-directions since $K_X$ and $K_Y$ are calculated for separate cell faces in the Arakawa C grid arrangement.  The value of $K_0$ is specified according to the approach in MM5 (Anthes and Warner, 1978):

$$K_0 \quad = \quad 3\times10^{-3}\frac{\Delta x \Delta y}{\Delta t}$$

A maximum value of $K_{X/Y}$ is set to maintain numerical stability for the given grid-specific timestep.  A minimum value is set to 1 m$^2$/s.  Horizontal diffusion is applied using an explicit simultaneous two-dimensional flux-divergence calculation.

Vertical transport and K-theory diffusion are both solved using implicit backward-Euler integration schemes.  Since implicit schemes are absolutely stable, only one solution step is necessary per driving time step.  Explicit approaches require potentially many sub-steps (on the order of 10-100) to maintain a stable solution, which introduces the potential for excessive numerical diffusion.  Whereas the vertical advection step is implicitly solved in a single step, K-theory vertical diffusion is implicitly solved over potentially several sub-steps, depending upon the magnitude of the vertical diffusivity relative to the vertical layer depths (CAMx uses the smaller of the current grid time step or a maximum 5 minute sub-step).  This ensures non-local diffusive coupling among all layers that exhibit high diffusivity, especially for long driving time steps on coarser grids that would otherwise only experience mixing between adjacent layers during a single implicit step.  Gridded vertical diffusion coefficients must be supplied to the model for the master grid via input file; the user may optionally supply vertical diffusion coefficients for any or all nested grids.

### 4.5.1  ACM2 Vertical Diffusion

The representation of sub-grid turbulent diffusion (or "mixing") in photochemical grid models has not significantly advanced for several decades.  Simple eddy viscosity (or "K-theory") first-order closure approaches have been used in most models.  As a "local" closure technique, K-theory only treats mass transfer cell-by-cell (horizontal) or layer-by-layer (vertical), analogously to the diffusion of heat through a solid medium.  Whereas K-theory adequately characterizes horizontal diffusion and weak vertical mixing during neutral and stable conditions, the shortcomings of K-theory are related to its inadequate treatment of deep vertical convective

boundary layer mixing. In convective situations, buoyant plumes deriving energy in the surface layer are quickly and efficiently mixed deep into the atmosphere within eddies that are usually much larger than the individual model layers. K-theory therefore mixes the convective boundary layer much less efficiently than commonly observed. This has been shown to have very important ramifications for chemistry, especially during transition periods between stable/neutral and convective conditions. Modelers have commonly adjusted for the lack of adequate vertical mixing by arbitrarily increasing the magnitude of the input vertical diffusivity fields.

A promising non-local mixing scheme was developed in the early 1990's called transilient theory (Raymond and Stull, 1990). This approach calculates the elements of a transilient matrix, where each element specifies the transfer rate from a given layer to any other layer, either adjacent or distant. In fact, K-theory is just a special case of transilient theory, in which transfer can only occur between adjacent layers above and below, leading to the trivially-solved "tri-diagonal" matrix. However, a fully populated transilient matrix is difficult to determine and until recently the approach has not been widely used in chemistry models.

The U.S. Environmental Protection Agency (EPA) has recently developed a new asymmetric convective model (ACM2) for the Models-3 Community Scale Air Quality (CMAQ) model (Pleim, 2007). This is considered a truncated, or simplified form of the general transilient mixing scheme in that it includes: (1) mixing among adjacent layers using K-theory (i.e, symmetrically along the diagonal of the transilient matrix); (2) rapid upward non-local mixing from the surface layer to all layers through the boundary layer (the convective aspect); and (3) slower compensating downward mixing layer-by-layer from the top of the boundary layer to the surface (the asymmetric aspect). All other matrix elements outside of these three transport paths are ignored. Figure 4-3 shows this approach schematically. During non-convective conditions, ACM2 reverts back to the local K-theory component. Thus, ACM2 includes the basic features of both local and the most important component of non-local exchange. Tests comparing ACM2 against standard K-theory result in more realistic profiles of ozone precursors, but usually minor impacts on surface ozone.
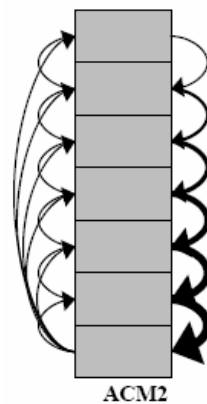


**Figure 4-3. Schematic representation of the turbulent exchange among layers within a vertical grid column during convective adjustment in the ACM2 (taken from Pleim [2007]).**

The ACM2 parameterization has been implemented in CAMx as an alternative to the K-theory approach. All variables needed to calculate the transfer rates are available from the existing input files, or are already calculated within CAMx for other purposes. The CAMx ACM2 option does not require that ACM2 be run within the meteorological model used to derive inputs for CAMx. However, EPA states that using ACM2 in both meteorological and chemistry models does lead to consistent boundary layer characterization. Meteorological interface programs (e.g., WRFCAMx, MM5CAMx, and RAMSCAMx) have been updated to include an option to generate vertical diffusivities in the same manner as the approach used within the CMAQ ACM2 algorithm, which performs its diffusivity calculations internally. The CMAQ ACM2 diffusivity calculation is a hybrid of two methodologies: (1) boundary layer scaling based on Hostlag and Boville (1993); and (2) local scaling according to Richardson number and vertical shear similar to Liu and Carroll (1996). The former is used within the stable boundary layer or if it is larger than the latter. The CAMx implementation of ACM2 supports OMP and MPI parallel processing, and all probing tools except the Integrated Process Rates algorithm of Process Analysis.

Note that ACM2 increases CAMx runtime considerably. Whereas the original CAMx K-theory solver is implicit and does not need to use small time steps, ACM2 and its K-theory counterpart both use explicit solvers, which must divide the model time step into many very small sub-steps to generate a stable solution. The slow-down can be exacerbated by using the much larger ACM2 vertical diffusivity values instead of the standard diffusivity options available in the CAMx meteorological preprocessors. The larger ACM2 diffusivity values further increase the number of integration sub-steps.

***NOTE: ACM2 does not work with the Decoupled Direct Method (DDM) or the Integrated Process Rate (IRP) component of the Process Analysis (PA) tool.***

## 4.6 Wet Deposition

Wet deposition is the predominant removal process for particles. Particles act as cloud condensation nuclei and subsequently the cloud droplets grow and collect into sufficiently large sizes to fall as precipitation. Additionally, particles that are entrained into the cloud, and that exist below precipitating clouds, can be directly scavenged by precipitation via accretion and impaction processes. The rates of nucleation and impaction depend upon cloud type (e.g., prolonged stratiform vs. vigorous convective development), precipitation rate, and particle size distribution.

Wet deposition can also be an important removal process for relatively soluble gaseous pollutants and this occurs through the following series of steps:

- Mixing of trace gas and condensed water in common air space;
- Absorption of gas molecules by water droplets;
- Possible aqueous-phase reactions of the pollutant within water droplets;
- Precipitation of droplets to the earth's surface;
- Diffusion of ambient gases into falling precipitation.

It is important to note that each of the above steps may be reversible, so that the overall wet deposition rate for gases depends on the net results of the forward and backward processes at each step.

The rate at which the first and fourth steps proceed depends on the frequency and nature of cloud formation and precipitation events.  For example, mid-latitude cyclonic storm events (e.g., winter storms) will result in different deposition rates than convective precipitation events such as summertime thunderstorms.  The rates at which the second, third, and fifth steps proceed depend on the extent to which the pollutant in question dissolves in water and its overall reaction rate once in solution.  Cloud water droplets can absorb gases from the air up the limit of their solubility in water.  For many pollutants this solubility far exceeds the amount of pollutant present in the air so that the distribution of the pollutant between the air and water droplets is determined by the Henry's Law constant, which is defined as the ratio of pollutant concentrations in the liquid-phase to the gas-phase at equilibrium.  High values for the Henry's law constant (greater than about 10,000 M/atm) indicate a strong tendency to dissolve in water droplets, whereas low values (less than about 100 M/atm) indicate a tendency to remain in the air (Seinfeld and Pandis, 1998).  Equilibrium between concentrations of pollutants in the air and in water droplets is usually established on time scales of minutes, so equilibrium conditions can generally be assumed to exist in the atmosphere.

If a pollutant partitions significantly into water droplets it can be removed by precipitation.  Averaged globally, highly soluble gases that are removed efficiently by wet deposition (e.g., nitric acid) are estimated to have lifetimes due to rainout of about 5 days (Warneck, 1989).  Clearly, on regional or local scales, lifetimes against wet deposition will depend upon the frequency and intensity of rainout events.  Gases that are removed less efficiently by wet deposition will have longer lifetimes.  For example, the corresponding global average lifetime of formaldehyde against rainout is estimated to be 14 days (Warneck, 1989).

The basic model implemented in CAMx is a scavenging approach in which the local rate of concentration change $\partial c/\partial t$ within or below a precipitating cloud depends on a scavenging coefficient $\Lambda$:

$$\frac{\partial c}{\partial t} \;=\; -\Lambda\, c$$

The scavenging coefficient is determined differently for gases and particles, based upon relationships described by Seinfeld and Pandis (1998).  Two components are calculated for gases: (1) direct diffusive uptake of ambient gases into falling precipitation; and (2) accretion of cloud droplets that contain dissolved gases.  Two components are also determined for particles: (1) impaction of ambient particles into falling precipitation with an efficiency that is dependent upon particle size; and (2) accretion of cloud droplets that contain particle mass.   Each of these processes is described below.

The external environmental inputs to the CAMx wet deposition algorithm include the three-dimensional gridded distribution of cloud and precipitation water contents, with the precipitation contents broken down into liquid, snow, and ice ("graupel").  Scavenging rate

equations were derived in terms of equivalent liquid precipitation rates, so the input precipitation water contents are internally translated into this metric.

The following general assumptions are made in the CAMx scavenging model:

1) Rain drops, snow flakes, and graupel particles are each separately represented by a single mean size, mass, and fall speed, which are determined from equivalent liquid precipitation rate;

2) There is no mixed-phased precipitation within a given grid cell – the dividing line between liquid rainfall and the two frozen forms is 273 K;

3) Snow is only associated with stratiform precipitation, and graupel only with convective precipitation;

4) Liquid cloud water is allowed to exist below 273 K – a linear ramp function is applied to apportion total cloud water into liquid form between 243-273 K (all cloud water is assumed to be in ice crystal form below 243 K);

5) All gasses can directly diffuse into or from liquid rainfall (only strong acids can diffuse into frozen precipitation) at a rate according to the precipitation's state of saturation, pollutant diffusivity, and aerodynamic considerations;

6) All gases can dissolve into liquid cloud water, which can be scavenged by all precipitation forms – dissolved gasses are in equilibrium with ambient concentrations according to Henry's Law;

7) PM is irreversibly scavenged directly by all precipitation forms via impaction, and by uptake into cloud water (liquid and ice) as condensation nuclei that is itself scavenged by all precipitation forms;

8) All in-cloud PM mass exists in cloud water (i.e., no "dry" aerosols exist in the interstitial air between cloud droplets) – all PM species and sizes are hygroscopic and internally mixed.

### 4.6.1 Precipitation Parameters

The mean raindrop diameter $d_d$ (m) and fall speed $v_d$ (m/s) are taken from the empirical estimates of Scott (1978). The drop diameter is related to rainfall rate $P$ (mm/hr), and the fall speed relationship has been modified to better agree with data provided by Seinfeld and Pandis (1998):

$$d_d = 9.0 \times 10^{-4} P^{0.21}$$

$$v_d = 3100 d_d$$

The precipitation water content $L_p$ (g/m$^3$) is related to rainfall rate by

$$L_p = \frac{P \rho_w}{3.6 \times 10^6 v_d}$$

where $\rho_w$ is liquid water density (g/m$^3$). This equation can be simplified to a dependency on just rainfall rate when the above relations for drop velocity and size are substituted. The resulting expression for rainfall rate as a function of precipitation water content is

$$P = \left( \frac{1 \times 10^7 L_p}{\rho_w} \right)^{1.27}$$

Locatelli and Hobbs (1974) developed power law equations relating average diameters, fall speeds, and masses for 15 precipitating ice "habits". We consolidated these relationships into two forms, termed "snow" and "graupel", by fitting new power law curves to the Locatelli and Hobbs data. For snow,

$$v_d = 0.83\, d_d{}^{0.20}$$

$$m_d = 0.035\, d_d{}^{1.8}$$

And for graupel,

$$v_d = 1.1\, d_d{}^{0.61}$$

$$m_d = 0.059\, d_d{}^{2.6}$$

Note that in these equations for ice, $d_d$ is in mm and crystal mass $m_d$ is in mg. By assuming that the number density and mass of snow/graupel crystals are equal to those for rain drops given equal precipitation water contents, we can relate the magnitudes of ice size and fall speed to equivalent liquid precipitation rate.

### 4.6.2 Gas Scavenging

Wet scavenging of gases by precipitation occurs within and below precipitating clouds. Below the cloud, the total gas concentration in a given grid cell is available for scavenging. Within a cloudy cell the total gas concentration must first be partitioned into an aqueous fraction $c_{aq}$ within cloud water and the remaining gaseous fraction $c_g$ within the interstitial air. Both aqueous and interstitial gasses within a cloudy cell are available for scavenging, but are removed at different rates as described below.

#### 4.6.2.1  Scavenging of Gases in Cloud Water

The aqueous concentration in liquid cloud water (or cloud ice in the case of strong acids) is determined by Henry's Law thereby assuming the solution exists in steady-state equilibrium. The Henry's Law constant for a given gas species $k_0$ (M/atm) specifies the ratio of pollutant mass in aqueous solution (M or mol/l$_{h2o}$) to its equilibrium partial pressure (atm) at standard pressure and temperature. This constant is adjusted for temperature $T$ and converted to a dimensionless molar ratio:

$$H = k_0 R\, T \exp\left[ A \left( \frac{1}{298} - \frac{1}{T} \right) \right]$$

where $R$ is the ideal gas constant (8.206×10$^{-2}$ l atm/mol K), and $A$ is the temperature dependence factor. Dissociation of ammonia, nitric acid, and sulfur dioxide as a function of cloud and rainwater pH is also considered in the solubility calculation. The effective Henry's

Law constant $H$ thus expresses the equilibrium ratio of the aqueous concentration $c_{aq}$ (mass per volume of water) to the gas concentration $c_g$ (mass per volume of air),

$$H = \frac{c_{aq}}{c_g}$$

which are related to total concentration $c$ by

$$c = c_g + c_{aq}\frac{L_c}{\rho_w}$$

where $L_c$ is cloud liquid water content (g/m$^3$).

The fraction of gases present in cloud water can be removed by precipitation via accretion of cloud water onto the falling hydrometeor (liquid or ice). As the hydrometeor falls, it sweeps a cylindrical volume per unit time equal to

$$V = \frac{\pi}{4}(d_d + d_c)^2 v_d$$

where $d_c$ is the size of cloud droplets. This implies that the ambient motion of cloud droplets is insignificant compared to the hydrometeor fall speed. Due to aerodynamic perturbations of air flow around the falling hydrometeor, a collection efficiency is applied, i.e., the fraction of cloud droplets within the collection volume that are scavenged by precipitation. For large hydrometeors with sizes greater than 0.5 mm and droplets 10-20 μm, we take this efficiency to be 0.9 (Seinfeld and Pandis, 1998). Also, we further assert that $(d_d + d_c)^2 \sim d_d^2$. Assuming then that a mono-disperse distribution of hydrometeors are falling through a mono-disperse distribution of cloud water droplets, the scavenging coefficient for precipitation collecting cloud water is

$$\Lambda_c = \frac{\pi}{4}d_d^2 v_d E N_d$$

where $E$ is the collection efficiency (0.9) and $N_d$ is the hydrometeor number density. The number density can be expressed in terms of equivalent rainfall rate, fall velocity, and drop size:

$$N_d = \frac{2.8\times10^{-7} P}{\pi d_d^3 v_d / 6}$$

Substituting the relationship between $N_d$ and rainfall parameters, then

$$\Lambda_c = 4.2\times10^{-7} \frac{E P}{d_d}$$

The cloud water scavenging coefficient is scaled by the ratio of aqueous pollutant concentration to total grid cell concentration to achieve the aqueous-phase scavenging coefficient:

$$\Lambda_a = \Lambda_c \frac{c_{aq} L_c}{c \rho_w}$$

### 4.6.2.2  Scavenging of Ambient Gases

Given the relatively short residence times of falling precipitation through a given grid cell, aqueous equilibrium between ambient gas and precipitation cannot be assumed and so the transfer of ambient gas into liquid rainfall (or ice in the case of strong acids) is explicitly calculated.  The maximum rate of transfer $W$ of a gas to a falling hydrometeor containing no pre-existing pollutant mass is

$$W = K_c H c_g$$

The mass transfer coefficient $K_c$ can be determined for a falling hydrometeor with speed $v_d$ and diameter $d_d$ by

$$K_c = \frac{D_g}{d_d}\left[2 + 0.6\left(\frac{v_d d_d}{\nu}\right)^{1/2}\left(\frac{\nu}{D_g}\right)^{1/3}\right]$$

where $D_g$ and $\nu$ are the molecular diffusivity of the gas species and air, respectively.

Following the methodology of Seinfeld and Pandis (1998), the rate of $c_{aq}$ increase can be represented by a mass balance with the rate of transport to the hydrometeor:

$$\frac{1}{6}\pi d_d^3 \frac{dc_{aq}}{dt} = \pi d_d^2 W$$

The expression for $W$ is substituted into the equation above, rearranged, and expressed in terms of rainfall velocity.  We then assume that through a given model layer the ambient gas concentration and hydrometeor pH and size is constant.  Multiplying by the number density of falling hydrometeors $N_d$ described above yields the gas-phase concentration scavenged by all drops falling through the layer:

$$\Lambda_g = 1.67\times10^{-6}\frac{P K_c}{d_d v_d}$$

Within cloudy layers, the gas-phase and aqueous-phase scavenging coefficients are added to provide the total in-cloud scavenging rate for gases, $\Lambda = \Lambda_g + \Lambda_a$.  For below-cloud scavenging, $\Lambda = \Lambda_g$.

### 4.6.2.3  Solubility Limits on Gas Scavenging

There is a chance for rainfall to become super-saturated for sparingly soluble gasses as it falls through a grid column.  The net scavenging coefficient for gases described above provides for the maximum potential uptake rate into clean rain water, so careful consideration must be

given to appropriately determine the sign and magnitude of ambient grid cell concentration change according to the degree of rainfall saturation.  The change in gas concentration is relaxed toward the difference between the maximum possible gas in solution for the given conditions $c_{eq}$, and the amount of pre-existing gas in solution from layers above $c_0$,

$$\Delta c \ = \ (c_{eq} - c_0)[1 - \exp(-\Lambda\,\Delta t)]$$

Here $c_{eq}$ is determined from the total liquid water in the cell (rain plus cloud water) and from Henry's law equilibrium according to the total gas concentration in the cell (ambient grid concentrations plus total gas in pre-existing solution).  If the concentration change is positive, mass is added to the rain water ($c_0$ is augmented) and removed from the grid cell; if negative, mass is removed from rain water ($c_0$ is decremented) and added to the grid cell.

### 4.6.3  Aerosol Scavenging

4.6.3.1  Scavenging of Aqueous Aerosols

All aerosols within cloudy layers are assumed to exist within cloud water.  Therefore, the scavenging coefficient for aqueous aerosols is exactly the same as for the scavenging of cloud droplets: $\Lambda = \Lambda_c$.

4.6.3.2  Scavenging of Dry Particles

Wet scavenging of dry particles only occurs below precipitating clouds.  We use the same scavenging coefficient as derived for the collection of cloud droplets:

$$\Lambda_c \ = \ 4.2\times 10^{-7}\,\frac{E\,P}{d_d}$$

For rain or graupel, the collection efficiency $E$ is a function of particle size $d_p$, and is given by Seinfeld and Pandis (1998) as:

$$
\begin{aligned}
E(d_p) \ = \ & \frac{4}{R_e S_c}\left(1 + 0.4\,R_e^{1/2}\,S_c^{1/3} + 0.16\,R_e^{1/2}\,S_c^{1/2}\right) \\[2mm]
& + \ 4\phi\left[\frac{\mu}{\mu_w} + \phi\left(1 + 2\,R_e^{1/2}\right)\right] \\[2mm]
& + \ \left(\frac{S_t - S^*}{S_t - S^* + 2/3}\right)^{3/2}
\end{aligned}
$$

where $\mu$ and $\mu_w$ are the kinematic viscosity of air (1.8×10$^{-5}$ kg/ms) and water (10$^{-3}$ kg/ms), respectively, $\phi = d_p/d_d$ is the ratio of particle size to hydrometeor size, $R_e$ is the Reynolds number for the hydrometeor, $S_c$ is the Schmidt number for the collected particle, and $S_t$ is the Stokes number of the collected particle.  The Reynolds number is given by

$$R_e \ = \ \frac{D_d v_d}{2\nu}$$

while the Schmidt number is

$$S_c = \frac{\nu}{D_p}$$

where $D_p$ is the particle Brownian diffusivity:

$$D_p = \frac{k\,T\,C}{3\pi\mu\,d_p}$$

Here, $k$ is the Boltzman constant ($1.38\times10^{-23}$ J/K) and $C$ is the Cunningham correction factor for small particles:

$$C = 1 + \frac{2\lambda}{d_p}\left[1.257 + 0.4\exp\left(-\frac{0.55d_p}{\lambda}\right)\right]$$

and where $\lambda$ is the mean free path of air ($6.5\times10^{-8}$ m).  The Stokes number is given by

$$S_t = \frac{v_d\,d_p^2\,\rho_p\,C}{9\mu\,d_d}$$

where $\rho_p$ is the particle density.  The $S^*$ parameter is given by

$$S^* = \frac{1.2 + \ln(1+R_e)/12}{1 + \ln(1+R_e)}$$

Note that particle size $d_p$ and density $\rho_p$ are affected by aerosol water content, which is determined from local humidity and PM deliquescence properties according to the ISORROPIA model (see Section 5).

Snow presents a complication for the efficiency calculation, since it is not a single solid mass but rather a collection of crystals arranged in a myriad of possible shapes that can lead to significant aerodynamic drag.  This drag affects particle collection efficiency.  To simplify the calculation, we use the value for E determined for rain and graupel, but set a lower limit for *E* of $1\times10^{-3}$ based on the work of Sauter and Wang (1989).

## 4.7  Dry Deposition

For many compounds, dry deposition can be as important as wet deposition as a removal process.  Due to the difficulty of making direct measurements of dry deposition and the need for a suitable model parameterization, dry deposition is often treated as a first-order removal mechanism, where the flux of a pollutant to the surface is the product of a characteristic deposition velocity and its concentration in the "surface layer" (i.e., the lowest model layer). Deposition velocities are derived from models that account for the reactivity, solubility, and diffusivity of gases, the sizes of particles, local meteorological conditions, and season-

dependent surface characteristics.  The factors affecting deposition are discussed in more detail below.

For a given species, particle size, and grid cell, CAMx determines a deposition velocity for each landuse type in that cell and then linearly combines them according to the fractional distribution of landuse.  The deposition flux is used as the lower boundary condition in the vertical diffusion algorithm.  Aerosol size spectra and species-dependent properties needed for the deposition velocity calculations are externally supplied to CAMx for all pollutant species via the chemistry parameters file; gridded landuse is supplied to the master grid and optionally any nested fine grids; the season is determined by the simulation date and location on the globe.

Movement of material along a path from the atmosphere, through any plant canopy, and onto the various plant and ground surfaces within and below the canopy is typically modeled by analogy to an electrical circuit.  Resistances in serial and parallel arrangements are used to represent the relative ease with which material moves through different portions of the deposition pathway.  Each branch of the circuit represents a different path by which material may be deposited.  For example, gaseous pollutants may transfer through the lowest layers of the atmosphere partially into a plant canopy, through the stomatal openings on plant leaves and into the plant mesophyll tissue.  Alternatively, the material may travel all the way through the plant canopy and deposit on the ground surface.

CAMx offers two dry deposition options: the original approach based on the work of Wesely (1989) and Slinn and Slinn (1980); and an updated approach based on the work of Zhang et al. (2001; 2003).  Both of these options are briefly described below.

### 4.7.1  The Wesely/Slinn Model

<u>4.7.1.1  Dry Deposition of Gases</u>

Wesely (1989) developed a resistance model that incorporates the major elements described above.  Deposition velocity $v_d$ is calculated from three primary resistances $r$ (s/m) in series:

$$V_d = \frac{1}{r_a + r_b + r_s}$$

The aerodynamic resistance $r_a$ represents bulk transport through the lowest model layer by turbulent diffusion, and operates equivalently for all gases and small particles.  The magnitude of this resistance depends on the intensity of turbulent motion, which in turn depends on solar insolation, wind speed, surface roughness, and near-surface temperature lapse rate.  In CAMx it is calculated from

$$r_a = \frac{1}{k\,u_*}\left[\ln\left(\frac{1}{z_o}\right) - \phi_h\right]$$

where $u_*$ is friction velocity (m/s), $k$ is von Karman's constant, $z$ is the lowest model layer midpoint height (m), $z_0$ is the surface roughness length (m), and $\phi_h$ is a stability correction term.  The surface layer parameterization of Louis (1979) is used to supply friction velocity and stability correction as a function of input surface meteorology and roughness length.

Roughness length is internally assigned according to season and the input gridded distribution of 11 landuse types as described in Section 3. In general, aerodynamic resistance is at a minimum on warm, sunny days with strong mixing due to surface heating and mechanical turbulence, and at a maximum on cool, calm nights when turbulent mixing is suppressed.

The quasi-laminar sublayer (or boundary) resistance $r_b$ represents molecular diffusion through the thin layer of air directly in contact with the particular surface to which material is being deposited. It is usually assumed to depend only on the molecular diffusivity of each pollutant species, and is given by

$$r_b = \frac{2 S_c^{2/3}}{k u_*}$$

where $S_c$ is the Schmidt number, or the ratio of air viscosity to species molecular diffusivity.

Over land, surface resistance $r_s$ is expressed as several more serial and parallel resistances that depend upon the physical and chemical properties of the surface in question:

$$r_s = \frac{1}{\dfrac{1}{r_{st} + r_m} + \dfrac{1}{r_{uc}} + \dfrac{1}{r_{dc} + r_{cl}} + \dfrac{1}{r_{ac} + r_{gs}}}$$

where the first set of parallel resistances represents the pathway into the stomatal ($r_{st}$) and mesophyll ($r_m$) portions of active plants, the second is the pathway into the upper canopy ($r_{uc}$), the third is the pathway into the lower canopy ($r_{dc}$ and $r_{cl}$), and the fourth is the pathway to the ground surface ($r_{ac}$ and $r_{gs}$). Many of these resistances are season- and landuse-dependent, and are built into Wesely's model; some in turn are adjusted within CAMx for solar insolation and surface wetness (vegetation is assumed to be unstressed). A few other resistances have been developed by Wesely for $SO_2$ and ozone, and so are scaled for each gaseous species based on the following pollutant properties:

- Molecular diffusivity (determined from molecular weight, $\sqrt{M_g / M_{H_2O}}$ );
- Henry's law solubility (*H*);
- Chemical reactivity toward oxidation of biological substances (*f*).

This allows the resistance approach to be used to estimate deposition velocities for a wide range of gaseous pollutants.

The surface resistances for strong acids (e.g., nitric, sulfuric, and hydrochloric acid, peroxides) are set to zero given their strong rates of update by biota and other surfaces (Huebert and Robert, 1995; Wesely and Hicks, 2000). The species for which surface resistance is set to zero are defined in the CAMx chemistry parameters file.

Over water, the surface resistance for all gas species other than ozone is based on some improvements adopted by Kumar et al. (1996) in UAM-AERO, following Sehmel (1980):

$$r_s = \frac{1}{3.9 \times 10^{-5} H T_s u_*}$$

where $T_s$ is surface temperature (K). For ozone, this equation has been updated to parametrically match the tendencies of measured ozone fluxes reported by Helmig et al. (2012) from ship-borne measurements:

$$r_s^{O3} = \frac{1}{1 \times 10^{-4} + 5 \times 10^{-6} H T_s^3 u_*}$$

where $T_s$ is in °C rather than K. The cubic temperature dependence fits the deposition velocity response to the range of sea surface temperatures reported in the Helmig et al. data. The additional $1 \times 10^{-4}$ term sets an upper limit on $r_s$ and a lower limit on deposition velocity so that the latter does not fall much below 0.01 cm/s. A lower limit of 1500 s/m was placed on $r_s$ such that ozone deposition over water does not exceed 6.5 cm/s, which is the upper limit in the cruise data.

### 4.7.1.2  Dry Deposition of Aerosols

Surface deposition of particles occurs via diffusion, impaction, and/or gravitational settling. Particle size is the dominant variable controlling these processes. The resistance approach of Slinn and Slinn (1980), as implemented in UAM-AERO (Kumar et al., 1996), has been adopted in CAMx. Particle deposition velocity for a given aerosol size is calculated using the following resistance equation:

$$v_d = v_{sed} + \frac{1}{r_a + r_b + r_a r_b v_{sed}}$$

where $v_{sed}$ is the gravitational settling (or sedimentation) velocity. This velocity is dependent on aerosol size and density:

$$v_{sed} = \frac{D^2 g C \rho_p}{18 \nu}$$

where $D$ is the log-mean particle diameter (m) of a given size section, $\rho_p$ is particle density (g/m$^3$), $g$ is gravitational acceleration, and $\nu$ is the viscosity of air. The factor $C$ is the Cunningham correction for small particles, as described earlier for wet scavenging of particles. Note that particle size and density are affected by aerosol water content, which is determined from local humidity and PM deliquescence properties according to the ISORROPIA model (see Section 5).

Aerodynamic resistance $r_a$ is identical to the value used for gaseous dry deposition. Resistance to diffusion through the quasi-laminar sub-layer layer depends on aerosol Brownian diffusion and inertial impaction. Particles are assumed to remain on a surface once they impact, so resuspension effects are ignored. Boundary resistance $r_b$ is given by

$$r_b \;=\; \frac{1}{u_*\left(S_c^{-2/3} + 10^{-3/S_t}\right)}$$

The stokes number $S_t$ is calculated from

$$S_t \;=\; \frac{v_{sed}\, u_*^2}{v\, g}$$

### 4.7.1.3  Specification of Season

The Wesely (1989) deposition algorithm specifies the various surface resistances by land cover type for five seasons:

- Spring
- Summer
- Fall
- Winter
- Winter with snow cover

CAMx internally defines a season map to determine four of these five seasons by month and latitude (Table 4-2).  Five latitude bands exist in each hemisphere:

- Tropical       < 20°
- Sub-tropical   20° to 35°
- Temperate      35° to 50°
- Cool           50° to 75°
- Polar          > 75°

The seasons in the Northern and Southern hemispheres are offset by six months.  This offset does not cause any discontinuity at the equator because all 12 months are defined as summer in the tropical band at the equator.  This season map is generalized and may not be ideal for all locations.  The season map is coded into data statements in the "`CAMx/chmdat.f`" subroutine and could be changed to better suit a specific region.

### 4.7.1.4  Specifying Snow Cover

The season map shown in Table 4-2 does not specify any snow cover because it is quite variable in space and time.  Gridded snow cover data are specified in the time-variant 2D surface input file (see Section 3).  The snow cover input is a binary value where 1 signifies that the grid cell is snow covered, while 0 is snow-free.  Snow covered grid cells are assigned the Wesely (1989) surface resistances for the category "winter with snow cover", regardless of the season.  Snow cover also impacts photolysis rates (see Section 5).

Generally, snow cover is taken from the meteorological models via the interface programs (e.g., WRFCAMx, MM5CAMx, RAMSCAMx).  Alternatively, snow cover data can be developed in several other ways:

**Table 4-2. Relationships between season and month/latitude used in the CAMx Wesely/Slinn dry deposition model. Exception: seasons for the area within 50N-75N and 15W-15E are internally set to those of latitude band 35-50 to account for regions of Europe in which the climate is influenced by the Gulf Stream.**

| Month | | Latitude Band | | | | |
|---|---|---|---|---|---|---|
| **Northern Hemisphere** | **Southern Hemisphere** | **< 20°** **Tropical** | **20° - 35°** **Sub-tropical** | **35° - 50°** **Temperate** | **50° - 75°** **Cool** | **> 75°** **Polar** |
| Jan | Jul | Summer | Winter | Winter | Winter | Winter |
| Feb | Aug | Summer | Spring | Winter | Winter | Winter |
| Mar | Sep | Summer | Spring | Spring | Winter | Winter |
| Apr | Oct | Summer | Spring | Spring | Spring | Winter |
| May | Nov | Summer | Summer | Spring | Spring | Winter |
| Jun | Dec | Summer | Summer | Summer | Summer | Spring |
| Jul | Jan | Summer | Summer | Summer | Summer | Summer |
| Aug | Feb | Summer | Summer | Summer | Summer | Fall |
| Sep | Mar | Summer | Summer | Fall | Fall | Winter |
| Oct | Apr | Summer | Fall | Fall | Fall | Winter |
| Nov | May | Summer | Fall | Fall | Winter | Winter |
| Dec | Jun | Summer | Fall | Winter | Winter | Winter |

- Spatially interpolated snow cover observations;

- Analyses of snow cover data included in existing metrological data sets, such as the NCEP North American Model (NAM);

- Analyses of snow cover based on a mix of observations, models and satellite-based information (e.g., SNODAS).

ENVIRON does not provide any pre-processors to develop snow cover data from external datasets, other than the meteorological interface programs.

### 4.7.2  The Zhang Model

At the time it was developed, the Wesely model was the most comprehensive algorithm applicable for regional-scale air quality modeling, but it no longer represents the current state of the science.  Furthermore, it was defined for a limited number of land cover types that were characterized according to typical eastern U.S. vegetation types, density, and seasonal conditions.  The deposition velocities calculated with the Wesely/Slinn model may not be sufficiently accurate outside the eastern U.S. or for atypical conditions (e.g., seasonal transitions, drought stress).  It was desirable to implement a dry deposition algorithm in CAMx that incorporates updates in theory as well as recent measurements.  One of the most important aspects of newer dry deposition schemes is the use of "leaf area index" (LAI) to scale pollutant uptake into biota.  The LAI is defined as the ratio of the one-sided green leaf area to a unit area of the ground.  This index characterizes the amount of vegetation present, and can be measured by satellites instruments at fairly high spatial resolution.

A recent LAI-based algorithm is used in Environment Canada's AURAMS air quality model (Zhang et al. 2003; Zhang et al. 2008).  This scheme is a state-of-the-science algorithm that possesses an updated representation of non-stomatal deposition pathways and has been

tested extensively through its use in daily air quality forecasting. It has been shown to reproduce observed fluxes of ozone and $SO_2$ with reasonable accuracy.

4.7.2.1  Dry Deposition of Gases

The gas resistance model of Zhang et al. (2003) invokes the same 3-resistance equation for deposition velocity as the Wesely (1989) model. The equations for aerodynamic resistance ($r_a$) and boundary resistance ($r_b$) are very similar to the Wesely (1989) formulations. However, Zhang et al. (2003) replace the surface resistance ($r_s$) equation with a new relationship for the overall canopy resistance:

$$r_c = \frac{1}{\frac{1-W_{st}}{r_{st}+r_m} + \frac{1}{r_{cut}} + \frac{1}{r_{ac}+r_{gs}}}$$

where $W_{st}$ is the fraction of stomatal blocking under wet conditions, $r_{cut}$ is the cuticle resistance, and all other resistances have similar meaning to the Wesely model. Stomatal resistance ($r_{st}$) is calculated using a sunlit/shade (so-called "two-big-leaf") stomatal resistance sub-model. Following Wesely (1989), values for $r_g$ and $r_{cut}$ are calculated for $SO_2$ and $O_3$ and then scaled for other gaseous species. Cuticle resistance is slightly different from that defined in traditional big-leaf models in that it also considers the aerodynamic and quasi-laminar resistances of individual leaves. This is done by parameterizing $r_{cut}$ as a function of friction velocity, similar to the concept of overall cuticle uptake considered in a multi-layer model framework.

LAI is used in functions for $r_{ac}$, and $r_{cut}$, where the LAI for any given day is linearly interpolated from monthly default LAI as a function of landuse type. To account for LAI effects on surface roughness ($z_0$), a similar daily LAI interpolation is applied to that parameter. Hence, the Zhang model does not require the specification of season, as all resistance equations are continuous over each month (note that CAMx automatically applies the 6-month offset for applications in the southern hemisphere).

For snow on the ground and leaves, both $r_{gs}$ and $r_{cut}$ are adjusted by a snow cover fraction, which is assumed to be 0.8 when snow cover is flagged for a grid cell in CAMx. Snow cover is defined through the input 2D surface file, as described in Section 3. For surfaces without canopies, $r_{gs}$ is defined as the resistance to any surface (e.g. soil, ice, snow and water), $r_{ac}$ is set to zero, and very large values are used for $r_{st}$, $r_m$ and $r_{cut}$.

Over water, the updated temperature-dependent ozone surface resistance equation described above for the Wesely scheme is also used for the Zhang scheme.

The Zhang scheme uses 26 landuse categories, whereas the Wesely scheme uses 11. Therefore, the CAMx landuse file was expanded to handle up to 26 categories (see Section 3). The Zhang model includes a set of embedded annual surface roughness ranges and monthly LAI specific to each of the 26 landuse categories. The capabilities of the scheme were extended by adding the option to use episode-specific (i.e., satellite-derived) LAI data. Satellite-based LAI data from

MODIS (MODerate-resolution Imaging Spectroradiometer)[2] can be processed into gridded LAI fields that are passed to CAMx as an optional record in the time-invariant 2D surface input file (see Section 3). The optional gridded LAI fields are used to scale the default landuse-specific LAI values. For each grid cell, a landuse-weighted default LAI is determined according to the landuse fractions present. An LAI scaling factor is then determined as the ratio of the input LAI to the landuse-weighted default LAI. This factor is used to scale the individual default LAI values for each landuse type in the grid cell, subject to the annual maximum to minimum range among the monthly default values. Figure 4-4 illustrates how the use of satellite LAI data introduces additional episode-specific variation into the LAI field.

In developmental tests, the Zhang dry deposition model has tended to generate lower ozone deposition rates relative to the Wesely model, which leads to higher ozone predictions overall. This effect is seasonally dependent and will vary with the definition of LAI. Ozone is less sensitive to the source of LAI (whether Zhang defaults or satellite-enhanced) than to the choice of deposition model.

## Zhang Embedded LAI Data
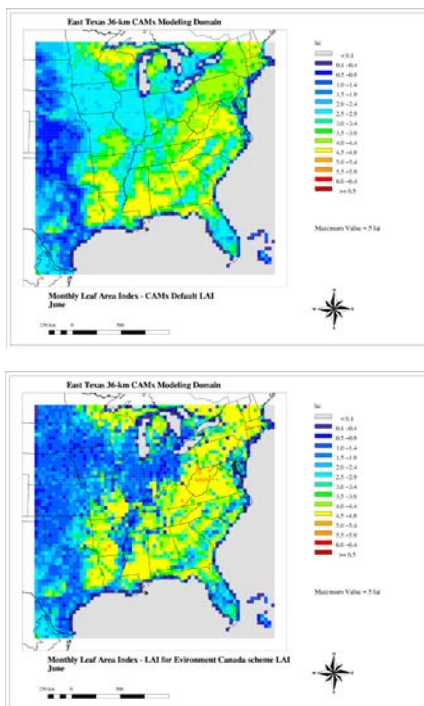


## LAI from Satellite
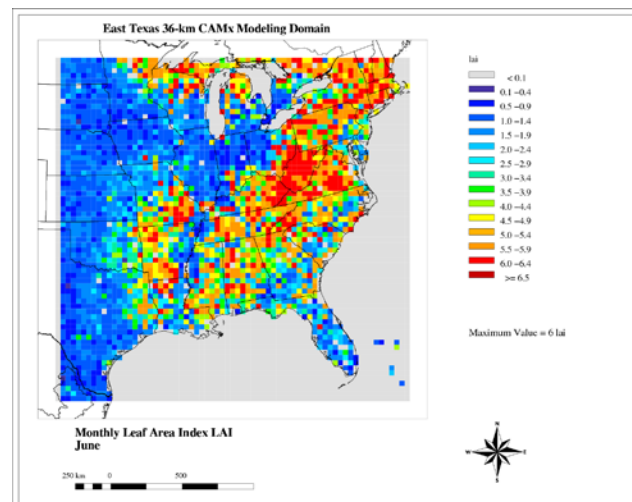
## Modified LAI using Satellite Data

**Figure 4-4. Comparison of monthly LAI data embedded in the Zhang dry deposition scheme against episode-specific LAI for June 2005.**

---

2 MODIS provides LAI at 250 meter spatial resolution and 16 day temporal resolution.

### 4.7.2.2  Dry Deposition of Aerosols

Many previous particle dry deposition models were evaluated against wind tunnel measurements, which may not be representative of field measurements.  Ruijgrok et al. (1995) showed that estimates from these early models differ greatly, especially in the range of 0.1-1.0 µm (by 2 to 3 orders of magnitude).  Theoretically, particles in this range deposit at rates much less than 0.01 cm/s, a value comparable only to laboratory (wind tunnel) studies.  According to Zhang et al. (2001), much higher values have been obtained in many field studies, including for sub-micron sulfate in which deposition velocities of one to two orders of magnitude higher have been measured.  Gallagher et al. (1997) state that much higher deposition velocity values, typically 1 cm/s or more for sub-micron aerosol deposition to a forest, are consistent across the aerosol size spectrum.  The Zhang et al. (2001) study developed a simple parameterization of particle dry deposition as a function of aerosol size and landuse that predicts higher deposition velocities for sub-micron aerosols, especially over rough vegetated surfaces.

The deposition of aerosols is based on the model of Slinn (1982), but using simplified empirical parameterizations to replace detailed canopy information.  The aerosol deposition velocity is defined as:

$$v_d \;\;=\;\; v_{sed} + \frac{1}{r_a + r_s}$$

where $v_{sed}$ and $r_a$ have identical meanings as the Slinn and Slinn (1980) definition described earlier for the Wesely/Slinn deposition model.  Note that in this case, the virtual serial resistance $r_a \cdot r_s \cdot v_{sed}$ has been removed, which results in higher values of deposition velocity.  The surface resistance is given by

$$r_s \;\;=\;\; \frac{1}{\varepsilon_0 u_* \left(E_B + E_{IM} + E_{IN}\right) R_1}$$

where the variable $E$ includes the collection efficiencies for Brownian diffusion, impaction, and interception, respectively, $R_1$ is a factor representing the fraction of particles that stick to the surface, and $\varepsilon_0$ is an empirical constant that is set to a value of 3.  The Brownian collection efficiency depends on the Schmidt number, while the impaction efficiency and $R_1$ depend on the Stokes number.

The collection efficiency by interception also exists if the particle passes an obstacle at a distance shorter than its physical dimensions (e.g., large particles passing near hairy leaves).  Zhang et al. (2001) adopted a simple equation for this term that is a function of particle diameter and a characteristic radius, for which default values are given for different landuse and seasonal categories.

Figures 4-5 and 4-6 compare estimated particle deposition velocities from the Zhang model, the Slinn and Slinn (1980) model, and the AERMOD model (EPA, 1998).  Calculations were made for daytime, neutrally stable conditions for a range of wind speeds and landuse categories.  Figure 4-6 shows that the Zhang model increases deposition velocities over forest by roughly an order

of magnitude for the 0.1-1 µm range, yet reduces deposition velocities above 1 µm.  Figure 4-6 clearly shows the Zhang model generates sub-micron deposition velocities that are ten times higher than the Slinn and Slinn (1980) model over the five landuse types tested.
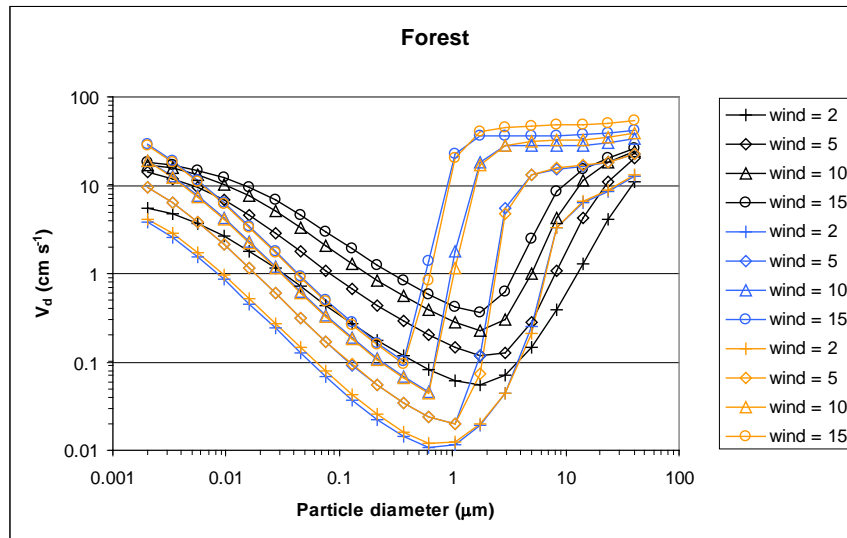


**Figure 4-5.  Comparison of particle dry deposition velocities as a function of size and wind speeds (m/s) for three models: black – Zhang et al. (2001); blue – Slinn and Slinn (1980); orange – AERMOD (EPA, 1998).  Results are shown for a forest landuse category during daytime neutral stability.  Particle density was set at 1.5 g/cm$^3$.**
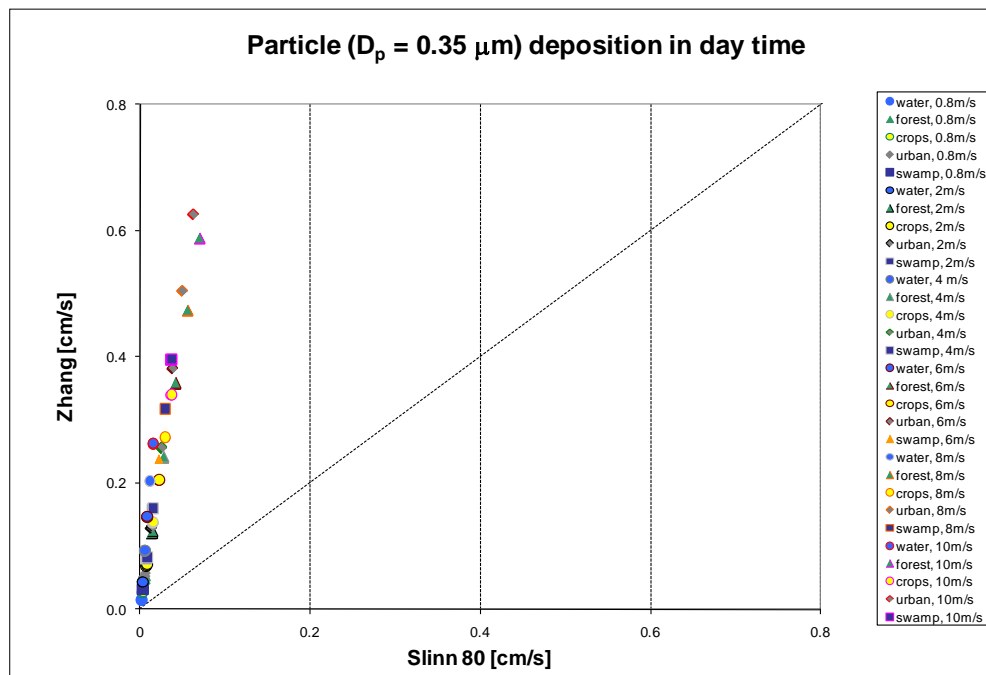


**Figure 4-6   Comparison of particle dry deposition velocities determined by the Zhang et al. (2001) and Slinn and Slinn (1980) models, as a function of landuse and wind speed during daytime neutrally stable conditions.  Particle density was set at 1.5 g/cm$^3$.**

# 5. CHEMISTRY MECHANISMS

The photochemical mechanisms currently supported in CAMx are listed in Table 5-1 and include the 2005 version of Carbon Bond (CB05; Yarwood et al., 2005b), version 6 of Carbon Bond (CB6; Yarwood et al., 2010; Yarwood et al., 2012a,b), and the 1999 version of the Statewide Air Pollution Research Center (SAPRC99) mechanism (Carter, 2000).  All are balanced for nitrogen conservation so that predicted NOy can be calculated as the sum of nitrogen containing species. All can be linked to optional modal and size-segregated primary and secondary particulate matter (PM) treatments.  The secondary PM chemistry includes organic and inorganic formation/partitioning from condensable gases derived from gas-phase chemistry, and aqueous inorganic chemistry.  The modal PM treatment also supports several optional mercury species. Additionally, there is an interface that allows a simpler user-defined chemical mechanism to be employed in the model (Mechanism 10).  A listing of the explicit species, reactions, and VOC species properties in Mechanisms 5 through 7, and the CB6 updates in Mechansims 1 and 2, are provided in Appendices A through E, respectively.

**Table 5-1.  Gas-phase chemical mechanisms currently implemented in CAMx.**

| Mechanism ID | Description |
|---|---|
| 5 | The fixed parameter version of the SAPRC99 gas-phase mechanism (Carter, 2000).  217 reactions and up to 114 species (76 state gases, up to 22 state particulates, and 16 radicals). |
| 6 | CB05 (Yarwood et al., 2005b).  156 reactions and up to 89 species (54 state gases, up to 22 state particulates, and 13 radicals). |
| 7 | CB6 (Yarwood et al., 2010).  218 reactions and up to 114 species (69 state gases, up to 22 state particulates, and 23 radicals). |
| 1 | Mechanism 7 with updates to include reactions involving oceanic iodine compounds (Yarwood et al., 2012b). |
| 2 | CB6 "Revision 1" (CB6r1; Yarwood et al., 2012a). |
| 10 | A user-defined simple chemistry mechanism can be developed for any gas and/or particulate species, which is defined by a "Mechanism 10" parameters file and solved within a user-supplied subroutine called "chem10.f." |

The selection of which mechanism to employ in a given CAMx application is determined by the "chemistry parameter" input file.  This file defines the mechanism number, the number of gas and aerosol species, and the number of reactions for the mechanism, lists the species by name with associated physico-chemical properties, lists the reaction rate constants and temperature dependencies for each reaction, and defines which reactions are photolytic.  Chemistry parameter input files for the CB05, CB6, and SAPRC99 listed in Table 5-1 are provided with CAMx and are not normally modified by users.  See Section 3 for additional information on the format and usage of these files.  Chemistry parameters files are specific to versions of CAMx. Always use chemistry parameters files with the right CAMx version number, do not attempt to use files for another CAMx version.

## 5.1 Gas-Phase Chemistry

### 5.1.1 Carbon Bond 2005

The Carbon Bond IV (CB4) mechanism was first developed by Gery et al. (1989), and subsequently underwent various updates in the mid 1990's to include revised PAN chemistry, additional radical-radical termination reactions and updated isoprene chemistry (Carter 1996; Whitten et al., 1996). Additional updates were then made to expand ozone modeling from urban to regional/rural environments and to support secondary aerosol chemistry, mercury and toxics (Yarwood et al., 2005a).

Mechanism 6 is the 2005 version of Carbon Bond (CB05) developed for EPA atmospheric modeling studies (Yarwood et al., 2005b). Updates in CB05 compared to the earlier CB4 mechanisms are:

- Updated rate constants based on 2003 – 2005 IUPAC and NASA evaluations.
- An extended inorganic reaction set for urban to remote tropospheric conditions.
- NOx recycling reactions to represent the fate of NOx over multiple days.
- Explicit organic chemistry for methane and ethane.
- Explicit methylperoxy radical, methyl hydroperoxide and formic acid.
- Lumped higher organic peroxides, organic acids and peracids.
- Internal olefin (R-HC=CH-R) species called IOLE.
- Higher aldehyde species ALDX making ALD2 explicitly acetaldehyde.
- Higher peroxyacyl nitrate species from ALDX called PANX.
- Lumped terpene species called TERP.

The CB05 was evaluated against smog chamber data from the Universities of North Carolina and California at Riverside. The new higher aldehyde and internal olefin species improve mechanism performance for these species and produce oxidants more rapidly at low VOC/NOx ratios. The new terpene species improves simulation of oxidants and PM from biogenic emissions. Several new organic peroxide species improve the simulation of oxidants that are involved in PM sulfate formation. The addition of explicit methylperoxy radical improves the simulation of hydrogen peroxide under low NOx conditions.

### 5.1.2 Carbon Bond Version 6

Mechanism 7 is version 6 of Carbon Bond (CB6; Yarwood et al., 2010). Several organic compounds that are long-lived and relatively abundant, namely propane, acetone, benzene and ethyne (acetylene), are added explicitly in CB6 so as to improve oxidant formation from these compounds as they are oxidized slowly at the regional scale. Alpha-dicarbonyl compounds (glyoxal and analogs), which can from secondary organic aerosol (SOA) via aqueous-phase reactions (Carlton et al., 2007), are added in CB6 to improve support for SOA modeling. Precursors to alpha-dicarbonyls in CB6 are aromatics, alkenes and ethyne. CB6 includes several updates to peroxy radical chemistry that will improve formation of hydrogen peroxide ($H_2O_2$) and therefore sulfate aerosol formation. The gas-phase reaction of dinitrogen pentoxide ($N_2O_5$) with water vapor is slower in CB6, which will reduce nighttime formation of nitric acid although

heterogeneous reactions on aerosol surfaces may dominate nitric acid formation at night (Brown et al, 2006). When CB6 is used in atmospheric models the heterogeneous reaction between $N_2O_5$ and water vapor should be included. CAMx includes the calculation of the heterogeneous $N_2O_5$ hydrolysis rate as a function of aerosol size, water content, and pH when PM is explicitly simulated; if no PM chemistry is included, CAMx sets the heterogeneous rate to the IUPAC (2006) $N_2O_5$ hydrolysis rate. The core inorganic chemistry mechanism for CB6 is based on evaluated data from the IUPAC tropospheric chemistry panel as of January, 2010 (Atkinson et al., 2010). IUPAC also is the primary source for photolysis data in CB6 with some data from the 2006 NASA/JPL data evaluation (Sander et al., 2006) or other sources for photolysis of some organic compounds. There are changes to the organic chemistry for alkanes, alkenes, aromatics and oxygenates. The most extensive changes are for aromatics and isoprene. Chemistry updates for aromatics were based on the updated toluene mechanism (CB05-TU) developed by Whitten et al. (2009) extended to benzene and xylenes. The isoprene mechanism was revised based on several recently published studies (Paulot et al., 2010; Peeters et al., 2010).

CB6 was evaluated using 339 experiments from several chambers at the University of California at Riverside and the Tennessee Valley Authority. The performance of CB6 and CB05 in simulating chamber studies was comparable for alkanes, alkenes, alcohols and aldehydes with both CB6 and CB05 performing well and exhibiting 20% or less bias for maximum ozone. For species that were explicitly added in CB6 (ethyne, benzene and ketones), CB6 performed much better than CB05. For aromatics, CB6 improved upon CB05 by reducing under prediction bias in maximum ozone to about 10% for benzene, toluene and xylene. For isoprene, both CB05 and CB6 show little bias for maximum ozone (less than 5%) but CB6 tended to form ozone too slowly. CB6 improved upon CB05 for simulating mixtures of VOCs. For mixtures without aromatics, both CB05 and CB6 showed minimal bias for maximum ozone. For mixtures including aromatics, both CB05 and CB6 under predicted maximum ozone but bias was reduced from about 30% for CB05 to about 20% for CB6.

### 5.1.3 Carbon Bond Version 6 with Iodine Chemistry

Mechanism 1 is an extension of CB6 chemistry that adds reactions involving ocean-borne iodine compounds. Atmospheric reactions of iodine atoms can destroy tropospheric ozone through series of chemical reactions. These reactions are referred to as catalytic cycles because the iodine is regenerated in the reactions and therefore one iodine atom can potentially destroy many ozone molecules. The efficiency of tropospheric ozone destruction by reactive iodine depends upon how effectively reactive iodine species are eliminated by other reactions. Emissions from oceans are the major source of atmospheric iodine (Carpenter, 2003), including methyl iodide ($CH_3I$), other iodo-methanes ($CH_2I_2$, $CH_2ICl$, $CH_2IBr$), larger alky iodides, and molecular iodine ($I_2$). Iodine emissions result both from biological and photochemical processes in ocean water (Moore and Tokarczyk, 1993; Moore and Zafirou, 1996). Photochemical processes that cause iodine emissions are linked to reactions of dissolved ozone and thereby to enhanced ozone deposition to oceanic waters (Ganzeveld et al., 2009; Helmig et al., 2012).

ENVIRON developed a chemical mechanism for iodine and ozone that is suitable for use in regional photochemical modeling of ozone (Yarwood et al., 2012b). The chemical reactions included in the mechanism (Appendix D) are based primarily on the recent review by Sommariva et al. (2012), with

references to other recent studies by Ordonez et al. (2012) and Mahajan et al. (2010).  The citations given for each reaction in Appendix D indicate the data source.  Notable differences between the mechanisms in Appendix D and Sommariva et al. (2012) are:

- Inclusion of reaction I23 (INO + I) which strongly limits daytime accumulation of INO;

- Inclusion of photolysis reactions I30 to I33 for iodocarbons in addition to $CH_3I$ (reaction I30).

- Condensation of the reactions forming iodine oxides larger than $I_2O_2$ to a single species IXOY which is defined as containing two I-atoms.

- Exclusion of a reaction between IO and $CH_3O_2$, which is uncertain (Sommariva et al., 2012) and does not have a large impact on model results in our tests (Yarwood et al., 2012b).

### 5.1.4  Carbon Bond Version 6, Revision 1

Mechanism 2 is referred to as CB6 revision 1 (CB6r1).  The major update in CB6r1 involves incorporating new NOx-recycling reactions involving certain classes of VOCs.  It is important that NOx-recycling be properly taken into account when modeling regional ozone formation, particularly in multi-day episodes where transport to NOx-limited regions is important.  Yarwood et al. (2012a) conducted new environmental chamber experiments at the University of California at Riverside to characterize NOx sinks and sources for several VOCs that are poorly understood.  At the same time, data of chamber experiments performed in Europe were obtained and formatted for use in mechanism evaluation and development.  The experimental data obtained were used to test and improve the mechanisms for isoprene and aromatics in CB6r1.  CB6r1 performed better than CB6 in simulating experiments for toluene, xylenes and mixtures combining aromatics with other VOCs.  CB6r1 includes NOx-recycling from photolysis of NTR (representing alkyl nitrates) and CRON (representing nitrocresols).  Results from Yarwood et al. (2012a) suggested that OH-reactions of isopropyl and isobutyl nitrate also lead to NOx recycling but the results were not conclusive because, under their specific experimental conditions, the isopropyl nitrate and isobutyl nitrate were mainly consumed by photolysis rather than OH reaction.  CB6r1 tentatively includes NOx recycling from the reaction of OH with NTR (a change from CB6) but we recommend conducting photochemical model sensitivity tests to evaluate the impacts of this change.

In the course of developing CB6r1 several errors in CB6 were identified and corrected.  These mechanism corrections were to the products of reactions 82 (XO2 + RO2), 86 (XO2N + RO2) and 112 (ALDX photolysis).  The rate constant for the reaction of OH with NO2 is uncertain with currently recommended values varying by 25%.  CB6r1 uses a rate constant at the middle of this range recommended by the NASA-JPL evaluation panel.

### 5.1.5  SAPRC 1999

Mechanism 5 is the SAPRC99 chemistry adapted for photochemical grid modeling by selecting a specific "fixed parameter" lumping scheme (Carter, 2000).  The SAPRC99 mechanism is included in CAMx because it has been tested extensively against environmental chamber data, it uses a different approach for VOC lumping than the Carbon Bond mechanisms, and has been adopted in several regulatory modeling applications in the U.S.

### 5.1.6 Implicit Gas-Phase Species

All photochemical mechanisms in CAMx employ fixed concentrations for molecular oxygen ($O_2$), molecular hydrogen ($H_2$), and methane ($CH_4$). Concentrations for these compounds are set to the following constant mixing ratios (i.e., they are not impacted by the chemical solution):

$$[O_2] \quad = 2.095 \times 10^5 \text{ ppm}$$
$$[H_2] \quad = 0.60 \text{ ppm}$$
$$[CH_4] \quad = 1.75 \text{ ppm}$$

### 5.1.7 Photolysis Rates

The rates of atmospheric photolysis reactions depend upon solar irradiance and therefore are sensitive to the amount of solar radiation transmitted through the atmosphere as well as reflected from the earth's surface (albedo). Photolysis rates are externally derived assuming clear-sky conditions as a function of five parameters: solar zenith angle, altitude above ground, total ozone column, surface albedo, and terrain height. The rates are provided to CAMx as a large lookup table that spans the range of conditions for each of the five dimensions. The lookup table is developed using a CAMx pre-processor that incorporates the Tropospheric Ultraviolet and Visible (TUV) radiative transfer model (NCAR, 2011). TUV employs a standard atmosphere density profile for Rayleigh scattering and other absorbers such as oxygen. User-specified ozone column values are used to scale a typical vertical ozone profile within TUV. A default aerosol profile from Elterman (1968) is combined with typical aerosol optical properties within TUV to account for haze.

The CAMx version of TUV is modified to output photolysis rate information in a format directly compatible with CAMx for the CB05, CB6, and SAPRC99 chemical mechanisms. See Sections 2 and 3 for more information on developing photolysis inputs.

As CAMx runs, the lookup rates are interpolated to the specific conditions in each grid cell. They are then adjusted for any local cloud cover and local aerosol attenuation (if PM is simulated). Additionally, solar angle-dependent temperature and pressure adjustments are applied to five key photolysis reactions ($NO_2$, $O_3$, acetaldehyde, and two formaldehyde reactions).

#### 5.1.7.1 Cloud and Aerosol Adjustments

Photochemistry is strongly influenced by the presence of clouds, which can both attenuate and enhance the actinic flux of ultraviolet (UV) and visible radiation responsible for photolysis. Their specific radiative impacts depend on many factors, including height, depth and fractional sky cover; water content; and water phase (i.e., liquid droplets or ice crystals). Aerosols also influence photochemistry according to their optical properties and mass loading as a function of altitude and depth. CAMx includes a fast in-line version of TUV (Emery et al., 2010) to calculate photolysis adjustment profiles through each cloudy, aerosol-laden grid column.

The in-line TUV is run twice for each grid column: first for non-cloudy conditions with the same Elterman (1968) aerosol profile used in the full-science TUV pre-processor, and second with clouds and simulated aerosols to derive a vertical profile of the cloudy:clear actinic flux ratio (in

the case that aerosols are not run in CAMx, the Elterman profile is used consistently). This ratio is then applied as a multiplicative factor to the clear-sky value in each grid cell. This approach maintains accuracy in the calculation of clear-sky photolysis rates, while allowing clouds and aerosols to be directly involved in radiative transfer calculations through each grid column.

TUV includes a calculation of integrated atmospheric density above the CAMx domain, based on the U.S. standard atmosphere, so that atmospheric attenuation of the UV stream is properly calculated entering the model top. Other aspects of the in-line TUV model were substantially streamlined to minimize runtimes. First, radiative calculations are performed for only a single representative wavelength (350 nm). Second, since absorption by gases occurs in rather narrow UV bands relative to the broad-band influence of clouds, the absorption from oxygen, ozone, nitrogen dioxide and sulfur dioxide were removed. Third, the extraterrestrial flux was not needed as it cancels out in the calculation of the cloudy: clear ratio. Finally, the plane-parallel version of the delta-Eddington approach was used in lieu of the more complex and expensive pseudo-spherical geometry. Preliminary tests against the full-science TUV showed that the streamlined version resulted in less than 1% differences in actinic flux ratio for a range of cloudy conditions (Emery et al., 2010).

Optical depth $\tau$ expresses the reduction of incident light $I_0$ through a light attenuating medium of depth $\Delta z$ according to

$$I \;=\; I_0 e^{-\tau}$$

The in-line TUV adjustment scheme utilizes cloud optical depth fields provided by the CAMx cloud/rain file, and aerosol optical depths calculated from the PM mass concentrations simulated by CAMx.

The CAMx meteorological interface pre-processors generate cloud water and optical depth fields from the variable fields present in the raw meteorological output files. Cloud optical depth is calculated in each model grid cell according to the approach of DelGenio et al. (1996) and Voulgarkakis et al. (2009), which satisfactorily approximates the effects of random cloud overlap according to

$$\tau \;=\; \frac{3\,L\,\Delta z}{2\,\rho_w\,r_d}\left(F_c\right)^{3/2}$$

where $L$ is cloud liquid water content (g/m$^3$), $\Delta z$ is the cell depth containing cloud water, $\rho_w$ is the density of liquid water ($10^6$ g/m$^3$), and $F_c$ is fractional cloud cover. The mean cloud droplet radius $r_d$ is not dependent on water phase, and is assumed to be a typical tropospheric value of $1.5\times10^{-5}$ m for liquid cloud water. TUV assumes constant Mie scattering parameters for clouds: a single scattering albedo of 0.99, and an asymmetry factor of 0.85.

When CAMx is run with PM, vertical haze opacity profiles are calculated from simulated aerosol concentration fields. When CAMx is run with only gas-phase chemistry without aerosols, photolysis rates are only adjusted for clouds. Aerosol optical parameters are best determined

from Mie theory, but in the interest of minimizing impacts to model speed and considering the degree of uncertainty in the simulated aerosol concentrations themselves, a simpler method was adopted.  Aerosols are assumed to exist as an external mixture of their component chemical species.  Aerosol light extinction (scattering and absorption) is a function of each species' concentration, extinction efficiency, and affinity for hygroscopic growth.  Total aerosol optical depth is determined by summing extinction over all species and multiplying by layer depth.

Dry extinction efficiencies and single-scattering albedos for each aerosol species, valid at 350 nm, are externally defined in the CAMx chemistry parameters file.  While these can be set by the user, the chemistry parameters files that are provided with the CAMx distribution include default values according to Takemura et al. (2002), as shown in Table 5-2.

**Table 5-2.  Default dry extinction efficiency and single-scattering albedo at 350 nm (Takemura et al., 2002) in the distributed CAMx chemistry parameters file.**

| Species | Dry Extinction Efficiency (m2/µg) | Single-Scattering Albedo |
|---|---|---|
| Sulfate | $7\times10^{-6}$ | 0.99 |
| Nitrate | $7\times10^{-6}$ | 0.99 |
| Ammonium | $7\times10^{-6}$ | 0.99 |
| Organics | $7\times10^{-6}$ | 0.80 |
| Elemental Carbon | $18\times10^{-6}$ | 0.25 |
| Crustal (Fine+Coarse) | $0.4\times10^{-6}$ | 0.70 |
| Sea salt (Na+Cl) | $1.5\times10^{-6}$ | 0.99 |

Takemura et al. provide extinction efficiencies and single-scattering albedos for sulfate, organics, soot, total dust, and sea salt; we have extended the sulfate values to nitrate and ammonium.  The asymmetry factor is internally set to a default value of 0.61 regardless of the composition of the aerosols.

Hygroscopic aerosols are also flagged in the chemistry parameters file.  For each flagged species, an internal growth factor is applied to the dry extinction efficiencies according to the relative humidity conditions in each grid cell.  The growth curve is taken from the Phase I report of the Federal Land Managers' Air Quality Related Values Workgroup (FLAG, 2000).  By default, the relative humidity growth factor is flagged for sulfate, nitrate, ammonium and sea salt; a single growth factor is applied for all hygroscopic species (Figure 5-1).  Minimum and maximum limits on relative humidity are set at 1% and 95%, respectively.

### 5.1.7.2  Effects of Surface Albedo and Snow Cover

Photolysis rates depend on the amount of solar radiation reflected from the earth's surface (albedo).  The grid-cell specific UV albedo is assigned within CAMx according to the input landuse types in the time-invariant 2D surface file (Tables 3-4 and 3-5).  This approach results in UV albedos that fall in the range 0.04 to 0.08 and are constant in time.  Analyses of reflected UV radiation recorded in satellite data (Herman and Celarier, 1997) report similar UV albedo values in the range 0.02-0.08 for surfaces not covered by snow.
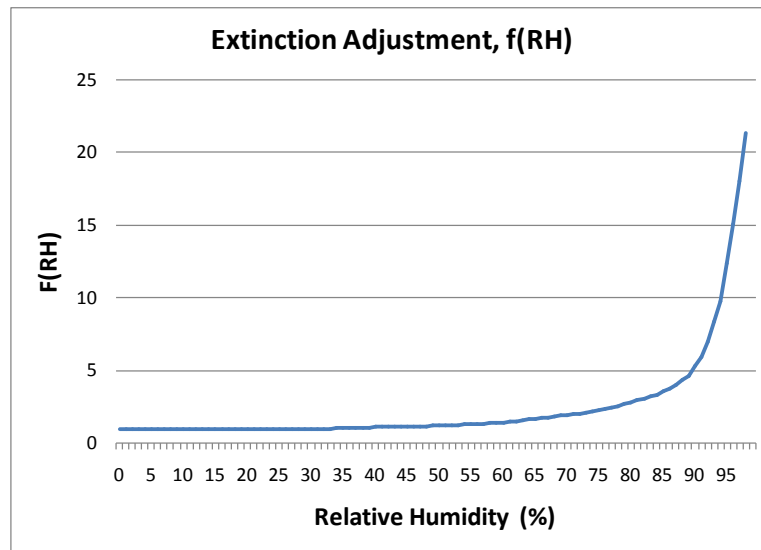
**Figure 5-1. Relative humidity adjustment factor applied to the dry extinction efficiency for hygroscopic aerosols (FLAG, 2000).**

Snow is much more reflective than other types of surfaces and so snow cover enhances the rates of photolysis reactions. Since most photolysis reactions depend upon ultra-violet radiation it is important to characterize the effect of snow cover on UV albedo. Measurements of the UV albedo for Antarctic snow report values of 0.96 to 0.98 over a wide range of snow grain sizes and solar zenith angles. However, these high values should be considered an upper limit to the reflectivity of snow cover because snow may not cover the entirety of the surface or all surface features, and because the snow may be aged or dirty. Satellite climatology shows surface albedos spanning a wide range of values from 0.2 to nearly 1.0. Potential reasons for this wide range of values include coarse resolution (1° latitude by 1.25° longitude) such that snow-covered and snow-free surfaces are combined, differences between rough and smooth land cover types (e.g., forest vs. open range land), and differences between new/clean and aged/dirty snow.

The CAMx photolysis rate input file is generated for five albedo ranges, two of which represent the non-snow range (0.04 – 0.08 ) and three that represent the snow range (0.2 – 0.5 – 0.8). CAMx determines the landuse-weighted average surface albedo in each grid cell and interpolates photolysis rates between the five albedos. For snow-covered grid cells defined in the time-variant 2D surface input file, CAMx currently uses the photolysis rates calculated for albedo of 0.5, because this is in the middle of the range reported by Herman and Celarier (1997). Use of the full range of snow albedo will be considered in future development.

### 5.1.8 Gas-Phase Chemistry Solvers

Solving the time evolution of gas-phase chemistry requires numerically integrating a set of ordinary differential equations (ODEs) and is among the most computationally expensive operations performed in a photochemical grid model. One reason for this is that the ODEs describing tropospheric chemistry are "stiff" – meaning that the chemical species involved have

widely varying production and/or decay times. The computational efficiency of the gas-phase chemistry solver strongly influences the overall efficiency of a grid model. CAMx includes three chemistry solvers that offer differing trade-offs between accuracy and efficiency.

The most accurate solution methods available for stiff ODEs are "Gear" type implicit solvers (Gear, 1971) such as LSODE (Hindmarsh, 1983). Gear solvers are stable when applied to "stiff" problems, such as gas-phase chemistry, but are generally too slow for routine use in grid model applications. Sun et al. (1994) developed an implicit-explicit hybrid (IEH) method based on LSODE that is accurate and much faster than LSODE. Hertel et al. (1993) developed an implementation of the Euler Backward Iterative (EBI) method that is very efficient and also accurate because it utilizes explicit algebraic formulae to solve several important groups of species (HOx, NOx, etc.) Hertel's EBI solver is the most efficient solver available in CAMx.

### 5.1.8.1 LSODE

CAMx includes the double precision version of the Livermore Solver for Ordinary Differential Equations (LSODE; Hindmarsh, 1983) distributed by the Netlib repository of numerical algorithms (http://www.netlib.org/). LSODE is too slow for everyday use but valuable as a reference method within CAMx. LSODE is based on Gear's method with numerical refinements to improve efficiency and ease of use (Radhakrishnan and Hindmarsh, 1993). Gear methods (Gear, 1971) are implicit and employ backwards-differentiation formulae to step forward in time by taking multiple steps. The converged solutions at each step are saved in a history matrix and used to predict the next solution. Thus, LSODE must initially take short time steps to build the history matrix and may then take progressively longer steps. LSODE is most efficient for long integration times (and inefficient for short integration times) and therefore least burdensome for coarse grid model applications that have relatively long coupling times between gas-phase chemistry and other processes, e.g., advection.

User-supplied information required by LSODE is essentially the error control parameters and the functions defining the system of ODEs, $\mathbf{f}(y,t)$, where $y$ is the vector of species concentrations and $t$ is time. Supplying a subroutine to evaluate the time derivatives of species concentrations ($\mathbf{f} = dy/dt$) is mandatory. Supplying a function to evaluate the Jacobian matrix ($\mathbf{J} = d\mathbf{f}/dy$) is optional since, if not supplied, LSODE can derive a numerical Jacobian by finite difference between repeated evaluations of $\mathbf{f}$. Supplying an algebraic Jacobian ensures accuracy, although a numerical Jacobian may be equally accurate if adequate precision (e.g., double precision) is employed. Supplying an algebraic Jacobian is more efficient when $\mathbf{J}$ is sparse, but for condensed mechanisms such as CB05 $\mathbf{J}$ is not sparse and the numerical Jacobian method is faster. CAMx uses the numerical Jacobian method with a relative error tolerance of $10^{-7}$ and an absolute error tolerance of $10^{-10}$.

### 5.1.8.2 IEH Solver

A stiffly-stable solver, such as LSODE, is only needed to solve the chemical species that have time constants comparable to or shorter than the integration time and which interact strongly with each other. Slowly changing species may be treated as constant for the duration of an LSODE solution and then solved outside LSODE using a simple explicit method. Sun et al. (1993) called this approach an implicit-explicit hybrid method and Chock et al. (1994) showed that IEH

methods offer useful computational efficiency and accuracy. The IEH method is faster than LSODE because fewer species are solved using the expensive Gear method, but less accurate than LSODE because of inaccuracy in the explicit method. The speed and accuracy of an IEH method is influenced by the designation of "fast" species to be solved implicitly and "slow" species to be solved explicitly.

The CAMx IEH solver designates species as fast, slow or steady-state (this designation is performed when mechanisms are implemented for the IEH solver and can't be changed by the user). Steady-state species are solved by assuming that they are in a quasi-stationary state (dy/dt = 0) with respect to other species and, therefore, that y = P/L, where P and L are respectively the production and loss rates for species y. Oxygen atoms, O($^1$D) and O($^3$P), are the most rapidly changing species in tropospheric chemistry mechanisms. Solving O-atoms with a steady-state assumption reduces stiffness and permits the single-precision version of LSODE to be used by the IEH solver. To ensure IEH solver accuracy with single precision, the Jacobian matrix is supplied algebraically to LSODE (see discussion, above). The relative error tolerance for LSODE within IEH is 5 x10$^{-5}$ and the absolute error tolerance is 10$^{-7}$. The O-atom concentrations are recalculated every time the derivatives (**f**) or Jacobian (**J**) are evaluated for LSODE. Slow species concentrations are calculated using rates evaluated at the middle of each IEH step. The IEH step size is limited to a few minutes for the slow species integration and multiple IEH steps are taken sequentially if needed.

### 5.1.8.3  EBI Solver

The backward Euler method solves concentrations (y) as y(t+h) = y(t) + h**f**, where f is the time derivative of species concentrations (**f**= dy/dt) evaluated at t+h. The method must be iterated to convergence in y(t+h) because species concentrations are interdependent. The basic EBI method is not efficient for stiff problems such as tropospheric chemistry because convergence is slow and the step size (h) must be short. Hertel et al. (1993) greatly improved the efficiency and accuracy of the method by developing analytical solutions to the EBI equation for groups of species that are strongly coupled (e.g. HOx and NOx/O$_3$). Time steps of up to 3 minutes are taken by the Hertel EBI solver in CAMx.

### 5.1.9  Chemical Mechanism Compiler

Each of the CAMx chemistry solvers relies upon equations that define the species time derivatives (**f** = dy/dt) and, in some cases, the Jacobian matrix (**J** = d**f**/dy) for each chemical mechanism. The preprocessor portion of the CAMx chemical mechanism compiler (CMC) reads a listing of the mechanism reactions and generates the Fortran statements for the rate equations and Jacobian matrix. This approach avoids potential errors resulting from coding equations by hand.

For the IEH and EBI chemistry solvers, the CMC preprocessor requires user input that determines how each species is solved. The CMC preprocessor could be used to generate many different solver implementations for a given mechanism, only some of which will be robust. The CMC preprocessor is not distributed with CAMx to avoid potential problems with users generating invalid chemistry solvers that produce unreliable results.

## 5.2  Aerosol Chemistry

The gas-phase chemistry of Mechanisms 5, 6 and 7 may be run alone (no aerosols) by simply setting the aerosol option keyword to "NONE" and omitting the entire list of aerosol species in the chemistry parameters file (see Section 3).  To model aerosols, the user sets the aerosol keyword to "INERT", "CF" or "CMU".  In all three cases, the user defines the number of size sections and their size ranges in a separate record in the chemistry parameters file.  The aerosol keyword "INERT" allows the user to define any number of arbitrarily-named inert particulate species to be carried by the model during a photochemical simulation (e.g., modeling the dispersion of only wind-blown dust).

Aerosol chemistry processes can be run together with gas-phase chemistry (Mechanism 5, 6, and 7) using two options for treating aerosol size distributions: the CF scheme and CMU scheme.  The CF scheme divides the size distribution into two static modes (coarse and fine).  Primary species can be modeled as fine and/or coarse particles, while all secondary (chemically-formed) species are modeled as fine particles only.  The CMU scheme employs a sectional approach that dynamically models the size evolution of each primary and secondary aerosol constituent across a number of fixed size sections.  The CF and CMU options require a minimum set of specific aerosol species with associated chemistry.  Aerosol water is explicitly treated in both CF and CMU options, which affects aerosol size and density.

### 5.2.1  Additional Gas-Phase Species

When either the CF or CMU aerosol option is selected, the following gas-phase species are added to model gas-aerosol interactions:

1) Ammonia (NH3) as a precursor for inorganic aerosol.
2) Gaseous sulfuric acid (SULF) as a precursor to sulfate aerosol.
3) Hydrogen chloride (HCL) as a product of acidified sea salt aerosol and aerosol precursor.
4) Condensable organic gases (CG1-CG7) as precursors to secondary organic aerosol (SOA) formation.
5) Organic gases that form CG species via oxidation reactions, namely toluene (TOLA), xylene (XYLA), monoterpenes (TRP), sesquiterpenes (SQT) and isoprene (ISP).

#### 5.2.1.1  SOA Precursors

Secondary organic aerosol (SOA) species exist in equilibrium with condensable gasses (CG) that can be produced by VOC oxidation:

$$VOC + oxidant \; \rightarrow \; CG \; \leftrightarrow \; SOA$$
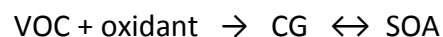
CG formation from VOC oxidation reactions (Table 5-3) is handled within the SOA module rather than the main gas-phase chemistry, as described below.  This approach has the following advantages: (1) separates the VOC precursors and lumping schemes for oxidant chemistry and SOA formation, e.g., for aromatics, different lumping schemes may be appropriate for oxidant and SOA formation; (2)  allows the same SOA mechanism to be used with different oxidant mechanisms; (3) allows inclusion of SOA precursors without explicitly defining oxidant reactions

**Table 5-3.  SOA precursor reactions included in CAMx.**

| Precursor | Reaction | CG Products[1] | $k_{298}$[2] $(ppm^{-1} min^{-1})$ |
|---|---|---|---|
| **Anthropogenic** | | | |
| Toluenes | TOLA + OH | 0.044 CG1 + 0.085 CG2 | 8.75E+03 |
| Xylenes | XYLA + OH | 0.027 CG1 + 0.118 CG2 | 3.71E+04 |
| **Biogenic** | | | |
| Isoprene | ISP + O | none | 5.32E+04 |
| | ISP + OH | 0.015 CG3 + 0.12 CG4 | 1.47E+05 |
| | ISP + O3 | none | 1.90E-02 |
| | ISP + NO3 | none | 9.96E+02 |
| Terpenes | TRP + O | 0.065 CG5 + 0.29 CG6 | 4.12E+04 |
| | TRP + OH | 0.065 CG5 + 0.29 CG6 | 7.76E+04 |
| | TRP + O3 | 0.065 CG5 + 0.29 CG6 | 1.33E-01 |
| | TRP + NO3 | 0.065 CG5 + 0.29 CG6 | 9.18E+03 |
| Sesquiterpenes | SQT + OH | 0.85 CG7 | 2.91E+05 |
| | SQT + O3 | 0.85 CG7 | 1.71E+01 |
| | SQT + NO3 | 0.85 CG7 | 2.81E+04 |

Notes:
1    Yield values are in ppm/ppm.
2    Rate constants are shown for 298 K and 1 atmosphere in $ppm^{-1} min^{-1}$.

– e.g., sesquiterpenes are explicit in the SOA module but their oxidant formation may be represented by surrogate species.

Emissions of SOA precursors must be provided separately from the emissions of oxidant precursors, e.g., isoprene emissions must be speciated both as ISOP for oxidant chemistry and ISP for SOA chemistry.  This "double counting" of emissions is correct because the species (e.g., ISOP and ISP) serve different purposes.  Ideally, emissions processors will develop VOC speciation schemes that suit both oxidant and SOA modeling.  In the absence of more refined information, emissions of SOA precursors may be set equal to emissions of oxidant precursors as follows: ISP = ISOP; TRP = TERP; TOLA = TOL or ARO1; XYLA = XYL or ARO2.

Some emitted VOCs are semi-volatile (SVOCs) and can condense directly to SOA, e.g., biogenic emissions of oxygenated VOCs.   SOA formation from SVOC emissions may be accounted for by including the SVOC in the CAMx emissions as one of the CGs listed in Table 5-4.  Choose a CG that has appropriate volatility properties, and account for any molecular weight difference between the SVOC and surrogate CG (moles CG emitted = moles SVOC x $MW_{SVOC}/MW_{CG}$).

### 5.2.2  Aerosol Processes

Aerosol processes are modeled using either the CF or CMU algorithm, depending on how the aerosol option keyword is set in the chemistry parameters file.  The CF and CMU aerosol chemistry algorithms both perform the following three processes:

**Table 5-4.  Properties of CG/SOA pairs.**

| Species | Molecular Weight (g mole$^{-1}$) | Saturation Concentration (µg m$^{-3}$ at 298 K) | Heat of vaporization (kJ mole$^{-1}$) |
|---|---|---|---|
| CG1/SOA1 | 150 | 7.82 | 66.8 |
| CG2/SOA2 | 150 | 227 | 66.8 |
| CG3/SOA3 | 130 | 0.726 | 42 |
| CG4/SOA4 | 130 | 136 | 42 |
| CG5/SOA5 | 180 | 3.92 | 75.5 |
| CG6/SOA6 | 180 | 55.8 | 75.5 |
| CG7/SOA7 | 210 | 0 | – |
| SOPA | 220 | – | – |
| SOPB | 220 | – | – |

1) Aqueous sulfate and nitrate formation in resolved cloud water using the RADM aqueous chemistry algorithm (Chang et al., 1987).

2) Partitioning of condensable organic gases (CG1-CG7) to secondary organic aerosols (SOA1-SOA7) to form a condensed "organic solution phase" using a semi-volatile, equilibrium scheme called SOAP (Strader et al., 1999).

3) Partitioning of inorganic aerosol constituents (sulfate, nitrate, ammonium, sodium, and chloride) between the gas and aerosol phases using the ISORROPIA thermodynamic module (Nenes et al., 1998, 1999).

4) Uptake of nitric acid by calcium in soil dust particles is calculated external to ISORROPIA.

The aqueous chemistry does not treat sub-grid scale clouds; clouds are assumed to either occupy the entirety of a grid cell volume, or be completely absent from it.  Cloudy grid cells are determined by cloud liquid water contents above a threshold of 0.05 g/m$^3$ as defined by input gridded cloud water fields.  Aqueous chemistry is calculated for each cloud grid cell at each model time step.  The SOAP and ISORRIOPA equilibrium algorithms are called on a unique aerosol "coupling" time step that is defined within the chemistry parameters file.  By default, the aerosol coupling time step is 15 minutes, and this is used for all grids in a simulation regardless of the grid-specific driving time step.

The CAMx SOA module consists of two parts: gas-phase oxidation chemistry that forms condensable gases (CGs), and equilibrium partitioning between gas and aerosol phases for each CG/SOA pair.  Table 5-3 lists the oxidation reactions and CG products.  The CG yields are expressed as ppm of CG formed per ppm of VOC reacted so that CG concentrations follow the CAMx convention for gases and are in ppm.  The physical properties of CG/SOA pairs are shown in Table 5-4.  The SOAs formed from the CGs are in units of µg/m$^3$ as are all other aerosol species.

Studies are starting to elucidate mechanisms for polymerization reactions in organic aerosol phases.  Polymerization increases the molecular weight of the condensed aerosol and reduces the volatility.  Detailed descriptions of polymerization will likely depend upon the chemical composition of the organic and inorganic aerosol phases (e.g., aerosol acidity).  Based on

limited available data we assumed that the SOA polymerized to a non-volatile form (i.e., moved permanently to the aerosol phase) with a lifetime of about 1 day (Kalberer et al., 2004). Polymerization slowly forms organic aerosol polymers called SOPA (anthropogenic) and SOPB (biogenic).

Uptake of nitric acid on mineral dust particles is one of the pathways of particle nitrate formation. For example, calcium in soil dust particles reacts with nitric acid to form calcium nitrate. Based on IMPROVE observations, we estimate 3.5% mass fraction of calcium in fine dust particles (FCRS), which is assumed to be fully neutralized by nitrate. Since the current ISORROPIA implementation in CAMx does not consider mineral cations other than sodium, nitrate uptake by calcium in soil dust is calculated external to ISORROPIA. CAMx outputs total particulate nitrate, i.e., the sum of particle nitrate determined by ISORROPIA and calcium nitrate.

Table 5-5 shows the aerosol species that can be included with the CF scheme. Some species must be present for this scheme ("Mandatory Species") to establish linkages between gas and aerosol phase chemistry. Other species are optional (meaning that they can be removed from the chemistry parameters input file), except that sodium and chloride must always be present or absent together (i.e., one cannot be present without the other). If sodium and chloride are not modeled then default background values are used within CAMx.

In the CMU scheme, CRST is used to identify all primary inert material, which replaces the CF species of FPRM, FCRS, CPRM, and CCRS in Table 5-5. Individual aerosol species names specify both the constituent and the size section using a set naming convention, e.g., PSO4_1 refers to particle sulfate in the section 1. The CMU scheme requires that the complete list of all aerosol species be present in the chemistry parameters file (i.e., no aerosol species are optional).

**Table 5-5.  List of PM species for the CAMx CF aerosol option.**

| Internal Label | Name | Mandatory Species |
|:---:|:---|:---:|
| PSO4 | Sulfate | X |
| PNO3 | Particulate Nitrate | X |
| PNH4 | Particulate Ammonium | X |
| PH2O | Aerosol Water Content | X |
| SOA1-2 | Anthropogenic SOA (see Tables 5-3, 5-4) | X |
| SOA3-7 | Biogenic SOA (see Table 5-3, 5-4) | X |
| SOPA | Polymerized anthropogenic SOA | X |
| SOPB | Polymerized biogenic SOA | X |
| NA | Sodium | |
| PCL | Particulate Chloride | |
| POA | Primary Organic Aerosol | |
| PEC | Primary Elemental Carbon | |
| FPRM | Fine Other Primary (diameter$\leq$2.5 µm) | |
| FCRS | Fine Crustal (diameter$\leq$2.5 µm) | |
| CPRM | Coarse Other Primary | |
| CCRS | Coarse Crustal | |

### 5.2.3  Aerosol Sectional Approach

Unlike the CF scheme, where each species is represented by a single particle size, the CMU scheme institutes an additional step to distribute the bulk aerosol concentrations from the aqueous/aerosol chemistry modules into each size bin.  For inorganic aerosol species, ISORROPIA yields the bulk aerosol composition at equilibrium. The aerosol size distribution is then determined by distributing the change in aerosol mass during the time step into each size bin using a weighting factor (Pandis et al., 1993).  The fraction $f_{i,k}$ of total flux of species $i$ between gas and aerosol phases that condenses onto or evaporates from an aerosol size section $k$ is given by,

$$ f_{i,k} = \frac{2\pi N_k d_k D_i \left(c_i - c_i^{eq}\right)/(\beta_k + 1)}{\sum_k 2\pi N_k d_k D_i \left(c_i - c_i^{eq}\right)/(\beta_k + 1)}, $$

where $N_k$ and $d_k$ are the number and mean diameter of particles in the section $k$, respectively, $D_i$, $c_i$, and $c_i^{eq}$ are the diffusivity, bulk gas-phase concentration, and equilibrium concentration at the particle surface of species $i$, respectively, $\beta_k = 2\lambda/ad_k$, $\lambda$ is the mean free path of air, and $a$ is the accommodation coefficient (Pandis et al., 1993).  Assuming that $c_i^{eq}$ is independent of particle size, the fraction is reduced to,

$$ f_{i,k} = \frac{N_k d_k /(\beta_k + 1)}{\sum_k N_k d_k /(\beta_k + 1)} = f_k. $$

The above weighting factor then depends on the surface area only.

For organic aerosols, SOAP calculates the bulk equilibrium composition.  Using the pseudo-ideal solution assumption (Strader et al., 1999), the effect of chemical composition of the particle can be incorporated into the weighting factor:

$$ f_{i,k} = \frac{N_k d_k \left(c_i - x_{i,k} c_i^*\right)/(\beta_k + 1)}{\sum_k N_k d_k \left(c_i - x_{i,k} c_i^*\right)/(\beta_k + 1)}. $$

where $x_{i,k}$ is the mole fraction of species $i$ in the section $k$ and $c_i^*$ is the effective saturation concentration of species $i$.  Since the fraction determines the composition of each size section, the above equation should be solved iteratively at each time step.  Assuming that the chemical composition changes slowly during a time step, however, the mole fractions can be approximated with those from the previous time step (Koo et al., 2003).

For cloud/fog droplets, RADM is used to calculate sulfate and nitrate formation in the bulk aqueous phase.  The added mass is then distributed into each size bin by a weighting factor which is based on the size-resolved aqueous chemistry model simulation results (Fahey and Pandis, 2001).

In addition, mathematical descriptions of nucleation and coagulation have been added to the CMU scheme.  The nucleation model employs the nucleation rate parameterization proposed by Russell et al. (1994).  The model assumes a linear sulfuric acid vapor concentration variation for the given time step of the aerosol module based on the initially available sulfuric acid and assigns all the nucleated mass to the first section of the distribution.  The coagulation rate of the aerosol particles is modeled according to Seinfeld and Pandis (1998).  A high-resolution distribution is used for the coagulation calculations by subdividing each section of the original distribution into 3 additional sections.

## 5.3  Mercury Chemistry

Mercury exists in the atmosphere as elemental mercury, Hg(0), and oxidized mercury, Hg(II) (Schroeder and Munthe, 1998).  Hg(II) can be inorganic (e.g., mercuric chloride, $HgCl_2$) or organic (e.g., methyl mercury, MeHg).  It can also be present as particulate mercury (e.g., mercuric oxide, HgO, or mercury sulfide, HgS).  In the global atmosphere, Hg(0) is the dominant form.  Hg(II) typically constitutes a few percent of total mercury and is predominantly in the gas phase.  MeHg concentrations in the atmosphere are negligible, about a factor of 10 to 30 lower than Hg(II) concentrations, based on analysis of precipitation samples conducted by Frontier Geosciences, Inc. (e.g., Seigneur et al., 1998).  However, Hg(II) becomes methylated in water bodies, where it can bioaccumulate in the food chain.  Hg(0) is sparingly soluble and is not removed significantly by wet deposition; its dry deposition velocity is also believed to be low. As a result, Hg(0) has a long atmospheric lifetime, on the order of several months, that is governed by its oxidation to Hg(II).  On the other hand, Hg(II) is quite soluble; it is consequently removed rapidly by wet and dry deposition processes.  Particulate mercury, Hg(p), is mostly present in the fine fraction of particulate matter ($PM_{2.5}$), although some Hg(p) may be present in coarse PM (e.g., Landis and Keeler, 2002).

Known transformations among inorganic mercury species include the gas-phase oxidation of Hg(0) to Hg(II), the aqueous-phase oxidation of Hg(0) to Hg(II), the aqueous-phase reduction of Hg(II) to Hg(0), various aqueous-phase equilibria of Hg(II) species, and the adsorption of Hg(II) to PM in both the gas-phase and aqueous-phase.  The inorganic mercury chemistry modules implemented in CAMx are based on our current knowledge of these transformations.  However, it should be noted that our knowledge of mercury chemistry continues to evolve as new laboratory data become available, and the Hg chemical kinetic mechanisms in CAMx and other models that treat the atmospheric fate of mercury will need to be revised accordingly.

Below, we provide additional details on the gas- and aqueous-phase mercury chemistry mechanisms implemented in CAMx, and the implementation approach.

### 5.3.1  Gas-Phase Chemistry

The gas-phase transformations include the oxidation of Hg(0) to Hg(II) by ozone ($O_3$) (Hall, 1995),  hydrogen peroxide ($H_2O_2$) (Tokos et al., 1998)  hydroxyl radicals (OH) (Sommar et al., 2001; Pal and Ariya, 2003; 2004), bromine (Br) (Ariya et al., 2002), and hypobromite (BrO) (Raofie and Ariya, 2003).  The oxidation of Hg(0) by $O_3$, $H_2O_2$, and OH are given by the following three reactions:

$$Hg(0)\,(g) + O_3\,(g) \rightarrow Hg(II)\,(g), \quad k = 3 \times 10^{-20}\ cm^3\ molec^{-1}s^{-1}$$

$$Hg(0)\,(g) + H_2O_2\,(g) \rightarrow Hg(OH)_2\,(g), \quad k = 8.5 \times 10^{-19}\ cm^3\ molec^{-1}s^{-1}$$

$$Hg(0)\,(g) + OH\,(g) \rightarrow Hg(OH)_2\,(g), \quad k = 8 \times 10^{-14}\ cm^3\ molec^{-1}s^{-1},$$
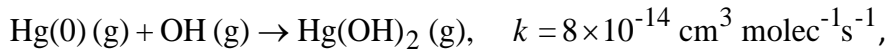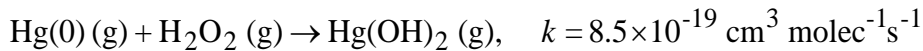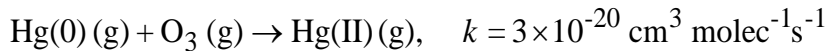
while oxidation by Bromine is based on a sequence of 5 reactions (Seigneur and Lohman, 2008):

$$Hg(0)\,(g) + Br\,(g) \rightarrow HgBr\,(g), \quad k_1 = 3.6 \times 10^{-13}\ P\left(\frac{T}{298}\right)^{-1.86}\ cm^3\ molec^{-1}s^{-1}$$

$$HgBr\,(g) \rightarrow Hg(0)\,(g), \quad k_2 = 3.9 \times 10^9\ \exp\left(\frac{-8537}{T}\right)\ s^{-1}$$

$$HgBr\,(g) + Br\,(g) \rightarrow HgBr_2\,(g), \quad k_3 = 2.5 \times 10^{-10}\left(\frac{T}{298}\right)^{-0.57}\ cm^3\ molec^{-1}s^{-1}$$

$$HgBr\,(g) + OH\,(g) \rightarrow HgBrOH\,(g), \quad k_4 = 2.5 \times 10^{-10}\left(\frac{T}{298}\right)^{-0.57}\ cm^3\ molec^{-1}s^{-1}$$

$$Hg(0)\,(g) + BrO\,(g) \rightarrow Hg(II)\,(g), \quad k_5 = 1 \times 10^{-15}\ cm^3\ molec^{-1}s^{-1}$$
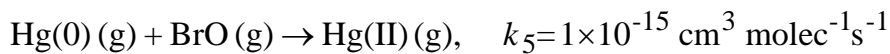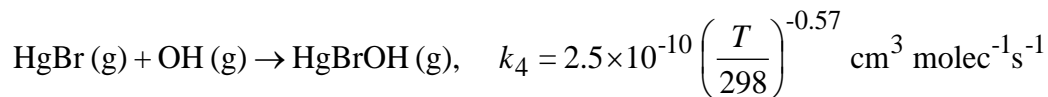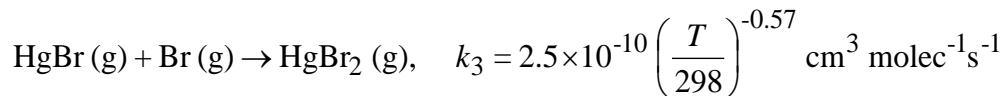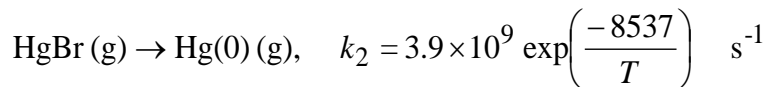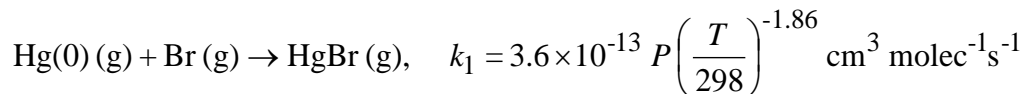
The reaction rate constants provided above are for temperatures in the range of 20 to 25°C; no temperature dependence information is available.  For the bromine reactions, $T$ is the temperature in degrees Kelvin, and $P$ is the pressure in atmospheres. The five reactions are treated as a single reaction, with an effective Hg(0) first-order rate constant that is a function of the individual reaction rates and the concentrations of Br, BrO and OH based on the assumption that Br, BrO and OH concentrations don't change by their reactions with mercury.  This treatment is similar to that of Holmes et al. (2006), who considered the oxidation of Hg(0) by bromine atoms with a set of three reactions. The effective first-order rate constant is calculated by the following expression:

$$k_{eff} = \frac{k_1[Br](k_3[Br] + k_4[OH])}{k_2 + k_3[Br] + k_4[OH]} + k_5[BrO] \quad s^{-1}$$

### 5.3.2  Adsorption of Hg(II) on PM

In the first implementation of mercury in CAMx, Hg(II) adsorption on PM was considered only in the aqueous phase (see below), using an adsorption coefficient derived from available experimental data (Seigneur et al., 1998; Ryaboshapko et al., 2002).  It is essential to also consider the adsorption of gaseous Hg species to PM because gas/particle conversion also affects Hg deposition (Lindberg et al., 2007).  Rutter and Schauer (2007a) reported results of laboratory work measuring the adsorption of reactive gaseous mercury (RGM) to atmospheric and synthetic particles as a function of temperature.  Their experimental results suggest that surface area rather than PM mass controls the partitioning process.  They reported three surface-area adsorption coefficients for urban PM (collected in Milwaukee, WI, and Riverside,

CA), ammonium sulfate and adipic acid, respectively. They expressed the surface-area adsorption coefficient ($K_{sa}$) as follows:

$$K_{sa} = Hg_{p,ads} / (RGM \cdot A_{sp} \cdot PM)$$

where $K_{sa}$ is in $m^3 m^{-2}$, $Hg_{p,ads}$ and RGM are in pg $m^{-3}$, $A_{sp}$ is the specific surface area of ambient PM in $m^2 \mu g^{-1}$ and PM is the ambient urban PM concentration in $\mu g\ m^{-3}$. Here, $Hg_{p,ads}$ refers only to the adsorbed RGM, i.e., it does not include non-volatile primary particulate mercury. Rutter and Schauer (2007a) also found that the $K_{sa}$ obtained for urban PM falls between that of ammonium sulfate (more RGM adsorption) and adipic acid (less RGM adsorption). Their laboratory experiments lead to the following value for $K_{sa}$ as a function of temperature (in K) for adsorption to urban PM:

$$K_{sa} = 10^{(4250/T - 10)} \qquad (1)$$

Rutter and Schauer's (2007b) experimental results also show a ten-fold increase in adsorption of RGM to sodium chloride compared to ammonium sulfate and organic particulate compounds (a larger increase was observed for sodium nitrate). Thus, the adsorption coefficient for RGM adsorption to sea-salt is about 10 times that for urban PM:

$$K_{sa} = 10^{(4250/T - 9)} \qquad (2)$$

Following the approach used in Vijayaraghavan et al. (2008), we treat all non-sea-salt PM as urban PM for simplicity and use Equation (1) to simulate RGM adsorption to all non-sea-salt PM. The adsorption to sea-salt PM is calculated using Equation (2). Thus, the effective adsorption coefficient for each aerosol size section is calculated as:

$$K_{sa,eff} = 10^{(4250/T - 9)} F_{ss} + 10^{(4250/T - 10)} (1 - F_{ss})$$

where $F_{ss}$ is the fraction of sea-salt in that size section. In the CAMx implementation, we assume that RGM is adsorbed on primary fine and coarse PM.

### 5.3.3 Aqueous-Phase Chemistry

The aqueous-phase chemistry includes the reduction of Hg(II) to Hg(0) via reaction with hydroperoxy radicals ($HO_2$) and by the formation of the sulfite complexes (at low HCl concentrations), $HgSO_3$ and $Hg(SO_3)_2^{2-}$, as well as the oxidation of Hg(0) to Hg(II) by dissolved $O_3$, OH, and $Cl_2$. Adsorption of Hg(II) species on atmospheric particulate matter (PM) is simulated using an adsorption coefficient (K = 34 L $g^{-1}$) recommended by Seigneur et al. (1998). The relevant reactions are listed below. Note that the gas-liquid equilibria and ionic equilibria of the non-mercury species (e.g., $SO_2$, $O_3$) involved in the mercury aqueous-phase chemistry are not shown here, since they are identical to those in the other CAMx mechanisms.

### 5.3.2.1  Gas-liquid Equilibria

$$\text{Hg}(0)\,(g) \Leftrightarrow \text{Hg}(0)\,(aq), \quad K = 0.11\,\text{M atm}^{-1} \text{ (Sanemasa, 1975; Clever et al., 1985)}$$

$$\text{HgCl}_2\,(g) \Leftrightarrow \text{HgCl}_2\,(aq), \quad K = 1.4 \times 10^6\,\text{M atm}^{-1} \text{ (Lindqvist and Rodhe, 1985)}$$

$$\text{Hg(OH)}_2\,(g) \Leftrightarrow \text{Hg(OH)}_2\,(aq), \quad K = 1.2 \times 10^4\,\text{M atm}^{-1} \text{ (Lindqvist and Rodhe, 1985)}$$
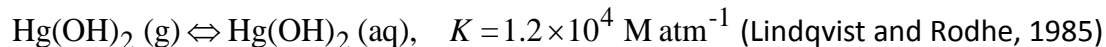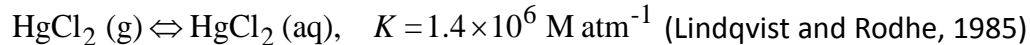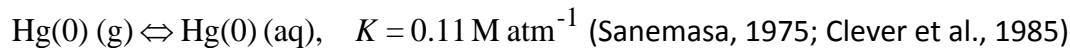
The Henry's Law constants listed above are for temperatures in the range of 20 to 25$^\text{o}$C. Temperature dependence information is available for the Hg(0) Henry's Law constant but the validity of this information for temperatures below 0$^\text{o}$C is not established.

### 5.3.2.2  Aqueous-phase Equilibria

$$\text{HgCl}_2\,(aq) \Leftrightarrow \text{Hg}^{2+} + 2\text{Cl}^-, \quad K = 10^{-14}\,\text{M}^2 \text{ (Sillen and Martel, 1964)}$$

$$\text{Hg(OH)}_2\,(aq) \Leftrightarrow \text{Hg}^{2+} + 2\text{OH}^-, \quad K = 10^{-22}\,\text{M}^2 \text{ (Sillen and Martel, 1964)}$$

$$\text{Hg}^{2+} + \text{SO}_3^{2-} \Leftrightarrow \text{HgSO}_3, \quad K = 2.1 \times 10^{13}\,\text{M}^{-1} \text{ (van Loon et al., 2001)}$$

$$\text{HgSO}_3 + \text{SO}_3^{2-} \Leftrightarrow \text{Hg(SO}_3)_2^{2-}, \quad K = 1 \times 10^{10}\,\text{M}^{-1} \text{ (van Loon et al., 2001)}$$
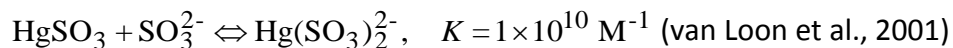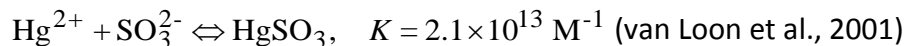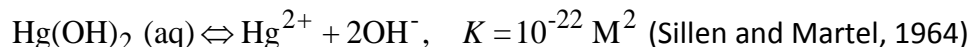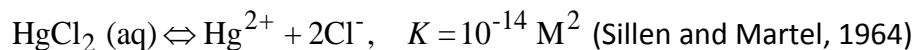
### 5.3.2.3  Adsorption of Hg(II) on PM in the Aqueous Phase

$$\text{Hg(II)}\,(aq) \Leftrightarrow \text{H(II)}\,(p), \quad K = 34\,\text{L g}^{-1} \text{ (Seigneur et al., 1998)}$$

### 5.3.2.4  Aqueous-phase Kinetics

$$\text{Hg}(0)\,(aq) + \text{O}_3\,(aq) \rightarrow \text{Hg}^{2+}, \quad k = 4.7 \times 10^7\,\text{M}^{-1}\text{s}^{-1} \text{ (Munthe, 1992)}$$

$$\text{Hg}(0)\,(aq) + \text{OH}\,(aq) \rightarrow \text{Hg}^{2+}, \quad k = 2 \times 10^9\,\text{M}^{-1}\text{s}^{-1} \text{ (Lin and Pehkonen, 1997)}$$

$$\text{HgSO}_3\,(aq) \rightarrow \text{Hg}(0)\,(aq), \quad k = 0.0106\,\text{s}^{-1} \text{ (van Loon et al., 2000)}$$

$$\text{Hg(II)}\,(aq) + \text{HO}_2\,(aq) \rightarrow \text{Hg}(0)\,(aq), \quad k = 1.7 \times 10^4\,\text{M}^{-1}\text{s}^{-1} \text{ (Pehkonen and Lin, 1998)}$$

$$\text{Hg}(0)\,(aq) + \text{HOCl}\,(aq) \rightarrow \text{Hg}^{2+}, \quad k = 2.09 \times 10^6\,\text{M}^{-1}\text{s}^{-1} \text{ (Lin and Pehkonen, 1998)}$$

$$\text{Hg}(0)\,(aq) + \text{OCl}^- \rightarrow \text{Hg}^{2+}, \quad k = 1.99 \times 10^6\,\text{M}^{-1}\text{s}^{-1} \text{ (Lin and Pehkonen, 1998)}$$
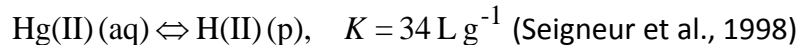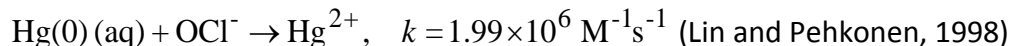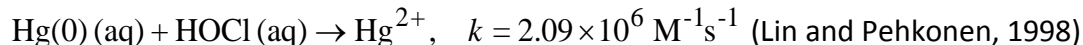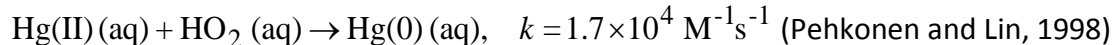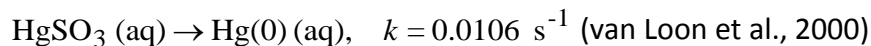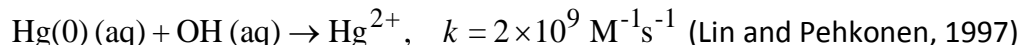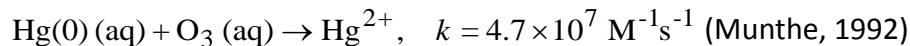
In the last two reactions listed above, HOCl and OCl$^-$ come from the dissolution and subsequent dissociation of molecular chlorine (Cl$_2$).  Note that Hg(II) (aq) refers to all divalent Hg species in solution (i.e., Hg$^{2+}$ + HgCl$_2$(aq) + Hg(OH)$_2$(aq) + HgSO$_3$ + Hg(SO$_3$)$_2^{2-}$).  The rate constants listed for the aqueous-phase kinetics are for temperatures in the range of 20 to 25$^\text{o}$C.  Temperature dependence information is available for the HgSO$_3$ reduction reaction.

As mentioned previously, the gas- and aqueous-phase Hg transformations presented above represent the state of the science from a decade ago (Ryaboshapko et al., 2002; Seigneur et al., 2001a, 2003a) and our knowledge of mercury chemistry continues to evolve.  For example,

Gardfeldt and Johnson (2003) challenged the aqueous-phase reduction of Hg(II) to Hg(0) by dissolved $HO_2$, suggesting that this pathway is unimportant.  There also seems to be some circumstantial evidence of reduction of Hg(II) to Hg(0) in power plant plumes from various experimental studies that is not accounted for in current treatments of Hg chemistry (e.g., Edgerton et al., 2001; Seigneur et al., 2001b).  Additional details are provided in a scoping study for mercury deposition conducted for the Midwest Regional Planning Organization by Seigneur et al. (2003b).

### 5.3.4  Implementation Approach

The approach used to implement the mercury transformation pathways, discussed above, into CAMx is based on the assumption that the mercury species concentrations are much smaller than those of the species with which they react.  Thus, the concentrations of the non-mercury species can be assumed to be constant during the mercury chemistry calculations and analytical solutions are available for both the gas-phase and aqueous-phase conversions.

The mercury chemistry discussed in the previous sections requires the concentrations of the following non-mercury species: $O_3$, $H_2O_2$, OH, $SO_2$, $HO_2$, $Cl_2$, HCl, Br, BrO and atmospheric particulate matter (PM).  The concentrations of most of these species are available from CAMx.  However, $Cl_2$, Br, and BrO are not explicitly simulated because the emissions data required to model these species are generally inadequate or unavailable.  Thus, we specify typical vertical profiles of $Cl_2$, Br, and BrO concentrations.  The $Cl_2$ concentrations are prescribed to be non-zero over oceans and zero elsewhere.  Also, daytime $Cl_2$ concentrations are lower than nighttime values to account for the fact that $Cl_2$ is photolyzed during the day.  The zenith angle is used for the determination of night/day.  A 2-D array of integer values (1 if ocean, 0 if not) is used to determine if the grid column is predominantly over ocean.  This array is initialized at the beginning of the simulation from an input file and is specific for the modeling domain and grid.  For Br and BrO, vertical profiles over land and ocean are prescribed, with higher values over ocean than over land.  During the night, the concentrations of these species are assumed to be zero, since the photolysis of Br2 is the primary source for these radicals.

The mercury aqueous-phase chemistry module also requires the specification of cloud liquid water content (LWC) and cloudwater pH.  Both these variables are available from CAMx – the mercury aqueous-phase chemistry module is invoked after the CAMx PM aqueous-phase chemistry calculations are performed, so the cloudwater pH has already been calculated.  Note that the PM aqueous-phase module (based on the RADM aqueous-phase chemistry module that is also used in Models-3/CMAQ) does not explicitly simulate the cloud chemistry of OH and $HO_2$ radicals.  The concentrations of these radicals can be reduced by their heterogeneous chemistry within clouds (e.g., Jacob, 2000; Jaegle et al., 2001).  In the CAMx implementation, we account for this by reducing the concentrations of OH and $HO_2$ radicals by factors of 2 and 10, respectively.

### 5.3.5  Chemistry Parameters for Mercury

The mercury chemistry module requires total PM concentrations, so mercury can only be modeled in conjunction with PM chemistry.  In CAMx, PM chemistry is modeled using

Mechanisms 5, 6 and 7. Mercury chemistry is selected by including mercury species among the list of modeled species for these three mechanisms. The CAMx mercury species names are:

HG0 – elemental gaseous mercury, or Hg(0)
HG2 – reactive gaseous mercury, or Hg(II)
HGP – primary particulate mercury, or Hg(P)
HGIIP – reactive gaseous mercury, or Hg(II) adsorbed onto fine PM
HGIIPC – reactive gaseous mercury, or Hg(II) adsorbed onto coarse PM

CAMx requires that all five or none of these species be included in a simulation. Therefore, mercury chemistry is not required for PM modeling, but if mercury chemistry is selected then all five mercury species must be modeled. All of the rate constants and equilibrium constants for the mercury chemistry module are hard-coded and so no mercury reaction rate data are included in the chemistry parameters input file (see Section 3). This is similar to the RADM aqueous chemistry and ISORROPIA inorganic aerosol equilibrium modules.

Several physical properties of the mercury species must be specified on the chemistry parameters file (see Figure 3-3a). The physical properties specified for the gas species (Henry's Law, molecular weight, surface reactivity) influence the deposition characteristics. The Henry constant for HG2 is assumed to be similar to that of $HNO_3$ because these two gases have similar solubility. The HG2 species represents $HgCl_2$ and $Hg(OH)_2$; the Henry constant for the former is $1.4 \times 10^6$ M atm$^{-1}$ and for the latter it is $1.2 \times 10^4$ M atm$^{-1}$. The surface resistance factor is set to zero for strong acids, such as $HNO_3$, that have a strong tendency to stick to surfaces – this forces the surface resistance calculated in the dry deposition algorithms to zero. The reactivity parameter for HG2 is set to 0, as for $HNO_3$.

The dry deposition of HG0 is set to zero by choosing a very low Henry constant (similar to CO). This is based on the assumption that natural emissions and dry deposition of HG0 balance each other over the modeling domain. This assumption is justified by the fact that the atmospheric lifetime of HG0 (about 1 year) greatly exceeds its residence time (days to weeks) within a regional modeling domain. If natural emissions of HG0 are not included in the mercury emissions inventory, the dry and wet deposition of HG0 should be zero by setting a Henry constant of smaller than $1 \times 10^{-8}$ M atm$^{-1}$. However, if natural emissions of Hg(0) are used in the CAMx simulation, the Henry constant should be set to 0.111 with a temperature factor of -4970 K (Clever et al., 1985).

## 5.4 Simple Chemistry Via Mechanism 10

CAMx offers three different chemical mechanisms for ozone and particulate matter modeling. However, the minimum level of chemistry is the CB05 mechanism for ozone (Table 5-1), which requires significant effort to prepare all of the input data, particularly with regard to emissions. There are many cases when air pollution problems could be investigated with a much simpler chemistry scheme. An example of this would include modeling $SO_2$ from a few specific sources over a relatively small region, and treating conversion to sulfate by assuming a representative decay rate. An approach was necessary to provide a simple and flexible scheme that can be

used for modeling chemical reactions other than the ozone or secondary PM reactions treated by the full-science mechanisms.

The new simple chemistry scheme is selected by specifying a mechanism ID of 10 in the chemistry parameters input file.  The specific chemical reactions to be modeled must be set in the subroutine `CAMx/chem10.f` in the source code directory.  The user must modify this subroutine to implement whatever reactions are desired.  Follow the guidelines for implementing reactions that are included in the subroutine.  This approach requires some knowledge from the user, but also provides complete flexibility in implementing reactions.

The simple chemistry has been tested using a modeling database for primary PM species in Cairo, Egypt (personal communication from Mr. Usama Faramawy, Egyptian Environmental Affairs Agency).  Results of the tests are shown in Figures 5-2 and 5-3.  A simple chemical reaction was implemented where the species PMT decayed to PM2 with a first-order rate constant of 10% per hour.  These species were selected because PMT has high emissions and PM2 has low emissions.  This modeling is not intended to represent any actual chemical reactions for PM species in Cairo, but rather is just a hypothetical testing scenario.  The expected result is that the chemical reaction will lower the concentration of PMT and raise the concentration of PM2.  Figure 5-2 shows the expected result, that the PMT concentration is lowered by the reaction.  The reduction in PMT becomes proportionately greater at longer downwind distances because there has been more time for reaction to take place.  Figure 5-3 shows the complementary increase in PM2 due to chemical production.

**No Chemical Decay**
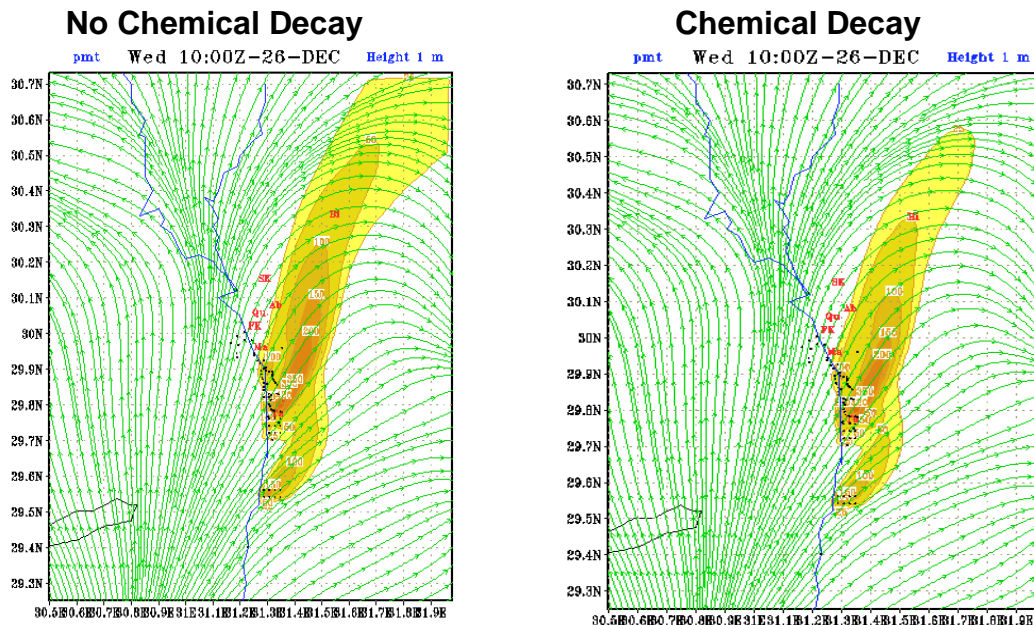


**Chemical Decay**



**Figure 5-2.  Impact of chemical decay on the concentration of the donor species PMT.**

**No Chemical Production**



**Chemical Production**
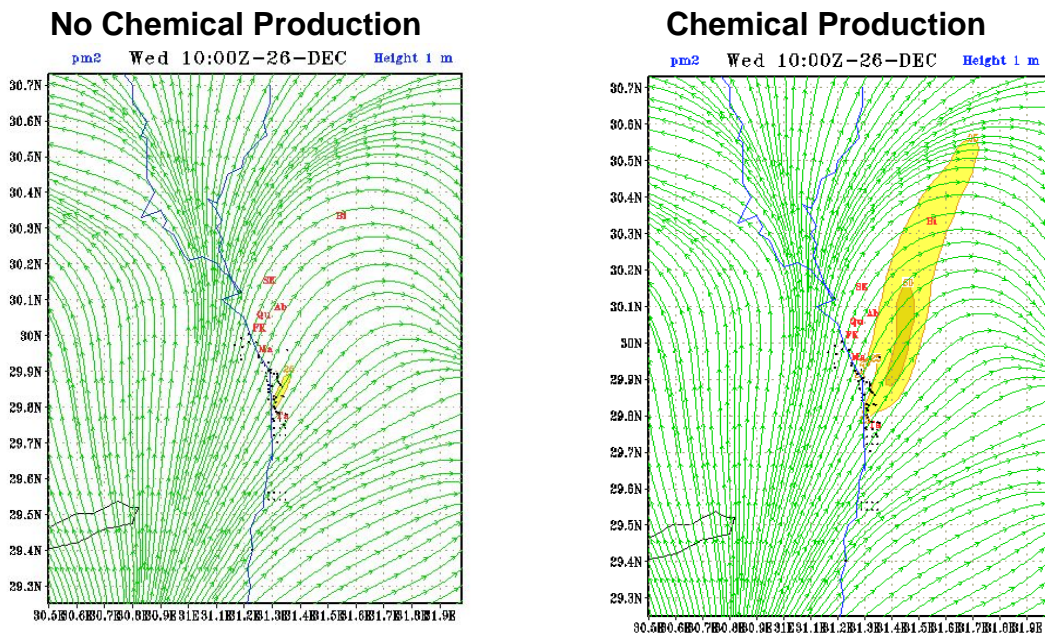


**Figure 5-3.  Impact of chemical production on the concentration of the recipient species PM2.**

## 6.  PLUME-IN-GRID SUBMODEL

Photochemistry is a highly non-linear problem because chemical reaction rates among most compounds depend upon their ambient concentrations.  In Eulerian air quality models, ambient concentrations depend on how well the modeling grid resolves emissions, transport, and chemical history.  Thus, grid resolution plays a vital role in the ability of the model to properly characterize photochemical conditions.  Increasing resolution should in theory lead to a better model as the time/space discretization tends toward a continuum.  However, practical and theoretical considerations suggest that the lower limit on horizontal grid spacing is about 1000 meters for Eulerian air quality models such as CAMx.  Nevertheless, even higher resolution is often necessary to adequately simulate chemistry within concentrated point source plumes.

As a result, many modern Eulerian models contain a Plume-in-Grid sub-model that tracks individual plume segments (or puffs) in a Lagrangian sense, accounting for plume-scale dispersion and chemical evolution, until such time as puff mass can be adequately represented within the larger grid model framework.  At this point the puff mass is added to the grid system as a virtual source, and that mass is then carried by the core grid model processes.  It is important to understand that the inclusion of a Lagrangian puff model within an Eulerian grid model is a forced construct.  The formulations of the two modeling approaches are fundamentally different and there is no theoretically "correct" methodology.  This explains the variety of Plume-in-Grid methodologies that are in use today.

There are two schools of thought regarding the appropriate times at which to transfer puff mass into the host model grid system.  The first primarily focuses on the physical size of puffs relative to grid cells.  It is assumed that once puffs are large enough to be adequately resolved by a grid, their mass should be added to the host cell.  The two principle problems associated with this approach are deciding what the appropriate size criteria are to be, and how to distribute puff mass into the grid system.  The second school focuses on the chemical maturity of the puffs (Gillani and Pleim, 1996), and the potential performance effects of dumping immature plume mixtures into a grid system.  The main problem seen with this approach is identifying chemically mature plume mixtures within an ever-evolving puff relative to ever-evolving grid chemistry.  Puffs may reach a stage of chemical maturity after very long simulation periods (say 24 hours), however it is unrealistic to assume that puffs will maintain physical coherence over such a long period given the cumulative effects of wind shears and mixing gradients.  In summary, neither of the above approaches is completely satisfactory and we strongly believe that further research is needed to develop new approaches to PiG modeling that adequately address <u>both</u> chemical maturity and physical size considerations.

Two CAMx Plume-in-Grid (PiG) approaches are available that provide different levels of chemical complexity.  Both approaches share common design features for puff initialization, puff structure, transport, and growth.  They deviate in how they treat chemistry and when they transfer mass from puffs to grid cells.  This section details the structure and functionality of both options.

The first PiG approach is aimed at treating the early chemical evolution of large $NO_x$ plumes when mostly inorganic gas-phase reactions are operative. The method is called the Greatly Reduced Execution and Simplified Dynamics (GREASD) PiG. The streamlining employed in this version was based upon our experiences in developing, utilizing, and studying the responses of more detailed PiG algorithms for large NOx plumes. The GREASD PiG model works with the Ozone and Particulate Source Apportionment Technology (OSAT/PSAT). This is possible because of the simplified approach used in GREASD PiG and because compatibility with the source apportionment Probing Tools was an explicit design objective.

The second approach treats the full suite of gas-phase photochemistry for all types of point sources and so by necessity incorporates much more chemical complexity than the first. This CAMx plume treatment is called the Incremental Reactions for Organics and NOx (IRON) PiG. Chemical processes are simulated within each plume segment using an "incremental chemistry" approach, whereby puffs carry the incremental contributions of the puff relative to the grid concentrations. Incremental puff concentrations can be positive or negative, depending upon the species and stage of plume evolution. A similar chemistry approach is used in the SCICHEM Lagrangian model (EPRI, 2000). IRON PiG supports the Reactive Tracer (RTRAC) Probing Tool. However, the incremental chemistry technique in IRON PiG is sufficiently complex as to prohibit the implementation of source apportionment Probing Tools. Furthermore, IRON PiG does not treat PM.

## 6.1  CAMx PiG Formulation

### 6.1.1  Basic Puff Structure and Diffusive Growth

Both GREASD and IRON PiG sub-models share a common physical structure and growth algorithm. A stream of plume segments (puffs) is released from a designated point source. Each puff possesses a longitudinal length and directional orientation defined by the separation of a leading and a trailing point. Initial separation of these points is determined by the wind vector at final plume rise. Each point is then subsequently and independently transported through the gridded wind fields, which directly accounts for puff stretching and changes to centerline orientation due to deforming shears. The official "position" of each puff is defined by the center point of each puff between the endpoints. This position defines the grid cell in which the puff resides for the calculation of diffusion and chemistry.

Like other puff models, the shape of each puff is characterized by a spread tensor, which is defined from a set of Gaussian standard deviations (so-called "sigmas") along the three spatial axes ($\sigma_x$, $\sigma_y$, $\sigma_z$). Diffusive growth is defined by the growth in these sigma values. The total cross-sectional width extends $\pm 1.5\sigma_y$ from puff centerline. Similarly, the total cross-sectional depth extends $\pm 1.5\sigma_z$ from puff centerline (with limits placed on depth by the ground and by capping stable layers aloft). The total longitudinal length is the distance between the puff endpoints with an additional $\pm 1.5\sigma_x$ added in each direction. Horizontal area and total volume are calculated using the formulae for an ellipse. Figure 6-1 presents a schematic representation of each puff in horizontal cross-section.
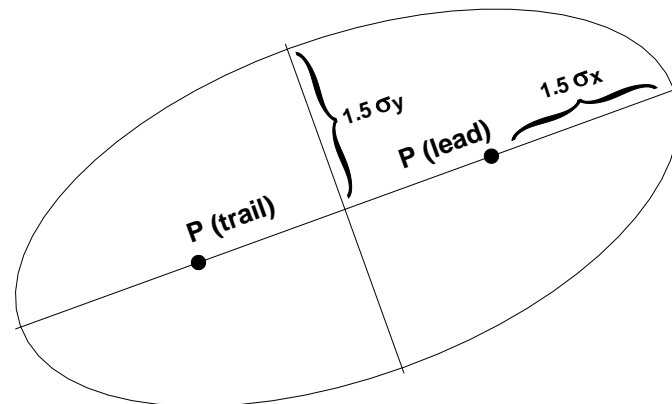
**Figure 6-1.  Schematic representation of CAMx PiG puff shape in the horizontal.  Directional orientation of the puff is arbitrary, and evolves during the age of the puff according to wind direction, shears and diffusive growth along its trajectory.**

We have developed an explicit solution approach for puff growth that shares SCICHEM theory and concepts (EPRI, 2000), but includes some simplifications.  SCICHEM solves predictive spatial moment equations with second-order closure that relate the evolution of the puff spread tensor ($\sigma_{ij}=\sigma_i\times\sigma_j$) to resolved mean shears and turbulent velocity statistics.  The Reynolds-averaged second-moment transport equation is given as

$$\frac{d\sigma_{ij}}{dt} \quad = \quad \sigma_{ik}\frac{\partial\overline{u}_j}{\partial x_k} + \sigma_{jk}\frac{\partial\overline{u}_i}{\partial x_k} + \frac{\left\langle x_i'\overline{u_j'c'}\right\rangle}{Q} + \frac{\left\langle x_j'\overline{u_i'c'}\right\rangle}{Q}$$

where $\overline{u}$ is the mean wind vector component, the primed values represent turbulent fluctuations from the mean, and the angle brackets denote integrals over space.  The Reynolds averaging process always introduces higher-order fluctuation correlations, and this is given by the turbulent flux moments $\left\langle x'\overline{u'c'}\right\rangle$, where $\overline{u'c'}$ represents the turbulent flux of concentration.  It is these last two diffusion terms that SCICHEM solves in its second-order closer scheme.

For sub-puff scale turbulence, SCICHEM employs the restriction that the only off-diagonal component of $\left\langle x'\overline{u'c'}\right\rangle$ to be considered is the symmetric horizontal term ($i=x$, $j=y$), and then only for the large-scale (meso to synoptic) contribution to puff deformation when puff scale reaches such dimensions.  In CAMx, we ignore this off-diagonal flux moment term altogether since puff mass is ultimately introduced to the grid when puff size is at the grid scale (1-50 km in practically all applications), and thus puffs never reach spatial scales at which this term becomes important.  SCICHEM also makes the assumption that the horizontal turbulence is

isotropic, $\langle x'\overline{u'c'}\rangle = \langle y'\overline{v'c'}\rangle$. This results in a single diffusivity equation for both $x$ and $y$ directions, and a single diffusivity for the $z$ direction:

$$K_x = K_y = \frac{\langle y'\overline{v'c'}\rangle}{Q}$$

$$K_z = \frac{\langle z'\overline{w'c'}\rangle}{Q}$$

In our approach for CAMx, we have adopted the SCICHEM second-order tendency equations to model the time-evolution of puff turbulent flux moments (represented by diffusivities $K_x=K_y$ and $K_z$) and their contribution to the evolution of puff spread (represented by the diagonal components of the puff spread tensor, $\sigma_x^2$, $\sigma_y^2$ and $\sigma_z^2$). Puff spread is defined for puff depth ($\sigma_z$), puff width ($\sigma_y$), and puff length ($\sigma_x$). We account for the effects of wind shears in the evolution of lateral and longitudinal spread, but assume that the evolution of vertical spread is solely the result of turbulent fluxes.

The resulting two Reynolds-averaged second-moment transport equations for CAMx PiG are:

$$\frac{d\sigma_z^2}{dt} \;=\; 2K_z$$

$$\frac{d\sigma_y^2}{dt} \;=\; 2\sigma_y^2 D \;+\; 2\sigma_y\sigma_z S_y \;+\; 2K_x$$

$$\frac{d\sigma_x^2}{dt} \;=\; 2\sigma_x^2 D \;+\; 2\sigma_x\sigma_z S_x \;+\; 2K_x$$

where $D$ is total explicit (grid-resolved) horizontal shear of horizontal wind (i.e., "deformation", see Section 4.5). $S$ is the explicit vertical shear of horizontal wind, which is broken down into puff-relative lateral and longitudinal components:

$$S_y \;=\; \left|\cos(\theta-\phi)\right|\left(\frac{du^2}{dz}+\frac{dv^2}{dz}\right)^{1/2}$$

$$S_y \;=\; \left|\sin(\theta-\phi)\right|\left(\frac{du^2}{dz}+\frac{dv^2}{dz}\right)^{1/2}$$

The difference between $\theta$ and $\phi$ represents the relative angle between the puff's longitudinal orientation and the direction of vertical shear; a cross-puff shear results in more lateral spread while along-puff shear results in more longitudinal spread. The explicit shear terms containing $D$ and $S$ may be toggled by the user: (1) shear effects may be applied to puff growth rates at all times; (2) shear effects may be applied only during neutral/unstable conditions; or (3) shear effects are never applied.

The SCICHEM tendency equation for the horizontal turbulent flux moment is

$$\frac{d}{dt}\langle y'\overline{v'c'}\rangle = Qq^2 - A\frac{q}{\Lambda}\langle y'\overline{v'c'}\rangle$$

where $A = 0.75$, $q^2 = \overline{v'v'}$, and $\Lambda$ is the horizontal turbulent length scale. Separate equations are given for two different boundary layer turbulence scales (shear- and buoyancy-produced), such that

$$\langle y'\overline{v'c'}\rangle = \langle y'\overline{v'c'}\rangle_{shear} + \langle y'\overline{v'c'}\rangle_{buoyancy}$$

Within the surface-based boundary layer, the horizontal velocity variance is given by

$$q^2_{buoyancy} = 0.13\,w_*^2\left[1+1.5\exp(z/z_i)\right]$$

$$q^2_{shear} = 2.5u_*^2(1-z/z_i)$$

where $u_*$ is the friction velocity, $w_*$ is the convective velocity scale, $z$ is height above the surface, and $z_i$ is the height of the surface-based boundary layer. The horizontal turbulent length scale is given by

$$\frac{1}{\Lambda^2_{shear}} = \frac{1}{(0.3\,z_i)^2} + \frac{1}{(0.65\,z)^2}$$

$$\Lambda_{buoyancy} = 0.3\,z_i$$

In the stable boundary layer, only the shear components of $q^2$ and $\Lambda$ are applied. Above the boundary layer, SCICHEM applies rough approximations for the velocity variance and turbulent length scale. In CAMx we have set these values to $q^2 = 0.25$ m$^2$/s$^2$, and $\Lambda = 1000$ m.

The SCICHEM tendency equation for the vertical turbulent flux moment is

$$\frac{d}{dt}\langle z'\overline{w'c'}\rangle = A\frac{q_v}{\Lambda_v}\left(QK_z^{eq} - \langle z'\overline{w'c'}\rangle\right)$$

where $q_v^2 = \overline{w'w'}$, $\Lambda_v$ is the vertical turbulent length scale, and $K_z^{eq}$ is the equilibrium diffusivity. Whereas a specific equation for $K_z^{eq}$ is formulated for SCICHEM, we have chosen to specify the value of this parameter from the gridded fields of vertical diffusivity in CAMx. Again SCICHEM gives separate equations for shear- and buoyancy-produced turbulence scales.

Within the surface-based boundary layer, the vertical velocity variance is given by

$$q_v^2\big|_{shear} = 1.5\,u_*^2(1-z/z_i)$$

$$q_v^2\big|_{buoyancy} = 1.1w_*^2(z/z_i)^{2/3}(1.05-z/z_i)$$

The vertical turbulent length scale for both shear and buoyancy is equal to $\Lambda_{shear}$ given above for horizontal length scale. Above the boundary layer, SCICHEM applies rough approximations for the velocity variance and turbulent length scale and we have adopted these for CAMx: $q_v^2 = 0.01$ m$^2$/s$^2$, and $\Lambda_v = 10$ m.

The external variables needed by PiG to complete the dispersion calculations include $z_i$, $u_*$ and $w_*$. All of these are available from an internal module in CAMx that calculates these boundary layer similarity theory parameters. Thus, no additional parameters are needed to be input to the model.

### 6.1.2 Puff Transport

A fresh set of new puffs are released from all PiG point sources within the modeling domain for the duration of the smallest time step among the master and all nested grids. The length of each puff is determined by the combination of the mean total wind speed at the height of final plume rise and time step. Limits are placed on maximum extruded length based on half the finest resolution in the given simulation. If winds and time-steps are such that the maximum allowed length is violated, then several puffs are automatically extruded from a given stack per time step. The user can also set a maximum time interval of release if more puffs (better plume resolution) are desired over the default automation. The orientation of the puff length is along the total wind vector. Total puff volume is determined by stack volumetric flow rate in conjunction with growth due to turbulent entrainment following the SCICHEM approach. Initially, $\sigma_x = \sigma_y$ and $\sigma_z$ values are explicitly calculated from this entrainment calculation.

The effects of resolved wind shear on plume deformation (i.e., at plume scales larger than individual puff scales) are treated using a "chained puff" approach (Figure 6-2). Points at the leading and trailing edges of the puff centerline are individually transported through the gridded wind fields, which directly accounts for puff stretching and changes to centerline orientation due to deforming shears. Since puffs can extend over multiple layers, layer density-weighted average wind components are determined for each endpoint based on the vertical coverage of the puff.

The "chain" aspect means that at least initially (as puffs are extruded from the stack) the trailing point of a puff emitted at time $t$ will be the leading point of a puff emitted at time $t+dt$. However, as the puffs are advected downstream, the leading point of one puff will deviate from the trailing point the puff behind it due to evolving puff depth and wind fields. Puff volume is conserved in convergent/divergent wind fields. Puff endpoints may move closer together or further apart, in wind fields that are slowing or accelerating downstream. We compute puff end-point separation changes and then adjust puff widths and depths to maintain constant puff volume. The change in computed puff endpoint spacing defines puff length tendencies, then puff depth tendencies are computed from grid-resolved vertical wind shear ($\partial w/\partial z$), and finally we determine the puff width tendencies required to conserve puff volume.

The official "position" of each puff is defined by the center point of each puff between the endpoints. This position defines which grid domain and grid cell the puff resides for the calculation of diffusion and chemistry. This definition holds even if the puff is sufficiently long
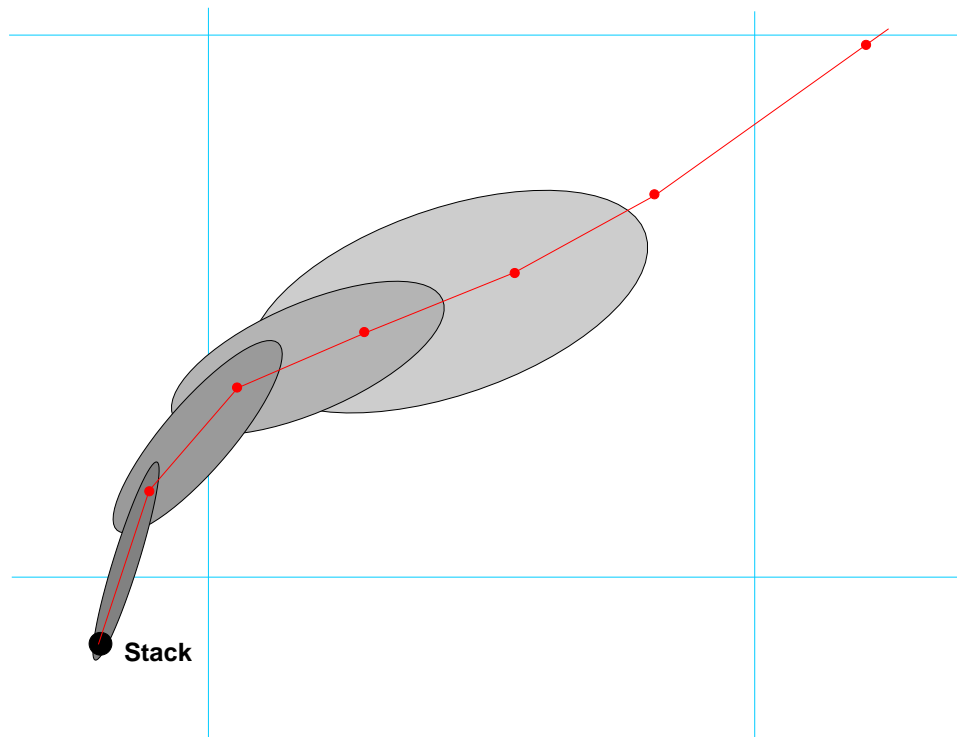
**Figure 6-2. Plan-view schematic representation of a chain of PiG puffs emitted from a point source into an evolving gridded wind field. The red line connected by dots represents puff centerlines, with dots representing leading and trailing points of each puff. The CAMx computational grid is denoted by the blue lines.**

that the endpoints are in different grid cells (or even different grid domains if near a domain boundary). With our definition for termination when horizontal area approaches grid cell area, the extents of the puff length should not extend across more than two grid cells.

## 6.2  IRON PiG

The IRON PiG model incorporates a complete treatment of gas-phase chemistry in point source pollutant plumes, while secondarily adding additional features central for treating toxic pollutants not normally carried by the standard CAMx chemical mechanisms. Several approaches have been developed to treat photochemistry within point source plume models. One of the more elegant methodologies is the incremental chemistry idea embodied in the SCICHEM model (EPRI, 2000). However, we found that the implementation of incremental chemistry in SCICHEM is very complex, especially in its handling of the chemistry of overlapping puffs, and not sufficiently flexible to allow for the adaptation of numerous chemistry mechanisms and/or solvers. In adopting this innovative approach for the IRON PiG, it was necessary to utilize an accurate numerical solution approach based on the LSODE chemical solver.

### 6.2.1  The Concept of Incremental Chemistry

For a second-order reaction between puff species *A* and *B*, the total reaction rate is given by:

$$R_T = k(P_A)(P_B)$$

(1)

where $P_A$ and $P_B$ are the total puff concentrations of each species.  The total puff concentrations can be expressed as the sum of the background and puff perturbation concentrations:

$$P_A = (c_A + C_A)$$

$$P_B = (c_B + C_B)$$

where *C* is the ambient concentration and *c* is the puff increment concentration (which can be positive or negative).  Thus the reaction rate is found to be:

or

$$R_T = k(c_A + C_A)(c_B + C_B)$$

$$R_T = k(c_A c_B + C_A c_B + c_A C_B + C_A C_B)$$

If we subtract the rate of change of the background,

$$R_{Ambient} = C_A C_B$$

(2)

by assuming that it is explicitly and separately treated by the grid model, we obtain the reaction rate for the puff increments:

$$R_P = k(c_A c_B + C_A c_B + c_A C_B)$$

(3)

Equation 3 is the basis of the SCICHEM incremental chemical kinetic solver.  One problem with this approach is the mixed terms, $C_A c_B$ and $c_A C_B$.  Most chemical solver packages are designed to solve rate equations for total concentration, as in Equation 1.  Thus, for the IRON PiG we developed an alternative numerical solution scheme for puff perturbation chemistry.  We note that the CAMx chemical solver can be independently applied to the rate equation for total puff concentrations, Equation 1, and to the rate equation for ambient concentrations, Equation 2. By subtraction of the two solutions, we obtain the solution to rate Equation 3.  This requires no modification to, and is obviously completely self-consistent with, the CAMx chemical solvers. Once the incremental puff reaction rates are obtained they are applied to the incremental puff mass to calculate the new (adjusted for chemistry) incremental concentrations.  These new puff increments are subsequently advected and dispersed by the transport portions of the PiG code.

### 6.2.2  Puff Constructs For Incremental Chemistry

The PiG sub-model includes three constructs designed specifically to facilitate the incremental chemistry approach:

- Treatments to handle puff-grid information exchange for puffs spanning multiple model layers;

- The concept of "virtual dumping" to handle the chemical impacts of large puffs that can overlap other puffs within a given grid column;
- The concept of multiple puff "reactor" cells to account for the chemical effects of concentration distributions within each puff.

Each of these is described below.

6.2.2.1  Puff Layer Spanning

The PiG is designed to chemically process point source plume mass within streams of puffs until such time that each puff can be adequately resolved on the horizontal grid.  Puffs are allowed to vertically span multiple grid model layers before they reach horizontal grid scales.  This introduces technical implications for defining "background" concentrations and ambient conditions for puff chemistry, as well as for transferring plume incremental mass to the grid. The solution employed is to:

1)  Assume that the vertical distribution of puff concentration is always uniform;

2)  Distribute puff mass transfer (via "leaking" and "dumping") to the grid according to the puff fractional coverage across each model layer and by density-weighting; and

3)  Determine mean background concentrations and other ambient conditions (e.g., temperature, humidity, etc.) over the puff vertical span via similar fractional layer-density weighting.

Horizontally, the mean background concentration and ambient conditions are taken from the single host grid column containing each puff center point, even if the puff is large and/or spans a horizontal cell interface.  As described earlier, puffs are considered to be elliptical in the horizontal, with the minor axis spanning the cross-wind puff width (defined as $\pm 1.5\sigma_y$), and the major axis spanning the along-wind puff length (defined as length $\pm 1.5\sigma_y$ on each end). However, given the complications associated with multiple layer spanning and mass-weighting of ambient inputs and dumped mass, puffs are rectangular and uniform in the vertical, with total puff depth defined as $\pm 1.5\sigma_z$.

6.2.2.2  Puff Overlap and the Idea of Virtual Dumping

The chemical effects of puff overlap were considered to be an important attribute of PiG. However, we wished to maintain a relatively simple approach, while appropriately accounting for the largest probable effects.  We assume that the largest effect is the condition in which older expansive puffs span significant fractions of their host grid cell, thereby potentially overlapping all other puffs contained within the same cell.  Instead of geometrically determining fractional overlap puff-by-puff, we instead introduce a process that we refer to as "virtual dumping."

For a given grid column, the mass from all puffs determined to be "sufficiently" large are temporarily dumped to the column, distributed according to each puff's vertical layer span, and added together along with the pre-existing grid concentrations.  This process is referred to as a "virtual dump" of puff mass to the grid column.  The criteria to determine a "sufficiently" large puff is the same that initiates puff mass leaking to the grid (as described below).  In this

approach, all large puffs contribute to the background chemistry step for other puffs occupying the same grid column. Double-counting of chemistry is avoided by not including a puff's contribution to the background while it's specific background and incremental chemical calculations are performed.

### 6.2.2.3  Multiple Puff Reactors

Accounting for full chemistry potentially introduces significant non-linear effects that are highly dependent upon the distribution of pollutant mass within each puff. Especially for ozone, aircraft flights through power plant plumes have often recorded wide concentration variations relative to ambient conditions: within the plume core where NOx remains concentrated, ozone is often depressed and follows $NO-NO_2$-ozone equilibrium, whereas on plume fringes where NOx is dilute and mixes with ambient VOC, ozone concentrations can exhibit concentration maxima. Past models have accounted for cross-plume chemistry variations through the use of reactors, with approaches ranging from multiple rectangular slabs to concentric shells.

The user may select multiple reactors as well to sub-divide the puff. Any number of reactors may be chosen (the default is 1). Multiple reactors simply divide the total puff volume evenly, and the initial mass assignments for newly emitted puffs are made using the standard error function that results in an initial Gaussian-like mass/concentration distribution among the reactors. This provides a mechanism for simulating the differing chemical processing that takes place in various concentration regimes. As the purpose of the reactors is merely to represent the range of photochemical conditions that are likely to occur at various locations within the puff as it undergoes differential shearing and mixing, there is no particular physical orientation assigned to these reactors with respect to each other or to the puff as a whole. Thus, there is no communication (i.e., diffusional mass exchange) between the reactors. The same background concentration chemistry applies to all reactors of a given puff. When puff mass is leaked or dumped, all reactors shed the same relative fraction of mass.

In summary, chemistry is solved for each puff "reactor" in three steps:

1) The layer-mean background (grid + overlapping puff) concentrations and environmental conditions over the volume occupied by the puff are stored and then chemically updated via the LSODE gas-phase chemistry mechanism;

2) The pre-updated mean background concentrations are added to the puff increments and the total concentrations are chemically updated; and

3) The updated results from step 1 are subtracted from the updated results of step 2 to provide the updated incremental concentrations.

An important consequence of this approach is that the incremental puff mass may be positive or negative. For example, a high-NOx puff that is destroying ambient ozone will have negative ozone increments. The puff increments are subsequently advected and dispersed by the transport portions of the PiG code. Note that the updated background concentrations, which include "virtual dumps" of mass from large puffs, are used for reference only in the puff incremental chemistry algorithm; the actual grid concentrations are updated in the grid chemistry routine.

6.2.2.4  Puff Dumping and PiG Rendering

Mass transfer from puff to grid can happen in two ways: slowly, termed "leaking", or suddenly, termed "dumping."  As described earlier, all mass is transferred to the vertical grid structure in a density-weighted fashion according to each puff's fractional layer coverage.  The process of leaking ensures that puff mass is transferred to the grid continuously, rather than in discrete lumps of pollutants with very different concentrations than those in the grid.  Sudden dumping can cause unphysical numerical shocks in the grid and can lead to unrealistic gridded concentration patterns that appear as "bullseyes".  The idea behind puff leakage is to account for turbulent shearing of mass from the main plume and its subsequent dispersion to the grid scale.  This rate of transfer should be directly proportional to the puff size relative to the grid scale.

Puff leakage is controlled by comparing the horizontal area of a puff to a specified leakage parameter, defined as a fraction of horizontal grid cell area.  When a puff is first emitted there is no leakage.  As the puff grows in volume the concentrations within the reactors are reduced accordingly by dilution.  When the puff area exceeds the leakage onset parameter, a fraction of the mass in each puff reactor is transferred to the grid.  This fraction is determined by the relative exceedance of the leakage parameter; initial leakage is slow as the exceedance is relatively small, but leakage rates grow as the puff continues to grow beyond the leakage parameter.

The reduced mass from leakage is compensated by a reduced effective volume, so that concentrations are not artificially diluted by leakage (an essential chemical imperative).  Thus, two distinct volumes are tracked: the actual volume (defined by the puff spread sigmas) and the effective volume.  While these are identical before leakage, they obviously deviate after leakage is initiated, and thereafter the relative deformation of the actual puff volume (via diffusion, shearing, etc.) is used to scale the deformation of effective puff volume.

Eventually the horizontal span of the puff will exceed the grid cell area, and the remaining mass is then dumped all at once to the grid.  However, because of the combination of photochemical processing and leakage, by the time a puff dumps the potential for producing numerical shocks is much reduced.  Furthermore, if the puff exceeds a user-defined maximum age, puff mass is transferred to the grid at the rate of 10% per timestep.

While the mass confined to the puffs at any given time has not yet affected the grid concentrations, it will eventually, so it can be somewhat misleading to sequester this mass from visualizations of a model simulation.  The puff mass can be optionally incorporated into the model average output files for visualization purposes (referred to as "PiG rendering").  Rendering employs a "virtual dump" of the puff masses into the average concentration array each time step.  As described for chemistry, virtual puff mass is added as an increment over the entire grid column according to fractional layer-density weighting over puff depth, thus diluting it's concentrations relative to that within the puff.  The actual puff mass remains within the puffs over the course of their lifetimes.  It should be noted that this visualization is available for 3-D average output files, and can produce some rather startling effects in output displays,

including very narrow virtual plumes, or streaks, representing mass moving through the grid in sub-grid puffs, but not subject to grid-scale eddy diffusion.

6.2.2.5  High Resolution Puff Sampling

PiG optionally employs surface-layer puff sampling of CB05, CB6, or SAPRC99 species on a user-defined grid of arbitrary horizontal resolution, similarly to the way nested grids are defined. Sampling grids are entirely passive, and intended to provide a display of the plume concentrations at scales much smaller than typically used for the finest computational grids (i.e., <1 km), primarily around and downwind of a source complex.  Sampled PiG concentrations are time-averaged like the output concentrations provided on the computational grids, and are written to files with similar format so that they may be readily viewed and manipulated with CAMx post-processing software.  Additional information on configuring and using PiG sampling grids is provided in Sections 2 and 4.

Given that the puffs constantly evolve via diffusive growth and reshaping due to deforming shears, the sampling procedure includes trigonometric calculations to define which sampling points are influenced by each puff.  This influence is determined according to the puffs' two-dimensional horizontal Guassian shape shown in Figure 6-1.  To include a sufficiently large percentage of mass across each puff for sampling, limits of $\pm 3\sigma_{x/y}$ in both horizontal dimensions are used to define the puffs' total elliptical area coverage.  Puffs are only sampled if they extend vertically into the model's surface layer.

Sampling grids are defined in the CAMx control file (see Section 2), and array dimensions must be set sufficiently large in the CAMx Fortran parameters file in `./Includes/camx.prm` (see Section 2).  An example of the type of plume detail that can be visualized using a sampling grid is provided in Figure 6-3.  In this case, a very fine 200 m sampling grid is set within a 4-km computational grid.

## 6.3  GREASD PiG

The GREASD PiG is designed for large NOx point sources, where inorganic chemistry is applicable only for early plume evolution with the intention of aging the NOx to mitigate the chemical effects of emitting fresh point source NO directly from the stack to the modeling grid. Therefore, this option should not be used for VOC sources.  The chemical limitations applied within GREASD PiG force the puffs to transfer their mass to the grid before full photochemical processing can develop, and usually before puffs reach size criteria relative to the grid spacing.

Concentrations and chemistry in GREASD PiG are treated with the same incremental techniques as described in Section 6.2 for IRON PiG.  In fact they are the same model, but with a distinct difference in the criteria that control when the puffs dump their incremental mass to the grid. The objective for GREASD PiG is to perform this dumping at about the time when non-linear organic chemistry starts to become important.  This was a specific design constraint that allowed source apportionment Probing Tools to be including into the PiG algorithm.  Kumar and Russell (1996) found that a PiG model with simplified inorganic chemistry produced results that were very similar to full chemistry.
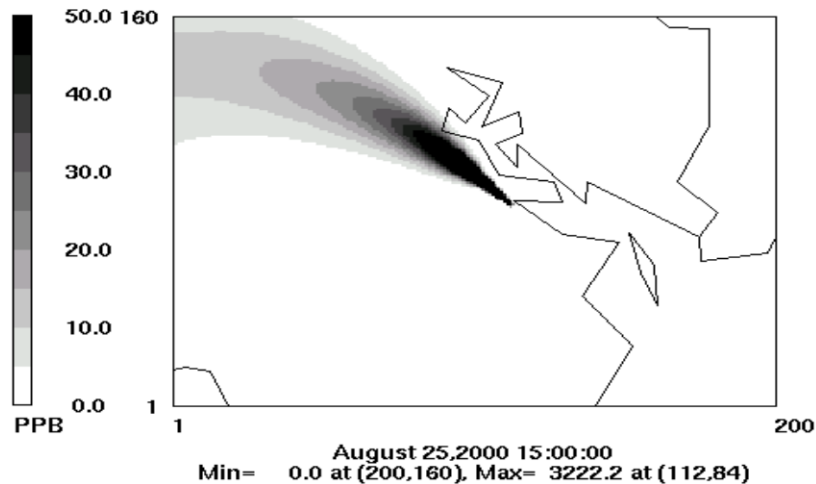
**Figure 6-3.  Example of a single point source PiG plume as depicted by a sampling grid with 200 m resolution (shown by the extent of the plot).  This sampling grid was set within a CAMx computational grid with 4-km resolution.  The source location is arbitrary and is emitting an inert tracer.**

EPRI (2000) describes the chemical evolution of large point source plumes in terms of three stages, as described below:

- Stage 1:  Early plume conditions where NOx concentrations are very high and radical concentrations are negligible – simple $NO/NO_2/O_3$ photostationary state applies along with the NO-NO self reaction;
- Stage 2:  Mid-range plume conditions where radical concentrations are sufficiently large to generate secondary inorganic acids like nitrate and sulfate;
- Stage 3:  Long-range plume conditions where sufficient mixing with the ambient air leads to the full range of gas-phase reactions involving VOC oxidation and ozone formation.

The GREASD PiG treats plume chemistry during Stages 1 and 2.  We define the onset of Stage 3 chemistry when the following criterion is met:

$$\frac{k[OH][CO] + k[OH][SO_2] + k[OH][VOC]}{k[OH][NO_2]} \; > \; 0.1$$

This conservative threshold ensures that GREASD puffs transfer all of their mass to the grid before the onset of any non-linear oxidant production, which is compatible with the source apportionment requirements.

## 6.4  Particulate Matter In PiG

Particulate chemistry in the CAMx PiG closely parallels the approach for gas-phase chemistry. The ISORROPIA, SOAP and RADM-AQ chemistry modules are called for each puff in the same manner and sequence as they are for the grid chemistry, but using the PiG incremental chemistry approach; i.e., by separate integrations for background and puff+background in order to determine the evolution of puff incremental PM concentrations.  Note that the PM capability in PiG was designed specifically for the static 2-mode PM chemistry only (CF), and not for the multi-section PM chemistry (CMU).  The PM capability is linked to the simper GREASD PiG option to limit the amount of non-linear chemistry in the PM treatment.  The addition of PM, and the PSAT Probing Tool, necessitated the addition of dry and wet deposition processes to the CAMx PiG.  These are described below.

### 6.4.1  PM Chemistry

The PiG performs gas and particulate chemical calculations for a given puff over each time step of the host grid where the puff resides.  This is done by calling a chemistry driver routine that is practically identical to the grid chemistry driver, except that layer-averaged ambient conditions over puff depth and PiG increments are passed to the chemistry algorithms rather than cell-specific conditions.  The driver routine contains the specific calls to all supported CAMx chemistry mechanism solvers, including the 2-mode (CF) PM algorithms.

Non-linear effects in gas-phase chemistry are transmitted to the PM and potentially amplified through the aqueous and equilibrium PM chemistry algorithms.  The implementation of PSAT in PiG prompted the need to limit the impact of such non-linearity in the plume chemistry similarly to the constraints imposed by OSAT for gas-phase chemistry.  Therefore, PM and PSAT can only be run using the GREASD PiG option.  Other limitations associated with running PM in PiG include:

- No puff leaking is allowed;
- No virtual dumping is allowed;
- No overlap chemistry is performed.

To maintain consistency with the grid chemistry, the PiG calls the aqueous PM chemistry algorithm at every time step for each puff that resides in a cloudy grid cell.  The remainder of the PM chemistry (ISORROPIA and SOAP) continues to be called on the PM "coupling" time step (default is 15 minutes), as these routines are not based on integrating conversion rates, but rather are equilibrium calculations independent of time step.

## 6.5  Deposition

The CAMx PiG treats the removal of gas and PM species from each puff via deposition processes.  Both dry and wet deposition calculations presented unique implementation issues for puffs.  The most difficult issue for both forms of deposition was how to manage deposition exchange between puffs and the ground in the case of negative puff concentration increments.

### 6.5.1  Dry Deposition

Dry deposition needs to consider the following: (1) the point at which puffs begin to deposit to the surface; (2) how to handle deposition through potentially deep puffs that may straddle several layers of varying stability since the puffs do not themselves resolve these stratifications or vertical concentration distributions; (3) managing deposition fluxes of negative concentration increments.  Our solution to issue (1) was to ignore dry deposition within puffs until they diffusively grow to the ground, although in reality deposition occurs on roughness elements that extend some distance above the nominal surface (trees, buildings, etc.).  We implemented a criterion that the bottom of the puff must extend to or below the midpoint of the surface layer, or below 10 m (whichever is larger), in order for dry deposition to be active.

Issue (2) can be handled in a variety of ways and complexity.  The current implementation institutes a simpler solution and we will consider more complicated improvements for future developments if evidence suggests that they would be necessary.  PiG utilizes pre-computed species-dependent deposition velocities derived for the grids.  Each puff in a particular grid cell is provided the host cell's deposition velocities for each species, and these are used to determine the flux of mass through the fraction of puff depth occupying the model's surface layer.

Issue (3) is unique to the incremental chemistry concept introduced with IRON PiG.  The flux of material depositing to the ground is given by $F = c \cdot v_d$, where by the normal definition a positive deposition velocity $v_d$ leads to a positive deposition flux to the ground.  If the puff increment $c$ is negative, then a negative flux is calculated (flux from ground to puff).  This is appropriate if we consider the following argument.  Dry deposition applied to a grid cell removes some pollutant mass from the entire volume.  If there is a puff existing in that cell with a negative concentration increment, then the amount of mass removed from the cell was over estimated if we consider the puff's contribution to total cell mass.  The negative deposition flux calculated for this puff leads to the addition of mass to the puff increment.  Adding mass to a negative increment reduces the magnitude of the increment, as expected for a deposition process.  This mass is taken from the grid cell's accumulated deposited mass to maintain accurate mass accounting within the model.

### 6.5.2  Wet Deposition

Wet deposition needs to consider the following: (1) how to handle scavenging of pollutants through potentially deep puffs that may straddle several layers of varying cloud and rain water contents but that do not themselves resolve vertical concentration distributions; (2) managing deposition fluxes of negative concentration increments in combination with the potential for mass to move in and out of rainwater as it falls (e.g., for slightly soluble gasses); (3) accounting for the initial pollutant concentrations in rainwater as they enter the top of each puff.

It was important to maintain consistency between the treatment of wet deposition and the approach for puff chemistry.  The chemistry relies on the assumption of vertically well-mixed puff reactors that can span multiple layers, and this is why layer-density weighted average ambient conditions are passed to the chemistry routines.  To maintain this assumption for wet deposition, a single scavenging rate is applied through the entire puff depth as effectively a

single layer of pollutant. This was found to be the simplest implementation approach. This single scavenging rate is calculated according to layer-density weighted average ambient cloud and rainwater contents.

Wet scavenging is performed throughout the entire depth of the puff to determine the amount of flux in or out of rainwater. Total concentrations (puff + background) are used to determine species-dependent scavenging rates using the identical algorithm as for grid removal. The rates are used to derive removal fractions, and these fractions are then applied directly to the puff incremental mass for each species. Removal fractions are considered positive for the standard case of mass moving from puff to rain. Note that negative puff mass increments in combination with a positive removal fraction lead to a reversal of the flux direction (rain to puff), and that is acceptable by an argument similar to that presented for dry deposition. We account for impacts on the mass budget appropriately by adding or subtracting from the wet deposition mass array according to the net fluxes into and out of rainwater, respectively.

We further assume that the top boundary condition for rainwater entering the top of each puff is zero. This means that the removal fraction is always positive (from puff to rain) in the single-layer puff. In contrast, for gridded concentrations the layer-by-layer buildup of slightly soluble species can lead to a reversal of fluxes (from rain to grid) if super saturation is diagnosed in a particular layer.

## 6.6 PiG Configuration

Selecting the individual elevated point sources to receive the PiG treatment is accomplished by setting their stack diameters negative within the header (time-invariant point list) section of the CAMx input point source file. CAMx will run correctly with these negative diameters even if the PiG algorithm is not invoked. CAMx preprocessors exist to ease the procedure of ranking elevated point sources by emission rate and flagging the sources that the user wishes to treat.

Invoking the CAMx PiG sub-model is controlled by keywords in the CAMx control file (`CAMx.in`), as described in Section 2. The choices are:

```
PiG_Submodel  = 'NONE',
PiG_Submodel  = 'GREASD',
PiG_Submodel  = 'IRON',
```

Note that the single choice between GREASD and IRON applies to all flagged point sources. It is not possible to make a single CAMx run with IRON PiG applied to a certain group of sources, and GREASD PiG applied to another group. Also note that GREASD must be selected to run PiG with OSAT, PM and PSAT; IRON must be selected to run PiG with the RTRAC Probing Tool. Several additional parameters are used to configure the PiG. It is important to note that all PiG configuration parameters exist in the CAMx Fortran parameters file (`./Includes/camx.prm`), as described in Section 2. PiG parameters are grouped together and briefly described at the end of that file. By effectively configuring the PiG submodel in the code, the default PiG configuration (as recommended by the model developers) is preset within the model distribution and alleviates the need for users to select settings on their own.

The default values are shown below:

```
parameter ( MXPIG   = 10000 )
parameter ( MXRECTR = 1 )
parameter ( FLEAK   = .25 )
parameter ( LEAKON  = .FALSE. )
parameter ( LVISPIG = .FALSE. )
parameter ( OVERLAP = .FALSE. )
parameter ( DXYMAX  = 0. )
parameter ( AGEMAX  = 18.*3600. )
parameter ( PIGMXDT = 300. )
parameter ( SHRFLG  = 1 )
```

Users should exercise thoughtful consideration when altering these default values.  A description of each of the remaining parameters is provided below, along with guidance in setting values.

### 6.6.1  Guidance on the Use of CAMx PiG

#### 6.6.1.1  PiG Keyword

The PiG keyword controls whether the PiG option is to be invoked in a CAMx simulation, and whether the emissions are treated with the GREASD or IRON options.  This keyword can be switched from NONE to GREASD or IRON on a model restart to invoke the PiG treatment at any point during a multi-day simulation.  To allow for this, it is not mandatory to provide CAMx with a pre-existing PiG output file upon a model restart – CAMx will not stop if this file is missing.  It is recommended that this file be provided on all subsequent restarts since the PiG output file is needed to reinitialize the PiG module, otherwise all mass contained in puffs at the end of the previous run will be lost.  If the PiG keyword is switched to NONE on a model restart, CAMx will continue the simulation without PiG, but all mass contained in puffs at the end of the previous run will be lost.

- Guidance:
  - Invoke GREASD or IRON PiG at any point during a multi-day simulation, or none at all.  Once PiG is started, provide CAMx with the PiG output file from the previous run for all subsequent model restarts so that no point source mass is lost.
  - GREASD PiG should be invoked for large NOx point sources only, since it does not provide any organic chemistry.  GREASD PiG does support PM chemistry (CF).  It can be run in conjunction with the OSAT and PSAT Probing Tools.  It does not support DDM, PA, or RTRAC.
  - IRON PiG can be invoked for any point sources to treat gas-phase chemical evolution using CB05, CB6 or SAPRC99 mechanisms.   IRON PiG does not treat particulate chemistry.  It can be run in conjunction with the RTRAC Probing Tool.  It does not support OSAT, PSAT, DDM, or PA.

Both GREASD and IRON options use the expensive LSODE chemistry solver exclusively, so users will notice a significant impact on run time, particularly if many (~thousands) puffs are to be carried and/or puffs are configured with many puff reactor cells (see below).  Since the lifetime

of GREASD puffs are much shorter than their IRON counterparts, GREASD PiG will run faster than IRON PiG for the same number of flagged sources. PiG chemistry is internally parallelized using OMP to maximize PiG speed performance.

6.6.1.2  Number of PiG Puffs

MXPIG sets the maximum number of PiG puffs to be expected during a simulation. It is used to statically allocate memory arrays for the PiG sub-model. A value of 10,000 is usually sufficient for most applications in which PiG is used; set this parameter to 1 if PiG is not used to conserve memory. If this parameter is exceeded during a simulation, the model will halt. If this happens, simply increase `MXPIG`, recompile the model executable, and restart the simulation.

- Guidance: Use the default value for most simulations, or set to 1 if PiG is not to be used. If the model stops because MXPIG is exceeded, increase its value, recompile, and restart the model.

6.6.1.3  Number of PiG Reactors

MXRECTR sets the number of puff reactors; when greater than 1, each puff is separated into that number of reactor cells and primary emissions are apportioned among them using a Gaussian distribution. Since chemistry is performed for each individual reactor cell (both background and puff+background), this parameter can affect the speed of chemical computations in the PiG. We have not seen a significant sensitivity to values greater than 1, but testing for each application is warranted.

- Guidance: Use the default of 1 for initial simulations, but test the sensitivity to this parameter for each unique application.

6.6.1.4  Leakage Parameters

FLEAK, LEAKON, and DXYMAX together control puff leakage to the computational grid and ultimately puff termination. When LEAKON is true, FLEAK and DXYMAX control when puffs begin to leak portions of reactor mass to the grid along their trajectory. When LEAKON is false, no leaking is performed and puffs maintain all of their mass until they reach sizes for termination, at which point all mass is directly introduced to the grid at that point. DXYMAX sets the maximum dimension that puff size will be compared to for leaking and termination; when it is zero, puff size will be compared to grid area, but when it is non-zero, puff size will be compared to the value of DXYMAX. FLEAK is the relative fraction of horizontal puff area to cell area, or DXYMAX, above which leaking will begin and continue until sufficient mass is shed and the puff is terminated. In the example above, puffs will begin to leak mass when they reach 25% of the host grid cell's area.

- Guidance: If LEAKON is set to true, maintain FLEAK at the default value of 0.25. Then test model sensitivity to different values of FLEAK and/or DXYMAX.
- Leaking is not allowed when PiG is run with PM.

### 6.6.1.5  Overlap Flag

OVERLAP controls whether puff overlap is to be treated in the background chemistry step.  As stated earlier, puffs only overlap if they meet the size criteria for leaking; all puffs smaller than this size do not overlap any other puffs in the same grid cell.

- Guidance:  We recommend that the OVERLAP flag remain set to the default value of "false".
- Overlap is not allowed when PiG is run with PM.

### 6.6.1.6  Virtual Puff Rendering

LVISPIG is a flag that turns on puff "rendering" to the computational grid average concentrations.  When it is false, the chemical effects of puff mass are not seen on the output average files until they either begin to leak mass to the grid and/or they are terminated and their mass is entirely introduced to the computation grid.  However, when the flag is true, all puff mass that resides in each grid column is summed, apportioned vertically to each grid cell according to puff vertical extent (via density and layer-depth weighting), converted to concentrations, and added to the average gridded concentrations for output.  This process is referred to as rendering since the effects of all puff mass can be readily visualized in the CAMx output.

- Guidance: This option has no impact on the actual CAMx chemical solution.  However, output average concentration files will be affected by puff rendering, and therefore could impact graphics of CAMx results and model performance measures.
- Virtual dumps are not allowed when PiG is run with PM.

### 6.6.1.7  Maximum Puff Age

AGEMAX is the age limit for all PiG puffs (IRON and GREASD).  When puffs reach this age limit, they are terminated and all of their mass is transferred to the host grid.

The assumption of a stream of coherent puffs becomes less valid with time as horizontal and vertical wind shears increase plume spread.  At some point the plume mass is better resolved on the grid than within puffs.  In CAMx the rate of puff expansion most often determines this transfer of mass, and the maximum puff age provides a safety check to ensure that puffs do not persist for unrealistic times in stable environments.  The maximum puff age should be set long enough to allow puffs to persist overnight, but a lifetime of longer than a day is probably not realistic.

- Guidance: limit puff age to 12-24 hours – we find that 18 hours works best since it will allow puffs emitted in the late afternoon to last through the night and into the following morning.  The purpose is to restrict growth-limited puffs to terminate over night simply as a result of age constraints.  Twelve hours is seen to be too short in this regard; puffs usually do not reach 24 hours of age before being terminated by grid constraints.

6.6.1.8  Maximum Puff Release Interval

PIGMXDT sets the maximum frequency of release and by default is set to 300 seconds (5 minutes).  This value should be adequate for most applications.  However, if the user wishes to improve plume resolution by increasing the number of puffs, the frequency of release can be increased by reducing the value of PIGMXDT.  This value supersedes the automated puff release rate that is determined by wind speed and grid size.

- Guidance: Maintain the default value of 300 s and allow PiG to use the automated PiG release frequency.  Set to a lower value if better plume resolution is desired; note that more puffs will be released and this could slow the model markedly.

6.6.1.9  Effects of Wind Shear on Puff Growth Rates

SHRFLG sets the approach by which to apply the effects of explicitly resolved (grid scale) wind shear on puff growth rates.  There are three options available to the user:

    0 = shear is never applied;
    1 = shear is applied only within the neutral/unstable boundary layer;
    2 = shear is always applied.

- Guidance: The application of wind shear can lead to large growth rates, especially during stable conditions at night, and this may over-dilute puff concentrations, lead to early transfer of puff mass to the grid, and have markedly reduced impacts on next-day ozone.  Shear has less relative impact on growth rates during the daytime because turbulent growth on its own leads to rapid plume dilution.   For these reasons, the default is to ignore the effects of shear during the night or when puffs are above the boundary layer.

# 7.  OZONE SOURCE APPORTIONMENT TECHNOLOGY

## 7.1  Introduction

Photochemical grid models are used to develop NO$_x$ and/or VOC emission reduction strategies to attain ozone air quality objectives.  Traditionally, the development of an ozone attainment strategy involves iteration through many photochemical grid model scenarios to identify which pollutants, source categories and source regions should be controlled.  It is impractical to analyze every potential control strategy and so there is potential for implementing controls on sources that contribute little to the high ozone levels or, conversely, not controlling sources that do contribute.

ENVIRON developed an ozone source attribution approach that has become known as the "Ozone Source Apportionment Technology", or OSAT (Yarwood et al., 1996).  This method was originally implemented in the Urban Airshed Model (UAM) and was then built into CAMx[3].  OSAT provides a method for estimating the contributions of multiple source areas, categories, and pollutant types to ozone formation in a single model run.  OSAT also includes a methodology for diagnosing the temporal relationships between ozone and emissions from groups of sources.  The capabilities of OSAT are summarized below along with an assessment of the strengths and limitations of the approach.

The main challenges in developing and implementing a methodology to track the spatial and temporal relationships between separate groups of emission sources and ozone formation are:

- Accounting not only for the presence of ozone precursors from a given source region at a given receptor location, but also accurately estimating the cumulative contribution to ozone production of those precursors while they were en-route to the receptor.
- Insuring compatibility with the underlying air quality model formulation so that derived source-receptor relationships will be consistent with model response to emission changes.
- Providing sufficient spatial and temporal resolution while managing, within practical constraints, the computer resources required to run the software tool.

OSAT uses multiple tracer species to track the fate of ozone precursor emissions (VOC and NO$_X$) and the ozone formation caused by these emissions within a simulation.  The tracers operate as spectators to the normal CAMx calculations so that the underlying CAMx predicted relationships between emission groups (sources) and ozone concentrations at specific locations (receptors) are not perturbed.  Tracers of this type are conventionally referred to as "passive tracers," however it is important to realize that the tracers in the OSAT track the effects of chemical reaction, transport, diffusion, emissions and deposition within CAMx.  In recognition of this, they are described here as "ozone reaction tracers."  The ozone reaction tracers allow ozone formation from multiple "source groupings" to be tracked simultaneously within a single simulation.  A source grouping can be defined in terms of geographical area and/or emission

---

[3] Note that the formulation of the Ozone Source Apportionment Technology differs slightly from earlier versions in that it accounts for the fact that ozone production and destruction occur simultaneously as it apportions ozone change among tracers.  Previously, OSAT only considered the net change in ozone in the apportionment algorithm.  The approach is described later in this section.

category.  Figure 7-1 provides an example of the way that a CAMx domain can be sub-divided into multiple source areas – 40 in this example.  Also, the emission inventory could be sub-divided into several source categories – two emission categories over 40 source regions would produce 80 separate source groupings.  So that all sources of ozone precursors are accounted, the CAMx boundary conditions and initial conditions are always tracked as separate source groupings.
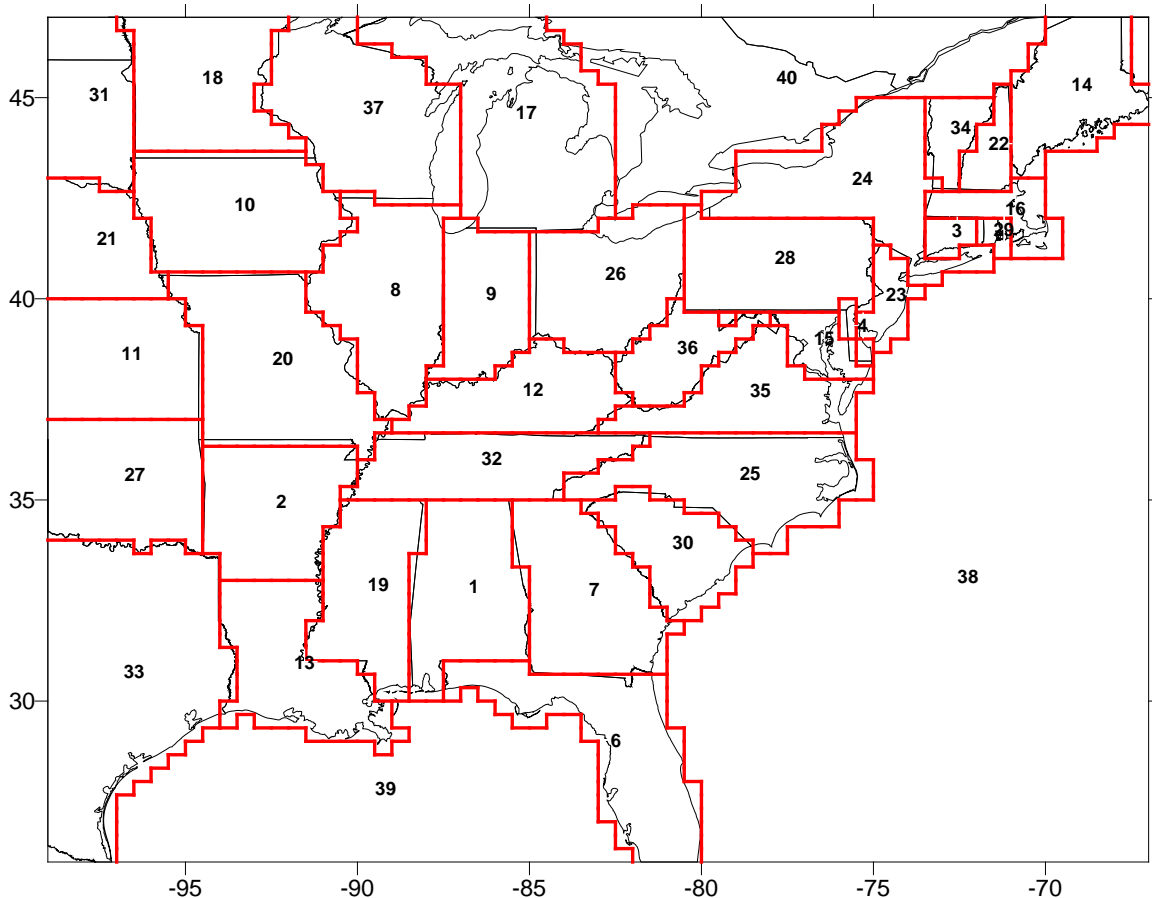


**Figure 7-1.  Example of the sub-division of a CAMx domain into separate areas for geographic source apportionment.**

The methodology is designed so that all ozone and precursor concentrations are attributed among the selected source groupings at all times.  Thus, for all receptor locations and times, the ozone (or ozone precursor concentrations) predicted by CAMx is attributed among the source groupings selected for OSAT.  The methodology also estimates the fractions of ozone arriving at the receptor that were formed en-route under VOC- or $NO_X$-limited conditions.  This information indicates how ozone concentrations at the receptor will respond to reductions in VOC and $NO_X$ precursor emissions.

An example display of the type of ozone source apportionment information available from OSAT is shown in Figure 7-2.  The figure shows information for the location of the region wide maximum hourly average ozone concentration (the hourly peak) for an example OSAT run (this run had 17 geographical source areas and a single emission group).  Summary information for scenario and receptor is shown in the center.  At top left, a bar chart shows how the total amount of ozone was attributed between initial conditions, boundary conditions and emissions, with the emissions contribution being divided between ozone formed under VOC and $NO_X$ limited conditions.  At top right, a pie chart shows the relative ozone contributions from initial conditions, boundary conditions and emissions, with the emissions contributions broken out by numbered geographical source areas.  Only the source areas with the largest ozone contribution are shown, the remaining source areas are lumped together under "All Others." The display shown in Figure 7-2 is only one of many ways in which OSAT results can be displayed to gain insight into ozone source-receptor relationships predicted by CAMx.  Figure 7-2 is shown here to illustrate the types of information available; displays like this are generated using post-processing software described later in this section.

An important feature of the ozone reaction tracer approach used in OSAT is that the normal CAMx calculations are not perturbed; thus, OSAT estimates the same ozone and precursor concentrations as CAMx.  Further, since the same inputs are used for meteorology, emissions etc., and the same numerical methods are employed throughout the model, the source-receptor relationships developed by OSAT inherently have a high degree of consistency with those present in CAMx.  The level of consistency between the source-receptor relationships developed by OSAT and CAMx is limited by three factors:

- The completeness of the conceptual methodology underlying the source apportionments;
- The limitations of the numerical methods employed by CAMx; and
- The non-linear nature of the ozone formation process.

The completeness of the source apportionment methodology was analyzed by performing a series of evaluations of OSAT results against UAM sensitivity tests (Yarwood et al., 1996).  These tests showed that the OSAT performed well in predicting both the spatial impacts of emissions from given source regions and the relative contributions of separate emission regions/groups to ozone.  OSAT cannot overcome numerical limitations inherent to CAMx (as well as other grid models).  The UAM evaluation tests referred to above suggested that a potentially serious numerical limitation was its horizontal advection solver.  As discussed below, the non-linear numerical limitations of advection algorithms were addressed in the OSAT design, and we believe that they probably pose greater problems for the use of CAMx in conventional control strategy evaluations than for OSAT (Yarwood et al., 1996).  This issue was one of the primary reasons for incorporating the Bott (1989) and PPM (Colella and Woodward, 1984) advection algorithms into CAMx and redesigning the three-dimensional transport scheme to be more mass consistent.  Further, the tracer transport routines were modified to directly use the advective fluxes diagnosed by the regular model advection solvers to minimize inconsistencies between tracers and regular model species.

## Contributions By Type

## Contributions By Source Area



Legend:
- NOx limited
- VOC limited
- Boundary
- Initial

| Receptor | = | **HourlyPeak** | | |
|---|---|---|---|---|
| **Time** | = | **16** | **To** | **17** |
| **Date** | = | **8/28/87** | | |
| **Scenario** | = | **Evaluation Test** | | |
| **Total Ozone** | = | **183** | **ppb** | |
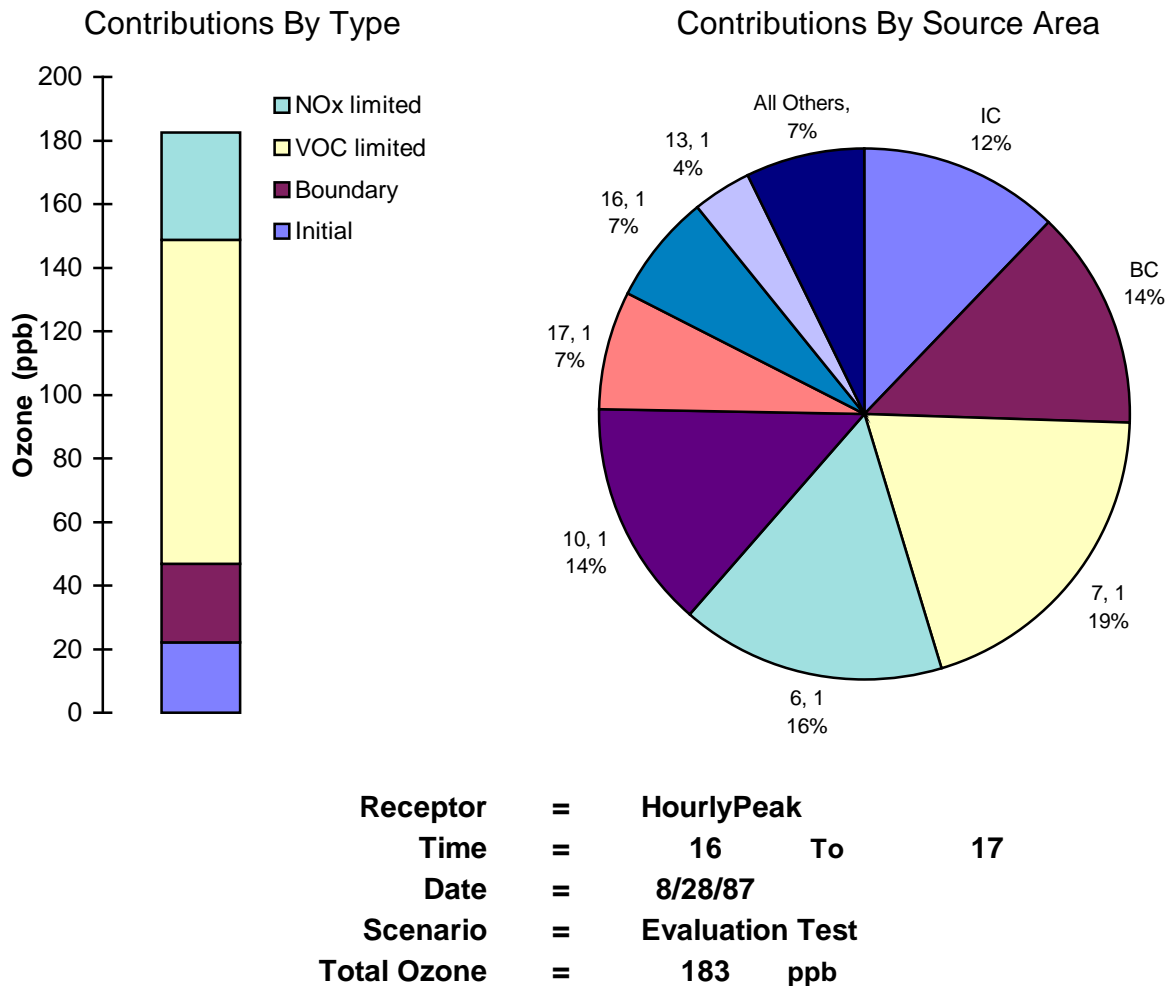
**Figure 7-2. Example display of ozone source apportionment information provided by OSAT for a run with 17 source areas and 1 emission group.**

The biggest limitation of this, or any other, ozone source apportionment approach likely results from the third factor mentioned above: namely, the non-linear nature of the chemical interactions between emissions from different source groupings. This means that as soon as the emission inventory is perturbed, the source receptor relationships begin to change. Thus, OSAT can only estimate the contribution to ozone from a specific source grouping under the current emissions scenario. It cannot directly quantify the ozone reductions that will result from an emission control strategy because the CAMx response may well be non-linear with the magnitude of the control applied (e.g. 20 percent or 60 percent control) and the presence/absence of other simultaneous controls on other source groupings.

However, this fundamental truth of photochemical modeling does not limit the usefulness of OSAT: arguably it increases its usefulness. At any rate, it suggests the following approach to control strategy development with OSAT. For the base CAMx scenario, OSAT could be used to identify specific source groupings for which ozone reductions from emissions controls would be

maximized.  Just as important, OSAT will identify source groupings for which emissions controls are not effective at reducing ozone concentrations. The most effective and feasible control measures identified in this way can be applied to the emission inventory, leading to a revised CAMx scenario with different (lower) emissions.  If additional controls are needed, OSAT could be applied again to identify the most effective control measures under the new conditions. Development of the control plan will still proceed by an iterative process, but OSAT can be used to guide the process to develop (and justify) more refined, better-targeted and more cost-effective ozone control strategies.

## 7.2  OSAT Formulation

CAMx has been extended to accommodate extra tracer species needed to perform ozone source apportionment.  For each user-specified source grouping (geographical area/emissions category) ozone reaction tracers track the fate of ozone precursor ($NO_X$ and VOC) emissions plus the ozone formation attributed to those emissions.  The methodology requires that all ozone precursors be tracked so that all contributions to ozone can be accounted for, thus ozone and precursors originating from the model boundary and initial concentrations are also tracked as separate source groupings.

There are four ozone-reaction tracers per source area to account for the contributions of emissions of separate source areas to the complex process of the ozone formation activity.  It is important to recall that the mass of $NO_X$ or VOC from a given source area that may be present at a given receptor at a selected hour is often not particularly relevant to the amount of ozone present there at that time.  Rather, it is the contribution to ozone formation activity of source areas' $NO_X$ and VOC emissions en-route to a receptor that must be determined.  The ozone-reaction tracers are designed to integrate these en-route contributions to ozone production/destruction activity.

Ozone formation involves both $NO_X$ and VOCs, and the $NO_X$ and VOCs participating in ozone formation in any particular grid cell/time step may have originated from different source groupings.  The ozone formation process can be controlled more by the availability of VOCs or $NO_X$, depending upon the relative abundance of both precursors, and ozone formation is described either as VOC limited or $NO_X$ limited, respectively.  When ozone production at a given location and time is $NO_X$ limited it makes sense to attribute ozone production to source groupings based on their contributions to the local $NO_X$ and similarly to allocate based on VOC contributions when ozone formation is VOC limited.  Consequently, separate tracers are used to track ozone formation occurring under $NO_X$ and VOC limited conditions.  The criterion used to determine whether ozone formation is occurring under locally $NO_X$ or VOC limited conditions is described in detail in a separate section below.

The four types of ozone-reaction tracers that are tracked for each source grouping (i.e., geographic area/source category, boundary conditions or initial conditions) are explained below.   The name of each tracer uniquely identifies the source grouping it represents:

$N_i$ = NO$_X$ tracer for source grouping *i*. Emitted with the same spatial and temporal distribution as NO$_X$ emissions for source grouping *i*. Decays with local $dNO_X/dt$ for each grid cell/time step.

$V_i$ = VOC tracer for source grouping *i*. Emitted with the same spatial and temporal distribution as VOC emissions for source grouping *i*. Decays with local $dVOC/dt$ for each grid cell/time step. Note that VOC tracers are defined as single carbon species, so their concentrations are numerically equal in ppb and ppbC units.

$O3V_i$ = Tracer of ozone formation under VOC limited conditions attributed to source grouping *i*. If ozone formation is determined to be VOC-limited for a given grid cell/time step, $O3V_i$ is formed in proportion to local $dO3/dt$ in proportion weighted by the distribution of VOC precursors ($V_i$).

$O3Ni$ = Tracer of ozone formation under NOX limited conditions attributed to source grouping *i*. If ozone formation is determined to be NOX-limited for a given grid cell/time step, $O3N_i$ is formed in proportion to local $dO_3/dt$ in proportion weighted by the distribution of NO$_X$ precursors ($N_i$).

### 7.2.1 Mass Consistency with CAMx

The ozone reaction tracer methodology was designed to be inherently mass consistent with CAMx. In other words, the sums of the individual ozone, NO$_X$, and VOC tracers (*i*) should remain consistent with their standard CAMx counterparts as follows:

$$\sum N_i = NO + NO_2$$

$$\sum V_i = \sum VOC_j \times C_j$$

$$\sum O3V_i + \sum O3N_i = O3$$

Note that VOC tracers are weighted by the carbon number of each VOC species ($C_j$). The validity of these relationships was evaluated and it was found that the chemistry, emissions, deposition, horizontal diffusion, and vertical diffusion algorithms maintained mass consistency on an overall and cell-by-cell basis. However, it was found that the horizontal and vertical advection algorithms inherently maintained mass consistency on an overall basis, but not a cell-by-cell basis. Accordingly, the advection algorithms for the ozone reaction tracers were modified as described below to maintain mass consistency.

### 7.2.2 Emissions

The tracer families, $N_i$ and $V_i$, track NO$_X$ and VOC emissions from each source grouping to allow attribution of ozone formation as it occurs throughout CAMx. The rates of emission of the $N_i$ and $V_i$ tracers are set equal to the total NO$_X$ and VOC emissions in the inventory for a source grouping, respectively. For the $V_i$ tracers, the emissions are set equal on a ppmC basis. For the initial condition (IC) source grouping, the $N_{IC}$ and $V_{IC}$ tracers are initialized from the CAMx initial concentration fields and receive no more mass input after the start of the simulation. For the

boundary condition (BC) source grouping, the fluxes of NO$_X$ and VOC entering CAMx from the boundaries are effectively interpreted as emissions of the $N_{BC}$ and $V_{BC}$ tracers at the model boundaries. Unlike emission source groupings, boundary and initial conditions also introduce ozone directly into CAMx. Since there is no way of determining whether the ozone in the boundary and initial conditions was formed under VOC or NO$_X$ limited conditions, this ozone is divided equally between *O3N* and *O3V* tracers. However, subsequent ozone formation within CAMx from boundary and initial condition VOCs and NO$_X$ is allocated to *O3V* and *O3N* tracers on the basis of whether ozone formation occurred under VOC or NO$_X$ limited conditions (discussed below).

### 7.2.3 Deposition

The $N_i$, $V_i$, $O3N_i$ and $O3V_i$ tracers are deposited at rates determined by the standard CAMx deposition calculation on a surface grid cell by grid cell basis. For NO$_X$, the deposition velocity for each tracer $N_i$ [$V_d(N_i)$] is set equal to the concentration weighted average of the deposition velocities for NO and NO$_2$:

$$V_d(N_i) \quad = \quad \frac{NO \times V_D(NO) + NO_2 \times V_D(NO_2)}{NO + NO_2} \qquad (1)$$

Similarly, the deposition velocity for each tracer $V_i$ is set equal to the concentration weighted average of the deposition velocities for the VOC species (the concentration weighting is performed on a ppmC basis). The deposition velocity for the *O3N* and *O3V* tracers is set equal to the ozone deposition velocity. Gridded fields of deposited OSAT tracer mass can optionally be output to a file for viewing or reporting.

### 7.2.4 Transport and Diffusion

Originally, the $N_i$, $V_i$, $O3N_i$ and $O3V_i$ tracers were advected and diffused by the CAMx algorithms. As mentioned above, testing of OSAT showed that the CAMx advection routines did not accurately preserve the spatial relationships between ozone reaction tracers and their corresponding CAMx species (i.e., between the sum of the *O3V* and *O3N* species and CAMx O$_3$). The distortion in any single model time-step was small, but the distortion built up over time to unacceptable levels. This was caused by non-linear dependences on the gradients of the advecting material, which can differ substantially between the standard model species and each of the OSAT tracers. This resulted in OSAT predictions that differed from the standard CAMx concentrations.

Such an outcome was inconsistent with the objectives in developing OSAT, so an alternative approach was adopted. As the horizontal and vertical transport operations are carried out for all CAMx species, the individual advective fluxes for ozone and each NO$_x$ and VOC species are reported by the advection solvers. The ozone and individual NO$_x$ and VOC fluxes are combined (and weighted by carbon number for VOC) and normalized by their respective weighted mean concentrations prior to advection. The equations below summarize this process, where $f^i$ is the flux of the core model species into or out of cell *i*, *C* is VOC carbon number, and $F^i$ is bulk normalized flux:

$$F_{NOx}^i \quad = \quad \frac{f_{NO}^i + f_{NO2}^i}{NO^i + NO2^i}$$

$$F_{VOC}^i \quad = \quad \frac{f_{PAR}^i \times C_{PAR} + f_{OLE}^i \times C_{OLE} + ...}{PAR^i \times C_{PAR} + OLE^i \times C_{OLE} + ...}$$

$$F_{O3}^i \quad = \quad \frac{f_{O3}^i}{O3^i}$$

These bulk normalized fluxes are used to advect each tracer species directly, rather than sending the tracers through the advection algorithms.  This approach has significantly improved consistency between tracer and regular model concentrations.

The OSAT tracers are sent to the standard CAMx routines for vertical diffusion and horizontal diffusion.  Since small deviations sometimes occur between the OSAT tracer concentrations and the regular CAMx species (due to numerical limitations), the ozone reaction tracer concentrations are renormalized after transport to be consistent with the standard CAMx concentration fields.  The renormalization is applied in the same subroutine as chemical change because this is computationally efficient.

### 7.2.5  Chemical Change

The $N_i$ tracer mass in each grid cell at each time step decays according to the chemical change in the CAMx predicted NO$_X$ ($\Delta NO_X$) weighted by the tracer contribution to the total of NO$_X$ tracers from all source groupings:

$$N_i^{new} \quad = \quad N_i^{old} + \Delta NO_x \times \frac{N_i^{old}}{\sum N_i^{old}} \qquad (2)$$

The $V_i$ tracer mass in each grid cell at each time step decays according to the chemical change in the CAMx predicted VOC ($\Delta VOC$) weighted by the tracer contribution to the total of VOC tracers from all source groupings.  However, because the reactivity of VOCs from different source groupings can be different, a weighting factor based on the OH-reactivity of each $V$ tracer ($kOH_i$) is also introduced.  The $kOH_i$ for each source grouping is calculated at the start of each simulation period (typically one day) by averaging the OH rate constants of the speciated VOC emissions for each source grouping.  The $V$ tracer mass in each grid cell at each time step decays at a rate determined by the following equation:

$$V_i^{new} \quad = \quad V_i^{old} + \Delta VOC \times \frac{V_i^{old} \times kOH_i}{\sum V_i^{old} \times kOH_i} \qquad (3)$$

The *O3N* and *O3V* tracers for each source grouping accumulate a weighted fraction of the ozone production activity ($PO_3$) and ozone destruction activity ($DO_3$) that occurs in each grid cell

at each time step.  The process of apportioning $PO_3$ and $DO_3$ across O3N and O3V tracers occurs as follows:

1. Determine whether the local (grid cell/time step) ozone production process is $NO_X$ or VOC limited.  As described in detail below, the determination is based on the ratio of the local $HNO_3$ and $H_2O_2$ production rates.  If the $H_2O_2/HNO_3$ production ratio is greater than 1/3 during a time step, then ozone formation is $NO_X$ limited.  If this ratio is less than or equal to 1/3, then ozone formation is VOC limited.

2. For allocating ozone production under conditions determined to be:

    (a) $NO_X$ limited:  allocate $PO_3$ across *O3N* tracers

$$O3N_i^{new} \quad = \quad O3N_i^{old} + PO_3 \times \frac{N_i^{old}}{\sum N_i^{old}} \qquad (4)$$

    (b) VOC limited:  allocate $PO_3$ across *O3v* tracers based on maximum incremental reactivity (MIR) factors

$$O3V_i^{new} \quad = \quad O3V_i^{old} + PO_3 \times \frac{V_i^{old} \times MIR_i}{\sum V_i^{old} \times MIR_i} \qquad (5)$$

3. For ozone destruction, allocate across all ozone tracers.

$$O3X_i^{new} \quad = \quad O3X_i^{old} + DO_3 \times \frac{X_i^{old}}{\sum X_i^{old}} \qquad (6)$$

where $X = N$ and $V$.

This is the algorithm used for OSAT.  The GOAT and APCA methods use different algorithms for allocating ozone production, as described below.

The MIRs used in equation (5) are the weighted average MIRs for the emissions in each source group.  The MIR approach was developed by Carter (1994) to approximate the ozone forming potential of VOCs accounting for both kinetic and mechanistic reactivity effects.  The MIR represents the ozone formation potential of the VOC mixture accounting for the VOC reactions with OH as well as the effects of all of the VOC products that produce ozone formation.  The VOC + OH reaction is the main VOC destruction mechanism so it is appropriate to weight the VOC destruction across the VOC reactive tracers by their composite reaction rate with OH (*kOH*).  The MIR factors for the CAMx SAPRC99, CB05, and CB6 mechanisms are shown in Tables A-3, B-3, and C-3, respectively.

### 7.2.5.1  Accounting for Ozone Destruction Reactions in OSAT

The original OSAT algorithm allocated chemical change to ozone tracers based on the total change in ozone ($\Delta O_3$) across a call to the gas-phase chemistry solver.  A positive $\Delta O_3$ was

equated to ozone production and ozone tracers were incremented according to the OSAT, APCA or GOAT rules for apportioning ozone production.  A negative $\Delta O_3$ was equated to ozone destruction and the destruction was distributed equally among all ozone tracers.  However, ozone production and destruction mechanisms operate simultaneously within the chemical mechanism and so the net change in ozone is the balance of production and destruction.  For example, VOC oxidation can drive photochemical ozone production at the same time that $O_3$ + VOC reactions directly consume ozone, and these processes may lead to a net increase or decrease in ozone depending mainly upon availability of NOx and sunlight.  OSAT has been modified to explicitly track several ozone destruction mechanisms as follows:

1)  $O_3$ + VOC reactions since these remove ozone;
2)  $O(^3P)$ + VOC reactions since these effectively remove ozone;
3)  $O(^1D)$ + $H_2O$ reaction since this effectively removes ozone;
4)  HOx + $O_3$ reactions that do not re-form ozone.

Ozone production is then calculated from the difference between $\Delta O_3$ and total ozone destruction ($PO3 = \Delta O_3 - DO3$).  The OSAT ozone tracers are adjusted first for ozone destruction (applied to all tracers) and second for ozone production (applied using the OSAT, APCA or GOAT rules).

The amount of ozone destruction is calculated using integrated reaction rates obtained from the Process Analysis (PA) Probing Tool; see Section 10.  It is easy to account for processes 1-3 using PA since the ozone destroyed is simply the integrated rates of the reactions involved.  Process 4 is less easy to identify but is very important as an ozone destruction mechanism in low NOx (rural) environments.  Therefore, accounting for process 4 is important to understanding long-range ozone transport.

The main reaction pathways between ozone and HOx (OH and $HO_2$) are shown in Figure 7-3.
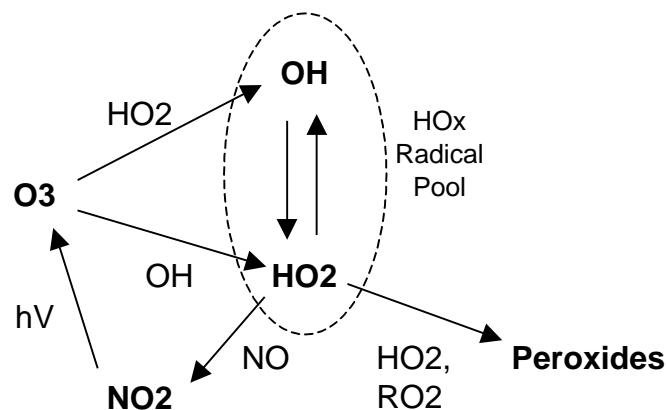


**Figure 7-3.  Daytime reactions of ozone with HOx (OH and $HO_2$) showing potential for reformation of ozone or ozone destruction via peroxide formation.**

Ozone reacts directly with both with OH and $HO_2$:

$$O_3 + OH \rightarrow O_2 + HO_2 (7) \qquad\qquad (7)$$
$$O_3 + HO_2 \rightarrow 2\ O_2 + OH \qquad\qquad (8)$$

Since OH and $HO_2$ radicals inter-convert rapidly during the daytime they can be viewed as a radical pool, called HOx.  During the daytime, there are two main sinks for HOx:

    (1) *propagation* by reaction with NO, which reforms ozone:

$$NO + HO_2 \rightarrow NO_2 + OH$$
$$NO_2 + h\nu \rightarrow NO + O(^3P)$$
$$\underline{O(^3P) + O_2 \rightarrow O_3}$$
$$\text{Net:}\quad HO_2 + O_2 + h\nu \rightarrow O_3 + OH$$
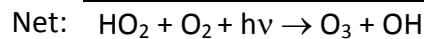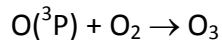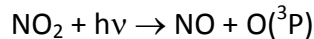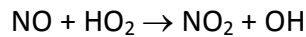
    (2) *termination* by reaction with $HO_2$ or $RO_2$ to form peroxides and other organic products, which prevents HOx from propagating to reform ozone:

$$HO_2 + HO_2 \rightarrow H_2O_2 + O_2$$
$$HO_2 + RO_2 \rightarrow ROOH + O_2$$
$$RO_2 + RO_2 \rightarrow \text{organic products} + O_2$$
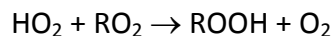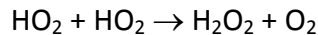
In the revised OSAT algorithms, the ozone destruction rate due to $O_3$ + HOx reactions is estimated as:

$$O_3\ \text{Destruction} \quad = \quad \text{Rate}_{(O_3 + HOx)} \times \left( \frac{\text{Rate}_{(HO_2\ term)}}{\text{Rate}_{(HO_2 + NO)} + \text{Rate}_{(HO_2\ term)}} \right)$$

This equation is the rate of $O_3$ + HOx reaction (i.e., the rates of [7] plus [8]) multiplied by a branching ratio that estimates the fraction of $O_3$ + HOx reactions that result in loss of ozone. The reaction of $O_3$ with $HO_2$ is the dominant destruction pathway for ozone under low NOx conditions at mid-latitudes (Wang et al., 2003).

Ozone destruction due to the $O_3$ + NO $\rightarrow$ $NO_2$ + $O_2$ titration reaction is explicitly <u>excluded</u> from the accounting of ozone destruction because it is hard to disentangle its role in ozone destruction and production.  Under high NOx (ozone titration) conditions and at night this reaction becomes clearly an ozone destruction pathway, and in these situations $\Delta O_3$ becomes negative and ozone destruction due to the $O_3$ + NO reaction is accounted for.  Under most daytime conditions, this reaction is part of the $O_3$, NO, $NO_2$ photo-stationary state and ozone can be reformed again when $NO_2$ photolyzes so this reaction is not clearly an ozone destruction pathway.

### 7.2.5.2  Distinguishing VOC-Limited from $NO_X$-Limited Ozone Formation

The classic trajectory model EKMA diagram can be used to distinguish VOC-limited from $NO_X$-limited trajectories and develop a classification based on initial VOC-to-$NO_X$ ratio.  However,

this approach classifies VOC- or $NO_X$-limited behavior based on the response of the peak ozone, which is the net response from several hours of photochemistry. In reality, many of the trajectories start out VOC-limited and become $NO_X$-limited during the course of the day essentially because the $NO_X$ is depleted more rapidly than the VOC. For OSAT, a more fundamental indicator of the instantaneous state of ozone formation with regard to VOC- or $NO_X$-limitation is required.

The sensitivity of ozone formation to VOCs and $NO_X$ at any given time is attributable to the fate of radicals. The radical pool is often referred to as odd-hydrogen ($HO_X$) and is most usefully considered as the sum of OH, $HO_2$ and $RO_2$ radicals. When $NO_X$ is plentiful, the main radical termination (i.e., $HO_X$ removal) pathway is nitric acid formation, i.e.:

$$OH + NO_2 (+M) \rightarrow HNO_3 (+M) \qquad (9)$$
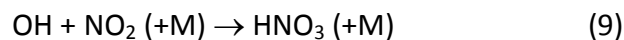
Under these conditions, ozone formation is limited by the rate at which radicals can be formed, which is generally described as the VOC-limited condition. Thus nitric acid ($HNO_3$) production is indicative of plentiful $NO_X$ and VOC-limited ozone formation.

When $NO_X$ is scarce, radical-radical reactions dominate $HO_X$ removal, e.g.:

$$HO_2 + HO_2 (+M) \rightarrow H_2O_2 + O_2 (+M) \qquad (10)$$

$$HO_2 + RO_2 \rightarrow ROOH + O_2 \qquad (11)$$
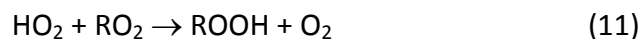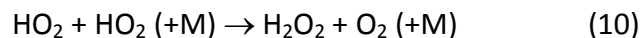
Under these conditions, ozone formation is limited by the availability of NO to react with $HO_2$ and $RO_2$ radicals, which is described as the $NO_X$-limited condition. $HO_2$ and $RO_2$ radicals that do not react with NO participate in peroxide formation. Thus, peroxide formation ($H_2O_2$ = hydrogen peroxide, or ROOH = organic hydroperoxides) is indicative of scarce $NO_X$ and $NO_X$-limited ozone formation.

Sillman (1995) has exploited this situation to develop useful indicators of VOC vs. $NO_X$ limited ozone formation based on the ratio of peroxide production to nitric acid production. Sillman proposed that the transition between these conditions occurs when:

$$(P_{H2O2} + P_{ROOH}) / P_{HNO3} = 0.5 \qquad (12)$$

The production rates of nitric acid ($P_{HNO3}$) and hydrogen peroxide ($P_{H2O2}$) in each CAMx grid cell at each time step are readily accessible. The balance between $P_{ROOH}$ and $P_{H2O2}$ depends upon the relative production of $HO_2$ and $RO_2$ radicals, and Sillman suggests that it is not highly variable within/across simulations. Accordingly, he proposes that equation (12) is equivalent to a transition point of:

$$P_{H2O2} / P_{HNO3} = 0.35 \qquad (13)$$

In other words, when this ratio exceeds 0.35 ozone formation is $NO_X$-limited, and when this ratio is less than 0.35 ozone formation is VOC-limited.

### 7.2.5.3  Evaluation of Sillman's $P_{H2O2}/P_{HNO3}$ Indicator

Equation (13) was evaluated as an indicator of VOC vs. $NO_X$-limited ozone formation for several trajectory model scenarios using the CB4 mechanism as implemented in the UAM.[4]  The ozone concentration for a scenario with an initial VOC/$NO_X$ ratio of 10 (0.3 ppmC of VOC, 30 ppb of $NO_X$) is shown in Figure 7-4.  Also plotted, against the right axis, is the ratio $P_{H2O2}/P_{HNO3}$.

Sillman's proposed $P_{H2O2}/P_{HNO3}$ transition point of 0.35 is shown by the dashed line.  Before about 12 noon, $P_{H2O2}/P_{HNO3}$ is less than 0.35 indicating VOC-limited ozone formation, whereas from about 12 noon to 7 PM $P_{H2O2}/P_{HNO3}$ exceeds 0.35 indicating $NO_X$-limited ozone formation. After 7 PM, $P_{H2O2}/P_{HNO3}$ falls below 0.35 again, but this is after the ozone peak when ozone is decreasing and the concepts of VOC and $NO_X$-limitation are no longer relevant.

In summary, the $P_{H2O2}/P_{HNO3}$ indicator suggested a transition from VOC to $NO_X$-limited ozone formation at about noon.  To investigate whether this prediction is corroborated by responses to emission controls, the trajectory model scenario was re-run with 30 percent reductions in initial concentrations and emissions of VOC and $NO_X$ (Figure 7-5).  Figure 7-5 shows that $NO_X$ controls started to be effective at about noon whereas VOC controls had maximum effect before noon.  This finding is even clearer in Figure 7-6, which shows the difference in ozone (control-base) for the reduced VOC and $NO_X$ cases.  Thus, the response of ozone to reducing VOC and $NO_X$ was found to be consistent with the prediction of the $P_{H2O2}/P_{HNO3}$ indicator.

The evaluation described above and shown in Figures 7-4 and 7-6 was repeated for two more scenarios with different base VOC/$NO_X$ ratios.  The results for a base VOC/$NO_X$ ratio of 20 (0.3 ppmC of VOC, 15 ppb of $NO_X$) are shown in Figure 7-7, and for a base VOC/$NO_X$ ratio of 5 (0.15 ppmC of VOC, 15 ppb of $NO_X$) are shown in Figure 7-8.  For a base VOC/$NO_X$ ratio of 20, Figure 7-7a shows that the transition from VOC to $NO_X$-limited ozone formation is predicted to occur at about 9:30 AM.  Figure 7-7b shows that this is confirmed by the response to VOC and $NO_X$ controls.  For a base VOC/$NO_X$ ratio of 5, Figure 7-8a shows that ozone formation is predicted to remain VOC-limited throughout the day.  Figure 7-8b confirms this by showing no net benefit from $NO_X$ control throughout the day.

---

[4] The scenarios begin at sunrise at 6 a.m. with 10 ppb of $O_3$ plus initial VOCs and $NO_X$.  There is no dilution, and 5 percent of the initial VOCs and $NO_X$ are added in each hour as emissions.
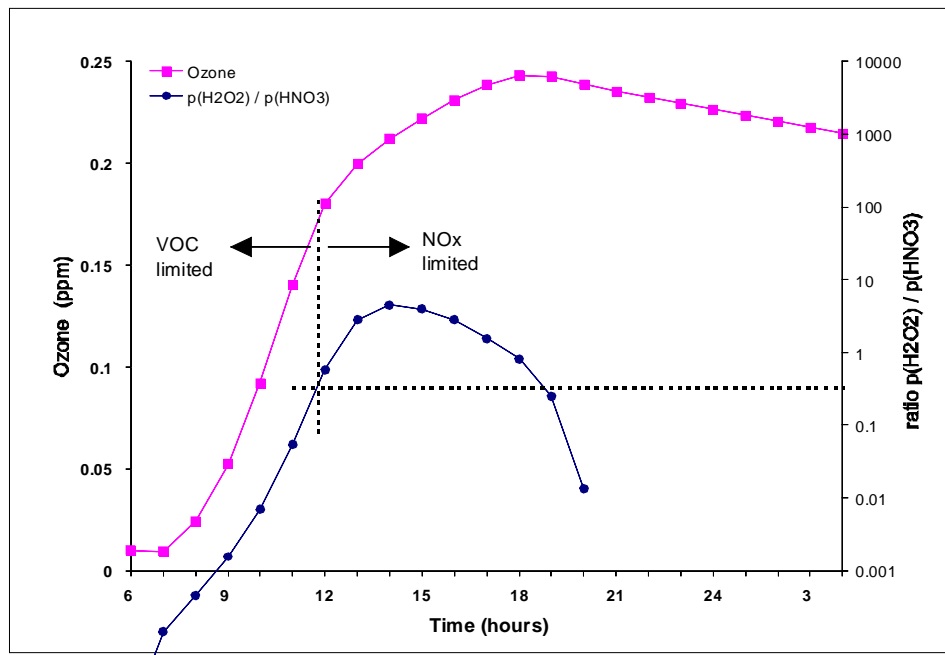
**Figure 7-4.** Box model simulation to evaluate $P_{H2O2}/P_{HNO3}$ indicator for VOC vs. NOx limited ozone formation (see text). Ozone is plotted against the left axis, $P_{H2O2}/P_{HNO3}$ is plotted against the right axis. For $P_{H2O2}/P_{HNO3}$ below 0.35 ozone formation is VOC limited. Thus, the transition from VOC to NOx limited ozone formation is predicted to occur about 12 noon. Initial VOC/NOx = 10:1.
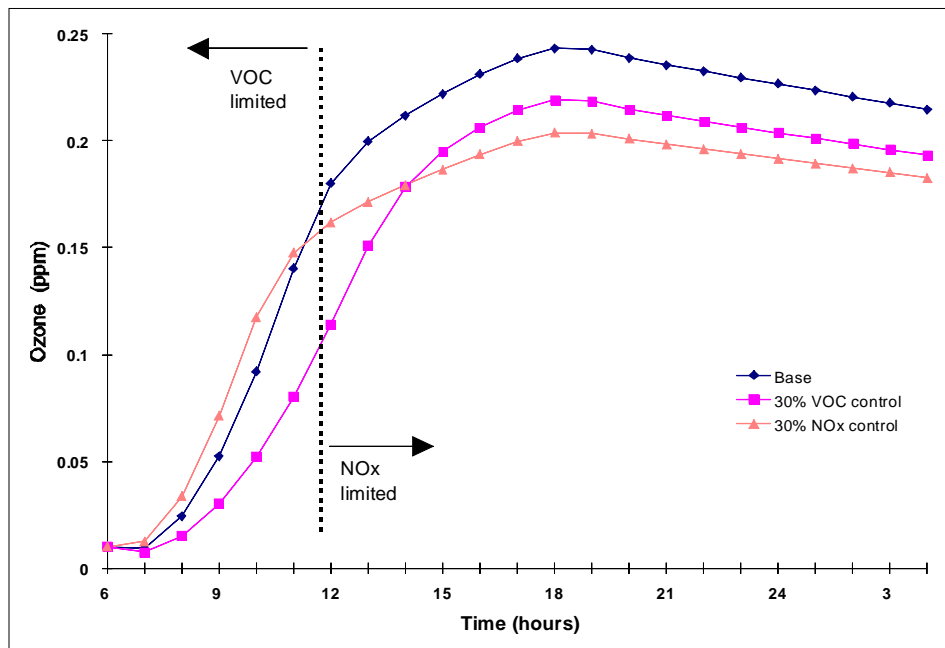


**Figure 7-5.** Effect on ozone of controlling VOC and NOx by 30 percent for the base scenario shown in Figure 7-4. The vertical dashed line shows the transition from VOC to NOx limited ozone formation for the base case derived in Figure 7-4. Initial base case VOC/NOx = 10:1.
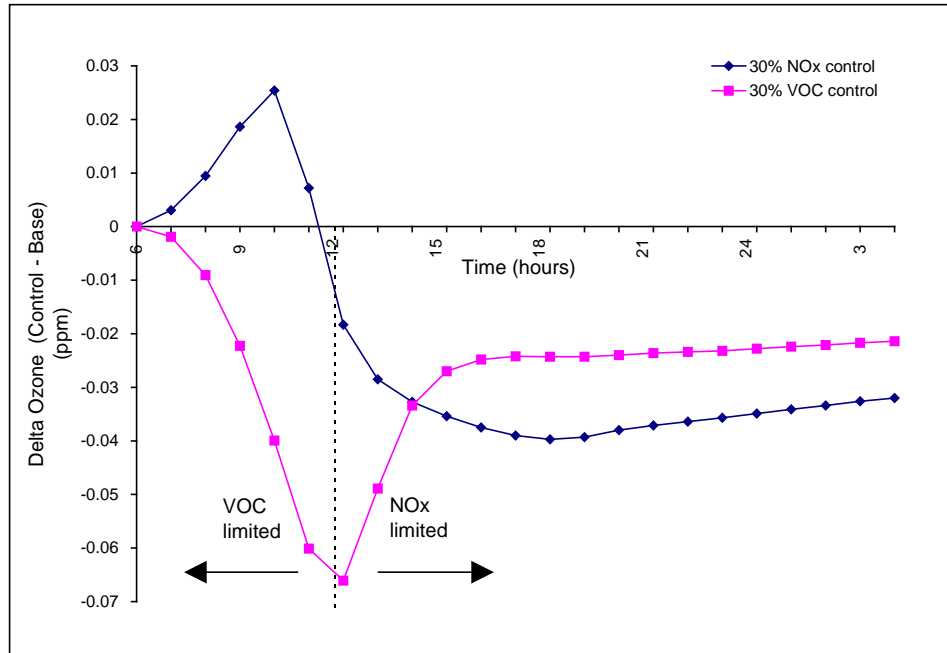
**Figure 7-6. Change in ozone (control-base) for the VOC and NOx control scenarios shown in Figure 7-5. The vertical dashed line shows the transition from VOC to NOx limited ozone formation for the base case derived in Figure 7-4. Initial base case VOC/NOx = 10:1.**
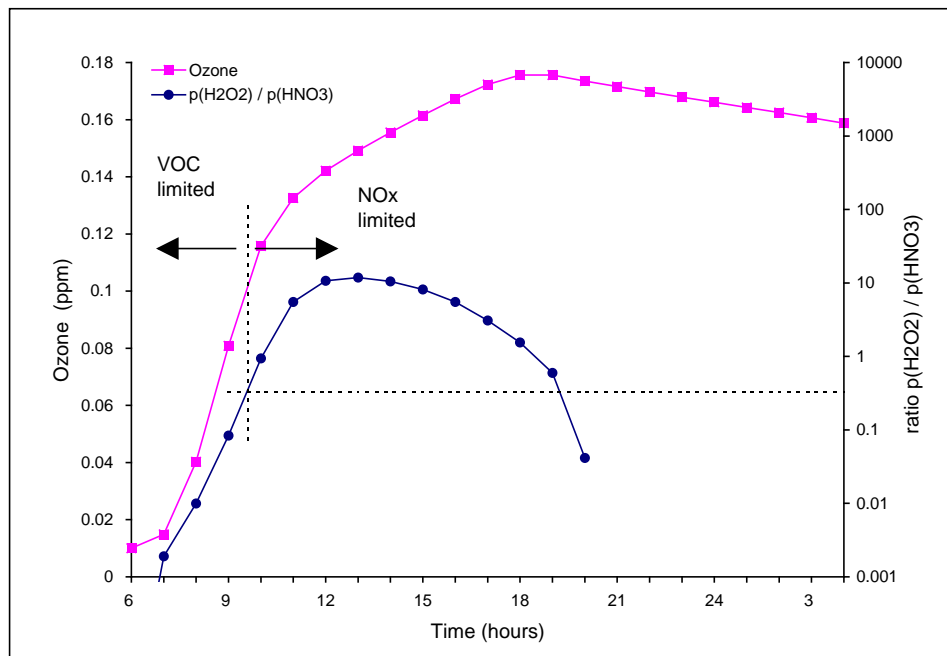


**Figure 7-7a. As Figure 7-4, but for an Initial VOC/NOx = 20:1.**
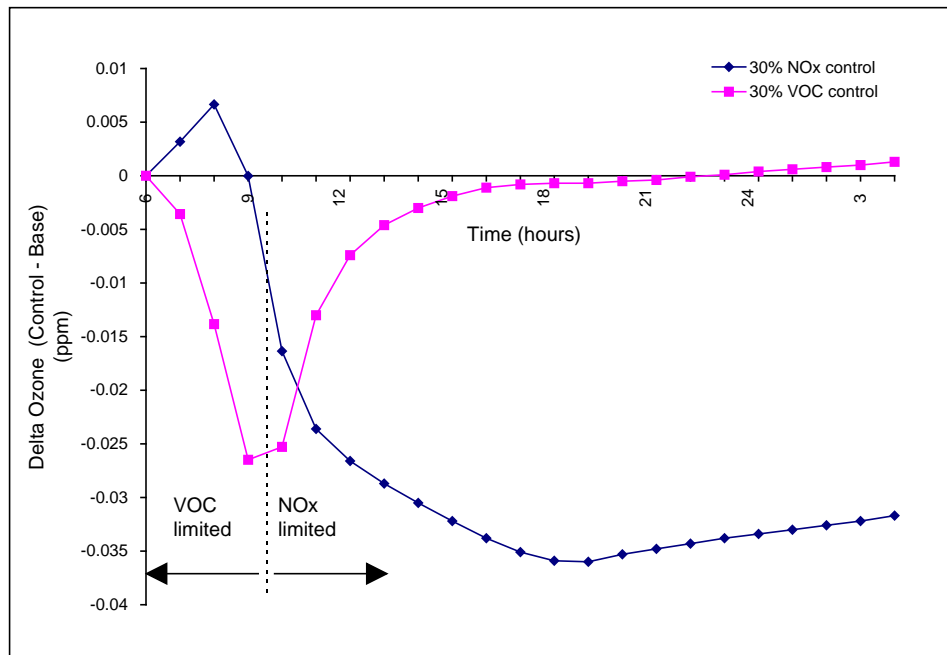
**Figure 7-7b.  As in Figure 7-6, but for an Initial VOC/NOx = 20:1.**
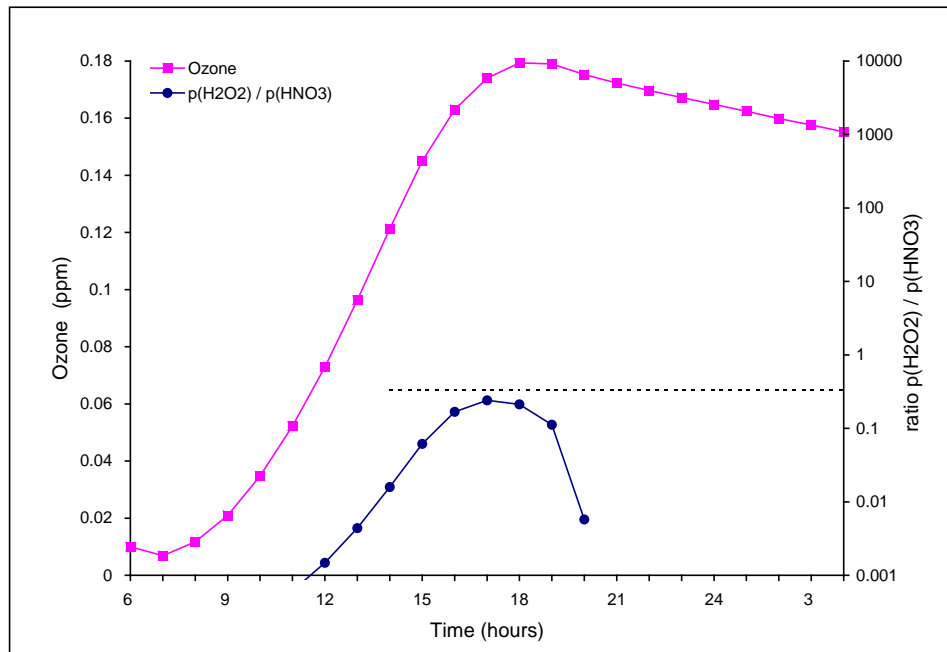


**Figure 7-8a.  As Figure 7-4, but for an Initial VOC/NOx = 5:1.**
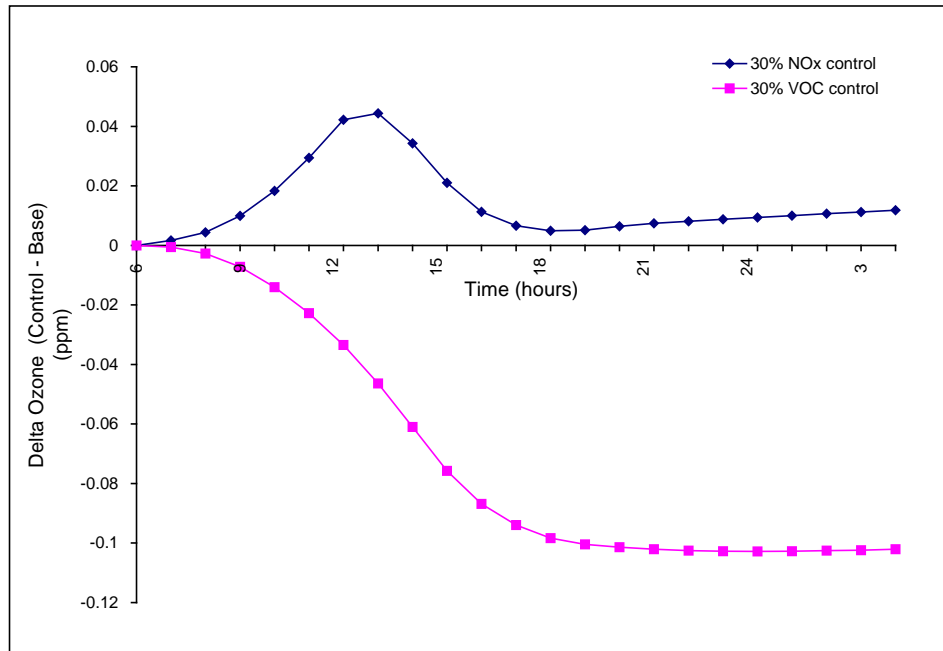
**Figure 7-8b.  As Figure 7-6, but for an Initial VOC/NOx = 5:1**

### 7.2.6  Alternative Chemical Apportionment Techniques

The formulation of OSAT described above was first methodology implemented into CAMx.
Several variations on OSAT are now available that use different algorithms to attribute ozone
contributions.  One advantage of the coding framework for OSAT is that it allows for easy
modification of the source attribution algorithm by modifying a single subroutine.  The
alternative methods currently available in CAMx are described below (other options are
possible).

> *Geographic Ozone Assessment Technology* (GOAT).  GOAT does not attempt to trace
> ozone production back to the source of the precursors, but rather ozone formation is
> tracked based on the geographic location where it occurred.  Thus ozone formation in a
> grid cell over "Area A" would be attributed to Area A even if the culpable emissions
> originated upwind in Area B.  The disadvantage of GOAT is its simplistic assumption
> regarding the basis for ozone culpability.  The advantages of GOAT are: (1) its freedom
> from assumptions about whether ozone formation is $NO_X$ or VOC limited; and (2) that its
> results may be more directly comparable to other emerging source attribution
> methodologies (e.g., trajectories, tracers, and possibly the spatial analysis component of
> Process Analysis).

> *Anthropogenic Precursor Culpability Assessment* (APCA).  APCA differs from OSAT in
> recognizing that certain emission groups are not controllable (e.g., biogenic emissions)
> and that apportioning ozone production to these groups does not provide information
> that is relevant to control strategies.  To address this, in situations where OSAT would
> attribute ozone production to non-controllable (i.e., biogenic) emissions, APCA re-

allocates that ozone production to the controllable portion of precursors that participated in ozone formation with the non-controllable precursor. In the case where biogenic emissions are the uncontrollable source category, APCA would only attribute ozone production to biogenic emissions when ozone formation is due to the interaction of biogenic VOC with biogenic $NO_X$. When ozone formation is due to biogenic VOC and anthropogenic $NO_X$ under VOC-limited conditions (a situation in which OSAT would attribute ozone production to biogenic VOC), APCA re-directs that attribution to the anthropogenic $NO_X$ precursors present. The use of APCA instead of OSAT results in more ozone formation attributed to anthropogenic $NO_X$ sources and less ozone formation attributed to biogenic sources. APCA is not really a "source apportionment" technique because it expresses biases as to which sources should be implicated (i.e., those that are controllable), hence it is referred to as a "culpability assessment." The APCA ozone allocation scheme is described in more detail below.

### 7.2.6.1 The APCA Technique

OSAT identifies which emission source regions, categories, and species (VOC and $NO_X$) that when reduced would have the greatest effect in reducing ozone concentrations. For the OTAG database, OSAT correctly identified biogenic VOC emissions as a major contributor to ozone formation, and if controlled, would result in efficient ozone reductions. However, biogenic emissions cannot be controlled; although scientifically and chemically correct, this information is irrelevant for the design of an ozone control strategy. The presence of a source category (biogenic emissions) that cannot be controlled requires special considerations when performing ozone source apportionment modeling for the purposes of aiding in the design of anthropogenic emission control strategies, or when performing an ozone precursor culpability analysis. (Note that some biogenic $NO_X$ emissions are soil $NO_X$ emissions, which are partly from fertilizers and thus are not truly "biogenic" in nature).

Biogenic versus anthropogenic ozone source apportionment, as a function of VOC and $NO_X$ precursor interactions, can be divided up into four ozone formation regimes as follows:

|  | Biogenic NOx | Anthropogenic NOx |
|---|---|---|
| Biogenic VOC | 1 | 2 |
| Anthropogenic VOC | 3 | 4 |

Regime 1 involves ozone formation due to the interaction between biogenic VOC and biogenic $NO_X$ and is truly "biogenic ozone". Regime 4 is true "anthropogenic ozone" and the OSAT attribution scheme will provide control strategy relevant information by allocating ozone formed in Regime 4 to the proper anthropogenic ozone precursors (VOC or $NO_X$). Difficulties arise in the mixed anthropogenic/biogenic regimes (Regimes 2 and 3) where precursors from both biogenic and anthropogenic sources participate in the ozone formation. Much of the ozone in the OTAG modeling is formed under Regime 2, although Regime 1 may have some influence on ozone formation in high biogenic $NO_X$ regions (e.g., the corn belt). To design effective control strategies, an ozone allocation scheme is needed that accounts for the special status of biogenic emissions as being uncontrollable.

In the APCA technique, only the true "biogenic ozone" (i.e., ozone formed under Regime 1) would be attributed to biogenic emissions, while ozone formed in the remainder of the regimes (2-4) would be allocated to anthropogenic emissions.  The standard OSAT approach is used to allocate ozone formed to anthropogenic VOC or $NO_X$ emissions when anthropogenic VOC and $NO_X$ emissions interact (i.e., Regime 4), and to allocate to biogenic VOC or $NO_X$ when these two precursors interact (Regime 1).  However, when ozone forms due to the interaction of biogenic and anthropogenic emissions (i.e., Regimes 2 and 3), the APCA technique differs from OSAT by allocating ozone formed to anthropogenic emissions; the ozone increment is allocated to anthropogenic $NO_X$ (if VOC-limited) or anthropogenic VOC (if $NO_X$-limited) precursors. Assuming that *N* and *V* are the $NO_X$ and reactivity-weighted VOC tracer concentrations in a grid cell from different source categories (e.g., biogenic sources and several anthropogenic emissions categories) that participated in the formation of an increment of ozone (O3), the APCA allocation scheme can be expressed mathematically as follows.

First, APCA defines the fraction of ozone formed due to the interaction of biogenic VOC with biogenic $NO_X$, which will be attributed to biogenic emissions (Regime 1):

$$F_{bio} \quad = \quad \min\left(\frac{V_{bio}}{V_{total}}, \frac{N_{bio}}{N_{total}}\right)$$

under VOC-limited conditions, APCA attributes the fraction of ozone formed to biogenic VOC emissions (Regime 1):

$$O3V_{bio} \quad = \quad F_{bio} \times O_3$$

It then attributes the fraction of ozone increment to anthropogenic VOC source groupings due to the interaction of anthropogenic VOC with anthropogenic and biogenic $NO_X$ (Regime 4):

$$O3V^i_{anthro} \quad = \quad \left(\frac{V^i_{anthro}}{V_{total}}\right) \times O_3, \quad i = 1,...,nanthro$$

Finally, the remainder of the ozone increment ($\Delta O3$), which would have been attributed to biogenic VOC in OSAT, is attributed to anthropogenic $NO_X$ (Regimes 2 and 3):

$$\Delta O3 \quad = \quad O_3 - O3V_{bio} - \sum_i O3V^i_{anthro}$$

$$O3N^i_{anthro} = \left(\frac{N^i_{anthro}}{N^{total}_{anthro}}\right) \times \Delta O_3, \quad i = 1,...,nanthro$$

Under $NO_X$-limited conditions, similar formulas are used, switching the *N* with *V* and *O3N* with *O3V*.  Since it is expected that biogenic VOC precursors will almost always be greater than biogenic $NO_X$ precursors (i.e., $F_{bio} = N_{bio}/N_{total}$), then under $NO_X$-limited conditions the APCA ozone allocation scheme will produce identical results to OSAT.

## 7.3  Running CAMx With OSAT

### 7.3.1  CAMx Control File

OSAT and its derivatives are invoked similarly to the other Probing Tools within the CAMx control file.  In the `&CAMx_Control` namelist module, the variable `Probing_Tool` must be set to "OSAT", "GOAT", or "APCA".  An additional namelist module called `&SA_Control` must then be provided in the control file to configure the OSAT portion of the model.  The additional namelist module is described below.  The order of the variables follows the template available with the source code.  Several examples of the OSAT portion of the CAMx run control file are shown in Figures 7-9(a-d).

**Description of OSAT Control in the CAMx Run Control File**

| | |
|---|---|
| `&SA_Control` | Label for the Probing Tool namelist module that configures the OSAT option; it must begin in column 2 |
| `&` | Flag ending a namelist module; it must be in column 2 |
| `SA_Summary_Output` | Logical flag used to limit the species written to the tracer concentration file to a subset of the PSAT treated species. If set to true, the output will be restricted to the following species: *O3N*, *O3V* |
| `SA_File_Root` | Character root output path/filename |
| `SA_Master_Sfc_Output` | Logical flag for master grid surface output (TRUE=OSAT concentration file will be output for all tracers, FALSE=OSAT concentration file will not be output) |
| `SA_Nested_Sfc_Output` | Logical flag for nested grid surface output (TRUE=OSAT concentration file will be output for all tracers, FALSE=OSAT concentration file will not be output) |
| `SA_Stratify_Boundary` | Logical flag to stratify boundary types (TRUE=separate tracer types will be used for the N, S, E, W, and Top boundaries, FALSE=a single tracer type will be used for all 5 boundaries) |
| `SA_Deposition_Output` | Logical flag to output deposited tracer mass to a file (TRUE=output deposited tracer mass, FALSE=do not generate a tracer deposition output file) |
| `SA_Number_of_Source_Regions` | Integer number of source regions for this run.  This must be the same as the number of source areas defined in the `SA_Source_Area_Map` file. |
| `SA_Number_of_Source_Groups` | Integer number of emission groups for this run.  Together with the `Use_Leftover_Group` flag, this determines the number |

of paired emission files that must be supplied (additional details below).

| | |
|---|---|
| `Use_Leftover_Group` | Logical flag to define a "leftover" emissions group (TRUE= calculate a "leftover" emissions group from the difference between the sum of the emission group files and the regular CAMx emission files, FALSE=do not calculate a "leftover" emissions group) |
| `SA_Receptor_Definitions` | Character input OSAT receptor definition path/filename. (This is an optional file). |
| `SA_Source_Area_Map` | Character array (by CAMx grid) input OSAT source area definition path/filename (required for master grid, optional for nested grids) |
| `SA_Master_Restart` | Character input master grid OSAT restart path/filename (ignored if `Restart=FALSE`) |
| `SA_Nested_Restart` | Character input nested grid OSAT restart path/filename (ignored if `Restart=FALSE` or `Number_of_Grids=1`) |
| `SA_Points_Group` | Character array (by source group) input OSAT elevated point source emissions path/filename (optional, ignored if `Point_Emissions=FALSE`) |
| `SA_Emiss_Group_Grid` | Character array (by source group, by CAMx grid) input OSAT gridded emissions path/filename (optional, ignored if `Gridded_Emissions=FALSE`) |

### 7.3.2  Specifying Emission Groups

OSAT can apportion ozone and ozone precursor concentrations among several emission categories.  To achieve this, the emissions for the separate groups must be supplied as sets of separate emissions files for each source group; a low level (gridded) file for each fine grid nest, and one elevated point source file.  The additional emission files must be in the CAMx emission file format, as described in Section 3.  If the group being separated has no elevated emissions (e.g. biogenics), the point source file name for the group can be left blank.  If the emission group being separated has no surface emissions (e.g. a utility), the surface file name for the group can be left blank for all grids.  APCA requires two or more emissions categories, with the first category being biogenic emissions.

Imagine a case where the emission inventory is split into three groups.  Three sets of emission files could be supplied that together have the same total emissions as the regular CAMx emissions files.  Alternatively, two sets of files could be supplied and the third calculated from the "leftover" emissions (i.e., the regular CAMx emissions minus the two groups specified).  Both approaches could be useful, depending upon the emissions files available to the user.

Accordingly, OSAT reads an input flag "`Use_Leftover_Group`" that can be set true or false. If a leftover group is selected, the model verifies that the group is not too small to calculate within the numerical precision of the computer (this also traps cases where the flag was set true in error). If no leftover group is selected, the model verifies that the total emissions for the groups supplied are equal to the regular model emissions, i.e., that a leftover group is not needed. In both cases, if appropriate conditions are not met, the model stops with a descriptive error message.

The number of emission file sets that need to be supplied for different model configurations is summarized in Table 7-1; the table also shows how the emissions groups are numbered, which is reflected in the tracer species names (defined below).

**Table 7-1. Numbers of emission file sets (i.e., low level files and point source file) needed for different model configurations.**

| Number of Emission Groups | Use Leftover Group | Number of Emission File Sets Needed | Numbering of Emission Groups and Tracer Species |
|---|---|---|---|
| 1 | Not Applicable | 0 | 0 |
| n>1 | False | n | 1,2,3,…n |
|  | True | n-1 | 1,2,3,…n |

When specifying additional point source files to resolve source category groupings, the list of point sources on each file must be identical (i.e., same number of sources, same order) to the regular model point source file. This formal restriction is necessary to ensure that point sources are correctly cross-referenced within CAMx. Thus, a point source file for a specific source group may need to contain records for sources that are not in the group: these records should have zero emissions.

Geographic resolution is superimposed on emission group resolution using the source area map described below. The source area map is defined using grid cells, which may not adequately resolve point source locations. To provide finer control of point source assignments to geographic areas, the source area can be specified for any source by putting the source area index in the (unused) `kcell` value on the point source file (see file description in section 3). This feature is referred to as "point source override."

```
&SA_Control

SA_File_Root                 = '$TRACOUT/CAMx.OSAT.9507$today',

SA_Master_Sfc_Output         = .true.,
SA_Nested_Sfc_Output         = .true.,
SA_Summary_Output            = .true.,
SA_Stratify_Boundary         = .false.,
SA_Deposition_Output         = .false.,
SA_Number_of_Source_Regions  = 19,
SA_Number_of_Source_Groups   = 1,
Use_Leftover_Group           = .false.,

SA_Receptor_Definitions  = '$TRACIN/receptor.cities ',
SA_Source_Area_Map(1)    = '$TRACIN/APCA.source.area.map',
SA_Source_Area_Map(2)    = ' ',

SA_Master_Restart        = ' ',
SA_Nested_Restart        = ' ',

SA_Points_Group(1)       = ' ',

SA_Emiss_Group_Grid(1,1) = ' ',
SA_Emiss_Group_Grid(1,2) = ' ',

&
```

**Figure 7-9a.  An example of OSAT input records in the CAMx run control file.  The options for this run are as follows: this is a two-grid run, master and nested grid surface concentrations are written to file, a single tracer type is to be used for all boundaries, 19 source regions, and one emission group (i.e., zero additional emission files and no leftover group).  This is the first day of the simulation (i.e., restart is false), so no OSAT restart files are supplied.**

```
&SA_Control

SA_File_Root                = '$TRACOUT/CAMx.OSAT.9507$today',

SA_Master_Sfc_Output        = .true.,
SA_Nested_Sfc_Output        = .true.,
SA_Summary_Output           = .true.,
SA_Stratify_Boundary        = .false.,
SA_Deposition_Output        = .false.,
SA_Number_of_Source_Regions = 19,
SA_Number_of_Source_Groups  = 1,
Use_Leftover_Group          = .false.,

SA_Receptor_Definitions  = '$TRACIN/receptor.cities ',
SA_Source_Area_Map(1)    = '$TRACIN/APCA.source.area.map',
SA_Source_Area_Map(2)    = ' ',

SA_Master_Restart           = '$TRACOUT/CAMx.OSAT.9507$yesterday.sa.inst',
SA_Nested_Restart           = '$TRACOUT/CAMx.OSAT.9507$yesterday.sa.finst',

SA_Points_Group(1)       = ' ',

SA_Emiss_Group_Grid(1,1) = ' ',
SA_Emiss_Group_Grid(1,2) = ' ',

&
```

**Figure 7-9b.  As in Figure 7-9(a), but in this case the run is a continuation, and so the restart flag is set to TRUE and a "Tracer Restart" files are supplied.**

```
&SA_Control

 SA_File_Root                  = '$TRACOUT/CAMx.OSAT.9507$today',

 SA_Master_Sfc_Output          = .true.,
 SA_Nested_Sfc_Output          = .true.,
 SA_Summary_Output             = .true.,
 SA_Stratify_Boundary          = .false.,
 SA_Deposition_Output          = .false.,
 SA_Number_of_Source_Regions   = 19,
 SA_Number_of_Source_Groups    = 3,
 Use_Leftover_Group            = .true.,

 SA_Receptor_Definitions   = '$TRACIN/receptor.cities ',
 SA_Source_Area_Map(1)     = '$TRACIN/APCA.source.area.map',
 SA_Source_Area_Map(2)     = ' ',

 SA_Master_Restart         = '$TRACOUT/CAMx.OSAT.9507$yesterday.sa.inst',
 SA_Nested_Restart         = '$TRACOUT/CAMx.OSAT.9507$yesterday.sa.finst',

 SA_Points_Group(1)        = ' ',
 SA_Points_Group(2)        = '$PTSRCE/utilpt.ng.$todate-07.ag.07cem1A-run11',

 SA_Emiss_Group_Grid(1,1) = '$TRACEMS/bio2.cc.$todate-95',
 SA_Emiss_Group_Grid(1,2) = '$TRACEMS/bio2.ff.$todate-95.ne',
 SA_Emiss_Group_Grid(2,1) = '$TRACEMS/util.cc.$todate-07.ag.07cem1A-run11',
 SA_Emiss_Group_Grid(2,2) = '$TRACEMS/util.ff.$todate-07.ag.07cem1A-run11',

 &
```

**Figure 7-9c.  As in Figure 7-9(a), but in this case the run is a continuation day of a run with three emission groups.  The three emission groups are defined by supplying two pairs of extra emission files for each grid (AREA group 1, AREA group 2, and POINT group 2), and setting the "Use_Leftover_Group" flag to TRUE for the model to calculate the third group internally.  The POINT group 1 filename is blank because group 1 is a category with no point source emissions (e.g., biogenics).**

```
&SA_Control

 SA_Master_Sfc_Output           = .true.,
 SA_Nested_Sfc_Output           = .true.,
 SA_Summary_Output              = .true.,
 SA_Stratify_Boundary           = .false.,
 SA_Deposition_Output           = .false.,
 SA_Number_of_Source_Regions    = 19,
 SA_Number_of_Source_Groups     = 3,
 Use_Leftover_Group             = .false.,

 SA_Receptor_Definitions   = '$TRACIN/receptor.cities ',
 SA_Source_Area_Map(1)     = '$TRACIN/APCA.source.area.map',
 SA_Source_Area_Map(2)     = ' ',

 SA_Master_Restart         = '$TRACOUT/CAMx.OSAT.9507$yesterday.sa.inst',
 SA_Nested_Restart         = '$TRACOUT/CAMx.OSAT.9507$yesterday.sa.finst',

 SA_Points_Group(1)        = ' ',
 SA_Points_Group(2)        = '$PTSRCE/utilpt.ng.$todate-07.ag.07cem1A-run11',
 SA_Points_Group(3)        = '$PTSRCE/remain.ng.$todate-07.ag.07cem1A-run11',

 SA_Emiss_Group_Grid(1,1) = '$TRACEMS/bio2.cc.$todate-95',
 SA_Emiss_Group_Grid(1,2) = '$TRACEMS/bio2.ff.$todate-95.ne',
 SA_Emiss_Group_Grid(2,1) = '$TRACEMS/util.cc.$todate-07.ag.07cem1A-run11',
 SA_Emiss_Group_Grid(2,2) = '$TRACEMS/util.ff.$todate-07.ag.07cem1A-run11',
 SA_Emiss_Group_Grid(3,1) = '$TRACEMS/remain.cc.$todate-07.ag.07cem1A-run11',
 SA_Emiss_Group_Grid(3,2) = '$TRACEMS/remain.ff.$todate-07.ag.07cem1A-run11',

 &
```

**Figure 7-9d.  As in Figure 7-9(c) (i.e. a continuation day of a run with three emission groups), but in this case all three emission groups are defined explicitly by supplying extra emission files (AREA group 1, AREA group 2, POINT group 2, AREA group 3, and POINT group 3).  Therefore, the "Use_Leftover_Group" flag is set to FALSE.  The POINT group 1 filename is blank because group 1 is a category with no point source emissions (e.g., biogenics).**

## 7.4 Input File Formats

### 7.4.1 Source Area Mapping

OSAT can apportion ozone and ozone precursor concentrations among several geographic regions within the modeling domain, as shown in Figure 7-1. The "source area mapping" file assigns each grid cell to a specific geographic source region. The format of the file is an array of integer numbers (i3) corresponding to the CAMx domain. Figure 7-10 shows the source area mapping file for the single grid corresponding to Figure 7-1. Since the CAMx domain in Figure 7-1 has 63 rows and 64 columns of cells, the file shown in Figure 7-10 has 63 lines with 64 numbers on each line. The first number (top left) always corresponds to the Northwest corner of the domain.

A source area map must be defined for the master grid and optionally any nested grids. The source area map for a nest is in the same format as the master grid source area map described above, but contains a number of rows and columns corresponding to the nested grid, ***including the boundary ("buffer") rows and columns***. Within a nest for which a nested grid source area map is supplied, the source areas as defined by this map will take precedence over the source areas defined by the master grid source area map. If a source area map is not provided for a specific nest the source area definition will be taken from the source area map of the parent grid.

### 7.4.2 Receptor Definition

Tracer concentrations for selected receptor locations are output to an ASCII file every hour. The receptors for each model run are defined in the "Receptor definition" input file. Three types of receptors are supported:

| | |
|---|---|
| POINT | a point specified in the coordinate system of the CAMx grid. Concentrations at the point are determined by bi-linear interpolation of the surrounding four master grid surface cells. |
| SINGLE CELL | a single surface grid cell identified by number. |
| CELL AVERAGE | a group of grid cells identified by number that are averaged together to provide multi-cell average tracer concentrations. |
| WALL OF CELLS | a group of grid cells defining a wall (i.e., a flux plane). |

For the receptor types that are defined by grid cell it is necessary to specify the grid containing the receptor. This is done by including the grid number on the receptor definition record. Grid numbers are defined using the internal CAMx grid ordering. The grid numbering as defined by CAMx is shown in a table in the .diag file. Each receptor can be identified by a 10 character name. The formats for specifying each receptor type are given in Table 7-2. An example receptor file is shown below:

```
31 31 31 31 18 18 18 18 18 18 18 18 18 18 37 37 37 37 17 17 17 17 17 17 17 17 17 17 17 17 40 40 40 40 40 40 40 40 40 40 40 40 40 40 40 40 40 40 40 40 40 40 40 40 14 14 14 14 14 40
31 31 31 31 31 18 18 18 18 18 18 18 18 18 37 37 37 37 37 17 17 17 17 17 17 17 17 17 17 17 40 40 40 40 40 40 40 40 40 40 40 40 40 40 40 40 40 40 40 40 40 40 40 40 14 14 14 14 14 40
31 31 31 31 31 18 18 18 18 18 18 18 18 37 37 37 37 37 37 37 17 17 17 17 17 17 17 17 17 17 17 40 40 40 40 40 40 40 40 40 40 40 40 40 40 40 40 40 40 40 40 40 40 14 14 14 14 14 14 40
31 31 31 31 31 18 18 18 18 18 18 18 18 37 37 37 37 37 37 37 37 17 17 17 17 17 17 17 17 17 17 40 40 40 40 40 40 40 40 40 40 40 40 40 40 40 40 40 40 40 40 40 40 14 14 14 14 14 14 40
31 31 31 31 31 18 18 18 18 18 18 18 37 37 37 37 37 37 37 37 37 37 17 17 17 17 17 17 17 17 17 40 40 40 40 40 40 40 40 40 40 40 40 40 40 40 40 40 40 40 40 40 40 14 14 14 14 14 14 40
31 31 31 31 31 18 18 18 18 18 18 18 37 37 37 37 37 37 37 37 37 37 37 17 17 17 17 17 17 17 17 17 17 40 40 40 40 40 40 40 40 40 40 40 40 40 40 40 22 14 14 14 14 14 14 14 14 14 14 14
31 31 31 31 31 18 18 18 18 18 18 18 37 37 37 37 37 37 37 37 37 37 37 17 17 17 17 17 17 17 17 17 17 40 40 40 40 40 40 40 40 40 40 40 40 24 24 24 24 24 34 34 34 34 22 14 14 14 14 14 14 14
31 31 31 31 31 18 18 18 18 18 18 18 37 37 37 37 37 37 37 37 37 37 37 17 17 17 17 17 17 17 17 17 17 40 40 40 40 40 40 40 40 40 40 40 40 24 24 24 24 24 34 34 34 34 22 14 14 14 14 14 14 14
31 31 31 31 31 18 18 18 18 18 18 18 37 37 37 37 37 37 37 37 37 37 37 17 17 17 17 17 17 17 17 17 17 40 40 40 40 40 40 40 40 40 40 40 40 24 24 24 24 24 34 34 34 22 22 14 14 14 14 14 38 38 38
31 31 31 31 31 18 18 18 18 18 18 18 37 37 37 37 37 37 37 37 37 37 37 17 17 17 17 17 17 17 17 17 17 40 40 40 40 40 40 40 40 40 40 40 40 24 24 24 24 24 34 34 34 22 22 14 14 14 14 14 38 38 38
31 31 31 31 31 10 10 10 10 10 10 10 10 10 10 37 37 37 37 37 37 37 37 37 37 17 17 17 17 17 17 17 17 40 40 40 40 40 40 40 40 40 40 40 40 24 24 24 24 24 24 24 24 24 34 34 22 22 22 14 14 38 38 38 38
31 31 31 31 31 10 10 10 10 10 10 10 10 10 10 10 37 37 37 37 37 37 37 37 37 37 17 17 17 17 17 17 17 17 40 40 40 40 40 40 40 40 40 40 40 40 24 24 24 24 24 24 24 24 24 34 22 22 22 14 14 38 38 38 38 38
21 21 21 31 31 10 10 10 10 10 10 10 10 10 10 37 37 37 37 37 37 37 37 37 37 37 24 24 24 24 34 22 22 22 16 16 38 38 38 38 38 38
21 21 21 21 21 10 10 10 10 10 10 10 10 10 10 10  8  8 37 37 37 37 37 17 17 17 17 17 17 17 17 40 40 40 40 24 24 24 24 24 24 24 24 24 24 16 16 16 16 16 16 16 38 38 38 38 38 38
21 21 21 21 21 10 10 10 10 10 10 10 10 10 10  8  8  8  8  8  8  8 17 17 17 17 17 17 17 17 17 40 26 26 26 28 24 24 24 24 24 24 24 24 24 24 16 16 16 16 16 16 16 38 38 38 38 38 38
21 21 21 21 21 21 10 10 10 10 10 10 10 10 10 10 10  8  8  8  8  8  9  9 17 17 17 17 17 17 17 26 26 26 26 26 28 28 28 28 28 28 28 28 28 28 24 24  3  3  3 29 29 16 16 16 38 38 38 38
21 21 21 21 21 21 10 10 10 10 10 10 10 10 10 10  8  8  8  8  8  9  9  9  9  9 26 26 26 26 26 26 26 26 28 28 28 28 28 28 28 28 28 28 24 24  3  3  3 29 29 16 16 16 38 38 38 38
21 21 21 21 21 21 10 10 10 10 10 10 10 10 10  8  8  8  8  8  8  9  9  9  9  9 26 26 26 26 26 26 26 26 28 28 28 28 28 28 28 28 28 28 23 24 24  3  3 24 24 29 16 16 16 38 38 38 38
21 21 21 21 21 21 10 10 10 10 10 10 10 10 10  8  8  8  8  8  8  9  9  9  9  9 26 26 26 26 26 26 26 26 28 28 28 28 28 28 28 28 28 23 23 24 24 24 24 38 38 38 38 38 38 38 38 38
21 21 21 21 21 21 21 20 20 20 20 20 20 20 20  8  8  8  8  8  8  9  9  9  9  9 26 26 26 26 26 26 26 26 28 28 28 28 28 28 28 28 28 23 23 24 24 38 38 38 38 38 38 38 38 38 38 38
21 21 21 21 21 21 21 20 20 20 20 20 20 20  8  8  8  8  8  8  9  9  9  9  9 26 26 26 26 26 26 26 26 28 28 28 28 28 28 28 28 23 23 23 38 38 38 38 38 38 38 38 38 38 38 38
11 11 11 11 11 11 11 11 20 20 20 20 20 20 20 20  8  8  8  8  8  8  9  9  9  9 26 26 26 26 26 26 26 26 36 36 36 15 36 36 15 15 15 15  4 28 23 23 38 38 38 38 38 38 38 38 38 38 38 38
11 11 11 11 11 11 11 11 20 20 20 20 20 20 20 20  8  8  8  8  8  9  9  9  9  9 26 26 26 26 26 26 26 26 36 36 36 36 36 36 36 36 35 15 15 15 15  4 23 23 23 38 38 38 38 38 38 38 38 38 38 38
11 11 11 11 11 11 11 11 11 20 20 20 20 20 20 20 20  8  8  8  8  9  9  9  9  9 12 12 26 26 26 26 36 36 36 36 36 36 35 35 35 15 15 15 15  4 23 38 38 38 38 38 38 38 38 38 38 38 38
11 11 11 11 11 11 11 11 11 20 20 20 20 20 20 20 20  8  8  8  8  9  9  9  9  9 12 12 12 12 12 12 12 36 36 36 36 36 35 35 35 35 35 15 15 15 15  4 38 38 38 38 38 38 38 38 38 38 38 38 38
11 11 11 11 11 11 11 11 11 20 20 20 20 20 20 20 20  8  8  8  9  9  9  9 12 12 12 12 12 12 12 12 36 36 36 36 36 35 35 35 35 35 35 35 35 38 38 38 38 38 38 38 38 38 38 38 38
11 11 11 11 11 11 11 11 11 20 20 20 20 20 20 20 20  8  8  8 12 12 12 12 12 12 12 12 12 12 12 12 36 36 36 35 35 35 35 35 35 35 35 35 35 38 38 38 38 38 38 38 38 38 38 38 38
11 11 11 11 11 11 11 11 11 20 20 20 20 20 20 20 20  8  8  8 12 12 12 12 12 12 12 12 12 12 12 12 36 36 36 35 35 35 35 35 35 35 35 35 35 38 38 38 38 38 38 38 38 38 38 38 38
27 27 27 27 27 27 27 27 27 20 20 20 20 20 20 20 20 12 12 12 12 12 12 12 12 12 12 12 12 35 35 35 35 35 35 35 35 35 35 35 35 35 35 38 38 38 38 38 38 38 38 38 38 38 38
27 27 27 27 27 27 27 27 27 20 20 20 20 20 20 20 20 32 32 32 32 32 32 32 32 32 32 32 32 32 32 25 25 25 25 25 25 25 25 25 25 25 25 38 38 38 38 38 38 38 38 38 38 38 38
27 27 27 27 27 27 27 27  2  2  2  2  2  2  2  2 20 32 32 32 32 32 32 32 32 32 32 32 32 32 32 25 25 25 25 25 25 25 25 25 25 25 25 38 38 38 38 38 38 38 38 38 38 38 38
27 27 27 27 27 27 27 27  2  2  2  2  2  2  2  2 32 32 32 32 32 32 32 32 32 32 32 32 32 32 32 25 25 25 25 25 25 25 25 25 25 25 25 25 38 38 38 38 38 38 38 38 38 38 38 38
27 27 27 27 27 27 27 27  2  2  2  2  2  2  2  2 32 32 32 32 32 32 32 32 32 32 32 32 32 25 25 25 30 30 25 25 25 25 25 25 25 25 25 25 38 38 38 38 38 38 38 38 38 38 38 38
27 27 27 27 27 27 27 27  2  2  2  2  2  2  2 19 19 19 19 19  1  1  1  1  1  7  7  7  7 30 30 30 30 30 30 25 25 25 25 25 25 25 25 38 38 38 38 38 38 38 38 38 38 38 38
27 27 27 27 27 27 27 27  2  2  2  2  2  2  2 19 19 19 19 19  1  1  1  1  1  7  7  7  7  7 30 30 30 30 30 30 25 25 25 25 25 25 25 25 38 38 38 38 38 38 38 38 38 38 38 38
33 33 33 33 33 27 33 33 27  2  2  2  2  2  2 19 19 19 19 19  1  1  1  1  1  1  7  7  7  7  7 30 30 30 30 30 30 30 25 25 25 25 25 25 25 38 38 38 38 38 38 38 38 38 38 38 38
33 33 33 33 33 33 33 33 33  2  2  2  2  2  2 19 19 19 19 19  1  1  1  1  1  1  7  7  7  7  7 30 30 30 30 30 30 38 38 38 38 38 38 38 38 38 38 38 38 38 38 38 38 38 38
33 33 33 33 33 33 33 33 33  2  2  2  2  2  2 19 19 19 19 19  1  1  1  1  1  1  7  7  7  7  7 30 30 30 30 30 38 38 38 38 38 38 38 38 38 38 38 38 38 38 38 38 38 38
33 33 33 33 33 33 33 33 33 13 13 13 13 13 19 19 19 19 19 19  1  1  1  1  1  1  7  7  7  7  7 30 30 30 30 38 38 38 38 38 38 38 38 38 38 38 38 38 38 38 38 38 38
33 33 33 33 33 33 33 33 33 13 13 13 13 13 19 19 19 19 19 19  1  1  1  1  1  1  7  7  7  7  7  7 30 30 30 38 38 38 38 38 38 38 38 38 38 38 38 38 38 38 38 38 38 38
33 33 33 33 33 33 33 33 33 13 13 13 13 13 19 19 19 19 19 19  1  1  1  1  1  1  7  7  7  7  7  7  7 30 30 38 38 38 38 38 38 38 38 38 38 38 38 38 38 38 38 38 38 38
33 33 33 33 33 33 33 33 33 13 13 13 13 13 19 19 19 19 19 19  1  1  1  1  1  1  7  7  7  7  7  7  7 38 38 38 38 38 38 38 38 38 38 38 38 38 38 38 38 38 38 38
33 33 33 33 33 33 33 33 33 13 13 13 13 13 13 13 19 19 19  1  1  6  6  6  6  6  7  7  7  7  7  7  7 38 38 38 38 38 38 38 38 38 38 38 38 38 38 38 38 38 38 38
33 33 33 33 33 33 33 33 33 13 13 13 13 13 13 13 19 19 19  1  1  6 39  6  6  6  6  6  6  6  6  6  6 38 38 38 38 38 38 38 38 38 38 38 38 38 38 38 38 38 38 38
33 33 33 33 33 33 33 33 33 13 39 13 13 13 13 13 13 39 39 39 39 39 39 39  6  6 39 39  6  6  6  6  6 38 38 38 38 38 38 38 38 38 38 38 38 38 38 38 38 38 38 38
33 33 33 33 33 33 33 33 39 39 39 39 39 39 39 39 39 13 39 39 39 39 39 39 39 39 39 39  6  6  6  6  6 38 38 38 38 38 38 38 38 38 38 38 38 38 38 38 38 38 38 38
33 33 33 33 33 33 33 39 39 39 39 39 39 39 39 39 39 39 39 39 39 39 39 39 39 39 39 39  6  6  6  6  6 38 38 38 38 38 38 38 38 38 38 38 38 38 38 38 38 38 38 38
33 33 33 33 33 33 39 39 39 39 39 39 39 39 39 39 39 39 39 39 39 39 39 39 39 39 39 39  6  6  6  6  6 38 38 38 38 38 38 38 38 38 38 38 38 38 38 38 38 38 38 38
33 33 33 33 39 39 39 39 39 39 39 39 39 39 39 39 39 39 39 39 39 39 39 39 39 39 39 39  6  6  6  6  6 38 38 38 38 38 38 38 38 38 38 38 38 38 38 38 38 38 38 38
33 33 33 33 39 39 39 39 39 39 39 39 39 39 39 39 39 39 39 39 39 39 39 39 39 39 39 39  6  6  6  6  6 38 38 38 38 38 38 38 38 38 38 38 38 38 38 38 38 38 38 38
33 33 33 33 39 39 39 39 39 39 39 39 39 39 39 39 39 39 39 39 39 39 39 39 39 39 39 39  6  6  6  6  6 38 38 38 38 38 38 38 38 38 38 38 38 38 38 38 38 38 38 38
33 33 33 33 39 39 39 39 39 39 39 39 39 39 39 39 39 39 39 39 39 39 39 39 39 39 39 39  6  6  6  6  6 38 38 38 38 38 38 38 38 38 38 38 38 38 38 38 38 38 38 38
```

**Figure 7-10.  Example source area mapping file for the domain and source areas shown in Figure 7-1.**

```
POINT                    City 1        461.520   3762.040
SINGLE CELL              Cell 1           1         45          18
CELL AVERAGE             Region 10        2          8
        31        19
        32        19
        33        19
        34        19
        31        18
        32        18
        33        18
        34        18
WALL OF CELLS           Boundary1        2         10          20
                                                   18          18
                                                    1           5
```

**Table 7-2.  Format for the receptor definition file.**

| Receptor Type | Line | Columns | Data |
|---|---|---|---|
| POINT | 1 | 1-15 | The word "POINT" |
| | 1 | 21-30 | Receptor name |
| | 1 | 31-40 | X co-ordinate |
| | 1 | 41-50 | Y co-ordinate |
| SINGLE CELL | 1 | 1-15 | The word "SINGLE CELL" |
| | 1 | 21-30 | Receptor name |
| | 1 | 31-40 | Grid Number |
| | 1 | 41-50 | X cell number |
| | 1 | 51-60 | Y cell number |
| CELL AVERAGE | 1 | 1-15 | The words "CELL AVERAGE" |
| | 1 | 21-30 | Receptor name |
| | 1 | 31-40 | Grid number |
| | 1 | 41-50 | The number of cells to average (M) |
| | 2-M | 1-10 | X cell number |
| | 2-M | 11-20 | Y cell number |
| WALL OF CELLS | 1 | 1-15 | The words "WALL OF CELLS" |
| | 1 | 21-30 | Receptor name |
| | 1 | 31-40 | Grid number |
| | 1 | 41-50 | X-cell begin |
| | 1 | 51-60 | X-cell end |
| | 2 | 41-50 | Y-cell begin |
| | 2 | 51-60 | Y-cell end |
| | 3 | 41-50 | Z-cell begin |
| | 3 | 51-60 | Z-cell end |

## 7.5  Output File Formats

OSAT writes several output files that are in Fortran binary format, as described in Section 3. These include the master and nested grid tracer instantaneous concentration files (`.sa.inst` and `.sa.finst`), the grid-specific surface tracer average concentration file

(`.sa.surf.grd`*nn*), and the grid-specific surface deposited mass file (`.sa.depn.grd`*nn*). These files are written in the same format as for the regular model species described in Section 3. In addition, OSAT writes out tracer concentrations for selected receptor locations to an ASCII file (`.sa.receptor`). The naming conventions for tracer species and the format of the receptor concentration file are discussed below.

### 7.5.1 Tracer Species Names

The names of tracer species uniquely identify the information carried by each species and, taken as a group, identify the model configuration in any run. Species names have less than ten characters, consistent with the UAM convention. The naming conventions are as follows:

Ozone Reaction Tracers

| | |
|---|---|
| Emission Sources | `SSSeeerrr` |
| where: | |

| | | |
|---|---|---|
| `SSS` | Species type, i.e., NOX, VOC, O3V or O3N | |
| `eee` | Emissions group: | |
| | | Single group, always 000 |
| | | Multiple groups, 001, 002, etc. |
| `rrr` | Region tracer released from, 001, 002, 003, etc. | |

| | |
|---|---|
| Initial/Boundary | `SSSeeerrr` |
| where: | |

| | |
|---|---|
| `SSS` | Species type, i.e., NOX, VOC, O3V or O3N |
| `eee` | Initial Concentrations: always 000 |
| | Boundary Concentrations not stratified by boundary: always 000 |
| | Boundary Concentrations stratified by boundary: WST, EST, STH, NTH, TOP indicating boundary of origin |
| `rrr` | IC for Initial Concentrations, BC for Boundary Concentrations |
| Examples: | `NOX000015, VOC002015, O3V000IC, O3NTOPBC` |

### 7.5.2 Receptor Concentration File

Hourly average tracer concentrations at user specific receptor locations are output to the "receptor concentration" file. The file is in comma delimited ASCII format suitable for importing into a spreadsheet (a spreadsheet postprocessing tool is available to visualize the data in this file, as described below). An example output file is shown in Figure 7-11. Two header lines at the top of the file identify the model version and the date the run was performed. Next, two lines identify the time period covered by the file and the averaging interval (generally one hour, determined by the CAMx simulation control file). Next, three lines define the model configuration and seven lines specify the numbers of tracer species that result from this configuration. The names of each tracer species are given on six lines ordered by tracer species type: the order in which species are listed here is the same as the order in which tracer concentrations are given later in the file.

```
CAMx, SOURCE APPORTIONMENT, VERSION -- 960315 ,
Mon Oct 26 10:37:34 1998                    ,

 File Duration ,      87238,      15.00,      87238,      24.00,
Average Interval ,    1.0000

Number of source areas        ,         17
Number of emission groupings ,          1
Number of tracer species       ,        144
Number of NOx species          ,         19
Number of VOC species          ,         19
Number of O3N species          ,         19
Number of O3V species          ,         19
Number of INERT TIME species ,         34
Number of DECAY TIME species ,         34


Tracer Names,
NOX000IC ,NOX000BC ,NOX001001,NOX001002,NOX001003,NOX001004,NOX001005 ..
VOC000IC ,VOC000BC ,VOC001001,VOC001002,VOC001003,VOC001004,VOC001005 ..
O3N000IC ,O3N000BC ,O3N001001,O3N001002,O3N001003,O3N001004,O3N001005 ..
O3V000IC ,O3V000BC ,O3V001001,O3V001002,O3V001003,O3V001004,O3V001005 ..
I23815001,I23815002,I23815003,I23815004,I23815005,I23815006,I23815007 ..
D23815001,D23815002,D23815003,D23815004,D23815005,D23815006,D23815007 ..


Number of receptors ,          6
  No,     Name,     Type,     Xloc,        Yloc,
    1, HourlyPeak,    1,              ,                ,
    2, Rubidoux  ,    0,       461.5,      3762.0,
    3, Pasadena  ,    0,       396.4,      3778.5,
    4, Lennox    ,    0,       373.0,      3755.0,
    5, Peak      ,    1,         45,          18,
    6, Region 10 ,    8,         31,          19,
                                  32,          19
                                    33,          19
                                    34,          19,
                                    31,          18,
                                    32,          18,
                                    33,          18,
                                    34,          18,

Time Varying Tracer Data,

 Data for Period,      87238,      15.00,      87238,      16.00,
  Receptor,     1,
1.3265E-02, 1.3544E-09, 1.0000E-16, 1.0974E-15, 1.0000E-16, 1.0000E-16 ..
1.2237E-01, 3.3869E-08, 1.0000E-16, 1.6165E-14, 1.0000E-16, 1.0000E-16 ..
8.7304E-02, 1.1926E-08, 1.0000E-16, 1.0000E-16, 1.0000E-16, 1.0000E-16 ..
9.0300E-02, 1.5269E-08, 1.0188E-16, 2.6997E-15, 1.0213E-16, 1.0162E-16 ..
1.0036E-16, 4.0640E-15, 1.0036E-16, 1.0036E-16, 1.0036E-16, 1.0029E-16 ..
1.0000E-16, 3.7563E-15, 1.0000E-16, 1.0000E-16, 1.0000E-16, 1.0000E-16 ..
1.4500E-02, 1.2663E-01, 1.7770E-01,
1.4500E-02, 1.2663E-01, 1.7770E-01,
  Receptor,     2,
(File continues with data for remaining receptors and hours)
```

**Figure 7-11.  Example Receptor Concentration File.  Lines ending with ".." are truncated to fit the page, and the file would continue with data for additional receptors and hours in the same format.**

The tracer species names are followed by the number of receptors and receptor names.  Note that the first receptor (receptor 1) is always the location of the hourly peak ozone.  Since the location of the hourly peak varies from hour to hour, the X and Y locations are left blank. Receptors 2 and higher are those specified in the "Receptor definition" file.  The tracer concentrations are reported in blocks with a date and time stamp at the head of each block. Within each block, receptors are reported in numerical order.  For each receptor, there are six lines of data for the tracer species identified at the heading "Tracer Names".  All values are in CAMx units of ppm.  At the bottom of the data block for each receptor are two lines with three numbers: these are the total tracer $NO_X$, VOC, and ozone (first line) and regular CAMx $NO_X$, VOC and ozone (second line).

## 7.6 Postprocessing

The tracer concentrations in the gridded surface concentration files can be displayed using any post-processing software normally used for displaying CAMx average file output formats.

The receptor concentration file contains information for all receptors and all hours within the model run that created the file.  A post-processing tool is available to allow the user to "browse" through the information contained in this file and prepare displays like Figure 7-2. The "browser" is a Microsoft Excel Spreadsheet macro that is controlled by a graphical user interface (GUI) allowing you to rapidly visualize results for any receptor.  To use this software, the user must have Microsoft Excel (tested for Office/Excel 2007).  The browser is provided at www.camx.com.

## 7.7 Steps In Developing Inputs And Running OSAT

Below is a simple methodological list of steps to follow in setting up and running OSAT.  The process is similar among the OSAT, PSAT, and DDM Probing Tools.

1) Define the source groups and regions that you wish to track.  Keep in mind that memory resources increase dramatically as the number of tracers grows.  Probing Tool applications with large numbers of tracers, tracer classes, nested grids or grid cells may exceed available memory.

2) Build a source region map (Figure 7-10) that defines the spatial allocation of tracer emissions.  For small domains or small number of regions, this can be done by hand.  We suggest using GIS software to develop complex source region maps on large grids.

3) Process the emissions inventory into the separate source group files that you want to track (e.g., mobile, area, point, biogenic, etc.).

   a) Consideration of potential source apportionment or sensitivity applications prior to any emissions processing can be very beneficial so that files by group are available for later use.

   b) Elevated point sources will automatically be assigned to the source region in which they reside.  However, you may override the region to which each individual point source is assigned (see the definition of `kcell` in Section 3, Elevated Point Source

File).  A point source region does not need to be defined in the source region map, e.g., you could have a map with two regions that split the domain in half, with a third region assigned arbitrarily to represent elevated point sources only.

4) Edit the CAMx control namelist file (Section 2).

   a) Set the `Probing_Tool` variable to the technology you wish to use (OSAT, APCA, GOAT).  This will activate the `&SA_Control` namelist module.

   b) Edit or add the `&SA_Control` namelist module (described earlier).  Provide the required information, including:
      - output paths
      - whether to stratify boundary conditions
      - number of source regions
      - number of source groups
      - whether to use the leftover group option
      - receptor definitions
      - list of input emission files by group.

   c) Note that APCA *requires* that the biogenic emission files for each grid are listed first. Several examples are shown in Figure 7-9.

5) Configure the CAMx source code to define the number of tracers, and build an executable.  This will ensure that you have sufficient memory for the Probing Tool application.

   a) Edit the file `Includes/camx.prm`

   b) Change the parameter `MXTRSP`, following the instructions provided in the file. CAMx is distributed with `MXTRSP = 1` to minimize memory requirements for standard applications of the model.  If you run OSAT with an insufficient value, the model will stop and tell you the required value of `MXTRSP` for your application.

   c) Execute the CAMx `Makefile` to build an executable program (Section 2).

6) Run CAMx and review the diagnostic output files to ensure that the model is correctly interpreting and running the Probing Tool configuration that you have specified.  Ensure that CAMx is generating the proper output files that you are expecting.  Review the table of emissions by source group and region.

7) Review gridded tracer fields using commonly available plotting programs.  Utilities such as PAVE or Verdi will read Probing Tool files directly.  Use of any other software may require specialized re-formatting procedures.

8) You may post-process OSAT receptor files using an Excel macro (OSAT_browser) that ENVIRON distributes at www.camx.com.

9) Probing Tool gridded tracer output files are written in the same Fortran binary format as the regular CAMx concentration output files.  You can post-process gridded output fields using any software that reads CAMx files, or you can adapt those programs or build your own software to generate specialized analysis and graphical products.

# 8. PARTICULATE SOURCE APPORTIONMENT TECHNOLOGY

Airborne particulate matter (PM) is widely recognized as an important pollution issue because it causes health problems and environmental degradation.  In recent years the emphasis on controlling PM has shifted toward fine PM (or PM2.5, with particle diameter less than 2.5 μm) because it is more strongly associated with serious health effects than coarse PM.  Knowing which sources contribute to PM2.5 is essential for developing effective control strategies.  Many components of PM2.5 are secondary pollutants and so photochemical models are important tools for PM air quality planning.  The Particulate Source Apportioning Technology (PSAT) has been developed for CAMx to provide PM source apportionment among specific geographic regions and source categories (Yarwood et al., 2004).  PM source apportionment information from PSAT is useful for:

1) Understanding model performance and thereby improving model inputs/formulation;

2) Performing culpability assessments to identify sources that contribute significantly to PM pollution;

3) Designing the most effective and cost-effective PM control strategies.

Source apportionment for primary PM is relatively simple to obtain from any air pollution model because their source-receptor relationships are essentially linear.  Gaussian steady-state models and Lagrangian puff models have been used extensively to model primary PM pollution from specific sources, which is a direct form of source apportionment.  The Gaussian and Lagrangian approaches work for primary PM because the models can assume that emissions from separate sources do not interact.  This assumption breaks down for secondary PM pollutants (e.g., sulfate, nitrate, ammonium, secondary organic aerosol) and so puff models may dramatically simplify the chemistry (to eliminate interactions between sources) so that they can be applied to secondary PM.  Eulerian photochemical grid models are better suited to modeling secondary pollutants because they account for chemical interactions between sources.  Grid models do not naturally provide source apportionment because the impact of all sources has been combined in the total pollutant concentration.  PSAT has been developed to retain the advantage of using a grid model to describe the chemistry of secondary PM formation and also to provide source apportionment.

This section starts by reviewing several approaches to PM source attribution in grid models that were considered when PSAT was designed.  Next, the PSAT algorithms are explained, and then example PSAT results are presented and compared to results from some other methods.

## 8.1 Approaches To PM Source Attribution In Grid Models

Several potential approaches were considered at the PSAT design stage and these are discussed below.  The approaches considered fall into two general categories, which we have called sensitivity analysis and reactive tracers.  The reactive tracer approaches also could be called tagged species approaches.   This section concludes with a discussion of an important fundamental difference between sensitivity analysis and source apportionment that explains why these two concepts should not be confused for secondary pollutants.

### 8.1.1 Sensitivity Analysis Methods

Sensitivity analysis methods measure the model output response to an input change, e.g., the change in sulfate concentration due to a change in SOx emissions. In general, sensitivity methods will not provide source apportionment if the relationship between model input and output is non-linear. For example, if sulfate formation is non-linearly related to SOx emissions, the sum of sulfate (SO4) sensitivities over all SOx sources will not equal the model total sulfate concentration. This concept is discussed in more depth later in this section.

Brute Force or Direct Method. The brute force method estimates first-order sensitivity coefficients (e.g., $\Delta SO4/\Delta SOx$) by making a small input change ($\Delta SOx$) and measuring the change in model output ($\Delta SO4$). This method is simple and can be applied to any model, but is inefficient because a complete model run is required for each sensitivity coefficient to be determined. Accuracy also may be an issue for the brute force method because ideally the input change ($\Delta SOx$) should be vanishingly small but for small input changes the output change may be contaminated by numerical precision or model "noise." For larger input changes, first-order sensitivities estimated by the brute force method may be distorted by non-linear chemical effects, e.g., a brute force coefficient ($\Delta SO4/\Delta SOx$) may be a mixture of first-order ($dSO4/dSOx$) and second-order ($d^2SO4/dSOx^2$) derivatives. High-order sensitivity coefficients also can be estimated by the brute force method.

Zero-Out Modeling. The zero-out method differs from the brute force method in that a specific emissions input is set to zero and the change in output measured. Zero-out modeling can be used with any model but is inefficient because a complete model simulation is required for each source. Accuracy also may be an issue if the zero-out method is applied to a small emissions source. This method has been used extensively for source attribution because it seems intuitively obvious that removing a source should reveal the source's impact. However, because zero-out modeling is a sensitivity method it does not provide source apportionment for non-linear systems because the sum of zero-out impacts over all sources will not equal the total concentration, as discussed in more depth later in this section.

Decoupled Direct Method (DDM). The DDM provides the same type of sensitivity information as the brute force method but using a computational method that is directly implemented in the host model (Dunker, 1981). The DDM has potential advantages of greater efficiency and accuracy relative to the brute force method (Dunker at al., 2002a) and the DDM implementation in CAMx (Dunker at al., 2002a,b) is currently being extended to PM species. Drawbacks of DDM are that the implementation is technically challenging, that using DDM for many sensitivities simultaneously requires large computer memory, and because DDM is a sensitivity method, it does not provide source apportionment for non-linear systems unless high-order sensitivities are calculated.

Other Sensitivity Methods. There are other sensitivity methods that provide similar information to DDM such as adjoint methods (e.g., Menut at al., 2000; Elbern and Schmidt, 1999) and automatic differentiation in FORTRAN (ADIFOR). They have similar advantages and disadvantages as DDM but may be less computationally efficient (Dunker et al., 2002a).

### 8.1.2  Reactive Tracer Methods

Reactive tracers (or tagged species) are extra species added to a grid model to track pollutants from specific sources.  For example, a standard grid model calculates concentrations for a species $X$ that has many sources and so the concentration of $X$ is the total concentration due to all sources.  A reactive tracer ($x_i$) is assigned to for each source ($i$) with the intention that the sum of the reactive tracers will equal total concentration ($X = \Sigma x_i$).  The challenge is to develop numerical algorithms for solving the reactive tracer concentrations that ensure that this equality is maintained.  Depending upon the formulation of the tracer algorithms, it may be possible to model tracers for a single source of interest and omit tracers for all other sources, or it may be necessary to include tracers for all sources (as is the case for PSAT).  Reactive tracers can potentially provide true source apportionment ($X = \Sigma x_i$), however the numerical value of the source apportionment will depend upon assumptions within the reactive tracer formulation.  In particular, for any process that is non-linear in species concentrations (e.g., chemistry) there is no unique way to assign the total concentration change to the reactive tracers.  This issue is discussed in more depth later in this section.

Source Oriented External Mixture (SOEM).  Kleeman and Cass (2001) developed an approach called SOEM that tracks primary PM from different source categories/regions using tagged species that are considered to represent seed particles.  Reactive tracers are added to track secondary PM and related gases from different source categories/regions, and source apportioned secondary PM condenses onto the seed particles.  Chemical change for secondary PM and related gases is accounted for by expanding the chemical mechanism to treat different source regions/categories as separate precursor and product species.  This requires thousands of chemical reactions and hundreds to thousands of chemical species, depending upon the number of source regions/categories.  The main advantage of the SOEM method is that it is potentially accurate, and the main disadvantage is computational demand.

PSAT and TSSA.  The PM Source Apportionment Technology (PSAT) uses reactive tracers to apportion primary PM, secondary PM and gaseous precursors to secondary PM among different source categories and source regions.  The PSAT methodology is described below.  PSAT was developed from the related ozone source apportionment method (OSAT) already implemented in CAMx (Dunker at al., 2002b).  Tonnesen and Wang (2004) are independently developing a method very similar to PSAT called Tagged Species Source Apportionment (TSSA) in the Community Multiscale Air Quality (CMAQ) modeling system.  Advantages of PSAT and TSSA are expected to be high efficiency and flexibility to study different source categories/regions.  The accuracy of the PSAT (and TSSA) source apportionment results must be evaluated, as for any other method.

### 8.1.3  Source Apportionment and Source Sensitivity

Consider a chemical species $X$ that has two sources $A$ and $B$ (so $X = x_A + x_B$) and which undergoes a second order self-reaction with rate constant $k$.  The rate of chemical change is:

$$\frac{dX}{dt} = -kX^2$$

$$\frac{dX}{dt} = -k\left(x_A + x_B\right)^2$$

$$\frac{dX}{dt} = -kx_A^2 - kx_B^2 - 2kx_A x_B$$

The homogeneous rate terms $kx_A^2$ and $kx_B^2$ clearly describe chemical change for pollutants from sources $A$ and $B$ ($x_A$ and $x_B$), but the inhomogeneous rate term $2kx_A x_B$ is not uniquely associated with either source $A$ or $B$. A reactive tracer (or tagged species) source apportionment method must deal with this inhomogeneous rate term either by developing rules to apportion the inhomogeneous term to sources $A$ and $B$ or by modifying the chemistry to eliminate the inhomogeneous term. For a sensitivity method, the homogeneous quadratic rate terms generate second-order homogeneous sensitivity coefficients ($s_{AA}$ and $s_{BB}$) and the inhomogeneous rate term generates a second-order inhomogeneous sensitivity coefficient ($s_{AB}$). Consequently, the total concentration of $X$ is incompletely described by the first-order sensitivity coefficients ($s_A$ and $s_B$) that resemble source apportionments.

The example presented above is a simple case of a non-linear chemical system that illustrates why source apportionment and source sensitivity are not the same thing for nonlinear systems. The implications are:

1) There is no unique source apportionment for chemical species that depend upon nonlinear reactions, such as secondary PM species and ozone. Nonetheless, reasonable source apportionment schemes can be developed and are useful tools for achieving the objectives listed in the introduction.

2) Sensitivity coefficients are not source apportionments for chemical species that depend upon nonlinear reactions, such as secondary PM species and ozone. Sensitivity coefficients are most applicable for predicting the model response to an input change (e.g., control strategy) and are very useful for this purpose (within the range of linear model response), but sensitivity coefficients should be used with care for source apportionment or culpability assessment. Likewise, source apportionments should be used with care for predicting model response to input changes.

## 8.2  PSAT Methodology

PSAT is designed to source apportion the following PM species (CF mode only) in CAMx:

- Sulfate (SO4)
- Particulate nitrate (NO3)
- Ammonium (NH4)
- Particulate mercury (Hg(p))

- Secondary organic aerosol (SOA)
- Six categories of primary PM:
  - Elemental carbon (EC)
  - Primary organic aerosol (POA)
  - Crustal fine (FCRS)
  - Other fine (FPRM)
  - Crustal coarse (CCRS)
  - Other coarse (CPRM)

The PSAT "reactive tracers" that are added for each source category/region (*i*) are described below.  In general, a single tracer can track primary PM species whereas secondary PM species require several tracers to track the relationship between gaseous precursors and the resulting PM.  Particulate nitrate and secondary organics are the most complex species to apportion because the emitted precursor gases (NO, VOCs) are several steps removed from the resulting PM species (NO3, SOA).  The PSAT tracers for each type of PM are listed below.  There is a PSAT convention that tracer names for particulate species begin with the letter "P."

Sulfur

| | |
|---|---|
| $SO2_i$ | Primary $SO_2$ emissions |
| $PS4_i$ | Particulate sulfate ion from primary emissions plus secondarily formed sulfate |

Nitrogen

| | |
|---|---|
| $RGN_i$ | Reactive gaseous nitrogen including primary NOx (NO + NO2) emissions plus nitrate radical (NO3), nitrous acid (HONO) and dinitrogen pentoxide (N2O5). |
| TPNi | Gaseous peroxyl acetyl nitrate (PAN) plus peroxy nitric acid (PNA) |
| NTRi | Organic nitrates (RNO3) |
| HN3i | Gaseous nitric acid (HNO3) |
| PN3i | Particulate nitrate ion from primary emissions plus secondarily formed nitrate |
| NH3i | Gaseous ammonia (NH3) |
| PN4i | Particulate ammonium ($NH_4$) |

Secondary Organic

| | |
|---|---|
| $ARO_i$ | Aromatic (toluene and xylene) secondary organic aerosol precursors |
| $ISP_i$ | Isoprene secondary organic aerosol precursors |
| $TRP_i$ | Terpene secondary organic aerosol precursors |
| SQT | Sesquiterpene secondary organic aerosol precursors |
| $CG1_i$ | Condensable gases from aromatics (low volatility products) |
| $CG2_i$ | Condensable gases from aromatics (high volatility products) |
| $CG3_i$ | Condensable gases from isoprene (low volatility products) |
| $CG4_i$ | Condensable gases from isoprene (high volatility products) |
| $CG5_i$ | Condensable gases from terpenes (low volatility products) |
| $CG6_i$ | Condensable gases from terpenes (high volatility products) |
| $CG7_i$ | Condensable gases from sesqiterpenes |
| $PO1_i$ | Particulate organic aerosol associated with CG1 |
| $PO2_i$ | Particulate organic aerosol associated with CG2 |

PO3$_i$     Particulate organic aerosol associated with CG3
PO4$_i$     Particulate organic aerosol associated with CG4
PO5$_i$     Particulate organic aerosol associated with CG5
PO6$_i$     Particulate organic aerosol associated with CG6
PO7$_i$     Particulate organic aerosol associated with CG7
PPA$_i$     Anthropogenic organic aerosol polymers (SOPA)
PPB$_i$     Biogenic organic aerosol polymers (SOPB)

Mercury

HG0$_i$     Elemental Mercury vapor
HG2$_i$     Reactive gaseous Mercury vapor
PHG$_i$     Particulate Mercury

Primary Particulate

PEC$_i$     Primary Elemental Carbon
POA$_i$     Primary Organic Aerosol
PFC$_i$     Fine Crustal PM
PFN$_i$     Other Fine Particulate
PCC$_i$     Coarse Crustal PM
PCS$_i$     Other Coarse Particulate

PSAT includes a total of 32 tracers for each source group (*i*) if source apportionment is applied to all types of PM.  Since source apportionment may not always be needed for all species, the PSAT implementation is flexible and allows source apportionment for any or all of the chemical classes in each CAMx simulation (i.e. the SO4, NO3, NH4, SOA, Hg and primary PM classes listed above).  For example, source apportionment for sulfate/nitrate/ammonium requires just 9 tracers per source group.

One fundamental assumption in PSAT is that PM should be apportioned to the primary precursor for each type of PM.  For example, SO4 is apportioned to SOx emissions, NO3 is apportioned to NOx emissions, NH4 is apportioned to NH3 emissions, etc.  As a source apportionment method, PSAT must account for all modeled sources of a PM species.   Consider two model species A and B that are apportioned by reactive tracers $a_i$ and $b_i$, respectively. Reactive tracers must be included for all sources of *A* and *B* including emissions, initial conditions and boundary conditions so that complete source apportionment is obtained, i.e., *A* = $\Sigma a_i$ and *B* = $\Sigma b_i$.

In PSAT, the general approach to modeling change over a model time step $\Delta t$ is illustrated for a chemical reaction $A \rightarrow B$.  The general equation for species destruction is:

$$a_i(t + \Delta t) \quad = \quad a_i(t) + \Delta A \frac{a_i}{\sum a_i}$$

Here, the relative apportionment of *A* is preserved as the total amount changes.  This equation applies to chemical removal of *A* and also to physical removal of *A* by processes such as deposition or transport out of a specific grid cell.

The general equation for species production (e.g, chemical production by the chemical reaction $A \rightarrow B$) is:

$$b_i(t + \Delta t) \quad = \quad b_i(t) + \Delta B \frac{a_i}{\sum a_i}$$

Here, production of *B* inherits the apportionment of the precursor *A*. The same equation applies for "production" of *B* in a specific grid cell due to emissions or transport. For the case where *B* increases due to emissions, $a_i$ is the apportionment of the emissions inventory. For the case where *B* increases due to transport, $a_i$ is the apportionment of the upwind grid cell.

In some cases, source category specific weighting factors ($w_i$) must be added to the equation for species destruction:

$$a_i(t + \Delta t) \quad = \quad a_i(t) + \Delta A \frac{w_i a_i}{\sum w_i a_i}$$

An example is chemical decay of the aromatic VOC tracers (ARO), which must be weighted by the average OH rate constant of each $ARO_i$. ARO tracers for different source groups have different average VOC reactivities because the relative amounts of toluenes and xylenes differ between source categories.

In some cases, source category specific weighting factors ($w_i$) must be added to the equation for species production:

$$b_i(t + \Delta t) \quad = \quad b_i(t) + \Delta B \frac{w_i a_i}{\sum w_i a_i}$$

An example is chemical production of condensable gases (CG1 or CG2) from aromatic VOC tracers, which must be weighted by aerosol yield weighting factors. The aerosol yield weighting factors depend upon the relative amounts of toluenes and xylenes in each source group.

Several aerosol reactions are treated as equilibria, $A \leftrightarrow B$. If *A* and *B* reach equilibrium at each time step, it follows that their source apportionments also reach equilibrium:

$$a_i(t + \Delta t) \quad = \quad [a_i(t) + b_i(t)]\left(\frac{A}{A + B}\right)$$

$$b_i(t + \Delta t) \quad = \quad [a_i(t) + b_i(t)]\left(\frac{B}{A + B}\right)$$

Examples are the equilibrium between gas phase nitric acid and aerosol nitrate, gas phase ammonium and aerosol ammonium, and condensable organic gases (CG) and secondary organic aerosols (SOA).

## 8.3  Testing PSAT

Initial PSAT testing was conducted for primary PM species (e.g., fine crustal material) because these species are the most straightforward to implement and test (i.e., no chemistry).  The results for primary PM species are not shown here but the tests were successful in that the sum of PSAT tracers over all source groups remained identical to the total model concentration ($A = \Sigma a_i$) for all grid cells and hours.  The primary PM tests confirmed the proper implementation of PSAT for all CAMx algorithms except chemistry.

The next stage of PSAT testing included the chemistry algorithms and results are shown here for two different types of testing for sulfate and nitrate.  Sulfate was tested by comparing PSAT to zero out results in full 3-D CAMx simulations.  As discussed above, zero out results are not expected to agree perfectly with PSAT because zero out does not give true source apportionment in non-linear systems.  However, non-linearity in sulfate formation chemistry is expected to be less important than for other secondary PM species making sulfate the best candidate for zero out testing.

The most complex PSAT chemistry algorithm is for nitrate.  Zero out tests were not used for nitrate because the relationship between NO emissions and nitric acid may be highly non-linear.  Therefore, 1-D (box model) tests were used to evaluate PSAT results for nitrate by comparing against the method used by Kleeman and Cass (2001) to track nitrate apportionment in the Source-Oriented External Mixture (SOEM) method, discussed above.

### 8.3.1  PSAT Sulfate Testing

The PSAT performance for sulfate was tested using a CAMx database developed by the Midwest RPO (MPRO) for PM and visibility modeling of the Eastern US.  The modeling was conducted from June 18 to July 21, 2001 and used a 36-km modeling grid with meteorology developed using the mesoscale model version 5 (MM5).  The modeling domain was sub-divided to geographic areas according to regional planning organizations (RPOs) responsible for developing regional visibility and PM control strategies in the U.S.  The sub division of the modeling domain to RPOs is shown in Figure 8-1 and the RPOs are labeled by their respective acronyms (MRPO, MANE-VU, VISTAS, CERAP and WRAP).  The state of Illinois (IL) was split out from the Midwest RPO (MPRO) to test the ability of PSAT to apportion the contribution from a single state.  Four hypothetical point sources were added near the middle of the MRPO, MANE-VU, VISTAS and CENRAP areas (shown by the + symbols in Figure 8-1) to test the ability of PSAT to track contributions from singe sources.  The hypothetical point sources were chosen to be generally representative of a large coal-fired electricity generating unit but do not represent actual sources at these locations.  In total, sulfate was apportioned to 11 source regions, including a remainder area for Canada, Mexico and over water, plus initial and boundary conditions.

The sulfate impacts from the hypothetical MRPO point source are compared in Figure 8-2 at a single hour (hour 15) on 28 June 2001.  The spatial distribution of sulfate impacts is very similar in the PSAT and zero out results as shown by the edge of the plume impacts (0.1 $\mu g/m^3$ level).  There are differences in the areas of larger impacts (e.g. the 1 and 2 $\mu g/m^3$ levels) and these are
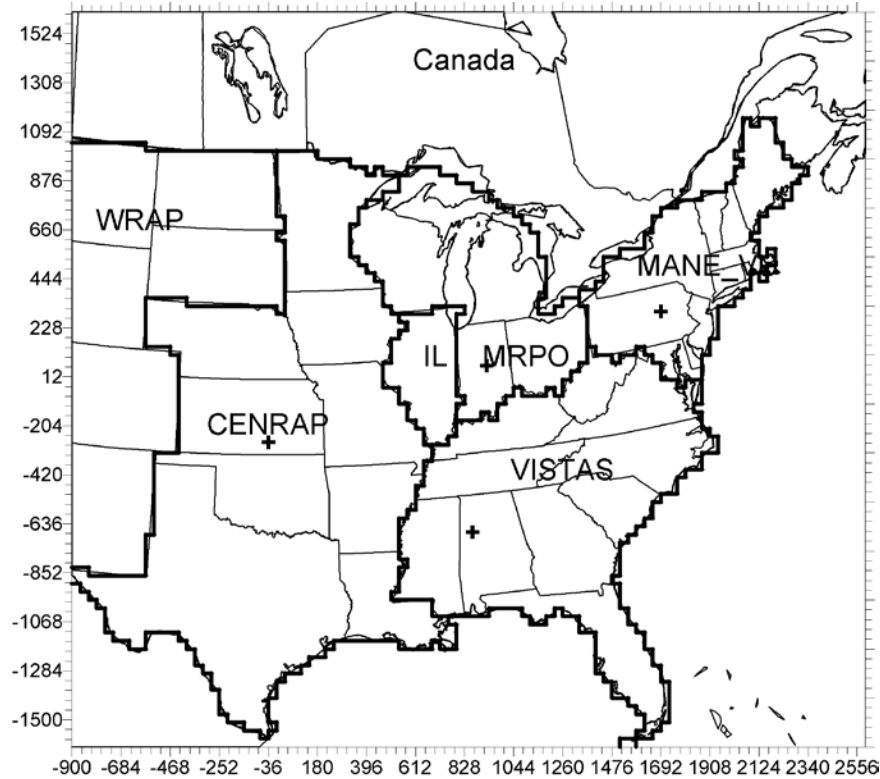
**Figure 8-1. The CAMx modeling domain for PSAT testing showing sub-division to geographic areas and locations of four hypothetical point sources (+ symbols).**
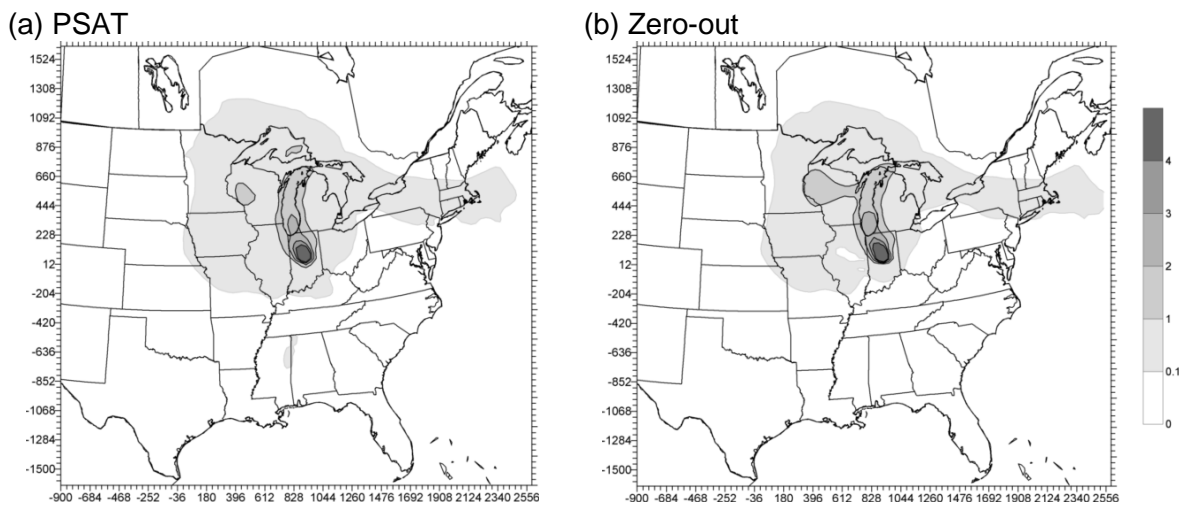


**Figure 8-2. Comparison of sulfate contributions (µg/m$^3$) from the hypothetical MRPO point source on 28 June 2001 at hour 15: (a) PSAT result; (b) Zero-out result.**

due to the effects of non-linear chemistry in the zero out test. As discussed above, sensitivity methods such as zero out do not provide accurate source apportionments for non-linear processes. Sulfate formation can be limited by the availability of oxidants, especially hydrogen peroxide in aqueous-phase chemistry, which will tend to depress the maximum impact levels inzero out runs as well as shift impacts further downwind (to where oxidant availability is no longer limiting). The oxidant limiting effect on zero out sulfate impacts is most easily seen from the 2 $\mu g/m^3$ level extending further downwind over Lake Michigan in the zero out result than the PSAT source apportionment result.

The episode average sulfate impacts from the hypothetical MRPO point source are compared in Figure 8-3 for the entire 28 June to July 21, 2001 modeling period. The spatial distribution of sulfate impacts is very similar in the PSAT and zero out results. The maximum impact occurs very close to the source and is higher in the PSAT result (2.2 $\mu g/m^3$) than the zero out result (1.8 $\mu g/m^3$) due to the effect of oxidant limitation on sulfate impacts determined by the zero out method.

The PSAT sulfate tests provided a comparison of the efficiency of the PSAT method compared to zero out modeling. Zero out modeling requires a new model run for each source contribution determined, so the incremental time for each "apportionment" is the same as for the model base case. In contrast, the marginal cost for each PSAT source apportionment was about 2% of the time required for the base case.
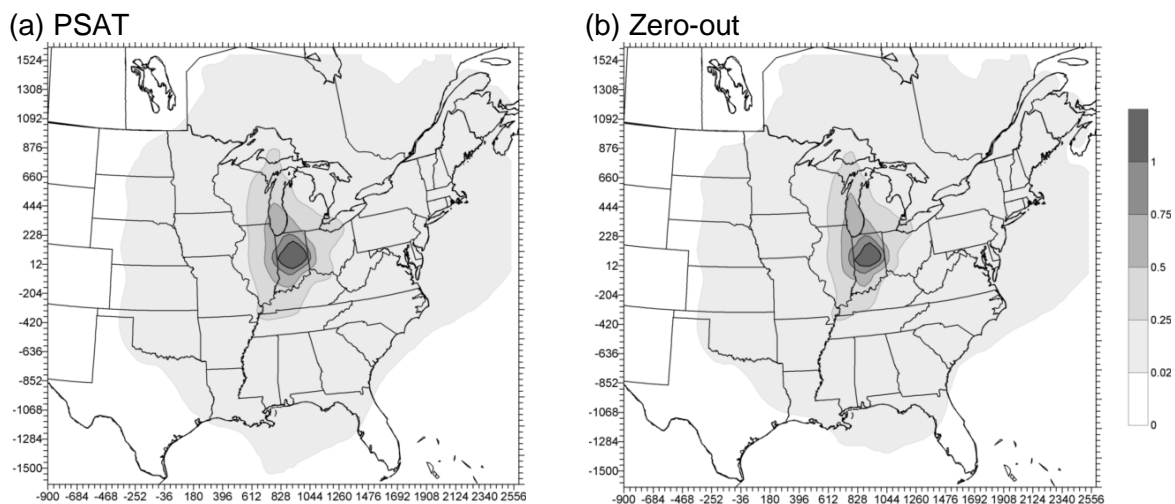


**Figure 8-3. Comparison of episode average (June 18 to July 21, 2001) sulfate contributions (µg/m³) from the hypothetical MRPO point source: (a) PSAT result; (b) Zero-out result.**

### 8.3.2 PSAT Nitrate Testing

The PSAT nitrate algorithms were tested using CAMx for a 1-D (box model) problem in order to focus upon the ability of the PSAT chemical algorithms to track nitrate apportionment. The box model problem was for summer conditions and PSAT was used to apportion nitrate between 20 ppb of initial NOx and 100 ppb of NOx emission injected continuously through the 24 hour run. The PSAT results were compared to the SOEM algorithm of Kleeman and Cass (2001) where the reactive nitrogen (NOy) reactions in the chemical mechanism are duplicated to provide two different types of NOy (think of them as "red" NOy and "blue" NOy). There was no ammonia in the box model so that nitric acid remained in the gas phase rather than forming PM nitrate.

The PSAT apportionment of NOy to initial conditions (ICs) and emissions during the 24 hour box model simulation is shown in Figure 8-4. The total NOy apportioned to ICs remains constant at 20 ppb throughout the simulation but the apportionment changes over time from NOx (RGN-IC) at the start to PAN (TPN-IC), organic nitrates (NTR-IC) and nitric acid (HN3-IC). The NOy apportioned to emissions increased linearly throughout the simulation and the apportionment also evolved as the NOx emissions (RGN-E) reacted. At the start of the simulation RGN (NOx) is dominated by ICs whereas late in the day (hour 18) RGN is dominated by emissions. The source apportionments shown in Figure 8-4 are reasonable and show necessary attributes (such as conserving the total 20 ppb of ICs).

The SOEM apportionment of NOy to ICs and emissions during the 24-hour box model simulation is shown in Figure 8-5. The time evolution of the source apportionments for the ICs and emissions is very similar for SOEM (Figure 8-5) and PSAT (Figure 8-4). It is not clear that either method is more "correct," or indeed that a correct source apportionment result exists for this test, but the consistency between the PSAT and SOME results is encouraging.

## 8.4 Running CAMx With PSAT

### 8.4.1 CAMx Control File

PSAT is invoked similarly to the OSAT Probing Tool within the CAMx control file. In the `&CAMx_Control` namelist module, the variable `Probing_Tool` must be set to "PSAT". An additional namelist module called `&SA_Control` must then be provided in the control file to configure the PSAT portion of the model – note that this is identically the same module as used for OSAT. The PSAT/OSAT namelist module is described in Section 7; the additional variables needed for PSAT are described below. The order of the variables follow the template available with the source code. An example of the PSAT portion of the CAMx run control file is shown in Figure 8-6. All other capabilities and I/O requirements for PSAT mirror those of OSAT.
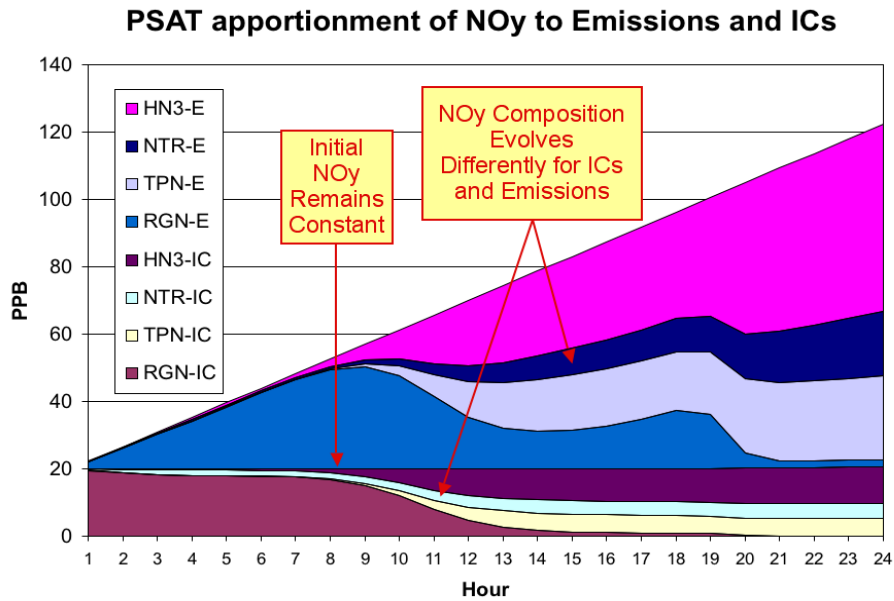
**Figure 8-4.  PSAT apportionment of reactive nitrogen (NOy) to initial conditions and emissions during a 24-hour box model simulation.**
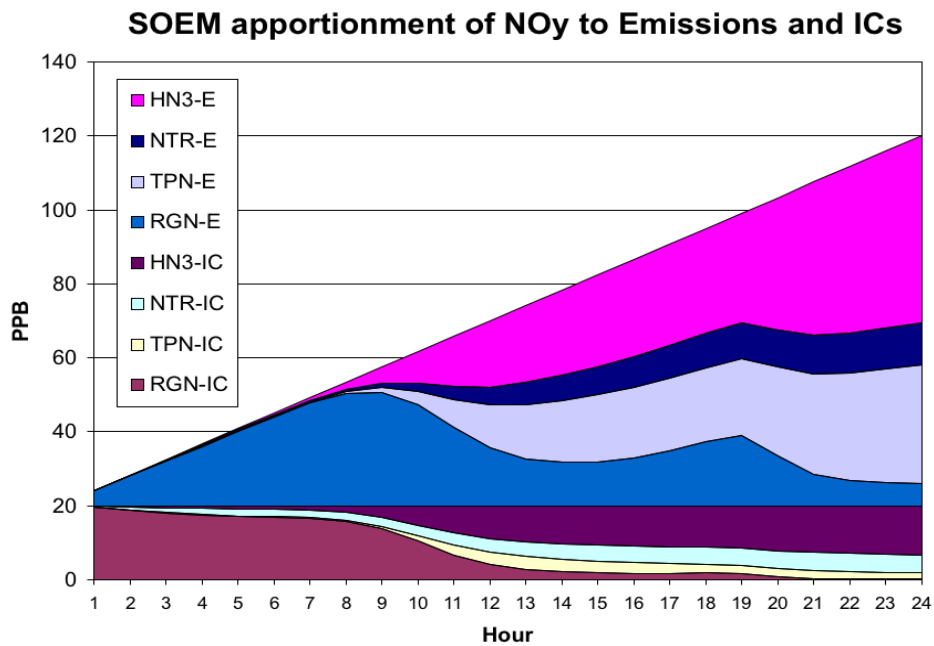


**Figure 8-5.  Source-Oriented External Mixture (SOEM) apportionment of reactive nitrogen (NOy) to initial conditions and emissions during a 24-hour box model simulation.**

**Description of PSAT Control in the CAMx Run Control File**

| | |
|---|---|
| `&SA_Control` | Label for the Probing Tool namelist module that configures the PSAT and OSAT options; it must begin in column 2 |
| `&` | Flag ending a namelist module; it must be in column 2 |
| `SA_Summary_Output` | Logical flag used to limit the species written to the tracer concentration file to a subset of the PSAT treated species. If set to true, the output will be restricted to the following species: O3N, O3V, PS4, PN3, PN4, PO1, PO2, PO3, PO4, PO5, PEC, POC, FCR, FPR, CCR, CPR, HG0, HG2, PHG |
| `PSAT_Treat_SULFATE_Class` | Logical flag to turn on the sulfate class of tracer species. |
| `PSAT_Treat_NITRATE_Class` | Logical flag to turn on the nitrate class of tracer species. |
| `PSAT_Treat_SOA_Class` | Logical flag to turn on the SOA class of tracer species. |
| `PSAT_Treat_PRIMARY_Class` | Logical flag to turn on the primary PM class of tracer species. |
| `PSAT_Treat_MERCURY_Class` | Logical flag to turn on the mercury class of tracer species. |
| `PSAT_Treat_OZONE_Class` | Logical flag to turn on the ozone class of tracer species. |

```
&SA_Control

 SA_File_Root              = '$TRACOUT/CAMx.OSAT.9507$today',
 SA_Summary_Output         = .true.,

 SA_Master_Sfc_Output       = .true.,
 SA_Nested_Sfc_Output       = .true.,
 SA_Stratify_Boundary       = .false.,
 SA_Deposition_Output       = .false.,
 SA_Number_of_Source_Regions = 19,
 SA_Number_of_Source_Groups  = 3,
 Use_Leftover_Group         = .false.,
 PSAT_Treat_SULFATE_Class   = .true.,
 PSAT_Treat_NITRATE_Class   = .true.,

 SA_Receptor_Definitions  = '$TRACIN/receptor.cities ',
 SA_Source_Area_Map(1)    = '$TRACIN/APCA.source.area.map',
 SA_Source_Area_Map(2)    = ' ',

 SA_Master_Restart         = '$TRACOUT/CAMx.OSAT.9507$yesterday.sa.inst',
 SA_Nested_Restart         = '$TRACOUT/CAMx.OSAT.9507$yesterday.sa.finst',

 SA_Points_Group(1)       = ' ',
 SA_Points_Group(2)       = '$PTSRCE/utilpt.ng.$todate-07.ag.07cem1A-run11',
 SA_Points_Group(3)       = '$PTSRCE/remain.ng.$todate-07.ag.07cem1A-run11',

 SA_Emiss_Group_Grid(1,1) = '$TRACEMS/bio2.cc.$todate-95',
 SA_Emiss_Group_Grid(1,2) = '$TRACEMS/bio2.ff.$todate-95.ne',
 SA_Emiss_Group_Grid(2,1) = '$TRACEMS/util.cc.$todate-07.ag.07cem1A-run11',
 SA_Emiss_Group_Grid(2,2) = '$TRACEMS/util.ff.$todate-07.ag.07cem1A-run11',
 SA_Emiss_Group_Grid(3,1) = '$TRACEMS/remain.cc.$todate-07.ag.07cem1A-run11',
 SA_Emiss_Group_Grid(3,2) = '$TRACEMS/remain.ff.$todate-07.ag.07cem1A-run11',

 &
```

**Figure 8-6.  This figure follows from Figure 7-9(d): it is a continuation day of a 2-grid run with three emission groups, and all three emission groups are defined explicitly by supplying extra emission files (AREA group 1, AREA group 2, POINT group 2, AREA group 3, and POINT group 3).  Therefore, the "Use_Leftover_Group" flag is set to FALSE.  The POINT group 1 filename is blank because group 1 is a category with no point source emissions (e.g., biogenics).  PSAT will trace PM sulfate and nitrate species only.**

## 8.5  Steps In Developing Inputs And Running PSAT

Below is a simple methodological list of steps to follow in setting up and running PSAT.  The process is similar among the OSAT, PSAT, and DDM Probing Tools.

1) Define the source groups and regions that you wish to track.  Keep in mind that memory resources increase dramatically as the number of tracers grows.  Probing Tool applications with large numbers of tracers, tracer classes, nested grids or grid cells may exceed available memory.
2) Build a source region map (Figure 7-10) that defines the spatial allocation of tracer emissions.  For small domains or small number of regions, this can be done by hand.  We suggest using GIS software to develop complex source region maps on large grids.
3) Process the emissions inventory into the separate source group files that you want to track (e.g., mobile, area, point, biogenic, etc.).
   a) Consideration of potential source apportionment or sensitivity applications prior to any emissions processing can be very beneficial so that files by group are available for later use.
   b) Elevated point sources will automatically be assigned to the source region in which they reside.  However, you may override the region to which each individual point source is assigned (see the definition of `kcell` in Section 3, Elevated Point Source File).  A point source region does not need to be defined in the source region map, e.g., you could have a map with two regions that split the domain in half, with a third region assigned arbitrarily to represent elevated point sources only.
4) Edit the CAMx control namelist file (Section 2).
   a) Set the `Probing_Tool` variable to the technology you wish to use (PSAT).  This will activate the `&SA_Control` namelist module.
   b) Edit or add the `&SA_Control` namelist module (described earlier).  Provide the required information, including:
      - output paths
      - whether to stratify boundary conditions
      - number of source regions
      - number of source groups
      - whether to use the leftover group option
      - receptor definitions
      - flags to turn on specific PM classes
      - list of input emission files by group.
5) Configure the CAMx source code to define the number of tracers, and build an executable.  This will ensure that you have sufficient memory for the Probing Tool application.
   a) Edit the file `Includes/camx.prm`
   b) Change the parameter `MXTRSP`, following the instructions provided in the file.  CAMx is distributed with `MXTRSP = 1` to minimize memory requirements for standard applications of the model.  If you run PSAT with an insufficient value, the model will stop and tell you the required value of `MXTRSP` for your application.

      c)   Execute the CAMx `Makefile` to build an executable program (Section 2).

6) Run CAMx and review the diagnostic output files to ensure that the model is correctly interpreting and running the Probing Tool configuration that you have specified.  Ensure that CAMx is generating the proper output files that you are expecting.  Review the table of emissions by source group and region.

7) Review gridded tracer fields using commonly available plotting programs.  Utilities such as PAVE or Verdi will read Probing Tool files directly.  Use of any other software may require specialized re-formatting procedures.

8) You may post-process PSAT receptor files using an Excel macro (OSAT_browser) that ENVIRON distributes at [www.camx.com](www.camx.com).

9) Probing Tool gridded tracer output files are written in the same Fortran binary format as the regular CAMx concentration output files.  You can post-process gridded output fields using any software that reads CAMx files, or you can adapt those programs or build your own software to generate specialized analysis and graphical products.

# 9. DECOUPLED DIRECT METHOD FOR SENSITIVITY ANALYSIS

Photochemical modelers have traditionally used sensitivity analysis both for model performance evaluation and emission control strategy design. The simplest approach to sensitivity analysis, often referred to as the "brute-force" approach, involves changing a model input parameter, rerunning the model, and then evaluating the change in model output. This approach requires an initial base run and a separate sensitivity run for each parameter to be investigated. For example, a model performance evaluation may use sensitivity simulations to evaluate the impact of changing the initial conditions (ICs), boundary conditions (BCs), biogenic emissions, anthropogenic emissions, etc. Sensitivity analysis is also used to aid control strategy design. For example, across-the-board VOC and $NO_x$ emission reductions are used to determine whether VOC and/or $NO_x$ reduction strategies are the most effective path to reduce ozone.

The advantages of the "brute force" method for sensitivity analysis are:

- Applicable to any model input parameter;
- Results are conceptually easy to explain and interpret.

The limitations of the "brute force" method are:

- Computationally inefficient;
- Sensitivity depends upon the magnitude of the perturbation if the model response is non-linear;
- Sensitivity derived from small perturbations may contain significant levels of uncertainty (numerical noise).

The last two points bear further explanation. If the model response to an input parameter depends upon non-linear components within the model (e.g., chemistry), then the relative magnitude or even sign of the output response may change for perturbations of different sizes. An example is the response of ozone to $NO_x$ reductions in a VOC-limited environment: smaller reductions in $NO_x$ emissions increase ozone levels whereas larger $NO_x$ reductions decrease ozone.

This situation can be illustrated mathematically. We define a "sensitivity coefficient" (*s*) which represents the change in concentration (*c*) with respect to some input parameter ($\lambda$), evaluated relative to the base state ($\lambda=\lambda_0$),

$$ s \quad = \quad \frac{\partial c}{\partial \lambda}\bigg|_{\lambda_o} $$

In general, $\lambda$ can be a vector (denoted as $\underline{\lambda}$), which contains multiple parameters related to processes in the model (e.g., rate constants) or inputs to the model (e.g., emissions). The response of concentration to a change in $\underline{\lambda}$ can be represented by a Taylor series of sensitivity coefficients:

$$c(\underline{x},t;\underline{\lambda}) \;=\; c(\underline{x},t;\underline{\lambda}_0) \;+\sum_{i=1}^{n}\frac{\partial c}{\partial \lambda_i}\bigg|_{\underline{\lambda}_o}(\lambda_i - \lambda_{i0})$$

$$+\frac{1}{2}\sum_{i=1}^{n}\sum_{j=1}^{n}\frac{\partial^2 c}{\partial \lambda_i \partial \lambda_j}\bigg|_{\underline{\lambda}_o}(\lambda_i - \lambda_{i0})(\lambda_j - \lambda_{j0})$$

$$+\ldots$$

where $n$ is the number of $\underline{\lambda}$ vector elements, $\underline{x}$ is the spatial dimension vector, and $t$ is time. In the ozone sensitivity example above, the non-linear response of ozone to large $NO_x$ emission reductions indicates that high-order sensitivity coefficients (curvatures and inflections) are significant relative to the first order sensitivity (linear response). As the magnitude of the input perturbation tends to zero, the output response will become dominated by the first-order sensitivity. Therefore, very small changes in the input parameter may be required to use the "brute force" method to estimate the first-order (local) sensitivity. The practical limitation to this approach is that since the change in output must be determined from the difference between two simulations, small levels of numerical uncertainty (noise) in two very similar outputs will contaminate the sensitivity calculation.

An alternative methodology for evaluating model sensitivity was developed by Dunker (1980 and 1981) called the decoupled direct method (DDM). The DDM can be used to calculate the same type of sensitivity coefficient as is available from the "brute force" method. The difference is that with DDM, sensitivity coefficients are calculated explicitly by specialized algorithms implemented in the host model. Thus, the DDM offers several advantages over the brute force method:

- Improved computational efficiency;
- Improved accuracy since sensitivities need not be contaminated by numerical noise;
- Multiple sensitivities can be calculated simultaneously

The degree to which these advantages are realized depends upon how the method is implemented, i.e., the algorithms employed and their coding. Fortunately, the performance of the DDM can be evaluated quantitatively by careful comparison of DDM sensitivities against "brute-force" sensitivities.

## 9.1 Implementation

The original implementation of the DDM in CAMx, which considers only first-order sensitivity, was performed in a joint project between Dr. Alan Dunker and ENVIRON with sponsorship from the Coordinating Research Council (http://www.crcao.com). A rigorous analysis of DDM was performed as part of that project, and excellent agreement was demonstrated (Dunker et al., 2002a). High-order DDM (HDDM; Hakami et al., 2003; Cohan et al., 2005) has since been implemented in CAMx through collaboration with Dr. Daniel Cohan (Rice University) with sponsorship from the Texas Commission on Environmental Quality (TCEQ). HDDM enables

CAMx to calculate second-order sensitivities along with first-order values. In the following discussion we use the term DDM generically to mean first and/or higher order sensitivity.

The CAMx DDM calculates sensitivity of predicted concentrations to pollutant sources (i.e., emissions, ICs and BCs) and to chemical rate constants. In the past, the implementation of DDM in other models (Dunker, 1981; Yang et al., 1997) has included sensitivities to other model input parameters (e.g., meteorological parameters). The CAMx implementation could be extended to other sensitivity parameters in the future.

The CAMx DDM sensitivity to be evaluated may bear a simple relationship to a model input parameter, such as scaling the ozone boundary concentration by a factor ($BC_{new} = \lambda \times BC_0$), or additively increasing the ozone boundary concentration by a constant amount everywhere ($BC_{new} = \lambda + BC_0$). To allow complete flexibility, the perturbations are specified by providing additional IC, BC, and/or emission input files with the same format as the regular model input files.

In mathematical terms, a regular model input file, for example the BC input file, represents some set of functions of space and time $f_i(\underline{x},t)$, where each chemical species $i$ can be defined by a unique function. An additional input file provided to the DDM represents another set of functions of space, time, and chemical species $g_i(\underline{x},t)$ that can be different from the regular input file. The scalar parameter $\lambda_i$ is then defined by

$$F_i\left(\underline{x},t\right) \;=\; f_i\left(\underline{x},t\right) + \lambda_i \times g_i\left(\underline{x},t\right).$$

Here, $\lambda_i \times g_i(\underline{x},t)$ is the perturbation, and the user desires information on how the model would respond if the input $f_i(\underline{x},t)$ is replaced by the input $F_i(\underline{x},t)$. The DDM calculates the first-order sensitivity $s_i^{(1)}(\underline{x},t)$ and second-order sensitivity $s_i^{(2)}(\underline{x},t)$ with respect to the scalar parameter $\lambda_i$. The Taylor series to second order then gives the estimate:

$$c_l\left(\underline{x},t;\lambda_i\right) \;=\; c_l\left(\underline{x},t;\lambda_i=0\right) + \lambda_i \times s_i^{(1)}\left(\underline{x},t\right) + \frac{1}{2}\lambda_i^2 \times s_i^{(2)}\left(\underline{x},t\right)$$

where $c_l(\underline{x};t;\lambda_i)$ is the estimated model result for species $l$ when $F_i(\underline{x},t)$ is used as input, and $c_l(\underline{x},t;\lambda_i=0)$ is the base case model result when $f_i(\underline{x},t)$ is used as input.

For example, to calculate the sensitivity of the predicted ozone concentration to scaling boundary ozone by a factor, CAMx would be provided with a DDM BC file that has the same ozone values as the regular model BC file. The sensitivity coefficient fields output by CAMx could then be used to estimate the resulting ozone concentration if the ozone BCs were increased by 20%, as follows:

$$c_{\lambda=0.2} \;=\; c_{\lambda=0} + 0.2 \times s^{(1)} + 0.5 \times 0.2^2 \times s^{(2)}$$

(For simplicity hereafter, the dependence on space, time, and chemical species will be omitted).

To calculate the sensitivity of the predicted ozone concentration to increasing boundary ozone by 10 ppb, CAMx would be provided with a DDM BC file that has a constant ozone value of 10 ppb. The sensitivity coefficient fields could be used to estimate the ozone concentration if the ozone BCs were increased by 10 ppb as follows:

$$c_{\lambda=1.0} \quad = \quad c_{\lambda=0} + 1.0 \times s^{(1)} + 0.5 \times 1.0^2 \times s^{(2)}$$

where each sensitivity is calculated according to a 10 ppb addition (thus sensitivities are scaled by unity). An alternative approach would be to provide CAMx with a DDM BC file that has a constant ozone value of 1 ppb. This perturbation would be associated with a new parameter $\lambda'$ and a new sensitivity coefficient $s'$. To estimate the ozone concentration if the ozone BC were increased by 10 ppb, one would use

$$c_{\lambda'=10} \quad = \quad c_{\lambda'=0} + 10.0 \times s'^{(1)} + 0.5 \times 10.0^2 \times s'^{(2)}$$

where each sensitivity is calculated according to a 1 ppb addition that must then be scaled by 10. This would give exactly the same estimate as the preceding approach in which CAMx is supplied with a DDM BC file that has an ozone value of 10 ppb everywhere because the two sensitivities are related by $s' = s \times 0.1$ (from the first to second approach, there has been only a change of the scalar variable from $\lambda$ to $\lambda'$).

These are examples of relatively simple sensitivities. A more complex example would be to calculate the sensitivity to morning (6-9 AM) $NO_x$ emissions in specific group of grid cells. In this case you would provide CAMx with a DDM emissions file where all values are zero except for the $NO_x$ emissions in the selected grid cells between 6 AM and 9 AM, which would have the same value as the regular emissions file. In this case the sensitivity coefficient for ozone might be interpreted as the increase (or decrease) in ozone concentration due to the selected emissions (however, caution is warranted because sensitivity coefficients are not directly equivalent to a source apportionment). More accurately, the sensitivity coefficient could be used to predict the concentration after a scalar change ($\lambda$) in the morning NOx emissions using the equation:

$$c_\lambda \quad = \quad c_{\lambda=0} + \lambda \times s^{(1)} + 0.5 \lambda^2 \times s^{(2)}$$

Any type of sensitivity perturbation can be described via an input file. However, the CAMx user interface also provides easy ways to define some sensitivities that are likely to be used frequently. In the first example above, the DDM BC file was described as having the "same ozone values as the regular model BC file." To make such a file you could copy the BC file and then remove (or zero out) all species but ozone. To avoid the effort of preparing an input file that is trivially different from the regular model file, the user interface allows you to select specific species from an input file to track - in this case ozone. It is possible to separately track the sensitivity to more than one species from the same file (e.g. ozone and NO). It is also possible to track the combined sensitivity to a group of species, such as $NO_x$, VOC, HRVOC, or ALL. The user interface also provides a simple way to track sensitivities to emissions from specific grid cells or groups of cells (sub-regions).

**9.1.1  Tracking Sensitivity Coefficients Within CAMx**

The conceptual approach in tracking DDM sensitivity coefficients is directly parallel to the way in which CAMx calculates three-dimensional concentration fields.  The concentration fields are calculated by a series of code modules that operate sequentially to represent the impact of different physical processes (emissions, advection, diffusion, chemistry, deposition, etc.) on the gridded concentrations.  Sensitivity coefficients are calculated by a parallel set of modules which operate in step with the CAMx modules to calculate gridded sensitivity coefficients.  For some processes (e.g., chemistry and horizontal advection), the sensitivity coefficient modules make use of information saved from the corresponding CAMx modules.  The need to employ this approach arises in cases where the CAMx algorithm depends non-linearly upon species concentrations.  In other cases, the sensitivity algorithm turns out to be identical to the CAMx algorithm (e.g., horizontal diffusion) and both concentrations and sensitivity coefficients can be processed by the single module.  Finally, there are cases where the sensitivity algorithm turns out to be identical to the CAMx algorithm, but a specialized module has been written for the sensitivity coefficients to improve the computational efficiency (e.g., vertical advection).

Priorities in the DDM coding implementation were:

- Ensuring accuracy by using consistent numerical methods for the concentrations and sensitivities;

- Ensuring accuracy by calculating the concentrations and sensitivities using the same time steps (for original DDM);

- Optimizing the efficiency of the sensitivity coefficient calculations without compromising accuracy;

- Providing a flexible User Interface that allows calculation of sensitivities to all sources and precursors;

- Ensuring that the DDM algorithms have minimal impact on computer resource requirements (memory and CPU time) when the DDM is not being used.

9.1.1.1  Horizontal Advection and Chemistry

Specialized modules were developed to calculate the effects of chemistry and horizontal advection upon DDM sensitivity coefficients.  These DDM modules are exactly matched to the numerical methods employed in the corresponding CAMx modules.  CAMx has two separate options for the horizontal advection solver (Bott and PPM) and three options for the gas phase chemistry solver (the EBI solver, IEH solver, and LSODE [Gear] solver).  The original first-order DDM implementation was developed for one advection solver (Bott) and one chemistry solver (EBI); it cannot be used with other solver options.  However, HDDM can be used with any advection solver and chemistry solver.

The implementation of DDM and HDDM algorithms into the chemistry solvers is performed using the chemical mechanism compiler (CMC).  Therefore, both DDM and HDDM are available for the CB05, CB6, and SAPRC99 chemical mechanisms, and will be available for additional mechanisms implemented in CAMx in the future.

### 9.1.1.2  Plume-in-Grid, ACM2, and Aerosol Processes

DDM and HDDM algorithms are not currently implemented for the Plume-in-Grid (PiG) submodel, the ACM2 vertical diffusion scheme, and any aerosol chemistry options currently available in CAMx.

### 9.1.1.3  Source Code

The coding of DDM algorithms involved the creation of several new subroutines for CAMx. These subroutines are all grouped in a separate directory (called DDM) under the main CAMx source code directory. It was necessary to add additional code for DDM in several existing CAMx subroutines, and the new code is clearly marked by comments.

### 9.1.2  Flexi-DDM

Although DDM is computationally much more efficient than the Brute-Force method, it does require much more additional CPU time and memory space over and above a standard CAMx run, which can be significant especially when many first and second-order sensitivities are requested for a nested grid run with multiple source categories and multiple source regions. The increased computational cost may not always be worthwhile if only part of the modeling domain is of interest. One way to enhance computational efficiency in such cases is to use one-way nesting, where BCs for a nested grid are extracted from the parent grid, and so subsequent runs with sensitivities are performed without outer grids. However, differences between the two nesting schemes (i.e. 1-way vs. 2-way) sometimes cause discrepancies in the model results. An alternative approach is to run the full 2-way nested model while "turning off" sensitivity calculations outside nested grids of interest.

CAMx provides a feature called "Flexi-DDM", which allows the user to turn off sensitivity calculations for selected grids (normally grids far outside the area of interest) to improve computational efficiency of DDM runs. This reduces CPU times but will not reduce memory requirements. Also, note that turning off sensitivity calculations for outer grids is only appropriate for certain types of sensitivity calculations: e.g., sensitivity to master grid BCs cannot be calculated with Flexi-DDM.

## 9.2  Running CAMX With DDM And HDDM

This section describes how to specify the sensitivity coefficients to be calculated and the additional input files that must be supplied. The DDM user interface was designed along similar lines to the Source Apportionment (OSAT/PSAT) user interface. This makes it easier to learn how to use both options and promotes consistency in analyses performed using OSAT/PSAT and DDM.

### Inputs in the CAMx Control File

DDM is invoked similarly to the other Probing Tools within the CAMx control file. In the `&CAMx_Control` namelist module, the variable `Probing_Tool` must be set to either "DDM" to utilize the original first-order implementation, or "HDDM" to utilize the high-order implementation. An additional namelist module called `&DDM_Control` must then be provided in the control file to configure the DDM portion of the model. The additional namelist

module is described below.  The order of the variables follow the template available with the source code.  An example of the DDM portion of the CAMx run control file is shown in Figure 9-1.

## Description of DDM Control in the CAMx Run Control File

&DDM_Control | Label for the Probing Tool namelist module that configures the DDM option; it must begin in column 2

& | Flag ending a namelist; it must be in column 2

DDM_File_Root | Character root output path/filename

DDM_Master_Sfc_Output | Logical flag for master grid surface output (TRUE=DDM file will be output for all sensitivities, FALSE=DDM file will not be output)

DDM_Nested_Sfc_Output | Logical flag for nested grid surface output (TRUE=DDM file will be output for all sensitivities, FALSE=DDM file will not be output)

DDM_Stratify_Boundary | Logical flag to stratify boundary types (TRUE=separate sensitivity types will be used for the N, S, E, W, and Top boundaries, FALSE=a single sensitivity type will be used for all 5 boundaries)

DDM_Number_of_Source_Regions | Integer number of source regions to be tracked.  This must be the same as the number of source areas defined in the DDM_Source_Area_Map file.  This value may be zero.

DDM_Number_of_Source_Groups | Integer number of emission groups to be tracked.  This determines the number of emission files that must be supplied (additional details below).  This value may be zero.

Number_of_IC_Species_Groups | Integer number of species or species groups in the initial conditions to be tracked.  This number may be between zero and the number of species being simulated plus four (allowing for the four species groups VOC, HRVOC, NOX, ALL).

IC_Species_Groups | Character array (by IC group) names of the species or species groups in the initial conditions to be tracked.  Allowed names are any species being simulated by the mechanism in use (e.g., O3, PAR, NO, etc.) plus the species groups NOX, VOC, HRVOC, and ALL.  It is permissible to specify both a species and a group containing that species, e.g., both NO and NOX.  Each name may have up to 10 characters.  Note that if you select a species that is not present on the IC file provided, the initial sensitivities

for that species will be set to zero. This variable may be left blank if the number of initial condition species groups is zero.

`Number_of_BC_Species_Groups`      Integer number of species or species groups in the boundary conditions to be tracked. This number may be between zero and the number of species being simulated plus four (allowing for the four species groups VOC, HRVOC, NOX, ALL).

`BC_species_Groups`      Character array (by BC group) names of the species or species groups in the boundary conditions to be tracked. See description for `IC_Species_Group` above.

`Number_of_EM_Species_Groups`      Integer number of species or species groups in the emissions to be tracked. This number may be between zero and the number of species being simulated plus four (allowing for the four species groups VOC, HRVOC, NOX, ALL).

`Emis_Species_Groups`      Character array (by emissions group) names of the species or species groups in the emissions to be tracked. See description for `IC_Species_Group` above.

`Number_of_Rate_Const_Groups`      Integer number of reaction rate sensitivity groups to be tracked. This number may be zero.

`Rate_Const_Groups`      Character string containing each reaction rate sensitivity group name and reaction numbers that belong to the group. Group name and reaction numbers are separated by colon (:) and each reaction number is separated by comma (,).

`Number_of_HDDM_Sens_Groups`   Integer number of second-order sensitivity groups to be tracked (additional details below). This number may be zero.

`HDDM_parameters`      Character array names of the first-order sensitivity parameters to which second-order sensitivity is computed. The naming of the first-order parameters is the same as the long name of sensitivities with the first 4 characters omitted (see DDM sensitivity naming conventions/formats below). For each HDDM sensitivity group, two first-order parameters are required (the same can be used twice). All the first-order parameters must be included in the modeling.

`DDM_Receptor_Definitions`      Character input DDM receptor definition path/filename

`DDM_Source_Area_Map`      Character array (by CAMx grid) input DDM source area definition path/filename (required for master grid, optional for nested grids). Source regions are defined using a map in the same format as an OSAT source area map (Section 7); however, DDM does not require that all parts of the modeling domain be

tracked, therefore it is permissible to define an area numbered zero in the source area map (emissions from those areas will not be tracked). The non-zero source region numbers must be between 1 and the number of regions.

| | |
|---|---|
| DDM_Calc_Grid | Logical array containing Flexi-DDM flag for each grid (.TRUE. = calculate sensitivities in the grid; .FALSE. = do not calculate sensitivities in the grid). |
| DDM_Initial_Conditions | The name of the sensitivity initial condition file. Leave the file name blank for restart days or if sensitivity to initial conditions is not being calculated. |
| DDM_Boundary_Conditions | The name of the sensitivity lateral boundary condition file. Leave the file name blank if sensitivity to boundary conditions is not being calculated. |
| DDM_Master_Restart | Character input master grid DDM restart path/filename (ignored if `Restart=FALSE`) |
| DDM_Nested_Restart | Character input nested grid DDM restart path/filename (ignored if `Restart=FALSE` or `Number_of_Grids=1`) |
| DDM_Points_Group | Character array (by source group) input DDM elevated point source emissions path/filename (optional, ignored if `Point_Emissions=FALSE`) |
| DDM_Emiss_Group_Grid | Character array (by source group, by CAMx grid) input DDM gridded emissions path/filename (optional, ignored if `Gridded_Emissions=FALSE`) |

```
&DDM_Control

DDM_File_Root                  = '$DDM_OUT/CAMx.08jul95.runA',
DDM_Master_Sfc_Output          = .true.,
DDM_Nested_Sfc_Output          = .true.,
DDM_Stratify_Boundary          = .false.,
DDM_Number_of_Source_Regions   = 4,
DDM_Number_of_Source_Groups    = 2,

Number_of_IC_Species_Groups = 1,
IC_Species_Groups(1)           = 'ALL',
Number_of_BC_Species_Groups = 1,
BC_species_Groups(1)           = 'ALL',
Number_of_EM_Species_Groups = 2,
Emis_Species_Groups(1)         = 'NOX',
Emis_Species_Groups(2)         = 'VOC',
Number_of_Rate_Const_Groups = 1,
Rate_Const_Groups(1)           = 'RXN1: 120,121,122',
Number_of_HDDM_Sens_Groups  = 3,
HDDM_parameters(1,1)           = 'EM0101NOX_',
HDDM_parameters(1,2)           = 'EM0101NOx_',
HDDM_parameters(2,1)           = 'EM0101VOC_',
HDDM_parameters(2,2)           = 'EM0101VOC_',
HDDM_parameters(3,1)           = 'EM0101NOX_',
HDDM_parameters(3,2)           = 'EM0101VOC_',

DDM_Receptor_Definitions  = '$DDM_IN/receptor.cities',
DDM_Source_Area_Map(1)    = '$DDM_IN/source_map.DDM.4areas',
DDM_Source_Area_Map(2)    = ' ',

DDM_Calc_Grid(1)               = .true.,
DDM_Calc_Grid(2)               = .true.,

DDM_Initial_Conditions    = ' ',
DDM_Boundary_Conditions   = '$DDM_IN/BC.08jul95',
DDM_Master_Restart        = '$DDM_OUT/CAMx.07jul95.runA.sa.inst',
DDM_Nested_Restart        = '$DDM_OUT/CAMx.07jul95.runA.sa.finst',

DDM_Points_Group(1)       = ' ',
DDM_Points_Group(2)       = '$DDM_PT/ptsr.ng.08jul95',

DDM_Emiss_Group_Grid(1,1) = '$DDM_EMIS/bio.cc.08jul95',
DDM_Emiss_Group_Grid(1,2) = '$DDM_EMIS/bio.ff.08jul95',
DDM_Emiss_Group_Grid(2,1) = '$DDM_EMIS/anthro.cc.08jul95',
DDM_Emiss_Group_Grid(2,2) = '$DDM_EMIS/anthro.ff.08jul95',
&
```

**Figure 9-1.  Example input of DDM options and filenames via the CAMx control file.  In this case, CAMx is run with two grids, and DDM is configure to track emissions from four source regions and two source groups (biogenic and anthropogenic).  Initial and boundary conditions are tracked as a single sensitivity called "ALL", while emissions are tracked with two sensitivities called "NOx" and "VOC". Sensitivity for a  single rate constant group will be calculated involving mechanism reaction numbers 120, 121, and 122.  Three groups of second-order sensitivities to biogenic VOC emissions (emissions group 1) from source region 1 will be computed ($d^2/dNOx^2$, $d^2/dVOC^2$ and $d^2/dNOxdVOC$).  No source region map is provided for the nested grid (the region assignments on the nest are defined by the master grid).  Initial condition sensitivity is not being tracked (no file provided), and only the group 2 point sources are tracked (no biogenic point sources are available).**

## 9.3  Approaches To Define IC, BC And Emissions Sensitivities

The description above shows how to specify the IC, BC and emissions files for DDM sensitivity calculations.  The formats for each of these files are identical to the CAMx input files of these types.  In many cases, users may choose to specify exactly the same file for a CAMx input file and a DDM input file.  (Be aware that some computer systems do not allow a file to be opened twice by the same application.  A work around for this problem is to copy or link the file "filename" to another file of different name, such as "filename.copy").

The user can perform many different sensitivity calculations in a single run according to the content of the DDM input files.  Take initial conditions (ICs) as an example.  If the same IC file is specified for both CAMx and DDM, the output sensitivity fields represent the sensitivity of the predicted concentrations to the ICs.  Therefore, simply scaling the output sensitivity coefficients fields provides the incremental concentrations resulting from scaling the ICs.

As another example, if a DDM emissions file is supplied to CAMx that has a constant VOC emission rate everywhere, the sensitivity will correspond to a uniform absolute increase in the VOC emission rate rather than a percentage increase as described above.  Another possibility would be a DDM emission file with a different spatial pattern than the CAMx input file.  The sensitivity coefficient would then correspond to changing both the geographic distribution and magnitude of emissions.  Still another possibility would be a DDM file that has zero emissions for all hours except midnight to 5 AM on the third simulated day.  The program would then calculate the sensitivity to early morning emissions on the third day.  In this case, just the concentrations could be simulated for the first two days and the DDM calculation begun on the third day, because sensitivities on the first two days are identically zero.

In short, the DDM input file can be arbitrary – different from the CAMx input file in the overall magnitude of concentrations or emissions, different in the geographic and temporal distribution, and different in the relative proportions of the chemical species.  However, the user must understand what perturbations are being considered in order to properly interpret the resulting output sensitivity coefficient fields.  Also, the user should recognize that as the size of perturbations increase, the second- and higher-order terms eventually become important, usually when the emissions are altered by more than 20-30% (a very crude, variable, and uncertain approximation).

## 9.4  DDM Output Files

The output file types for a DDM simulation are described in Table 9-1.  These files have the same format as corresponding concentration output files, described in Section 2.

**Table 9-1.  DDM output file suffix names.**

| File Name Suffix | DDM File Type |
|---|---|
| `.ddm.inst` | Binary master grid instantaneous sensitivity file at end of simulation (used for restart), 3-D, all sensitivities, $\mu$mol m$^{-3}$ parameter$^{-1}$ units. |
| `.ddm.finst` | Binary nested grid instantaneous sensitivity file at end of simulation (used for restart), 3-D, all sensitivities, $\mu$mol m$^{-3}$ parameter$^{-1}$ units. |
| `.ddm.grd`*nn* | Binary average sensitivity file for grid *nn*, 2-D, surface layer sensitivities only for affected species requested in the CAMx average file, ppm parameter$^{-1}$ units. |
| `.ddm.receptor` | Text hourly average sensitivities at user specific receptor locations.  This file is in comma delimited ASCII format suitable for importing into a spreadsheet. |

## 9.5  DDM Sensitivity Coefficient Names

Each DDM sensitivity coefficient tracks the influence of a species from a specific source (the *influencing species*) on a predicted concentration (the *affected species*).  The sensitivity coefficient names are constructed to show this relationship, as follows:

{Affected Species}{Pollutant Source}{Influencing Species}

This is a lot of information to encode in a name that must conform to the ten character limit imposed by the binary I/O file formats.  Because of this, two naming systems are used in CAMx:

- Long Names - these names are easy to read, but since they are more than ten characters in length they cannot be used in sensitivity coefficient binary output files.  If an alternate I/O format is implemented in the future it may be possible to use the long names on sensitivity output files.
- Short Names - these convey the same information as the long names but require more practice to learn.  They are used in the sensitivity coefficient binary output files.

At the start of each CAMx run a concordance of Long and Short sensitivity coefficient names is written to the diagnostic output file (.diag file).  An example concordance is shown in Figure 9-2, and a detailed explanation of the naming convention follows.

```
  Affected     Influencing   Source                          Long          Short
  Species        Species      Type     Group  Region         Name          Name
--------------------------------------------------------------------------------------
NO             NO            EM          1       2      NO__EM0102NO__   01E0102001
NO2            NO            EM          1       2      NO2_EM0102NO__   02E0102001
O3             NO            EM          1       2      O3__EM0102NO__   03E0102001
PAN            NO            EM          1       2      PAN_EM0102NO__   04E0102001
NXOY           NO            EM          1       2      NXOYEM0102NO__   05E0102001
OLE            NO            EM          1       2      OLE_EM0102NO__   06E0102001
PAR            NO            EM          1       2      PAR_EM0102NO__   07E0102001
TOL            NO            EM          1       2      TOL_EM0102NO__   08E0102001
XYL            NO            EM          1       2      XYL_EM0102NO__   09E0102001
FORM           NO            EM          1       2      FORMEM0102NO__   10E0102001
ALD2           NO            EM          1       2      ALD2EM0102NO__   11E0102001
ETH            NO            EM          1       2      ETH_EM0102NO__   12E0102001
CRES           NO            EM          1       2      CRESEM0102NO__   13E0102001
MGLY           NO            EM          1       2      MGLYEM0102NO__   14E0102001
OPEN           NO            EM          1       2      OPENEM0102NO__   15E0102001
PNA            NO            EM          1       2      PNA_EM0102NO__   16E0102001
CO             NO            EM          1       2      CO__EM0102NO__   17E0102001
HONO           NO            EM          1       2      HONOEM0102NO__   18E0102001
H2O2           NO            EM          1       2      H2O2EM0102NO__   19E0102001
HNO3           NO            EM          1       2      HNO3EM0102NO__   20E0102001
ISOP           NO            EM          1       2      ISOPEM0102NO__   21E0102001
MEOH           NO            EM          1       2      MEOHEM0102NO__   22E0102001
ETOH           NO            EM          1       2      ETOHEM0102NO__   23E0102001
ISPD           NO            EM          1       2      ISPDEM0102NO__   24E0102001
NTR            NO            EM          1       2      NTR_EM0102NO__   25E0102001
```

**Figure 9-2**. Example concordance of long and short sensitivity coefficient names from the CAMx diagnostic output file.

### 9.5.1 Initial Condition Sensitivity Names

Long Name              **NNNNIC_____MMMM**

where:

| | |
|---|---|
| **NNNN** | Affected species name with trailing underscore to pad blanks |
| **IC** | Indicates the sensitivity coefficient is for initial conditions |
| **_____** | Four underscores to pad the name to 14 characters |
| **MMMM** | Influencing species name with trailing underscore to pad blanks |

Examples:              FORMIC_____VOC_
                       O3__IC_____O3__

Short Name             **nnI_____mmm**

where:

| | |
|---|---|
| **nn** | Affected species number |
| **I** | Indicates the sensitivity coefficient is for initial conditions |
| **_____** | Four underscores to pad the name to 10 characters |
| **mmm** | Influencing species number or name of a species group (NOX, VOC, HRVOC or ALL). |

Examples:          `10I_____VOC` (where FORM is species number 10)
                   `03I_____003` (where O3 is species number 3)

## 9.5.2 Boundary Condition Sensitivity Names

Long Name          **NNNNBCRRR_MMMM**

where:

| | |
|---|---|
| **NNNN** | Affected species name with trailing underscore to pad blanks |
| **BC** | Indicates the sensitivity coefficient is for boundary conditions |
| **RRR** | NTH, STH, EST, WST or TOP if stratified by boundary; ALL if not stratified by boundary |
| **_** | Underscore to pad the name to 14 characters |
| **MMMM** | Influencing species name with trailing underscore to pad blanks |

Examples:          `FORMBCALL_VOC_`
                   `O3___BCTOP_O3___`

Short Name         **nnBRRR_mmm**

where:

| | |
|---|---|
| **nn** | Affected species number |
| **B** | Indicates the sensitivity coefficient is for initial conditions |
| **RRR** | NTH, STH, EST, WST or TOP if stratified by boundary; ALL if not stratified by boundary |
| **_** | Underscore to pad the name to 10 characters |
| **mmm** | Influencing species number or name of a species group (NOX, VOC, HRVOC or ALL) |

Examples:          `10BALL_VOC` (where FORM is species number 10)
                   `03BTOP_003` (where O3 is species number 3)

## 9.5.3 Emissions Sensitivity Names

Long Name          **NNNNEMGGRRMMMM**

where:

| | |
|---|---|
| **NNNN** | Affected species name with trailing underscore to pad blanks |
| **EM** | Indicates the sensitivity coefficient is for emissions |
| **GG** | Emissions group number |
| **RR** | Emissions region number |
| **MMMM** | Influencing species name with trailing underscore to pad blanks |

Examples:          `FORMEM0103VOC_`
                   `O3___EM0201O3___`

Short Name                  **nnEGGRRmmm**

where:

| | |
|---|---|
| **nn** | Affected species number |
| **E** | Indicates the sensitivity coefficient is for emissions |
| **GG** | Emissions group number |
| **RR** | Emissions region number |
| **mmm** | Influencing species number or name of a species group (NOX, VOC, HRVOC or ALL) |

Examples:                   `10E0103VOC`  (where FORM is species number 10)

                            `03E0201003`     (where O3 is species number 3)

### 9.5.4 Reaction Rate Sensitivity Names

Long Name                   **NNNNRATE___MMMM**

where:

| | |
|---|---|
| **NNNN** | Affected species name with trailing underscore to pad blanks |
| **RATE** | Indicates the sensitivity coefficient is for rate constants |
| **___** | Two underscores to pad the name to 14 characters |
| **MMMM** | Reaction rate sensitivity group name with trailing underscore to pad blanks |

Examples:                   `NO__RATE__RXN1`
                            `O3__RATE__R28_`

Short Name                  **nnRATE_mmm**

where:

| | |
|---|---|
| **nn** | Affected species number |
| **RATE** | Indicates the sensitivity coefficient is for rate constants |
| **_** | Underscore to pad the name to 10 characters |
| **mmm** | Reaction rate sensitivity group number |

Examples:                   `01RATE_001`  (where NO is species number 1)
                            `03RATE_002`  (where O3 is species number 3)

### 9.5.5 HDDM Sensitivity Names

Long Name                   **NNNNHDDMLLLMMM**

where:

| | |
|---|---|
| `NNNN` | Affected species name with trailing underscore to pad blanks |
| `HDDM` | Indicates the sensitivity coefficient is second-order |
| `LLL` | The index of the first 1$^{st}$-order sensitivity parameter in the internal list of the 1st-order parameters |
| `MMM` | The index of the second 1$^{st}$-order sensitivity parameter in the internal list of the 1st-order parameters |

Examples:          `NO__HDDM001001`
                   `O3__HDDM001002`

Short Name          `nnEGGRRmmm`

where:

| | |
|---|---|
| `nn` | Affected species number |
| `HDDM` | Indicates the sensitivity coefficient is second-order |
| `ll` | The index of the first 1$^{st}$-order sensitivity parameter in the internal list of the 1st-order parameters |
| `mm` | The index of the second 1$^{st}$-order sensitivity parameter in the internal list of the 1st-order parameters |

Examples:          `01HDDM0101`   (where NO is species number 1)
                   `03HDDM0102`  (where O3 is species number 3)

## 9.6  Steps In Developing Inputs And Running DDM

Below is a simple methodological list of steps to follow in setting up and running DDM.  The process is similar among the OSAT, PSAT, and DDM Probing Tools.

1) Define the source groups and regions that you wish to track.  Keep in mind that memory resources increase dramatically as the number of sensitivities grows.  Probing Tool applications with large numbers of sensitivities, nested grids or grid cells may exceed available memory.

5) Build a source region map (Figure 7-10) that defines the spatial allocation of emission sensitivities.  For small domains or small number of regions, this can be done by hand.  We suggest using GIS software to develop complex source region maps on large grids.

6) Process the emissions inventory into the separate source group files that you want to track (e.g., mobile, area, point, biogenic, etc.).

   a) Consideration of potential source apportionment or sensitivity applications prior to any emissions processing can be very beneficial so that files by group are available for later use.

   b) Elevated point sources will automatically be assigned to the source region in which they reside.  However, you may override the region to which each individual point source is assigned (see the definition of `kcell` in Section 3, Elevated Point Source

File).  A point source region does not need to be defined in the source region map, e.g., you could have a map with two regions that split the domain in half, with a third region assigned arbitrarily to represent elevated point sources only.

7) Edit the CAMx control namelist file (Section 2).

   a) Set the `Probing_Tool` variable to the technology you wish to use (DDM, HDDM). This will activate the `&DDM_Control` namelist module.

   b) Edit or add the `&DDM_Control` namelist module (described earlier).  Provide the required information, including:
   - output paths
   - whether to stratify boundary conditions
   - number of source regions
   - number of source groups
   - numbers and names of IC, BC, emissions, rate constant, and HDDM groups
   - receptor definitions
   - IC/BC input files
   - list of input emission files by group.

8) Configure the CAMx source code to define the number of tracers, and build an executable.  This will ensure that you have sufficient memory for the Probing Tool application.

   a) Edit the file `Includes/camx.prm`

   b) Change the parameter `MXTRSP`, following the instructions provided in the file. CAMx is distributed with `MXTRSP = 1` to minimize memory requirements for standard applications of the model.  If you run DDM with an insufficient value, the model will stop and tell you the required value of `MXTRSP` for your application.

   c) Execute the CAMx `Makefile` to build an executable program (Section 2).

9) Run CAMx and review the diagnostic output files to ensure that the model is correctly interpreting and running the Probing Tool configuration that you have specified.  Ensure that CAMx is generating the proper output files that you are expecting.  Review the table of emissions by source group and region.

10) Review gridded tracer fields using commonly available plotting programs.  Utilities such as PAVE or Verdi will read Probing Tool files directly.  Use of any other software may require specialized re-formatting procedures.

11) Probing Tool gridded tracer output files are written in the same Fortran binary format as the regular CAMx concentration output files.  You can post-process gridded output fields using any software that reads CAMx files, or you can adapt those programs or build your own software to generate specialized analysis and graphical products.

# 10.  PROCESS ANALYSIS

Process Analysis (PA) allows for in-depth analysis of photochemical model performance by revealing the contributions from individual physical and chemical processes operating within the model (Jeffries and Tonnesen, 1994).  Using PA, one can more fully understand the complex interactions between the different processes, explain simulation results within the context of the model formulation, and improve the design of control strategies.

A conventional model performance evaluation employs statistical and graphical methods to analyze predicted concentrations against observed concentrations.  This answers the basic question: "How well is the model replicating measurements?"  While such comparisons are necessary to summarize performance, they are far from sufficient to determine whether the model is adequately representing the real situation.  This is because compensating errors among various model processes can result in predictions that serendipitously agree with limited observations but for the wrong reasons.  In contrast PA provides information on how the specific model predictions were obtained, which can be interpreted to improve model performance and/or inform control strategy decisions.

## 10.1  Process Analysis In CAMx

Three components of PA are implemented in CAMx:

1) **Integrated Processes Rate (IPR) analysis.**  The IPR method provides detailed process rate information for each physical process in CAMx (i.e., advection, diffusion, deposition, emissions, and chemistry) for selected grid cells and selected species (Wang, Langstaff, and Jeffries, 1995).  The IPR outputs can be analyzed to determine what processes governed the model-predicted concentrations at any time and place.  IPR information has often been plotted as a time series of process contributions for specific cells or groups of cells.  IPR outputs have also been used to check the mass balance in the host model, i.e., to determine whether model concentrations are fully explained by the diagnosed process information or whether unexpected artifacts are occurring.  The IPR data are relatively easy to interpret and can be analyzed using simple tools such as spreadsheets.  Currently, only the IPR analysis has been extended to the PM modules in CAMx.  IPR does not work with the ACM2 vertical diffusion option.

2) **Integrated Reaction Rate (IRR) analysis**.  The IRR method provides detailed reaction rate information for all reactions in the chemical mechanism for selected grid cells (Jeffries and Tonnesen, 1994).  The IRR data can be analyzed to determine how the chemical changes occurring in the model are related to the chemical mechanism.  For example, by analyzing rate information over groups of reactions it is possible to quantify chemically meaningful attributes such as radical initiation rates, radical propagation efficiencies, chain lengths, etc.  Since these analyses tend to be complex, IRR data generally require post-processing to be useful.  IRR is implemented for the SAPRC99, CB05 and CB6 chemical mechanisms (mechanism numbers 5 through 7, respectively: see Chapter 5, Table 5-1).

3) **Chemical Process Analysis (CPA)**. CPA is related to the IRR method but is designed to be more user friendly and accessible. As mentioned above, IRR data are generally only useful after the data have been post-processed into chemically meaningful parameters. With CPA, a selection of useful parameters is calculated from IRR data within CAMx and then output to gridded files (Tonnesen and Dennis, 2000). The gridded CPA files use the same format as the gridded concentration outputs and can be visualized and processed using standard post-processing tools. CPA is implemented for the SAPRC99, CB05, and CB6 chemical mechanisms (mechanism numbers 5 through 7: see Chapter 5, Table 5-1).

### 10.1.1 Integrated Process Rate Analysis

The specific processes that are reported by IPR are listed in Table 10-1. This information is output for each chemical species selected for inclusion in the average concentration output file, and for each grid cell selected for analysis. The process rates are integrated across each model output time interval (normally hourly). Taken together, this information provides a complete description of how the species concentration changed across the output time interval and the magnitude of all of the processes that caused this change. Information is output in the concentration units used internally within CAMx ($\mu$mole/m$^3$ for gases, $\mu$g/m$^3$ for PM species). A gas conversion factor (ppm/$\mu$mole/m$^3$) specific to the grid cell/time period is also output to allow conversion to mixing ratio (ppm) for comparison of gas species with CAMx average concentration outputs. For PM species, the conversion factor is always 1. Grid cell volume is also output to allow aggregation across grid cells.

For most of the process rates listed in Table 10-1 the interpretation is straightforward, the rate is simply the concentration change caused by the named process across the output time interval. The sign convention is such that a positive flux always tends to increase the cell concentration. Further explanation is provided for several processes below:

*Plume-in-Grid change*: The grid cell concentration change caused by Plume-in-Grid puffs that transferred mass to the grid cell during the output time interval.

*Point source emissions*: Does not include point sources selected for PiG treatment as these are reported in Plume-in-Grid Change.

*Dilution in the vertical*: CAMx allows for layer interface heights to change over time which can lead to a "dilution" term for affected grid cells.

*Boundary diffusion*: In some cases this term will be zero by definition, namely: the bottom boundary of surface layer grid cells; the top boundary of top layer grid cells; any lateral boundary that coincides with a nest boundary.

*Dry deposition*: This term is zero by definition for all grid cells above the surface layer.

**Table 10-1.  Process information reported by the IPR option.**

| IPR Parameter | Process Information | Units[a] |
|:---:|:---|:---:|
| 1 | Initial concentration | $\mu$mole/m$^3$ ($\mu$g/m$^3$) |
| 2 | Gas phase chemistry | $\mu$mole/m$^3$ ($\mu$g/m$^3$) |
| 3 | Gridded emissions | $\mu$mole/m$^3$ ($\mu$g/m$^3$) |
| 4 | Point source emissions | $\mu$mole/m$^3$ ($\mu$g/m$^3$) |
| 5 | Plume-in-Grid change | $\mu$mole/m$^3$ ($\mu$g/m$^3$) |
| 6 | West boundary advection | $\mu$mole/m$^3$ ($\mu$g/m$^3$) |
| 7 | East boundary advection | $\mu$mole/m$^3$ ($\mu$g/m$^3$) |
| 8 | South boundary advection | $\mu$mole/m$^3$ ($\mu$g/m$^3$) |
| 9 | North boundary advection | $\mu$mole/m$^3$ ($\mu$g/m$^3$) |
| 10 | Bottom boundary advection | $\mu$mole/m$^3$ ($\mu$g/m$^3$) |
| 11 | Top boundary advection | $\mu$mole/m$^3$ ($\mu$g/m$^3$) |
| 12 | Dilution in the vertical | $\mu$mole/m$^3$ ($\mu$g/m$^3$) |
| 13 | West boundary diffusion | $\mu$mole/m$^3$ ($\mu$g/m$^3$) |
| 14 | East boundary diffusion | $\mu$mole/m$^3$ ($\mu$g/m$^3$) |
| 15 | South boundary diffusion | $\mu$mole/m$^3$ ($\mu$g/m$^3$) |
| 16 | North boundary diffusion | $\mu$mole/m$^3$ ($\mu$g/m$^3$) |
| 17 | Bottom boundary diffusion | $\mu$mole/m$^3$ ($\mu$g/m$^3$) |
| 18 | Top boundary diffusion | $\mu$mole/m$^3$ ($\mu$g/m$^3$) |
| 19 | Dry deposition | $\mu$mole/m$^3$ ($\mu$g/m$^3$) |
| 20 | Wet deposition | $\mu$mole/m$^3$ ($\mu$g/m$^3$) |
| 21 | Inorganic aerosol chemistry | $\mu$mole/m$^3$ ($\mu$g/m$^3$) |
| 22 | Oganic aerosol chemistry | $\mu$mole/m$^3$ ($\mu$g/m$^3$) |
| 23 | Aqueous aerosol chemistry | $\mu$mole/m$^3$ ($\mu$g/m$^3$) |
| 24 | Final concentration | $\mu$mole/m$^3$ ($\mu$g/m$^3$) |
| 25 | Units conversion | ppm/($\mu$mole/m$^3$) (N/A)[b] |
| 26 | Average cell volume | m$^3$ |

a  Units in the parentheses are for PM species.
b  Unit conversion factor for PM species is always 1.


### 10.1.2  Integrated Reaction Rate Analysis

IRR provides the integrated rate of each gas-phase chemical reaction in units of ppm hr$^{-1}$ for each grid cell selected for process analysis.  Reaction rates are accumulated (integrated) within the chemistry solver at the time steps being used to solve the chemical equations, and output at the CAMx output time interval (usually 1 hour).

### 10.1.3  Chemical Process Analysis

The CPA method calculates a pre-determined set of parameters as listed in Table 10-2.  The CPA parameters are calculated for all grid cells in either the surface layer or all layers.  The selection between surface layer or all layer CPA outputs is determined by the "3-D average  file" flag specified in the CAMx Control File (see Section 2).  This is based on the premise that 3-D CPA information will be interpreted in conjunction with 3-D concentration fields.

**Table 10-2.  Chemical Process Analysis (CPA) variables calculated in CAMx for the CB6, CB05 and SAPRC99 mechanisms.   Concentrations are ppb; production and destruction are ppb/hr; photolysis rates are hr$^{-1}$, ratios are unitless.**

| CB6 | CB05 | SAPRC99 | Description |
|---|---|---|---|
| **Ozone and Oxidant Production and Loss** | | | |
| OxProd | OxProd | OxProd | Production of Ox = Ozone + NOy-NO |
| OxLoss | OxLoss | OxLoss | Destruction of Ox |
| PO3_net | PO3_net | PO3_net | Net ozone produced |
| PO3_VOCsns | PO3_VOCsns | PO3_VOCsns | Net ozone produced under VOC sensitive conditions |
| PO3_NOxsns | PO3_NOxsns | PO3_NOxsns | Net ozone produced under NOx sensitive conditions |
| PH2O2_PHN3 | PH2O2_PHN3 | PH2O2_PHN3 | Ratio of $H_2O_2$ produced / $HNO_3$ produced.  Greater than 0.35 means NOx sensitive ozone production |
| O3_dest | O3_dest | O3_dest | Ozone destruction by chemical reactions |
| **Radical Initiation** | | | |
| OH_new | OH_new | OH_new | New OH produced (initiated) |
| HO2_new | HO2_new | HO2_new | New $HO_2$ produced |
| HOx_new | HOx_new | HOx_new | New HOx (HOx = OH+$HO_2$) produced |
| newOH_O1D | newOH_O1D | newOH_O1D | Production of OH from ozone photolysis |
| newOH_HONO | newOH_HONO | newOH_HONO | Production of OH from HONO photolysis |
| nOH_O3_OLE | nOH_O3_OLE | nOH_O3_OLE | Production of OH from ozone-alkene reactions |
| nwHO2_HCHO | nwHO2_HCHO | nwHO2_HCHO | Production of $HO_2$ from formaldehyde photolysis |
| RO2_new | RO2_new | RO2_new | New $RO_2$ produced |
| **Radical Propagation** | | | |
| OHw_CO | OHw_CO | OHw_CO | OH reacted with carbon monoxide |
| OHw_CH4 | OHw_CH4 | OHw_CH4 | OH reacted with methane |
| OHw_ETHA | OHw_ETHA | OHw_ALK1 | OH reacted with alkanes |
| OHw_PRPA | OHw_PAR | OHw_ALK2 | |
| OHw_PAR | | OHw_ALK3 | |
| | | OHw_ALK4 | |
| | | OHw_ALK5 | |
| OHw_BENZ | | | OH reacted with benzene |
| OHw_TOL | OHw_TOL | OHw_ARO1 | OH reacted with toluene and mono-substituted aromatics |
| OHw_XYL | OHw_XYL | OHw_ARO2 | OH reacted with xylenes and poly-substituted aromatics |
| OHw_ETH | OHw_ETH | OHw_ETHE | OH reacted with ethane |
| OHw_OLE | OHw_OLE | OHw_OLE1 | OH reacted with terminal alkenes (R–HC=$CH_2$, e.g. propene) |
| OHw_IOLE | OHw_IOLE | OHw_OLE2 | OH reacted with internal alkenes (R–HC=CH–R, e.g. 2-butene) |
| OHw_ISOP | OHw_ISOP | OHw_ISOP | OH reacted with isoprene |
| OHw_TERP | OHw_TERP | OHw_TERP | OH reacted with terpenes |
| OHw_ETHY | | | OH reacted with ethyne |
| OHw_all_HC | OHw_all_HC | OHw_all_HC | OH reacted with all organic compounds (including CO) |
| ISOPwOx | ISOPwOx | ISOPwOx | Isoprene reacted with $O_3$, $NO_3$ and O($^3$P) |
| TERPwOx | TERPwOx | TERPwOx | Terpenes reacted with $O_3$, $NO_3$ and O($^3$P) |
| OH_rctd | OH_rctd | OH_rctd | Total OH reacted |

| CB6 | CB05 | SAPRC99 | Description |
|-----|------|---------|-------------|
| HO2_rctd | HO2_rctd | HO2_rctd | Total HO2 reacted |
| HOx_rctd | HOx_rctd | HOx_rctd | Total HOx reacted |
| RO2_rctd | RO2_rctd | RO2_rctd | Total $RO_2$ reacted |
| OHfromHO2 | OHfromHO2 | OHfromHO2 | OH produced from reactions of $HO_2$ |
| Y_OHperHO2 | Y_OHperHO2 | Y_OHperHO2 | Yield of OH per $HO_2$ reacted (= OHfromHO2 / HO2_rctd) |
| **Radical Termination and HOx Chain Length** | | | |
| OH_term | OH_term | OH_term | OH terminated |
| HO2_term | HO2_term | HO2_term | $HO_2$ terminated |
| HOx_term | HOx_term | HOx_term | HOx terminated |
| RO2_term | RO2_term | RO2_term | $RO_2$ terminated |
| HOx_CL | HOx_CL | HOx_CL | HOx chain length ( = HOx_rctd / {2 x  HOx_new} ) |
| **Formaldehyde Production** | | | |
| HCHOp_eth | HCHOp_eth | HCHOp_ethe | Formaldehyde produced from ethene |
| HCHOp_ole | HCHOp_ole | HCHOp_ole1 | Formaldehyde from terminal alkenes (R–HC=CH$_2$, e.g. propene) in the first generation of products |
| HCHOp_iole | HCHOp_iole | HCHOp_ole2 | Formaldehyde from internal alkenes (R–HC=CH–R, e.g. 2-butene) in the first generation of products |
| HCHOp_terp | HCHOp_terp | HCHOp_terp | Formaldehyde from terpenes in the first generation of products |
| HCHOp_isop | HCHOp_isop | HCHOp_isop | Formaldehyde from isoprene in the first generation of products |
| HCHOp_ispd | HCHOp_ispd | HCHOp_ispd | Formaldehyde from isoprene daughter products (isoprod, methacrolein and methylvinylketone) |
| HCHOp_Tot | HCHOp_Tot | HCHOp_Tot | Total formaldehyde produced |
| **NOy Reactions** | | | |
| HNO3_OHNO2 | HNO3_OHNO2 | HNO3_OHNO2 | Nitric acid produced from OH reacting with $NO_2$ |
| HNO3_NO3HC | HNO3_NO3HC | HNO3_NO3HC | Nitric acid produced from $NO_3$ reacting with organics |
| HNO3_N2O5 | HNO3_N2O5 | HNO3_N2O5 | Nitric acid produced from $N_2O_5$ reacting with water |
| PANprodNet | PANprodNet | PANSprdNet | Net PAN produced (sum of several for SAPRC99) |
| PANlossNet | PANlossNet | PANSlosNet | Net PAN destroyed (sum of several for SAPRC99) |
| RNO3_prod | RNO3_prod | RNO3prod | Organic nitrates ($RNO_3$) produced |
| NOxrecycl | NOxrecycl | NOxrecycl | Nitrates ($HNO_3$ and $RNO_3$) recycled to NOx |
| NOw_HO2 | NOw_HO2 | NOw_HO2 | NO reacted with $HO_2$ (forming $NO_2$) |
| NOw_RO2s | NOw_RO2s | NOw_RO2s | NO reacted with $RO_2$ (forming $NO_2$) |
| NOw_RCO3s | NOw_RCO3s | NOw_RCO3s | NO reacted with $RCO_3$ (forming $NO_2$) |
| **Photolysis** | | | |
| J_NO2 | J_NO2 | J_NO2 | $NO_2$ photolysis rate |
| J_O3O1D | J_O3O1D | J_O3O1D | $O_3$ photolysis rate to O($^1$D) atoms |
| J_CLDADJ | J_CLDADJ | J_CLDADJ | Cloud/haze adjustment factor |
| **Radical Concentrations** | | | |
| OH | OH | OH | OH radical concentration |
| HO2 | HO2 | HO2 | $HO_2$ radical concentration |

## 10.2 Running Process Analysis

PA can be used with most of the physical options available for the "core" CAMx model, e.g., the various advection and chemistry mechanisms/solvers. However, PA cannot be used at the same time as the other CAMx "Probing Tool" options (e.g., OSAT, PSAT, DDM, or RTRAC) because the Probing Tools share internal data structures to minimize the total memory resources required by CAMx. IPR cannot be used with the ACM2 diffusion option.

PA is invoked similarly to the other Probing Tools within the CAMx control file. In the `&CAMx_Control` namelist module, the variable `Probing_Tool` must be set to either "PA" (generates all PA output), "IPR", or "IRR". Table 10-3 summarizes the types of process analysis performed for each keyword and the output files that are produced.

**Table 10-3. Process analysis keywords and associated CAMx output files.**

| Process Analysis Key Word | | | Output | File |
|---|---|---|---|---|
| IPR | IRR | PA | Filename | Contains |
| Yes | No | Yes | `*.ipr` | Integrated process rate (IPR) information for all selected cells |
| No | Yes | Yes | `*.irr` | Integrated reaction rate (IRR) information for all selected cells |
| No | Yes | Yes | `*.cpa.grd`*nn* | Chemical process analysis (CPA) parameters for grid *nn* |

An additional namelist module called `&PA_Control` must then be provided in the control file to configure the PA portion of the model. The additional namelist module is described below. The order of the variables follow the template available with the source code. An example of the PA portion of the CAMx run control file is shown in Figure 10-1.

The rules for defining PA domains are as follows:

1) They must be contained within a single CAMx grid;
2) They may not include cells that contain a nested grid;
3) They may contain as few as 1 grid cells;
4) They may contain up to all of the grid cells in a CAMx grid provided that this does not violate the second rule;
5) They may intersect or overlap – the same grid cell may be in several process analysis domains.

## Description of PA Control in the CAMx Run Control File

| | |
|---|---|
| `&PA_Control` | Label for the Probing Tool namelist module that configures the PA option; it must begin in column 2 |
| `&` | Flag ending a namelist; it must be in column 2 |
| `PA_File_Root` | Character root output path/filename |
| `Number_of_PA_Domains` | Integer number of PA analysis domains to be evaluated during the simulation. |
| `Within_CAMx_Grid` | Integer array (by PA domain) pointer into the CAMx grid within which the PA domain exists (1=master grid, etc.). Use the CAMx internal grid number reported in the *.diag file. Note that this may differ from the nest order provided by the user in the CAMx control file. |
| `PA_Beg_I_Index` | Integer array (by PA domain) grid column containing western edge of PA domain. |
| `PA_End_I_Index` | Integer array (by PA domain) grid column containing eastern edge of PA domain. |
| `PA_Beg_J_Index` | Integer array (by PA domain) grid row containing southern edge of PA domain. |
| `PA_End_J_Index` | Integer array (by PA domain) grid row containing northern edge of PA domain. |
| `PA_Beg_K_Index` | Integer array (by PA domain) grid layer containing bottom of PA domain. |
| `PA_End_K_Index` | Integer array (by PA domain) grid layer containing top of PA domain. |

```
&PA_Control

 PA_File_Root           = 'CAMx.OTAG.950707.PA',

 Number_of_PA_Domains = 2,
 Within_CAMx_Grid(1)  = 1,
 PA_Beg_I_Index(1)    = 8,
 PA_End_I_Index(1)    = 12,
 PA_Beg_J_Index(1)    = 9,
 PA_End_J_Index(1)    = 13,
 PA_Beg_K_Index(1)    = 1,
 PA_End_K_Index(1)    = 5,


 Within_CAMx_Grid(2)  = 2,
 PA_Beg_I_Index(2)    = 107,
 PA_End_I_Index(2)    = 110,
 PA_Beg_J_Index(2)    = 78,
 PA_End_J_Index(2)    = 82,
 PA_Beg_K_Index(2)    = 1,
 PA_End_K_Index(2)    = 7,


 &
```

**Figure 10-1.  Example section of a CAMx control file specifying options for Process Analysis.**


### 10.2.1  Setting CAMx Parameters

PA stores information in data structures that are dimensioned using FORTRAN parameter statements.  These parameters must be large enough to accommodate the PA configuration specified in the CAMx control file.  If one of these parameters is exceeded CAMx will stop with an error message stating that a parameter must be changed and the model recompiled.  It is always a good idea to do a complete rebuild (use the Unix command "make clean") when a parameter is changed.  The parameters that may need to be changed are in two include files, "procan.inc" and "camx.prm".

**procan.inc**

>  MXPADOM – The maximum number of Process Analysis domains.

>  MXPACEL – The maximum number of Process Analysis cells over all domains

**camx.prm**

>  MXTRSP – This parameter defines gridded data structures that are used by several probing tools.  For PA the data structures store chemical process analysis (CPA) variables, so MXTRSP must be set to at least the value of MXCPA (set in procan.inc) which is 99.

### 10.2.2 Output File Formats

CAMx may output up to four files containing PA information according to the PA option selected (see Table 10-3). All of these files are in Fortran binary format to conserve disk space. Two files (the `*.ipr` and `*.irr` files) contain information for just the grid cells selected for PA. The formats for these files are not described here since two Fortran post-processor programs are provided to extract data from these files in a comma-delimited ASCII format. The files containing CPA information (the `*.cpa.grdnn`) are gridded files covering the same area as the regular model average files (`*.avrg.grdnn`). The gridded CPA files have the same format as a regular model average file as described in Section 3.

## 10.3  Postprocessing

Two post-processors are provided to read the binary `*.ipr` and `*.irr` output files and extract PA data for further analysis. The CPA output files can be visualized directly.

### 10.3.1 IPR Output Files

The Fortran program "`ext_ipr`" extracts IPR data from one or more CAMx `*.ipr` binary files and reformats the data to comma delimited ASCII format (`.csv`) suitable for subsequent analysis (e.g., using spreadsheets). The "`ext_ipr`" program performs the following tasks:

- Reads and outputs the descriptive header of the `*.ipr` file;
- Optionally combines data from several consecutive `*.ipr` files to provide multi-day output;
- Selects data for an individual cell within a PA sub-domain or aggregates data over multiple cells within a PA sub-domain;
- Outputs the selected IPR data in `.csv` format in either ppb or molar units for gas species; PM species are in either µg/m$^3$ or mass units..

A sample script to run the "`ext_ipr`" program is provided with its source code, and the script includes a description of how to use the program. Also included is a spreadsheet macro that can read the `.csv` format and prepare several plots. This macro is described below.

#### 10.3.1.1  Aggregating Cells

The "`ext_ipr`" program can combine IPR information across several cells. This is useful for analyzing the contributions of model processes to a geographic area that spans multiple cells (e.g., an urban area). For simplicity, the multi-cell area must be defined as a rectangular box. The capability of aggregating IPR information across vertical layers is particularly important during the day because vertical columns of cells within the mixed layer become strongly coupled on time scales shorter than one hour. Thus, if the process contributions for a surface grid cell are analyzed during the day vertical diffusion will often completely dominate all other processes. In this situation, it is more informative to analyze a column of cells extending from the surface to the approximate height of the mixed layer.

When the "`ext_ipr`" program aggregates information across grid cells it accounts for differences in cell volume. If the output for aggregate cells is requested in ppb units, the output

from CAMx in molar units is converted to ppb using the volume-weighted average units conversion factor for the cells being aggregated.

10.3.1.2  IPR Time Series Analysis

One useful approach to analyzing IPR data is to plot the contributions of several processes as a time series.  Figures 10-2 through 10-4 present examples of this approach from the CAMx test case that is distributed with the model.  The figures show process contributions to the PM$_{2.5}$ sulfate and nitrate concentrations in a multi-cell area around Chicago on June 13 and 14, 2002, and are intended solely as an illustration of how PA can be used.  The figures were prepared using the "`ext_ipr`" program described above and the spreadsheet macro "`process_analysis_macro.xls`."  The macro reads an output file from "`ext_ipr`" and prepares three charts:

1) Bar chart of the contribution from each process averaged over the duration of the PA data.  This is useful to see which processes were important (Figure 10-2).

2) Bar chart showing the time series of contributions from all major processes.  To reduce the number of processes being displayed, advection and diffusion information for each boundary is combined into a single transport term, and any series with zero contribution is excluded from the chart.  Also, the three PM chemistry processes (organic, inorganic and aqueous-phase aerosol chemistry) are aggregated to a single net term (Heterogeneous Chemistry).  An example of this chart is shown in Figure 10-3.

3) Bar chart showing the time series of contributions from major processes with lateral boundary transport and all chemistry processes shown as a single net term.  An example of this chart is shown in Figure 10-4.  For a small region lateral boundary transport often leads to large positive and negative terms that approximately cancel (e.g., inflow from the east and outflow to the west).  This chart provides a comparison of the net effect of lateral boundary transport relative to other processes, whereas the second chart resolves the transport by boundary.  Comparing Figures 10-3 and 10-4, based on the same data, shows the difference between these two analysis approaches.

**10.3.2  IRR Output Files**

The Fortran program "`ext_irr`" extracts IRR data from one or more CAMx `*.irr` binary files and reformats the data for subsequent analysis. The "`ext_irr`" program performs the following tasks:

- Reads and outputs the descriptive header of the `*.irr` file;

- Optionally combines data from several consecutive `*.irr` files to provide multi-day output;

- Selects data for an individual cell or multiple cells within a PA sub-domain;

- Optionally, outputs the selected IRR data to a `.csv` format ASCII file;

- Optionally, outputs the selected IRR data to a UAM average format binary file.
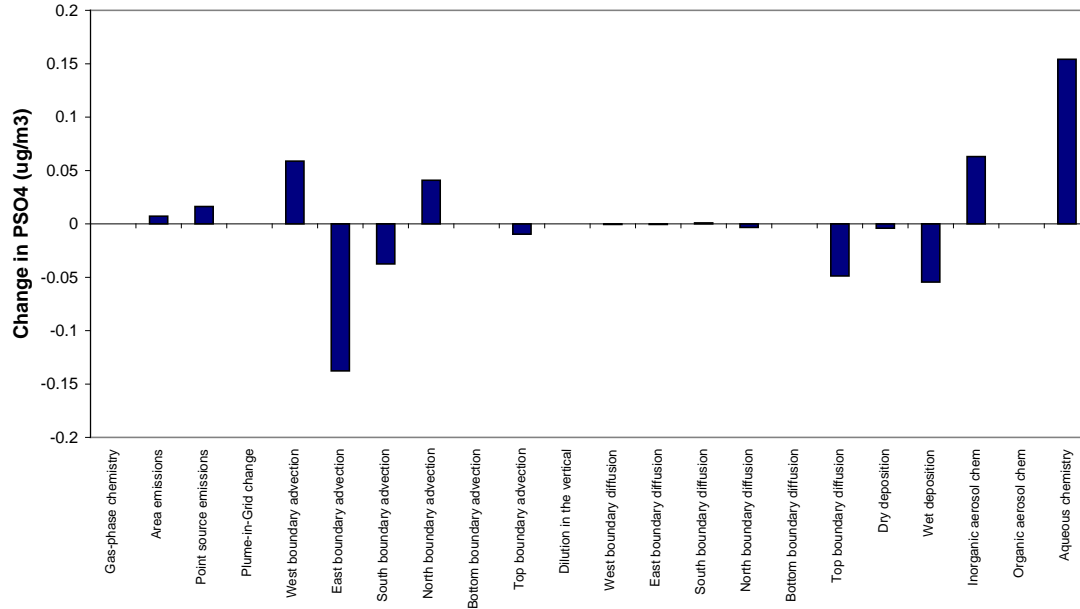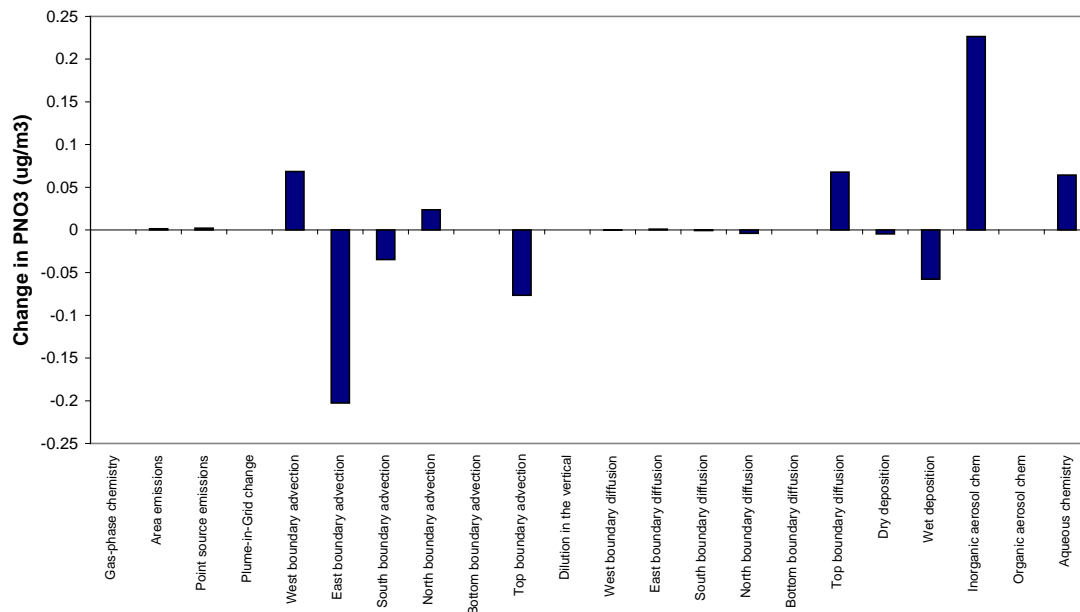
Figure 10-2. Time-averaged IPR analysis for PSO4 and PNO3 on June 13 and 14, 2002; all of the processes are plotted individually.

**Hourly PSO4 Change from Different Processes in Chicago Area.**
**Run = postproc_test**
**Grid cells used from grid number 1: (43, 47) to (52, 56) using layers 1 to 5**



**Hourly PNO3 Change from Different Processes in Chicago Area.**
**Run = postproc_test**
**Grid cells used from grid number 1: (43, 47) to (52, 56) using layers 1 to 5**
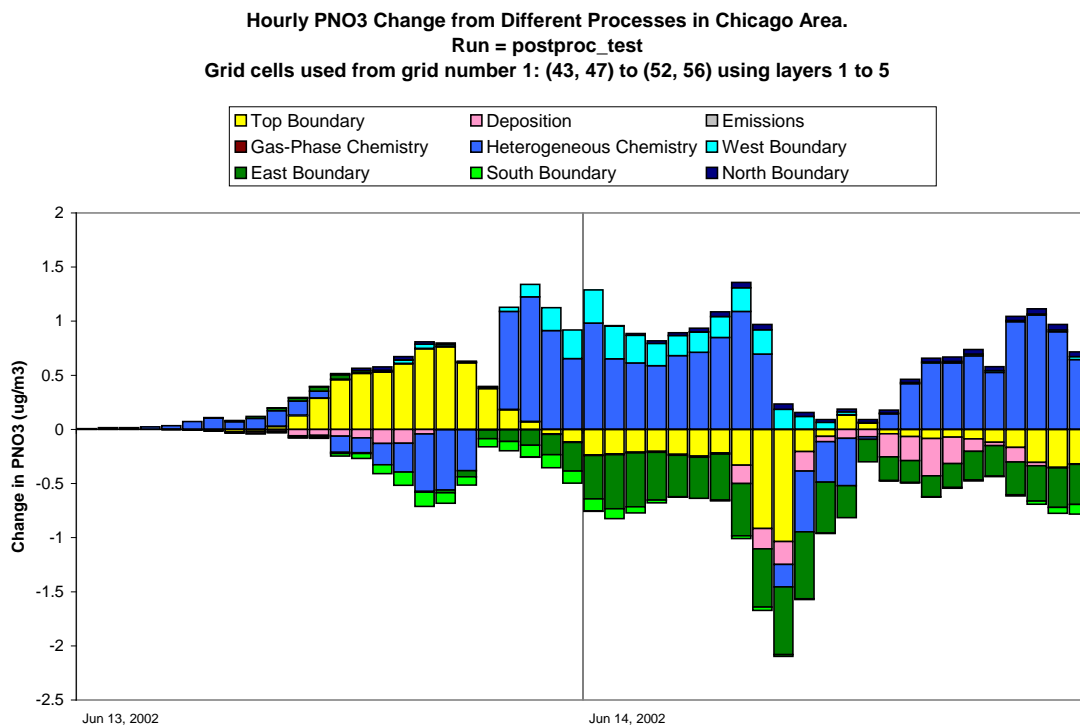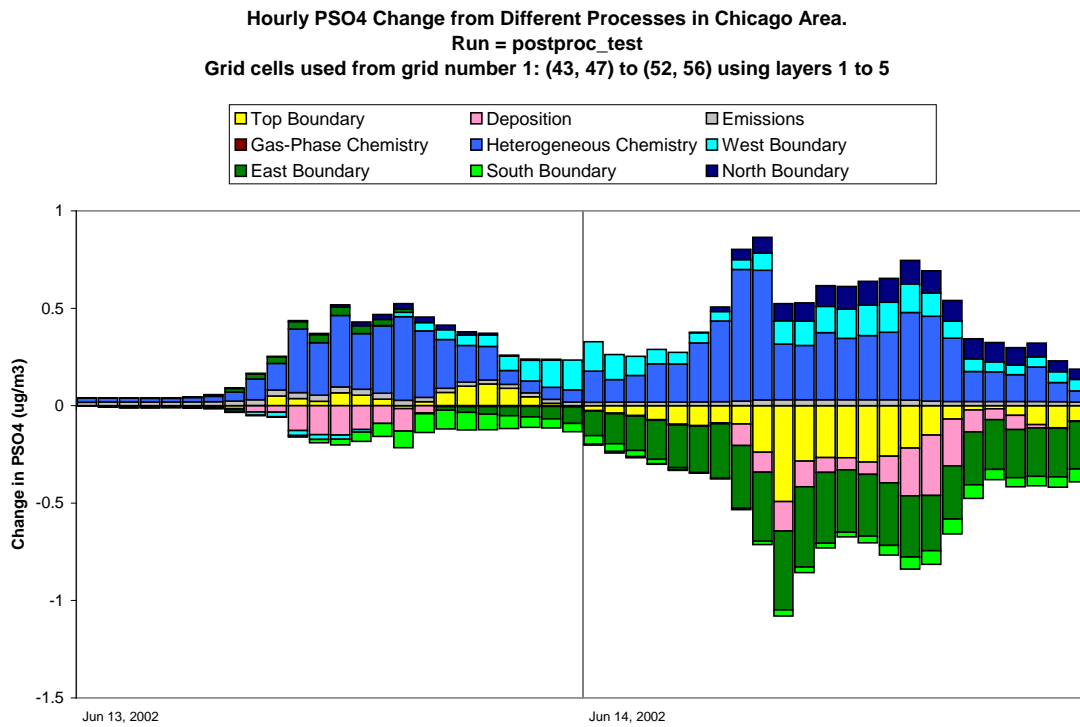


**Figure 10-3. IPR time series analysis for PSO4 and PNO3; Lateral boundary/Chemistry terms are not aggregated.**

**Hourly PSO4 Change from Different Processes in Chicago Area.**
**Run = postproc_test**
**Grid cells used from grid number 1: (43, 47) to (52, 56) using layers 1 to 5**



**Hourly PNO3 Change from Different Processes in Chicago Area.**
**Run = postproc_test**
**Grid cells used from grid number 1: (43, 47) to (52, 56) using layers 1 to 5**
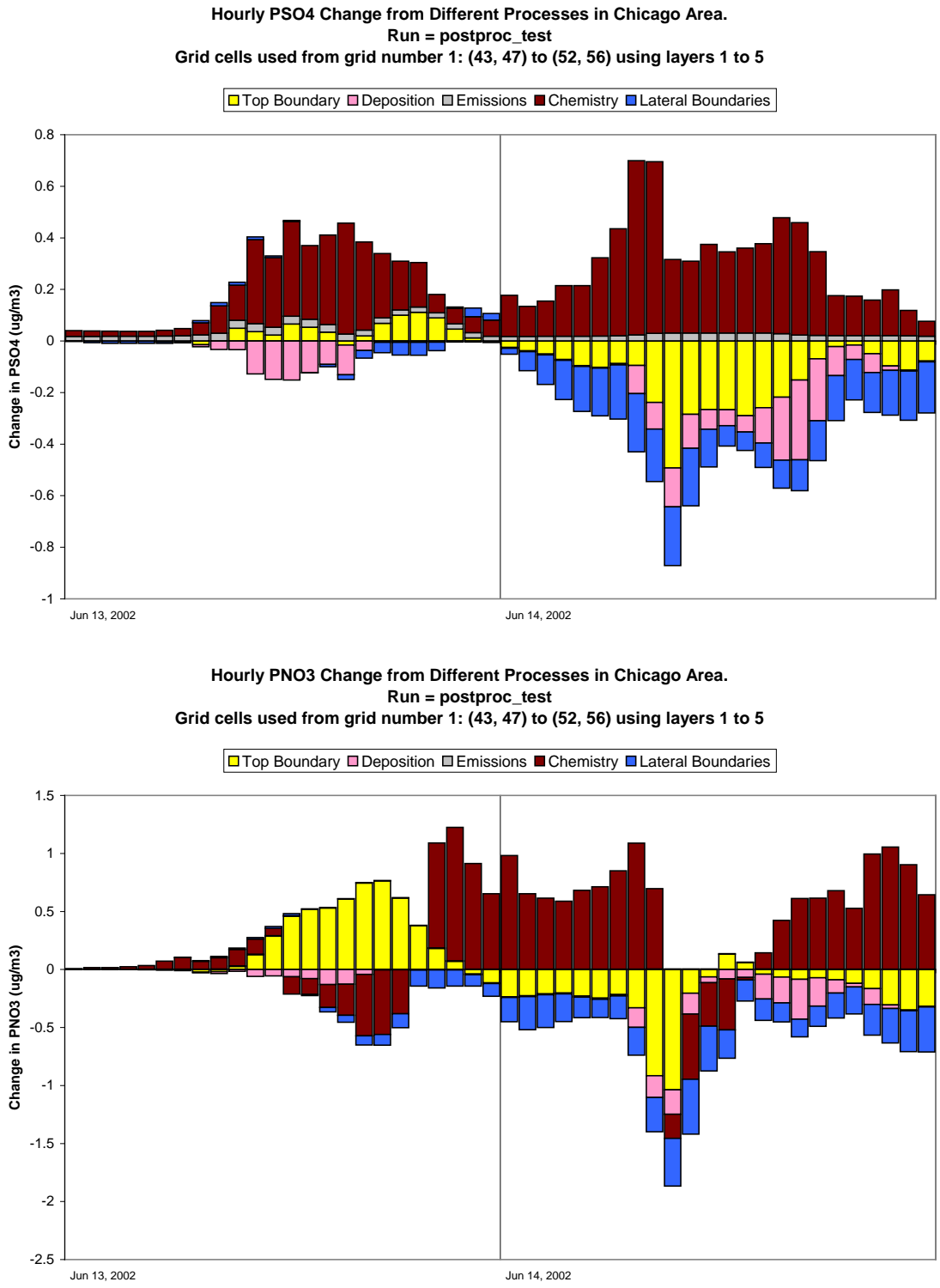


**Figure 10-4. IPR time series analysis for PSO4 and PNO3; Lateral boundary/Chemistry terms are aggregated to a single net term, in contrast to Figure 10-3.**

The ASCII IRR data are suitable for subsequent analysis (e.g., using spreadsheets) but at this time there is no "pre-packaged" analysis available comparable to the macro for analyzing IPR data. The binary IRR output from "ext_irr" can be displayed using any post-processing software that can display CAMx average concentration outputs.

### 10.3.3 CPA Output Files

CPA results are output from CAMx as gridded files in the same format as the average concentration files, and therefore can be visualized using any post-processing software that can display CAMx concentration outputs. These files may optionally include just the surface layer or all layers according to how the "3-D output" flag is set in the CAMx control file. Surface layer species concentrations reflect the balance between several model processes including surface emissions/deposition, vertical mixing, and chemical reactions in surface (and possibly aloft) grid cells. In contrast, the CPA output data are grid cell specific and reflect chemical change in single grid cells. The fact that vertical mixing tends to average species concentrations over multiple layers whereas CPA variables are layer specific may complicate and bias the interpretation of CPA results. A solution is to place both the concentrations and CPA variables on a comparable basis by averaging them over all layers within the planetary boundary layer.

A post-processor (VERTAVG) was developed to average CPA variables and concentrations over multiple layers contained within the depth of the planetary boundary layer (PBL). The PBL depth varies in space and time according to the strength and vertical extent of turbulent mixing. Vertical turbulent mixing is specified for CAMx by the input diffusivity (Kv) fields. The VERTAVG processor reads CAMx Kv, height, temperature, and pressure input files, and then calculates the PBL depth for each grid column at each hour. VERTAVG also reads a CAMx 3-D output file of CPA variables (or species concentrations) and calculates air-mass weighted PBL values for each grid column at each hour. The output from VERTAVG is a 2-D file in average file format where the single layer represents the PBL average values rather than surface layer values.

VERTAVG appends two extra variables to the file being processed to aid with interpretation and to make clear that the data have been vertically averaged. The added variables are:

- PBL_Z is the diagnosed height of the PBL for each grid column.
- PBL_I is the layer index of the top layer within the diagnosed PBL for each grid column.

CAMx must be run using the option to create 3-D species concentration (and therefore CPA) output files in order to use VERTAVG.

An example of how CPA can be used to evaluate a particular CAMx modeling application is provided below.

## 10.4  CPA Demonstration

CAMx simulations were performed with CPA for an existing Los Angeles modeling database (Yarwood et al., 2003).  The analysis focused on chemical explanations for differences in ozone predictions with the CB4 and SAPRC99 mechanisms.  CPA was used to investigate several aspects of atmospheric chemistry that are important to understanding model performance and control strategy development:

- Determining geographic areas of high ozone productivity;
- Classifying geographic areas as being "VOC-sensitive" or "NOx- sensitive" with respect to ozone production;
- Quantifying the initiation, propagation and termination of radical species such as hydroxyl (OH) radical that drive ozone formation chemistry;
- Investigating the efficiency of radical utilization in ozone production as measured by the "HOx chain length";
- Determining the contribution of biogenic (isoprene) emissions to VOC reactivity and ozone production;
- Determining geographic areas of photochemical ozone destruction;
- Investigating how NOx emissions are converted to NOz;
-  Quantifying recycling of NOy from chemically inactive (NOz) to active (NOx) forms.

The Los Angeles (LA) modeling episode was August 3–7, 1997 during the Southern California Ozone Study (SCOS).  The modeling domain covered 65 by 40, 5-km grid cells as shown in Figure 10-5.  CAMx was run with 10 layers extending between a surface layer of 60 m and a model top at 4 km.  The photochemistry of ozone formation was simulated in CAMx using two different condensed chemical mechanisms:
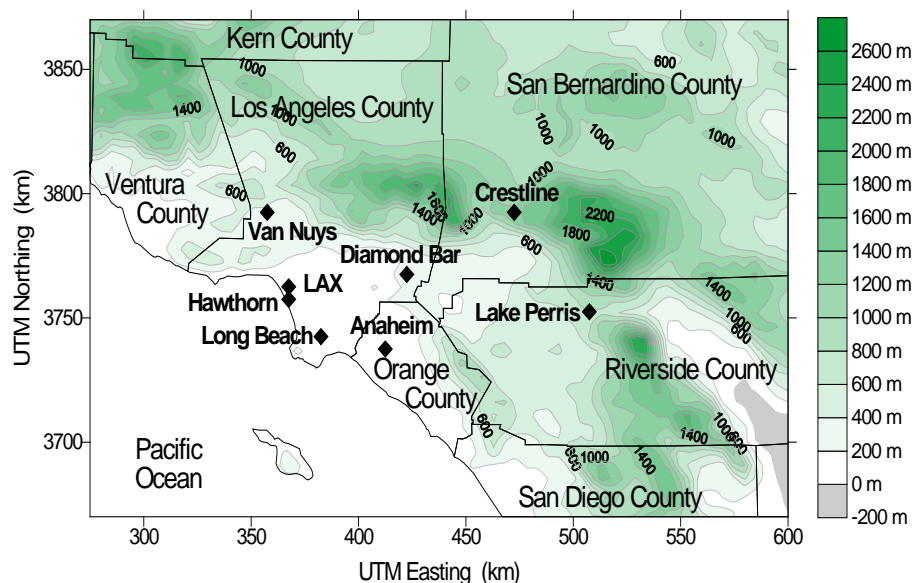


**Figure 10-5.  The CAMx Los Angeles modeling domain (Yarwood et al., 2003).**

- The CB4 mechanism (Gery et al., 1989) with updates for low-NO$_x$ conditions and isoprene reactions, carrying 37 species and 96 reactions (this mechanism is no longer available in CAMx).
- The fixed stoichiometry version of the SAPRC99 mechanism (Carter, 2000).  This is implemented in CAMx as "Mechanism 5" and has 74 species and 211 reactions.

The analysis of CPA results for Los Angeles is shown for 2 PM on August 5, 1997.  This was the day with the highest observed ozone during the episode period and 2 PM is the time when modeled ozone production rates were high in many areas just before the peak concentration levels were modeled.  The CPA results were averaged over all layers within the PBL using the VRTAVG post-processor described above.  Figure 10-6 shows the diagnosed PBL depth for the modeling domain at this time.

### 10.4.1  Ozone Production

The PBL average ozone levels with CB4 and SAPRC99 are compared in Figure 10-7.  SAPRC99 (right) produces up to about 30 ppb more ozone throughout the Los Angeles basin.  The chemical process analysis sought to explain how SAPRC99 makes more ozone than CB4 and the potential consequences.  One consequence is response to emission changes.  The NOx emission inventory was reduced by 50% and the ozone response measured as a relative reduction factor (RRF = Control Case ozone / Base Case ozone) is shown in Figure 10-8.  CB4 showed both greater ozone increases (yellow/red) and decreases (green/blue) than SAPRC99 in response to the 50% NOx emissions cut.
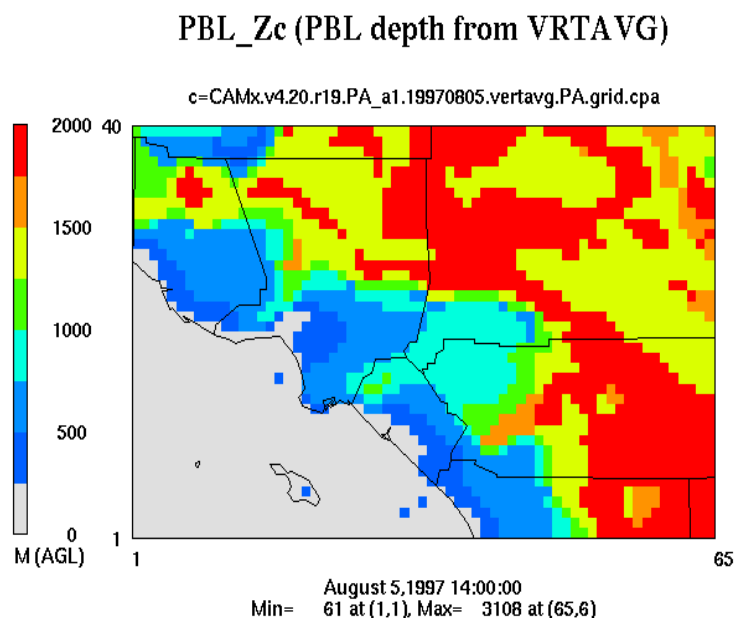


**Figure 10-6.  PBL depth (m) diagnosed by VRTAVG for 14:00 on August 5, 1997.**

**CB4**                                                        **SAPRC99**
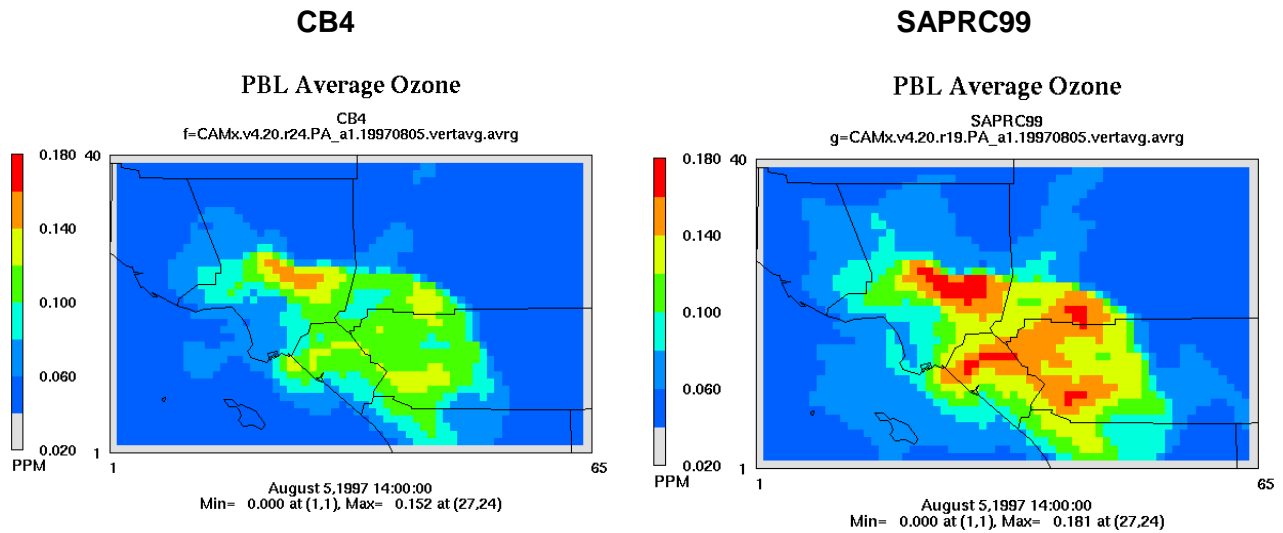


**Figure 10-7.  PBL average ozone (ppb) at 14:00 on August 5, 1997.**

**CB4**                                                        **SAPRC99**
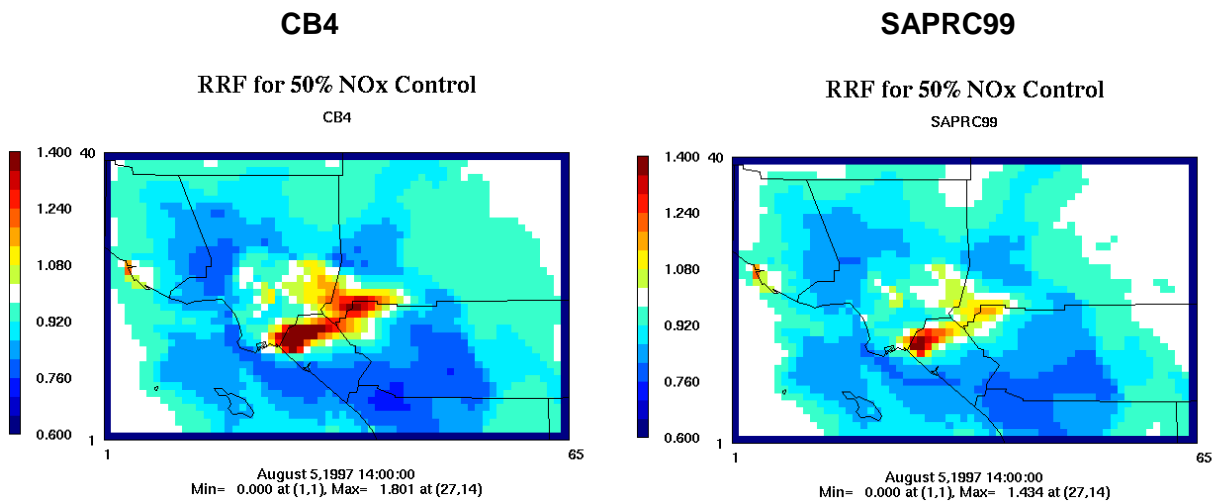


**Figure 10-8.  Relative response of ozone to a 50% NOx emission reduction at 14:00 on August 5, 1997.**

The ozone production rate (ppb/hr) during this same time is compared in Figure 10-9.  As expected from the ozone concentrations (Figure 10-7), SAPRC99 has higher peak ozone production rates than CB4 by about 5 to 10 ppb/hr.  Comparing the ozone production rates (Figure 10-10) reveals that SAPRC99 produces ozone faster especially in the central area of the Los Angeles basin and directs the chemical process analysis toward understanding this phenomenon.

**CB4**
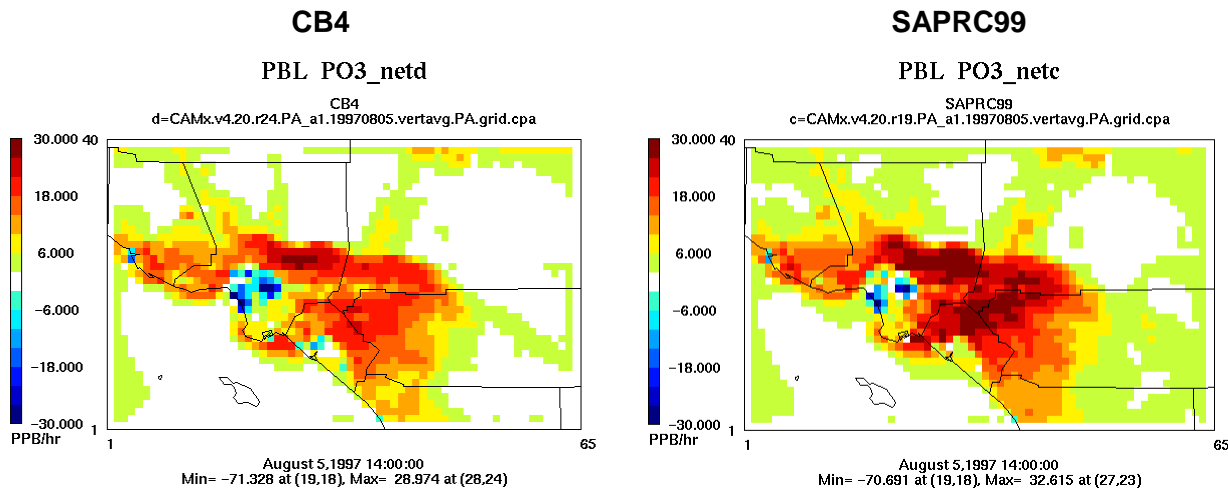
**SAPRC99**



Figure 10-9.  Ozone production rate (ppb/hr) at 14:00 on August 5, 1997.
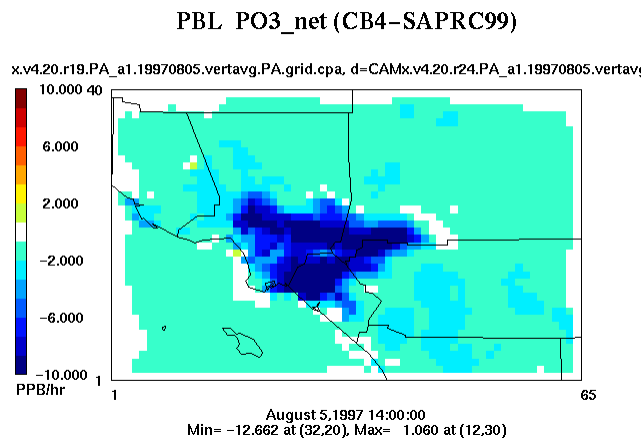


**Figure 10-10.  Difference (CB4-SAPRC99) in ozone production rate (ppb/hr) at 14:00 on August 5, 1997.**

### 10.4.2  Ozone Sensitivity to NOx and VOC

Understanding the sensitivity of ozone to NOx and VOC precursors is important to control strategy design.  Several methods have been proposed for differentiating ozone sensitivity to precursors based on chemical indicators, such as the ratio of the production rates of hydrogen peroxide and nitric acid ($P_{H2O2}/P_{HNO3}$).  This method is implemented in CPA and used to designate grid cells as VOC-sensitive or NOx-sensitive at each model time step (i.e., every few minutes) by defining $P_{H2O2}/P_{HNO3}$ of 0.35 and higher as the NOx-sensitive regime.  The $P_{H2O2}/P_{HNO3}$ indicator ratio is reported as the CPA variable (PH2O2_PHN3; Figure 10-11) and the NOx-sensitive and VOC-sensitive ozone production rates are accumulated as the CPA variables PO3_NOxsns (Figure 10-12) and PO3_VOCsns (Figure 10-13), respectively.

## CB4                                                    SAPRC99

PBL  PH2O2_PHN3d (Ratio PH2O2/PHNO3)          PBL  PH2O2_PHN3c (Ratio PH2O2/PHNO3)
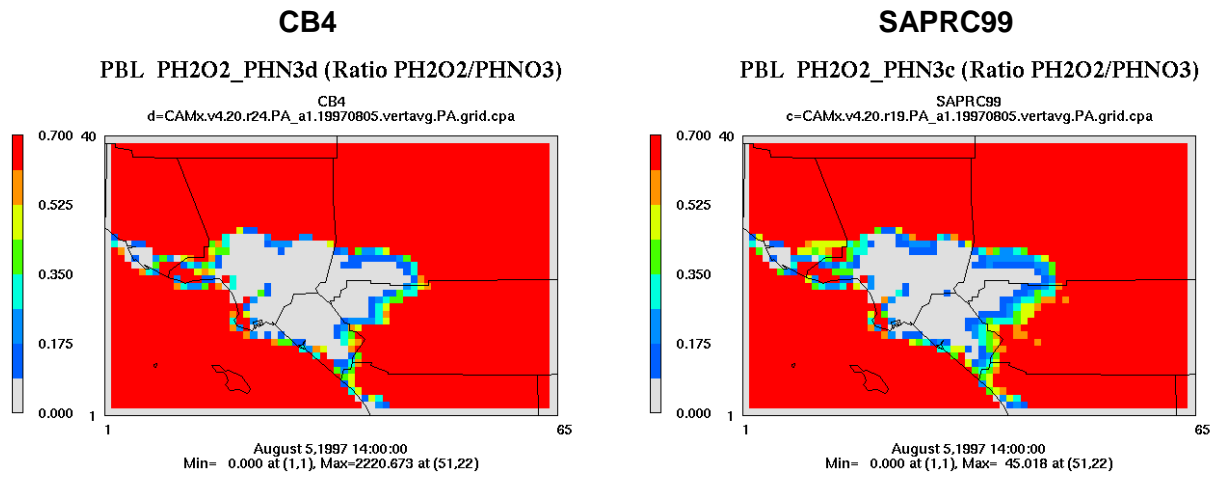


**Figure 10-11.  Ratio of instantaneous production rates for hydrogen peroxide to nitric acid ($H_2O_2$ produced / $HNO_3$ produced) at 14:00 on August 5, 1997.**

## CB4                                                    SAPRC99

PBL  PO3_NOxsnsd                              PBL  PO3_NOxsnsc
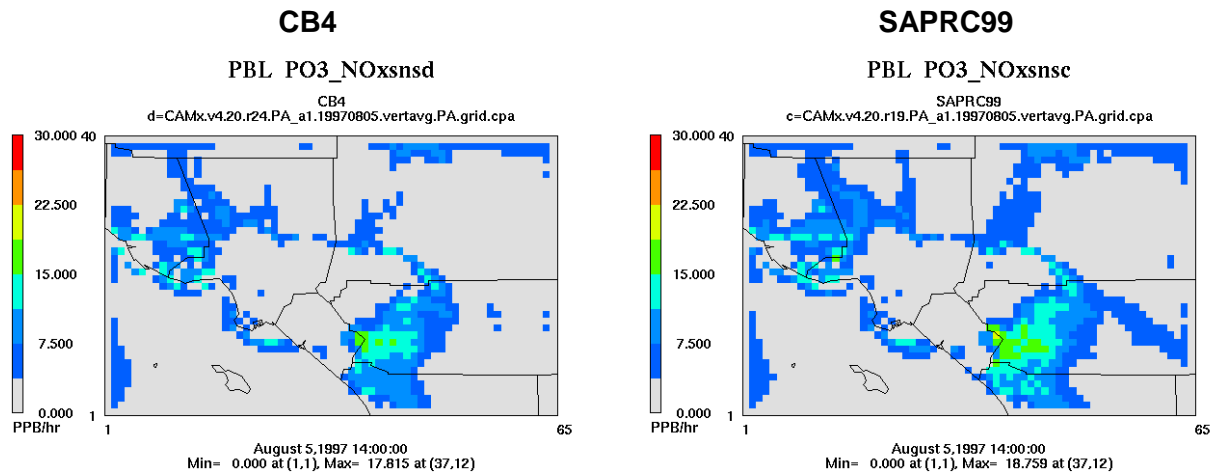


**Figure 10-12.  Ozone production rate in areas defined as NOx-sensitive by the $P_{H2O2}/P_{HNO3}$ indicator ratio at 14:00 on August 5, 1997.**

**CB4**                                                        **SAPRC99**
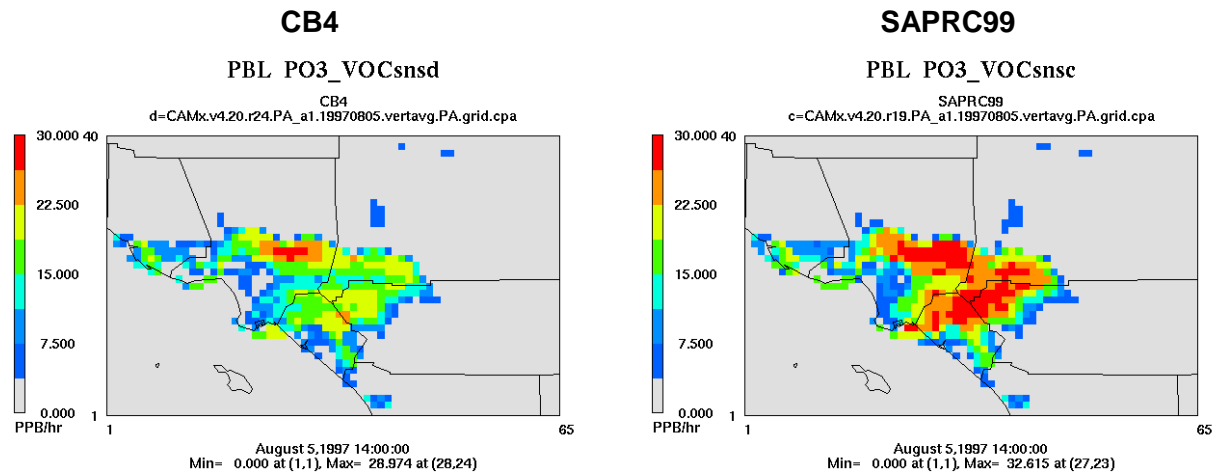


**Figure 10-13.  Ozone production rate in areas defined as VOC-sensitive by the $P_{H2O2}/P_{HNO3}$ indicator ratio at 14:00 on August 5, 1997.**

The $P_{H2O2}/P_{HNO3}$ indicator ratio at 14:00 on August 5, 1997 (Figure 10-11) shows a sharp transition from VOC-sensitive in high NOx emission urban/suburban areas to NOx-sensitive in lower NOx emission rural areas.  The transition in indicator ratio occurs at almost the same location with the CB4 and SAPRC99 mechanisms even though the ozone production rates differ between the mechanisms.

Ozone production rates are much lower in the NOx-sensitive areas than VOC-sensitive areas (Figures 10-12 and 10-13).  SAPRC99 predicts much higher ozone production rates than CB4 in VOC-sensitive areas, and this is where the major difference between the mechanisms is found.  The important question is: how is SAPRC99 more reactive than CB4 under VOC-sensitive conditions?  Potential explanations include:

- SAPRC99 has greater radical production for VOC-sensitive conditions and therefore converts NO more rapidly to $NO_2$.
- SAPRC99 has stronger NOx removal mechanisms (NOx sinks) than CB4 for VOC-sensitive conditions and therefore more rapidly achieves NOx concentrations that maximize ozone production.

CPA can be used to evaluate these (and other) potential hypotheses for how SAPRC99 and CB4 are different.

### 10.4.3  Radical Production

Radicals are molecular fragments with an unpaired electron and they generally are highly reactive in the atmosphere.  The hydroxyl radical (OH) initiates many VOC degradation reactions whereas peroxy radicals ($HO_2$ and $RO_2$) convert NO to $NO_2$ thereby triggering ozone production.

The CAMx implementation of CPA calculates initiation rates of OH, HO$_2$ and RO$_2$ radicals. Initiation means the creation of "new" radicals from reactions of stable molecules such as photolysis or ozonolysis.  Figure 10-14 compares the production of new HOx (the sum of OH and HO$_2$) by CB4 and SAPRC99 (HOx_new).  SAPRC99 has stronger HOx initiation than CB4 in the VOC-sensitive area where the mechanisms differ.  However, HOx radicals can be formed in propagation reactions as well as initiation reactions.  The total production of HO$_2$ can be determined from the amount of HOx reacting because these quantities will always be in balance (because HOx radicals have lifetimes much shorter than a second).
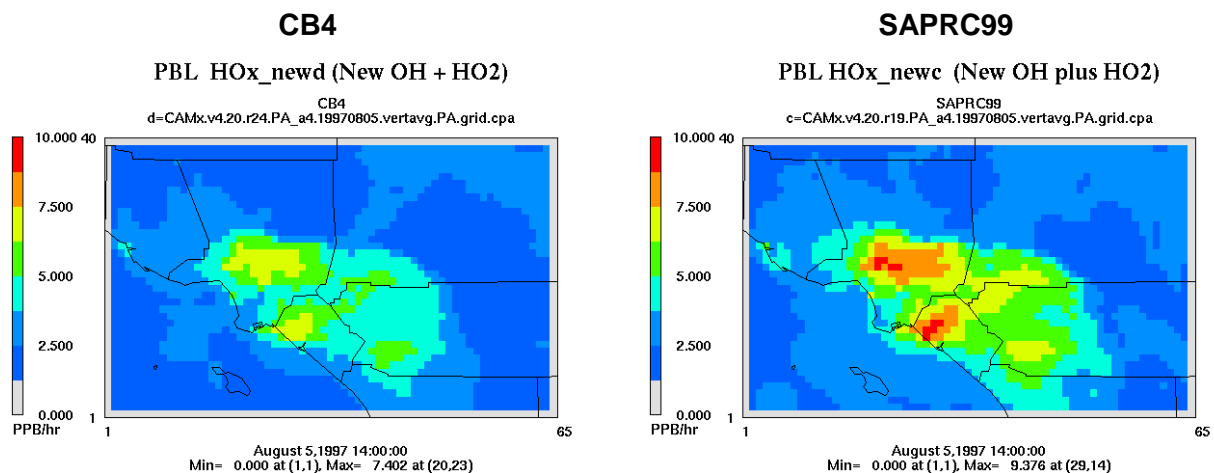


**Figure 10-14.  HOx radical initiation rate (ppb/hour) at 14:00 on August 5, 1997.**

The HOx radical reaction rate (HOx_rctd) is compared in Figure 10-15.  Once again, SAPRC99 has more HOx radical reaction (and therefore HOx radical production) than CB4 in VOC-sensitive areas.

The amount of HOx radicals reacting (Figure 10-15) is greater than the amount of new HOx radicals initiated (Figure 10-14) because of chain reactions that propagate radicals, such as:

1.  OH and HO$_2$ inter-conversion, e.g.
    OH + O$_3$ $\rightarrow$ HO$_2$ + O$_2$
    HO$_2$ + O$_3$ $\rightarrow$ OH + O$_2$

2.  OH and HO$_2$ propagation through RO$_2$ radicals, e.g.
    OH + VOC $\rightarrow$ RO$_2$ + products
    RO$_2$ + NO $\rightarrow$ HO$_2$ + products
    HO$_2$ + NO $\rightarrow$ OH + NO$_2$

**CB4**                                                                                    **SAPRC99**
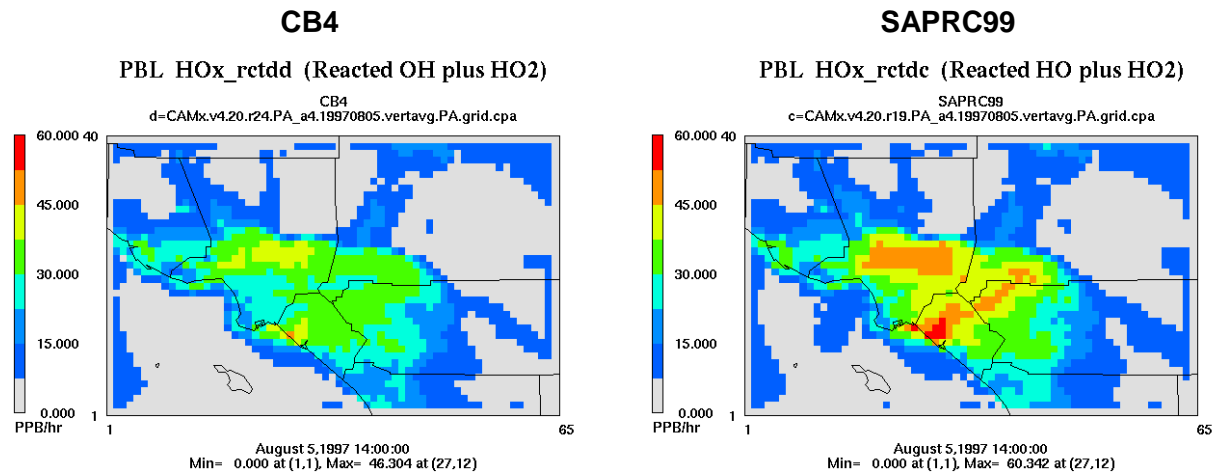


**Figure 10-15. HOx radical reaction rate (ppb/hour) at 14:00 on August 5, 1997.**

Every time that an OH radical propagates via a chain of reactions and reforms OH (or $HO_2$ propagates back to $HO_2$) may be considered as one cycle of HOx propagation.  The HOx chain length is the number of cycles completed by the average HOx radical and depends upon atmospheric conditions.  HOx propagation could be relatively more efficient for OH than $HO_2$, or vice-versa, but this distinction disappears as the HOx chain length becomes large (> 2) and HOx can cycle between OH and $HO_2$ many times.  Therefore, CAMx CPA just calculates a combined HOx chain length that averages OH and $HO_2$ together.

The HOx chain length can be calculated simply as HOx_rctd/(2×HOx_new).  The number 2 appears here because one chain is considered to require two HOx reactions to return the HOx radical back to its initial form (e.g., OH $\rightarrow$ $HO_2$ $\rightarrow$ OH).  Using this approach enables consistent HOx chain length calculations for the CB4 and SAPRC99 mechanisms.

The CB4 and SAPRC99 chain lengths (HOx_CL) for 14:00 on August 5, 1997 are compared in Figures 10-16 and 10-17.  The HOx chain length for SAPRC99 is longer than for CB4 in the VOC-sensitive areas (Figure 10-16) and this combines with the greater HOx initiation for SAPRC99 than CB4 (Figure 10-14) to give SAPRC99 more overall HOx production in the VOC-sensitive area.  The HOx chain length values calculated by CPA may be interpreted using the following guidelines:

- HOx_CL should never be less than 0.5 because of the way chain length is being defined.
  - Chain length of 0.5 means that all newly produced HOx "terminates" at the first reaction.
- HOx_CL is low (1-2) in areas where NO is scarce (radicals can not propagate) or $NO_2$ is very high (radicals are scavenged).
  - OH or $HO_2$ terminating immediately is likely to result in ozone destruction.
- HOx_CL is high (>2) in areas where NO levels favor efficient radical propagation and rapid ozone production.
  - The area of HOx_CL of ~2.5 and higher corresponds to the VOC-sensitive area.

## CB4

## SAPRC99

PBL HOx_CLd (HOx Chain Length)

PBL HOx_CLc (HOx Chain Length)
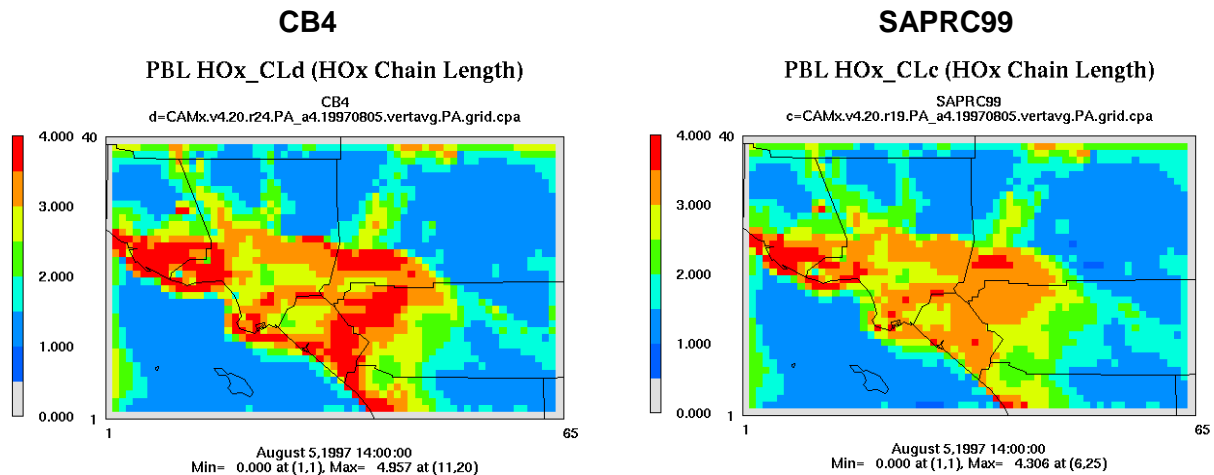


**Figure 10-16.  HOx chain length at 14:00 on August 5, 1997.**

PBL HOx_CL (HOx Chain Length)
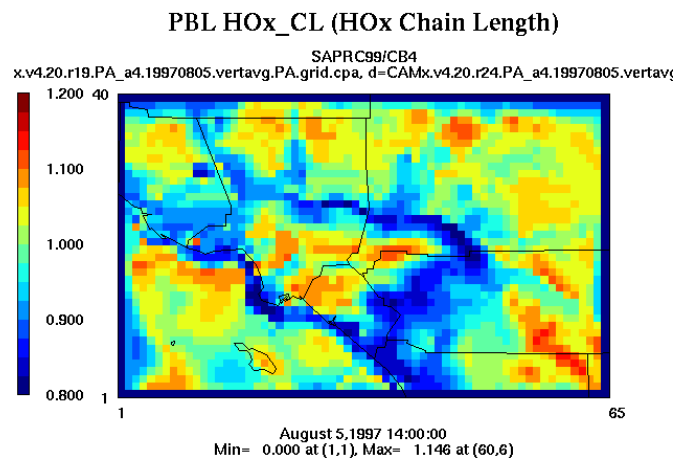


**Figure 10-17.  Ratio of the HOx chain length for CB4 to SAPRC99 at 14:00 on August 5, 1997.**

Organic peroxy ($RO_2$) radicals also are important because they convert NO to $NO_2$ and because they are potential sources of HOx radicals.  $RO_2$ is comprised of many different organic radicals produced from different VOCs and the CB4 and SAPRC99 mechanisms classify $RO_2$ radicals using different lumping schemes and names.  Accordingly, the CAMx CPA just compares the total amount of $RO_2$ radicals reacting (RO2_rctd) as a measure of the influence of $RO_2$ on ozone production chemistry.

The $RO_2$ reaction rates for CB4 and SAPRC99 are compared in Figure 10-18.  SAPRC99 has a much higher $RO_2$ reaction rate, and therefore $RO_2$ production rate, than CB4 in the VOC-sensitive area.  The area where SAPRC99 has higher $RO_2$ production closely corresponds with the area where SAPRC99 has higher ozone production (Figure 10-13).

**CB4**                                                          **SAPRC99**
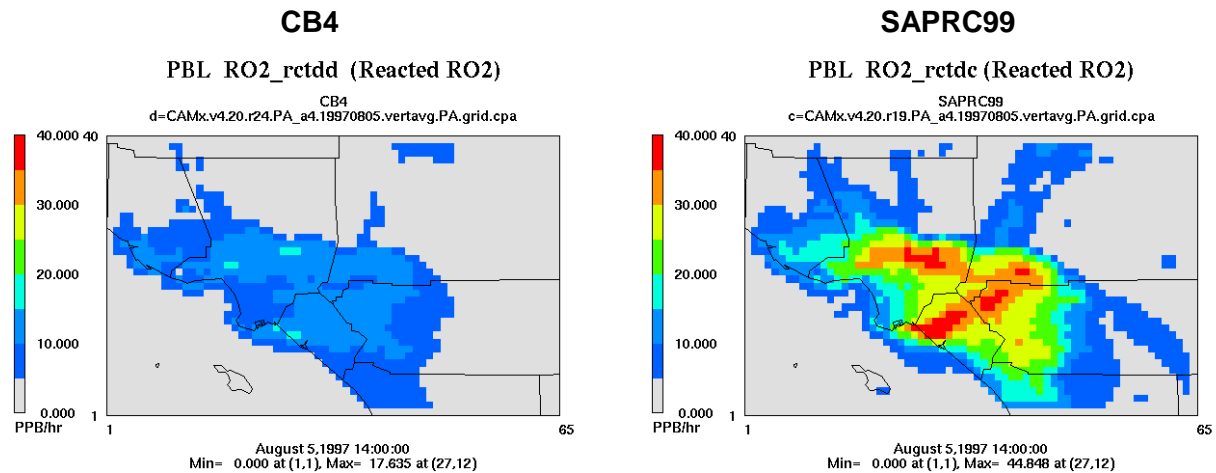


**Figure 10-18.  RO₂ organic peroxy radical reaction rate (ppb/hour) at 14:00 on August 5, 1997.**

### 10.4.4  NOy Reactions

Reactive nitrogen (NOy) comprises NOx and its reaction products (NOz):

- NOx = NO + $NO_2$
- NOz = HONO + PAN + $HNO_3$ organic nitrates + other minor N-species
- NOy = NOx + NOz

CAMx CPA reports several parameters that track the conversion of oxidized nitrogen between active (NOx) and inactive forms (NOz).  Here, active means able to participate directly in ozone producing reactions, i.e., NO and $NO_2$.

### 10.4.4.1  OH + $NO_2$ Reaction

The most important atmospheric reaction converting NOx to NOz is the reaction of OH with $NO_2$ to for nitric acid ($HNO_3$).  Converting $NO_2$ to $HNO_3$ promotes ozone formation in high NOx environments by overcoming the NOx inhibition effect.  The rate constant for the OH + $NO_2$ reaction has changed in recent years and CB4 has a slightly higer (~10%) value than SAPRC99.  However, the rate at which OH radicals convert $NO_2$ to $HNO_3$ depends upon both the reaction rate constant and the OH concentration.  Figure 10-19 compares the CB4 and SAPRC99 conversion rate for $NO_2$ to $HNO_3$ by reaction with OH (HNO3_OHNO2).  The conversion rate is higher in SAPRC99 than CB4 because the higher OH concentration in SAPRC99 more than offsets the lower OH + $NO_2$ reaction rate in SAPRC99 than CB4.  This shows that the OH + $NO_2$ reaction rate alone does not explain differences in reactivity between SAPRC99 and CB4.

**CB4**                                                          **SAPRC99**
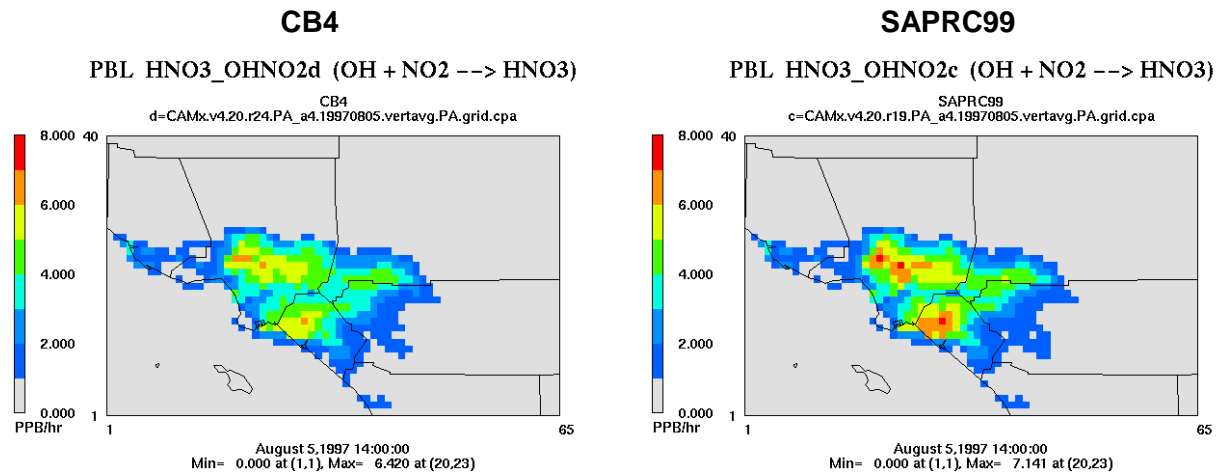


**Figure 10-19.  Conversion rate (ppb/hr) for NO$_2$ to HNO$_3$ by reaction with OH at 14:00 on August 5, 1997.**

10.4.4.2  NOx Recycling

Both the CB4 and SAPRC99 mechanisms include reactions that slowly convert reactive nitrogen from inactive (NOz) back to active (NOx) forms. Potentially important "NOx recycling" reactions are:

- OH reaction with nitric acid
- Nitric acid photolysis
- Organic nitrate photolysis
-  OH reaction with organic nitrates

The original CB4 mechanism (Gery et al., 1989) includes only the first of these reactions, whereas SAPRC99 includes the first three reactions.  The CB05 mechanism includes all four of these reactions.

The amount of NOz recycled back to NOx (NOxrecycl) for the CB4 and SAPRC99 mechanisms is compared in Figure 10-20.  As expected, NOx recycling is greater for SAPRC99 than CB4 because SAPRC99 includes more reaction pathways.  The NOx recycling rate is slow (tenths of ppb/hour of NOx produced) and these reactions will only influence ozone chemistry in regions where NOx emissions are low.  The NOx recycling reactions play little role in ozone production for large urban areas.  NOx recycling will be more important in rural areas between urban areas and may influence ozone transport.

**CB4** **SAPRC99**
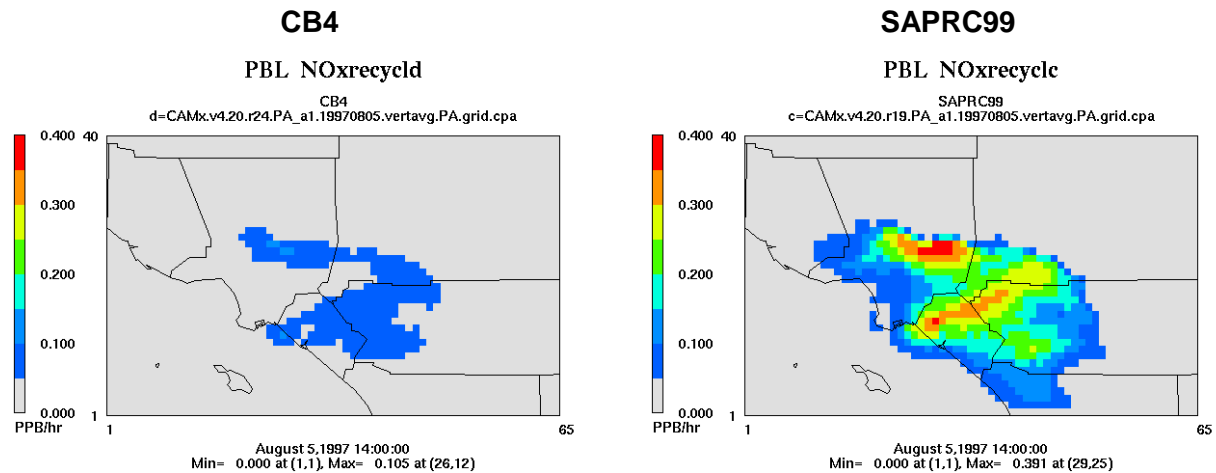


**Figure 10-20. Rate of NOx recycling (ppb/hr) from NOz at 14:00 on August 5, 1997.**

### 10.4.5 Ozone Destruction

The CB4 and SAPRC99 mechanisms include reactions that can destroy ozone as well as produce ozone. Some ozone destruction pathways are well-known, e.g., ozone titration by NO and ozone reaction with alkenes:

$$NO + O_3 \rightarrow NO_2 + O_2$$
$$alkene + O_3 \rightarrow products$$
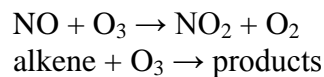
Reactions with radicals such as the HOx cycle discussed above also can destroy ozone:

$$OH + O_3 \rightarrow HO_2 + O_2$$
$$HO_2 + O_3 \rightarrow OH + O_2$$
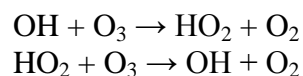
Whether or not the HOx cycle results in net ozone destruction or production depends upon the availability of NOx.

The CAMx CPA calculates the ozone destruction rate (O3_dest) due to these processes. Figure 10-21 compares the ozone destruction rate for CB4 and SAPRC99. There is rapid ozone destruction by NO-titration in high NOx emission areas for both CB4 and SAPRC99. Outside of high NOx emission areas, ozone destruction occurs at moderate rates of about 1-4 ppb/hr even as net ozone production is occurring at the same time (Figure 10-9). The net ozone production shown in Figure 10-9 is the sum of ozone production and destruction reactions. Simultaneous ozone destruction and production represents a replacement of "old ozone" by "new ozone." Since "old ozone" is effectively transported ozone, the rate of ozone destruction has implications for ozone transport analyses and evaluating the balance between ozone transport and local ozone production in causing ozone pollution. The ozone destruction rates seen here outside high NOx emission areas of a few ppb/hour are small compared to the ozone
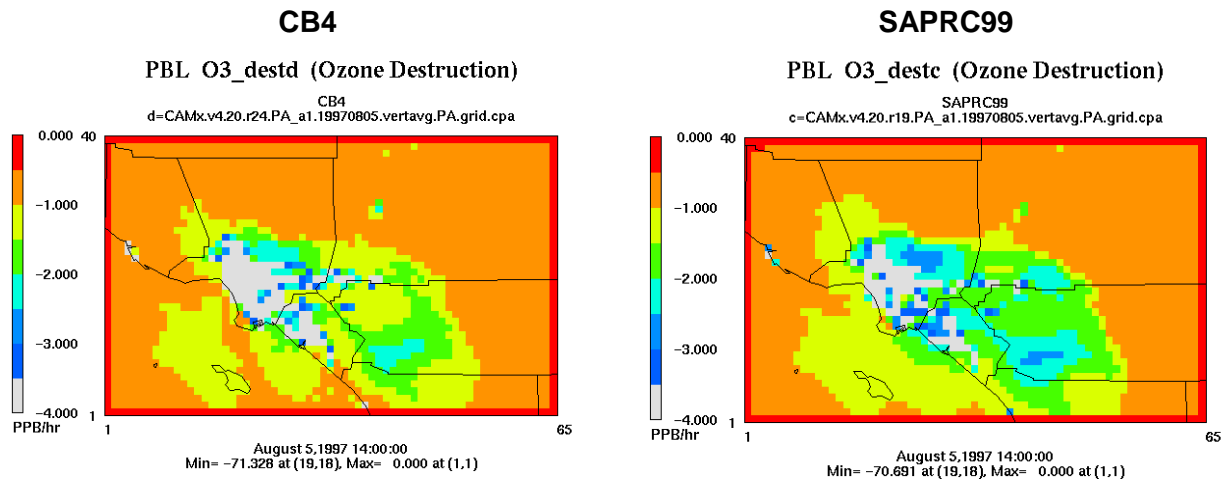
**Figure 10-21.  Ozone destruction rate by chemical reactions (ppb/hr) at 14:00 on August 5, 1997.**

production rates of many ppb/hour, but would be significant if combined with multi-hour, or multi-day, transport times.

### 10.4.6  Role of Biogenic VOC

The CAMx CPA reports the amount of OH reacting with VOCs included in the reaction mechanism.  The VOCs in the CB4 and SAPRC99 mechanism are different because of differences in the lumping approach.  Direct comparisons are possible for explicit species (e.g., isoprene, ethylene), for species that are effectively the same (TOL and ALK1; XYL and ALK2) and for groups of lumped compounds (PAR and the sum of ALK1 to ALK5).

One way to use the CPA variables for OH + VOC reactions is to evaluate the role of biogenic isoprene.  Figure 10-22 shows the fractional contribution of isoprene to all OH + VOC reactions. The contribution of isoprene to OH + VOC reactions is very similar for the CB4 and SAPRC99 mechanisms.  Isoprene is much less important as an OH reaction partner for the Los Angeles area than in the Eastern US because the area is dry and has relatively low biomass, and also has relatively high anthropogenic VOC emissions.  Note that the analysis shown in Figure 10-22 indicates where isoprene reactions are occurring, but not where ozone is produced as a consequence of isoprene reactions.

**CB4**

**SAPRC99**

PBL  ISOPwOHd/(OHw_all_HCd+0.0001)

PBL  ISOPwOHc/(OHwHCc+0.0001)

CB4
d=CAMx.v4.20.r24.PA_a1.19970805.vertavg.PA.grid.cpa

SAPRC99
c=CAMx.v4.20.r19.PA_a1.19970805.vertavg.PA.grid.cpa

August 5,1997 14:00:00
Min=  0.000 at (1,1), Max=  0.268 at (17,34)

August 5,1997 14:00:00
Min=  0.000 at (1,1), Max=  0.211 at (17,34)
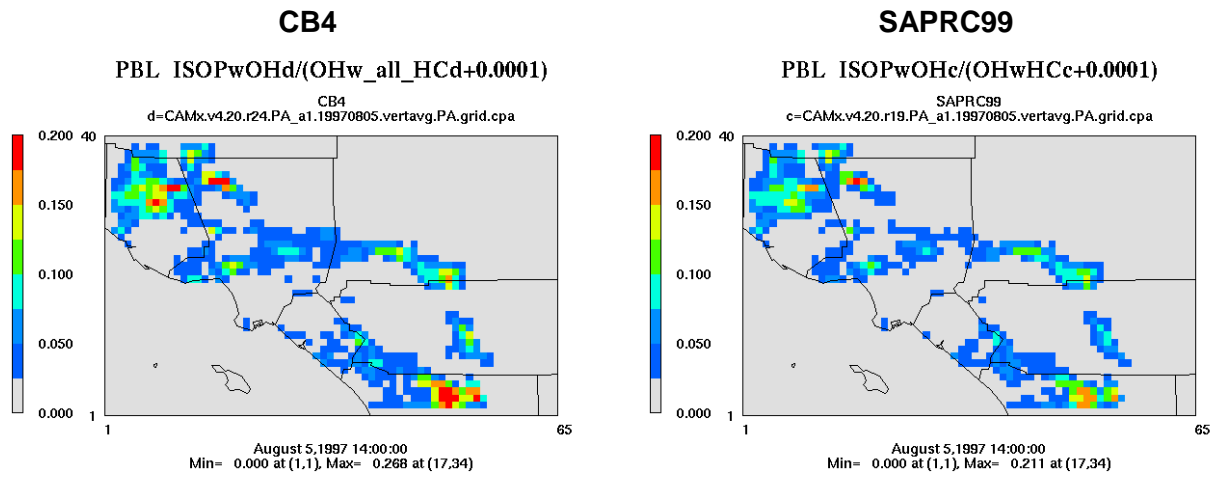
**Figure 10-22.  OH + isoprene as a fraction of OH + VOC reactions at 14:00 on August 5, 1997.**

## 11. REACTIVE TRACERS

The CAMx reactive tracer algorithm provides a flexible approach for simulating the emission, dispersion, chemistry, and deposition of multiple trace gas and particulate tracers on the computational grid(s) and within the IRON PiG treatment. Originally developed to model air toxics, it was extended and generalized to be able to track a variety of user-defined organic and inorganic species.

Reactive tracers are carried separately from the core model photochemical/PM chemistry mechanisms, and thus can be used to address a variety of issues, separately or in combination:

- Reactive and inert gaseous and particle air toxic compounds;
- Chemical decay of individual VOC compounds into multiple generations of daughter products;
- Source tagging of primary emitted inert and reactive compounds from specific source types/classes, or from individual stacks, facilities and/or complexes.

The reactive tracer algorithm is implemented as a CAMx "Probing Tool" and thus shares model data structures with other Probing Tools such as the Ozone/Particulate Source Apportionment Technology (OSAT/PSAT) and the Decoupled Direct Method (DDM/HDDM). This streamlines the CAMx code, improves efficiency, and maximizes consistency with the core model since it allows reactive tracer calculations for emissions, transport, and deposition to use the existing CAMx algorithms. However, this means that reactive tracers cannot be used simultaneously with other Probing Tools.

The reactive tracer implementation employs two approaches to define tracer chemistry. The original approach, referred to as RTRAC, allows tracers to decay and form multiple generations of daughter products through photolysis and user-specified thermal reactions with ozone and radicals (OH, $NO_3$) that are extracted from the core gas-phase chemistry (CB05, CB6, or SAPRC99). The newer approach, referred to as the RTRAC Chemical Mechanism Compiler (RTCMC), allows the user to externally define a full chemistry mechanism with no limits on complexity (within available computer resources). RTCMC can also access any gas-phase concentrations from the core gas-phase mechanism as well. Neither option allows chemistry for particulate tracers.

## 11.1 Description of RTRAC

Reactive tracers are defined for each CAMx run by providing an RTRAC chemistry parameters file similar to that used for the core model. The examples in Figure 11-1 and 11-2 illustrate an RTRAC air toxics application using the older CB4 and SAPRC99 chemical mechanisms, respectively (ENVIRON, 2002; Morris et al., 2003). The number and names of the tracers are arbitrary; i.e. information on the tracer species' chemical identities, structure, reaction pathways, and kinetics are kept separate from the core model. Consistent with the chemistry parameters files used for CB4 and SAPRC99, the physical characteristics for each reactive tracer must be specified for deposition calculations, and their reaction pathways and rates must be defined.

```
CAMx Version          |VERSION6.0
Description           |MATES Toxics for CRC project A-42
No of gas tracers     |6
No of aero tracers    |8
No photolysis rxns    |4
No thermal rxns       |12
Gas Tracers
No.   Name      P/S   SNAM  lower bnd    H-law    T-fact      Molwt  Reactvty   Rscale
  1   PACET     PRIM        1.00E-12  6.30e+03   -6492.       44.00      0.0      1.0
  2   HCHO      PRIM        1.00E-12  6.30e+03   -6492.       30.00      0.0      1.0
  3   BENZ      PRIM        1.00E-12  1.80e-01       0.       78.00      0.0      1.0
  4   BUTA      PRIM        1.00E-12  1.00e-02       0.       54.00      0.0      1.0
  5   SACET     SEC   ALD2  1.00E-12  6.30e+03   -6492.       44.00      0.0      1.0
  6   SFORM     SEC   FORM  1.00E-12  6.30e+03   -6492.       30.00      0.0      1.0
Aero Tracers
No.   Name      lower bnd    Density   Low cut Upper cut
  7   DSLF      1.00E-09      1.5       0.10      2.50
  8   ECF       1.00E-09      1.5       0.10      2.50
  9   CRF       1.00E-09      1.5       0.10      2.50
 10   CR6F      1.00E-09      1.5       0.10      2.50
 11   DSLC      1.00E-09      1.5       2.50     10.00
 12   ECC       1.00E-09      1.5       2.50     10.00
 13   CRC       1.00E-09      1.5       2.50     10.00
 14   CR6C      1.00E-09      1.5       2.50     10.00
Photolysis reactions
Toxic      Rxn #     Factor
PACET        45        1.0
SACET        45        1.0
HCHO         39        1.6
SFORM        39        1.6
Thermal reactions and rates
Toxic      React A(ppm-1min-1)      Ea(K)          B      Tref
PACET      OH     8.2015E+03 -3.1099E+02      0.0     300.0
PACET      NO3    2.0689E+03  1.8599E+03      0.0     300.0
HCHO       OH     1.6699E+03 -6.4815E+02      2.0     300.0
HCHO       NO3    4.1377E+03  2.5161E+03      0.0     300.0
BENZ       OH     3.6944E+03  1.9978E+02      0.0     300.0
BUTA       OH     2.1871E+04 -4.4787E+02      0.0     300.0
BUTA       O3     4.8766E+01  2.5000E+03      0.0     300.0
BUTA       NO3    2.1871E+04  1.4890E+03      0.0     300.0
SACET      OH     8.2015E+03 -3.1099E+02      0.0     300.0
SACET      NO3    2.0689E+03  1.8599E+03      0.0     300.0
SFORM      OH     1.6699E+03 -6.4815E+02      2.0     300.0
SFORM      NO3    4.1377E+03  2.5161E+03      0.0     300.0
```

**Figure 11-1. Example RTRAC chemistry input file for modeling the MATES toxic species using CB4 as the host chemical mechanism (CB4 is no longer available in CAMx).**

```
CAMx Version        |VERSION6.0
Description         |Toxics for CRC project A-42 with SAPRC99 host mechanism
No of gas tracers   |14
No of aero tracers  |0
No photolysis rxns  |8
No thermal rxns     |28
Gas Tracers
No.   Name     P/S    SNAM   lower bnd      H-law     T-fact    Diffrat   Reactvty   Rscale
  1   mPACET   PRIM           1.00E-12    6.30e+03    -6492.      1.56       0.0       1.0
  2   mPFORM   PRIM           1.00E-12    6.30e+03    -6492.      1.29       0.0       1.0
  3   mBENZ    PRIM           1.00E-12    1.80e-01       0.      2.08       0.0       1.0
  4   mBUTA    PRIM           1.00E-12    1.00e-02       0.      1.73       0.0       1.0
  5   SACET    SEC    CCHO    1.00E-12    6.30e+03    -6492.      1.56       0.0       1.0
  6   SFORM    SEC    HCHO    1.00E-12    6.30e+03    -6492.      1.29       0.0       1.0
  7   oPACET   PRIM           1.00E-12    6.30e+03    -6492.      1.56       0.0       1.0
  8   oPFORM   PRIM           1.00E-12    6.30e+03    -6492.      1.29       0.0       1.0
  9   oBENZ    PRIM           1.00E-12    1.80e-01       0.      2.08       0.0       1.0
 10   oBUTA    PRIM           1.00E-12    1.00e-02       0.      1.73       0.0       1.0
 11   pPACET   PRIM           1.00E-12    6.30e+03    -6492.      1.56       0.0       1.0
 12   pPFORM   PRIM           1.00E-12    6.30e+03    -6492.      1.29       0.0       1.0
 13   pBENZ    PRIM           1.00E-12    1.80e-01       0.      2.08       0.0       1.0
 14   pBUTA    PRIM           1.00E-12    1.00e-02       0.      1.73       0.0       1.0
Photolysis reactions
Toxic        Rxn #     Factor
mPACET        131       1.0
oPACET        131       1.0
pPACET        131       1.0
SACET         131       1.0
mPFORM        123       1.6
oPFORM        123       1.6
pPFORM        123       1.6
SFORM         123       1.6
Thermal reactions and rates
Toxic        React A(ppm-1min-1)      Ea(K)          B       Tref
mPACET        OH     8.2015E+03 -3.1099E+02        0.0      300.0
mPACET        NO3    2.0689E+03  1.8599E+03        0.0      300.0
oPACET        OH     8.2015E+03 -3.1099E+02        0.0      300.0
oPACET        NO3    2.0689E+03  1.8599E+03        0.0      300.0
pPACET        OH     8.2015E+03 -3.1099E+02        0.0      300.0
pPACET        NO3    2.0689E+03  1.8599E+03        0.0      300.0
mPFORM        OH     1.6699E+03 -6.4815E+02        2.0      300.0
mPFORM        NO3    4.1377E+03  2.5161E+03        0.0      300.0
oPFORM        OH     1.6699E+03 -6.4815E+02        2.0      300.0
oPFORM        NO3    4.1377E+03  2.5161E+03        0.0      300.0
pPFORM        OH     1.6699E+03 -6.4815E+02        2.0      300.0
pPFORM        NO3    4.1377E+03  2.5161E+03        0.0      300.0
mBENZ         OH     3.6944E+03  1.9978E+02        0.0      300.0
oBENZ         OH     3.6944E+03  1.9978E+02        0.0      300.0
pBENZ         OH     3.6944E+03  1.9978E+02        0.0      300.0
mBUTA         OH     2.1871E+04 -4.4787E+02        0.0      300.0
mBUTA         O3     4.8766E+01  2.5000E+03        0.0      300.0
mBUTA         NO3    2.1871E+04  1.4890E+03        0.0      300.0
oBUTA         OH     2.1871E+04 -4.4787E+02        0.0      300.0
oBUTA         O3     4.8766E+01  2.5000E+03        0.0      300.0
oBUTA         NO3    2.1871E+04  1.4890E+03        0.0      300.0
pBUTA         OH     2.1871E+04 -4.4787E+02        0.0      300.0
pBUTA         O3     4.8766E+01  2.5000E+03        0.0      300.0
pBUTA         NO3    2.1871E+04  1.4890E+03        0.0      300.0
SACET         OH     8.2015E+03 -3.1099E+02        0.0      300.0
SACET         NO3    2.0689E+03  1.8599E+03        0.0      300.0
SFORM         OH     1.6699E+03 -6.4815E+02        2.0      300.0
SFORM         NO3    4.1377E+03  2.5161E+03        0.0      300.0
```

**Figure 11-2. Example RTRAC chemistry input file for modeling toxic species with SAPRC99 as the host chemical mechanism.**

The structure of the RTRAC tracer definition provides complete flexibility in the selection of the compounds and tracers to be included in each analysis. The user is able to easily alter or expand the compounds as needed.

For gas species, the required deposition parameters are the Henry's Law constant and molecular weight $M_g$, the latter of which defines a diffusivity parameter according to $\sqrt{M_g / M_{H_2O}}$ . The deposition calculation for gases that react in plant tissue also needs a reactivity parameter that describes whether a species reacts when dissolved inside leaf tissues (Wesely, 1989). This parameter is intended for modeling the deposition of reactive species, such as ozone, and should be set to zero for air toxics. The deposition calculation for gasses also uses an "Rscale" factor to adjust the surface resistance. This is used to set the surface resistance to zero for strong acids (e.g., $HNO_3$) and should be set to 1.0 for modeling air toxics.

The deposition calculation for particles requires the particle density and size associated with each species. The particle size is calculated as the geometric mean of the lower and upper cut points (see Figure 11-1). If possible, the particle size and density should be based on the measured size of particles associated with each RTRAC species (e.g., for a compound associated with soot particles, use a density and size representing the soot).

The emission rates for the RTRAC species are provided by an extra set of emission files (surface and/or point source). Emissions of gases are in moles per time period (normally moles/hour), whereas particles are in micro-grams per time period. The emissions file format is the same as for a regular CAMx emissions file, as described in Section 3.

### 11.1.1 RTRAC Gas-Phase Chemistry

The RTRAC chemistry calculations use a special chemistry module. Chemistry may be modeled for primary and secondary gas species, meaning that tracers can be formed from the decay of primary tracers or from the decay of host model species (e.g., secondary formaldehyde). The chemical decay of gaseous tracers can account for thermal reactions with ozone ($O_3$), hydroxyl radical (OH) and nitrate radical ($NO_3$), as well as photolysis. The algorithms are coded so that all chemical decay pathways are zero by default and only become non-zero if decay rates are explicitly specified in the input file (see Figure 11-1). The example RTRAC chemistry input file in Figure 11-1 shows how thermal reactions are specified by naming the tracer and oxidant, and providing reaction rate parameters. Note that the RTRAC chemical reaction rates depend on the rates and parameters provided in the RTRAC input file, and <u>not</u> the rates in the host model chemical mechanism; however the host model does provide the oxidizing species concentrations (i.e., $O_3$, OH, and $NO_3$).

11.1.1.1 Thermal Reactions

Thermal reactions with oxidants are modeled as second order reactions:

$$R \quad = \quad k\left[tracer\right]\left[oxidant\right]$$

where *R* is the decay rate and the rate constant *k* is defined using the generalized temperature dependent rate expression:

$$k \;=\; A\left(\frac{T}{300}\right)^{B} \exp\left(\frac{-E_a}{T}\right)$$

The Arrhenius factor (*A*) must be in units (ppm$^{-1}$min$^{-1}$), the activation energy (*E$_a$*) must be Kelvin and *B* is dimensionless.  This is the same as expression 3 in Table 3-3a.  Oxidant concentrations for the decay calculation are obtained from the CAMx photochemical simulation for each grid cell at each time step.  RTRAC can be used with either CB05, CB6, or SAPRC99 chemical mechanisms that are available in the current version of CAMx (see Section 5).  Choosing between the core mechanisms will influence the RTRAC chemical decay rates by changing the oxidant concentrations in the host model.

### 11.1.1.2  Photolysis

Photolysis reactions are specified by naming the tracer undergoing photolysis and providing a ratio of the tracer photolysis rate to one of the photolysis reactions in the host photochemical mechanism.  For example, Figure 11-1 shows that there are both primary and secondary acetaldehyde reactive tracers (PACET and SACET) and the photolysis rate for both species is set equal to reaction 45.  Reaction 45 in the old CB4 mechanism was photolysis of ALD2, which is based on acetaldehyde.  Figure 11-1 also shows that there are two types of formaldehyde in the MATES toxics modeling (PFORM and SFORM).  Modeling the photolysis of formaldehyde with RTRAC is complicated by the fact that the CB4 mechanism included two photolysis reactions for formaldehyde (reactions 38 and 39).  The solution shown in Figure 11-1 was to model formaldehyde photolysis as 1.6 times the rate of CB4 reaction 39.  The CAMx host mechanisms are discussed in Section 5 and are defined by the ASCII chemistry parameters files (Section 3) and mechanism listings distributed with CAMx and available from the CAMx web page (www.camx.com).

### 11.1.1.3  Secondary Species

RTRAC allows for formation of secondary/daughter products related to the chemical decay of one of the primary tracers.  Secondary species can also be subject to chemical decay, just like primary species, if the user desires.  Therefore, the RTRAC chemistry module allows decay reactions (thermal and photolysis) to be specified for secondary species using the same method as for primary species.  In this manner, concentrations of secondary species are determined by the balance between chemical production and destruction.  RTRAC requires that any secondary daughter tracers must be specified after their parent tracer in the chemistry parameters input file.

RTRAC also allows tracers that track the secondary formation of any species that is included in the host chemical mechanism.  For example, in Figure 11-1 the species SFORM is used to track secondary formaldehyde, and so SFORM is defined as a secondary species and identified with the host species FORM.  This means that the RTRAC chemistry module will identify the chemical production of FORM in each grid cell at each time step, and add this chemical production to the

SFORM tracer. Since SFORM is intended to track only secondary formaldehyde, no primary emissions should be included for SFORM.

### 11.1.1.4  Example for Defining Chemical Rate Data

Reaction rate data for many gases can be found in rate constant compilations such as IUPAC (2001), JPL (2001) and Calvert et al. (2000, 2002). For the examples shown in Figures 11-1 and 11-2, rate constants were obtained from a study by Harley and Cass (1995) that modeled detailed VOCs for Los Angeles. Photolysis rates were calculated using the Tropospheric Ultra-violet Visible (TUV) model (NCAR, 2011), which is available as a CAMx pre-processor. TUV includes photolysis data (cross-sections and quantum yields) for many species, and data for other species are included in IUPAC (2001), JPL (2001) and Calvert et al. (2002).

### 11.1.1.5  Chemical Decay Rates for Near-Source Modeling

The RTRAC algorithm can output hourly chemical decay rates at user-specified locations for input to an external point-source dispersion model (e.g., a Gaussian plume/puff model) for subsequent sub-grid scale "fenceline" modeling. The objective is to allow the grid model (CAMx) to provide local decay rate information to any plume-scale model of the user's choice.

If subgrid-scale near-source modeling is to be conducted using an external model, then the user provides the locations of each of the target emission complexes using the CAMx Probing Tools receptor file input format. Figure 11-3 displays an example RTRAC receptor input file for the five point source complexes modeled by ENVIRON (2002) and Morris et al. (2003). At each grid cell, hourly decay rates for each RTRAC compound and every vertical layer are output and can then be interfaced with the user-selected plume model.

```
SINGLE CELL          Test Cell          1        42        44
SINGLE CELL          Test Cell          1        41        36
SINGLE CELL          Test Cell          1        39        36
SINGLE CELL          Test Cell          1        50        43
SINGLE CELL          Test Cell          1        34        48
```

**Figure 11-3.  Example RTRAC receptor input file identifying the grid cells with locations of point source complexes where hourly decay rates will be output for subgrid-scale point source modeling (see format for OSAT receptor file in Table 7-2).**

### 11.1.2  RTRAC Source-Receptor Relationships and Double Counting

Separate families of reactive tracer compounds can be simulated by providing separate emission inputs similarly to OSAT/PSAT (see Section 7). Tracking separate families of RTRAC tracers allows for source apportionment and can be used to avoid double counting when an external plume model is used to obtain near-source impacts. For example, in the RTRAC air toxics example application discussed previously (ENVIRON, 2002; Morris et al., 2003), separate air toxic emission inputs were provided to source apportion on-road mobile sources, area plus

non-road sources, point sources, and secondarily formed species. Furthermore, separate families of air toxic tracers were also specified for each point source complex to be modeled by the external plume model, so that total concentrations could include the local point source impacts (plume model) plus the regional contributions from all other sources (CAMx RTRAC).

## 11.2 Description Of RTCMC

Like RTRAC, the purpose of RTCMC is to add tracer species to a CAMx "core model" simulation and have the tracers undergo chemical changes that depend, in part, upon the evolution of CAMx core model species. The RTCMC approach differs from the original RTRAC approach by allowing arbitrarily complex chemical reaction schemes, but it is exactly like RTRAC in every other respect. The current implementation of RTCMC is for gas-phase reactions, i.e., gas-phase tracers reacting with each other and/or gas-phase host model species. The core model's photochemical mechanisms remain intact and separate from the reactive tracer chemistry.

### 11.2.1 RTCMC Gas-Phase Chemistry

The RTCMC allows users to input, in a text-based (ASCII) format, a set of chemical reactions (mechanism) for certain target species to be treated by the CAMx Reactive Tracer Probing Tool. RTCMC is an extension of the original RTRAC algorithm that reads (and solves) a completely independent, user-defined chemical mechanism for reactive tracers that can utilize concentrations of any photochemical species from the core model mechanism. Upon startup, RTCMC compiles information on the chemical mechanism and configures the reactive tracer chemistry solver. During the model simulation, the RTCMC chemistry solver receives ambient pollutant information from the core photochemical mechanism and uses this to calculate the evolution of RTRAC species.

The format of the RTCMC input file is essentially the same as the "IMC" input file format of the SCICHEM Lagrangian puff model (EPRI, 2000). An example IMC format file is shown in Figure 11-4. There are four sections in an IMC file that are identified by a keyword at the start of each section, as follows:

| | |
|---|---|
| `#Control` | Configuration information identified by keywords |
| `#Species` | Names of chemical species and associated data |
| `#Table` | Photolysis rate data for any photolytic reactions |
| `#Equations` | Chemical reactions and thermal rate constants |

The IMC file uses space-delimited ASCII format. Leading white space at the start of any line will be ignored. CAMx reads the IMC file as *case insensitive*.

The hash symbol (#) before each section keyword marks the start of a section and should be reserved for this purpose. The four sections should appear in the order shown above. The only section that may be unnecessary in some cases (i.e., if there are no photolytic reactions) is the `#Table` section and guidance on handling this case is provided below.

```
#Control
    rate_species_units = 'ppm'
    rate_time_units = 'min'
    solver = 'dlsode'
    Jacobian = 'numeric'
#Species, Type, Ambient, Tolerance, deposition vel, wet scav
O3        A     1.0      1.0E-12    0.0             0.0
OH        A     1.0      1.0E-12    0.0             0.0
ATRAC     F     1.0      1.0E-12    0.010           0.0
BTRAC     F     1.0      1.0E-12    0.001           0.0
CTRAC     F     1.0      1.0E-12    0.020           0.0
DTRAC     F     1.0      1.0E-12    0.001           0.0
ETRAC     F     1.0      1.0E-12    0.030           0.0
FTRAC     F     1.0      1.0E-12    0.001           0.0
#Table
  0         0.       15.       30.      45.        60.        75.
       80.        86.       87.       88.
  1 4.1590E-04 4.0600E-04 3.7540E-04 3.27E-04 2.6040E-04 9.4990E-05
2.9930E-05 4.8590E-06 8.3030E-08 1.0000E-09
#Equations
  1 [ATRAC]               -> (2.0)[BTRAC] ; 0 0.000E-00
  2 (1.5)[CTRAC] + [OH]  -> (0.5)[DTRAC] ; 1 4.2000E+04
  3 [ETRAC] + [O3]       -> [FTRAC]      ; 1 1.8000E-02
```

**Figure 11-4.  Example RTCMC chemistry input file.**

### 11.2.1.1  The Control Section

According to the SCICHEM documentation, the `#Control` section of the IMC file must always have at least three lines, as follows:

```
#CONTROL
    &CONTROL
    &END
```

The first line is the keyword identifying the control section.  The second and third lines are additional keywords denoting the start and end of the control section.  Note, however, that CAMx ignores the `&CONTROL` and `&END` lines.

One or more control options may be specified using keywords, inserted one per line, ahead of the closing `&END` line, like this:

```
#CONTROL
    &CONTROL
      Keyword = 'option'
      Keyword = 'option'
    &END
```

The keywords used by CAMx and SCICHEM are listed in Table 11-1 and are case insensitive.  Not all keywords are used by both models, and CAMx will ignore any non-recognized keyword.  A "=" symbol must separate each keyword and option.  The option must be enclosed within

**Table 11-1.  Keywords, options and default values for the Control section of the IMC file.**

| Keyword | Used by SCICHEM | Used by CAMx | Options Allowed by CAMx |
|---|:---:|:---:|---|
| `Ambient file` | ● | | n/a |
| `Species_units` | ● | | n/a |
| `Emission_units` | ● | | n/a |
| `Rate_species_units` | ● | ● | molecules/cm$^3$ (*default*) <br> ppm |
| `Rate_time_units` | ● | ● | seconds (*default*) <br> minutes <br> hours |
| `Solver` | | ● | DLSODE (*default*) <br> SLSODE <br> Rosenbrock |
| `Rtol` | ● | ● | Real number (*default = 1.0E-5*) |
| `Atol` | | ● | Real number (*default = 1.0E-18*) |
| `Jacobian` | | ● | Numeric (*default*) <br> Algebraic |

single quotes.  In practice, only the first six letters of each keyword and the first three letters of each option are considered and you may abbreviate accordingly (i.e., `keywor = 'opt'`).

All CAMx recognized keywords have a default option that will be used if the keyword is omitted, meaning that the CAMx RTCMC may be run without specifying any keywords provided that that all other input data (e.g., rate constants) are consistent with the defaults.  The allowed keyword options in Table 11-1 are discussed below:

`Rate_species_units`
> The concentration units for thermal rate constant expressions.

`Rate_time_units`
> The time units for photolysis and thermal rate constant expressions.

`Solver`
> The name of the numerical integrator to be used as the chemistry solver.  SLSODE and DLSODE are, respectively, the single and double precision versions of the Livermore Solver for Ordinary Differential Equations (Hindmarsh 1983).  The Rosenbrock solver is the double precision RODAS solver (Hairer and Wanner, 1991).

`Rtol`
> The relative error tolerance (convergence criterion) employed for all chemical species by the chemistry solver.

`Atol`
> The absolute error tolerance (convergence criterion) employed for all chemical species by the chemistry solver.  CAMx does not use species-specific `Atol` values that may appear in the species section, as discussed below.

`Jacobian`

The chemistry solvers employ a Jacobian matrix of first-order derivatives of each chemical species with respect to all species. The Jacobian matrix is constructed automatically by the RTCMC. This option controls whether the Jacobian is constructed algebraically or numerically. Both options may be used with the double precision solvers and numeric may be more efficient. The algebraic option is strongly recommended for the single precision SLSODE solver (because single precision may be inadequate for constructing a numeric Jacobian by finite difference).

### 11.2.1.1.1 Concentration Units

CAMx does not use the `Species_units` or `Emission_units` keywords and will ignore them if they are present. CAMx will output RTCMC species average concentrations in ppm units. Emissions of RTCMC species must be provided in moles/hour.

### 11.2.1.1.2 Setting Error Tolerances

All three RTCMC chemistry solvers use the `Rtol` and `Atol` parameters specified in the control section to manage errors in predicted concentrations. CAMx does not use the species-specific `Atol` values that may appear in the species section because it is difficult to select reliable `Atol` values for each species. The error (*err*) in the predicted concentration (*con*) for species *i* should be roughly less than:

$$err(i) = rtol \times con(i) + atol$$

The combined `Rtol` and `Atol` determine accuracy. Setting `Atol` to zero will result in pure relative error control. Relative error control has the advantage of being easily understood (the errors should be smaller than X percent) but suffers the disadvantage of excessive computational resources that may be expended to manage errors in species concentrations that are essentially zero. Note that RTCMC sets a concentration floor of 1.0E-16 ppm.

The default settings for `Rtol` and `Atol` listed in Table 11-1 should be generally applicable because they are conservative and effectively result in pure relative error control. We recommend against setting `Rtol` greater than 0.001. Appropriate settings for `Atol` depend upon the magnitude of concentration predictions and the need for accurate predictions in high vs. low concentration areas (e.g., plume centerline vs. out of plume).

Do not request infeasible accuracy from single precision SLSODE by setting `Rtol` and `Atol` smaller than about 1.0E-7.

### 11.2.1.2  The Species Section

The species section of the IMC file lists chemical species and associated data. All chemical species referred to in the equation section must appear in the species section. Extra species may appear in the species section, but including numerous extra species may cause a run-time error by exceeding the memory available for storing species information (if this happens, delete some of the unused species from the species section).

The first line is the keyword identifying the species section.  The following information must be provided for each listed species:

`Name`

        Species names may be up to 8 characters and must start with a letter.  They are case insensitive.  Accurate names are important because other CAMx input data (e.g., emissions, boundary conditions) will be matched to RTRAC species by name.

`Type`

        There are four permissible species types identified by first letter: Ambient (A), Fast (F), Slow (S), and Equilibrium (E).  Setting the species type is discussed in more detail below.

`Ambient`

        The ambient value is not used by CAMx, but is used by SCICHEM.  Provide a real number (e.g., 0.0).

`Atol`

        Species specific error tolerances are not used by CAMx, but are used by SCICHEM.  Provide a real number (e.g., 0.0).

`Dep`

        The species deposition velocity in m/s.  This deposition velocity will be used for all land surface types, which is a simplification compared to the CAMx dry deposition scheme.  Provide a real number (e.g., 0.0).

`Wet Scav`

        The wet scavenging coefficient is not used by CAMx.  For SCICHEM, this is a washout ratio.  CAMx does not use the washout ratio because this approach is incompatible with the CAMx wet deposition algorithms.  Provide a real number (e.g., 0.0).

`MW`

        The molecular weight is not needed by CAMx.  Provide a real number (e.g., 1.0).

### 11.2.1.2.1  Choosing the Species Type

The `Type` for each RTCMC species should be set according to: (a) whether the species concentration should be obtained from the core model or modeled using the RTCMC; and (b) the most accurate and efficient numerical method for performing chemistry within RTCMC.

All species to be obtained from the core model (e.g., $O_3$, OH, NO, $NO_2$, $H_2O$, M, $O_2$) must be set to type `Ambient`.  This rule will be enforced by CAMx and, for example, the species O3 must be set to type `A`, because it is part of all the core chemical mechanisms.

Species that are solved by the RTCMC may be type `F`, `S` or `E`.  The recommended default type is `F` (fast) in which case chemistry will be performed using the selected chemistry solver (e.g., DLSODE).  Species that undergo slow chemical change (lifetime of hours or longer) may be set to type `S` (slow) with potential gain in efficiency but some loss in accuracy.  Species that undergo extremely rapid chemical change (lifetime smaller than a second) may be set to type `E` (equilibrium) and solved using a steady-state approximation with some gain in efficiency but some loss in accuracy.  The Rosenbrock solver does not work well with species types `S` or `E`.  Equilibrium species may be used effectively with the single precision SLSODE solver to avoid the need for double precision.  You should use types `S` or `E` with caution and evaluate both

computational speed and concentration accuracy by comparing against results with using type `F`.

11.2.1.3  The Table Section

The table section of the IMC file provides photolysis rates for any photolytic reactions in the RTCMC mechanism.  It must contain at least two lines:

```
#Table
0  zenith1, zenith2, zenith3, …
```

The first line is the keyword identifying the table section.  The second line must begin with 0 (zero) followed by a list of space-delimited zenith angles (in degrees) starting with zero degrees and ascending to the largest angle.  If the largest zenith angle specified is less than 90 degrees a value of 90 degrees is implicitly added to the list.  By default, up to 15 zenith angles are allowed (this may be changed as described under adjustable parameters, below).  If the final zenith angle is not 90 degrees, no more than 14 angles should be listed to allow the 15th angle to be implicitly set to 90 degrees.

If the reaction mechanism has no photolytic reactions, include just the first two lines (keyword followed by zenith angles) in the table section.  If the reaction mechanism includes photolytic reactions, list them one reaction per space-delimited line after the zenith angles:

```
reaction_ID, rate1, rate2, rate3, …
```

The `reaction_ID` must be the integer identification number of the photolytic reaction followed by the photolysis rate at each zenith angle, from zero to the largest angle.  Photolysis reactions are first order and have rate units of reciprocal time to be provided in the `Rate_time_units` specified in the control section of the IMC file.  A photolysis rate of zero is implicitly assumed at 90 degrees unless you specify otherwise.

11.2.1.4  The Equations Section

The equations section of the IMC file lists the chemical reactions and rate constants for the RTCMC reaction mechanism and must contain at least two lines:

```
#Equations
reaction_ID [Reactants] > (Stoichiometry) [Products] ; Rate_Constant
```

The first line is the keyword identifying the equations section and must be followed by at least one reaction line.  Reaction lines list reactions and rate constants and are delimited by white space and separators.  The `reaction_ID` and the `Reactants` must be separated by white space.  The `Reactants` and `Products` must be separated by a right arrow symbol (the right arrow may be preceded by characters, e.g., `=>` or `->`).  The `Products` and the `Rate_Constant` must be separated by a semi-colon.

The `reaction_ID` must be an integer value that uniquely identifies each reaction.  Reactions identifiers need not be in order or continuous.

The name of `Reactants` and `Products` must be enclosed within square brackets, begin with a letter, and not exceed 8 characters in length.  All species names used in the equations section must also appear in the species section.  Zero to three reactants are allowed.  Zero to 20 products are allowed (the maximum is a user adjustable parameter).  Reactant and product names may be preceded by a stoichiometric coefficient enclosed within round brackets.  If the stoichiometric coefficient is omitted it is assumed to be unity.

Rate constants are specified using SCICHEM conventions and must be in the units specified by the keywords `Rate_species_units` and `Rate_time_units` in the control section (the defaults are molecules cm$^{-3}$ and seconds, respectively).  SCICHEM supports numerous rate constant expression types and CAMx should interpret all of them correctly, although not all have been thoroughly tested.  Table 11-2 defines a sub-set of the SCICHEM rate constant expression types that are recommended for use with CAMx.  The format for specifying rate expressions is the integer expression type followed by a list of the numerical values required by that expression type.  It is important that rate expressions are defined in units that are consistent with the reaction order, and Table 11-3 defines how the reaction order and rate constant unit dimensions may be determined.

The CAMx output "diag" file lists diagnostic information on the mechanism and rate constant expressions read by from the IMC file.  You should review this diagnostic output to ensure that CAMx correctly read and configured the RTCMC chemistry mechanism.

## 11.3  Reactive Tracers In IRON PiG

RTRAC/RTCMC calculations for emissions and chemistry have been integrated into the IRON PiG algorithms.  There are two ways in which RTRAC tracers may enter a PiG plume: as primary emissions from specifically flagged sources within the RTRAC point source file, or by formation of secondary species from decay of primary plume emissions.  There is no entrainment of tracers from the grid to the plume as this is likely to result in negative tracer concentrations, especially if the entrained tracer is a secondary product of a host model species (e.g., secondary formaldehyde).  Tracers are assumed to have negligible impact on PiG puff chemistry or oxidant levels.  If the tracer concentration in the plume is high enough to enhance or suppress the plume oxidant levels, then the photochemical impacts of the tracer can be accounted for by separately adding the tracer emissions into the host model lumped emissions; e.g., for tracing high concentrations of propene and butene in a plume, one would track the propene/butene concentrations using RTRAC tracers but also add CB-OLE or SAPRC99-OLE1 emissions to the plume to account for the oxidant impacts.

**Table 11-2a.  Recommended SCICHEM rate constant expression types for use in CAMx.**

| Expression Type | Description | Expression |
|---|---|---|
| 0 | Photolysis | $k = 0$ |
| 1 | Constant | $k = k_0$ |
| 2 | General temperature dependence | $k = A T^{-c} e^{(B/T)}$ |
| 3 | Troe-type temperature and pressure dependence | $k = \left[ \dfrac{k^0[M]}{1 + k^0[M]/k^\infty} \right] F^G$ $$k^0 = A T^B$$ $$k^\infty = C T^D$$ $$F = 0.6$$ $$G = \left\{ 1 + \left[ \log\left( k^0[M]/k^\infty \right) \right]^2 \right\}^{-1}$$ |
| 8 | Equilibrium with a previously defined reaction ($k_{ref}$) | $k = k_{ref} A e^{(B/T)}$ |
| 13 | Lindemann - Hinshelwood as used for OH + HNO3 | $k = k_0 + \dfrac{k_3[M]}{1 + k_3[M]/k_2}$ $$k_0 = A e^{(B/T)}$$ $$k_2 = C e^{(D/T)}$$ $$k_3 = E e^{(F/T)}$$ |
| 7 | Simple pressure dependence used for OH + CO | $k = k_0(1 + 0.6P)$ |

**Table 11-2b.  Parameters required by SCICHEM rate constant expression types.**

| Expression Type | Parameters | | | | | |
|---|---|---|---|---|---|---|
| | **1** | **2** | **3** | **4** | **5** | **6** |
| 0 | *0* | | | | | |
| 1 | $k_o$ | | | | | |
| 2 | *A* | *B* | *C* | | | |
| 3 | *A* | *B* | *C* | *D* | | |
| 8 | $k_{ref}$ | *A* | *B* | | | |
| 13 | *A* | *B* | *C* | *D* | *E* | *F* |
| 7 | $k_o$ | | | | | |

**Table 11-3.  Determining the reaction order and consequent unit dimensions for rate constants.**

| Number of Reactants | Reaction Order | Concentration Unit Dimension | Time Unit Dimension |
|---|---|---|---|
| 0 | Zero | None | $Time^{-1}$ |
| 1 | First | None | $Time^{-1}$ |
| 2 | Second | $Concentration^{-1}$ | $Time^{-1}$ |
| 3 | Third | $Concentration^{-2}$ | $Time^{-1}$ |

RTRAC checks to ensure that it is reading its own input point source file.  RTRAC and host model point source files must have the same number of sources in the same order; however, the list of species on each file may be different, and the sources flagged to receive the PiG treatment may vary.  A pre-processor program was coded to help prepare consistent RTRAC and host model point source files.

Tracers released from PiG sources decay according to the oxidant and photolytic environment of the plume using user-supplied chemical rate parameters (as described earlier).  Oxidant concentrations for the decay calculation are obtained from the CAMx PiG incremental photochemical simulation for each puff at each time step.  RTRAC tracers in each puff reactor are updated based on the *total* oxidant concentrations for the reactor, i.e., puff increment plus puff ambient/background.  RTRAC enforces a rule that no secondary tracer formation from the decay of host model species are allowed if IRON PiG is active (e.g., no secondary formaldehyde tracer formation is allowed with IRON PiG).  Secondary tracer production from primary tracer decay is allowed.

Tracers are transferred from the PiG to the grid using the same approach as for any other host model species (see Section 6).  Tracer concentrations at any point are the superposition of the grid concentration plus any collocated PiG puffs.

### 11.3.1  Integration of RTRAC Puff Sampling

RTRAC optionally employs surface-layer IRON puff sampling of tracers on a user-defined sampling grid (see Section 6).  Sampling grids are entirely passive, and intended to provide a display of the reactive tracer plume concentrations at scales much smaller than typically used for the finest computational grids (i.e., <1 km).

Figure 11-5 shows an example plume of hypothetical tracer "TRAC1" emitted from a point source in the center of the image as displayed on a 1-km sampling grid.  The finest core model computational mesh contains 4-km grid spacing and covers a much broader area than shown in the figure.
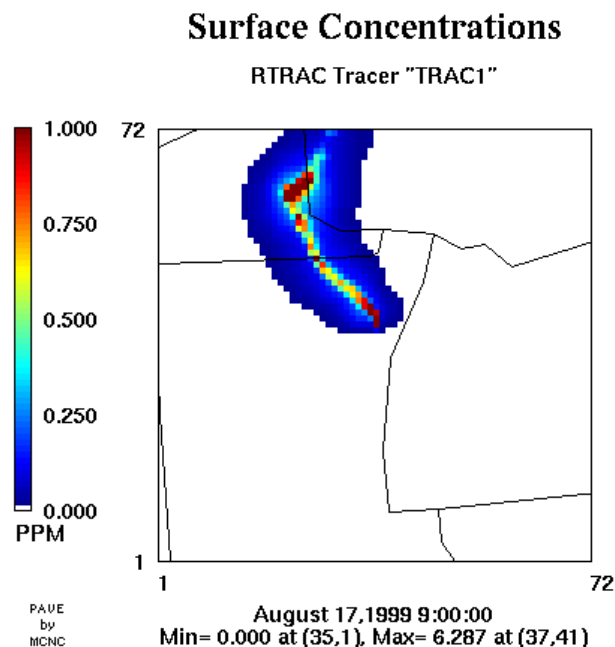


**Figure 11-5.  Example RTRAC tracer plume emanating from a large point source and displayed on a surface sampling grid with 1-km grid spacing.  The figure illustrates the entire extent of the sampling grid.**

## 11.4  Running CAMx With Reactive Tracers

### 11.4.1  CAMx Control File

RTRAC is invoked similarly to the other Probing Tools within the CAMx control file.  In the `&CAMx_Control` namelist module, the variable `Probing_Tool` must be set to "RTRAC" or "RTCMC".  An additional namelist module called `&RT_Control` must then be provided in the control file to configure the RTRAC portion of the model.  The additional namelist module is described below. The order of the variables follows the template available with the source code.  Figure 11-6 provides an example of the RTRAC control module.

**Description of RTRAC Control in the CAMx Run Control File**

| | |
|---|---|
| `&RT_Control` | Label for the Probing Tool namelist module that configures the RTRAC option; it must begin in column 2 |
| `&` | Flag ending a namelist; it must be in column 2 |
| `RT_File_Root` | Character root output path/filename |
| `RT_Initial_Conditions` | Character input master grid RTRAC initial conditions path/filename (optional, ignored if `Restart=TRUE`) |
| `RT_Boundary_Conditions` | Character input master grid RTRAC boundary conditions path/filename (optional) |
| `RT_Master_Restart` | Character input master grid RTRAC restart path/filename (ignored if `Restart=FALSE`) |
| `RT_Nested_Restart` | Character input nested grid RTRAC restart path/filename (ignored if `Restart=FALSE` or `Number_of_Grids=1`) |
| `RT_Chemistry_Parameters` | Character input RTRAC chemistry parameters path/filename, or RTCMC IMC chemistry definition path/filename |
| `RT_Receptor_Definitions` | Character input RTRAC receptor definition path/filename (optional) |
| `RT_Point_Sources` | Character input RTRAC elevated point source emissions path/filename (optional, ignored if `Point_Emissions=FALSE`) |
| `RT_Emiss_Grid` | Character array (by CAMx grid) input RTRAC gridded emissions path/filename (optional, ignored if `Gridded_Emissions=FALSE`) |
| `RT_PiG_Sample` | Logical sampling grid flag for RTRAC IRON PiG output; sampling grids are defined in the main `&CAMx_Control` namelist (TRUE=sampling grid output will be generated, FALSE=sampling grid output will not be generated) |

```
&RT_Control

 RT_File_Root              = 'CAMx6.test.020614',

 RT_Initial_Conditions    = ' ',
 RT_Boundary_Conditions   = ' ',
 RT_Master_Restart        = 'CAMx6.test.020613.rt.inst',
 RT_Nested_Restart        = 'CAMx6.test.020613.rt.finst',

 RT_Chemistry_Parameters  = 'CAMx6.chemparam.rtrac_test',
 RT_Receptor_Definitions  = 'receptor.rtrac.test',
 RT_Point_Sources         = 'pt.rtrac.test',
 RT_Emiss_Grid(1)         = 'emiss.rtrac.36km',
 RT_Emiss_Grid(2)         = 'emiss.rtrac.12km',
 RT_Emiss_Grid(3)         = 'emiss.rtrac.04km',

 RT_PiG_Sample            = .true.,

 &
```

**Figure 11-6.  Example input of RTRAC options and filenames within the CAMx control file.**

As with the output for the host model and other Probing Tools, a "root" file name is specified and suffixes are added depending upon the type of output produced.  A separate root name for RTRAC (and other Probing Tools) allows the user to direct the output to a completely different path.  RTRAC writes several output files that are in Fortran binary format, as described in Section 3.  These include the master and nested grid tracer instantaneous concentration files (`.rt.inst` and `.rt.finst`), the grid-specific surface tracer average concentration file (`.rt.surf.grd`*nn*).  These files are written in the same format as for the regular model species described in Section 3.

The "`RT_Chemistry_Parameter`" namelist variable specifies the path/filename of either the RTRAC chemistry parameters file or the RTCMC IMC chemistry definition file.  The choice of which type of file format is read is set according the main "`Probing_Tool`" variable (i.e., `RTRAC` or `RTCMC`).

RTRAC/IRON PiG sampling grids are invoked in the RTRAC namelist by setting a logical flag.  If set to TRUE, the user must provide the number of sampling grids and the grid parameters of each in the main `&CAMx_Control` namelist.  Sampling grids are set identically to the way nested grids are specified for the host model, with one exception: there are no vertical levels to define (sampling grids are currently only 2-D surface fields).  The same rules that apply for the specification of nested grids holds for the specification of all sampling grids (see Sections 3, 4, and 6 of the User's Guide).  The "mesh factor" sets the resolution or cell size of the sampling

grid relative to the master grid.  The CAMx diagnostic output file provides information on the location and size of each sampling grid to help ensure proper setup.

## 11.4.2  User Adjustable Parameters

Once the RTRAC/RTCMC chemistry parameters/definition file is established, the user should be sure that a sufficient allocation of memory is provided for this Probing Tool.  This is done by examining the main Probing Tool parameter and common block file in `Includes/camx.prm`.  The parameter `MXTRSP` should be set to the total number of species defined in the chemistry parameters file.  If sampling grids are to be used, the user should ensure that sufficient memory is available to define the size of sampling grid arrays.  This is also set in `Includes/camx.prm`.

User adjustable parameters for RTCMC are set in the CAMx include file `Includes/rtcmcchm.inc`.  If an error is encountered at model start up because one of these RTCMC parameter has been exceeded, consult the list of parameters in Table 11-4 and then change the parameter appropriately in the `rtcmcchm.inc` include file.  Rebuild the CAMx executable (we recommend performing a "`make clean`" before making a new CAMx executable) after changing any RTCMC parameter.

**Table 11-4.  RTCMC parameters default settings in the `Includes/rtcmcchm.inc` include file.**

| Name | Description | Default |
|---|---|---|
| MXRX | maximum number of RTCMC reactions | 20 |
| MXPHOT | maximum number of photolysis reactions | 10 |
| MXZEN | maximum number of photolysis reaction zenith angles | 15 |
| MXRCT | Maximum number of reactants in each reaction | 3 |
| MXPRD | maximum number of products in each reaction | 20 |
| MXEQM | maximum number of equilibrium species | 5 |
| MXSLO | maximum number of slow species | 25 |

## 12. REFERENCES

Anthes, R.A. and T.T. Warner. 1978. Development of Hydrodynamic Models Suitable for Air Pollution and Other Mesometeorological Studies. *Mon. Wea. Rev.*, **106**, 1045-1078.

Ariya, P.A., A. Khalizov and A. Gidas. 2002. Reactions of gaseous mercury with atomic and molecular halogens: kinetics, product studies, and atmospheric implications. *J. Phys. Chem.*, **106**, 7310-7320.

Archibald, A.T., M.C. Cooke, S.R. Utembe, D.E. Shallcross, R.G. Derwent, M.E. Jenkin. 2010. Impacts of mechanistic changes on HOx formation and recycling in the oxidation of isoprene. *Atmos. Chem. Phys.*, **10**, 8097-8118, doi:10.5194/acp-10-8097-2010.

Atkinson, R.A., D.L. Baulch, R.A. Cox, J.N. Crowley, R.F. Hampson, R.G. Hynes, M.E. Jenkin, J.A. Kerr, M.J. Rossi, J. Troe. 2010. "Evaluated kinetic and photochemical data for atmospheric chemistry - IUPAC subcommittee on gas kinetic data evaluation for atmospheric chemistry." January 3, 2010 web version available at http://www.iupac-kinetic.ch.cam.ac.uk/index.html.

Bloss, C., V. Wagner, M.E. Jenkin, R. Volkamer, W.J. Bloss, J.D. Lee, D.E. Heard, K. Wirtz, M. Martin-Reviejo, G. Rea, J.C. Wenger, M.J. Pilling. 2005. Development of a detailed chemical mechanism (MCMv3.1) for the atmospheric oxidation of aromatic hydrocarbons. *Atmo. Chem. Phys.*, **5**, 641–644.

Bott, A. 1989. A Positive Definite Advection Scheme Obtained by Nonlinear Renormalization of the Advective Fluxes. *Mon. Wea. Rev.,* **117**, 1006-1015.

Calvert, J.G., R. Atkinson, J.A. Kerr, S. Madronich, G.K. Moortgat, T.H. Wallington and G. Yarwood. 2000. *The Mechanisms of Atmospheric Oxidation of the Alkenes*. Oxford University Press, New York, New York.

Calvert, J.G., R. Atkinson, K.H. Becker, R.M. Kamens, J.H. Seinfeld, T.H. Wallington and G. Yarwood. 2002. *The Mechanisms of Atmospheric Oxidation of the Aromatic Hydrocarbons*. Oxford University Press, New York, New York.

Carlton, A.G., B.J. Turpin, K.E. Altieri, S. Seitzinger, A. Reff, H.-J. Lim, B. Ervens. 2007. Atmospheric oxalic acid and SOA production from glyoxal: Results of aqueous photooxidation experiments. *Atmos. Environ.,* **41**, 7588-7602.

Carpenter, L.J. 2003. Iodine in the marine boundary layer. *Chemical Reviews*, **103**, 4953-4962.

Carter, W.P.L. 1994. Development of ozone reactivity scales for volatile organic compounds. *J. Air & Waste Manage. Assoc.*, **44**, 881-899.

Carter, W.P.L. 1996. Condensed Atmospheric Photooxidation Mechanisms for Isoprene. *Atmos. Environ.,* **30**, 4275-4290.

Carter, W.P.L. 2000. Programs and Files Implementing the SAPRC-99 Mechanism and its Associates Emissions Processing Procedures for Models-3 and Other Regional Models. January 31, 2000. http://pah.cert.ucr.edu/~carter/SAPRC99.htm.

Carter, W.P.L, G.S. Tonnesen, and G. Yarwood. 2002. Investigation of VOC Reactivity Effects in Existing Regional Air Quality Models. Draft Report to American Chemistry Council for the NARSTO Reactivity Research Working Group. September.

Chang, J.S., R.A. Brost, I.S.A. Isaksen, S. Madronich, P. Middleton, W.R. Stockwell, and C.J, Walcek. 1987. A Three-dimensional Eulerian Acid Deposition Model: Physical Concepts and Formulation. *J. Geophys. Res.*, **92**, 14,681-14,700.

Chock, D.P., S.L. Winkler, and P. Sun. 1994. Comparison of stiff chemistry solvers for air quality models. *Environ. Sci. Technol.*, **28**, 1882-1892.

Clever, H., S.A. Johnson and E.M. Derrick. 1985. The solubility of mercury and some sparingly soluble mercury salts in water and aqueous solutions. *J. Phys. Chem. Ref. Data*, **14**, 631-680.

Cohan, D. S., A. Hakami, Y. Hu, and A. G. Russell. 2005. Nonlinear Response of Ozone to Emissions: Source Apportionment and Sensitivity Analysis. *Environ. Sci. Technol.*, **39**, 6739-6748.

Colella, P., and P.R. Woodward. 1984. The Piecewise Parabolic Method (PPM) for Gas-dynamical Simulations. *J. Comp. Phys.*, **54**, 174-201.

Del Genio, A.D., M.S. Yao, W. Kovari, K.K.W. Lo. 1996. A prognostic cloud water parameterization for global climate models. *J. Climate*, **9**, 270-304.

Dunker, A. M. 1980. The response of an atmospheric reaction-transport model to changes in input functions. *Atmos. Environ*., **14**, 671-679.

Dunker, A.M. 1981. Efficient calculations of sensitivity coefficients for complex atmospheric models. *Atmos. Environ*. **15**, 1155-1161.

Dunker A.M., G. Yarwood, J.P. Ortmann, G.M. Wilson. 2002a. The decoupled direct method for sensitivity analysis in a three-dimensional air quality model – implementation, accuracy and efficiency. *Environ. Sci. Technol.*, **36,** 2965-2976.

Dunker A.M., G. Yarwood, J.P. Ortmann, G.M. Wilson. 2002b. Comparison of source apportionment and source sensitivity of ozone in a three-dimensional air quality model. *Environ. Sci. Technol.*, **36,** 2953-2964.

Edgerton, E.S., B.E. Hartsell and J.J. Jansen. 2001. Atmospheric mercury measurements at a rural and urban site near Atlanta, GA, USA. *6th International Conference on Mercury as a Global Pollutant*, 15-19 October 2001, Minamata, Japan.

Elbern, H. and H. Schmidt. 1999. A four-dimensional variational chemistry data assimilation scheme for Eulerian chemistry transport modeling. *J. Geophys. Res.*, **104**, 18583-18598.

Elterman, L. 1968. "UV, Visible, and IR Attenuation for Altitudes to 50 km, 1968." US Air Force Cambridge Research Laboratory Report, AFCRL 68-0153.

Emery, C., J. Jung, J. Johnson, G. Yarwood, S. Madronich, G.Grell.  2010.  Improving the Characterization of Clouds and their Impact on Photolysis Rates within the CAMx Photochemical Grid Model.  Prepared for the Texas Commission on Environmental Quality, Austin, TX.  Prepared by ENVIRON International Corporation, Novato, CA (August 27, 2010).

ENVIRON. 2002.  Development, Application, and Evaluation of an Advanced Photochemical Air Toxics Modeling System.  Prepared for the Coordinating Research Council, Alpharetta, GA, and the U.S. Department of Energy, Office of Heavy Vehicle Technologies (September 27, 2002).  Available from www.crcao.com.

EPA.  1990.  User's Guide for the Urban Airshed Model-Volume I; User's Manual for UAM(CB-IV).  U.S. Environmental Protection Agency, Research Triangle Park, NC, EPA-450/4-90-007a.

EPA.  1998.  User's Guide for the AERMOD Meteorological Preprocessor (Revised Draft).  Prepared by the U.S. Environmental Protection Agency, Research Triangle Park, NC (November, 1998).

EPRI.  2000.  SCICHEM Version 1.2: Technical Documentation.  Final Report prepared by ARAP/Titan Corporation, Princeton, NJ, for EPRI, Palo Alto, CA.  December 2000 (1000713).

Fahey, K.M. and S.N. Pandis. 2001.  Optimizing model performance: variable size resolution in cloud chemistry modeling.  *Atmos. Environ.* **35**, 4471-4478.

FLAG.  2000.  "Federal Land Managers' Air Quality Related Values Workgroup (FLAG), Phase I Report."  Prepared by the US Forest Service, Air Quality Program; National Park Service, Air Resources Division; and US Fish and Wildlife Service, Air Quality Branch (December 2000).

Gallagher, W.M., K.M. Beswick, J. Duyzer, H. Westrate, T.W. Choularton, J.P. Hummelsho.  1997.  Measurements of aerosol fluxes to Speulder forest using a micrometeorological technique.  *Atmos. Environ.*, **31**, 359 – 373.

Ganzeveld, L., D. Helmig, C. W. Fairall, J. Hare, and A. Pozzer.  2009.  Atmosphere-ocean ozone exchange: A global modeling study of biogeochemical, atmospheric, and waterside turbulence dependencies.  *Global Biogeochem. Cycles*, **23**, GB4021, doi:10.1029/2008GB003301.

Gardfeldt, K. and M. Johnson.  2003.  Is bimolecular reduction of Hg(II) complexes possible in aqueous systems of environmental importance?  *J. Phys. Chem.*, **107**, 4478-4482.

Gear, C.W.  1971.  *Numerical Initial Value Problems in Ordinary Differential Equations.*  Prentice-Hall, Englewood Cliffs, NJ.

Gery, M.W., G.Z. Whitten, J.P. Killus, and M.C. Dodge.  1989.  A Photochemical Kinetics Mechanism for Urban and Regional Scale Computer Modeling.  *J. Geophys. Res.*, **94**, 925-956.

Gillani, N. V. and J. E. Pleim.  1996.  Sub-grid-scale Features of Anthropogenic Emissions of $NO_X$ and VOC in the Context of Regional Eulerian Models.  *Atmos. Environ.,* **30**, 2043-2059.

Hairer, E., and G. Wanner.  1991.  "Solving ordinary differential equations II Stiff and differential-algebraic problems." Springer-Verlag, Berlin.

Hakami, A., M. T. Odman, and A. G. Russell.  2003.  High-order, direct sensitivity analysis of multidimensional air quality models.  *Environ. Sci. Technol.*, **37**, 2442-2452.

Hall, B.  1995.  The gas-phase oxidation of elemental mercury by ozone.  *Water Air Soil Pollut.*, **80**, 301-315.

Harley R. A., and G. R. Cass.  1995.  Modeling the Atmospheric Concentrations of Individual Volatile Organic Compounds.  *Atmos. Environ*. **29**, No. 8, 905-922.

Helmig, D., E.K. Lang, L. Bariteau, P. Boylan, C.W. Fairall, L. Ganzeveld, J.E. Hare, J. Hueber, M. Pallandt.  2012.   Atmospherie-ocean ozone fluxes during the TexAQS 2006, STRATUS 2006, GOMECC 2007, GasEx 2008 and AMMA 2008 Cruises.  *J. Geophys. Res.*, **117**, D04305, doi:10.1029/2011JD015955.

Herman, J.R. and E. A. Celarier.  1997.  Earth surface reflectivity climatology at 340-380 nm from TOMS data.  *J. Geophys. Res.*, **102**, No. 23.

Hertel O., R. Berkowics, J. Christensen and O. Hov.  1993.  Test of two numerical schemes for use in atmospheric transport-chemistry models.  *Atmos. Env.*, **27**, 2591-2611.

Hesstvedt, E., Hov, O., and Isaksen, I. S. A.  1978.  Quasi-steady state approximation in air pollution modeling: comparison of two numerical schemes for oxidant prediction. *Int. J. Chem. Kin.*, **10**, 4148-4156.

Hindmarsh, A.C.  1980.  "LSODE and LSODI, two new initial value ordinary differential equation solvers."  ACM SIGNUM Newsletter, Volume 15 ,  Issue 4  (December).

Hindmarsh, A.C.  1983.  ODEPACK, a Systematized Collection of ODE Solvers.  In *Numerical Methods for Scientific Computation,* **55**, R.S. Stepleman, Ed., North-Holland, New York.

Holmes, C.D., D.J. Jacob, and X. Yang.  2006.  Global lifetime of elemental mercury against oxidation by atomic bromine in the free troposphere.  *Geophys. Res. Lett.*, **33**, L20808, doi:10.1029/2006GL027176.

Holtslag, A.A.M, and B.A. Boville.  1993.  Local versus non-local boundary layer diffusion in a global climate model.  *J. Climate*, **6**, 1825-1842.

Hu, D., M. Tolocka, Q. Li, R.M. Kamens.  2007.  A kinetic mechanism for predicting secondary organic aerosol formation from toluene oxidation in the presence of NOx and natural sunlight.  *Atmos. Environ.*, **41**, 6478–6496.

Huebert, B.J., and C.H. Robert.  1985.  The Dry Deposition of Nitric Acid to Grass.  *J. Geophys. Res.*, **90**(D1), 2085-2090 (doi:10.1029/JD090iD01p02085).

IUPAC.  1992.  Evaluated Kinetic and Photochemical Data for Atmospheric Chemistry. Supplement IV.  IUPAC Subcommittee on Gas Kinetic Data Evaluation for Atmospheric Chemistry (R. Atkinson, D.L. Baulch, R. A. Cox, R. F. Hampson, Jr., J. A. Kerr, and J. Troe). *Journal of Physical and Chemical Reference Data,* **21**, No. 6, 1125-1568.

IUPAC.  2001.  Evaluated kinetic and photochemical data for atmospheric chemistry.  IUPAC Subcommittee for Gas Kinetic Data Evaluation.  Available at http://www.iupac-kinetic.ch.cam.ac.uk/index.html.  December, 2001.

Jacob, D.J.  2000.  Heterogeneous chemistry and tropospheric ozone.  *Atmos. Environ.*, **34**, 2131-2159.

Jaegle, L., D.J. Jacob, W.H. Brune and P.O. Wennberg.  2001.  Chemistry of $HO_x$ radicals in the upper troposphere.  *Atmos. Environ.*, **35**, 469-489.

Jeffries, H. E., and G.S. Tonnesen. 1994.  Comparison of two photochemical reaction mechanisms using a mass balance and process analysis.  *Atmos. Environ.*, **28**, 2991-3003.

JPL.  2001.  Chemical Kinetics and Photochemical Data for Stratospheric Modeling --Evaluation 13.  NASA Jet Propulsion Laboratory publication 00-3.  Available at http://jpldataeval.jpl.nasa.gov.  February, 2001.

Kalberer, M.,  D. Paulson, M. Sax, M. Steinbacher, J. Dommen, A. S. H. Prevot, R. Fisseha, E. Weingartner, V. Franhevich, R. Zenob, and U. Balternsperger.  2004.  Identification of polymers as major components of atmospheric organic aerosols, *Science*, **303**, 1659-1662.

Kleeman, M.J. and G.R. Cass.  2001.  A 3D Eulerian source-oriented model for an externally mixed aerosol.  *Environ. Sci. and Technol.*, **35,** 4834-4848.

Koo, B., A.S. Ansari, and S.N. Pandis.  2003.  Integrated Approaches to Modeling the Organic and Inorganic Atmospheric Aerosol Components.  *Atmos. Environ.*, **37**, 4757-4768.

Kumar, N., F.W. Lurmann, A.S. Wexler, S. Pandis, and J.H. Seinfeld.  1996.  Development and Application of a Three Dimensional Aerosol Model.  Presented at the A&WMA Specialty Conference on Computing in Environmental Resource Management, Research Triangle Park, NC, December 2-4, 1996.

Kumar, N. and A. G. Russell.  1996.  Development of a Computationally efficient, Reactive Sub-Grid-Scale Plume Model and the Impact in the Northeastern United States Using Increasing Levels of Chemical Detail.  *J. Geophys. Res.,* **101**, 16,737-16,744.

Landis, M.S. and G. Keeler.  2002.  Atmospheric mercury deposition to Lake Michigan during the Lake Michigan Mass Balance Study.  *Environ. Sci. Technol.,* **36**, 4518-4524.

Lambert, J. D.  1973.  *Computational Methods in Ordinary Differential Equations.*  John Wiley and Sons Ltd.  New York.

Lin, C.J. and S.O. Pehkonen.  1997.  Aqueous-free radical chemistry of mercury in the presence of iron oxides and ambient aerosol.  *Atmos. Environ.*, **31**, 4125-4137.

Lin, C.J. and S.O. Pehkonen.  1998.  Oxidation of elemental mercury by aqueous chlorine (HOCl/OCl⁻): Implications for tropospheric mercury chemistry.  *J. Geophys. Res.*, **103**, 28093-28102.

Lindberg, S., O.R. Bullock, R. Ebinghaus, D. Engstrom, X. Feng, W. Fitzgerald, N. Pirrone, E. Prestbo, and C. Seigneur.  2007.  A synthesis of progress and uncertainties in attributing the sources of mercury in deposition.  *Ambio*, **36**, 19-33.

Lindqvist, O. and H. Rodhe. 1985. Atmospheric mercury - a review. *Tellus*, **37B**, 136-159.

Liu, M. and J. Carroll. 1996. A high resolution air pollution model suitable for dispersion studies in complex terrain. *Mon. Wea. Rev.*, **124**, 10, 2396-2409.

Louis, J.F. 1979. A Parametric Model of Vertical Eddy Fluxes in the Atmosphere. *Bound. Lay. Meteor.* **17**, 187-202.

Mahajan, A. S., J.M.C., Plane, H. Oetjen, L Mendes, R.W. Saunders, A. Saiz-Lopez, C.E. Jones, L.J. Carpenter, and G.B. McFiggans. 2010. Measurement and modelling of tropospheric reactive halogen species over the tropical Atlantic Ocean. *Atmos. Chem. Phys.*, **10**, 4611-4624, doi:10.5194/acp-10-4611-2010.

Mentel, Th.F., D. Bleilebens and A. Wahner. 1996. A Study of Nighttime Nitrogen Oxide Oxidation in a Large Reaction Chamber -- The Fate of $NO_2$, $N_2O_5$, and $O_3$ at Different Humidities. *Atmos. Environ.,* **30**, 4007–4020.

Menut L., R. Vautard, M. Beekmann, C. Honoré. 2000. Sensitivity of Photochemical Pollution using the Adjoint of a Simplified Chemistry-Transport Model. *Journal of Geophysical Research – Atmospheres,* **105,** (D12) 15,379-15,402.

Moore, R. and Tokarczyk, R. 1993. Volatile Biogenic Halocarbons in the Northwest Atlantic. *Global Biogeochem. Cy.*, **7**, 195–210,

Moore, R. and Zafiriou, O. 1994. Photochemical production of methyl iodide in seawater. *J. Geophys. Res.*, **99**, 16415–16420, doi:10.1029/94JD00786.

Morris, R.E., S. Lau, and G. Yarwood. 2003. "Development and Application of an Advanced Air Toxics Hybrid Photochemical Grid Modeling System." Presented at 96th Annual Conference and Exhibition of the A&WMA, San Diego, California (June 2003).

Munthe, J. 1992. The aqueous oxidation of elemental mercury by ozone. *Atmos. Environ., Part A*, **26**, 1461-1468.

NASA. 1997. Chemical Kinetics and Photochemical Data for Use in Stratospheric Modeling, *JPL Publication 97-4.* Jet Propulsion Laboratory, California Institute of Technology, Pasadena, California. January 15.

NCAR. 2011. The Tropospheric Visible and Ultraviolet (TUV) Radiation Model web page. National Center for Atmospheric Research, Atmospheric Chemistry Division, Boulder, Colorado, http://cprm.acd.ucar.edu/Models/TUV/index.shtml.

Nenes, A, C. Pilinis, and S.N. Pandis. 1998. ISORROPIA: A New Thermodynamic Model for Multiphase Multicomponent Inorganic Aerosols. *Aquatic Geochemistry*, 4, 123-152.

Nenes, A, C. Pilinis, and S.N. Pandis. 1999. Continued Development and Testing of a New Thermodynamic Aerosol Module for Urban and Regional Air Quality Models. *Atmos. Environ*. 33, 1553-1560.

Novelli, P.C., P.M. Lang, K.A. Masarie, D.F. Hurst, R. Myers, and J.W. Elkins. 1999. Molecular hydrogen in the troposphere: global distribution and budget*. J. Geophys. Res.*, **104**, 30: 427-30,444.

Odman, M. T. and Ingram, C. L.  1993.  Multiscale Air Quality Simulation Platform (MAQSIP): Source Code Documentation and Validation.  Technical report, 83 pp., ENV-96TR002, MCNC–North Carolina Supercomputing Center, Research Triangle Park, North Carolina, 1996.

Ordóñez, C., J.-F. Lamarque, S. Tilmes, D.E. Kinnison, E.L. Atlas, D.R. Blake, G. Sousa Santos, G. Brasseur, and A. Saiz-Lopez.  2012.  Bromine and iodine chemistry in a global chemistry-climate model: description and evaluation of very short-lived oceanic sources.  *Atmos. Chem. Phys.*, **12**, 1423-1447, doi:10.5194/acp-12-1423-2012.

Pal, B., and P.A. Ariya.  2003.  Atmospheric reactions of gaseous mercury with ozone and hydroxyl radical: kinetics and product studies.  *J. Phys*, **107**, 189–192.

Pal, B. and P.A. Ariya.  2004.  Gas-phase HO·-initiated reactions of elemental mercury: Kinetics, product studies and atmospheric implications.  *Environ. Sci. Technol.,* **38**, 5555-5566.

Pandis, S.N., A.S. Wexler, and J.H. Seinfeld.  1993.  Secondary organic aerosol formation and transport, II, Predicting the ambient secondary organic aerosol size distribution.  *Atmos. Environ.,* **27A**, 2403-2416.

Paulot, F., J.D. Crounse, H.G. Kjaergaard, J.H. Kroll, J.H. Seinfeld, P.O. Wennberg.  2009a.  "Isoprene photooxidation:  new insights into the production of acids and organic nitrates."  *Atmos. Chem. Phys.*, **9**, 1479-1501.

Paulot, F, J.D. Crounse, H.G. Kjaergaard, A. Kurten, J.M. St.Clair, J.H. Seinfeld, P.O. Wennberg.  2009b.  "Unexpected Epoxide Formation in the Gas-Phase Photooxidation of Isoprene."  *Science*, **325**, 730-733.

Peeters, J., Nguyen, T.L., Vereecken, L., 2009. HOx radical regeneration in the oxidation of isoprene. Physical Chemistry and Chemical Physics 11, 5935-5939

Pehkonen, S.O. and C.J. Lin.  1998.  Aqueous photochemistry of divalent mercury with organic acids.  *J. Air Waste Manage. Assoc.*, **48**, 144-150.

Perring, A.E., A. Wisthaler, M. Graus, P.J. Wooldridge, A.L. Lockwood, L.H. Mielke, P.B. Shepson, A. Hanset, R.C. Cohen.  2009.  "A product study of the isoprene+NO3 reaction."  *Atmos. Chem. Phys.*, **9**, 4945-4956.

Pleim, J.  2007.  "A combined local and nonlocal closure model for the atmospheric boundary layer.  Part I: Model description and testing."  *J. Appl. Met. and Clim.*, **46**, 1383-1395.

Radhakrishnan, K. and A.C.  Hindmarsh. 1993.  *Description and Use of LSODE, the Livermore Solver for Ordinary Differential Equations*.  NASA reference Publication 1327.  Lawrence Livermore National Laboratory, Livermore, CA.

Raofie, F. and P.A. Ariya.  2003.  Reactions of BrO with mercury: kinetic studies.  *J. Phys. IV*, **107**, 1119–1121.

Raymond, W. and R. Stull.  1990.  Application of Transilient Turbulence Theory to Mesoscale Numerical Weather Forecasting.  *Mon. Wea. Rev.*, **118**, 2471-2499.

Ruijgrok, W., C.I. Davidson, K.W. Nicholson. 1995. Dry deposition of particles – implications and recommendations for mapping of deposition over Europe. *Tellus*, **47B**, 587 – 601.

Russell, L.M., S.N. Pandis, and J.H. Seinfeld. 1994. Aerosol production and growth in the marine boundary layer. *J. Geophys. Res.,* **99**, 20989-21003.

Rutter, A.P., and J.J. Schauer. 2007a. The effect of temperature on the gas-particle partitioning of reactive mercury in atmospheric aerosols. *Atmos. Environ.*, **41**, 8647-8657.

Rutter, A.P.; Schauer, J.J. 2007. The impact of aerosol composition on the particle to gas partitioning of reactive mercury. *Environ. Sci. Technol.*, **41**, 3934-3939.

Ryaboshapko, A., R. Bullock, R. Ebinghaus, I. Ilyin, K. Lohman, J. Munthe, G. Petersen, C. Seigneur and I. Wängberg. 2002. Comparison of mercury chemistry models. *Atmos. Environ.*, **36**, 3881-3898.

Sanemasa, I. 1975. The solubility of elemental mercury vapor in water. *Bull. Chem. Soc. Jpn.*, **48**, 1795-1798.

Schroeder, W.H. and J. Munthe. 1998. Atmospheric mercury – An overview. *Atmos. Environ.*, **32**, 809-822.

Scott, B.C. 1978. Parameterization of sulfate removal by precipitation. J. Appl. Meteor., 17, 1375-1389

Sehmel, G.A. 1980. Particle and Gas Deposition, a Review. *Atmos. Environ.,* **14**, 983-1011.

Seigneur, C., H. Abeck, G. Chia, M. Reinhard, N.S. Bloom, E. Prestbo and P. Saxena. 1998. Mercury adsorption to elemental carbon (soot) particles and atmospheric particulate matter. *Atmos. Environ.*, **32**, 2649-2657.

Seigneur, C., P. Karamchandani, K. Lohman, K. Vijayaraghavan and R.-L. Shia. 2001a. Multiscale modeling of the atmospheric fate and transport of mercury. *J. Geophys. Res*., **106**, 27795-27809.

Seigneur, C., P. Karamchandani, K. Lohman and J. Jansen. 2001b. Modeling of mercury in power plant plumes. *6$^{th}$ International Conference on Mercury as a Global Pollutant*, 15-19 October 2001, Minamata, Japan.

Seigneur, C., K. Vijayaraghavan, K. Lohman and P. Karamchandani. 2003a. Modeling the atmospheric fate and transport of mercury over North America. *Fuel Processing Technol*., in press.

Seigneur, C., P. Karamchandani, K. Vijayaraghavan, K. Lohman and G. Yelluru. 2003d. *Scoping Study for Mercury Deposition in the Upper Midwest.* AER Report CP149-03-01a, prepared for the Midwest Regional Planning Organization, Des Plaines, IL.

Seigneur, C. and K. Lohman. 2008. Effect of bromine chemistry on the atmospheric mercury cycle. *J. Geophys. Res.*, **113**, D23309, doi:10.1029/2008JD010262.

Seinfeld, J.H., and S.N. Pandis. 1998. *Atmospheric Chemistry and Physics, From Air Pollution to Climate Change*. John Wiley and Sons, Inc., NY.

Sillen, G.L. and A.E. Martell, (Eds.).  1964.  Stability constants of metal ion complexes, *Spec. Publ. Chem. Soc.*, **17**, 754.

Sillman, S.  1995.  The Use of $NO_y$, $H_2O_2$, and $HNO_3$ as Indicators for Ozone - $NO_X$-Hydrocarbon Sensitivity in Urban Locations.  *J. Geophys. Res.*, **100**, 14,175-14,188.

Slinn, S.A. and W.G.N. Slinn.  1980.  Predictions for particle deposition on natural waters. *Atmos. Environ.*, **24**, 1013-1016.

Slinn, W.G.N.  1982.  Predictions for particle deposition to vegetative surfaces. Atmos. Environ., **16**, 1785-1794.

Smagorinsky, J.  1963.  General Circulation Experiments with the Primitive Equations: I. The Basic Experiment.  *Mon. Wea. Rev.*, **91**, 99-164.

Sommar, J., K. Gårdfeldt, D. Strömberg and X. Feng.  2001.  A kinetic study of the gas-phase reaction between the hydroxyl radical and atomic mercury.  *Atmos. Environ.*, **35**, 3049-3054.

Sommariva R., W.J. Bloss, and R. von Glasow.  2012.  Uncertainties in gas-phase atmospheric iodine chemistry.  *Atmospheric Environment*, **57**, 219–232, doi:10.1016/j.atmosenv.2012.04.032.

Strader, R., C. Gurciullo, S.N. Pandis, N. Kumar, and F.W. Lurmann.  1998.  Development of gas-phase chemistry, secondary organic aerosol, and aqueous-phase chemistry modules for PM modeling.  Final report for CRC Project A21-1 prepared for the Coordinating Research Council, Atlanta, GA by Sonoma Technology, Inc., Petaluma, CA, STI-97510-1822-FR, October.

Strader, R., F. Lurmann, and S.N. Pandis.  1999.  Evaluation of secondary organic aerosol formation in winter.  *Atmos. Environ.,* **33**, 4849-4863.

Sun, P., D.P. Chock, and S.L. Winkler.  1994.  An Implicit-Explicit Hybrid Solver for a System of Stiff Kinetic Equations.  *J. Comp. Phys.,* **115**.

Takamura, T., T. Nakajima, O. Dubovik, B.N. Holben, S. Kinne.  2002.  Single-scattering albedo and radiative forcing of various aerosol species with a global three-dimensional model. J. Climate, 15(4), 333-352.

Tanaka, P.L., D.T. Allen, E.C. McDonald-Buller, S. Chang, Y. Kimura, C.B. Mullins, G. Yarwood, J.D. Neece.  2000.  Development of a chlorine mechanism for use in the carbon bond IV chemistry model.  *Journal of Geophysical Research*. Vol. 108(D4), 4145.

Tokos, J.J.S., B. Hall, J.A. Calhoun, and E.M. Prestbo.  1998.  Homogeneous gas-phase reaction of $Hg^0$ with $H_2O_2$, $O_3$, $CH_3I$, and $(CH_3)_2S$: Implications for atmospheric Hg cycling.  *Atmos. Environ.*, **32**, 823-827.

Tonnesen, G.S. and R.L. Dennis.  2000.  Analysis of radical propagation efficiency to assess ozone sensitivity to hydrocarbons and NOx.  Part 1: Local indicators of odd oxygen production sensitivity.  *J. Geophys. Res.*, **105**, 9213-9225.

Tonnesen G. and B. Wang.  2004.  CMAQ Tagged Species Source Apportionment, July 22, 2004; http://www.wrapair.org/forums/aoh/meetings/040722/UCR_tssa_tracer_v2.ppt.

Turner, D.B., T. Chico, and A. Catalano.  1986.  TUPOS: A Multiple Source Gaussian Dispersion Algorithm Using On-Site Turbulence Data.  U.S Environmental Protection Agency, Research Triangle Park, North Carolina (EPA-600/8-86/010).

Turner, D.B. and R.H. Schulze.  2007.  *Practical Guide to Atmospheric Dispersion Modeling*.  Air and Waste Management Association.

van Loon, L., E. Mader, and S.L. Scott.  2000.  Reduction of the aqueous mercuric ion by sulfite: UV spectrum of $HgSO_3$ and its intramolecular redox reactions.  *J. Phys. Chem.*, **104**, 1621-1626.

van Loon, L.L., E.A. Mader, and S.L. Scott.  2001.  Sulfite stabilization and reduction of the aqueous mercuric ion: kinetic determination of sequential formation constants.  *J. Phys. Chem.*, **105**, 3190-3195.

Vijayaraghavan, K., P. Karamchandani, C. Seigneur, R. Balmori, and S.-Y. Chen.  2008.  Plume-in-grid modeling of atmospheric mercury.  *J. Geophys. Res.*, **113**, D24305, doi:10.1029/2008JD010580.

Voulgarakis, A., N.H. Savage, O. Wild, G.D. Carver, K.C. Clemitshaw, J.A. Pyle.  2009.  Upgrading photolysis in the p-TOMCAT CTM: model evaluation and assessment of the role of clouds.  *Geoscientific Model Development*, **2**, 59-72.

Wang, Y., et al.  2003.  Springtime photochemistry at northern mid and high latitudes.  *J. Geophys. Res.*, **108(**D4), 8358.

Wang, Z., J. E. Langstaff, and H.E. Jeffries.  1995.  The Application of the Integrated Process Rate Analysis Method for Investigation of Urban Airshed Model (UAM) Sensitivity to Speciation in VOC Emissions Data.  Air & Waste Management Association annual meeting, San Antonio, TX.

Warneck, P.  1989.  *The Chemistry of the Natural Atmosphere*.  Academic Press, New York, NY.

Wesely, M.L.  1989.  Parameterization of Surface Resistances to Gaseous Dry Deposition in Regional-Scale Numerical Models.  *Atmos. Environ.*, **23**, 1293-1304.

Wesely, M.L., and B.B. Hicks.  2000.  A review of the current status of knowledge on dry deposition.  *Atmos. Environ.*, **34**, 2261.

Whitten, G., H.P. Deuel, C.S. Burton, and J.L. Haney.  1996.  Memorandum to OTAG Participants "Overview of the Implementation of an Updated Isoprene Chemistry Mechanism in CB4/UAM-V." (Revised Memorandum, July 22).

Whitten, G.Z., G. Heo, Y. Kimura, E. McDonald-Buller, D.T. Allen, W.P.I. Carter, , G. Yarwood.  2010.  "A New Condensed Toluene Mechanism for Carbon Bond: CB05-TU." *Atmos. Environ.*, doi: 10.1016/j.atmosenv.2009.12.029.

Yamartino, R.  2000.  Refinement of Horizontal Diffusion in Photochemical Grid Models.  Presented at the American Meteorological Society 11th Joint Conference on the Applications of Air Pollution Meteorology with the Air and Waste Management Association, Long Beach, CA, January 9-13.

Yang, Y.J., J.G. Wilkinson, and A.G. Russell, 1997: Fast direct sensitivity analysis of multidimensional photochemical models, *Environ. Sci. Technol.*, **31**, 2859-2868.

Yarwood, G., R.E. Morris, M.A. Yocke, H. Hogo and T. Chico. 1996. Development of a Methodology for Source Apportionment of Ozone Concentration Estimates from a Photochemical Grid Model. Presented at the 89th AWMA Annual Meeting, Nashville TN, June 23-28.

Yarwood, G., T.E. Stoeckenius, G. Wilson, R.E. Morris, and M.A. Yocke. 1996. Development of a Methodology to Assess Geographic and Temporal Ozone Control Strategies for the South Coast Air Basin. Prepared for South Coast Air Quality Management District, Diamond Bar, CA.

Yarwood, G., T.E. Stoeckenius, J.G. Heiken, A.M. Dunker. 2003. Modeling Weekday/Weekend Ozone Differences in the Los Angeles Region for 1997. *J. Air & Waste Manage. Assoc.*, **53**, 864.

Yarwood, G., R.E. Morris, G.M. Wilson. 2004. Particulate Matter Source Apportionment Technology (PSAT) in the CAMx Photochemical Grid Model. Proceedings of the 27th NATO/ CCMS International Technical Meeting on Air Pollution Modeling and Application. Springer Verlag (Available from http://camx.com/publ/pdfs/_____Yarwood_ITM_paper.pdf).

Yarwood. G., G.Z. Whitten, and S. Rao. 2005a. "Updates to the Carbon Bond 4 Photochemical Mechanism." Prepared for the Lake Michigan Air Directors Consortium, Des Plains, Illinois.

Yarwood. G., S. Rao, M. Yocke, and G.Z. Whitten. 2005b. Updates to the Carbon Bond chemical mechanism: CB05. Final Report prepared for US EPA. Available at http://www.camx.com/publ/pdfs/CB05_Final_Report_120805.pdf.

Yarwood, G., J. Jung, G. Z. Whitten, G. Heo, J. Mellberg and E. Estes. 2010. "Updates to the Carbon Bond Mechanism for Version 6 (CB6)." Presented at the 9th Annual CMAS Conference, Chapel Hill, October.

Yarwood, G., H. Gookyoung, W.P.L. Carter, G.Z. Whitten. 2012a. "Environmental Chamber Experiments to Evaluate NOx Sinks and Recycling in Atmospheric Chemical Mechanisms." Final Report prepared for the Texas Air Quality Research Program, University of Texas, Austin, Texas (AQRP Project 10-042, February 2012).

Yarwood, G., J. Jung, U. Nopmongcol, C. Emery. 2012b. "Improving CAMx Performance in Simulating Ozone Transport from the Gulf of Mexico." Final Report prepared for the Texas Commisision on Environmental Quality, Austin, Texas (September 2012).

Zaveri, R.A. and L.K. Peters. 1999. A new lumped structure photochemical mechanism for large-scale applications. *J. Geophys. Res.*, **104**, 30387-30416.

Zhang, L., S. Gong, J. Padro, L. Barrie. 2001. A size-segregated particle dry deposition scheme for an atmospheric aerosol module. *Atmos. Environ.*, **35**, 549-560.

Zhang, L., J. R. Brook, and R. Vet. 2003. A revised parameterization for gaseous dry deposition in air-quality models. *Atmos. Chem. Phys.*, **3**, 2067–2082.

Zhang, X., S. Kondragunta, C. Schmidt, and F. Kogan.  2008.  Near real time monitoring of biomass burning particulate emissions (PM2.5) across contiguous United States using multiple satellite instruments.  *Atmospheric Environment,* **42**, 6959-6972.

# Appendix A

# CAMx Mechanism 5

# SAPRC99 Gas-Phase Chemistry

## Table A-1.  Reactions and rate constants for the SAPRC99 mechanism (Mechanism 5).

| Reaction Number | Reactants | Products | $k_{298}$[1] $(ppm^{-n} min^{-1})$ |
|---|---|---|---|
| 1 | NO2 | NO + O | Photolysis |
| 2 | O + O2 + M | O3 + M | 2.105E-05 |
| 3 | O + O3 | 2O2 | 1.175E+01 |
| 4 | O + NO + M | NO2 + M | 3.676E-03 |
| 5 | O + NO2 | NO + O2 | 1.435E+04 |
| 6 | O + NO2 | NO3 | 2.690E+03 |
| 7 | O3 + NO | NO2 + O2 | 2.682E+01 |
| 8 | O3 + NO2 | O2 + NO3 | 5.202E-02 |
| 9 | NO + NO3 | 2NO2 | 3.849E+04 |
| 10 | NO + NO + O2 | 2NO2 | 7.104E-10 |
| 11 | NO2 + NO3 | N2O5 | 2.268E+03 |
| 12 | N2O5 | NO2 + NO3 | 3.169E+00 |
| 13 | N2O5 + H2O | 2HNO3 | 3.841E-07 |
| 14 | NO2 + NO3 | NO + NO2 + O2 | 9.689E-01 |
| 15 | NO3 | NO + O2 | Photolysis |
| 16 | NO3 | NO2 + O | Photolysis |
| 17 | O3 | O + O2 | Photolysis |
| 18 | O3 | O1D + O2 | Photolysis |
| 19 | O1D + H2O | 2OH | 3.250E+05 |
| 20 | O1D + M | O + M | 4.248E+04 |
| 21 | OH + NO | HONO | 1.094E+04 |
| 22 | HONO | OH + NO | Photolysis |
| 23 | HONO | HO2 + NO2 | Photolysis |
| 24 | OH + HONO | NO2 | 9.549E+03 |
| 25 | OH + NO2 | HNO3 | 1.326E+04 |
| 26 | OH + NO3 | HO2 + NO2 | 2.954E+04 |
| 27 | OH + HNO3 | NO3 + H2O | 2.176E+02 |
| 28 | HNO3 | OH + NO2 | Photolysis |
| 29 | OH + CO | HO2 | 3.081E+02 |
| 30 | OH + O3 | HO2 | 9.794E+01 |
| 31 | HO2 + NO | OH + NO2 | 1.244E+04 |
| 32 | HO2 + NO2 | HNO4 | 0.000E+00 |
| 33 | HNO4 | HO2 + NO2 | 0.000E+00 |
| 34 | HNO4 | 0.61HO2 + 0.61NO2 + 0.39OH + 0.39NO3 | Photolysis |
| 35 | HNO4 + OH | NO2 | 0.000E+00 |
| 36 | HO2 + O3 | OH | 2.763E+00 |
| 37 | HO2 + HO2 | HO2H + O2 | 4.235E+03 |
| 38 | HO2 + HO2 + H2O | HO2H + O2 + H2O | 2.348E-01 |
| 39 | NO3 + HO2 | 0.8OH + 0.8NO2 + 0.2HNO3 | 5.909E+03 |
| 40 | NO3 + NO3 | 2NO2 + O2 | 3.373E-01 |
| 41 | HO2H | 2OH | Photolysis |
| 42 | HO2H + OH | HO2 | 2.504E+03 |
| 43 | OH + HO2 |  | 1.641E+05 |
| 44 | OH + SO2 | HO2 + SULF | 1.444E+03 |
| 45 | OH + H2 | HO2 | 9.898E+00 |
| 46 | CXO2 + NO | NO2 + HCHO + HO2 | 1.076E+04 |
| 47 | CXO2 + HO2 | COOH + O2 | 7.691E+03 |
| 48 | CXO2 + NO3 | HCHO + HO2 + NO2 | 1.920E+03 |
| 49 | CXO2 + CXO2 | MEOH + HCHO + O2 | 3.914E+02 |
| 50 | CXO2 + CXO2 | 2HCHO + 2HO2 | 1.581E+02 |
| 51 | RO2R + NO | NO2 + HO2 | 1.334E+04 |
| 52 | RO2R + HO2 | ROOH | 2.200E+04 |
| 53 | RO2R + NO3 | NO2 + O2 + HO2 | 3.398E+03 |

| Reaction Number | Reactants | Products | $k_{298}$[1] $(ppm^{-n} min^{-1})$ |
|---|---|---|---|
| 54 | RO2R + CXO2 | HO2 + 0.75HCHO + 0.25MEOH | 2.954E+02 |
| 55 | RO2R + RO2R | HO2 | 5.170E+01 |
| 56 | R2O2 + NO | NO2 | 1.334E+04 |
| 57 | R2O2 + HO2 | HO2 | 2.200E+04 |
| 58 | R2O2 + NO3 | NO2 | 3.398E+03 |
| 59 | R2O2 + CXO2 | CXO2 | 2.954E+02 |
| 60 | R2O2 + RO2R | RO2R | 5.170E+01 |
| 61 | R2O2 + R2O2 | | 5.170E+01 |
| 62 | RO2N + NO | RNO3 | 1.334E+04 |
| 63 | RO2N + HO2 | ROOH | 2.200E+04 |
| 64 | RO2N + CXO2 | HO2 + 0.25MEOH + 0.5MEK + 0.5PROD + 0.75HCHO | 2.954E+02 |
| 65 | RO2N + NO3 | NO2 + O2 + HO2 + MEK | 3.398E+03 |
| 66 | RO2N + RO2R | HO2 + 0.5MEK + 0.5PROD | 5.170E+01 |
| 67 | RO2N + R2O2 | RO2N | 5.170E+01 |
| 68 | RO2N + RO2N | MEK + HO2 + PROD | 5.170E+01 |
| 69 | CCO3 + NO2 | PAN | 1.548E+04 |
| 70 | PAN | CCO3 + NO2 | 3.123E-02 |
| 71 | CCO3 + NO | CXO2 + NO2 | 3.152E+04 |
| 72 | CCO3 + HO2 | 0.75CO3H + 0.25CO2H + 0.25O3 | 2.084E+04 |
| 73 | CCO3 + NO3 | CXO2 + NO2 | 5.909E+03 |
| 74 | CCO3 + CXO2 | CO2H + HCHO | 1.425E+04 |
| 75 | CCO3 + RO2R | CO2H | 1.108E+04 |
| 76 | CCO3 + R2O2 | CCO3 | 1.108E+04 |
| 77 | CCO3 + RO2N | CO2H + PROD | 1.108E+04 |
| 78 | CCO3 + CCO3 | 2CXO2 | 2.295E+04 |
| 79 | RCO3 + NO2 | PAN2 | 1.783E+04 |
| 80 | PAN2 | RCO3 + NO2 | 2.661E-02 |
| 81 | RCO3 + NO | NO2 + CCHO + RO2R | 4.132E+04 |
| 82 | RCO3 + HO2 | 0.75RC3H + 0.25RC2H + 0.25O3 | 2.084E+04 |
| 83 | RCO3 + NO3 | NO2 + CCHO + RO2R | 5.909E+03 |
| 84 | RCO3 + CXO2 | RC2H + HCHO | 1.425E+04 |
| 85 | RCO3 + RO2R | RC2H | 1.108E+04 |
| 86 | RCO3 + R2O2 | RCO3 | 1.108E+04 |
| 87 | RCO3 + RO2N | RC2H + PROD | 1.108E+04 |
| 88 | RCO3 + CCO3 | CXO2 + CCHO + RO2R | 2.295E+04 |
| 89 | RCO3 + RCO3 | 2CCHO + 2RO2R | 2.295E+04 |
| 90 | BZCO + NO2 | PBZN | 2.024E+04 |
| 91 | PBZN | BZCO + NO2 | 1.873E-02 |
| 92 | BZCO + NO | NO2 + BZO + R2O2 | 4.132E+04 |
| 93 | BZCO + HO2 | 0.75RC3H + 0.25RC2H + 0.25O3 | 2.084E+04 |
| 94 | BZCO + NO3 | NO2 + BZO + R2O2 | 5.909E+03 |
| 95 | BZCO + CXO2 | RC2H + HCHO | 1.425E+04 |
| 96 | BZCO + RO2R | RC2H | 1.108E+04 |
| 97 | BZCO + R2O2 | BZCO | 1.108E+04 |
| 98 | BZCO + RO2N | RC2H + PROD | 1.108E+04 |
| 99 | BZCO + CCO3 | CXO2 + BZO + R2O2 | 2.295E+04 |
| 100 | BZCO + RCO3 | CCHO + RO2R + BZO + R2O2 | 2.295E+04 |
| 101 | BZCO + BZCO | 2BZO + 2R2O2 | 2.295E+04 |
| 102 | MCO3 + NO2 | MPAN | 1.783E+04 |
| 103 | MPAN | MCO3 + NO2 | 2.127E-02 |
| 104 | MCO3 + NO | NO2 + HCHO + CCO3 | 4.132E+04 |
| 105 | MCO3 + HO2 | 0.75RC3H + 0.25RC2H + 0.25O3 | 2.084E+04 |
| 106 | MCO3 + NO3 | NO2 + HCHO + CCO3 | 5.909E+03 |
| 107 | MCO3 + CXO2 | RC2H + HCHO | 1.425E+04 |
| 108 | MCO3 + RO2R | RC2H | 1.108E+04 |
| 109 | MCO3 + R2O2 | MCO3 | 1.108E+04 |
| 110 | MCO3 + RO2N | 2RC2H | 1.108E+04 |
| 111 | MCO3 + CCO3 | CXO2 + HCHO + CCO3 | 2.295E+04 |
| 112 | MCO3 + RCO3 | HCHO + CCO3 + CCHO + RO2R | 2.295E+04 |
| 113 | MCO3 + BZCO | HCHO + CCO3 + BZO + R2O2 | 2.295E+04 |
| 114 | MCO3 + MCO3 | 2HCHO + 2CCO3 | 2.295E+04 |
| 115 | TBUO + NO2 | RNO3 | 3.545E+04 |

| Reaction Number | Reactants | Products | $k_{298}$ [1] $(ppm^{-n} min^{-1})$ |
|---|---|---|---|
| 116 | TBUO | ACET + CXO2 | 5.923E+04 |
| 117 | BZO + NO2 | NPHE | 5.620E+04 |
| 118 | BZO + HO2 | PHEN | 2.200E+04 |
| 119 | BZO | PHEN | 6.000E-02 |
| 120 | BZNO + NO2 | 2XN | 5.620E+04 |
| 121 | BZNO + HO2 | NPHE | 2.200E+04 |
| 122 | BZNO | NPHE | 6.000E-02 |
| 123 | HCHO | 2HO2 + CO | Photolysis |
| 124 | HCHO | CO | Photolysis |
| 125 | HCHO + OH | HO2 + CO | 1.359E+04 |
| 126 | HCHO + HO2 | HCO3 | 1.167E+02 |
| 127 | HCO3 | HO2 + HCHO | 9.060E+03 |
| 128 | HCO3 + NO | HC2H + NO2 + HO2 | 1.076E+04 |
| 129 | HCHO + NO3 | HNO3 + HO2 + CO | 8.477E-01 |
| 130 | CCHO + OH | CCO3 | 2.341E+04 |
| 131 | CCHO | CO + HO2 + CXO2 | Photolysis |
| 132 | CCHO + NO3 | HNO3 + CCO3 | 4.027E+00 |
| 133 | RCHO + OH | 0.034RO2R + 0.001RO2N + 0.965RCO3 + 0.034CO + 0.034CCHO | 2.954E+04 |
| 134 | RCHO | CCHO + RO2R + CO + HO2 | Photolysis |
| 135 | RCHO + NO3 | HNO3 + RCO3 | 5.421E+00 |
| 136 | ACET + OH | HCHO + CCO3 + R2O2 | 2.840E+02 |
| 137 | ACET | CCO3 + CXO2 | Photolysis |
| 138 | MEK + OH | 0.37RO2R + 0.042RO2N + 0.616R2O2 + 0.492CCO3 + 0.096RCO3 + 0.115HCHO + 0.482CCHO + 0.37RCHO | 1.741E+03 |
| 139 | MEK | CCO3 + CCHO + RO2R | Photolysis |
| 140 | MEOH + OH | HCHO + HO2 | 1.351E+03 |
| 141 | COOH + OH | 0.35HCHO + 0.35OH + 0.65CXO2 | 8.111E+03 |
| 142 | COOH | HCHO + HO2 + OH | Photolysis |
| 143 | ROOH + OH | RCHO + 0.34RO2R + 0.66OH | 1.625E+04 |
| 144 | ROOH | RCHO + HO2 + OH | Photolysis |
| 145 | GLY | 2CO + 2HO2 | Photolysis |
| 146 | GLY | HCHO + CO | Photolysis |
| 147 | GLY + OH | 0.63HO2 + 1.26CO + 0.37RCO3 | 1.625E+04 |
| 148 | GLY + NO3 | HNO3 + 0.63HO2 + 1.26CO + 0.37RCO3 | 1.424E+00 |
| 149 | MGLY | HO2 + CO + CCO3 | Photolysis |
| 150 | MGLY + OH | CO + CCO3 | 2.216E+04 |
| 151 | MGLY + NO3 | HNO3 + CO + CCO3 | 3.584E+00 |
| 152 | BACL | 2CCO3 | Photolysis |
| 153 | PHEN + OH | 0.24BZO + 0.76RO2R + 0.23GLY | 3.885E+04 |
| 154 | PHEN + NO3 | HNO3 + BZO | 5.584E+03 |
| 155 | CRES + OH | 0.24BZO + 0.76RO2R + 0.23MGLY | 6.204E+04 |
| 156 | CRES + NO3 | HNO3 + BZO | 2.024E+04 |
| 157 | NPHE + NO3 | HNO3 + BZNO | 5.584E+03 |
| 158 | BALD + OH | BZCO | 1.906E+04 |
| 159 | BALD | | Photolysis |
| 160 | BALD + NO3 | HNO3 + BZCO | 3.867E+00 |
| 161 | METH + OH | 0.5RO2R + 0.416CO + 0.084HCHO + 0.416MEK + 0.084MGLY + 0.5MCO3 | 4.962E+04 |
| 162 | METH + O3 | 0.008HO2 + 0.1RO2R + 0.208OH + 0.1RCO3 + 0.45CO + 0.2HCHO + 0.9MGLY + 0.333HC2H | 1.670E-03 |
| 163 | METH + NO3 | 0.5HNO3 + 0.5RO2R + 0.5CO + 0.5MCO3 + 0.5XN | 6.762E+00 |
| 164 | METH + O | RCHO | 9.365E+03 |
| 165 | METH | 0.34HO2 + 0.33RO2R + 0.33OH + 0.67CCO3 + 0.67CO + 0.67HCHO + 0.33MCO3 | Photolysis |
| 166 | MVK + OH | 0.3RO2R + 0.025RO2N + 0.675R2O2 + 0.675CCO3 + 0.3HCHO + 0.675RCHO + 0.3MGLY | 2.796E+04 |
| 167 | MVK + O3 | 0.064HO2 + 0.05RO2R + 0.164OH + 0.05RCO3 + 0.475CO + 0.1HCHO + 0.95MGLY + 0.351HC2H | 6.765E-03 |
| 168 | MVK + O | 0.45RCHO + 0.55MEK | 6.382E+03 |
| 169 | MVK | 0.3CXO2 + 0.7CO + 0.7PROD + 0.3MCO3 | Photolysis |
| 170 | ISPD + OH | 0.67RO2R + 0.041RO2N + 0.289MCO3 + 0.336CO + 0.055HCHO + 0.129CCHO + 0.013RCHO + 0.15MEK + 0.332PROD + 0.15GLY + 0.174MGLY | 9.144E+04 |

| Reaction Number | Reactants | Products | $k_{298}^{1}$ $(ppm^{-n} min^{-1})$ |
|---|---|---|---|
| 171 | ISPD + O3 | 0.4HO2 + 0.048RO2R + 0.048RCO3 + 0.285OH + 0.498CO + 0.125HCHO + 0.047CCHO + 0.21MEK + 0.023GLY + 0.742MGLY + 0.1HC2H + 0.372RC2H | 6.175E-03 |
| 172 | ISPD + NO3 | 0.799RO2R + 0.051RO2N + 0.15MCO3 + 0.572CO + 0.15HNO3 + 0.227HCHO + 0.218RCHO + 0.008MGLY + 0.572RNO3 + 0.278XN | 1.477E+02 |
| 173 | ISPD | 1.233HO2 + 0.467CCO3 + 0.3RCO3 + 1.233CO + 0.3HCHO + 0.467CCHO + 0.233MEK | Photolysis |
| 174 | PROD + OH | 0.379HO2 + 0.473RO2R + 0.07RO2N + 0.029CCO3 + 0.049RCO3 + 0.213HCHO + 0.084CCHO + 0.558RCHO + 0.115MEK + 0.329PROD | 2.216E+04 |
| 175 | PROD | 0.96RO2R + 0.04RO2N + 0.515R2O2 + 0.667CCO3 + 0.333RCO3 + 0.506HCHO + 0.246CCHO + 0.71RCHO | Photolysis |
| 176 | RNO3 + OH | 0.338NO2 + 0.113HO2 + 0.376RO2R + 0.173RO2N + 0.596R2O2 + 0.01HCHO + 0.439CCHO + 0.213RCHO + 0.006ACET + 0.177MEK + 0.048PROD + 0.31RNO3 + 0.352XN | 1.152E+04 |
| 177 | RNO3 | NO2 + 0.341HO2 + 0.564RO2R + 0.095RO2N + 0.152R2O2 + 0.134HCHO + 0.431CCHO + 0.147RCHO + 0.02ACET + 0.243MEK + 0.435PROD | Photolysis |
| 178 | DCB1 + OH | RCHO + RO2R + CO | 7.386E+04 |
| 179 | DCB1 + O3 | 1.5HO2 + 0.5OH + 1.5CO + GLY | 2.954E-03 |
| 180 | DCB2 + OH | R2O2 + RCHO + CCO3 | 7.386E+04 |
| 181 | DCB2 | RO2R + 0.5CCO3 + 0.5HO2 + CO + R2O2 + 0.5GLY + 0.5MGLY | Photolysis |
| 182 | DCB3 + OH | R2O2 + RCHO + CCO3 | 7.386E+04 |
| 183 | DCB3 | RO2R + 0.5CCO3 + 0.5HO2 + CO + R2O2 + 0.5GLY + 0.5MGLY | Photolysis |
| 184 | CH4 + OH | CXO2 | 9.402E+00 |
| 185 | ETHE + OH | RO2R + 1.61HCHO + 0.195CCHO | 1.258E+04 |
| 186 | ETHE + O3 | 0.12OH + 0.12HO2 + 0.5CO + HCHO + 0.37HC2H | 2.346E-03 |
| 187 | ETHE + NO3 | RO2R + RCHO + XN | 3.022E-01 |
| 188 | ETHE + O | 0.5HO2 + 0.2RO2R + 0.3CXO2 + 0.491CO + 0.191HCHO + 0.25CCHO + 0.009GLY | 1.077E+03 |
| 189 | ISOP + OH | 0.907RO2R + 0.093RO2N + 0.079R2O2 + 0.624HCHO + 0.23METH + 0.32MVK + 0.357ISPD | 1.450E+05 |
| 190 | ISOP + O3 | 0.266OH + 0.066RO2R + 0.008RO2N + 0.126R2O2 + 0.192MCO3 + 0.275CO + 0.592HCHO + 0.1PROD + 0.39METH + 0.16MVK + 0.204HC2H + 0.15RC2H | 1.897E-02 |
| 191 | ISOP + NO3 | 0.187NO2 + 0.749RO2R + 0.064RO2N + 0.187R2O2 + 0.936ISPD + 0.813RNO3 | 9.958E+02 |
| 192 | ISOP + O | 0.01RO2N + 0.24R2O2 + 0.25CXO2 + 0.24MCO3 + 0.24HCHO + 0.75PROD | 5.318E+04 |
| 193 | TERP + OH | 0.75RO2R + 0.25RO2N + 0.5R2O2 + 0.276HCHO + 0.474RCHO + 0.276PROD | 1.221E+05 |
| 194 | TERP + O3 | 0.567OH + 0.033HO2 + 0.031RO2R + 0.18RO2N + 0.729R2O2 + 0.123CCO3 + 0.201RCO3 + 0.157CO + 0.235HCHO + 0.205RCHO + 0.13ACET + 0.276PROD + 0.001GLY + 0.031BACL + 0.103HC2H + 0.189RC2H | 1.014E-01 |
| 195 | TERP + NO3 | 0.474NO2 + 0.276RO2R + 0.25RO2N + 0.75R2O2 + 0.474RCHO + 0.276RNO3 + 0.25XN | 9.714E+03 |
| 196 | TERP + O | 0.147RCHO + 0.853PROD | 4.830E+04 |
| 197 | ALK1 + OH | RO2R + CCHO | 3.752E+02 |
| 198 | ALK2 + OH | 0.246OH + 0.121HO2 + 0.612RO2R + 0.021RO2N + 0.16CO + 0.039HCHO + 0.155RCHO + 0.417ACET + 0.248GLY + 0.121HC2H | 1.533E+03 |
| 199 | ALK3 + OH | 0.695RO2R + 0.07RO2N + 0.559R2O2 + 0.236TBUO + 0.026HCHO + 0.445CCHO + 0.122RCHO + 0.024ACET + 0.332MEK | 3.515E+03 |
| 200 | ALK4 + OH | 0.835RO2R + 0.143RO2N + 0.936R2O2 + 0.011CXO2 + 0.011CCO3 + 0.002CO + 0.024HCHO + 0.455CCHO + 0.244RCHO + 0.452ACET + 0.11MEK + 0.125PROD | 6.486E+03 |
| 201 | ALK5 + OH | 0.653RO2R + 0.347RO2N + 0.948R2O2 + 0.026HCHO + 0.099CCHO + 0.204RCHO + 0.072ACET + 0.089MEK + 0.417PROD | 1.378E+04 |
| 202 | ARO1 + OH | 0.224HO2 + 0.765RO2R + 0.011RO2N + 0.055PROD + 0.118GLY + 0.119MGLY + 0.017PHEN + 0.207CRES + 0.059BALD + 0.491DCB1 + 0.108DCB2 + 0.051DCB3 | 8.793E+03 |
| 203 | ARO2 + OH | 0.187HO2 + 0.804RO2R + 0.009RO2N + 0.097GLY + 0.287MGLY + 0.087BACL + 0.187CRES + 0.05BALD + 0.561DCB1 + 0.099DCB2 + 0.093DCB3 | 3.900E+04 |
| 204 | OLE1 + OH | 0.91RO2R + 0.09RO2N + 0.205R2O2 + 0.732HCHO + 0.294CCHO + 0.497RCHO + 0.005ACET + 0.119PROD | 4.770E+04 |
| 205 | OLE1 + O3 | 0.155OH + 0.056HO2 + 0.022RO2R + 0.001RO2N + 0.076CXO2 + 0.345CO | 1.574E-02 |

| Reaction Number | Reactants | Products | $k_{298}$[1] $(ppm^{-n} min^{-1})$ |
|---|---|---|---|
| | | + 0.5HCHO + 0.154CCHO + 0.363RCHO + 0.001ACET + 0.215PROD + 0.185HC2H + 0.05CO2H + 0.119RC2H | |
| 206 | OLE1 + NO3 | 0.824RO2R + 0.176RO2N + 0.488R2O2 + 0.009CCHO + 0.037RCHO + 0.024ACET + 0.511RNO3 + 0.489XN | 1.862E+01 |
| 207 | OLE1 + O | 0.45RCHO + 0.437MEK + 0.113PROD | 7.208E+03 |
| 208 | OLE2 + OH | 0.918RO2R + 0.082RO2N + 0.001R2O2 + 0.244HCHO + 0.732CCHO + 0.511RCHO + 0.127ACET + 0.072MEK + 0.061BALD + 0.025METH + 0.025ISPD | 9.339E+04 |
| 209 | OLE2 + O3 | 0.378OH + 0.003HO2 + 0.033RO2R + 0.002RO2N + 0.137R2O2 + 0.197CXO2 + 0.137CCO3 + 0.006RCO3 + 0.265CO + 0.269HCHO + 0.456CCHO + 0.305RCHO + 0.045ACET + 0.026MEK + 0.006PROD + 0.042BALD + 0.026METH + 0.073HC2H + 0.129CO2H + 0.303RC2H | 1.576E-01 |
| 210 | OLE2 + NO3 | 0.391NO2 + 0.442RO2R + 0.136RO2N + 0.711R2O2 + 0.03CXO2 + 0.079HCHO + 0.507CCHO + 0.151RCHO + 0.102ACET + 0.001MEK + 0.015BALD + 0.048MVK + 0.321RNO3 + 0.288XN | 1.072E+03 |
| 211 | OLE2 + O | 0.013HO2 + 0.012RO2R + 0.001RO2N + 0.012CO + 0.069RCHO + 0.659MEK + 0.259PROD + 0.012METH | 3.087E+04 |
| 212 | ETOH + OH | 0.05RO2R + 0.95HO2 + 0.081HCHO + 0.96CCHO | 4.919E+03 |
| 213 | MTBE + OH | 0.743RO2R + 0.078RO2N + 0.381R2O2 + 0.162CXO2 + 0.016TBUO + 0.234HCHO + 0.024ACET + 0.719MEK + 0.007PROD | 4.343E+03 |
| 214 | MBUT + OH | 0.935RO2R + 0.065RO2N + 0.311HCHO + 0.624CCHO + 0.311RCHO + 0.624ACET | 9.346E+04 |
| 215 | MBUT + O3 | 0.099OH + 0.099HO2 + 0.365CO + 0.3HCHO + 0.7RCHO + 0.015ACET + 0.259HC2H + 0.285RC2H | 1.374E-02 |
| 216 | MBUT + NO3 | 0.935RO2R + 0.065RO2N + 0.935RCHO + 0.934ACET + RNO3 | 1.760E+01 |
| 217 | MBUT + O | 0.45RCHO + 0.55MEK | 2.969E+04 |

Notes:

1. Rate constants are shown for 298 K and 1 atmosphere in units of ppm and minutes.  See the CAMx chemistry parameters file for the temperature and pressure dependencies (Section 3).

**Table A-2.  Explicit species in the SAPRC99 mechanism (Mechanism 5).**

| Species Name | Description |
|---|---|
| NO2 | Nitrogen dioxide |
| NO | Nitric oxide |
| O3 | Ozone |
| O | Oxygen atom in the $O^3(P)$ electronic state |
| NO3 | Nitrate radical |
| N2O5 | Dinitrogen pentoxide |
| HNO3 | Nitric acid |
| O1D | Oxygen atom in the $O^1(D)$ electronic state |
| OH | Hydroxyl radical |
| HONO | Nitrous acid |
| HO2 | Hydroperoxy radical |
| CO | Carbon monoxide |
| HNO4 | Peroxynitric acid |
| HO2H | Hydrogen peroxide |
| SO2 | Sulfur dioxide |
| SULF | Sulfuric acid (gaseous) |
| CXO2 | Methylperoxy radical |
| HCHO | Formaldehyde |
| COOH | Methyl hydroperoxide |
| MEOH | Methanol |
| RO2R | Organic peroxy radical converting NO to NO2 with HO2 production |
| ROOH | Organic hydroperoxide |
| R2O2 | Organic peroxy radical converting NO to NO2 |
| RO2N | Organic peroxy radical converting NO to organic nitrate |
| RNO3 | Organic nitrate |
| MEK | Methylethyl ketone |
| PROD | Organic product |
| CCO3 | Acetylperoxy radical |
| PAN | Peroxyacetyl nitrate |
| CO3H | Peroxyacetic acid |
| CO2H | Acetic acid |
| RCO3 | Higher acylperoxy radical (based on propylperoxy) |
| PAN2 | Higher peroxyacetyl nitrate (based on peroxypropyl nitrate) |
| CCHO | Acetaldehyde |
| RC3H | Higher percarboxylic acid |
| RC2H | Higher carboxylic acid |
| BZCO | Peroxybenxoyl radical |
| PBZN | Peroxybenzoyl nitrate |
| BZO | Phenoxy radical |
| MCO3 | Peroxyacyl radical from methacrolein |
| MPAN | PAN compound from methacrolein |
| TBUO | Tertiary-butoxy radical |
| ACET | Acetone |
| NPHE | Nitrophenol |
| PHEN | Phenol |
| BZNO | Nitrophenol reaction product |
| XN | Other nitrogen containing product |
| HCO3 | Adduct from HO2 plus formaldehyde |
| HC2H | Formic acid |
| RCHO | Higher aldehyde (based on propionaldehyde) |
| GLY | Glyoxal |
| MGLY | Methylglyoxal |
| BACL | Biacetyl |
| CRES | Cresol |
| BALD | Benzaldehyde |

| Species Name | Description |
|---|---|
| METH | Methacrolein |
| MVK | Methylvinyl ketone |
| ISPD | Isoprene product |
| DCB1 | Aromatic ring opening dicarbonyl product |
| DCB2 | Aromatic ring opening dicarbonyl product |
| DCB3 | Aromatic ring opening dicarbonyl product |
| ETHE | Ethene |
| ISOP | Isoprene |
| TERP | Terpene |
| ALK1 | Lumped alkane 1 |
| ALK2 | Lumped alkane 2 |
| ALK3 | Lumped alkane 3 |
| ALK4 | Lumped alkane 4 |
| ALK5 | Lumped alkane 5 |
| ARO1 | Lumped aromatic 1 |
| ARO2 | Lumped aromatic 2 |
| OLE1 | Lumped olefin 1 |
| OLE2 | Lumped olefin 2 |
| ETOH | Ethanol |
| MTBE | Methyl tertiary butyl ether |
| MBUT | Methylbutenol |

**Table A-3.  Properties of VOC species in the SAPRC99 mechanism: molecular weights, average carbon numbers, $k_{OH}$ values (ppm$^{-1}$min$^{-1}$) and maximum incremental reactivity (MIR) values (mole $O_3$/mole VOC).**

| Species | Molecular Weight | Carbon Number | Average $k_{OH}$[1] | MIR |
|---|---|---|---|---|
| ALK1 | 46.81 | 1.88 | 3.75E+02 | 0.39 |
| ALK2 | 47.02 | 2.65 | 1.53E+03 | 0.80 |
| ALK3 | 57.72 | 2.92 | 3.51E+03 | 2.19 |
| ALK4 | 73.23 | 4.36 | 6.49E+03 | 3.11 |
| ALK5 | 106.97 | 6.42 | 1.38E+04 | 4.95 |
| ETHE | 28.05 | 2 | 1.26E+04 | 5.44 |
| OLE1 | 61.68 | 3.99 | 4.77E+04 | 9.73 |
| OLE2 | 79.05 | 5.67 | 9.34E+04 | 10.98 |
| ISOP | 68.12 | 5 | 1.45E+05 | 12.62 |
| TERP | 136.24 | 10 | 1.22E+05 | 8.54 |
| ARO1 | 100.47 | 7.27 | 8.79E+03 | 6.72 |
| ARO2 | 113.93 | 8.58 | 3.90E+04 | 15.36 |
| HCHO | 30.03 | 1 | 1.36E+04 | 6.49 |
| CCHO | 44.05 | 2 | 2.34E+04 | 5.79 |
| RCHO | 67.32 | 3.66 | 2.95E+04 | 9.45 |
| BALD | 108.21 | 7.15 | | |
| ACET | 58.08 | 3 | | |
| MEK | 72.82 | 4.03 | | |
| PROD | 106.44 | 6.48 | | |
| MEOH | 32.04 | 1 | 1.35E+03 | 1.34 |
| GLY | 58.04 | 2 | | |
| MGLY | 72.06 | 3 | | |
| BACL | 101.31 | 6.37 | | |
| PHEN | 94.11 | 6 | | |
| CRES | 115.38 | 7.52 | | |
| METH | 56.06 | 3 | | |
| MVK | 112.17 | 7 | | |
| ISPD | 70.45 | 4.03 | | |
| ETOH | 46.07 | 2 | 4.92E+03 | 1.62 |
| MTBE | 88.15 | 5 | 4.34E+03 | 1.43 |
| MBUT | 86.13 | 5 | 9.35E+04 | 9.12 |

Notes:

1. $k_{OH}$ values are given to assist in assigning VOC species to SAPRC99 lumped species.

# Appendix B

# CAMx Mechanism 6

# CB05 Gas-Phase Chemistry

### Table B-1.  Reactions and rate constants for the CB05 mechanism (Mechanism 6).

| Reaction Number | Reactants | Products | $k_{298}{}^1$ $(ppm^{-n} min^{-1})$ |
|---|---|---|---|
| 1 | NO2 | NO + O | Photolysis |
| 2 | O + O2 + M | O3 + M | 2.220E-05 |
| 3 | O3 + NO | NO2 | 2.888E+01 |
| 4 | O + NO2 | NO | 1.513E+04 |
| 5 | O + NO2 | NO3 | 4.852E+03 |
| 6 | O + NO | NO2 | 2.459E+03 |
| 7 | NO2 + O3 | NO3 | 4.765E-02 |
| 8 | O3 | O | Photolysis |
| 9 | O3 | O1D | Photolysis |
| 10 | O1D + M | O + M | 4.368E+04 |
| 11 | O1D + H2O | 2 OH | 3.250E+05 |
| 12 | O3 + OH | HO2 | 1.071E+02 |
| 13 | O3 + HO2 | OH | 2.853E+00 |
| 14 | NO3 | NO2 + O | Photolysis |
| 15 | NO3 | NO | Photolysis |
| 16 | NO3 + NO | 2 NO2 | 3.920E+04 |
| 17 | NO3 + NO2 | NO + NO2 | 9.691E-01 |
| 18 | NO3 + NO2 | N2O5 | 1.742E+03 |
| 19 | N2O5 + H2O | 2 HNO3 | 3.693E-07 |
| 20 | N2O5 + H2O + H2O | 2 HNO3 | 6.554E-11 |
| 21 | N2O5 | NO3 + NO2 | 3.168E+00 |
| 22 | NO + NO + O2 | 2 NO2 | 7.114E-10 |
| 23 | NO + NO2 + H2O | 2 HONO | 1.820E-11 |
| 24 | NO + OH | HONO | 1.094E+04 |
| 25 | HONO | NO + OH | Photolysis |
| 26 | OH + HONO | NO2 | 7.184E+03 |
| 27 | HONO + HONO | NO + NO2 | 1.477E-05 |
| 28 | NO2 + OH | HNO3 | 1.545E+04 |
| 29 | OH + HNO3 | NO3 | 2.280E+02 |
| 30 | HO2 + NO | OH + NO2 | 1.196E+04 |
| 31 | HO2 + NO2 | PNA | 0.000E+00 |
| 32 | PNA | HO2 + NO2 | 0.000E+00 |
| 33 | OH + PNA | NO2 | 0.000E+00 |
| 34 | HO2 + HO2 | H2O2 | 4.319E+03 |
| 35 | HO2 + HO2 + H2O | H2O2 | 2.397E-01 |
| 36 | H2O2 | 2 OH | Photolysis |
| 37 | OH + H2O2 | HO2 | 2.504E+03 |
| 38 | O1D + H2 | OH + HO2 | 1.625E+05 |
| 39 | OH + H2 | HO2 | 9.887E+00 |
| 40 | OH + O | HO2 | 4.861E+04 |
| 41 | OH + OH | O | 2.773E+03 |
| 42 | OH + OH | H2O2 | 9.298E+03 |
| 43 | OH + HO2 | | 1.641E+05 |
| 44 | HO2 + O | OH | 8.670E+04 |
| 45 | H2O2 + O | OH + HO2 | 2.517E+00 |
| 46 | NO3 + O | NO2 | 1.477E+04 |
| 47 | NO3 + OH | HO2 + NO2 | 3.250E+04 |
| 48 | NO3 + HO2 | HNO3 | 5.170E+03 |
| 49 | NO3 + O3 | NO2 | 1.477E-02 |
| 50 | NO3 + NO3 | 2 NO2 | 3.375E-01 |
| 51 | PNA | 0.61 HO2 + 0.61 NO2 + 0.39 OH + 0.39 NO3 | Photolysis |
| 52 | HNO3 | OH + NO2 | Photolysis |
| 53 | N2O5 | NO2 + NO3 | Photolysis |

| Reaction Number | Reactants | Products | $k_{298}$[1] $(ppm^{-n} min^{-1})$ |
|---|---|---|---|
| 54 | XO2 + NO | NO2 | 1.307E+04 |
| 55 | XO2N + NO | NTR | 1.307E+04 |
| 56 | XO2 + HO2 | ROOH | 1.160E+04 |
| 57 | XO2N + HO2 | ROOH | 1.160E+04 |
| 58 | XO2 + XO2 | | 1.005E+02 |
| 59 | XO2N + XO2N | | 1.005E+02 |
| 60 | XO2 + XO2N | | 1.005E+02 |
| 61 | NTR + OH | HNO3 + HO2 + 0.33 FORM + 0.33 ALD2 + 0.33 ALDX - 0.66 PAR | 2.604E+02 |
| 62 | NTR | NO2 + HO2 + 0.33 FORM + 0.33 ALD2 + 0.33 ALDX - 0.66 PAR | Photolysis |
| 63 | SO2 + OH | SULF + HO2 | 1.313E+03 |
| 64 | ROOH + OH | XO2 + 0.5 ALD2 + 0.5 ALDX | 8.412E+03 |
| 65 | ROOH | OH + HO2 + 0.5 ALD2 + 0.5 ALDX | Photolysis |
| 66 | OH + CO | HO2 | 3.376E+02 |
| 67 | OH + CH4 | MEO2 | 9.371E+00 |
| 68 | MEO2 + NO | FORM + HO2 + NO2 | 1.132E+04 |
| 69 | MEO2 + HO2 | MEPX | 7.503E+03 |
| 70 | MEO2 + MEO2 | 1.37 FORM + 0.74 HO2 + 0.63 MEOH | 5.194E+02 |
| 71 | MEPX + OH | 0.7 MEO2 + 0.3 XO2 + 0.3 HO2 | 1.098E+04 |
| 72 | MEPX | FORM + HO2 + OH | Photolysis |
| 73 | MEOH + OH | FORM + HO2 | 1.346E+03 |
| 74 | FORM + OH | HO2 + CO | 1.330E+04 |
| 75 | FORM | 2 HO2 + CO | Photolysis |
| 76 | FORM | CO | Photolysis |
| 77 | FORM + O | OH + HO2 + CO | 2.340E+02 |
| 78 | FORM + NO3 | HNO3 + HO2 + CO | 8.568E-01 |
| 79 | FORM + HO2 | HCO3 | 1.167E+02 |
| 80 | HCO3 | FORM + HO2 | 9.054E+03 |
| 81 | HCO3 + NO | FACD + NO2 + HO2 | 8.272E+03 |
| 82 | HCO3 + HO2 | MEPX | 1.860E+04 |
| 83 | FACD + OH | HO2 | 5.909E+02 |
| 84 | ALD2 + O | C2O3 + OH | 6.631E+02 |
| 85 | ALD2 + OH | C2O3 | 2.047E+04 |
| 86 | ALD2 + NO3 | C2O3 + HNO3 | 3.520E+00 |
| 87 | ALD2 | MEO2 + CO + HO2 | Photolysis |
| 88 | C2O3 + NO | MEO2 + NO2 | 2.961E+04 |
| 89 | C2O3 + NO2 | PAN | 1.548E+04 |
| 90 | PAN | C2O3 + NO2 | 1.986E-02 |
| 91 | PAN | C2O3 + NO2 | Photolysis |
| 92 | C2O3 + HO2 | 0.8 PACD + 0.2 AACD + 0.2 O3 | 2.082E+04 |
| 93 | C2O3 + MEO2 | 0.9 MEO2 + 0.9 HO2 + FORM + 0.1 AACD | 1.582E+04 |
| 94 | C2O3 + XO2 | 0.9 MEO2 + 0.1 AACD | 2.356E+04 |
| 95 | C2O3 + C2O3 | 2 MEO2 | 2.294E+04 |
| 96 | PACD + OH | C2O3 | 1.156E+03 |
| 97 | PACD | MEO2 + OH | Photolysis |
| 98 | AACD + OH | MEO2 | 1.156E+03 |
| 99 | ALDX + O | CXO3 + OH | 1.036E+03 |
| 100 | ALDX + OH | CXO3 | 2.932E+04 |
| 101 | ALDX + NO3 | CXO3 + HNO3 | 9.602E+00 |
| 102 | ALDX | MEO2 + CO + HO2 | Photolysis |
| 103 | CXO3 + NO | ALD2 + NO2 + HO2 + XO2 | 3.098E+04 |
| 104 | CXO3 + NO2 | PANX | 1.548E+04 |
| 105 | PANX | CXO3 + NO2 | 1.986E-02 |
| 106 | PANX | CXO3 + NO2 | Photolysis |
| 107 | PANX + OH | ALD2 + NO2 | 4.432E+02 |
| 108 | CXO3 + HO2 | 0.8 PACD + 0.2 AACD + 0.2 O3 | 2.082E+04 |
| 109 | CXO3 + MEO2 | 0.9 ALD2 + 0.9 XO2 + HO2 + 0.1 AACD + 0.1 FORM | 1.582E+04 |
| 110 | CXO3 + XO2 | 0.9 ALD2 + 0.1 AACD | 2.356E+04 |
| 111 | CXO3 + CXO3 | 2 ALD2 + 2 XO2 + 2 HO2 | 2.294E+04 |
| 112 | CXO3 + C2O3 | MEO2 + XO2 + HO2 + ALD2 | 2.294E+04 |
| 113 | OH + ETHA | 0.991 ALD2 + 0.991 XO2 + 0.009 XO2N + HO2 | 3.545E+02 |
| 114 | OH + ETOH | HO2 + 0.9 ALD2 + 0.05 ALDX + 0.1 FORM + 0.1 XO2 | 4.711E+03 |
| 115 | PAR + OH | 0.87 XO2 + 0.13 XO2N + 0.11 HO2 + 0.06 ALD2 - 0.11 PAR + 0.76 ROR + | 1.196E+03 |

| Reaction Number | Reactants | Products | $k_{298}$ [1] $(ppm^{-n}\, min^{-1})$ |
|---|---|---|---|
| | | 0.05 ALDX | |
| 116 | ROR | 0.96 XO2 + 0.6 ALD2 + 0.94 HO2 - 2.1 PAR + 0.04 XO2N + 0.02 ROR + 0.5 ALDX | 1.316E+05 |
| 117 | ROR | HO2 | 9.600E+04 |
| 118 | ROR + NO2 | NTR | 2.216E+04 |
| 119 | O + OLE | 0.2 ALD2 + 0.3 ALDX + 0.3 HO2 + 0.2 XO2 + 0.2 CO + 0.2 FORM + 0.01 XO2N + 0.2 PAR + 0.1 OH | 5.773E+03 |
| 120 | OH + OLE | 0.8 FORM + 0.33 ALD2 + 0.62 ALDX + 0.8 XO2 + 0.95 HO2 - 0.7 PAR | 4.727E+04 |
| 121 | O3 + OLE | 0.18 ALD2 + 0.74 FORM + 0.32 ALDX + 0.22 XO2 + 0.1 OH + 0.33 CO + 0.44 HO2 - PAR | 1.634E-02 |
| 122 | NO3 + OLE | NO2 + FORM + 0.91 XO2 + 0.09 XO2N + 0.56 ALDX + 0.35 ALD2 - PAR | 7.356E-01 |
| 123 | O + ETH | FORM + 1.7 HO2 + CO + 0.7 XO2 + 0.3 OH | 1.077E+03 |
| 124 | OH + ETH | XO2 + 1.56 FORM + 0.22 ALDX + HO2 | 1.204E+04 |
| 125 | O3 + ETH | FORM + 0.63 CO + 0.13 HO2 + 0.13 OH + 0.37 FACD | 2.605E-03 |
| 126 | NO3 + ETH | NO2 + XO2 + 2 FORM | 3.096E-01 |
| 127 | IOLE + O | 1.24 ALD2 + 0.66 ALDX + 0.1 HO2 + 0.1 XO2 + 0.1 CO + 0.1 PAR | 3.398E+04 |
| 128 | IOLE + OH | 1.3 ALD2 + 0.7 ALDX + HO2 + XO2 | 9.354E+04 |
| 129 | IOLE + O3 | 0.65 ALD2 + 0.35 ALDX + 0.25 FORM + 0.25 CO + 0.5 O + 0.5 OH + 0.5 HO2 | 3.095E-01 |
| 130 | IOLE + NO3 | 1.18 ALD2 + 0.64 ALDX + HO2 + NO2 | 5.731E+02 |
| 131 | TOL + OH | 0.44 HO2 + 0.08 XO2 + 0.36 CRES + 0.56 TO2 | 8.751E+03 |
| 132 | TO2 + NO | 0.9 NO2 + 0.9 HO2 + 0.9 OPEN + 0.1 NTR | 1.196E+04 |
| 133 | TO2 | CRES + HO2 | 2.520E+02 |
| 134 | OH + CRES | 0.4 CRO + 0.6 XO2 + 0.6 HO2 + 0.3 OPEN | 6.056E+04 |
| 135 | CRES + NO3 | CRO + HNO3 | 3.250E+04 |
| 136 | CRO + NO2 | NTR | 2.068E+04 |
| 137 | CRO + HO2 | CRES | 8.125E+03 |
| 138 | OPEN | C2O3 + HO2 + CO | Photolysis |
| 139 | OPEN + OH | XO2 + 2 CO + 2 HO2 + C2O3 + FORM | 4.432E+04 |
| 140 | OPEN + O3 | 0.03 ALDX + 0.62 C2O3 + 0.7 FORM + 0.03 XO2 + 0.69 CO + 0.08 OH + 0.76 HO2 + 0.2 MGLY | 1.490E-02 |
| 141 | OH + XYL | 0.7 HO2 + 0.5 XO2 + 0.2 CRES + 0.8 MGLY + 1.1 PAR + 0.3 TO2 | 3.706E+04 |
| 142 | OH + MGLY | XO2 + C2O3 | 2.511E+04 |
| 143 | MGLY | C2O3 + HO2 + CO | Photolysis |
| 144 | O + ISOP | 0.75 ISPD + 0.5 FORM + 0.25 XO2 + 0.25 HO2 + 0.25 CXO3 + 0.25 PAR | 5.318E+04 |
| 145 | OH + ISOP | 0.912 ISPD + 0.629 FORM + 0.991 XO2 + 0.912 HO2 + 0.088 XO2N | 1.473E+05 |
| 146 | O3 + ISOP | 0.65 ISPD + 0.6 FORM + 0.2 XO2 + 0.066 HO2 + 0.266 OH + 0.2 CXO3 + 0.15 ALDX + 0.35 PAR + 0.066 CO | 1.898E-02 |
| 147 | NO3 + ISOP | 0.2 ISPD + 0.8 NTR + XO2 + 0.8 HO2 + 0.2 NO2 + 0.8 ALDX + 2.4 PAR | 9.954E+02 |
| 148 | NO2 + ISOP | 0.2 ISPD + 0.8 NTR + XO2 + 0.8 HO2 + 0.2 NO + 0.8 ALDX + 2.4 PAR | 2.216E-04 |
| 149 | OH + ISPD | 1.565 PAR + 0.167 FORM + 0.713 XO2 + 0.503 HO2 + 0.334 CO + 0.168 MGLY + 0.252 ALD2 + 0.21 C2O3 + 0.25 CXO3 + 0.12 ALDX | 4.963E+04 |
| 150 | O3 + ISPD | 0.114 C2O3 + 0.15 FORM + 0.85 MGLY + 0.154 HO2 + 0.268 OH + 0.064 XO2 + 0.02 ALD2 + 0.36 PAR + 0.225 CO | 1.049E-02 |
| 151 | NO3 + ISPD | 0.357 ALDX + 0.282 FORM + 1.282 PAR + 0.925 HO2 + 0.643 CO + 0.85 NTR + 0.075 CXO3 + 0.075 XO2 + 0.15 HNO3 | 1.477E+00 |
| 152 | ISPD | 0.333 CO + 0.067 ALD2 + 0.9 FORM + 0.832 PAR + 1.033 HO2 + 0.7 XO2 + 0.967 C2O3 | Photolysis |
| 153 | TERP + O | 0.15 ALDX + 5.12 PAR | 5.318E+04 |
| 154 | TERP + OH | 0.75 HO2 + 1.25 XO2 + 0.25 XO2N + 0.28 FORM + 1.66 PAR + 0.47 ALDX | 9.997E+04 |
| 155 | TERP + O3 | 0.57 OH + 0.07 HO2 + 0.76 XO2 + 0.18 XO2N + 0.24 FORM + 0.001 CO + 7 PAR + 0.21 ALDX + 0.39 CXO3 | 1.128E-01 |
| 156 | TERP + NO3 | 0.47 NO2 + 0.28 HO2 + 1.03 XO2 + 0.25 XO2N + 0.47 ALDX + 0.53 NTR | 9.833E+03 |

Notes:

[1]    Rate constants are shown for 298 K and 1 atmosphere in units of ppm and minutes.  See the CAMx chemistry parameters file for the temperature and pressure dependencies (Section 3).

**Table B-2.  Explicit species in the CB05 mechanism (Mechanism 6).**

| Species Name | Description |
|---|---|
| NO | Nitric oxide |
| NO2 | Nitrogen dioxide |
| O3 | Ozone |
| O | Oxygen atom in the $O^3(P)$ electronic state |
| O1D | Oxygen atom in the $O^1(D)$ electronic state |
| OH | Hydroxyl radical |
| HO2 | Hydroperoxy radical |
| H2O2 | Hydrogen peroxide |
| NO3 | Nitrate radical |
| N2O5 | Dinitrogen pentoxide |
| HONO | Nitrous acid |
| HNO3 | Nitric acid |
| PNA | Peroxynitric acid ($HNO_4$) |
| CO | Carbon monoxide |
| FORM | Formaldehyde |
| ALD2 | Acetaldehyde |
| C2O3 | Acetylperoxy radical |
| HCO3 | Adduct from HO2 plus formaldehyde |
| PAN | Peroxyacetyl nitrate |
| ALDX | Propionaldehyde and higher aldehydes |
| CXO3 | C3 and higher acylperoxy radicals |
| PANX | C3 and higher peroxyacyl nitrates |
| XO2 | NO to NO2 conversion from alkylperoxy ($RO_2$) radical |
| XO2N | NO to organic nitrate conversion from alkylperoxy ($RO_2$) radical |
| NTR | Organic nitrate ($RNO_3$) |
| ETOH | Ethanol |
| MEO2 | Methylperoxy radical |
| MEOH | Methanol |
| MEPX | Methylhydroperoxide |
| FACD | Formic acid |
| ETHA | Ethane |
| ROOH | Higher organic peroxide |
| AACD | Acetic and higher carboxylic acids |
| PACD | Peroxyacetic and higher peroxycarboxylic acids |
| PAR | Paraffin carbon bond (C-C) |
| ROR | Secondary alkoxy radical |
| ETH | Ethene |
| OLE | Terminal olefin carbon bond (R-C=C) |
| IOLE | Internal olefin carbon bond (R-C=C-R) |
| ISOP | Isoprene |
| ISPD | Isoprene product (lumped methacrolein, methyl vinyl ketone, etc.) |
| TERP | Terpene |
| TOL | Toluene and other monoalkyl aromatics |
| XYL | Xylene and other polyalkyl aromatics |
| CRES | Cresol and higher molecular weight phenols |
| TO2 | Toluene-hydroxyl radical adduct |
| OPEN | Aromatic ring opening product |
| CRO | Methylphenoxy radical |
| MGLY | Methylglyoxal and other aromatic products |
| SO2 | Sulfur dioxide |
| SULF | Sulfuric acid (gaseous) |

**Table B-3.  Properties of VOC species in the CB05 mechanism: carbon numbers, $k_{OH}$ values ($ppm^{-1}min^{-1}$) and maximum incremental reactivity (MIR) values (mole $O_3$/mole VOC).**

| Species | Carbon Number | Average $k_{OH}$ | MIR |
|---------|---------------|------------------|--------|
| PAR | 1 | 1.20E+03 | 0.319 |
| ETHA | 2 | 3.54E+02 | 0.109 |
| MEOH | 1 | 1.35E+03 | 0.361 |
| ETOH | 2 | 4.71E+03 | 1.042 |
| ETH | 2 | 1.20E+04 | 4.370 |
| OLE | 2 | 4.73E+04 | 8.235 |
| IOLE | 4 | 9.35E+04 | 13.109 |
| ISOP | 5 | 1.47E+05 | 11.555 |
| TERP | 10 | 1.00E+05 | 8.824 |
| FORM | 1 | 1.33E+04 | 4.496 |
| ALD2 | 2 | 2.05E+04 | 4.454 |
| ALDX | 2 | 2.93E+04 | 6.807 |
| TOL | 7 | 8.75E+03 | 2.941 |
| XYL | 8 | 3.71E+04 | 14.790 |

# Appendix C

# CAMx Mechanism 7

# CB6 Gas-Phase Chemistry

**Table C-1. Reactions and rate constants/parameters for the CB6 mechanism (Mechanism 7).**

| Number | Reactants and Products | k$_{298}$ | Rate Parameters | | | Notes |
| | | | A | E$_a$ | B | |
|---|---|---|---|---|---|---|
| 1 | NO2 = NO + O | Photolysis | | | | a |
| 2 | O + O2 + M = O3 + M | 5.78E-34 | 5.68E-34 | 0.0 | -2.60 | a |
| 3 | O3 + NO = NO2 | 1.73E-14 | 1.40E-12 | 1310.0 | 0.00 | a |
| 4 | O + NO + M = NO2 + M | 1.01E-31 | 1.00E-31 | 0.0 | -1.60 | a |
| 5 | O + NO2 = NO | 1.03E-11 | 5.50E-12 | -188.0 | 0.00 | a |
| 6 | O + NO2 = NO3 | 2.11E-12 | Falloff, F=0.60 ,N=1.00 | | | a |
| | | k$_0$ | 1.30E-31 | 0.0 | -1.50 | |
| | | k$_\infty$ | 2.30E-11 | 0.0 | 0.24 | |
| 7 | O + O3 = | 7.96E-15 | 8.00E-12 | 2060.0 | 0.00 | a |
| 8 | O3 = O | Photolysis | | | | a |
| 9 | O3 = O1D | Photolysis | | | | a |
| 10 | O1D + M = O + M | 3.28E-11 | 2.23E-11 | -115.0 | 0.00 | a |
| 11 | O1D + H2O = 2 OH | 2.14E-10 | 2.14E-10 | | | a |
| 12 | O3 + OH = HO2 | 7.25E-14 | 1.70E-12 | 940.0 | 0.00 | a |
| 13 | O3 + HO2 = OH | 2.01E-15 | 2.03E-16 | -693.0 | 4.57 | a |
| 14 | OH + O = HO2 | 3.47E-11 | 2.40E-11 | -110.0 | 0.00 | a |
| 15 | HO2 + O = OH | 5.73E-11 | 2.70E-11 | -224.0 | 0.00 | a |
| 16 | OH + OH = O | 1.48E-12 | 6.20E-14 | -945.0 | 2.60 | a |
| 17 | OH + OH = H2O2 | 5.25E-12 | Falloff, F=0.50 ,N=1.13 | | | a |
| | | k$_0$ | 6.90E-31 | 0.0 | -0.80 | |
| | | k$_\infty$ | 2.60E-11 | 0.0 | 0.00 | |
| 18 | OH + HO2 = | 1.11E-10 | 4.80E-11 | -250.0 | 0.00 | a |
| 19 | HO2 + HO2 = H2O2 | 2.90E-12 | k = k1 + k2[M] | | | a |
| | | k1 | 2.20E-13 | -600.0 | 0.00 | |
| | | k2 | 1.90E-33 | -980.0 | 0.00 | |
| 20 | HO2 + HO2 + H2O = H2O2 | 6.53E-30 | k = k1 + k2[M] | | | a |
| | | k1 | 3.08E-34 | -2800.0 | 0.00 | |
| | | k2 | 2.66E-54 | -3180.0 | 0.00 | |
| 21 | H2O2 = 2 OH | Photolysis | | | | a |
| 22 | H2O2 + OH = HO2 | 1.70E-12 | 2.90E-12 | 160.0 | 0.00 | a |
| 23 | H2O2 + O = OH + HO2 | 1.70E-15 | 1.40E-12 | 2000.0 | 0.00 | a |
| 24 | NO + NO + O2 = 2 NO2 | 1.95E-38 | 3.30E-39 | -530.0 | 0.00 | a |
| 25 | HO2 + NO = OH + NO2 | 8.54E-12 | 3.45E-12 | -270.0 | 0.00 | a |
| 26 | NO2 + O3 = NO3 | 3.52E-17 | 1.40E-13 | 2470.0 | 0.00 | a |
| 27 | NO3 = NO2 + O | Photolysis | | | | b |
| 28 | NO3 = NO | Photolysis | | | | b |
| 29 | NO3 + NO = 2 NO2 | 2.60E-11 | 1.80E-11 | -110.0 | 0.00 | a |
| 30 | NO3 + NO2 = NO + NO2 | 6.56E-16 | 4.50E-14 | 1260.0 | 0.00 | b |
| 31 | NO3 + O = NO2 | 1.70E-11 | 1.70E-11 | | | a |
| 32 | NO3 + OH = HO2 + NO2 | 2.00E-11 | 2.00E-11 | | | a |
| 33 | NO3 + HO2 = OH + NO2 | 4.00E-12 | 4.00E-12 | | | a |
| 34 | NO3 + O3 = NO2 | 1.00E-17 | 1.00E-17 | | | c,k |
| 35 | NO3 + NO3 = 2 NO2 | 2.28E-16 | 8.50E-13 | 2450.0 | 0.00 | b |

| Number | Reactants and Products | k$_{298}$ | Rate Parameters | | | Notes |
|---|---|---|---|---|---|---|
| | | | A | E$_a$ | B | |
| 36 | NO3 + NO2 = N2O5 | 1.24E-12 | Falloff, F=0.35 ,N=1.33 | | | a |
| | | k$_0$ | 3.60E-30 | 0.0 | -4.10 | |
| | | k$_\infty$ | 1.90E-12 | 0.0 | 0.20 | |
| 37 | N2O5 = NO3 + NO2 | 4.46E-02 | Falloff, F=0.35 ,N=1.33 | | | a |
| | | k$_0$ | 1.30E-03 | 11000.0 | -3.50 | |
| | | k$_\infty$ | 9.70E+14 | 11080.0 | 0.10 | |
| 38 | N2O5 = NO2 + NO3 | Photolysis | | | | a |
| 39 | N2O5 + H2O = 2 HNO3 | 1.00E-22 | 1.00E-22 | | | a |
| 40 | NO + OH = HONO | 9.77E-12 | Falloff, F=0.81 ,N=0.87 | | | a |
| | | k$_0$ | 7.40E-31 | 0.0 | -2.40 | |
| | | k$_\infty$ | 3.30E-11 | 0.0 | -0.30 | |
| 41 | NO + NO2 + H2O = 2 HONO | 5.00E-40 | 5.00E-40 | | | c,l |
| 42 | HONO + HONO = NO + NO2 | 1.00E-20 | 1.00E-20 | | | c,m |
| 43 | HONO = NO + OH | Photolysis | | | | a |
| 44 | HONO + OH = NO2 | 5.98E-12 | 2.50E-12 | -260.0 | 0.00 | a |
| 45 | NO2 + OH = HNO3 | 1.06E-11 | Falloff, F=0.60 ,N=1.00 | | | b |
| | | k$_0$ | 1.80E-30 | 0.0 | -3.00 | |
| | | k$_\infty$ | 2.80E-11 | 0.0 | 0.00 | |
| 46 | HNO3 + OH = NO3 | 1.54E-13 | k = k1+k3M/(1+k3M/k2) | | | a |
| | | k1 | 2.40E-14 | -460.0 | 0.00 | |
| | | k2 | 2.70E-17 | -2199.0 | 0.00 | |
| | | k3 | 6.50E-34 | -1335.0 | 0.00 | |
| 47 | HNO3 = OH + NO2 | Photolysis | | | | a |
| 48 | HO2 + NO2 = PNA | 1.38E-12 | Falloff, F=0.60 ,N=1.00 | | | a |
| | | k$_0$ | 1.80E-31 | 0.0 | -3.20 | |
| | | k$_\infty$ | 4.70E-12 | 0.0 | 0.00 | |
| 49 | PNA = HO2 + NO2 | 8.31E-02 | Falloff, F=0.60 ,N=1.00 | | | a |
| | | k$_0$ | 4.10E-05 | 10650.0 | 0.00 | |
| | | k$_\infty$ | 4.80E+15 | 11170.0 | 0.00 | |
| 50 | PNA = 0.59 HO2 + 0.59 NO2 + 0.41 OH + 0.41 NO3 | Photolysis | | | | a |
| 51 | PNA + OH = NO2 | 3.24E-12 | 3.20E-13 | -690.0 | 0.00 | a |
| 52 | SO2 + OH = SULF + HO2 | 8.12E-13 | Falloff, F=0.53 ,N=1.10 | | | a |
| | | k$_0$ | 4.50E-31 | 0.0 | -3.90 | |
| | | k$_\infty$ | 1.30E-12 | 0.0 | -0.70 | |
| 53 | C2O3 + NO = NO2 + MEO2 + RO2 | 1.98E-11 | 7.50E-12 | -290.0 | 0.00 | a |
| 54 | C2O3 + NO2 = PAN | 1.05E-11 | Falloff, F=0.30 ,N=1.00 | | | a |
| | | k$_0$ | 2.70E-28 | 0.0 | -7.10 | |
| | | k$_\infty$ | 1.20E-11 | 0.0 | -0.90 | |
| 55 | PAN = NO2 + C2O3 | 3.31E-04 | Falloff, F=0.30 ,N=1.00 | | | a |
| | | k$_0$ | 4.90E-03 | 12100.0 | 0.00 | |
| | | k$_\infty$ | 5.40E+16 | 13830.0 | 0.00 | |
| 56 | PAN = 0.6 NO2 + 0.6 C2O3 + 0.4 NO3 + 0.4 MEO2 + 0.4 RO2 | Photolysis | | | | a |
| 57 | C2O3 + HO2 = 0.41 PACD + 0.15 AACD + 0.15 O3 + 0.44 MEO2 + 0.44 RO2 + 0.44 OH | 1.39E-11 | 5.20E-13 | -980.0 | 0.00 | a |
| 58 | C2O3 + RO2 = C2O3 | 1.30E-11 | 8.90E-13 | -800.0 | 0.00 | a |
| 59 | C2O3 + C2O3 = 2 MEO2 + 2 RO2 | 1.55E-11 | 2.90E-12 | -500.0 | 0.00 | a |
| 60 | C2O3 + CXO3 = MEO2 + ALD2 + XO2H + 2 RO2 | 1.55E-11 | 2.90E-12 | -500.0 | 0.00 | a |

| Number | Reactants and Products | k₂₉₈ | Rate Parameters | | | Notes |
|---|---|---|---|---|---|---|
| | | | A | Eₐ | B | |
| 61 | CXO3 + NO = NO2 + ALD2 + XO2H + RO2 | 2.10E-11 | 6.70E-12 | -340.0 | 0.00 | a |
| 62 | CXO3 + NO2 = PANX | 1.16E-11 | Falloff, F=0.30 ,N=1.00 | | | a |
| | | | k₀ | 3.00E-28 | 0.0 | -7.10 | |
| | | | k∞ | 1.33E-11 | 0.0 | -0.90 | |
| 63 | PANX = NO2 + CXO3 | 3.68E-04 | Falloff, F=0.30 ,N=1.00 | | | a |
| | | | k₀ | 1.70E-03 | 11280.0 | 0.00 | |
| | | | k∞ | 8.30E+16 | 13940.0 | 0.00 | |
| 64 | PANX = 0.6 NO2 +0.6 CXO3 + 0.4 NO3 + 0.4 ALD2 + 0.4 XO2H + 0.4 RO2 | Photolysis | | | | a |
| 65 | CXO3 + HO2 = 0.41 PACD + 0.15 AACD + 0.15 O3 + 0.44 ALD2 + 0.44 XO2H + 0.44 RO2 + 0.44 OH | 1.39E-11 | 5.20E-13 | -980.0 | 0.00 | a |
| 66 | CXO3 + RO2 = 0.8 ALD2 + 0.8 XO2H + 0.8 RO2 | 1.30E-11 | 8.90E-13 | -800.0 | 0.00 | a |
| 67 | CXO3 + CXO3 = 2 ALD2 + 2 XO2H + 2 RO2 | 1.71E-11 | 3.20E-12 | -500.0 | 0.00 | a |
| 68 | RO2 + NO = NO | 8.03E-12 | 2.40E-12 | -360.0 | 0.00 | a |
| 69 | RO2 + HO2 = HO2 | 7.03E-12 | 4.80E-13 | -800.0 | 0.00 | a |
| 70 | RO2 + RO2 = | 3.48E-13 | 6.50E-14 | -500.0 | 0.00 | a |
| 71 | MEO2 + NO = FORM + HO2 + NO2 | 7.70E-12 | 2.30E-12 | -360.0 | 0.00 | a |
| 72 | MEO2 + HO2 = 0.9 MEPX + 0.1 FORM | 5.21E-12 | 3.80E-13 | -780.0 | 0.00 | a |
| 73 | MEO2 + C2O3 = FORM + 0.9 HO2 + 0.9 MEO2 + 0.1 AACD + 0.9 RO2 | 1.07E-11 | 2.00E-12 | -500.0 | 0.00 | a |
| 74 | MEO2 + RO2 = 0.685 FORM + 0.315 MEOH + 0.37 HO2 + RO2 | 3.48E-13 | k = kref*K | | | a |
| | | k(ref) | ref = 70 | | | |
| | | K | 1.00E+00 | 0.0 | 0.00 | |
| 75 | XO2H + NO = NO2 + HO2 | 9.04E-12 | 2.70E-12 | -360.0 | 0.00 | a |
| 76 | XO2H + HO2 = ROOH | 9.96E-12 | 6.80E-13 | -800.0 | 0.00 | a |
| 77 | XO2H + C2O3 = 0.8 HO2 + 0.8 MEO2 + 0.2 AACD + 0.8 RO2 | 1.30E-11 | k = kref*K | | | a |
| | | k(ref) | ref = 58 | | | |
| | | K | 1.00E+00 | 0.0 | 0.00 | |
| 78 | XO2H + RO2 = 0.6 HO2 + RO2 | 3.48E-13 | k = kref*K | | | a |
| | | k(ref) | ref = 70 | | | |
| | | K | 1.00E+00 | 0.0 | 0.00 | |
| 79 | XO2 + NO = NO2 | 9.04E-12 | k = kref*K | | | a |
| | | k(ref) | ref = 75 | | | |
| | | K | 1.00E+00 | 0.0 | 0.00 | |
| 80 | XO2 + HO2 = ROOH | 9.96E-12 | k = kref*K | | | a |
| | | k(ref) | ref = 76 | | | |
| | | K | 1.00E+00 | 0.0 | 0.00 | |
| 81 | XO2 + C2O3 = 0.8 MEO2 + 0.2 AACD + 0.8 RO2 | 1.30E-11 | k = kref*K | | | a |
| | | k(ref) | ref = 58 | | | |
| | | K | 1.00E+00 | 0.0 | 0.00 | |
| 82 | XO2 + RO2 = RO2 | 3.48E-13 | k = kref*K | | | a |
| | | k(ref) | ref = 70 | | | |
| | | K | 1.00E+00 | 0.0 | 0.00 | |
| 83 | XO2N + NO = NTR | 9.04E-12 | k = kref*K | | | a |
| | | k(ref) | ref = 75 | | | |
| | | K | 1.00E+00 | 0.0 | 0.00 | |

| Number | Reactants and Products | k₂₉₈ | Rate Parameters | | | Notes |
|---|---|---|---|---|---|---|
| | | | A | Eₐ | B | |
| 84 | XO2N + HO2 = ROOH | 9.96E-12 | k = kref*K | | | a |
| | | k(ref) | ref = 76 | | | |
| | | K | 1.00E+00 | 0.0 | 0.00 | |
| 85 | XO2N + C2O3 = 0.8 HO2 + 0.8 MEO2 + 0.2 AACD + 0.8 RO2 | 1.30E-11 | k = kref*K | | | a |
| | | k(ref) | ref = 58 | | | |
| | | K | 1.00E+00 | 0.0 | 0.00 | |
| 86 | XO2N + RO2 = RO2 | 3.48E-13 | k = kref*K | | | a |
| | | k(ref) | ref = 70 | | | |
| | | K | 1.00E+00 | 0.0 | 0.00 | |
| 87 | MEPX + OH = 0.6 MEO2 + 0.6 RO2 + 0.4 FORM + 0.4 OH | 1.00E-11 | 5.30E-12 | -190.0 | 0.00 | a |
| 88 | MEPX = MEO2 + RO2 + OH | Photolysis | | | | a |
| 89 | ROOH + OH = 0.54 XO2H + 0.06 XO2N + 0.6 RO2 + 0.4 OH | 6.05E-12 | 3.20E-12 | -190.0 | 0.00 | a |
| 90 | ROOH = HO2 + OH | Photolysis | | | | a |
| 91 | NTR + OH = HNO3 + XO2H + RO2 | 8.10E-13 | 8.10E-13 | | | a,c |
| 92 | NTR = NO2 + XO2H + RO2 | Photolysis | | | | a,c |
| 93 | FACD + OH = HO2 | 4.50E-13 | 4.50E-13 | | | a |
| 94 | AACD + OH = MEO2 + RO2 | 6.93E-13 | 4.00E-14 | -850.0 | 0.00 | a |
| 95 | PACD + OH = C2O3 | 6.93E-13 | 4.00E-14 | -850.0 | 0.00 | a |
| 96 | FORM + OH = HO2 + CO | 8.49E-12 | 5.40E-12 | -135.0 | 0.00 | a |
| 97 | FORM = 2 HO2 + CO | Photolysis | | | | a |
| 98 | FORM = CO + H2 | Photolysis | | | | a |
| 99 | FORM + O = OH + HO2 + CO | 1.58E-13 | 3.40E-11 | 1600.0 | 0.00 | b |
| 100 | FORM + NO3 = HNO3 + HO2 + CO | 5.50E-16 | 5.50E-16 | | | a |
| 101 | FORM + HO2 = HCO3 | 7.90E-14 | 9.70E-15 | -625.0 | 0.00 | a |
| 102 | HCO3 = FORM + HO2 | 1.51E+02 | 2.40E+12 | 7000.0 | 0.00 | a |
| 103 | HCO3 + NO = FACD + NO2 + HO2 | 5.60E-12 | 5.60E-12 | | | a |
| 104 | HCO3 + HO2 = 0.5 MEPX + 0.5 FACD + 0.2 OH + 0.2 HO2 | 1.26E-11 | 5.60E-15 | -2300.0 | 0.00 | a |
| 105 | ALD2 + O = C2O3 + OH | 4.49E-13 | 1.80E-11 | 1100.0 | 0.00 | b |
| 106 | ALD2 + OH = C2O3 | 1.50E-11 | 4.70E-12 | -345.0 | 0.00 | a |
| 107 | ALD2 + NO3 = C2O3 + HNO3 | 2.73E-15 | 1.40E-12 | 1860.0 | 0.00 | a |
| 108 | ALD2 = MEO2 + RO2 + CO + HO2 | Photolysis | | | | a |
| 109 | ALDX + O = CXO3 + OH | 7.02E-13 | 1.30E-11 | 870.0 | 0.00 | c,n |
| 110 | ALDX + OH = CXO3 | 1.91E-11 | 4.90E-12 | -405.0 | 0.00 | a |
| 111 | ALDX + NO3 = CXO3 + HNO3 | 6.30E-15 | 6.30E-15 | | | a |
| 112 | ALDX = ALD2 + XO2H + RO2 + CO + HO2 | Photolysis | | | | f |
| 113 | GLYD + OH = 0.2 GLY + 0.2 HO2 + 0.8 C2O3 | 8.00E-12 | 8.00E-12 | | | a |
| 114 | GLYD = 0.74 FORM + 0.89 CO + 1.4 HO2 + 0.15 MEOH + 0.19 OH + 0.11 GLY + 0.11 XO2H + 0.11 RO2 | Photolysis | | | | a,b,f |
| 115 | GLYD + NO3 = HNO3 + C2O3 | 2.73E-15 | 1.40E-12 | 1860.0 | 0.00 | a |
| 116 | GLY + OH = 1.7 CO + 0.3 XO2 + 0.3 RO2 + HO2 | 9.70E-12 | 3.10E-12 | -340.0 | 0.00 | a |
| 117 | GLY = 2 HO2 + 2 CO | Photolysis | | | | a,q |
| 118 | GLY + NO3 = HNO3 + CO + HO2 + XO2 + RO2 | 2.73E-15 | 1.40E-12 | 1860.0 | 0.00 | a |
| 119 | MGLY = C2O3 + HO2 + CO | Photolysis | | | | a |
| 120 | MGLY + NO3 = HNO3 + C2O3 + XO2 + RO2 | 2.73E-15 | 1.40E-12 | 1860.0 | 0.00 | a |
| 121 | MGLY + OH = C2O3 + CO | 1.31E-11 | 1.90E-12 | -575.0 | 0.00 | a |

| Number | Reactants and Products | k₂₉₈ | Rate Parameters | | | Notes |
|---|---|---|---|---|---|---|
| | | | A | Eₐ | B | |
| 122 | H2 + OH = HO2 | 6.70E-15 | 7.70E-12 | 2100.0 | 0.00 | a |
| 123 | CO + OH = HO2 | 2.28E-13 | k = k1 + k2[M] | | | a |
| | | k1 | 1.44E-13 | 0.0 | 0.00 | |
| | | k2 | 3.43E-33 | 0.0 | 0.00 | |
| 124 | CH4 + OH = MEO2 + RO2 | 6.37E-15 | 1.85E-12 | 1690.0 | 0.00 | a |
| 125 | ETHA + OH = 0.991 ALD2 + 0.991 XO2H + 0.009 XO2N + RO2 | 2.41E-13 | 6.90E-12 | 1000.0 | 0.00 | a |
| 126 | MEOH + OH = FORM + HO2 | 8.95E-13 | 2.85E-12 | 345.0 | 0.00 | a |
| 127 | ETOH + OH = 0.95 ALD2 + 0.9 HO2 + 0.1 XO2H + 0.1 RO2 + 0.078 FORM + 0.011 GLYD | 3.21E-12 | 3.00E-12 | -20.0 | 0.00 | a |
| 128 | KET = 0.5 ALD2 + 0.5 C2O3 + 0.5 XO2H +0.5 CXO3 + 0.5 MEO2 + RO2 - 2.5 PAR | Photolysis | | | | a |
| 129 | ACET = 0.38 CO + 1.38 MEO2 + 1.38 RO2 + 0.62 C2O3 | Photolysis | | | | a |
| 130 | ACET + OH = FORM + C2O3 + XO2 + RO2 | 1.76E-13 | 1.41E-12 | 620.6 | 0.00 | a |
| 131 | PRPA + OH = 0.71 ACET + 0.26 ALDX + 0.26 PAR + 0.97 XO2H + 0.03 XO2N + RO2 | 1.07E-12 | 7.60E-12 | 585.0 | 0.00 | a |
| 132 | PAR + OH = 0.11 ALDX + 0.76 ROR + 0.13 XO2N + 0.11 XO2H + 0.76 XO2 + RO2 - 0.11 PAR | 8.10E-13 | 8.10E-13 | | | c |
| 133 | ROR = 0.2 KET + 0.42 ACET + 0.74 ALD2 + 0.37 ALDX + 0.04 XO2N + 0.94 XO2H + 0.98 RO2 + 0.02 ROR - 2.7 PAR | 2.15E+04 | 5.70E+12 | 5780.0 | 0.00 | a,c |
| 134 | ROR + O2 = KET + HO2 | 3.78E+04 | 1.50E-14 | 200.0 | 0.00 | a,c |
| 135 | ROR + NO2 = NTR | 3.29E-11 | 8.60E-12 | -400.0 | 0.00 | a,c |
| 136 | ETHY + OH = 0.7 GLY + 0.7 OH + 0.3 FACD + 0.3 CO + 0.3 HO2 | 7.52E-13 | Falloff, F=0.37 ,N=1.30 | | | a |
| | | k₀ | 5.00E-30 | 0.0 | -1.50 | |
| | | k∞ | 1.00E-12 | 0.0 | 0.00 | |
| 137 | ETH + O = FORM + HO2 + CO + 0.7 XO2H + 0.7 RO2 + 0.3 OH | 7.29E-13 | 1.04E-11 | 792.0 | 0.00 | c,o |
| 138 | ETH + OH = XO2H + RO2 + 1.56 FORM + 0.22 GLYD | 7.84E-12 | Falloff, F=0.48 ,N=1.15 | | | a,g |
| | | k₀ | 8.60E-29 | 0.0 | -3.10 | |
| | | k∞ | 9.00E-12 | 0.0 | -0.85 | |
| 139 | ETH + O3 = FORM + 0.51 CO + 0.16 HO2 + 0.16 OH + 0.37 FACD | 1.58E-18 | 9.10E-15 | 2580.0 | 0.00 | a,g |
| 140 | ETH + NO3 = 0.5 NO2 + 0.5 NTR + 0.5 XO2H + 0.5 XO2 + RO2 + 1.125 FORM | 2.10E-16 | 3.30E-12 | 2880.0 | 0.00 | a,g |
| 141 | OLE + O = 0.2 ALD2 + 0.3 ALDX + 0.1 HO2 + 0.2 XO2H + 0.2 CO + 0.2 FORM + 0.01 XO2N + 0.21 RO2 + 0.2 PAR + 0.1 OH | 3.91E-12 | 1.00E-11 | 280.0 | 0.00 | c,o |
| 142 | OLE + OH = 0.781 FORM + 0.488 ALD2 + 0.488 ALDX + 0.976 XO2H + 0.195 XO2 + 0.024 XO2N + 1.17 RO2 - 0.73 PAR | 2.86E-11 | Falloff, F=0.50 ,N=1.13 | | | a,g |
| | | k₀ | 8.00E-27 | 0.0 | -3.50 | |
| | | k∞ | 3.00E-11 | 0.0 | -1.00 | |
| 143 | OLE + O3 = 0.295 ALD2 + 0.555 FORM + 0.27 ALDX + 0.15 XO2H + 0.15 RO2 + 0.334 OH +0.08 HO2 + 0.378 CO + 0.075 GLY + 0.075 MGLY + 0.09 FACD + 0.13 AACD + 0.04 H2O2 - 0.79 PAR | 1.00E-17 | 5.50E-15 | 1880.0 | 0.00 | a,g |
| 144 | OLE + NO3 = 0.5 NO2 + 0.5 NTR + 0.48 XO2 + 0.48 XO2H + 0.04 XO2N + RO2 + 0.5 FORM + 0.25 ALD2 + 0.375 ALDX - PAR | 9.54E-15 | 4.60E-13 | 1155.0 | 0.00 | a,g |

| Number | Reactants and Products | k$_{298}$ | Rate Parameters | | | Notes |
|---|---|---|---|---|---|---|
| | | | A | E$_a$ | B | |
| 145 | IOLE + O = 1.24 ALD2 + 0.66 ALDX + 0.1 XO2H + 0.1 RO2 + 0.1 CO + 0.1 PAR | 2.30E-11 | 2.30E-11 | | | c,o |
| 146 | IOLE + OH = 1.3 ALD2 + 0.7 ALDX + XO2H + RO2 | 5.99E-11 | 1.05E-11 | -519.0 | 0.00 | a,g |
| 147 | IOLE + O3 = 0.732 ALD2 + 0.442 ALDX + 0.128 FORM + 0.245 CO + 0.5 OH + 0.3 XO2H + 0.3 RO2 + 0.24 GLY + 0.06 MGLY + 0.29 PAR + 0.08 AACD + 0.08 H2O2 | 1.57E-16 | 4.70E-15 | 1013.0 | 0.00 | a,g |
| 148 | IOLE + NO3 = 0.5 NO2 + 0.5 NTR + 0.48 XO2 + 0.48 XO2H + 0.04 XO2N + RO2 + 0.5 ALD2 + 0.625 ALDX + PAR | 3.70E-13 | 3.70E-13 | | | a,g |
| 149 | ISOP + OH = ISO2 + RO2 | 9.99E-11 | 2.70E-11 | -390.0 | 0.00 | a |
| 150 | ISO2 + NO = 0.117 INTR + 0.883 NO2 + 0.803 HO2 + 0.66 FORM + 0.66 ISPD + 0.08 XO2H + 0.08 RO2 + 0.05 IOLE + 0.042 GLYD + 0.115 PAR + 0.038 GLY + 0.042 MGLY + 0.093 OLE + 0.117 ALDX | 8.13E-12 | 2.39E-12 | -365.0 | 0.00 | r,s |
| 151 | ISO2 + HO2 = 0.88 ISPX + 0.12 OH + 0.12 HO2 + 0.12 FORM + 0.12 ISPD | 7.78E-12 | 7.43E-13 | -700.0 | 0.00 | r,s |
| 152 | ISO2 + C2O3 = 0.709 HO2 + 0.583 FORM + 0.583 ISPD + 0.071 XO2H + 0.044 IOLE + 0.037 GLYD + 0.102 PAR + 0.034 GLY + 0.037 MGLY + 0.082 OLE + 0.103 ALDX + 0.8 MEO2 + 0.2 AACD + 0.871 RO2 | 1.30E-11 | k = kref*K | | | r,s |
| | | k(ref) | ref = 58 | | | |
| | | K | 1.00E+00 | 0.0 | 0.00 | |
| 153 | ISO2 + RO2 = 0.803 HO2 + 0.66 FORM + 0.66 ISPD + 0.08 XO2H + 0.05 IOLE + 0.042 GLYD + 0.115 PAR + 0.038 GLY + 0.042 MGLY + 0.093 OLE + 0.117 ALDX + 1.08 RO2 | 3.48E-13 | k = kref*K | | | r,s |
| | | k(ref) | ref = 70 | | | |
| | | K | 1.00E+00 | 0.0 | 0.00 | |
| 154 | ISO2 = 0.8 HO2 + 0.04 OH + 0.04 FORM + 0.8 ISPD | 1.00E+00 | 1.00E+00 | | | j,t |
| 155 | ISOP + O3 = 0.6 FORM + 0.65 ISPD + 0.15 ALDX + 0.2 CXO3 + 0.35 PAR + 0.266 OH + 0.2 XO2 + 0.2 RO2 + 0.066 HO2 + 0.066 CO | 1.27E-17 | 1.03E-14 | 1995.0 | 0.00 | c |
| 156 | ISOP + NO3 = 0.35 NO2 + 0.65 INTR + 0.64 XO2H + 0.33 XO2 + 0.03 XO2N + RO2 + 0.35 FORM + 0.35 ISPD | 6.74E-13 | 3.03E-12 | 448.0 | 0.00 | u |
| 157 | ISPD + OH = 0.095 XO2N + 0.379 XO2 + 0.318 XO2H + 0.792 RO2 + 0.843 PAR + 0.379 C2O3 + 0.209 CXO3 + 0.379 GLYD + 0.24 MGLY + 0.24 FORM + 0.067 OLE + 0.079 CO + 0.028 ALDX | 3.38E-11 | 6.31E-12 | -500.0 | 0.00 | r,s |
| 158 | ISPD + O3 = 0.02 ALD2 + 0.15 FORM + 0.225 CO + 0.85 MGLY + 0.36 PAR + 0.114 C2O3 + 0.064 XO2H + 0.064 RO2 + 0.268 OH + 0.09 HO2 | 7.10E-18 | 4.17E-15 | 1900.0 | 0.00 | c |
| 159 | ISPD + NO3 = 0.643 CO + 0.282 FORM + 0.357 ALDX + 1.282 PAR + 0.85 HO2 + 0.075 CXO3 + 0.075 XO2H + 0.075 RO2 + 0.85 NTR + 0.15 HNO3 | 1.00E-15 | 1.00E-15 | | | c |
| 160 | ISPD = 0.333 CO + 0.067 ALD2 + 0.9 FORM + 0.832 PAR + 0.333 HO2 + 0.7 XO2H + 0.7 | Photolysis | | | | c,f |

| Number | Reactants and Products | k₂₉₈ | Rate Parameters | | | Notes |
|---|---|---|---|---|---|---|
| | | | A | Eₐ | B | |
| | RO2 + 0.967 C2O3 | | | | | |
| 161 | ISPX + OH = 0.904 EPOX + 0.933 OH + 0.067 ISO2 + 0.067 RO2 + 0.029 IOLE + 0.029 ALDX | 7.77E-11 | 2.23E-11 | -372.0 | 0.00 | r,s |
| 162 | EPOX + OH = EPX2 + RO2 | 1.51E-11 | 5.78E-11 | 400.0 | 0.00 | r,s |
| 163 | EPX2 + HO2 = 0.275 GLYD + 0.275 GLY + 0.275 MGLY + 1.125 OH + 0.825 HO2 + 0.375 FORM + 0.074 FACD + 0.251 CO + 2.175 PAR | 7.78E-12 | 7.43E-13 | -700.0 | 0.00 | r,s |
| 164 | EPX2 + NO = 0.275 GLYD + 0.275 GLY + 0.275 MGLY + 0.125 OH + 0.825 HO2 + 0.375 FORM + NO2 + 0.251 CO + 2.175 PAR | 8.13E-12 | 2.39E-12 | -365.0 | 0.00 | r,s |
| 165 | EPX2 + C2O3 = 0.22 GLYD + 0.22 GLY + 0.22 MGLY + 0.1 OH + 0.66 HO2 + 0.3 FORM + 0.2 CO + 1.74 PAR + 0.8 MEO2 + 0.2 AACD + 0.8 RO2 | 1.30E-11 | k = kref*K | | | a,r,s |
| | | k(ref) | ref = 58 | | | |
| | | K | 1.00E+00 | 0.0 | 0.00 | |
| 166 | EPX2 + RO2 = 0.275 GLYD + 0.275 GLY + 0.275 MGLY + 0.125 OH + 0.825 HO2 + 0.375 FORM + 0.251 CO + 2.175 PAR + RO2 | 3.48E-13 | k = kref*K | | | a,r,s |
| | | k(ref) | ref = 70 | | | |
| | | K | 1.00E+00 | 0.0 | 0.00 | |
| 167 | INTR + OH = 0.63 XO2 + 0.37 XO2H + RO2 + 0.444 NO2 + 0.185 NO3 + 0.104 INTR + 0.592 FORM + 0.331 GLYD + 0.185 FACD + 2.7 PAR + 0.098 OLE + 0.078 ALDX + 0.266 NTR | 3.10E-11 | 3.10E-11 | | | r,s |
| 168 | TERP + O = 0.15 ALDX + 5.12 PAR | 3.60E-11 | 3.60E-11 | | | c |
| 169 | TERP + OH = 0.75 XO2H + 0.5 XO2 + 0.25 XO2N + 1.5 RO2 + 0.28 FORM + 1.66 PAR + 0.47 ALDX | 6.77E-11 | 1.50E-11 | -449.0 | 0.00 | c |
| 170 | TERP + O3 = 0.57 OH + 0.07 XO2H + 0.69 XO2 + 0.18 XO2N + 0.94 RO2 + 0.24 FORM + 0.001 CO + 7 PAR + 0.21 ALDX + 0.39 CXO3 | 7.63E-17 | 1.20E-15 | 821.0 | 0.00 | c |
| 171 | TERP + NO3 = 0.47 NO2 + 0.28 XO2H + 0.75 XO2 + 0.25 XO2N + 1.28 RO2 + 0.47 ALDX + 0.53 NTR | 6.66E-12 | 3.70E-12 | -175.0 | 0.00 | c |
| 172 | BENZ + OH = 0.53 CRES + 0.352 BZO2 + 0.352 RO2 + 0.118 OPEN + 0.118 OH + 0.53 HO2 | 1.22E-12 | 2.30E-12 | 190.0 | 0.00 | a,d,e |
| 173 | BZO2 + NO = 0.918 NO2 + 0.082 NTR + 0.918 GLY + 0.918 OPEN + 0.918 HO2 | 9.04E-12 | 2.70E-12 | -360.0 | 0.00 | d,h |
| 174 | BZO2 + C2O3 = GLY + OPEN + HO2 + MEO2 + RO2 | 1.30E-11 | k = kref*K | | | a,d,h |
| | | k(ref) | ref = 58 | | | |
| | | K | 1.00E+00 | 0.0 | 0.00 | |
| 175 | BZO2 + HO2 = | 1.49E-11 | 1.90E-13 | -1300.0 | 0.00 | d |
| 176 | BZO2 + RO2 = GLY + OPEN + HO2 + RO2 | 3.48E-13 | k = kref*K | | | a,d,h |
| | | k(ref) | ref = 70 | | | |
| | | K | 1.00E+00 | 0.0 | 0.00 | |
| 177 | TOL + OH = 0.18 CRES + 0.65 TO2 + 0.72 RO2 + 0.1 OPEN + 0.1 OH + 0.07 XO2H + 0.18 HO2 | 5.63E-12 | 1.80E-12 | -340.0 | 0.00 | a,d,e |
| 178 | TO2 + NO = 0.86 NO2 + 0.14 NTR + 0.417 GLY + 0.443 MGLY + 0.66 OPEN + 0.2 XOPN + 0.86 HO2 | 9.04E-12 | 2.70E-12 | -360.0 | 0.00 | d,h |
| 179 | TO2 + C2O3 = 0.48 GLY + 0.52 MGLY + 0.77 | 1.30E-11 | k = kref*K | | | a,d,h |

| Number | Reactants and Products | k₂₉₈ | Rate Parameters | | | Notes |
|--------|------------------------|------|-----------------|---|---|-------|
| | | | A | Eₐ | B | |
| | OPEN + 0.23 XOPN + HO2 + MEO2 + RO2 | k(ref) | ref = 58 | | | |
| | | K | 1.00E+00 | 0.0 | 0.00 | |
| 180 | TO2 + HO2 = | 1.49E-11 | 1.90E-13 | -1300.0 | 0.00 | d |
| 181 | TO2 + RO2 = 0.48 GLY + 0.52 MGLY + 0.77 | 3.48E-13 | k = kref*K | | | a,d,h |
| | OPEN + 0.23 XOPN + HO2 + RO2 | k(ref) | ref = 70 | | | |
| | | K | 1.00E+00 | 0.0 | 0.00 | |
| 182 | XYL + OH = 0.155 CRES + 0.544 XLO2 + 0.602 RO2 + 0.244 XOPN + 0.244 OH + 0.058 XO2H + 0.155 HO2 | 1.85E-11 | 1.85E-11 | | | d,e,p |
| 183 | XLO2 + NO = 0.86 NO2 + 0.14 NTR + 0.221 GLY + 0.675 MGLY + 0.3 OPEN + 0.56 XOPN + 0.86 HO2 | 9.04E-12 | 2.70E-12 | -360.0 | 0.00 | d,h |
| 184 | XLO2 + HO2 = | 1.49E-11 | 1.90E-13 | -1300.0 | 0.00 | d |
| 185 | XLO2 + C2O3 = 0.26 GLY + 0.77 MGLY + 0.35 | 1.30E-11 | k = kref*K | | | a,d,h |
| | OPEN + 0.65 XOPN + HO2 + MEO2 + RO2 | k(ref) | ref = 58 | | | |
| | | K | 1.00E+00 | 0.0 | 0.00 | |
| 186 | XLO2 + RO2 = 0.26 GLY + 0.77 MGLY + 0.35 | 3.48E-13 | k = kref*K | | | a,d,h |
| | OPEN + 0.65 XOPN + HO2 + RO2 | k(ref) | ref = 70 | | | |
| | | K | 1.00E+00 | 0.0 | 0.00 | |
| 187 | CRES + OH = 0.06 CRO + 0.12 XO2H + HO2 + 0.13 OPEN + 0.732 CAT1 + 0.06 CO + 0.06 XO2N + 0.18 RO2 + 0.06 FORM | 4.12E-11 | 1.70E-12 | -950.0 | 0.00 | d |
| 188 | CRES + NO3 = 0.3 CRO + HNO3 + 0.24 XO2 + 0.36 XO2H + 0.48 ALDX + 0.24 FORM + 0.24 MGLY + 0.12 OPEN + 0.1 XO2N + 0.7 RO2 + 0.24 CO | 1.40E-11 | 1.40E-11 | | | d |
| 189 | CRO + NO2 = CRON | 2.10E-12 | 2.10E-12 | | | d |
| 190 | CRO + HO2 = CRES | 5.50E-12 | 5.50E-12 | | | d |
| 191 | CRON + OH = CRNO | 1.53E-12 | 1.53E-12 | | | d |
| 192 | CRON + NO3 = CRNO + HNO3 | 3.80E-12 | 3.80E-12 | | | d |
| 193 | CRNO + NO2 = 2 NTR | 2.10E-12 | 2.10E-12 | | | d |
| 194 | CRNO + O3 = CRN2 | 2.86E-13 | 2.86E-13 | | | d |
| 195 | CRN2 + NO = CRNO + NO2 | 8.50E-12 | 2.54E-12 | -360.0 | 0.00 | d |
| 196 | CRN2 + HO2 = CRPX | 1.88E-11 | 2.40E-13 | -1300.0 | 0.00 | d |
| 197 | CRPX = CRNO + OH | Photolysis | | | | a,d |
| 198 | CRPX + OH = CRN2 | 3.59E-12 | 1.90E-12 | -190.0 | 0.00 | d |
| 199 | XOPN = CAO2 + 0.7 HO2 + 0.7 CO + 0.3 C2O3 + RO2 | Photolysis | | | | d,p |
| 200 | XOPN + OH = CAO2 + MGLY + XO2H + RO2 | 9.00E-11 | 9.00E-11 | | | d,p |
| 201 | XOPN + O3 = 1.2 MGLY + 0.5 OH + 0.6 C2O3 + 0.1 ALD2 + 0.5 CO + 0.3 XO2H + 0.3 RO2 | 2.02E-17 | 1.08E-16 | 500.0 | 0.00 | d,p |
| 202 | XOPN + NO3 = 0.5 NO2 + 0.5 NTR + 0.45 XO2H + 0.45 XO2 + 0.1 XO2N + RO2 + 0.25 OPEN + 0.25 MGLY | 3.00E-12 | 3.00E-12 | | | d,p |
| 203 | OPEN = OPO3 + HO2 + CO | Photolysis | | | | d,p |
| 204 | OPEN + OH = 0.6 OPO3 + 0.4 CAO2 + 0.4 RO2 | 4.40E-11 | 4.40E-11 | | | d,p |
| 205 | OPEN + O3 = 1.4 GLY + 0.24 MGLY + 0.5 OH + 0.12 C2O3 + 0.08 FORM + 0.02 ALD2 + 1.98 CO + 0.56 HO2 | 1.01E-17 | 5.40E-17 | 500.0 | 0.00 | d,p |

| Number | Reactants and Products | k₂₉₈ | Rate Parameters | | | Notes |
|---|---|---|---|---|---|---|
| | | | A | Eₐ | B | |
| 206 | OPEN + NO3 = OPO3 + HNO3 | 3.80E-12 | 3.80E-12 | | | d,p |
| 207 | CAT1 + OH = CAO2 + RO2 | 7.00E-11 | 7.00E-11 | | | d |
| 208 | CAT1 + NO3 = CRO + HNO3 | 1.70E-10 | 1.70E-10 | | | d |
| 209 | CAO2 + NO = 0.86 NO2 + 0.14 NTR + 1.2 HO2 + 0.344 FORM + 0.344 CO | 8.50E-12 | 2.54E-12 | -360.0 | 0.00 | d |
| 210 | CAO2 + HO2 = | 1.88E-11 | 2.40E-13 | -1300.0 | 0.00 | d |
| 211 | CAO2 + C2O3 = HO2 + 0.4 GLY + MEO2 + RO2 | 1.30E-11 | k = kref*K | | | d |
| | | k(ref) | ref = 58 | | | |
| | | K | 1.00E+00 | 0.0 | 0.00 | |
| 212 | CAO2 + RO2 = HO2 + 0.4 GLY + RO2 | 3.48E-13 | k = kref*K | | | d |
| | | k(ref) | ref = 70 | | | |
| | | K | 1.00E+00 | 0.0 | 0.00 | |
| 213 | OPO3 + NO = NO2 + XO2H + RO2 + ALDX | 1.00E-11 | 1.00E-11 | | | d |
| 214 | OPO3 + NO2 = OPAN | 1.16E-11 | k = kref*K | | | d |
| | | k(ref) | ref = 62 | | | |
| | | K | 1.00E+00 | 0.0 | 0.00 | |
| 215 | OPAN = OPO3 + NO2 | 9.92E-05 | Falloff, F=0.30 ,N=1.00 | | | d |
| | | k₀ | 4.60E-04 | 11280.0 | 0.00 | |
| | | k∞ | 2.24E+16 | 13940.0 | 0.00 | |
| 216 | OPO3 + HO2 = 0.41 PACD + 0.15 AACD + 0.15 O3 + 0.44 ALDX + 0.44 XO2H + 0.44 RO2 + 0.44 OH | 1.39E-11 | k = kref*K | | | d |
| | | k(ref) | ref = 57 | | | |
| | | K | 1.00E+00 | 0.0 | 0.00 | |
| 217 | OPO3 + C2O3 = MEO2 + XO2 +ALDX + 2 RO2 | 1.55E-11 | k = kref*K | | | d |
| | | k(ref) | ref = 59 | | | |
| | | K | 1.00E+00 | 0.0 | 0.00 | |
| 218 | OPO3 + RO2 = 0.8 XO2H + 0.8 RO2 + 0.8 ALDX + 0.2 AACD | 1.30E-11 | k = kref*K | | | d |
| | | k(ref) | ref = 58 | | | |
| | | K | 1.00E+00 | 0.0 | 0.00 | |

Table notes:

$k_{298}$ is the rate constant at 298 K and 1 atmosphere using units molecules cm$^{-3}$ and s$^{-1}$

See Table C-2 for species names

See the CAMx chemistry parameters file for the temperature and pressure dependencies (Section 3).

| | | | | | |
|---|---|---|---|---|---|
| a | IUPAC: Atkinson et al., (2010) | h | Arey et al. (2009) | o | Cvetanovic (1987) |
| b | JPL: Sander et al., (2006) | i | Hu et al. (2007) | p | Calvert et al. (2002) |
| c | CB05: Yarwood et al (2005b) | j | Archibald et al. (2010) | q | Feierabend et al. (2009) |
| d | CB05-TU: Whitten et al., 2010) | k | Hjorth et al. (1992) | r | Paulot et al. (2009a) |
| e | Bloss et al. (2005) | l | Kaiser and Wu (1977) | s | Paulot et al. (2009b) |
| f | SAPRC-99: Carter (2000) | m | Jeffries et al. (2002) | t | Peeters et al. (2009) |
| g | Calvert et al. (2000) | n | Herron (1988) | u | Perring et al. (2009) |

### Table C-2.  Explicit species in the CB6 mechanism (Mechanism 7).

| Species | Description |
|---|---|
| AACD | Acetic acid |
| ACET | Acetone |
| ALD2 | Acetaldehyde |
| ALDX | Propionaldehyde and higher aldehydes |
| BENZ | Benzene |
| BZO2 | Peroxy radical from OH addition to benzene |
| C2O3 | Acetylperoxy radical |
| CAO2 | Peroxy radical from aromatic degradation products |
| CAT1 | Methyl-catechols |
| CO | Carbon monoxide |
| CRES | Cresols |
| CRN2 | Peroxy radical from nitro-cresol |
| CRNO | Alkoxy radical from nitro-cresols |
| CRO | Alkoxy radical from cresol |
| CRON | Nitro-cresols |
| CRPX | Nitro-cresol hydroperoxides |
| CXO3 | C3 and higher acylperoxy radicals |
| EPOX | Epoxide formed from ISPX reaction with OH |
| EPX2 | Peroxy radical from EPOX reaction with OH |
| ETH | Ethene |
| ETHA | Ethane |
| ETHY | Ethyne |
| ETOH | Ethanol |
| FACD | Formic acid |
| FORM | Formaldehyde |
| GLY | Glyoxal |
| GLYD | Glycolaldehyde |
| H2O2 | Hydrogen peroxide |
| HCO3 | Adduct from HO2 plus formaldehyde |
| HNO3 | Nitric acid |
| HO2 | Hydroperoxy radical |
| HONO | Nitrous acid |
| INTR | Organic nitrates from ISO2 reaction with NO |
| IOLE | Internal olefin carbon bond (R-C=C-R) |
| ISO2 | Peroxy radical from OH addition to isoprene |
| ISOP | Isoprene |
| ISPD | Isoprene product (lumped methacrolein, methyl vinyl ketone, etc.) |
| ISPX | Hydroperoxides from ISO2 reaction with HO2 |
| KET | Ketone carbon bond (C=O) |
| M | Air |
| MEO2 | Methylperoxy radical |
| MEOH | Methanol |
| MEPX | Methylhydroperoxide |
| MGLY | Methylglyoxal |
| N2O5 | Dinitrogen pentoxide |
| NO | Nitric oxide |
| NO2 | Nitrogen dioxide |
| NO3 | Nitrate radical |
| NTR | Organic nitrates |
| O | Oxygen atom in the $O^3(P)$ electronic state |

| Species | Description |
|---------|-------------|
| O1D | Oxygen atom in the $O^1(D)$ electronic state |
| O3 | Ozone |
| OH | Hydroxyl radical |
| OLE | Terminal olefin carbon bond (R-C=C) |
| OPAN | Peroxyacyl nitrate (PAN compound) from OPO3 |
| OPEN | Aromatic ring opening product (unsaturated dicarbonyl) |
| OPO3 | Peroxyacyl radical from OPEN |
| PACD | Peroxyacetic and higher peroxycarboxylic acids |
| PAN | Peroxyacetyl Nitrate |
| PANX | C3 and higher peroxyacyl nitrate |
| PAR | Paraffin carbon bond (C-C) |
| PNA | Peroxynitric acid |
| PRPA | Propane |
| RO2 | Operator to approximate total peroxy radical concentration |
| ROOH | Higher organic peroxide |
| ROR | Secondary alkoxy radical |
| SO2 | Sulfur dioxide |
| SULF | Sulfuric acid (gaseous) |
| TERP | Monoterpenes |
| TO2 | Peroxy radical from OH addition to TOL |
| TOL | Toluene and other monoalkyl aromatics |
| XLO2 | Peroxy radical from OH addition to XYL |
| XO2 | NO to NO2 conversion from alkylperoxy (RO2) radical |
| XO2H | NO to NO2 conversion (XO2) accompanied by HO2 production |
| XO2N | NO to organic nitrate conversion from alkylperoxy (RO2) radical |
| XOPN | Aromatic ring opening product (unsaturated dicarbonyl) |
| XYL | Xylene and other polyalkyl aromatics |

**Table C-3. Properties of VOC species in the CB6 mechanism: carbon numbers, $k_{OH}$ values (ppm$^{-1}$min$^{-1}$) and maximum incremental reactivity (MIR) values (mole $O_3$/mole VOC).**

| Species | Carbon Number | Average $k_{OH}$ | MIR |
|---------|---------------|------------------|-----|
| PAR | 1 | 1.20E+03 | 0.509 |
| ETHA | 2 | 3.54E+02 | 0.135 |
| MEOH | 1 | 1.35E+03 | 0.48 |
| ETOH | 2 | 4.71E+03 | 1.53 |
| ETH | 2 | 1.20E+04 | 4.95 |
| OLE | 2 | 4.73E+04 | 9.66 |
| IOLE | 4 | 9.35E+04 | 16 |
| ISOP | 5 | 1.47E+05 | 12.7 |
| TERP | 10 | 1.00E+05 | 9.91 |
| FORM | 1 | 1.33E+04 | 4.87 |
| ALD2 | 2 | 2.05E+04 | 5.8 |
| ALDX | 2 | 2.93E+04 | 8.35 |
| TOL | 7 | 8.75E+03 | 7.39 |
| XYL | 8 | 3.71E+04 | 20.5 |
| PRPA | 3 | 1. 58E+03 | 0.541 |
| ETHY | 2 | 1.80E+03 | 1.39 |
| BENZ | 6 | 1.11E+03 | 0.487 |
| ACET | 3 | 2.60E+02 | 0.564 |
| KET | 1 | 0.0 | 4.86 |

# Appendix D

# CAMx Mechanism 1

# CB6 Gas-Phase Chemistry with Iodine Chemistry

**Table D-1.  Listing of the chemical mechanism for iodine and ozone.**

| Number | Reactants and Products | $k_{298}$ | Rate Parameters | | | Notes |
|---|---|---|---|---|---|---|
| | | | A | $E_a$ | B | |
| I1 | I + O3 = IO | 1.30E-12 | 2.10E-11 | 830.0 | 0.00 | a |
| I2 | I + HO2 = HI | 3.87E-13 | 1.50E-11 | 1090.0 | 0.00 | a |
| I3 | I + NO = INO | 3.76E-13 | Falloff, F=0.60 ,N=1.00 | | | a |
| | | $k_0$ | 1.80E-32 | 0.0 | -1.00 | |
| | | $k_\infty$ | 1.70E-11 | 0.0 | 0.00 | |
| I4 | I + NO2 = INO2 | 5.24E-12 | Falloff, F=0.63 ,N=1.00 | | | a |
| | | $k_0$ | 3.00E-31 | 0.0 | -1.00 | |
| | | $k_\infty$ | 6.60E-11 | 0.0 | 0.00 | |
| I5 | I2 = 2 I | Photolysis | | | | a |
| I6 | I2 + OH = HOI + I | 2.10E-10 | 2.10E-10 | | | a |
| I7 | I2 + NO3 = I + INO3 | 1.50E-12 | 1.50E-12 | | | a |
| I8 | HI + OH = I | 7.00E-11 | 1.60E-11 | -440.0 | 0.00 | |
| I9 | IO = I + O | Photolysis | | | | a |
| I10 | IO + NO = I + NO2 | 1.96E-11 | 7.15E-12 | -300.0 | 0.00 | a |
| I11 | IO + NO2 = INO3 | 3.55E-12 | Falloff, F=0.40 ,N=1.00 | | | a |
| | | $k_0$ | 7.70E-31 | 0.0 | -5.00 | |
| | | $k_\infty$ | 1.60E-11 | 0.0 | 0.00 | |
| I12 | IO + HO2 = HOI | 8.57E-11 | 1.40E-11 | -540.0 | 0.00 | a |
| I13 | IO + IO = 0.4 I + 0.4 OIO + 0.6 I2O2 | 9.88E-11 | 5.40E-11 | -180.0 | 0.00 | a,b |
| I14 | HOI = I + OH | Photolysis | | | | a |
| I15 | HOI + OH = IO | 5.00E-12 | 5.00E-12 | | | c |
| I16 | OIO = I | Photolysis | | | | d |
| I17 | OIO + NO = IO + NO2 | 6.78E-12 | 1.10E-12 | -542.0 | 0.00 | a |
| I18 | OIO + OH = HIO3 | 4.72E-10 | Falloff, F=0.30 ,N=1.00 | | | e |
| | | $k_0$ | 1.50E-27 | 0.0 | -3.93 | |
| | | $k_\infty$ | 5.50E-10 | -46.0 | 0.00 | |
| I19 | OIO + IO = IXOY | 1.00E-10 | 1.00E-10 | | | f |
| I20 | OIO + OIO = IXOY | 1.50E-10 | 1.50E-10 | | | f |
| I21 | I2O2 = I + OIO | 1.00E+01 | 1.00E+01 | | | g |
| I22 | I2O2 + O3 = IXOY | 1.00E-12 | 1.00E-12 | | | h |
| I23 | INO + I = I2 +  NO | 1.66E-10 | 1.66E-10 | | | i |
| I24 | INO + INO = I2 + 2 NO | 1.28E-14 | 8.40E-11 | 2620.0 | 0.00 | a |
| I25 | INO2 = I + NO2 | Photolysis | | | | a |
| I26 | INO2 + INO2 = I2 + 2 NO2 | 1.73E-15 | 4.70E-13 | 1670.0 | 0.00 | a |
| I27 | INO3 = I + NO3 | Photolysis | | | | j |
| I28 | INO3 + I = I2 + NO3 | 5.58E-11 | 9.10E-11 | 146.0 | 0.00 | g |
| I29 | CH3I = I + MEO2 | Photolysis | | | | a |
| I30 | MI2 = 2.000 I + FORM | Photolysis | | | | a |
| I31 | MIB = I + XO2 + FORM | Photolysis | | | | a |
| I32 | MIC = I + XO2 + FORM | Photolysis | | | | a |
| I33 | IALK = I + XO2H + ALDX | Photolysis | | | | a,k |

Table notes:

k$_{298}$ is the rate constant at 298 K and 1 atmosphere using units of molecules cm$^{-3}$ and s$^{-1}$

See Table D-2 for species names

See Table D-3 for information on photolysis reactions

MEO2, FORM and ALDX in reactions I29 – I33 are Carbon Bond species names and should be changed for use with a different base mechanism

References are indicated in the notes column as follows:

| | | | | | |
|---|---|---|---|---|---|
| a | Atkinson et al. (2010) – IUPAC | e | Plane et al. (2006) | i | van den Bergh et al. (1976) |
| b | Sommariva et al. (2012) | f | Gomez-Martin et al. (2007) | j | Joseph et al. (2007) |
| c | Riffault et al. (2005) | g | Kaltsoyannis et al. (2008) | k | Taatjes et al. (2012) |
| d | Sander et al. (2011) – JPL | h | Saunders et al. (2005) | l | Cotter et al. (2001) |

## Table D-2.  Model species names and properties in the chemical mechanism for iodine and ozone.

| Model Species Name | Description | Chemical Formula | | | | | | | M. Wt. (g) | Henry Constant | | |
|---|---|---|---|---|---|---|---|---|---|---|---|---|
| | | C | H | O | N | Cl | Br | I | | H$_{298}$ (M atm$^{-1}$) | A (K) | Notes |
| I2 | molecular iodine | | | | | | | 2 | 253.8 | 3.10E+00 | -4600 | |
| I | iodine atom | | | | | | | 1 | 126.9 | 8.00E-02 | -2300 | |
| IO | iodine monoxide | | | 1 | | | | 1 | 142.9 | 8.00E-02 | -2300 | Same as I |
| OIO | iodine dioxide | | | 2 | | | | 1 | 158.9 | 1.00E+00 | -3300 | Same as OClO |
| I2O2 | diiodine dioxide | | | 2 | | | | 2 | 285.8 | 1.00E+06 | -4000 | Large value |
| IXOY | condensable iodine oxides | | | 3 | | | | 2 | 301.8 | 1.00E+06 | -4000 | Large value |
| HI | hydrogen iodide | | 1 | | | | | 1 | 127.9 | 1.00E+06 | -9800 | Accounting for dissociation |
| HOI | hypoiodous acid | | 1 | 1 | | | | 1 | 143.9 | 4.10E+02 | -4000 | |
| HIO3 | iodic acid | | 1 | 3 | | | | 1 | 175.9 | 1.00E+06 | -4000 | |
| INO | nitrosyl iodide | | | 1 | 1 | | | 1 | 156.9 | 5.00E-02 | -4000 | Same as ClNO |
| INO2 | nitryl iodide | | | 2 | 1 | | | 1 | 172.9 | 3.00E-01 | -4000 | Same as BrNO$_2$ |
| INO3 | iodine nitrate | | | 3 | 1 | | | 1 | 188.9 | 1.00E+06 | -4000 | Same as BrNO$_3$ (large) |
| CH3I | iodomethane | 1 | 3 | | | | | 1 | 141.9 | 1.40E-01 | -4300 | |
| MIC | chloroiodomethane | 1 | 2 | | | 1 | | 1 | 176.4 | 8.90E-01 | -4300 | |
| MIB | bromoiodomethane | 1 | 2 | | | | 1 | 1 | 219.9 | 8.90E-01 | -4300 | Same as CH$_2$ICl |
| MI2 | diiodomethane | 1 | 2 | | | | | 2 | 267.8 | 2.30E+00 | -5000 | |
| IALK | alkyl iodides | 3 | 7 | | | | | 1 | 170.0 | 6.30E-02 | -4000 | |

Table notes:

H$_{298}$ is the Henry Constant at 298 K and T factor is the temperature dependence (K)

Henry constant data from http://www.mpch-mainz.mpg.de/~sander/res/henry.html

Henry constants are for the exact compound unless noted otherwise under comments

Default value for temperature dependence (A) is 4000 K

Frequently it is useful to characterize the photolysis rate for one reaction as a ratio to another reaction, although the reference reaction should be selected so that the ratio has little dependence upon zenith angle. Photolysis rate ratios for iodine compounds are listed below with the reference reactions defined in the footnote to Table D-3.

$$
\begin{aligned}
j(I2) &= 0.922 \ \times j(NO3\_NO2) \\
j(IO) &= 18.5 \ \times j(NO2) \\
j(OIO) &= 0.907 \ \times j(NO3\_NO2) \\
j(HOI) &= 10.1 \ \times j(NO2) \\
j(INO2) &= 0.509 \ \times j(NO2) \\
i(INO3) &= 522.2 \ \times j(FORM\_M) \\
j(CH3I) &= 1.15 \ \times j(HNO3) \\
j(MI2) &= 198.2 \ \times j(FORM\_M) \\
j(MIB) &= 14.2 \ \times j(FORM\_R) \\
j(MIC) &= 4.21 \ \times j(FORM\_R) \\
j(IALK) &= 2.31 \ \times j(HNO3)
\end{aligned}
$$

**Table D-3. Photolysis rates ($s^{-1}$) for iodine-containing species and reference reactions.**

| Species Name | Solar Zenith Angle (degrees) | | | | | | | | | |
|---|---|---|---|---|---|---|---|---|---|---|
| | **0** | **10** | **20** | **30** | **40** | **50** | **60** | **70** | **78** | **86** |
| I2 | 1.51E-01 | 1.50E-01 | 1.47E-01 | 1.43E-01 | 1.36E-01 | 1.27E-01 | 1.12E-01 | 8.88E-02 | 5.80E-02 | 1.35E-02 |
| IO | 1.72E-01 | 1.72E-01 | 1.67E-01 | 1.60E-01 | 1.50E-01 | 1.34E-01 | 1.12E-01 | 8.00E-02 | 4.48E-02 | 1.10E-02 |
| OIO | 1.48E-01 | 1.47E-01 | 1.45E-01 | 1.41E-01 | 1.34E-01 | 1.25E-01 | 1.11E-01 | 8.78E-02 | 5.75E-02 | 1.30E-02 |
| HOI | 9.55E-02 | 9.47E-02 | 9.22E-02 | 8.78E-02 | 8.12E-02 | 7.17E-02 | 5.87E-02 | 4.05E-02 | 2.20E-02 | 5.60E-03 |
| INO2 | 4.83E-03 | 4.78E-03 | 4.65E-03 | 4.43E-03 | 4.08E-03 | 3.60E-03 | 2.93E-03 | 2.02E-03 | 1.09E-03 | 2.80E-04 |
| INO3 | 2.40E-02 | 2.38E-02 | 2.28E-02 | 2.12E-02 | 1.88E-02 | 1.58E-02 | 1.18E-02 | 7.18E-03 | 3.50E-03 | 9.60E-04 |
| CH3I | 7.82E-06 | 7.65E-06 | 7.15E-06 | 6.33E-06 | 5.25E-06 | 3.98E-06 | 2.62E-06 | 1.33E-06 | 5.50E-07 | 1.26E-07 |
| IALK | 1.56E-05 | 1.53E-05 | 1.43E-05 | 1.27E-05 | 1.05E-05 | 7.97E-06 | 5.22E-06 | 2.65E-06 | 1.10E-06 | 2.52E-07 |
| MI2 | 9.33E-03 | 9.20E-03 | 8.78E-03 | 8.07E-03 | 7.07E-03 | 5.75E-03 | 4.15E-03 | 2.40E-03 | 1.11E-03 | 2.87E-04 |
| MIB | 5.93E-04 | 5.83E-04 | 5.52E-04 | 5.02E-04 | 4.30E-04 | 3.42E-04 | 2.38E-04 | 1.32E-04 | 5.92E-05 | 1.47E-05 |
| MIC | 1.78E-04 | 1.75E-04 | 1.65E-04 | 1.48E-04 | 1.26E-04 | 9.90E-05 | 6.82E-05 | 3.70E-05 | 1.63E-05 | 3.98E-06 |
| NO2 | 9.58E-03 | 9.50E-03 | 9.22E-03 | 8.73E-03 | 8.02E-03 | 7.00E-03 | 5.60E-03 | 3.73E-03 | 1.95E-03 | 5.27E-04 |
| NO3_NO2 | 1.63E-01 | 1.62E-01 | 1.60E-01 | 1.55E-01 | 1.48E-01 | 1.38E-01 | 1.22E-01 | 9.70E-02 | 6.37E-02 | 1.46E-02 |
| FORM_R | 4.17E-05 | 4.10E-05 | 3.88E-05 | 3.53E-05 | 3.05E-05 | 2.42E-05 | 1.68E-05 | 9.08E-06 | 3.95E-06 | 9.20E-07 |
| FORM_M | 4.63E-05 | 4.58E-05 | 4.38E-05 | 4.07E-05 | 3.60E-05 | 2.98E-05 | 2.20E-05 | 1.31E-05 | 6.27E-06 | 1.68E-06 |
| HNO3 | 6.77E-06 | 6.62E-06 | 6.20E-06 | 5.50E-06 | 4.57E-06 | 3.45E-06 | 2.25E-06 | 1.12E-06 | 4.43E-07 | 9.28E-08 |

Table notes:
Rates calculated for an ozone column of 300 Dobson units, surface albedo of 0.04, and height above ground of 640 m
NO3_NO2 means $NO_3$ photolysis producing $NO_2$
FORM_R means formaldehyde photolysis producing radical products (HCO + H)
FORM_M means formaldehyde photolysis producing molecular products (CO + $H_2$)

**References**

Atkinson, R.A., D.L. Baulch, R.A. Cox, J.N. Crowley, R.F. Hampson, R.G. Hynes, M.E. Jenkin, J.A. Kerr, M.J. Rossi, and J. Troe.  2010.  "Evaluated kinetic and photochemical data for atmospheric chemistry - IUPAC subcommittee on gas kinetic data evaluation for atmospheric chemistry." 3 January 2010 web version available from http://www.iupac-kinetic.ch.cam.ac.uk/index.html

Cotter E.S.N., N.J. Booth, and C.E. Canosa-Mas, R.P. Wayne.  2001.  Release of iodine in the atmospheric oxidation of alkyl iodides and the fates of iodinated alkoxy radicals. *Atmospheric Environment*, **35**, 2169–2178.

Gómez-Martín, J.C., P. Spietz, and J.P. Burrows.  2007.  Kinetic and mechanistic studies of the I2/O3 photochemistry.  *Journal of Physical Chemistry*, **111**, 306–320.

Joseph, D.M., S.H. Ashworth and J.M.C. Plane.  2005.  The absorption cross-section and photochemistry of OIO.  *Journal of Photochemistry and Photobiology A – Chemistry*, **176**, 68–77.

Kaltsoyannis, N., Plane, and J.M.C.  2008.  Quantum chemical calculations on a selection of iodine-containing species (IO, OIO, $INO_3$, $IO_2$, $I_2O_3$, $I_2O_4$ and $I_2O_5$) of importance in the atmosphere.  *Physical Chemistry Chemical Physics*, **10**, 1723–1733.

Plane, J.M.C., Joseph, D.M., Allan, B.J., Ashworth, S.H., and Francisco, J.S.  2006.  An experimental and theoretical study of the reactions OIO + NO and OIO + OH.  *Journal of Physical Chemistry*, **110**, 93–100.

Riffault, V., Y. Bedjanian, and G. Poulet.  2005.  Kinetic and mechanistic study of the reactions of OH with IBr and HOI.  *Journal of Photochemistry and Photobiology A – Chemistry*, **176**, 155–161.

Sander, S.P., R.R. Friedl, D. M. Golden, M. J. Kurylo, G. K. Moortgat, P. H. Wine, A. R. Ravishankara, C. E. Kolb, M. J. Molina, B. J Finlayson-Pitts, R. E. Huie, and V. L. Orkin.  2006.  "Chemical Kinetics and Photochemical Data for use in Atmospheric Studies, Evaluation Number 15.  NASA Jet Propulsion Laboratory."  July.  Available from http://jpldataeval.jpl.nasa.gov/download.html.

Saunders, R.W., and J.M.C. Plane.  2005.  Formation pathways and composition of iodine oxide ultra-fine particles.  *Environmental Chemistry*, **2**, 299–303.

Sommariva R., W.J. Bloss, and R. von Glasow.  2012.  Uncertainties in gas-phase atmospheric iodine chemistry.  *Atmospheric Environment*, **57**, 219–232.  doi:10.1016/j.atmosenv.2012.04.032.

van den Bergh, H. and Troe, J.  1976.  Kinetic and thermodynamic properties of INO and $INO_2$ intermediate complexes in iodine recombination.  *J. Chem. Phys.*, **64**, 736–742.